Etude expérimentale et modélisation du procédé continu ensemencé de copolymérisation en dispersion du système styrène/acrylonitrile en milieu polyol

Bruno Salvador

▶ **To cite this version:**

Bruno Salvador. Etude expérimentale et modélisation du procédé continu ensemencé de copolymérisation en dispersion du système styrène/acrylonitrile en milieu polyol. Génie des procédés. Institut National Polytechnique de Lorraine, 2004. Français. NNT : 2004INPL041N . tel-01752316

HAL Id: tel-01752316
https://hal.univ-lorraine.fr/tel-01752316

Submitted on 1 Jun 2021

HAL is a multi-disciplinary open access archive for the deposit and dissemination of scientific research documents, whether they are published or not. The documents may come from teaching and research institutions in France or abroad, or from public or private research centers.

L'archive ouverte pluridisciplinaire **HAL**, est destinée au dépôt et à la diffusion de documents scientifiques de niveau recherche, publiés ou non, émanant des établissements d'enseignement et de recherche français ou étrangers, des laboratoires publics ou privés.

UNIVERSITÉ DE LORRAINE

AVERTISSEMENT

Ce document est le fruit d'un long travail approuvé par le jury de soutenance et mis à disposition de l'ensemble de la communauté universitaire élargie.

Il est soumis à la propriété intellectuelle de l'auteur. Ceci implique une obligation de citation et de référencement lors de l'utilisation de ce document.

D'autre part, toute contrefaçon, plagiat, reproduction illicite encourt une poursuite pénale.

Contact : ddoc-theses-contact@univ-lorraine.fr

LIENS

Code de la Propriété Intellectuelle. articles L 122. 4
Code de la Propriété Intellectuelle. articles L 335.2- L 335.10
http://www.cfcopies.com/V2/leg/leg_droi.php
http://www.culture.gouv.fr/culture/infos-pratiques/droits/protection.htm

INSTITUT NATIONAL
POLYTECHNIQUE DE LORRAINE

Ecole Nationale Supérieure
des Industries Chimiques

CENTRE NATIONAL DE LA
RECHERCHE SCIENTIFIQUE

Laboratoire des Sciences
du Génie Chimique

Thèse

présentée en vue de l'obtention du titre de

DOCTEUR
DE L'INSTITUT NATIONAL POLYTECHNIQUE DE LORRAINE

Spécialité : Génie des Procédés

par

Bruno SALVADOR
Ingénieur E.N.S.I.C.

Etude Expérimentale et Modélisation du Procédé Continu Ensemencé de Copolymérisation en Dispersion du Système Styrène/Acrylonitrile en Milieu Polyol

Experimental Study and Modeling of the Seeded Continuous Dispersion Copolymerization of the Styrene/Acrylonitrile System in Polyol Medium

---

Soutenue le 2 Juillet 2004 devant le jury

Président :	M. SARDIN	Professeur à l'E.N.S.I.C.
Rapporteurs :	B. W. BROOKS	Professeur à l'Université de Loughborough
	H. VAN DER WAL	Dow Global Technology Leader
Examinateurs :	C. FONTEIX	Professeur à l'E.N.S.G.S.I.
	A. PETIT	Maître de Conférences à l'E.N.S.I.C.
	F. PLA	Professeur à l'E.N.S.I.C.
Invité :	F. VAN DAMME	Dow Analytical Sciences

A mes Parents et à mon frère

A mes Grands-Parents

A la mémoire de mémé Renée et pépé Marcel

de mémé Césarine et pépé François

et de tonton René

A tous ceux que j'aime

A tous ceux qui m'aiment

ACKNOWLEDGEMENTS

This work is the result of the collaboration between the "Laboratoire des Sciences du Génie Chimique" and Dow Benelux N.V. It has been realized at the "Laboratoire des Sciences du Génie Chimique" in the research group "Génie de la Réaction Chimique". I would like to thank Prof. Hans-Günther LINTZ and Prof. Michel SARDIN, successively directors of the laboratory, for their welcome.

I would like to thank Prof. Fernand PLA for having welcomed me in his team "Génie des Procédés de Polymérisation".

I would like to thank Prof. Fernand PLA and Dr. Alain PETIT, the directors of my Ph.D. and also Prof. Christian FONTEIX, for their scientific help, their trust, the discussions we had and their encouragements during these years.

I would like to express my sincere gratitude to Prof. B.W. BROOKS, Professor at the Loughborough University and to Dr. Hanno Van der Wal, Global Technology Leader at Dow Benelux, for having agreed to judge this work.

I would like to thank Prof. Michel Sardin for having agreed to be president of the jury.

It has been a real pleasure to work with people from Dow at Terneuzen, who were always very kind and helpful.

I would like to thank particularly Dr. Hanno Van der WAL, Dr. Freddy Van DAMME, Dr. Jean-Paul MASY and Dr. Graeme FOGG from Dow for all the very interesting discussions that we had during these years and for their help.

I am also very grateful to Dr. Freddy Van DAMME and to all the people from the analytical department of Dow, who brought me a tremendous support during this work.

I would like to thank the PIBV team, and particularly Peter MULLAERT, Christiaan HIENSCH and Paul Van KOUTEREN, who taught me how to produce copolymer polyols with safety, zen and humor, and who helped me so much to go through all the technical problems.

Je tiens également à remercier toutes les personnes travaillant à l'ENSIC sans qui ce projet n'aurait pas pu être possible et particulièrement le personnel de la bibliothèque, de l'atelier, de l'antenne informatique, de la comptabilité et de l'administration.

Je remercie également les permanents du GP2 pour leur aide et leur sympathie durant ces quelques années et en particulier Sandrine, Cornélius et Jean.

Les déjà docteurs, Silvère, Marc, Manu, Olivier et Mathilde, qui m'ont accueilli dans ces murs et m'ont appris les ficelles du métier ainsi que les futurs docteurs Yannick, Rabih, Matthieu, Alexandra, Virginie, Thierry et Georges, pour leur chaleur et pour les liens qu'ils ont créé entre nous tous. Vraiment, ce fût agréable de travailler parmi vous.

I also thank all the roommates who have shared a bit of their life with me and who made me travel at home : Chafik, Katrin, Tatiana, Jialin, Jiang, Jérémy, Jeanette, Birte, Monica, Pedro, Matthieu and Gabi.

Un grand merci à toutes mes "infirmières" qui m'ont tant aidé après cette opération du genoux : Hélène, Céline, Navi, Maggi, Lucie, Valou, Elise, Rachel, Leïla, Sandrine, Alex, Virginie, Matthieu, Rabih, Cyril, Birte, Monica... et bien sur ma maman.

Un grand merci également à Didier, Yumiko & Joachim, Christelle & Philippe, Dom, Anne, Sylvie, Cyril & Sosana, Atsushi & Hiroko et à Kiki, avec qui j'ai beaucoup appris et pour toute l'énergie qu'ils m'ont donné.

J'ai aussi une très forte pensée pour Fred, Lucia, Tina, Valou, Jagna, Méloche, Rachel, Hélène, Célin, Virginie, Maggi, Emilie, Laura, Navi, Nico, Sara et Maud qui m'ont donné un peu de leur amitié et de leur amour.

And a special thank to :

Sarah Putsine, Rose & Paul, Anne-Lize & Gilou, Iggy et à tous les merveilleux clowns que j'ai rencontré.

Maggi et Benjamin mes partenaires trapézistes et échassiers,

Mes amis du projet Idiot qui fera un jour le tour du monde : Aurel, Cams, Seb et Cyril,

Ishrann, Jean et Aurore de la "Cie Pendule",

Rachel et toutes les "Braguettes Magiques",

Stéphanie et Yannick, mes collègues et amis marionnettistes de la "Cie Aristophane & Michichi",

Et tous les autres...

AVERTISSEMENT POUR LE LECTEUR

A la demande de la compagnie Dow Benelux et avec l'accord exceptionnel de Mr. Le Président de l'Institut National Polytechnique de Lorraine, cette thèse a été rédigée en anglais.

Le lecteur pourra trouver un long résumé en français de ces travaux à la fin du manuscrit.

RÉSUMÉ

Ces travaux de recherche ont pour but d'étudier et de modéliser un procédé continu ensemencé de copolymérisation en dispersion d'acrylonitrile et de styrène en milieu polyol : l'influence des conditions expérimentales sur les propriétés physiques des copolymères polyols produits est examinée à dessein de mieux comprendre les mécanismes mis en jeu et de développer un modèle de tendances pour le procédé global.

La première partie concerne l'étude expérimentale du procédé. L'influence du rapport des compositions en styrène et acrylonitrile, la température de réaction et les concentrations en agent de transfert, amorceur et stabilisant précurseur, sur les propriétés des copolymères polyols, est étudiée. Cela permet d'établir les différentes relations existant entre la distribution de masses molaires, le niveau de greffage, la viscosité, la distribution de tailles de particules et le site de la polymérisation. Cette étude montre également la complexité des phénomènes de stabilisation de particules qui interviennent.

La seconde partie présente la modélisation du procédé ainsi que l'identification des paramètres inconnus de ce modèle. En effet, un modèle destiné à prévoir les masses molaires moyennes, les conversions ainsi que le niveau de greffage des copolymères polyols est développé malgré la complexité du procédé et le manque de précision de certaines des mesures. Un algorithme d'évolution permet, en utilisant un nombre important d'expériences, d'identifier ces paramètres. Une validation préliminaire du travail est effectuée et permet de définir avec plus de précision les futures voies de recherche dans le domaine.

Mots-Clefs : Copolymérisation en dispersion, Modélisation, Algorithme d'évolution, Copolymère polyol

ABSTRACT

The aim of this work is to study and model the continuous seeded dispersion copolymerization of acrylonitrile with styrene in polyol medium : the influence of the process conditions on the physical properties of the copolymer polyols produced is investigated in order to better understand the different mechanisms involved and to develop a tendency model for the whole process.

The first part deals with the experimental study of the process. The influence of the styrene to acrylonitrile ratio, the temperature and the concentrations of the chain transfer agent, the initiator, and the precursor stabilizer, on the physical properties of copolymer polyols are studied. This allows to understand better the relationships between the molecular weight distributions, the grafting level, the viscosity, the particle size distributions, and the locus of polymerization. This study shows also the complexity of the phenomena involved in the particle stabilization.

The second part presents the modeling of the overall process and the identification of the parameters of this model. Indeed, a model intended to forecast the average molecular weights, the conversions and the grafting level in the copolymer polyols is developed in spite of the process complexity and the lack of accuracy of some of the measurements. An evolutionary algorithm allows then, with a consequent number of experiments realized, to identify the unknown parameters of this model. A preliminary validation of the work is presented and helps to define the ways to go further with this research.

Key words : Dispersion polymerization, Modeling, Evolutionary algorithm, Copolymer polyol

TABLE OF CONTENTS

Acknowledgements.....5

Résumé.....9

Abstract.....10

Table of contents.....11

Notations.....15

List of tables.....35

List of Figures.....41

Introduction.....51

Chapter 1. Dispersion Polymerization : General Bibliography

INTRODUCTION.....59

1. HETEROGENEOUS POLYMERIZATION PROCESSES.....59

1.1 GENERAL FEATURES OF HETEROGENEOUS POLYMERIZATION PROCESS.....59
1.2 EMULSION POLYMERIZATION.....60
1.3. SUSPENSION POLYMERIZATION AND DISPERSION POLYMERIZATION IN AQUEOUS MEDIUM.....60
1.4. PRECIPITATION POLYMERIZATION AND DISPERSION PRECIPITATION.....62

2. DEVELOPMENT OF THE DISPERSION POLYMERIZATION PROCESS.62

2.1. FIRST GENERATION : 1950S TO THE 1970S.....62
2.2. SECOND GENERATION : 1980S.....62
2.3. THIRD GENERATION : 1990S.....63

3. STERIC STABILIZATION.....65

3.1. THE ATTRACTIVE AND REPULSIVE FORCES.....65
3.2. THERMODYNAMIC APPROACH OF STERIC STABILIZATION.....67
3.3. STABILIZER STRUCTURES AND CONFORMATIONS.....68

4. MECHANISM AND MODELING OF DISPERSION POLYMERIZATION..70

4.1. GENERAL MECHANISM.....70
4.2. PARTICLE NUCLEATION.....70
4.3. PARTICLE GROWTH.....72
4.4. THERMODYNAMICS.....72

4.5. AGGLOMERATION AND RENUCLEATION : PARTICLE SIZE DISTRIBUTION 81
4.6. DISPERSION COPOLYMERIZATION 82

5. MAIN EXPERIMENTAL PARAMETERS INFLUENCING DISPERSION POLYMERIZATION 82

5.1. DILUENT SOLVENCY 82
5.2. MONOMERS 82
5.3. TEMPERATURE 83
5.4. INITIATOR 83
5.5. CHAIN TRANSFER AGENT 83
5.6. STABILIZER, PRECURSOR STABILIZER 83
5.7. AGITATION SPEED 84

6. COPOLYMER POLYOLS (CPP) 84

6.1. FLEXIBLE POLYURETHANE FOAMS 84
6.2. POLYETHER POLYOL 86
6.3. GRAFTED COPOLYMER POLYOL 89
6.4. EXAMPLES OF GRAFTED COPOLYMER POLYOL PRODUCED BY DOW CHEMICAL AND APPLICATIONS 90

CONCLUSION 91

Chapter 2 : Experimental Techniques

INTRODUCTION 95

1. PRODUCTION OF CPP LATEX 95

1.1. PREMIX FORMULATION 95
1.2. CONTINUOUS PRIMARY REACTOR AND ITS ENVIRONMENT 99

2. ANALYTICAL METHODS TO FOLLOW CPP PROPERTIES 103

2.1. ISOLATION OF THE SOLIDS FROM CPP : WASHING / CENTRIFUGATION WITH HEXANE-ETHYL ACETATE MIXTURES 104
2.2. HEADSPACE GAS CHROMATOGRAPHY (HSGC) / FLAME IONIZATION DETECTOR (FID) 104
2.3. GEL PERMEATION CHROMATOGRAPHY (GPC) – UV DETECTOR 105
2.4. PARTICLE SIZE DISTRIBUTION 108
2.5. RHEOMETRY 112
2.6. NUCLEAR MAGNETIC RESONANCE (NMR) : ^{1}H AND ^{13}C 114
2.7. MINIPULSED NUCLEAR MAGNETIC RESONANCE 116
2.8. NIC DERIVATIZATION FOLLOWED BY GPC – FLUORESCENCE 117
2.9. LIQUID CHROMATOGRAPHY ON SILICA GEL / UV DETECTOR 118

CONCLUSION 120

Chapter 3 : Experimental Study of the Process

INTRODUCTION 123

1. PRELIMINARY STUDIES 123

1.1. NDM AND MONOMER PARTITIONING 123
1.2. "NATURAL" GRAFTING 124
1.3. RELATIONSHIP BETWEEN GRAFTING AND VISCOSITY 126

2. EXPERIMENTAL RESULTS 127

2.1 EXPERIMENTAL DESIGN 127
2.2. STUDY OF THE STEADY STATE REGIME 128
2.3. RESULTS 129
2.4. RELATIONSHIPS BETWEEN THE DIFFERENT CPP PROPERTIES 150

CONCLUSION 153

Chapter 4 : Modeling

INTRODUCTION 157

1. MAIN ASSUMPTIONS 157

1.1. STYRENE-ACRYLONITRILE COPOLYMERIZATION 157
1.2. MONOMER UNITS 162
1.3. GRAFTING 163
1.4. THERMODYNAMICS 166
1.5. CAPTURE BY PARTICLES 167
1.6. PARTICLE STABILIZATION : MODEL FOR AVERAGE PARTICLE SIZE 168
1.7. KINETIC SCHEME 170

2. THE DEFINITION OF THE SYSTEM 173

2.1. BALANCE ON THE TOTAL CONCENTRATIONS OF THE SPECIES IN THE REACTOR 173
2.2. BALANCE ON THE CONCENTRATIONS OF FREE SPECIES IN THE REACTOR 174
2.3. BALANCE ON RADICALS, DEAD POLYMER CHAINS AND MOMENTS IN THE REACTOR 177
2.4. CALCULATION OF DATA TO BE COMPARED TO THE MEASUREMENTS 179

3. ESTIMATION OF THE STEADY STATE REGIME 185

CONCLUSION 187

Chapter 5 : Parameter identification

INTRODUCTION 191

1. PRINCIPLES OF EVOLUTIONARY ALGORITHM AND PARAMETER IDENTIFICATION 191

1.1. INTRODUCTION AND VOCABULARY 191
1.2. PRINCIPLE 192
1.3. DESCRIPTION OF THE COMPONENTS OF THE GENETIC OR EVOLUTIONARY ALGORITHM 192
1.4. PARAMETER IDENTIFICATION 194

2. DEFINITION OF THE PARAMETERS TO IDENTIFY 195
2.1. FIXED PARAMETERS 195
2.2. IDENTIFIED PARAMETERS 195
2.3. EXPERIMENTAL DATA CONSIDERED 197
3. RESULTS AND DISCUSSION 198
3.1. RESULTS 198
3.2. AVERAGE MOLECULAR WEIGHTS 201
3.3. SOLIDS AND RESIDUAL CONCENTRATIONS OF ACRYLONITRILE, STYRENE AND NDM 205
3.4. SAN COPOLYMER COMPOSITION 205
3.5. SERUM : WT-% OF SAN DISSOLVED AND % OF GRAFTED SAN 211
3.6. % OF GRAFTED SAN IN WHOLE CPP (HMW) AND WT-% OF POLYOL IN SOLIDS ..214
3.7. SAUTER MEAN DIAMETER 217
4. VALIDATION AND DISCUSSION 219
4.1. VALIDATION ON STANDARD RUNS CARRIED OUT AT T = 130°C 219
4.2. CONFIDENCE INTERVAL OF THE IDENTIFIED PARAMETERS 221
4.3. GRAFTING MODELING AND PATH FORWARD 222
CONCLUSION 223

Conclusions and recommendations 225

List of References 231

ANNEXES

Annex 1 : Main works done on dispersion precipitation from the 1980s to now 245

Annex 2 : Experimental Procedures 251

Annex 3 : Tables and figures of Chapter 3 261

Annex 4 : Calculations 305

Annex 5 : Tables and Figures of Chapter 5 337

Résumé Long 357

NOTATIONS

Abbreviations	Meaning
A	Acrylonitrile
AA	Acrylic acid
AIBN	Azo(bis-iso-butyronitrile)
AMBN	Azo(bis-methylbutyronitrile)
AN	Acrylonitrile
B	Styrene
BMA	N-butylmethacrylate
CPP	Copolymer polyol
C6	Hexane
CSTR	Continuous stirred tank reactor
CTA	Chain transfer agent
DABCO T12	Dibutyltin dilaurate
DCM	Dichloromethane
DMA	N,N-dimethylacrilamide
DMAEMA	2-(dimethylamino) ethylmethacrylate
DMC	2-Chloro-1,3-dimethylimidazolinium chloride
DMSO	Dimethyl sulfoxide
EGDMA	Ethylene glycol dimethacrylate
EMA	Ethyl methacrylate
EO	Ethylene oxide
EtOAc	Ethyl acetate
FID	Flame ionization detector
GC	Gas chromatography
GMA	Glycidil methacrylate
GPC	Gel permeation chromatography
HEMA	2-Hydroxyethyl methacrylate
HMW	High molecular weight grafted SAN copolymer
HPC	(Hydroxypropyl)cellulose
HPMC	Hydroxypropyl methylcellulose
HSGC	Headspace gas chromatography

I	Initiator
KOH	Potassium hydroxide
LC	Liquid chromatography
LALLS	Low Angle Laser Light Scattering
LMW	Low molecular weight grafted SAN copolymer
mMA	Methyl acrylate macromonomer
MMA	Methyl methacrylate
NDM	Normal-dodecamethyl mercaptan
NIC	Naphthyl Isocyanate
NMP	N-methyl pyrolidone
NMR	Nuclear magnetic resonance
NVC	N-vinyl carbazole
PAA	Poly(acrylic acid)
PDMS	Poly(dimethylsiloxane) monomethacrylate
PEI	Poly(ethyleneimine)
PEtOZO	Poly(2-ethyl-2-oxazoline)
PIDS	Polarization intensity differential scattering
PHEMA	Poly(2-hydroxyethyl methacrylate)
PFOA	Poly(1,1-dihydroperfluorooctyl acrylate)
PO	Propylene oxide
PPIE	Poly(propionylimino) ethylene
PVME	Polyvinylmethylether
PVP	Poly(N-vinylpyrrolidone)
PVPAc	Poly(vinylpyrrolidone vinylacetate) copolymer
SAN	Poly(styrene -co- acrylonitrile)
SEM	Scanning electron microscopy
Sty	Styrene
TBC	4-*tert*-butylcatechol
TDI	Toluene diisocyanate
THF	Tetrahydrofuran
TMSPMA	3-(trimetoxysilyl)propyl methacrylate
T27	Trigonox 27 (peroxide initiator)
UV	Ultraviolet
VMDAS	Vinylmethyldiacetoxysilane

VMDES	Vinylmethyldiethoxysilane
VTES	Vinyltriethoxysilane
VTMS	Vinyltrimethoxysilane

Nomenclature	Meaning	Unit
a	Sphere radius	m
a	Parameter of the model (see Eq. 4.42 and 4.43)	m $(mol\ kg^{-1})^{1/3}$
A	Constant	-
A*	Effective constant of Hamaker (see Eq 1.1)	-
[A]	Concentration of acrylonitrile in the reactor	$mol\ m^{-3}$
A_c	Quantity of acrylonitrile in the continuous phase	mol
$[A]_c$	Concentration of acrylonitrile in the continuous phase	$mol\ m^{-3}$
$[A]_e$	Concentration of acrylonitrile in the premix	$mol\ m^{-3}$
A_p	Quantity of acrylonitrile inside particles	mol
$[A]_p$	Concentration of free acrylonitrile inside particles	$mol\ m^{-3}$
$[A_P]$	Concentration of monomers A incorporated in the polymer chains	$mol\ m^{-3}$
$\left[A^*_{i,0}\right]_c$	Concentration of oligoradicals terminated by acrylonitrile, having i monomeric units and 0 graft, in the continuous phase	$mol\ m^{-3}$
$\left[A^*_{i,1}\right]_c$	Concentration of oligoradicals terminated by acrylonitrile, having i monomeric units and 1 graft unit (polyol), in the continuous phase	$mol\ m^{-3}$
$\left[A^*_{i,3}\right]_c$	Concentration of oligoradicals terminated by acrylonitrile, having i monomeric units and 3 graft units (S5200), in the continuous phase	$mol\ m^{-3}$
$\left[A^*_{i,0}\right]_p$	Concentration of oligoradicals terminated by acrylonitrile, having i monomeric units and 0 graft, inside the particles	$mol\ m^{-3}$
$\left[A^*_{i,1}\right]_p$	Concentration of oligoradicals terminated by acrylonitrile, having i monomeric units and 1 graft unit (polyol),, inside the particles	$mol\ m^{-3}$
$\left[A^*_{i,3}\right]_p$	Concentration of oligoradicals terminated by acrylonitrile, having i monomeric units and 3 graft units (S5200), inside the particles	$mol\ m^{-3}$

$[A_T]$	Total concentration of acrylonitrile in the reactor (free and incorporated)	mol m^{-3}
$\left[A^*_{T,0}\right]_c$	Total concentration of all oligoradicals terminated by acrylonitrile having 0 graft in the continuous phase	mol m^{-3}
$\left[A^*_{T,1}\right]_c$	Total concentration of all oligoradicals terminated by acrylonitrile having 1 graft unit (polyol) in the continuous phase	mol m^{-3}
$\left[A^*_{T,3}\right]_c$	Total concentration of all oligoradicals terminated by acrylonitrile having 3 graft units (S5200) in the continuous phase	mol m^{-3}
$\left[A^*_{T,0}\right]_p$	Total concentration of all oligoradicals terminated by acrylonitrile having 0 graft inside particles	mol m^{-3}
$\left[A^*_{T,1}\right]_p$	Total concentration of all oligoradicals terminated by acrylonitrile 1 graft unit (polyol) inside particles	mol m^{-3}
$\left[A^*_{T,3}\right]_p$	Total concentration of all oligoradicals terminated by acrylonitrile 3 graft units (S5200) inside particles	mol m^{-3}
B	Constant	-
[B]	Concentration of styrene in the reactor	mol m^{-3}
B_c	Quantity of styrene in the continuous phase	mol
$[B]_c$	Concentration of free styrene in the continuous phase	mol m^{-3}
$[B]_e$	Concentration of styrene in the premix	mol m^{-3}
B_p	Quantity of styrene inside particles	mol
$[B]_p$	Concentration of styrene inside particles	mol m^{-3}
$[B_P]$	Concentration of monomers B incorporated in the polymer chains	mol m^{-3}
$\left[B^*_{i,0}\right]_c$	Concentration of oligoradicals terminated by styrene, having i monomeric units and 0 graft, in the continuous phase	mol m^{-3}
$\left[B^*_{i,1}\right]_c$	Concentration of oligoradicals terminated by styrene, having i monomeric units and 1 graft unit (polyol) in the continuous phase	mol m^{-3}
$\left[B^*_{i,3}\right]_c$	Concentration of oligoradicals terminated by styrene, having i monomeric units and 3 graft units (S5200) in the continuous phase	mol m^{-3}

$\left[B_{i,0}^{*}\right]_p$	Concentration of oligoradicals terminated by styrene, having i monomeric units and 0 graft, inside the particles	mol m^{-3}
$\left[B_{i,1}^{*}\right]_p$	Concentration of oligoradicals terminated by styrene, having i monomeric units and 1 graft unit (polyol), inside the particles	mol m^{-3}
$\left[B_{i,3}^{*}\right]_p$	Concentration of oligoradicals terminated by styrene, having i monomeric units and 3 graft units (S5200), inside the particles	mol m^{-3}
$[B_T]$	Total concentration of styrene in the reactor (free and incorporated)	mol m^{-3}
$\left[B_{T,0}^{*}\right]_c$	Total concentration of all oligoradicals terminated by styrene having 0 graft in the continuous phase	mol m^{-3}
$\left[B_{T,1}^{*}\right]_c$	Total concentration of all oligoradicals terminated by styrene having 1 graft unit (polyol) in the continuous phase	mol m^{-3}
$\left[B_{T,3}^{*}\right]_c$	Total concentration of all oligoradicals terminated by styrene having 3 graft units (S5200) in the continuous phase	mol m^{-3}
$\left[B_{T,0}^{*}\right]_p$	Total concentration of all oligoradicals terminated by styrene having 0 graft inside particles	mol m^{-3}
$\left[B_{T,1}^{*}\right]_p$	Total concentration of all oligoradicals terminated by styrene 1 graft unit (polyol) inside particles	mol m^{-3}
$\left[B_{T,3}^{*}\right]_p$	Total concentration of all oligoradicals terminated by styrene 3 graft units (S5200) inside particles	mol m^{-3}
c	Continuous phase	-
C	Constant	-
c_A	Weight fraction of monomers A in the feed	-
C_A	Weight fraction of monomers A in the copolymer	-
c_B	Weight fraction of monomers B in the feed	-
C_B	Weight fraction of monomers B in the copolymer	-
Coef	Random number in the range [–0.1 ; 1.1]	-
[CTA]	Concentration of chain transfer agent in the reactor	mol m^{-3}
CTA_c	Quantity of chain transfer agent in the continuous phase	mol
$[CTA]_c$	Concentration of chain transfer agent in the continuous phase	mol m^{-3}
$[CTA]_e$	Concentration of chain transfer agent in the premix	mol m^{-3}

CTA_p	Quantity of chain transfer agent inside particles	mol
$[CTA]_p$	Concentration of chain transfer agent inside particles	mol m^{-3}
$[CTA_T]$	Total concentration of chain transfer agent in the reactor	mol m^{-3}
D	Constant	-
$\overline{D}$	Effective mean diffusion coefficient for radical capture	m^2 particle^{-1} s^{-1}
D_i	Diffusion coefficient of an oligoradical having i monomeric units in the surrounding medium	m^2 particle^{-1} s^{-1}
$\overline{D}_0$	Mean diffusion coefficient for ungrafted species	m^2 particle^{-1} s^{-1}
$\overline{D}_1$	Mean diffusion coefficient for species with 1 graft unit (polyol)	m^2 particle^{-1} s^{-1}
$\overline{D}_3$	Mean diffusion coefficient for species with 3 graft units (S5200)	m^2 particle^{-1} s^{-1}
d_{max}	Mean diameter of spheres of same maximum length	m
d_{min}	Mean diameter of spheres of same minimum length	m
d_p	Particle diameter	m
d_{sed}	Mean diameter of spheres having the same sedimentation rate	m
d_{sieve}	Mean diameter of spheres passing through the same sieve aperture	m
d_v	Mean diameter of spheres of same volume	m
d_w	Mean diameter of spheres of same weight	m
D[1, 0]	Number-length mean diameter	m
D[2, 0]	Number-surface mean diameter	m
D[3, 0]	Number-volume mean diameter	m
D[3, 2]	Sauter mean diameter	m
D[4, 3]	De Brouckere mean diameter	m
E	Exponential factor	J mol^{-1}
ΔE_i^v	Energy of vaporization of species i	J
F	Maximum likelihood estimator	-
f_A	Mole fraction of monomers A in the feed	-
F_A	Mole fraction of monomers A in the copolymer	-
f_B	Mole fraction of monomers B in the feed	-
F_B	Mole fraction of monomers B in the copolymer	-
f_c	Initiator efficiency in the continuous phase	-

F_{crit}	Critical value of the maximum likelihood estimator	-
F_i	Correction factor to account for the reversibility of radical absorption and potential barrier to absorption	-
F_{mut}	Value of the maximum likelihood estimator of a mutant	-
f_p	Initiator efficiency inside particles	-
F_{parent}	Value of the maximum likelihood estimator of a parent	
g	Gel effect parameter (see Eq. 1.12)	-
[G]	Concentration of S5200 in the reactor	mol m^{-3}
$[G]_e$	Concentration of S5200 in the premix	mol m^{-3}
g(L)	Volume particule size distribution	m^3
gel1	Gel effect coefficient (adjustable parameters of the model)	-
gel2	Gel effect coefficient (adjustable parameters of the model)	-
ΔG_M	Gibbs free energy of mixing	J
$\left[G^*_{0,3}\right]_c$	Concentration of S5200 molecules activated by action of primary radicals on its vinyl bond or by H-abstraction on PO groups	mol m^{-3}
$\left[G^*_{i,3}\right]_c$	Concentration of oligoradicals having i monomeric units and a terminal graft S5200 in the continuous phase	mol m^{-3}
$\left[G^*_{i,3}\right]_p$	Concentration of oligoradicals having i monomeric units and a terminal graft S5200 adsorbed at the particles surface	mol m^{-3}
$[G_T]$	Total concentration of S5200 in the reactor (free or incorporated)	mol m^{-3}
$\left[G^*_{T,3}\right]_c$	Total concentration of oligoradicals terminated by a graft S5200 in the continuous phase	mol m^{-3}
$\left[G^*_{T,3}\right]_p$	Total concentration of oligoradicals terminated by a graft S5200 adsorbed at the particles surface	mol m^{-3}
H	Height of inner cone (see Eq. 2.23)	m
H_A	Partitioning coefficient of acrylonitrile	-
H_B	Partitioning coefficient of styrene	-
H_{CTA}	Partitioning coefficient of the chain transfer agent	-
H_I	Partitioning coefficient of the initiator	-
ΔH_i^v	Enthalpy of vaporization of species i	J
ΔH_M	Enthalpy change on mixing	J
H_0	Distance between two particle surfaces (see Eq. 1.1)	m

i	Index giving the number of monomer units in SAN chains	
[I]	Concentration of initiator in the reactor	mol m^{-3}
I_c	Quantity of initiator in the continuous phase	mol
$[I]_c$	Concentration of initiator in the continuous phase	mol m^{-3}
$[I]_e$	Concentration of the initiator in the premix	mol m^{-3}
I_p	Quantity of initiator inside particles	mol
$[I]_p$	Concentration of initiator inside particles	mol m^{-3}
j	Index giving the number of monomeric units(j = 0 : no graft, j = 1 : graft = polyol solvent ; j = 3 : graft = S5200)	-
J	Sum of the squares of differences between theory and experiments for a given data	-
$\overline{J}_a^0$	Rate of absorption of ungrafted species	mol m^{-3} s^{-1}
$\overline{J}_a^1$	Rate of absorption of species grafted with the solvent	mol m^{-3} s^{-1}
$\overline{J}_a^3$	Rate of absorption of species grafted with S5200	mol m^{-3} s^{-1}
$\overline{J}_p$	Mean rate of precipitation	mol m^{-3} s^{-1}
k	Index giving the number of acrylonitrile elements in SAN chains	-
K	Constant (see Eq. 1.9)	m
$\overline{k}_a^0$	Constant of absorption of ungrafted species	m $particle^{-1}$ s^{-1}
$\overline{k}_a^1$	Constant of absorption of species grafted with the solvent	m $particle^{-1}$ s^{-1}
$\overline{k}_a^3$	Constant of absorption of species grafted with S5200	m $particle^{-1}$ s^{-1}
Kc	Proportional action	-
k_d	Kinetic constant of decomposition	s^{-1}
K_D	Constant of calibration of GPC (see Eq. 2.2)	-
$\overline{k}_e$	Average entry rate coefficient (see Eq. 1.6)	m^3 $particle^{-1}$ s^{-1}
k_{ei}	Entry rate coefficient of oligoradicals of length I (see Eq. 1.4)	m^3 $particle^{-1}$ s^{-1}
$\overline{k}_p$	Average propagation reaction constant (see Eq. 1.15)	m^3 mol^{-1} s^{-1}
$\overline{K}_p$	Constant of precipitation	s^{-1}
k_{pAA}	Kinetic rate constant for the homopropagation of acrylonitrile	m^3 mol^{-1} s^{-1}
k_{pAB}	Kinetic rate constant for the cross-propagation of acrylonitrile with styrene	m^3 mol^{-1} s^{-1}

k_{pAG}	Kinetic rate constant for the cross-propagation of acrylonitrile with S5200	$m^3 mol^{-1} s^{-1}$
k_{pBA}	Kinetic rate constant for the cross-propagation of styrene with acrylonitrile	$m^3 mol^{-1} s^{-1}$
k_{pBB}	Kinetic rate constant for the homopropagation of styrene	$m^3 mol^{-1} s^{-1}$
k_{pBG}	Kinetic rate constant for the cross-propagation of styrene with S5200	$m^3 mol^{-1} s^{-1}$
k_{GA}	Kinetic rate constant for the reaction of the radicals G* on acrylonitrile	$m^3 mol^{-1} s^{-1}$
k_{GB}	Kinetic rate constant for the reaction of the radicals G* on styrene	$m^3 mol^{-1} s^{-1}$
$\overline{k}_{p_0}$	Average propagation reaction constant under conditions at which the propagation is not diffusionally controlled (diluted systems) (see Eq. 1.15)	$m^3 mol^{-1} s^{-1}$
k_{RA}	Kinetic rate constant for the initiation on styrene by primary radicals	$m^3 mol^{-1} s^{-1}$
k_{RB}	Kinetic rate constant for the initiation on acrylonitrile by primary radicals	$m^3 mol^{-1} s^{-1}$
k_{RG}	Kinetic rate constant for the initiation on S5200 by primary radicals	$m^3 mol^{-1} s^{-1}$
$k_{RG,ng}$	Kinetic rate constant for the hydrogen abstraction of primary radicals on S5200 (natural grafting)	$m^3 mol^{-1} s^{-1}$
$k_{RS,ng}$	Kinetic rate constant for the hydrogen abstraction of primary radicals on the solvent (natural grafting)	$m^3 mol^{-1} s^{-1}$
k_{SA}	Kinetic rate constant for the reaction of the radicals S* on acrylonitrile	$m^3 mol^{-1} s^{-1}$
k_{SB}	Kinetic rate constant for the reaction of the radicals S* on styrene	$m^3 mol^{-1} s^{-1}$
$\overline{k}_t$	Average termination rate constant (see Eq. 1.10)	$m^3 mol^{-1} s^{-1}$
$\overline{k}_{t_0}$	Average termination reaction constant under conditions at which the termination is not diffusionally controlled (diluted systems) (see Eq. 1.11)	$m^3 mol^{-1} s^{-1}$
k_{tcAA}	Kinetic rate constant for the homotermination by combination of oligoradicals terminated by acrylonitrile	$m^3 mol^{-1} s^{-1}$

k_{tcAB}	Kinetic rate constant for the cross-termination by combination of oligoradicals terminated by acrylonitrile and by styrene	$m^3\ mol^{-1}\ s^{-1}$
k_{tcBB}	Kinetic rate constant for the homotermination by combination of oligoradicals terminated by styrene	$m^3\ mol^{-1}\ s^{-1}$
k_{tdGA}	Kinetic rate constant for the termination by dismutation of oligoradicals terminated by S5200 and by acrylonitrile	$m^3\ mol^{-1}\ s^{-1}$
k_{tdGB}	Kinetic rate constant for the termination by dismutation of oligoradicals terminated by S5200 and by styrene	$m^3\ mol^{-1}\ s^{-1}$
$k_{tr,A}$	Kinetic rate constant of the transfers of the oligoradicals terminated by acrylonitrile to the chain transfer agent	$m^3\ mol^{-1}\ s^{-1}$
$k_{tr,AG}$	Kinetic rate constant of the transfers of the oligoradicals terminated by acrylonitrile to S5200	$m^3\ mol^{-1}\ s^{-1}$
$k_{tr,AS}$	Kinetic rate constant of the transfers of the oligoradicals terminated by acrylonitrile to the solvent	$m^3\ mol^{-1}\ s^{-1}$
$k_{tr,B}$	Kinetic rate constant of the transfers of the oligoradicals terminated by styrene to the chain transfer agent	$m^3\ mol^{-1}\ s^{-1}$
$k_{tr,BG}$	Kinetic rate constant of the transfers of the oligoradicals terminated by styrene to S5200	$m^3\ mol^{-1}\ s^{-1}$
$k_{tr,BS}$	Kinetic rate constant of the transfers of the oligoradicals terminated by styrene to the solvent	$m^3\ mol^{-1}\ s^{-1}$
$k_{tr,GS}$	Kinetic rate constant of the transfers of the oligoradicals terminated by S5200 to the solvent	$m^3\ mol^{-1}\ s^{-1}$
l	Index giving the number of styrene elements in SAN copolymers	-
l_{crit}	Critical chain length	-
M	Molecular weight	$g\ mol^{-1}$
m_A	Weight of acrylonitrile in the reactor	kg
M_A	Molecular weight of acrylonitrile	$g\ mol^{-1}$
M_{AN}	Molecular weight of acrylonitrile	$g\ mol^{-1}$
m_B	Weight of styrene in the reactor	kg
M_B	Molecular weight of styrene	$g\ mol^{-1}$
$m^c_{B_{SAN}}$	Weight of the styrene elements contained in SAN copolymer in the continuous phase	kg

$m^{c}_{B_{SAN-grafted}}$	Weight of the styrene elements contained in grafted SAN copolymer in the continuous phase	kg
$m^{p}_{B_{SAN}}$	Weight of the styrene elements contained in SAN copolymer inside particles	kg
$m^{p}_{B_{SAN-grafted}}$	Weight of the styrene elements contained in grafted SAN copolymer inside particles	kg
m_{CPP}	Weight in the reactor	kg
M_{EO}	Molecular weight of ethylene oxide	g mol^{-1}
M_G	Molecular weight of the graft S5200	g mol^{-1}
m^{p}_{Grafi}	Weight of the grafts contained in the solid phase	kg
M_i	Torques exerting on inner cylinder	N m
M_I	Molecular weight of the initiator	g mol^{-1}
$\left[M_i^*\right]$	Concentration of the oligoradical species with DP = i	mol m^{-3}
$\bar{M}_n$	Number-average molecular weight	g mol^{-1}
$\bar{M}^{c}_{n}$	Number-average molecular weight of the SAN chains in the continuous phase	g mol^{-1}
M_o	Torques exerting on outer cylinder	N m
m^{c}_{SAN}	Weight of SAN copolymer in the continuous phase	kg
m_{serum}	Weight of the serum phase in the reactor	kg
m_{solid}	Weight of the solid phase in the reactor	kg
M_{S5200}	Molecular weight of S5200	g mol^{-1}
M_{PO}	Molecular weight of propylene oxide	g mol^{-1}
M_{Polyol}	Molecular weight of the solvent	g mol^{-1}
M_S	Molecular weight of the solvent	g mol^{-1}
M_{SAN}	Molecular weight of SAN copolymer	g mol^{-1}
m^{p}_{SAN}	Weight of the SAN copolymer inside particles	kg
M_{Sty}	Molecular weight of styrene	g mol^{-1}
M_u	Average molecular weight of the monomer unit	g mol^{-1}
$\left[M_T^*\right]$	Global concentration of all the oligoradicals M_i^*	mol m^{-3}
$\bar{M}_W$	Weight average molecular weight	g mol^{-1}
$\bar{M}_{W_{crit}}$	Value of $\bar{M}_W$ at which chain entanglement begins	g mol^{-1}

$\bar{M}_w^c$	Weight-average molecular weight of the SAN chains in the continuous phase	g mol^{-1}
n	Adjustable parameters (see Eq. 1.11)	-
n	Parameter of the gamma function (see Eq. 2.9)	-
n	Mean number of grafts per SAN chain (see Eq. 3.6)	-
$\tilde{n}$	Radical number per particle (see Eq. 1.9)	-
Na	Avogadro number	-
ne	Total number of experiments	-
N_G	Number of grafts S5200 in the reactor	-
n(L)	Number particle size distribution	-
nm	Number of different types of measurement used for the identification	-
N_p	Number of polymer particles in the reactor	-
N_S	Number of grafts polyol in the reactor	-
p	Particle phase	-
P_c	Critical pressure	Pa
$[P_{i,0}]_c$	Concentration of dead polymer having i monomeric units and 0 graft, in the continuous phase	mol m^{-3}
$[P_{i,1}]_c$	Concentration of dead polymer having i monomeric units and 1 graft unit (polyol) in the continuous phase	mol m^{-3}
$[P_{i,3}]_c$	Concentration of dead polymer having i monomeric units and 3 graft units (S5200) in the continuous phase	mol m^{-3}
$[P_{i,0}]_p$	Concentration of dead polymer having i monomeric units and 0 graft inside particles	mol m^{-3}
$[P_{i,1}]_p$	Concentration of dead polymer having i monomeric units and 1 graft unit (polyol) inside particles	mol m^{-3}
$[P_{i,3}]_p$	Concentration of dead polymer having i monomeric units and 3 graft units (S5200) inside particles	mol m^{-3}
$[P_{T,0}]_c$	Total concentration of dead polymer having 0 graft in the continuous phase	mol m^{-3}
$[P_{T,1}]_c$	Total concentration of dead polymer having 1 graft unit (polyol) in the continuous phase	mol m^{-3}

$\left[P_{T,3}^{*}\right]_c$	Total concentration of dead polymer having 3 graft units (S5200) in the continuous phase	mol m^{-3}
$\left[P_{T,0}^{*}\right]_p$	Total concentration of dead polymer having 0 graft inside particles	mol m^{-3}
$\left[P_{T,1}^{*}\right]_p$	Total concentration of dead polymer having 1 graft unit (polyol) inside particles	mol m^{-3}
$\left[P_{T,3}^{*}\right]_p$	Total concentration of dead polymer having 3 graft units (S5200) inside particles	mol m^{-3}
Q_e	Volume flow at the reactor inlet	m^3 s^{-1}
Q_s	Volume flow at the reactor outlet	m^3 s^{-1}
Q_{sm}	Mass flow at the outlet of the reactor	kg s^{-1}
r	Particle radius	m
R	Gaz constant (= 8,314)	J mol^{-1} K^{-1}
R	Cone radius (see Eq. 2.25)	m
r_a	Radius of interaction (see Eq. 1.10)	m
r_A	Coefficient of reactivity of acrylonitrile ($= k_{pAA}/k_{pAB}$)	-
R_{Ai}	Rate of absorption of radical species of length i (see Eq. 1.4)	mol s^{-1} m^{-1}
Ran	Random number from 0 to 1	-
r_B	Coefficient of reactivity of styrene ($= k_{pBB}/k_{pBA}$)	-
Residual AN	Weight ratio of residual acrylonitrile in the reactor	wt-%
Residual NDM	Weight ratio of residual NDM in the reactor	ppm
Residual Sty	Weight ratio of residual styrene in the reactor	wt-%
R_g	Radius of gyration	m
$R_{g,G}$	Radius of gyration of S5200	m
$R_{g,S}$	Radius of gyration of the solvent	m
R_{Gi}	Coefficient of reactivity of oligaradicals terminated by S5200 with styrene ($= k_{pGi}/k_{pGG}$)	-
R_i	Radius of inner cylinder	m
R_{iG}	Coefficient of reactivity of oligaradicals with a terminal i (A or B) with the S5200 macromeres ($= k_{piG}/k_{pii}$)	-
R_o	Radius of outer cylinder	m

R_{TA}	Transfer reactivity of the oligoradicals terminated by acrylonitrile to the chain transfer agent ($= k_{tr,A}/k_{pAA}$)	-
R_{TB}	Transfer reactivity of the oligoradicals terminated by styrene to the chain transfer agent ($= k_{tr,B}/k_{pBB}$)	-
$[R^*]_c$	Concentrations of primary radicals coming from initiator decomposition and transfers to chain transfer agent in the continuous phase	mol m^{-3}
$[R^*]_p$	Concentrations of primary radicals coming from initiator decomposition and transfers to chain transfer agent inside the particles	mol m^{-3}
[S]	Concentration of the solvent in the reactor	mol m^{-3}
$[S]_e$	Concentration of the solvent in the premix	mol m^{-3}
$[S_T]$	Total concentration of the solvent in the reactor	mol m^{-3}
S_0	Original signal, (see Eq. 2.35)	-
ΔS_M	Entropy change on mixing	J
S_p	Total surface of the particles	m^2
S_τ	Signal at time is τ (see Eq. 2.35)	-
$[S^*_{0,1}]_c$	Concentration of polyol molecules (solvent) activated by H-abstraction on PO groups by primary radicals issued from T27 (peroxide)	mol m^{-3}
t	Time	s
Δt	Step of time	s
T	Temperature	K
T_2	Relaxation time (see Eq. 2.35)	s
T_2^*	Apparent relaxation time (see Eq. 2.35)	s
T_c	Critical temperature	K
T_{gA}	Glass transition temperature of acrylonitrile	K
T_{gB}	Glass transition temperature of styrene	K
T_I	Integration action	-
V	Volume of the reactor	m^3
V_c	Volume of the continuous phase in the reactor	m^3
$\overline{V_i}$	Molar volume of species i	m^3 mol^{-1}
V_u	Average molecular volume of the monomeric unit	mol m^{-3}

V_A	van der Waals attraction potential (see Eq 1.1)	J
V_E	Elution volume	m^3
V_I	Interstitial volume inside the column	m^3
V_F	Free volume in the polymer particles	m^3
$V_{F_{crit}}$	Free volume at which chain entanglement begins in Eq. 1.11 and free volume at which $\overline{k}_p$ begins to decrease in Eq. 1.15	m^3
V_p	Total volume of the particles in the reactor	m^3
V_P	Volume of the pores	m^3
V_S	Steric interaction potential	J
V_T	Total interaction potential	J
x	Vector containing the different parameters of the model that are investigated	-
X^{child}	Vector of the children containing the different parameters of the model that are investigated	-
x_p	Weight fraction of polymer in the particles swollen by the monomers	-
$X^{parent1}$	Vector of the parent n°1 containing the different parameters of the model that are investigated	-
$X^{parent2}$	Vector of the parent n°2 containing the different parameters of the model that are investigated	-
Y_B	Composition in weight of styrene in the SAN copolymer	-
Y_k	Copolymer composition in the monomer k	-
Z_{exp}	Matrix containing all the experimental data obtained for the different experiments	-
Z_{theo}	Matrix containing all the theoretical data obtained for the different experiments for a given set of parameters	-

Greek symbols	**Meaning**	**Unit**
β	Gap angle (see Eq. 2.24)	°
β_{gel}	Gell effect constant (see Eq. 1.14)	-
χ_{ij}	Interaction parameter per molecule of compound i with compound j	-
χ_{iP_k}	Interaction parameter of component i with homopolymer k	-
χ_{ij}^H	Enthalpic term of the interaction parameter between the species i and j	-

χ_{ij}^{S}	Entropic term of the interaction parameter between the species i and j	-
δ	Thickness of the stabilizing layer (see Eq. 1.2)	m
δ_i	Hildebrand solubility parameter of species i (see Eq. 1.17)	$J^{1/2}\ m^{-3/2}$
δ_d	Hansen cohesive energy density representing dispersion contributions	$J^{1/2}\ m^{-3/2}$
${}^{m}\delta_d$	Hansen cohesive energy density representing dispersion contributions of a mixture	$J^{1/2}\ m^{-3/2}$
δ_h	Hansen cohesive energy density representing hydrogen bonding contributions	$J^{1/2}m^{-3/2}$
${}^{m}\delta_h$	Hansen cohesive energy density representing hydrogen bonding contributions of a mixture	$J^{1/2}m^{-3/2}$
δ_{mix}	Mixture solubility parameter of the continuous phase	$J^{1/2}\ m^{-3/2}$
δ_p	Hansen cohesive energy density representing polarity contributions	$J^{1/2}\ m^{-3/2}$
${}^{m}\delta_p$	Hansen cohesive energy density representing polarity contributions of a mixture	$J^{1/2}\ m^{-3/2}$
δ_t	Total Hansen cohesive energy density	$J^{1/2}\ m^{-3/2}$
${}^{m}\delta_t$	Total Hansen cohesive energy density of a mixture	$J^{1/2}\ m^{-3/2}$
$\Delta_{i,0}^{c}$	Distribution of oligoradicals terminated by acrylonitrile, having i monomer units and 0 graft, in the continuous phase	-
$\Delta_{i,1}^{c}$	Distribution of oligoradicals terminated by acrylonitrile, having i monomer units and 1 graft unit (polyol), in the continuous phase	-
$\Delta_{i,3}^{c}$	Distribution of oligoradicals terminated by acrylonitrile, having i monomer units and 3 graft units (S5200), in the continuous phase	-
$\Delta_{i,0}^{p}$	Distribution of oligoradicals terminated by acrylonitrile, having i monomer units and 0 graft, inside the particles	-
$\Delta_{i,1}^{p}$	Distribution of oligoradicals terminated by acrylonitrile, having i monomer units and 1 graft unit (polyol), inside the particles	-
$\Delta_{i,3}^{p}$	Distribution of oligoradicals terminated by acrylonitrile, having i monomer units and 3 graft units (S5200), inside the particles	-
$\varphi(M)$	Distribution of the molecular weights	-

γ	Interfacial tension	$N\ m^{-1}$
$\dot{\gamma}$	shear rate	s^{-1}
Γ	Gamma function	-
$\Gamma^{c}_{i,0}$	Distribution of oligoradicals terminated by styrene, having i monomer units and 0 graft, in the continuous phase	-
$\Gamma^{c}_{i,1}$	Distribution of oligoradicals terminated by styrene, having i monomer units and 1 graft unit (polyol), in the continuous phase	-
$\Gamma^{c}_{i,3}$	Distribution of oligoradicals terminated by styrene, having i monomer units and 3 graft units (S5200), in the continuous phase	-
$\Gamma^{p}_{i,0}$	Distribution of oligoradicals terminated by styrene, having i monomer units and 0 graft, inside the particles	-
$\Gamma^{p}_{i,1}$	Distribution of oligoradicals terminated by styrene, having i monomer units and 1 graft unit (polyol), inside the particles	-
$\Gamma^{p}_{i,3}$	Distribution of oligoradicals terminated by styrene, having i monomer units and 3 graft units (S5200), inside the particles	-
$\lambda^{c}_{1,0}$	Moment of order 1 of oligoradicals terminated with acrylonitrile, having 0 graft, in the continuous phase	-
$\lambda^{c}_{1,1}$	Moment of order 1 of oligoradicals terminated with acrylonitrile, having 1 graft unit (polyol), in the continuous phase	-
$\lambda^{c}_{1,3}$	Moment of order 1 of oligoradicals terminated with acrylonitrile, having 3 graft units (S5200), in the continuous phase	-
$\lambda^{c}_{2,0}$	Moment of order 2 of oligoradicals terminated with acrylonitrile, having 0 graft, in the continuous phase	-
$\lambda^{c}_{2,1}$	Moment of order 2 of oligoradicals terminated with acrylonitrile, having 1 graft unit (polyol), in the continuous phase	-
$\lambda^{c}_{2,3}$	Moment of order 2 of oligoradicals terminated with acrylonitrile, having 3 graft units (S5200), in the continuous phase	-
$\lambda^{p}_{1,0}$	Moment of order 1 of oligoradicals terminated with acrylonitrile, having 0 graft, inside particles	-

$\lambda_{1,1}^{p}$	Moment of order 1 of oligoradicals terminated with acrylonitrile, having 1 graft unit (polyol), inside particles	-
$\lambda_{1,3}^{p}$	Moment of order 1 of oligoradicals terminated with acrylonitrile, having 3 graft units (S5200), inside particles	-
$\lambda_{2,0}^{p}$	Moment of order 2 of oligoradicals terminated with acrylonitrile, having 0 graft, inside particles	-
$\lambda_{2,1}^{p}$	Moment of order 2 of oligoradicals terminated with acrylonitrile, having 1 graft unit (polyol), inside particles	-
$\lambda_{2,3}^{p}$	Moment of order 2 of oligoradicals terminated with acrylonitrile, having 3 graft units (S5200), inside particles	-
η	Viscosity	Pa s
$\eta_{1,0}^{c}$	Moment of order 1 of oligoradicals terminated with styrene, having 0 graft, in the continuous phase	-
$\eta_{1,1}^{c}$	Moment of order 1 of oligoradicals terminated with styrene, having 1 graft unit (polyol), in the continuous phase	-
$\eta_{1,3}^{c}$	Moment of order 1 of oligoradicals terminated with styrene, having 3 graft units (S5200), in the continuous phase	-
$\eta_{2,0}^{c}$	Moment of order 2 of oligoradicals terminated with styrene, having 0 graft, in the continuous phase	-
$\eta_{2,1}^{c}$	Moment of order 2 of oligoradicals terminated with styrene, having 1 graft unit (polyol), in the continuous phase	-
$\eta_{2,3}^{c}$	Moment of order 2 of oligoradicals terminated with styrene, having 3 graft units (S5200), in the continuous phase	-
$\eta_{1,0}^{p}$	Moment of order 1 of oligoradicals terminated with styrene, having 0 graft, inside particles	-
$\eta_{1,1}^{p}$	Moment of order 1 of oligoradicals terminated with styrene, having 1 graft unit (polyol), inside particles	-
$\eta_{1,3}^{p}$	Moment of order 1 of oligoradicals terminated with styrene, having 3 graft units (S5200), inside particles	-
$\eta_{2,0}^{p}$	Moment of order 2 of oligoradicals terminated with styrene, having 0 graft, inside particles	-
$\eta_{2,1}^{p}$	Moment of order 2 of oligoradicals terminated with styrene, having 1 graft unit (polyol), inside particles	-

$\eta_{2,3}^{p}$	Moment of order 2 of oligoradicals terminated with styrene, having 3 graft units (S5200), inside particles	-
ϕ_c	Cross-termination coefficient in the continuous phase	
ϕ_p	Cross-termination coefficient in the particles	-
ϕ_i^l	Volume fraction of the compound i in the phase l	-
ϕ_v	Shape factor (see Eq. 2.18)	-
$\mu_{1,0}^{c}$	Moment of order 1 of dead polymer chains having 0 graft in the continuous phase	-
$\mu_{1,1}^{c}$	Moment of order 1 of dead polymer chains having 1 graft unit (polyol) in the continuous phase	-
$\mu_{1,3}^{c}$	Moment of order 1 of dead polymer chains having 3 graft units (S5200) in the continuous phase	-
$\mu_{2,0}^{c}$	Moment of order 2 of dead polymer chains having 0 graft in the continuous phase	-
$\mu_{2,1}^{c}$	Moment of order 2 of dead polymer chains having 1 graft unit (polyol) in the continuous phase	-
$\mu_{2,3}^{c}$	Moment of order 2 of dead polymer chains having 3 graft units (S5200) in the continuous phase	-
$\mu_{1,0}^{p}$	Moment of order 1 of dead polymer chains having 0 graft inside particles	-
$\mu_{1,1}^{p}$	Moment of order 1 of dead polymer chains having 1 graft unit (polyol) inside particles	-
$\mu_{1,3}^{p}$	Moment of order 1 dead polymer chains having 3 graft units (S5200) inside particles	-
$\mu_{2,0}^{p}$	Moment of order 2 of dead polymer chains having 0 graft inside particles	-
$\mu_{2,1}^{p}$	Moment of order 2 of dead polymer chains having 1 graft unit (polyol) inside particles	-
$\mu_{2,3}^{p}$	Moment of order 2 of dead polymer chains having 3 graft units (S5200) inside particles	-
$\nu_{1,3}^{c}$	Moment of order 1 of oligoradicals terminated by S5200 in the continuous phase	-

$\nu_{2,3}^{c}$	Moment of order 2 of oligoradicals terminated by S5200 in the continuous phase	-
$\nu_{1,3}^{p}$	Moment of order 1 of oligoradicals terminated by S5200 inside particles	-
$\nu_{2,3}^{p}$	Moment of order 2 of oligoradicals terminated by S5200 inside particles	-
Ω	Angular velocity	rad s^{-1}
$\Omega_{i,0}^{c}$	Distribution of dead polymer chains having i monomer units and 0 graft in the continuous phase	-
$\Omega_{i,1}^{c}$	Distribution of dead polymer chains having i monomer units and 1 graft unit (polyol) in the continuous phase	-
$\Omega_{i,3}^{c}$	Distribution of dead polymer chains having i monomer units and 3 graft units (S5200) in the continuous phase	-
$\Omega_{i,0}^{p}$	Distribution of dead polymer chains having i monomer units and 0 graft inside the particles	-
$\Omega_{i,1}^{p}$	Distribution of dead polymer chains having i monomer units and 1 graft unit (polyol) inside the particles	-
$\Omega_{i,3}^{p}$	Distribution of dead polymer chains having i monomer units and 3 graft units (S5200) inside the particles	-
$\Pi_{i,3}^{c}$	Distribution of oligoradicals terminated by S5200 having i monomer units in the continuous phase	-
$\Pi_{i,3}^{p}$	Distribution of oligoradicals terminated by S5200 having i monomer units inside the particles	-
ρ	Particle density	kg m^{-3}
ρ_A	Density of acrylonitrile	kg m^{-3}
ρ_{PA}	Density of the monomer A once it is incorporated in the polymer	kg m^{-3}
ρ_B	Density of styrene	kg m^{-3}
ρ_{PB}	Density of the monomer B once it is incorporated in the polymer	kg m^{-3}
ρ_s	Density of the solvent	kg m^{-3}
τ	Parameter of the gamma function (see Eq. 2.10)	-
τ	Shear stress (see Eq. 2.21)	Pa
τ	Time after the pulse (see Eq. 2.35)	s

LIST OF TABLES

Table name	Page
Table 1.1 : Characteristics of free-radical heterogeneous polymerization processes.	61
Table 1.2 : Thermodynamic types of steric stabilization.	68
Table 1.3 : Hansen's parameters of monomers and polymers (Bandrup, 1989).	77
Table 1.4 : Hansen's parameters estimated by Van Kravelen method.	77
Table 1.5 : Common recipes for flexible polyurethane foam production.	86
Table 2.1 : Properties of Styrene and Acrylonitrile	95
Table 2.2 : ^{1}H-NMR spectrum analysis.	115
Table 3.1 : Experimental design for CPP process study	128
Table 3.2 : Deconvolution of the molecular weight distribution of run n°9.	131
Table 3.3 : Deconvolution of the molecular weight distribution of run n°10.	135
Table 3.4 : Deconvolution of the molecular weight distribution of run n°19.	138
Table 3.5 : Deconvolution of the molecular weight distribution of standard run n°31.	138
Table 3.6 : Estimation of the number, n, of grafts S5200 by grafted SAN chain from experimental data	151
Table 4.1 : Kinetic constants of homopropagation and homotermination of styrene and acrylonitrile at 120 °C and 140 °C from the literature.	158
Table 4.2 : Reactivity ratios between acrylonitrile (A) and styrene (B) in bulk and in solution polymerizations.	160
Table 4.3 : Reactivity ratios from literature for styrene and acrylonitrile reacting with silanes.	163
Table 5.1 : Parameters of the model identified using the genetic algorithm.	196
Table 5.2 : Parameters of the model concerning natural grafting.	197
Table 5.3 : Results of parameter identification at 140°C and 120°C.	199
Table 5.4 : Broad and absolute measurement.	202
Table 5.5 : Data simulated with the standard conditions.	219
Table 5.6 : Values of the parameters at 130 °C.	220

Table A1.1 : Bibliography list on dispersion polymerization from the 1980s to now. 247

Table A3.1 : Average molecular weights of whole CPP of runs done with Sty/AN = 60/40 (-1) and S5200 = 1 wt-% (-1) 263

Table A3.2.a : Average molecular weights of whole CPP of runs done with Sty/AN = 60/40 (-1) and S5200 = 3 wt-% (1) 263

Table A3.2.b : Average molecular weights of whole CPP of runs done with Sty/AN = 60/40 (-1) and S5200 = 3 wt-% (1) 263

Table A3.3 : Average molecular weights of whole CPP of runs done with Sty/AN = 80/20 (1) and S5200 = 1 wt-% (-1) 264

Table A3.4 : Average molecular weights of whole CPP of runs done with Sty/AN = 80/20 (1) and S5200 = 3 wt-% (1) 264

Table A3.5 : Average molecular weights of whole CPP of runs done with Sty/AN = 70/30 (0) and S5200 = 2 wt-% (0) 264

Table A3.6 : Residual concentrations and conversions of monomers and NDM and Wt-% solids of runs done with Sty/AN = 60/40 (-1) and S5200 = 1 wt-% (-1) 265

Table A3.7.a : Residual concentrations and conversions of monomers and NDM and Wt-% solids of runs done with Sty/AN = 60/40 (-1) and S5200 = 3 wt-% (1) 265

Table A3.7.b : Residual concentrations and conversions of monomers and NDM and Wt-% solids of runs done with Sty/AN = 60/40 (-1) and S5200 = 3 wt-% (1) 265

Table A3.8 : Residual concentrations and conversions of monomers and NDM and Wt-% solids of runs done with Sty/AN = 80/20 (1) and S5200 = 1 wt-% (-1) 266

Table A3.9 : Residual concentrations and conversions of monomers and NDM and Wt-% solids of runs done with Sty/AN = 80/20 (1) and S5200 = 3 wt-% (1) 266

Table A3.10 : Residual concentrations and conversions of monomers and NDM and Wt-% solids of runs done with Sty/AN = 70/30 (0) and S5200 = 2 wt-% (0) 266

Table A3.11 : Viscosities of stripped CPP and serum, and Sauter mean particle diameters of runs done with Sty/AN = 60/40 (-1) and S5200 = 1 wt-% (-1) 267

Table A3.12.a : Viscosities of stripped CPP and serum, and Sauter mean particle diameters of runs done with Sty/AN = 60/40 (-1) and S5200 = 3 wt-% (1) 267

Table A3.12.b : Viscosities of stripped CPP and serum, and Sauter mean particle diameters of runs done with Sty/AN = 60/40 (-1) and S5200 = 3 wt-% (1) 267

Table A3.13 : Viscosities of stripped CPP and serum, and Sauter mean particle diameters of runs done with Sty/AN = 80/20 (1) and S5200 = 1 wt-% (-1) 268

Table A3.14 : Viscosities of stripped CPP and serum, and Sauter mean particle diameters of runs done with Sty/AN = 80/20 (1) and S5200 = 3 wt-% (1) 268

Table A3.15 : Viscosities of stripped CPP and serum, and Sauter mean particle diameters of runs done with Sty/AN = 70/30 (0) and S5200 = 2 wt-% (0) 268

Table A3.16 : Grafting from LC-UV in solids, whole CPP and serum of runs done with Sty/AN = 60/40 (-1) and S5200 = 1 wt-% (-1) 269

Table A3.17 : Grafting from LC-UV in solids, whole CPP and serum of runs done with Sty/AN = 60/40 (-1) and S5200 = 3 wt-% (1) 269

Table A3.18 : Grafting from LC-UV in solids, whole CPP and serum of runs done with Sty/AN = 80/20 (1) and S5200 = 1 wt-% (-1) 269

Table A3.19 : Grafting from LC-UV in solids, whole CPP and serum of runs done with Sty/AN = 80/20 (1) and S5200 = 3 wt-% (1) 270

Table A3.20 : Grafting from LC-UV in solids, whole CPP and serum of runs done with Sty/AN = 70/30 (0) and S5200 = 2 wt-% (0) 270

Table A3.21 : Composition of solids (wt-% of polyol, Sty, AN), composition of soluble SAN and quantity of soluble SAN in the serum phase of runs done with Sty/AN = 60/40 (-1) and S5200 = 1 wt-% (-1) 270

Table A3.22 : Composition of solids (wt-% of polyol, Sty, AN), composition of soluble SAN and quantity of soluble SAN in the serum phase of runs done with Sty/AN = 60/40 (-1) and S5200 = 3 wt-% (1) 271

Table A3.23 : Composition of solids (wt-% of polyol, Sty, AN), composition of soluble SAN and quantity of soluble SAN in the serum phase of runs done with Sty/AN = 80/20 (1) and S5200 = 1 wt-% (-1) 271

Table A3.24 : Composition of solids (wt-% of polyol, Sty, AN), composition of soluble SAN and quantity of soluble SAN in the serum phase of runs done with Sty/AN = 80/20 (1) and S5200 = 3 wt-% (1) 271

Table A3.25 : Composition of solids (wt-% of polyol, Sty, AN), composition of soluble SAN and quantity of soluble SAN in the serum phase of runs done with Sty/AN = 70/30 (0) and S5200 = 2 wt-% (0) 272

Table A3.26 : Comparison between two methods used to measure the polyol content 272

Table A3.27 : SAN in serum of runs done with Sty/AN = 60/40 (-1) and S5200 = 1 wt-% (-1) 272

Table A3.28 : SAN in serum of runs done with Sty/AN = 60/40 (-1) and S5200 = 3 wt-% (1) 273

Table A3.29 : SAN in serum of runs done with Sty/AN = 80/20 (1) and S5200 = 1 wt-% (-1) 273

Table A3.30 : SAN in serum of runs done with Sty/AN = 80/20 (1) and S5200 = 3 wt-% (1) 273

Table A3.31 : SAN in serum of runs done with Sty/AN = 70/30 (0) and S5200 = 2 wt-% (0) 273

Table A5.1 : Comparison of the number-average molecular weights of experiments carried out at 140 °C obtained experimentally and given by the model. 339

Table A5.2 : Comparison of the number-average molecular weights of the experiments carried out at 120 °C obtained experimentally and given by the model. 339

Table A5.3 : Comparison of the weight-average molecular weights of the experiments done at 140 °C obtained experimentally and given by the model. 340

Table A5.4 : Comparison of the weight-average molecular weights of the experiments done at 120 °C obtained experimentally and given by the model. 340

Table A5.5 : Comparison of the quantities of solid of the experiments done at 140 °C obtained experimentally and given by the model. 341

Table A5.6 : Comparison of the quantities of solid of the experiments done at 120 °C obtained experimentally and given by the model. 341

Table A5.7 : Comparison of the quantities of residual acrylonitrile of the experiments done at 140 °C obtained experimentally and given by the model. 342

Table A5.8 : Comparison of the quantities of residual acrylonitrile of the experiments done at 120 °C obtained experimentally and given by the model. 342

Table A5.9 : Comparison of the conversions in residual acrylonitrile of the experiments done at 140 °C obtained experimentally and given by the model. 343

Table A5.10 : Comparison of the conversions in residual acrylonitrile of the experiments done at 120 °C obtained experimentally and given by the model. 343

Table A5.11 : Comparison of the quantities of residual styrene of the experiments done at 140 °C obtained experimentally and given by the model. 344

Table A5.12 : Comparison of the quantities of residual styrene of the experiments done at 120 °C obtained experimentally and given by the model. 344

Table A5.13 : Comparison of the conversions in residual styrene of the experiments done at 140 °C obtained experimentally and given by the model. 345

Table A5.14 : Comparison of the conversions in residual styrene of the experiments done at 120 °C obtained experimentally and given by the model. 345

Table A5.15 : Comparison of the quantities of residual NDM of the experiments done at 140 °C obtained experimentally and given by the model. 346

Table A5.16 : Comparison of the quantities of residual NDM of the experiments done at 120 °C obtained experimentally and given by the model. 346

Table A5.17 : Comparison of the conversions in residual NDM of the experiments done at 140 °C obtained experimentally and given by the model. 347

Table A5.18 : Comparison of the conversions in residual NDM of the experiments done at 120 °C obtained experimentally and given by the model. 347

Table A5.19 : Comparison of the compositions in acrylonitryle of the SAN copolymers of the experiments done at 140 °C obtained experimentally and given by the model. 348

Table A5.20 : Comparison of the compositions in acrylonitryle of the SAN copolymers of the experiments done at 120 °C obtained experimentally and given by the model. 348

Table A5.21 : Comparison of the quantities of copolymer SAN dissolved in the serum of the experiments done at 140 °C obtained experimentally and given by the model. 349

Table A5.22 : Comparison of the quantities of copolymer SAN dissolved in the serum of the experiments done at 120 °C obtained experimentally and given by the model. 349

Table A5.23 : Comparison of the proportions of copolymer SAN grafted in the serum of the experiments done at 140 °C obtained experimentally and given by the model. 350

Table A5.24 : Comparison of the proportions of copolymer SAN grafted in the serum of the experiments done at 120 °C obtained experimentally and given by the model. 350

Table A5.25 : Comparison of the proportions of copolymer SAN grafted in the whole CPP of the experiments done at 140 °C obtained experimentally and given by the model. 351

Table A5.26 : Comparison of the proportions of copolymer SAN grafted in the whole CPP of the experiments done at 120 °C obtained experimentally and given by the model. 351

Table A5.27 : Comparison of the quantities of polyol grafted to the solid of the experiments done at 140 °C obtained experimentally and given by the model. 352

Table A5.28 : Comparison of the quantities of polyol grafted to the solid of the experiments done at 120 °C obtained experimentally and given by the model. 352

Table A5.29 : Comparison of de Sauter diameters of the experiments done at 140 °C obtained experimentally and given by the model. 353

Table A5.30 : Comparison of de Sauter diameters of the experiments done at 120 °C obtained experimentally and given by the model. 353

LIST OF FIGURES

Figure name	Page
Figure 1.1 : Schematic representation of the close approach of sterically stabilized particles.	66
Figure 1.2 : Potential energy against distance of separation, h, for sterically stabilized particles with varying depth of steric barrier.	67
Figure 1.3 : Possible structures of stabilizer copolymers : a-e, grafted copolymers ; f-i, block copolymers.	69
Figure 1.4 : Two types of grafted surfaces : **a)** "mushroom" conformation at low grafting density, **b)** "brush" conformation at high grafting density.	70
Figure 1.5 : Models for particle nucleation.	71
Figure 1.6 : Cross-linking in polyurethane polymers.	85
Figure 2.1 : Polyether polyol.	96
Figure 2.2 : Thermal dissociation of Trigonox 27 initiator.	97
Figure 2.3 : GPC chromatogram of a sample of S5200.	98
Figure 2.4 : Species that may also be present in S5200 samples.	98
Figure 2.5 : Scheme of the laboratory rig.	100
Figure 2.6 : Agitation device of the reactor.	100
Figure 2.7 : Schema of all the analytical methods used.	103
Figure 2.8 : GPC calibration curve : molecular weight vs. elution volume.	105
Figure 2.9 : Different possible descriptions for a particle.	108
Figure 2.10 : General principle of Scanning Electron Microscope.	112
Figure 2.11 : Cone & Cup sensor.	113
Figure 2.12 : Cone & Plate sensor.	114
Figure 2.13. : Chromatogram of the DCM blank.	119
Figure 2.14 : HL400 chromatogram without baseline subtraction.	119
Figure 2.15 : HL400 chromatogram after baseline subtraction.	120
Figure 3.1 : Monol-SAN diblock and monol-g-SAN copolymers.	124

Figure 3.2 : Number molecular weight distribution of the runs n° 8 (low NDM, low T27), n° 9 (high NDM, low T27), n° 10 (low NDM, high T27) and n° 11 (high NDM, high T27) done with low styrene (Sty/AN=60/40), high S5200 (3 wt-%) and low T (120 °C). 132

Figure 3.3 : Weight molecular weight distribution of the runs n° 8 (low NDM, low T27), n° 9 (high NDM, low T27), n° 10 (low NDM, high T27) and n° 10 (high NDM, high T27) done with low styrene (Sty/AN=60/40), high S5200 (3 wt-%) and low T (120 °C). 132

Figure 3.4 : Deconvolution of the number molecular weight distribution of the run n° 9 done with Sty/AN=60/40, S5200 =3 wt-%, NDM = 0.45 wt-%, T27 = 0.10 wt-% and T=120 °C. 133

Figure 3.5 : Deconvolution of the weight molecular weight distribution of the run n° 9 done with Sty/AN=60/40, S5200 =3 wt-%, NDM = 0.45 wt-%, T27 = 0.10 wt-% and T=120 °C. 133

Figure 3.6 : Deconvolution of the number molecular weight distribution of the run n° 10 done with Sty/AN=60/40, S5200 =3 wt-%, NDM = 0.15 wt-%, T27 = 0.2 wt-% and T = 120 °C. 134

Figure 3.7 : Deconvolution of the weight molecular weight distribution of the run n° 10 done with Sty/AN=60/40, S5200 =3 wt-%, NDM = 0.15 wt-%, T27 = 0.20 wt-% and T=120 °C. 134

Figure 3.8 : Deconvolution of the number molecular weight distribution of the run n° 19 done with Sty/AN=80/20, S5200 =1 wt-%, NDM = 0.45 wt-%, T27 = 0.10 wt-% and T=140 °C. 136

Figure 3.9 : Deconvolution of the weight molecular weight distribution of the run n° 19 done with Sty/AN=80/20, S5200 =1 wt-%, NDM = 0.45 wt-%, T27 = 0.10 wt-% and T=140 °C. 136

Figure 3.10 : Deconvolution of the number molecular weight distribution of the standard run n° 31 done with Sty/AN=70/30, S5200 =2 wt-%, NDM = 0.30 wt-%, T27 = 0.15 wt-% and T=130 °C. 137

Figure 3.11 : Deconvolution of the weight molecular weight distribution of the standard run n° 31 done with Sty/AN=70/30, S5200 =2 wt-%, NDM = 0.30 wt-%, T27 = 0.15 wt-% and T=130 °C. 137

Figure 3.12 : Influence of NDM and Sty/AN ratio on the viscosity of stripped CPP. 140

Figure 3.13 : Influence of the T27 concentration on the CPP viscosity. 141

Figure 3.14 : Volume particle size distributions of run n° 31 done with standard conditions (0.30 wt-% NDM, 0.15 wt-% T27, T=130°C, 2 wt-% S5200 and Sty/AN = 70/30. 142

Figure 3.15 : Influence of the NDM concentration on % graft of whole CPP. 145

Figure 3.16 : Influence of the Sty/AN ratio on the % Graft of whole CPP. 146

Figure 3.17 : Influence of the T27 concentration on % graft of whole CPP. 146

Figure 3.18 : Influence of the temperature on % graft of whole CPP. 147

Figure 3.19 : Influence of the S5200 concentration on % graft of whole CPP. 147

Figure 4.1 : Dependence of the instantaneous copolymer weight composition C_B on the comonomer feed c_B for radical copolymerisation of acrylonitrile-styrene system. 160

Figure 4.2 : Radii of gyrations of polyol and S5200. 169

Figure 5.1 : Scheme of the genetic algorithm. 193

Figure 5.2 : Number-average molecular weights ; Measurements vs. modeling using the parameters identified at 140 °C. 203

Figure 5.3 : Number-average molecular weights ; Measurements vs. modeling using the parameters identified at 120 °C. 203

Figure 5.4 : Weight-average molecular weights ; Measurements vs. modeling using the parameters identified at 140 °C. 204

Figure 5.5 : Weight-average molecular weights ; Measurements vs. modeling using the parameters identified at 120 °C. 204

Figure 5.6 : Solids quantities ; Measurements vs. modeling, using the parameters identified at 140 °C. 206

Figure 5.7 : Solids quantities ; Measurements vs. modeling, using the parameters identified at 120 °C. 206

Figure 5.8 : Conversions of acrylonitrile ; Measurements vs. modeling using the parameters identified at 140 °C. 207

Figure 5.9 : Conversions of acrylonitrile ; Measurements vs. modeling using the parameters identified at 120 °C. 207

Figure 5.10. : Conversions of styrene ; Measurements vs. modeling using the parameters identified at 140 °C. 208

Figure 5.11 : Conversions of styrene ; Measurements vs. modeling using the parameters identified at 120 °C. 208

Figure 5.12. : Conversions of NDM ; Measurements vs. modeling using the parameters identified at 140 °C. 209

Figure 5.13 : Conversions of NDM ; Measurements vs. modeling using the parameters identified at 120 °C. 209

Figure 5.14 : Composition of AN of the SAN copolymer : Measurements vs. modeling using the parameters identified at 140 °C. 210

Figure 5.15 : Composition of AN of the SAN copolymer: Measurements vs. modeling using the parameters identified at 120 °C. 210

Figure 5.16 : Quantity of SAN copolymer dissolved in the serum : Measurements vs. modeling using the parameters identified at 140 °C. 212

Figure 5.17 : Quantity of SAN copolymer dissolved in the serum : Measurements vs. modeling using the parameters identified at 120 °C. 212

Figure 5.18 : Proportion of SAN grafted dissolved in the serum : Measurements vs. modeling using the parameters identified at 140 °C. 213

Figure 5.19 : Proportion of SAN grafted dissolved in the serum : Measurements vs. modeling using the parameters identified at 120 °C. 213

Figure 5.20 : Proportion of SAN grafted in the whole CPP : Measurements vs. modeling using the parameters identified at 140 °C. 214

Figure 5.21 : Proportion of SAN grafted in the whole CPP: Measurements vs. modeling using the parameters identified at 120 °C. 214

Figure 5.22 : Quantity of polyol in the solids: Measurements vs. modeling using the parameters identified at 140 °C. 216

Figure 5.23 : Quantity of polyol in the solids : Measurements vs. modeling using the parameters identified at 120 °C. 216

Figure 5.24 : Quantity of SAN copolymer dissolved in the serum: Measurements vs. modeling using the parameters identified at 140 °C. 218

Figure 5.25 : Quantity of SAN copolymer dissolved in the serum: Measurements vs. modeling using the parameters identified at 120 °C. 218

Figure A2.1 : Equipment for the filterability test. 257

Figure A3.1. : Evolution of Mn and Mw versus time during the production of different CPP samples : standard runs n° 33 and n° 34 (Sty/AN = 70/30, S5200 = 2 wt-%, NDM = 0.30 wt-%, T27 = 0.15 wt-%, T = 130 °C) and the unstable run n° 36 (Sty/AN = 60/40, S5200 = 3 wt-%, NDM = 0.15 wt-%, T27 = 0.10 wt-%, T = 120 °C). 274

Figure A3.2. : Evolution of the surface area moment mean diameter versus time during the production of standard CPP samples (Sty/AN = 70/30, S5200 = 2 wt-%, NDM = 0.30 wt-%, T27 = 0.15 wt-%, T = 130 °C). 274

Figure A3.3. : Evolution of the surface area moment mean diameter versus time during the production of CPP during the runs n° 37 (low T27, low T), n° 39 (high T27, low T), n° 41 (low T27, low T) and n° 43 (high T27, low T) done with high NDM (0.45 wt-%), low styrene (Sty/AN = 60/40) and high S5200 (3 wt-%). 275

Figure A3.4. : Evolution of the surface area moment mean diameter versus time during the production of CPP during the runs n° 36 (low T27, low T), n° 38 (high T27, low T), n° 40 (low T27, low T) and n° 42 (high T27, low T) done with low NDM (0.15 wt-%), low styrene (Sty/AN = 60/40) and high S5200 (3 wt-%). 275

Figure A3.5.a : Evolution of the volume particle size distributions with time of the run n° 34 done with a standard recipe (Sty/AN=70/30, S5200 = 2 wt-%, NDM = 0.30 wt-%, T27 = 0.15 wt-% and T = 130 °C). 276

Figure A3.5.b : Evolution of the volume particle size distributions with time of the run n° 34 done with a standard recipe (Sty/AN=70/30, S5200 = 2 wt-%, NDM = 0.30 wt-%, T27 = 0.15 wt-% and T = 130 °C). 276

Figure A3.6.a : Evolution of the volume particle size distributions with time of the run n° 42 done with low styrene (Sty/AN=60/40), high S5200 (3 wt-%), low NDM (0.15 wt-%), high T27 (0.20 wt-%) and high T (140 °C). 277

Figure A3.6.b : Evolution of the volume particle size distributions with time of the run n° 42 done with low styrene (Sty/AN=60/40), high S5200 (3 wt-%), low NDM (0.15 wt-%), high T27 (0.20 wt-%) and high T (140 °C). 277

Figure A3.7.a : Evolution of the volume particle size distributions with time of the run n° 36 done with low styrene (Sty/AN=60/40), high S5200 (3 wt-%), low NDM (0.15 wt-%), low T27 (0.10 wt-%) and low T (120 °C). 278

Figure A3.7.b : Evolution of the volume particle size distributions with time of the run n° 36 done with low styrene (Sty/AN=60/40), high S5200 (3 wt-%), low NDM (0.15 wt-%), low T27 (0.10 wt-%) and low T (120 °C). 278

Figure A3.8 : Number molecular weight distribution of the runs n° 1 (high NDM, low T27), n° 2 (low NDM, high T27) and n° 3 (high NDM, high T27) done with low styrene (Sty/AN=60/40), low S5200 (1 wt-%) and low T (120 °C). 279

Figure A3.9 : Weight molecular weight distribution of the runs n° 1 (high NDM, low T27), n° 2 (low NDM, high T27) and n° 3 (high NDM, high T27) done with low styrene (Sty/AN=60/40), low S5200 (1 wt-%) and low T (120 °C). 279

Figure A3.10 : Number molecular weight distribution of the runs n° 4 (low NDM, low T27), n° 5 (high NDM, low T27), n° 6 (low NDM, high T27) and n° 7 (high NDM, high T27) done with low styrene (Sty/AN=60/40), low S5200 (1 wt-%) and high T (140 °C). 280

Figure A3.11 : Weight molecular weight distribution of the runs n° 4 (low NDM, low T27), n° 5 (high NDM, low T27), n° 6 (low NDM, high T27) and n° 7 (high NDM, high T27) done with low styrene (Sty/AN=60/40), low S5200 (1 wt-%) and high T (140 °C). 280

Figure A3.12 : Number molecular weight distribution of the runs n° 12 (low NDM, low T27), n° 13 (high NDM, low T27), n° 14 (low NDM, high T27) and n° 15 (high NDM, high T27) done with low styrene (Sty/AN=60/40), high S5200 (3 wt-%) and high T (140 °C). 281

Figure A3.13 : Weight molecular weight distribution of the runs n° 12 (low NDM, low T27), n° 13 (high NDM, low T27), n° 14 (low NDM, high T27) and n° 15 (high NDM, high T27) done with low styrene (Sty/AN=60/40), high S5200 (3 wt-%) and high T (140 °C). 281

Figure A3.14 : Number molecular weight distribution of the runs n° 16 (low NDM, high T27) and n° 17 (high NDM, high T27) done with high styrene (Sty/AN=80/20), low S5200 (1 wt-%) and low T (120 °C). 282

Figure A3.15 : Weight molecular weight distribution of the runs n° 16 (low NDM, high T27) and n° 17 (high NDM, high T27) done with high styrene (Sty/AN=80/20), low S5200 (1 wt-%) and low T (120 °C). 282

Figure A3.16 : Number molecular weight distribution of the runs n° 18 (low NDM, low T27), n° 19 (high NDM, low T27), n° 20 (low NDM, high T27) and n° 21 (high NDM, high T27) done with high styrene (Sty/AN=80/20), low S5200 (1 wt-%) and high T (140 °C). 283

Figure A3.17 : Weight molecular weight distribution of the runs n° 18 (low NDM, low T27), n° 19 (high NDM, low T27), n° 20 (low NDM, high T27) and n° 21 (high NDM, high T27) done with high styrene (Sty/AN=80/20), low S5200 (1 wt-%) and high T (140 °C). 283

Figure A3.18 : Number molecular weight distribution of the runs n° 22 (low NDM, low T27), n° 23 (high NDM, low T27), n° 24 (low NDM, high T27) and n° 25 (high NDM, high T27) done with high styrene (Sty/AN=80/20), high S5200 (3 wt-%) and low T (120 °C). 284

Figure A3.19 : Weight molecular weight distribution of the runs n° 22 (low NDM, low T27), n° 23 (high NDM, low T27), n° 24 (low NDM, high T27) and n° 25 (high NDM, high T27) done with high styrene (Sty/AN=80/20), high S5200 (3 wt-%) and low T (120 °C). 284

Figure A3.20 : Number molecular weight distribution of the runs n° 26 (low NDM, low T27), n° 27 (high NDM, low T27), n° 28 (low NDM, high T27) and n° 29 (high NDM, high T27) done with high styrene (Sty/AN=80/20), high S5200 (3 wt-%) and high T (140 °C). 285

Figure A3.21 : Weight molecular weight distribution of the runs n° 26 (low NDM, low T27), n° 27 (high NDM, low T27), n° 28 (low NDM, high T27) and n° 29 (high NDM, high T27) done with high styrene (Sty/AN=80/20), high S5200 (3 wt-%) and high T (140 °C). 285

Figure A3.22 : Number molecular weight distribution of the standard runs n° 31 and n° 32 done with Sty/AN=70/30, S5200 =2 wt-%, NDM = 0.30 wt-%, T27 = 0.15 wt-% and T=130 °C. 286

Figure A3.23 : Weight molecular weight distribution of the standard runs n° 31 and n° 32 done with Sty/AN=70/30, S5200 =2 wt-%, NDM = 0.30 wt-%, T27 = 0.15 wt-% and T=130 °C. 286

Figure A3.24 : Volume particle size distributions of runs n° 2 (high T27 and low T), n°4 (low T27 and high T) and n°6 (high T27 and high T) done with Sty/AN=60/40, low S5200 (1 wt-%) and low NDM (0.15 wt-%). 287

Figure A3.25 : Volume particle size distributions of runs n° 1 (low T27 and low T), n°3 (high T27 and high T), n°5 (low T27 and high T) and n°7 (high T27 and high T) done with Sty/AN=60/40, low S5200 (1 wt-%) and high NDM (0.45 wt-%). 287

Figure A3.26 : Volume particle size distributions of runs n° 8 (low T27 and low T), n°10 (high T27 and low T), n°12 (low T27 and high T) and n°14 (high T27 and high T) done with Sty/AN=60/40, S5200 = 3 wt-% and low NDM. 288

Figure A3.27 : Volume particle size distributions of runs n° 9 (low T27 and low T), n°11 (high T27 and high T), 13 (low T27 and high T) and n°15 (high T27 and high T) done with Sty/AN=60/40, S5200 = 3 wt-% and high NDM. 288

Figure A3.28 : Volume particle size distributions of runs n° 16 (high T27 and high T), n°18 (low T27 and high T) and n°20 (high T27 and high T) done with Sty/AN=80/20, S5200 = 1 wt-% and low NDM. 289

Figure A3.29 : Volume particle size distributions of runs n°19 (low T27 and high T) and n°21 (high T27 and high T) done with Sty/AN=80/20, S5200 = 1 wt-% and high NDM. 289

Figure A3.30 : Volume particle size distributions of runs n° 22 (low T27 and low T), n°24 (high T27 and low T), n°26 (low T27 and high T) and n°28 (high T27 and high T) done with Sty/AN=80/20, S5200 = 3 wt-% and low NDM. 290

Figure A3.31 : Volume particle size distributions of runs n° 23 (low T27 and low T), n°25 (high T27 and low T), n°27 (low T27 and high T) and n°29 (high T27 and high T) done with Sty/AN=80/20, S5200 = 3 wt-% and high NDM. 290

Figure A3.32 : SEM pictures and particle sizes distributions of the **run n° 4** done with low NDM (0.15 wt-%), low T27 (0.10 wt-%), high temperature (140°C), low styrene (Sty/AN = 60/40) and low S5200 (1 wt-%). 291

Figure A3.33 : SEM pictures and particle sizes distributions of the **run n° 5** done with high NDM (0.45 wt-%), low T27 (0.10 wt-%), high temperature (140°C), low styrene (Sty/AN = 60/40) and low S5200 (1 wt-%). 291

Figure A3.34 : SEM pictures and particle sizes distributions of the **run n° 10** done with low NDM (0.15 wt-%), high T27 (0.20 wt-%), low temperature (130°C), low styrene (Sty/AN = 60/40) and high S5200 (3 wt-%). 291

Figure A3.35 : SEM pictures and particle sizes distributions of the **run n° 11** done with high NDM (0.45 wt-%), high T27 (0.20 wt-%), low temperature (130°C), low styrene (Sty/AN = 60/40) and high S5200 (3 wt-%). 292

Figure A3.36 : SEM pictures and particle sizes distributions of the **run n° 18** done with low NDM (0.15 wt-%), low T27 (0.10 wt-%), high temperature (140°C), high styrene (Sty/AN = 80/20) and low S5200 (1 wt-%). 292

Figure A3.37 : SEM pictures and particle sizes distributions of the **run n° 19** done with high NDM (0.45 wt-%), low T27 (0.10 wt-%), high temperature (140°C), high styrene (Sty/AN = 80/20) and low S5200 (1 wt-%). 292

Figure A3.38 : SEM pictures and particle sizes distributions of the **run n° 26** done with low NDM (0.15 wt-%), low T27 (0.10 wt-%), high temperature (140°C), high styrene (Sty/AN = 80/20) and high S5200 (3 wt-%). 293

Figure A3.39 : SEM pictures and particle sizes distributions of the **run n° 27** done with high NDM (0.45 wt-%), low T27 (0.10 wt-%), high temperature (140°C), high styrene (Sty/AN = 80/20) and high S5200 (3 wt-%). 293

Figure A3.40 : SEM pictures and particle sizes distributions of the standard **run n° 31** done with high NDM = 0.30 wt-%, T27 = 0.15 wt-%, T = 130°C, Sty/AN = 70/30) and S5200 = 2 wt-%). 293

Figure A3.41 : LC-UV chromatograms of grafted SAN from samples n° 2 (low NDM) and 3 (high NDM), both at high T27, low T, low styrene and low S5200. 294

Figure A3.42 : LC-UV chromatograms of grafted SAN from samples n° 4 (low NDM) and 5 (high NDM), both at low T27, high T, low styrene and low S5200. 294

Figure A3.43 : LC-UV chromatograms of grafted SAN from samples n° 6 (low NDM) and 7 (high NDM), both at high T27, high T, low styrene and low S5200. 294

Figure A3.44 : LC-UV chromatograms of grafted SAN from samples n° 10 (low NDM, high T27), 9 (high NDM, low T27), and 11 (high NDM, high T27), all at low T, low styrene and high S5200. 295

Figure A3.45 : LC-UV chromatograms of grafted SAN from samples n° 22 (low NDM) and 23 (high NDM), both at low T27, low T, high styrene and high S5200. 295

Figure A3.46 : LC-UV chromatograms of grafted SAN from samples n° 24, 26 and 28 (low NDM) and 25, 27 and 29 (high NDM), all at high styrene and high S5200. 295

Figure A3.47 : LC-UV chromatograms of grafted SAN from samples n° 10 (low styrene) and 23 (high styrene), both at low NDM, high T27, low T and high S5200, and a sample of HL400 (Sty/AN= 60/40). 296

Figure A3.48 : LC-UV chromatograms of grafted SAN from samples n° 24 (low NDM, high T27, low T), 25 (high NDM, high T27, low T) and 30 (high NDM, high T27, high T), all at high styrene and high S5200. 296

Figure A3.49 : LC-UV chromatograms of grafted SAN from samples n° 24 (low NDM, high T27, low T), 25 (high NDM, high T27, low T), 27 (high NDM, low T27, high T) and 29 (high NDM, high T27, high T), all at high styrene and high S5200. 296

Figure A3.50 : Example of ^{13}C NMR chromatogram of solids from a sample of standard HL 400 copolymer polyol. 297

Figure A3.51 : Example of ^{1}H NMR chromatogram of solids from a sample of standard HL 400 copolymer polyol. 298

Figure A3.52 : Examples of ^{1}H NMR chromatograms of solids from CPP samples : expansion in the 3.2-3.8 ppm region of the polyol. 299

Figure A3.53 : Examples of chromatograms obtained by NIC-derivatization of solids followed by GPC-Fluorescence. 300

Figure A3.54 : Number molecular weight distribution of SAN polymer dissolved in serum coming from samples n°2 (high T27, low T), n° 4 (low T27, high T) and n° 6 (high T27, high T) done with Sty/AN = 60/40, S5200=1 wt-% and NDM=0.15 wt-%. 301

Figure A3.55 : Number molecular weight distribution of SAN polymer dissolved in serum coming from samples n°1 (low T27, low T), n°3 (high T27, low T), n° 5 (low T27, high T) and n° 7 (high T27, high T) done with Sty/AN = 60/40, S5200=1 wt-% and NDM=0.45 wt-%. 301

Figure A3.56 : Weight molecular weight distribution of SAN polymer dissolved in serum coming from samples n°2 (high T27, low T), n° 4 (low T27, high T) and n° 6 (high T27, high T) done with Sty/AN = 60/40, S5200=1 wt-% and NDM=0.15 wt-%. 302

Figure A3.57 : Weight molecular weight distribution of SAN polymer dissolved in serum coming from samples n°1 (low T27, low T), n°3 (high T27, low T), n° 5 (low T27, high T) and n° 7 (high T27, high T) done with Sty/AN = 60/40, S5200=1 wt-% and NDM=0.45 wt-%. 302

Figure A3.58 : Number molecular weight distribution of SAN polymer dissolved in serum coming from samples n°22 (low NDM), and n° 23 (high NDM) done with Sty/AN = 80/20, S5200 = 1 wt-% and T27 = 0.10 wt-%. 303

Figure A3.59 : Weight molecular weight distribution of SAN polymer dissolved in serum coming from samples n°22 (low NDM), and n° 23 (high NDM) done with Sty/AN = 80/20, S5200 = 1 wt-% and T27 = 0.10 wt-%. 303

Figure A4.1 : The Euler's Gamma function. 334

Figure A5.1 : Residual acrylonitrile : Measurements vs. modeling using the parameters identified at 140 °C. 354

Figure A5.2 : Residual acrylonitrile : Measurements vs. modeling using the parameters identified at 120 °C. 354

Figure A5.3 : Residual styrene : Measurements vs. modeling using the parameters identified at 140 °C. 355

Figure A5.4 : Residual styrene : Measurements vs. modeling using the parameters identified at 120 °C. 355

Figure A5.5 : Residual NDM : Measurements vs. modeling using the parameters identified at 140 °C. 356

Figure A5.6 : Residual NDM : Measurements vs. modeling using the parameters identified at 140 °C. 356

INTRODUCTION

This work is the result of the collaboration between Dow Benelux N.V., Terneuzen (NL), and the team of polymerization process engineering of the "Laboratoire des Sciences du Génie Chimique", Nancy. The industrial challenge is to improve the knowledge of the copolymer polyols produced by dispersion polymerization of styrene and acrylonitrile in polyol medium in order to improve the quality of this product and to reduce one of the major problem related to the fouling inside the continuous stirred tank reactor.

1. Generalities

Among all polymerization processes, dispersion polymerization is one of the most complex. It has been developed by Osmond et al. (1962) from Imperial Chemical Industries Society and it can be considered as a particular case of precipitation polymerization. Its origin is closely linked to the development of the painting and coating industry.

The principle of this process can be summed up as follows : typically, polymer particles are formed in a homogeneous medium that contains the monomer dissolved in a solvent, the initiator and a stabilizer. The solvent must be a non-solvent of the polymer. Indeed, during the polymerization, the resulting macromolecules precipitate to form particles which flocculation is avoided by the presence of the stabilizer.

According to Kawaguchi (2000), the history of dispersion polymerization began during the 1950s. Until the 1970s, aliphatic hydrocarbons were used as a medium in almost all cases. The first generation of dispersion polymerization generated organic dispersions of submicrometer particles with high solid fractions and low viscosity, the so-called NAD (non aqueous dispersion), and was employed for coatings and industry use. Compared with this, dispersion polymerization of the 1980s should be considered to belong to a second generation. It used polar solvents as a medium, and the main purpose was to prepare micrometer-ordered monodisperse particles. The third generation operated in the 1990s and aimed for the same purpose with design of functional particles and considerations towards the environment.

Today, copolymer polyols (CPPs) are produced via radical dispersion copolymerization of styrene and acrylonitrile in polyol medium within Dow Chemical in Freeport, Terneuzen and Zwijndrecht using both continuous stirred tank reactor and batch reactor processes. The batch process is an internal Dow Chemical development, while the rights to use the Union Carbide Company continuous process were obtained via an acquisition of a former British Petroleum plant in Belgium in July 1998.

CPPs have been used since the 1960s (Kuryla et al., 1966) as raw materials for the manufacture of urethane elastomers and foams and they have grown to be one of the major building blocks for the flexible polyurethanes industry. The application of CPP in automotive high resilient (HR) molding formulations and in furnitures improves processing and increases foam hardness. CPPs bring weight and cost reductions in the foaming process and this results in energy savings during the use of these molded parts in car transportation seats.

2. Copolymer polyols production : a complex process

During dispersion polymerization the nucleation process starts in an essentially homogeneous solution containing monomer, initiator, chain transfer agent and polyol. The first step involves production of radicals resulting from the decomposition of the initiator, which in turn react with the monomers to form growing oligoradicals. Each oligoradical has an extended configuration,

but then collapses into a condensed state when is reached a certain threshold molecular weight depending on its solubility in the medium. Precipitation depends on the molecular weight, the styrene to acrylonitrile ratio of these growing radicals, the temperature and the monomer concentration. Therefore, the condensed oligomer radicals constitute new primary particles. Due to van der Waal's attractive forces, these particles attract one another, either with other primary particles or with other existing larger particles, which are not completely covered with steric stabilizer.

Thus, the mechanism by which poly(styrene-co-acrylonitrile) CPP particles grow is due to particle agglomeration and also to bulk polymerization inside particles, which are swollen by the monomers. Therefore, the partitioning of the monomers, initiator and chain transfer agent between the two phases is of major importance in this process.

Moreover, the nature and the structure of the stabilizer is also an important key of the dispersion polymerization process. Actually, the copolymer polyols made in this work are produced by using both a stabilizer precursor (S5200) and a preformed stabilizer (seed). S5200 results from the transesterification of a small amount of vinyltrimethoxysilane (VTMS) with a polyether triol. Then, the grafting of S5200 is supposed to happen *in situ* through the copolymerization of its Si-C=C bond with the styrene/acrylonitrile system, providing a polyol grafted poly(styrene-co-acrylonitrile) to serve as the final particle steric stabilizer. The reactivity of the steric stabilizer precursor with both styrene and acrylonitrile is very low and the reactivity of the precursor with itself is extremely low, which are the ideal conditions to be a good steric stabilizer. The preformed stabilizer (seed) is produced by radical polymerization of an excess of the precursor stabilizer with the monomers. Therefore, the seed contains both soluble and insoluble SAN polymeric material.

Fine dispersions of macromolecules may be stabilized to prevent flocculation by solvated polymeric or oligomeric species that adsorb onto the dispersed polymeric particle surface. Indeed, the SAN polymer portion of the grafted block copolymer is adsorbed onto the surface of the SAN polymer particles with the polyol portion of the block copolymer projecting into the polyol solvent and forming a repulsive sheath around the particle when sufficient material is adsorbed so that particle interaction and touching is prevented. In order to obtain a stable dispersion, it is required that the continuous liquid phase is a good solvent for the adsorbed polymer, that the particle surface is completely covered by the adsorbed stabilizer, which must be firmly attached, and that the thickness of the steric barrier is sufficient to prevent flocculation.

Nevertheless it is believed that other mechanisms, so called "natural grafting", occurs during the polymerization. Indeed, an initiator radical or any other polymeric radical can abstract an hydrogen from the polyol backbone (solvent) creating a radical on the polyol. Thus, the polyol backbone can behave as a chain transfer agent, initiating a new polymerization of present monomers. This kind of mechanisms leads to *in situ* formation of a polyol-SAN stabilizer macromolecule, which does not provide the same stabilizing power as S5200-SAN stabilizer. Therefore, the nature and the structure of the stabilizer is very complex and depends on many experimental conditions.

The different aspects of the process briefly exposed above show the complexity of this heterogeneous polymerization process where occur particularly polymerization in both phases, precipitation, *in situ* formation of the stabilizer and particle stabilization in order to prevent renucleation and agglomeration. All these mechanisms depend on the experimental conditions and act on the quality of the final dispersion.

3. Objectives

The objective of the work is to obtain a copolymer polyol material with the lowest viscosity and optimum filterability but with the maximum amount of solids. In order to reach this goal it is necessary to improve the stabilizer technology and to understand the influence of the process conditions on the final product.

Therefore the different objectives were to answer to the following questions concerning the process :

a) What is exactly the structure of the stabilizer molecule ?

b) What is the kinetics of the stabilizer precursor – styrene – acrylonitrile polymerization ?

c) What is the kinetics of adsorption onto the SAN surface ?

d) What is the effect of the stabilizer grafting on SAN solubility and CPP viscosity ?

e) What is the partitioning of monomers between the two phases with temperature ?

f) Where does the radical reaction take place (polyol or solids phase) and how does the splitting occur ?

In order to investigate the maximum of these issues, an experimental study of the process must be realized and a model must be developed in order to forecast the main characteristics of the copolymer polyols produced.

As the continuous stirred tank reactor process is used commercially, only this process will be studied. This project will reveal the effect of temperature, initiator, chain transfer agent, monomers and precursor concentration on the overall styrene and acrylonitrile kinetics. Part of this study will concern the partitioning of monomers, chain transfer agent and initiator over the two phases with temperature.

4. Scope of the research

This dissertation is composed of five chapters. The first one will expose the general bibliography about dispersion polymerization and copolymer polyols. This process will be compared with other types of heterogeneous polymerization processes and a chronological review presenting the main works realized in this field will be exposed. Then, the principal aspects of the mechanisms involved during this complex polymerization process (including steric stabilization, particles nucleation and growth, thermodynamics and modeling) will be developed in more details. Finally, a general overview of the influence of the main process parameters on the final dispersions will be presented before a review of the use of the copolymer polyols in polyurethane industry.

Chapter 2 will present the different experimental techniques used to study the copolymer polyol production at a laboratory scale. This chapter will be divided in two parts : the first part will present the different reactants and the devices used to run the continuous dispersion copolymerization while the second will expose the analytical techniques used to study the CPP properties.

Then, chapter 3 will provide the experimental tendencies. Experimental results obtained in order to support the modeling part will be presented and the influence of the process conditions on the CPP properties will be exposed.

The last part of this work deals with the modeling of the process. This part is actually divided in two chapters. Chapter 4 will present the hypotheses leading to the model and the resulting system of equations, which constitute the simulator, while chapter 5 will present the mathematical tools used to solve this system and to identify the unknown parameters of the model at the temperatures of work. Then, the results will be discussed taking into account the complexity of the subject and the accuracy of the measurements.

A general conclusion presenting the main results of this work and some recommendations will be exposed at the end of this dissertation.

CHAPTER 1
DISPERSION POLYMERIZATION : GENERAL BIBLIOGRAPHY

INTRODUCTION **59**

1. HETEROGENEOUS POLYMERIZATION PROCESSES **59**

1.1 GENERAL FEATURES OF HETEROGENEOUS POLYMERIZATION PROCESS 59
1.2 EMULSION POLYMERIZATION 60
1.3. SUSPENSION POLYMERIZATION AND DISPERSION POLYMERIZATION IN AQUEOUS MEDIUM 60
1.4. PRECIPITATION POLYMERIZATION AND DISPERSION PRECIPITATION 62

2. DEVELOPMENT OF THE DISPERSION POLYMERIZATION PROCESS **62**

2.1. FIRST GENERATION : 1950S TO THE 1970S 62
2.2. SECOND GENERATION : 1980S 62
2.3. THIRD GENERATION : 1990S 63
2.3.1. Mechanism and modeling *63*
2.3.2. Functional particles *64*
2.3.3. Dispersion polymerization in supercritical carbon dioxide *65*

3. STERIC STABILIZATION **65**

3.1. THE ATTRACTIVE AND REPULSIVE FORCES 65
3.2. THERMODYNAMIC APPROACH OF STERIC STABILIZATION 67
3.3. STABILIZER STRUCTURES AND CONFORMATIONS 68

4. MECHANISM AND MODELING OF DISPERSION POLYMERIZATION **70**

4.1. GENERAL MECHANISM 70
4.2. PARTICLE NUCLEATION 70
4.3. PARTICLE GROWTH 72
4.3.1. Radical Entry *72*
4.3.2. Polymerization within the polymer particles *73*
4.4. THERMODYNAMICS 74
4.4.1. Polymer solubility and precipitation *75*
4.4.2. Monomer Partitioning, locus of polymerization *79*
4.5. AGGLOMERATION AND RENUCLEATION : PARTICLE SIZE DISTRIBUTION 81
4.6. DISPERSION COPOLYMERIZATION 82

5. MAIN EXPERIMENTAL PARAMETERS INFLUENCING DISPERSION POLYMERIZATION 82

5.1. DILUENT SOLVENCY 82
5.2. MONOMERS 82
5.3. TEMPERATURE 83
5.4. INITIATOR 83
5.5. CHAIN TRANSFER AGENT 83
5.6. STABILIZER, PRECURSOR STABILIZER 83
5.7. AGITATION SPEED 84

6. COPOLYMER POLYOLS (CPP) 84

6.1. FLEXIBLE POLYURETHANE FOAMS 84
6.2. POLYETHER POLYOL 86
6.3. GRAFTED COPOLYMER POLYOL 89
6.4. EXAMPLES OF GRAFTED COPOLYMER POLYOL PRODUCED BY DOW CHEMICAL AND APPLICATIONS 90

CONCLUSION 91

Introduction

The present chapter will expose in a first part generalities concerning the dispersion polymerization, which will be compared with other types of heterogeneous polymerization processes in order to understand its particularities. Then, a chronological review of the main works done in the area will be presented. Further, the steric stabilization, which is the key of the process will be explained theoretically before presenting globally the mechanisms and the different models used to describe this kind of process, particularly, the nucleation step, the particle growth and the thermodynamic equilibrium between the dispersed solid phase and the continuous phase. Finally, a review of the influence of the main process parameters on the final dispersions will be exposed.
In a second part, generalities concerning the so-called "copolymer polyols" (CPPs) will be presented. Firstly, the use of polyols in the production of flexible polyurethane foams will be explained before describing the production by dispersion polymerization and the composition of polyether polyols, and then, of grafted copolymer polyols. The characteristics and the use of some examples of CPPs produced industrially will illustrate this presentation. Finally, the two main processes used industrially to produce copolymer polyols, batch and continuous processes, will be exposed briefly.

1. Heterogeneous polymerization processes

1.1 General features of heterogeneous polymerization process

According to Arshady (1992, 1999), heterogeneous polymerization processes are usually two-phase systems in which the starting monomer(s) and/or the resulting polymer are in the form of a fine dispersion in an immiscible liquid. The polymerization initiator may be soluble in the monomer or the liquid, and it may or may not be present within the polymer particles during their formation. In addition to the monomer, polymerization medium and the initiator, one or more additives is also added to the polymerization mixture to emulsify the monomer, and/or to stabilize the monomer droplets and the resulting polymer particles (Abad et al., 1995). Various combinations of the above-named possibilities are employed under empirically adjusted conditions to produce spherical (or irregularly shaped) polymer particles within relatively narrow size ranges from about 50 nm to 1-2 mm. There are four basic two-phases processes employed for chain growth polymerization : emulsion, suspension, dispersion, and precipitation, which are clearly distinguished on the basis of the following criteria.

1) Initial state of the polymerization mixture,
2) Kinetics of polymerization,
3) Mechanism of particle formation,
4) Shape and size of the final polymer particles.

The monomer is usually referred to as the "monomer phase" or the "dispersed phase". The liquid phase containing the dispersed monomer is defined as the "polymerization medium", or "medium" for the sake of brevity. The polymerization medium may also be referred to as the "continuous phase" or the "serum". In addition to the monomer(s) and the polymerization medium, another liquid (which must be miscible with the monomer and immiscible with the medium) may also be added to the monomer. This liquid is known as the "monomer diluent", or "diluent". The use of the term solvent is deliberately avoided by Arshady (1999) because the

diluent may be a good, poor or non-solvent, or a precipitant for the polymer. Polymerizations mixtures composed of an aqueous phase are generally classified in oil-in-water (O/W) or water-in-oil (W/O) systems. The main characteristics of each type of polymerization process are presented below and summed up in table 1.1.

1.2 Emulsion polymerization

In emulsion polymerization, the monomer in insoluble (or scarcely soluble) in the continuous phase (water), but it is emulsified in it by the aid of a surfactant. Under these conditions, the monomer is present in the form of droplets (about 1-10 μm or larger) or partly in the form of soap-coated micelles (about 5-10 nm), depending on the nature and concentration of the emulsifier. A small percentage of the monomer is also molecularly dissolved in the medium. Initiator is present in the continuous phase, where the initiating radicals are produced, and is not soluble in the monomer. According to Harkins (1947), the oligoradicals formed in the continuous phase are either surrounded by the dissolved monomer and emulsifier molecules, or they enter an already present monomer-swollen micelle and polymerization proceeds within the micelle with monomer droplets functioning as reservoirs. The emulsion polymerization process has the advantage of being able to simultaneously attain both high molecular weights and high reaction rates. Polymer latex particles prepared by this process are in the submicron size range, usually in the range of 50-300 nm.

The more commonly employed emulsion defined above is known as oil-in-water (O/W) system. Emulsion of water soluble monomers can also be carried out in exactly the same way by water-in-oil (W/O) systems, in the presence of a (W/O) emulsifier, and an oil soluble initiator. Certain monomer mixtures can also be polymerized in oil-in-oil (O/O) systems.

1.3. Suspension polymerization and dispersion polymerization in aqueous medium

In suspension polymerization (also called pearl polymerization), the initiator is soluble in the monomer, and these two are insoluble in the polymerization medium. It is carried out by suspending the monomer as droplets (100-10000 μm in diameter) in the continuous aqueous phase. This suspension is maintained by mechanical agitation and the addition of stabilizers. The initiator is soluble in the monomer droplets and is often referred to as oil-soluble initiator. Each monomer droplet in a suspension is considered to be a small bulk polymerization system. The kinetics of polymerization follows bulk or solution polymerization, depending on the absence or presence of a monomer diluent in the monomer droplets. Under these conditions, the monomer droplets are converted directly to the corresponding polymer beads of approximately the same size.

The term "dispersion polymerization in aqueous medium" has been used to describe a particular process for the preparation of polymer particles in the size range between suspension and emulsion, namely, around 10 μm in diameter. The mechanism of polymerization is the same as in suspension polymerization. It is often referred to as micro-suspension polymerization. The smaller polymer particles prepared in this system, compared to suspension particles, are due to a higher amount of polymeric stabilizer.

Oil-in-water and oil-in-oil systems can also be carried out in suspension processes.

Table 1.1. Characteristics of free-radical heterogeneous polymerization processes

Type of polymerization	Emulsion (O/W)	Precipitation	Dispersion	Dispersion in water	Suspension
Continuous phase	Water	Water or organic liquids	Organic liquids or alcohol-water mixtures	Water	Water
Monomer	-Low solubility in water -Droplets -Micelles / particles	Soluble in the continuous phase	Soluble in the continuous phase	-Low solubility in water -Droplets	-Low solubility in water -Droplets
Initiator	Soluble in water	Soluble in the continuous phase	Soluble in the continuous phase	Soluble in water	Soluble in the monomer
Stabilizer	Ionic/non-ionic emulsifiers	none	Soluble polymer stabilizers	High level of ionic stabilizers	Low level of ionic stabilizers
Initial medium	Multi-phases	Homogeneous phase	Homogeneous phase	Two phases	Two phases
Polymerization loci	2 (medium and next inside particles)	1 (medium)	2 (medium and inside particles)	1 (inside particles)	1 (inside particles)
Kinetics	High rates due to radical isolation	Gel effect possible	Gel effect possible	Gel effect possible	Gel effect possible
Product	Stable latex, 50 to 500 nm	Coarse precipitate or coagulum	Stable latex 0.1 to 0.5 μm, dispersions until 20 μm possible	Stable latex, around 10 μm	Rough suspensions 20 to 2000 μm

1.4. Precipitation polymerization and dispersion precipitation

According to Arshady (1999), precipitation polymerization involves an initially homogeneous reaction mixture, but the polymer precipitates from the monomer solution and the monomer will not merge into the polymer. Therefore the locus of polymerization is the solution, and the polymer continues to precipitate from it. The precipitation aggregates and finally becomes macroscopic particles or coagulum. Typical examples include polymerization of acrylonitrile in bulk, and styrene in hexane or ethanol.

On the other hand, in dispersion polymerization, as polymerization starts, a phase that is rich in polymer segregates from the continuous phase by separation. When the surface of the segregated polymer phase is stabilized, the polymer becomes a sphere (particle) and maintains a dispersion state. Polymerization after this occurs in both the continuous and polymer phases, and the contribution of each phase to polymerization depends on the partition of monomer between the two phases.

2. Development of the dispersion polymerization process

Several reviews of dispersion polymerization have been published since the first book written on the subject (Barret, 1975) in aliphatic solvents. Croucher and Winnik (1987, 1990), Walbridge (1989) and Ober (1990) focused on the second generation of studies done in polar solvents. Cawse (1997) and Kawaguchi (2000) are the more recent authors to present a global view concerning the knowledge on this process.

2.1. First generation : 1950s to the 1970s

The first works about dispersion polymerization, mainly realized by the ICI researchers, dealt essentially with aliphatic hydrocarbons as a medium and was the subject of a book edited by Barret (1975). Many examples of free-radical polymerization, ionic polymerization and polycondensations that can be processed by the way of dispersion polymerization were exposed.

The main applications of these polymer dispersions were for film-forming compositions in the surface coatings field and for paints, particularly for automotive applications. In addition, a number of related surface coating applications such as adhesives, polishes, textile impregnants, encapsulants of pigments, and fiber coatings were reported.

2.2. Second generation : 1980s

When the first works presented in Barret's book dealt with particles smaller than 2 μm, the works, which followed, focused on the ways to control particle size and to achieve narrow particle size distribution in the range of 1 to 20 μm. Indeed, monodisperse particles are required for a number of applications, including the production of toners, preparation of instrument calibration standards, development of packing materials for chromatography, and performing of biomedical and biomedical analysis (Araujo & Pinto, 2000).

In the 1980s, there was also a considerable interest in generalizing the results to more polar solvents as the continuous phase by which the range of monomers that can be polymerized using this method is greatly widened. A view of the different systems that have been studied from the 1980s to now are shown in table A1.1 of annex 1. Methyl methacrylate, styrene and mixtures of these have been the most studied monomer systems. Hydrophilic polymers such as (hydroxypropyl)cellulose (HPC), poly(acrylic acid) (PAA) and poly(N-vinylpyrrolidone) (HPC) have been mainly used for the preparation of polystyrene latex particles in alcohol media. They

were used as precursor stabilizers that react *in situ* with radicals to provide amphiphilic graft polymers that stabilize sterically the particles, as it will be explained latter.

Corner (1981) reported a dispersion polymerization method for the production of polystyrene particles in aqueous ethanol media using poly(acrylic acid) as a steric stabilizer. Almog et al. (1982) produced monodispersed polystyrene and poly(methyl methacrylate) particles up to 5 μm using a quaternary ammonium salt surfactant with a polymeric steric stabilizer. Ober and co-workers (Ober et al., 1985, 1986), (Lok & Ober, 1985), (Ober & Hair, 1987) produced polystyrene particles up to 9 μm by polymerizing styrene in ether/alcohol systems in the presence of different nonionic cellulosic polymers as steric stabilizers. They also achieved large monosize styrene / butyl methacrylate copolymer particles (Ober & Lok, 1987), (Ober, 1990).

Researchers of Lehigh University (USA) produced uniform polystyrene particles in 1-10 μm range and up to 40% solid contents in ethanol (Tseng et al., 1986). Some experiments were done to incorporate onto particles some functional groups such as hydroxyl, carboxyl, amine, amide, silane, polydimethylsiloxane and silacrown. They also attempted to present a mechanism for particle formation and growth. Further, Lu et al. (1988), studied particularly the partitioning of styrene between ethanol and solid particles, and the locus of polymerization.

Croucher and Winnik (1987) discussed the requirements necessary to prepare polymer particles by dispersion polymerization. They reviewed the state of knowledge in the area with particular emphasis being given to control the particle size and size distribution by varying the composition of mixed solvents, the temperature and the initiator concentration.

2.3. Third generation : 1990s

2.3.1. Mechanism and modeling

Following the works done in the 1980s, several studies tried to understand the mechanism of dispersion polymerization for various systems in order to control particle monodispersity. A list of the different systems studied are presented in table A1.1 of annex 1 and some of them are presented in more details below, in order to show the different experimental conditions investigated.

Paine and co-workers investigated the different important key factors involved in the dispersion polymerization of styrene in polar solvents : the grafting mechanism (Paine, 1990a) and its visualization over the particles surface (Paine et al., 1990a), the solvency control (Paine, 1990b) and the influence of different reaction parameters (Paine et al., 1990b).

Following the works of Almog et al. (1982), Kobayashi et al. (1990, 1992) studied the preparation of micron-sized monodispersed PMMA particles and the effect on the particle size of the concentrations of the stabilizer (PEtOZO, PEI), the monomer and the initiator.

Tuncel et al. (1993) studied the dispersion polymerization of styrene in different alcohol/water media and the effect of initiator, stabilizer concentrations, alcohol/water ratio and monomer/dispersion ratio on particle sizes and dispersity.

Lehigh university researchers followed their work on dispersion polymerization by producing monodisperse PMMA particles (Shen et al., 1993, 1994) and describing the influence of several key polymerization parameters on particle size including temperature, initiator type and concentration, stabilizer concentration and molecular weight, monomer concentration, co-stabilizer type and concentration, solvency and the use of a crosslinking agent. Hattori et al. (1993) prepared monodisperse poly(divinylbenzene) and poly(styrene-co-divinylbenzene)

particles in the 0.4-3 μm range in methanol and studied the effects of polymerization parameters, such as monomer concentration, the co-solvent, and the presence of oxygene. Hu et al. (1995) Investigated the process variables that act on the preparation of monodisperse micron-size poly(butadiene-co-styrene) particles in ethanol, such as the monomer/ethanol ratio and the agitation.

Kawaguchi et al. (1995, 1996) studied the dispersion polymerization of N-butylmethacrylate (BMA) in methanol/water media and the effect on particle size of the structure and the molecular weight of the poly(ethylene oxide) (PEO) macromonomers, the initial BMA, initiator, and macromonomer concentrations, the temperature and the composition of the solvent. He recently reviewed the knowledge in the area of dispersion polymerization (Kawaguchi, 2000).

Saenz & Asua (1995, 1998) studied the same system and the effect of the nitrogen purge, the monomer purification, the type of agitation, the presence of costabilizer, the stabilizer concentration, the ethanol/water ratio, the monomers ratio, the temperature and the initiator concentration on the particle size distribution.

Lacroix-Desmazes and Guyot (1995, 1996a) used maleic, styrenic and methacrylic macromonomers of poly(ethylene oxide) and related polymerizable surfactants (surfmers) as stabilizers in the dispersion polymerization of styrene in ethanol-water mixtures. They also focused on the formation and the prediction of final size of PS and PMMA particles (Lacroix-Desmazes & Guyot, 1996b). Lacroix-Desmazes and Guillot (1997) investigated the locus of polymerization by studying the partitioning of styrene between ethanol/water medium and the solid phase.

These studies have shown that dispersion polymerizations depends on numerous reaction parameters and that the process is highly sensitive to small changes in the parameters leading sometimes to contradictory results. From these experimental studies, different works tried to provide some mathematical models for dispersion polymerization in polar media to forecast monomer partitioning, particle size and molecular weight distributions : Paine (1990c), Chernyshev et al. (1997), Lacroix-Desmazes & Guillot (1997), Ahmed & Poehlein (1997a, 1997b), Saenz & Asua (1999), Cao et al. (1999, 2000c), Arauja & Pinto (2000) and Yasuda et al. (2001a, 2001b).

2.3.2. Functional particles

Following the work done by Tseng et al. (1986), some researchers tried to incorporate a variety of functional groups onto the particles through copolymerization in order to obtain monosize polymeric particles in the micron size range for diverse biomedical applications (i.e., chromatographic separation of biological macromolecules, scintigraphic imaging, cell labeling, and separation). Lee et al. (1994) obtained acrylic polymer particles with polar surface functionality (acids and alcohols) and that can be transferred in basic aqueous medium. Tuncel et al. (1994) produced monodisperse polystyrene particles carrying basic functional groups (i.e., hydroxyl, carboxyl, or amino) on their surfaces as they provide important advantages for coupling of ligands onto polystyrene particles. Cao et al. (2000b) produced micron-size functional uniform PMMA particles by dispersion copolymerization in methanol/ water medium.

The copolymer polyols (CPP) studied in this work are actually part of this kind of functional particles as the alcohol groups of polyols that stabilized Styrene-Acrylonitrile particles react further with isocyanates during the production of polyurethane foams, as it will be exposed deeper at the end of this chapter.

2.3.3. Dispersion polymerization in supercritical carbon dioxide

Since a decade, the solvent-intensive polymer industries have looked for alternatives to reduce or/and eliminate the negative impact of harmful solvent emissions on the environment. Supercritical CO_2 ($scCO_2$) represents an alternative to both the use of toxic and flammable organic solvents and the generation of large volumes of aqueous waste. Moreover, the use of $scCO_2$ as a dispersion medium for free-radical polymerizations of vinyl monomers allows the easy isolation of polymer as a free-flowing powder through a simple reduction in the CO_2 pressure. Carbon dioxide has a relatively low critical temperature (T_c=31.1 °C) and a moderate critical pressure (P_c= 72 bar). Depending on the temperature and pressure conditions, $scCO_2$ can exhibit "liquid like" densities and at the same time "gas like" viscosities. Near its critical point, $scCO_2$ has a dissolving power similar to that of liquids. As with all supercritical fluids, $scCO_2$ offers mass-transfer advantages over conventional solvents because of its low viscosity and surface tension. Another important fact is that its thermodynamic and transport properties are easily adjustable, as they can be altered by small changes in pressure and/or temperature. Nevertheless, one major drawback of $scCO_2$ is its poor solvency power for most hydrocarbon polymers. However, amorphous fluorinated polymers and/or organosiloxane polymers exhibit appreciable solubility in $scCO_2$, and, therefore, have been employed by the choice of at least one suitable fluorinated or siloxane comonomer.

Since the first report on polymerization of vinyl monomers in $scCO_2$ by DeSimone and coworkers (1992), many papers have been reported dealing with the polymerization of various monomers (e.g., methyl methacrylate, styrene, vinyl pyrrolidone, acrylonitrile, etc) by DeSimone et al. (1994), Hsiao et al. (1995), Shaffer et al. (1996) and Canelas et al. (1996). O'Neil et al. (1998a, 1998b) studied more particularly the particle growth regime and the particle formation regime for dispersion polymerization of methyl methacrylate in $scCO_2$. A limited number of copolymerizations have been investigated : Galia et al. (2003) studied the dispersion copolymerization of methyl methacrylate and N,N-dimethylacrylamide (DMA).

Most of the reported studies have been focused on experimental investigations of process parameters (e.g., pressure, temperature, stabilizer concentration, etc) and the type of stabilizer on the polymerization kinetics and product morphology. A recent publication of Chatzidoukas et al. (2003) develops a comprehensive mathematical model for the quantitative prediction of the time evolution of monomer conversion and molecular weight distribution in the free-radical dispersion polymerization of methyl methacrylate in $scCO_2$.

3. Steric stabilization

According to Napper (Napper, 1977, 1983), steric stabilization is a generic term that takes into account all aspects of the stabilization of colloidal particles by non-ionic macromolecules. According to Osmond and Waite (Barret, 1975), this colloidal stability is achieved by the interposition of repulsive forces of sufficient magnitude to overcome the inherent attractive forces of electromagnetic origin that arise as particles approach each other. In the absence of any repulsive forces, the particles rapidly aggregate.

3.1. The attractive and repulsive forces

The attractive forces that operate between two adjacent particles are called the van der Waals forces. Different models describe the source of the attractive forces : the interaction between permanent dipoles (Keesom force), the interaction between a permanent dipole in one molecule

and a dipole induces by it in a second molecule (Debye force) and the interaction between two transient dipoles (the quantum-mechanical attraction of London).

For two spheres of radius a, Van der Waals' attraction, V_A, is :

$$V_A \approx -A^* \frac{a}{12H_0}, \qquad (1.1)$$

where A^* is the effective constant of Hamaker and H_0 is the distance between the two particle surfaces. This equation is valid only if $a >> H_0$, that is to say if the particles are closed to each other.

The more common repulsive forces are the electrostatic forces, which are generated in aqueous media, however, these forces are not generally available for stabilizing particles in organic liquids. The steric stabilization results from a mechanical effect. This means that the repulsion forces act only if the polymer layers are in contact with each other. Considering two surfaces, each covered by a layer of adsorbed polymer chains : when they approach to each other to within a distance less than the combined thickness of the adsorbed layers, δ, an interaction between the polymer layers will occur (figure 1.1). The polymer segment density increases from the interpenetration or compression of the polymer sheaths when two particles approach one another. According to Walbridge (1989), the osmotic diffusion of solvent into the region of increased polymer concentration generates a repulsive force, causing the particles to separate.

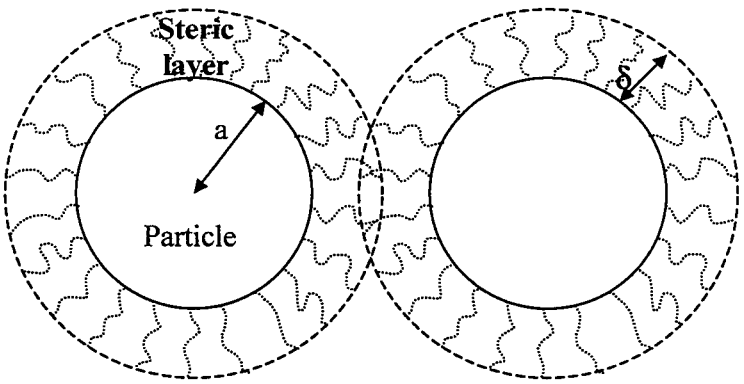

Figure 1.1 : Schematic representation of the close approach of sterically stabilized particles

Napper (1977) precises that the term "steric stabilization" is correct in that the effect derives from the spatial or configurational interactions of polymer molecules. It should not be confused with the steric effects of organic chemistry, which are concerned with the very short-range repulsions between substituent groups in a molecule.

For polymer colloids stabilized by firmly attached solvated polymer layers, the thickness of the layer, δ, is such that, at the point of closest approach, Van der Waals' attraction, V_A, between the particles is reduced to a level at which the particles separate spontaneously by thermal motion. Figure 1.2 shows schematically the potential energy as a function of the distance of separation for two sterically stabilized particles and for different barrier thicknesses. V_S is the steric interaction and V_T is the total interaction potential.

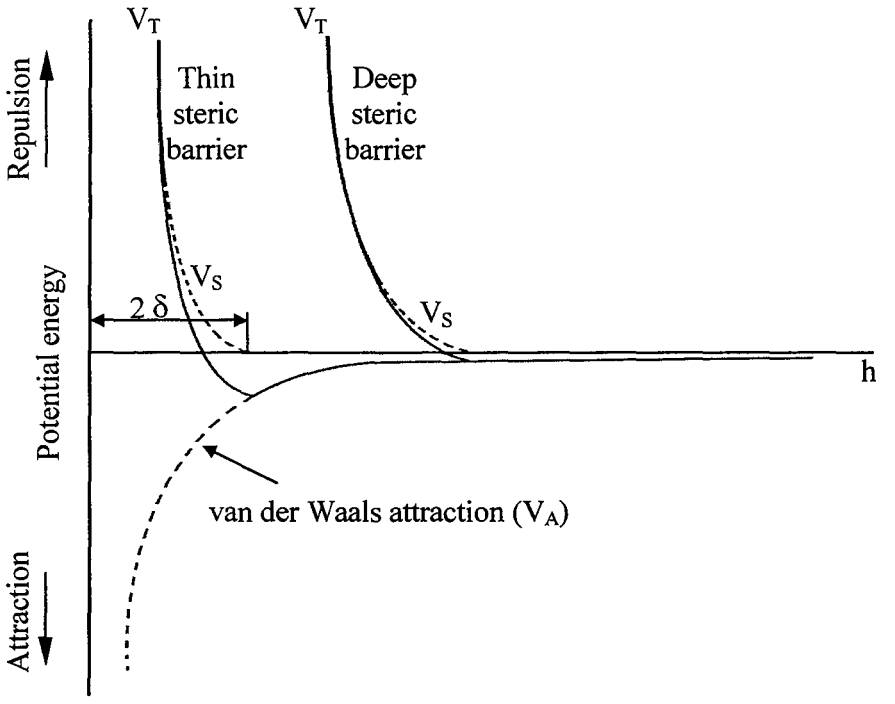

Figure 1.2 : Potential energy against distance of separation, h, for sterically stabilized particles with varying depth of steric barrier

Unlike electrostatic stabilization, there is no long-range repulsion and the particles are subject only to attractive forces until the outer fringes of the adsorbed stabilizer polymer are in physical contact. Here, Van der Waals' attraction can be estimated from Eq. 1.1, using $H_0 = 2\,\delta$:

$$V_A \approx -A^* \frac{a}{24\delta}. \qquad (1.2)$$

This equation shows that the stabilization is all the more efficient than the polymer layer is thicker. This thickness is besides closely linked to the molecular weight of the stabilizer and its density in the layer. It shows also that the attraction increases with the particle size, a. The more the size increases, the more the thickness of the stabilizer layer must be important.

The existence of a secondary minimum, i.e. a small net attraction, is quite probable for strongly attracting particles or for shallow steric barriers as it can be seen on figure 1.2. The colloid stability is therefore dependent on the dimensions and the solution properties of the adsorbed polymer, under the local conditions of temperature, concentration and pressure, and on the size and nature of the particle core.

3.2. Thermodynamic approach of steric stabilization

Napper (1977) proposed a thermodynamic approach of steric stabilization by considering the Gibbs free energy of mixing,

$$\Delta G_M = \Delta H_M - T\Delta S_M, \qquad (1.3)$$

associated to the interpenetration of macromolecular chains when two sterically stabilized particles get closed together. ΔH_m is the enthalpy change on mixing, T is the absolute temperature and ΔS_m is the entropy change on mixing. Flocculation happens if $\Delta G_M < 0$. The border case $\Delta G_M = 0$ corresponds to the theta conditions for the stabilizer polymer, and corresponds to the apparition of the flocculation. The Theta conditions are the ideal conditions where the dimensions are not perturbed, that is to say that there is no interaction with the solvent or between the segments of a molecule. Therefore, only $\Delta G_M > 0$ corresponds to a stable system.

Three types of stabilization are therefore distinguished as presented below in table 1.2. If both ΔH_M and ΔS_M are positive but $\Delta H_M > T\Delta S_M$, the enthalpy change on close approach opposes flocculation whereas the entropy change promotes it. As the enthalpic contribution is dominant, this is referred to as enthalpic stabilization. Moreover, enthalpically stabilized dispersions are characterized by flocculation on heating.

Table 1.2 : Thermodynamic types of steric stabilization

ΔH_M	ΔS_M	$\lvert\Delta H_M\rvert/T\lvert\Delta S_M\rvert$	ΔG_M	Type	Flocculation
+	+	>1	+	Enthalpic	On heating UCFT
-	-	<1	+	Entropic	On cooling LCFT
+	-	>1 or <1	+	Combined enthalpic - entropic	Not accessible

UCFT and LCFT : respectively Upper and Lower Critical Flocculation Temperature

An opposite situation occurs if both ΔH_M and ΔS_M are negative and $|\Delta H_M| < T|\Delta S_M|$. In this situation, the entropy term opposes flocculation whereas the enthalpy term favours it. It is therefore called entropic stabilization and it is characterized by flocculation on cooling.

The third category is characterized by ΔH_M being positive and ΔS_M being negative so that both the enthalpy and entropy terms contribute to stability. Therefore, dispersions stabilized by combined enthalpic-entropic stabilization cannot in principle be flocculated at any accessible temperature.

3.3. Stabilizer structures and conformations

Napper (1977) noticed that the best way to obtain sterically stabilized lattices is to generate the latex particles in the presence of a preformed steric stabilizer. The stabilizer may also be generated *in situ* by the grafting of a suitable precursor on the polymer.

The stabilizers that provide the best stability are amphipathic block or graft copolymers. Indeed, the most effective stabilizers consist of both anchor groups and stabilizing moieties. The stabilizing moieties must be soluble in the dispersion medium to be effective whereas the most efficient anchor groups functions are nominally insoluble in the dispersion medium and must have a composition similar to that of the polymer particles to stabilize. The different structures answering to these criteria have been summed up by Barret (1975) in figure 1.3. There are block or graft copolymers.

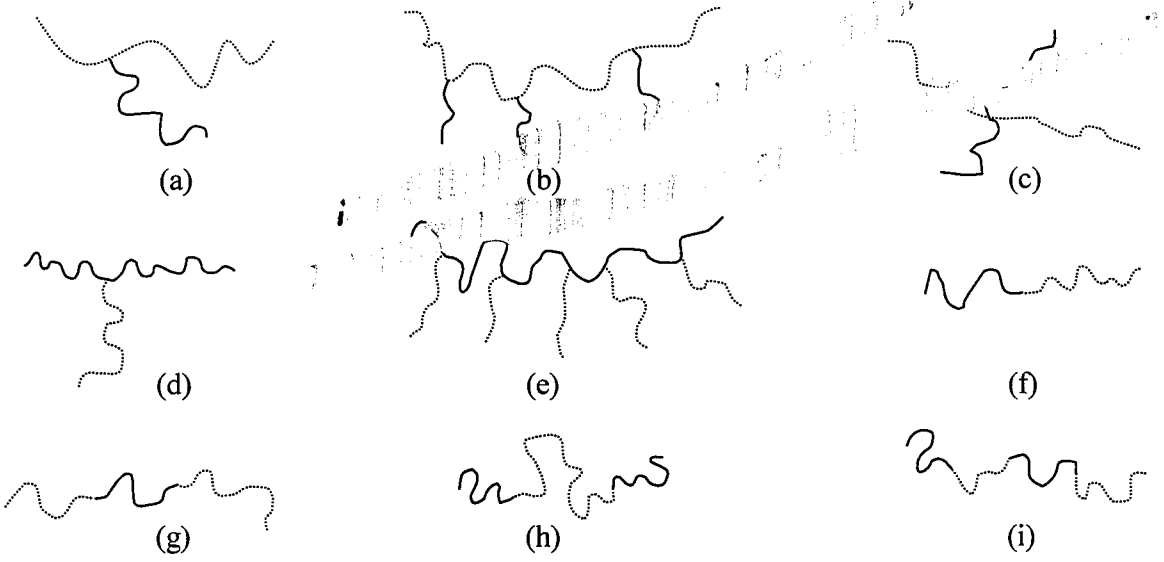

Figure 1.3 : Possible structures of stabilizer copolymers : a-e, grafted copolymers ; f-i, block copolymers
(—) soluble chain , (.....) insoluble chain

Grafted copolymers are produced *in situ* by using a precursor either sensible to transfers, or having a copolymerizable group. If it is sensible to transfers, the primary radicals issued from initiator decomposition may abstract an hydrogen from the precursor chain, which allows to initiate the polymerization of the polymer to stabilize. These kind of precursors are called "transurfs" ((Guyot, 1999), (Guyot et al., 1999)). If the polymer precursors have a copolymerizable group (maleic, vinylic, methacrylic,...), they are macromonomers that can copolymerize with the monomers, and are called "surfmers".

The purpose of the anchor polymer is to prevent the stabilizing moieties attached to one particle from moving away from the interaction zone on the approach of a second particle. The stabilizing moieties could escape from the stress of the interaction zone by two different mechanisms : first, the stabilizer molecules could move laterally around the surface of the particle while remaining attached to the particle, or secondly, the stabilizers may in some circumstances be desorbed from the particle surface. Ensuring that the particle surfaces are fully coated can prevent lateral movement of the adsorbed grafts. Desorption can be eliminated by attaching the stabilizing moieties to suitably insoluble polymer chains that anchor the moieties to the particles, either physically or chemically by covalent linkage between the anchor group and the dispersed polymer.

As seen before, the molecular weight of the stabilizing moieties is important, as it is linked to their hydrodynamic volumes, because it determines the segment density distribution function. The minimum coverage is realized by chains disposed like adjacent "mushrooms" as described on figure 1.4.a. The grafting density can be increased leading to a "brush" conformation (figure 1.4.b) and therefore a thicker region of constant concentration (de Gennes, 1987). R_g is the radius of gyration of the graft.

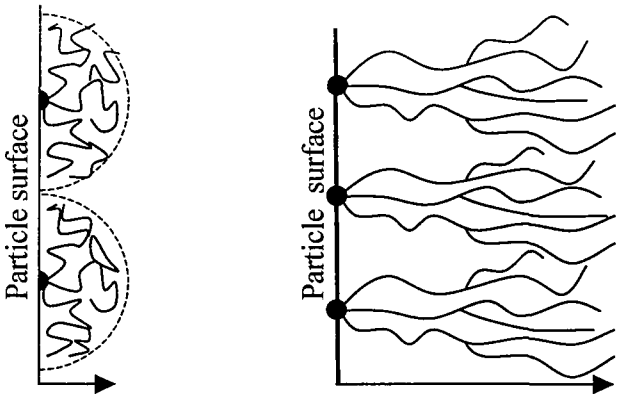

Figure 1.4 : Two types of grafted surfaces :
a) "mushroom" conformation at low grafting density,
b) "brush" conformation at high grafting density.

4. Mechanism and Modeling of Dispersion Polymerization

4.1. General mechanism

The general mechanism of dispersion polymerization may be divided in four stages in the batch process (Cao et al., 2000c). Firstly, the pre-polymerization stage, during which the monomers, dispersant, initiator and chain transfer agent are dissolved in the medium and the reaction system is homogeneous prior to polymerization. Secondly, the nucleation stage, during which Oligoradicals, polymers and grafted-copolymer stabilizers (if the stabilizer is not preformed) are produced in this solution. The key feature is the *in situ* formation of the stabilizer by chain transfer or by copolymerization as explained before. These oligoradicals precipitate to form unstable nuclei. Different nucleation models can be taken into account : self-nucleation or aggregative nucleation. A new phase appears therefore, but the solution polymerization dominates the reaction. Thirdly, the particle stabilization stage, during which the nuclei coalesce and may be hindered by the stabilizer until the particles are stabilized providing "mature" particles. Finally, the particle growth stage, during which all particles have enough stabilizer and the number of particles becomes constant. The particles grow by absorption of monomer, initiator, chain transfer agent, oligo-radicals, stabilizer and by the capture of unstable nuclei before they mature into stable particles, but also by bulk polymerization. Therefore, following this mechanism, the particle size distribution should be relatively narrow, even monodisperse. In this stage there are two polymerization loci, namely the monomer-swollen polymer particles and the continuous phase. Particular points of this mechanism and related models will be discussed below.

4.2. Particle Nucleation

Barret (1975) reviewed related theories and proposed several models for particle nucleation in dispersion polymerization, as shown on figure 1.5.

Among these models, the nucleation in the monomer-swollen micelles cannot be considered as the major particle formation mechanism in the dispersion polymerization since, before polymerization, the system is clear and homogeneous.

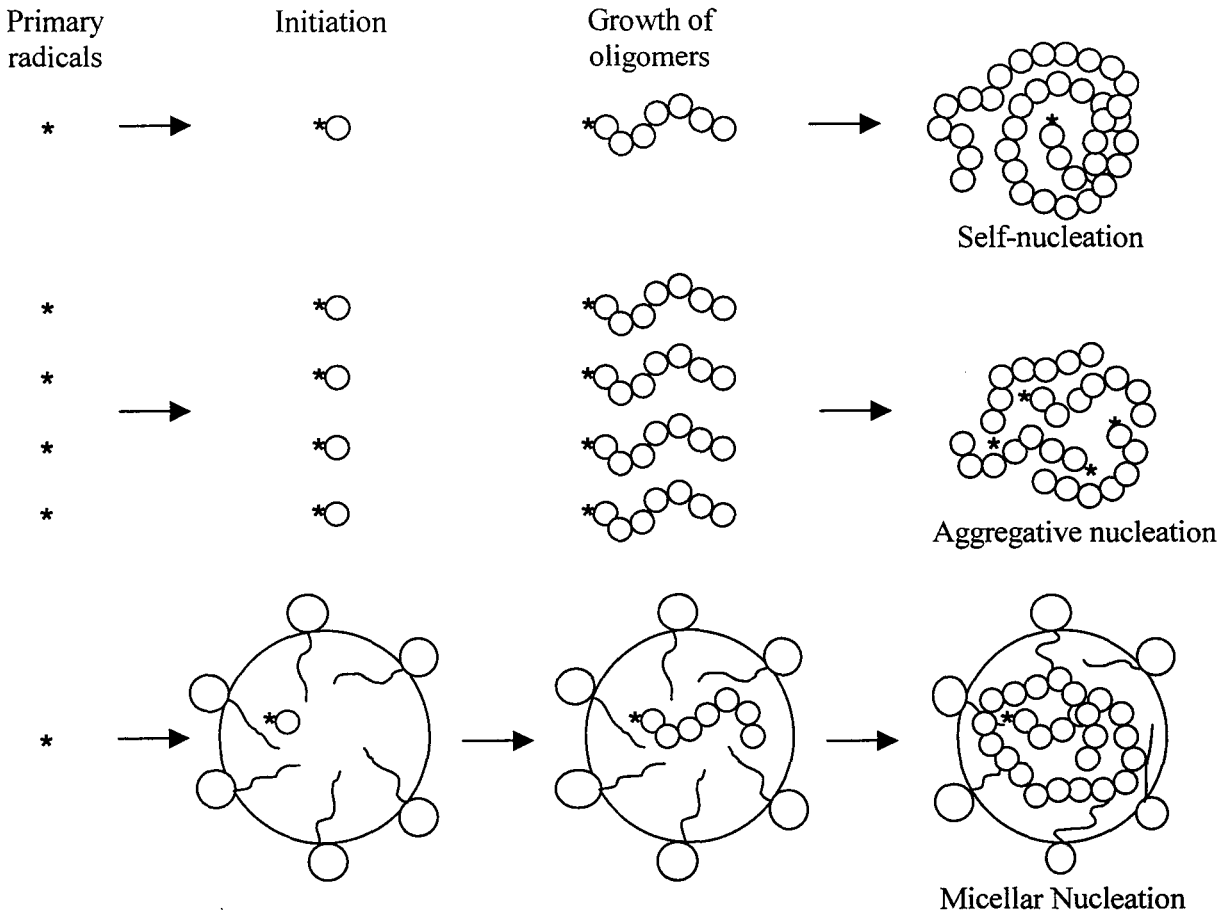

Figure 1.5 : Models for particle nucleation

If the particle nucleation is mainly based on the self-nucleation mechanism, each individual oligomer chain initiated by a primary radical forms a new particle nucleus as soon as it reaches a critical chain length. This can be checked experimentally as an increase of the initiator concentration would increase the number of particle nuclei, which in turn would decrease the particle size of the final particles. This critical chain length depends on the solubility of the polymer in the continuous phase that will be discussed further.

However, if the particle nucleation is based on aggregative nucleation, the oligomer chains formed by solution polymerization associate with each other increasingly as their molecular weight and concentration rise. At the same time, the stabilizer adsorbs onto the aggregates to form stable particle nuclei. Therefore, increasing the initiator concentration induces an increase in the instantaneous concentration of oligomeric radicals, which in turn increases the degree of aggregation of the oligomeric radicals to form larger permanent particle nuclei, and thus, larger final particles sizes. For instance, experimental results obtained by Lu (1988) show that the particles size of the final polystyrene dispersion in ethanol increases with increasing initiator concentration, which may imply that this system follows aggregative nucleation.

With the aggregative nucleation model, the chain length at which the oligoradicals precipitate should be lower than the critical chain length at which they would precipitate in a self-nucleation model.

4.3. Particle growth

The rate of radical formation within the monomer-swollen polymer particles comes from two sources : the rate of absorption by the particles of the radicals produced in the continuous phase, and the rate of generation of primary radicals within the particles, arising from the partition of initiator.

4.3.1. Radical Entry

Different models have been proposed for the capture of oligomeric radicals. Paine (1990a) has expressed the capture of oligomeric radicals by diffusion kinetics. He has shown that, for styrene in ethanol, when particles with a diameter of 1 μm are formed, the vast majority of the oligomeric radicals are captured before terminating in the continuous phase, that means that polymerization occurs mainly within the particles. According to him, when 3-4 μm particles are formed, a majority of oligoradicals terminate in the continuous phase, and when 10 μm particles are formed, most of the radicals initiated in the continuous phase terminate there as well.

Ahmed & Poehlein (1997a) applied Fick's law of diffusion to the absorption process, taking into account the concentration gradient of radicals at the particle surface and neglecting the concentration of oligoradicals at particle surface in front of their concentration in the continuous phase. For large particles the rate of absorption of radical species with a degree of polymerization (DP) i, M_i^*, from the continuous phase, is given by the following expression :

$$R_{Ai} = k_{ei}\pi d_p^2 N_p \left[M_i^*\right]_c , \tag{1.4}$$

where $k_{ei} = 2D_i F_i / d_p$. (1.5)

k_{ei} is the entry rate coefficient expressed in m^3 per particle per second, d_p is the swollen radius of the polymer particles, N_p is the number of polymer particles per m^3, and D_i is the diffusion coefficient of a radical with DP = i in the surrounding medium. F_i is a correction factor to account for the reversibility of the radicals absorption and the potential barrier to absorption.

The total absorption rate is expressed in terms of an average absorption coefficient, $\overline{k_e}$:

$$\overline{k_e} = \sum_{i=1}^{Z-1} \frac{k_{ei}\left[M_i^*\right]_c}{\left[M_T^*\right]_c}, \tag{1.6}$$

$$\text{where } \left[M_T^*\right]_c = \sum_{i=1}^{Z-1} \left[M_i^*\right]_c , \tag{1.7}$$

is the total concentration of radicals in the continuous phase.

Z is here the critical chain DP at which the oligoradicals precipitate in an self-nucleation model.

The absorption coefficient is, in turn, expressed in terms of an effective average diffusion coefficient for radical capture, $\overline{D}$, which include the correction factor F_i :

$$\overline{k_e} = 2\overline{D}/d_p . \tag{1.8}$$

Ahmed & Poehlein (1997b) found from the simulation of batch dispersion polymerization of styrene in ethanol, with poly(vinylpyrrolidone) as precursor stabilizer, $\overline{D} = 2.86\ 10^{-12}\ m^2s^{-1}$ at 60°C and $\overline{D} = 2.86\ 10^{-13}\ m^2s^{-1}$ at 80°C. Hansen and Ugelstad (1982) found $\overline{D} = 10^{-10}\ m^2s^{-1}$ in

water for emulsion polymerization of styrene. Araujo & Pinto (2000) assumed that $\overline{D} = 6\ 10^{-11}$ m^2s^{-1} for dispersion polymerization of styrene in ethanol.

Yasuda et al. (2001a) considered that the termination of oligomer radicals in the continuous phase can be neglected, indicating that the rate of absorption of radicals is equal to the rate of radical production in the continuous phase.

4.3.2. Polymerization within the polymer particles

In dispersion polymerization, the polymer particles are rather large (by comparison with emulsion polymerization as shown in table 1.1 at the beginning of this chapter) and may contain a high number of radicals per particle. Moreover as the particles may contain a high volume fraction of polymer, the conditions may be closed to those of bulk polymerization. Therefore, the effect due to high viscosity must be considered : the cage effect concerning initiation, the glass effect concerning propagation and the gel effect concerning termination.

a) The cage effect

According to Yasuda et al. (2001a), Araujo and Pinto (2000), Saenz and Asua (1999), and as previously suggested by Lu (1988), the high internal viscosity of the polymer particles may promote a cage effect (Odian, 1981). The efficiency factor of primary radicals decreases exponentially for a high polymer volume fraction (Ahmed & Poehlein, 1997a). This means that radicals generated within the polymer particles are likely to terminate before any significant growth can be attained, as diffusion of radicals through the polymer mass is seriously impaired. This means that radicals present within the polymer particles come mainly from the continuous phase. As the entering chains are relatively long, it may be difficult for radicals to diffuse towards the core of the particle. This would lead to a heterogeneous distribution of radicals that is to say to a radical concentration gradient along the particle radius, as believed to occur in conventional emulsion polymerization by anchoring of the hydrophilic part of the entering radical to the particle surface. Araujo & Pinto (2000) proposed, to express the radical number per particle as a function of the particle diameter : $\tilde{n} = K \cdot d_p^2$ (1.9)

with K is assumed to be equal to 3.0 10^{11} cm^{-2} and d_p is the particle diameter (in cm).

b) The gel effect

The viscosity in the polymer particles is relatively high as the polymer concentration in the particle is high. Therefore the bimolecular termination is expected to become kinetically controlled by the diffusion of polymer chains and thus the termination rate constant may be reduced by several orders of magnitude and cause a large increase in the average number of radicals per particle and an acceleration in the rate of polymerization. Such behavior is referred to as the gel effect or Trommsdorff effect and Norrish-Smith effect in recognition of the early workers in the field (Odian, 1981).

Saenz and Asua (1999) recalled that under these conditions the termination rate constant should be given by:

$$\overline{k}_t = 4\pi (D_1 + D_2) r_a Na, \quad (1.10)$$

where D_1 and D_2 are the diffusion coefficients of the polymer chains involved in the termination reaction and r_a is the radius of interaction. However, as this approach leads to a chain length which depends on the termination rate and as it involves heavy computational load, average gel effect factors were developed. For example, different works ((Lu, 1988), (Ahmed & Poehlein,

1997), (Saenz & Asua, 1999)) referred to the free volume theories for viscosity-controlled termination reactions proposed by Marten and Hamielec (1978, 1982) :

$$\bar{k}_t = \bar{k}_{t_0}\left(\frac{\bar{M}_{W_{crit}}}{\bar{M}_W}\right)^n Exp\left\{-A\left(\frac{1}{V_F}-\frac{1}{V_{F_{crit}}}\right)\right\}, \tag{1.11}$$

where $\bar{M}_W$ is the weight average molecular weight, $\bar{M}_{W_{crit}}$ the value of $\bar{M}_W$ at which chain entanglement begins, V_F the free volume in the polymer particles, $V_{F_{crit}}$ the free volume at which chain entanglement begins, $\bar{k}_{t_0}$ the average termination reaction constant under conditions at which the termination is not diffusionally controlled (diluted systems) and n and A are adjustable parameters.

Nevertheless, Eq. (1.11) is difficult to use as it depends on the composition of the polymer. Saenz and Asua (1999) considered the following empirical equation for their model :

$$\bar{k}_t = \bar{k}_{t_0} g\,, \tag{1.12}$$

$$\text{with, } g = \frac{\left(\bar{k}_t\right)_x}{\left(\bar{k}_{t_0}\right)_{x=0}} = Exp\left(-\left(Bx + Cx^2 + Dx^3\right)\right) \tag{1.13}$$

where x is the fraction of polymer in the polymer particles, and B, C and D are parameters of the model, which have been identified from experimental results.

Yasuda et al. (2001) considered a simple model for gel effect :

$$\bar{k}_t = \bar{k}_{t_0}\beta_{gel}\,, \tag{1.14}$$

where β_{gel} was determined empirically.

c) The glass effect

If the glass transition temperature of the resulting polymer is higher than the polymerization temperature, at high volume fractions of polymer in the particles, a glass-transition state occurs with the result that the propagation reaction rate is also controlled by the diffusion of monomer to the reactive sites (Lu, 1988). Ahmed and Poehlein (1997) used the semi-empirical relation proposed by Marten and Hamielec (1978) in terms of fractional free volume of the system to account for the reduction of the propagation rate with increasing the conversion :

$$\bar{k}_p = \bar{k}_{p_0} Exp\left\{-A\left(\frac{1}{V_F}-\frac{1}{V_{F_{crit}}}\right)\right\} \tag{1.15}$$

where $V_{F_{crit}}$ is here the free volume at which $\bar{k}_p$ begins to decrease and B is an adjustable parameter. $\bar{k}_{p_0}$ is the average propagation reaction constant under conditions at which the propagation is not diffusionally controlled (diluted systems).

4.4. Thermodynamics

The precipitation of the polymer formed leads to a heterogeneous system consisting in a polymer phase (particles) and a continuous phase. The particles contain polymer, monomers, initiator, chain transfer agent and eventually a minor amount of solvent. Below, are presented

the main models concerning polymer solubility and the partitioning of the different species between the two phases, which determines the locus of polymerization and therefore all the characteristics of the resulting latex.

4.4.1. Polymer solubility and precipitation

Two notions are developed here : a way to qualitatively forecast the solubility of a polymer in a medium, and the determination of the critical chain length at which a polymer precipitates in a given medium.

a) Cohesive Energy Density and Solubility (Hildebrand) Parameters

The process for dissolving an amorphous polymer in a solvent is governed by the Gibbs-free energy of mixing, given by Eq. 1.3 : $\Delta G_m = \Delta H_m - T\Delta S_m$.

A negative ΔG_m predicts that the process will occur spontaneously. Since the dissolution of high-molecular-weight macromolecules is always connected with a large increase in entropy, the enthalpy term (the sign and magnitude of ΔH_m) is the deciding factor in determining the sign of the Gibbs free energy change. Solubility parameters were developed to describe the enthalpy of mixing of simple liquids (non polar, non-associating solvents), but have been extended to polar solvents and polymers.

Hildebrand and Scott (1949) proposed that :

$$\Delta H_m = V\left(\left(\frac{\Delta E_1^v}{\overline{V}_1}\right)^{1/2} - \left(\frac{\Delta E_2^v}{\overline{V}_2}\right)^{1/2}\right)^2 \phi_1\phi_2, \qquad (1.16)$$

where V is the volume of the mixture, ΔE_i^v is the energy of vaporization of species i that is to say the energy change upon isothermal vaporization of the saturated liquid i to the ideal gas state at infinite volume, $\overline{V}_i$ is the molar volume of species i, and ϕ_i is the volume fraction of species i in the mixture. The cohesive energy density, $\Delta E_i^v/\overline{V}_i$, is the energy of vaporization per unit volume.

The Hildebrand solubility parameter, has been defined as the square root of the cohesive energy density and describes the attractive strength between molecules of the material :

$$\delta_i = \left(\frac{\Delta E_i^v}{\overline{V}_i}\right)^{1/2}. \qquad (1.17)$$

The dimensions of δ are $(cal/cm^3)^{1/2} = 2.046\ 10^3\ (J/m^3)^{1/2} = 2.046\ (MPa)^{1/2}$.

The enthalpy change of mixing per unit volume can then be rewritten as follows for a binary mixture :

$$\Delta H_m/V = (\delta_1 - \delta_2)^2 \phi_1\phi_2. \qquad (1.18)$$

In order for ΔG_m to be less than zero, the heat of mixing must be smaller than the entropic term. ΔG_m will always be less than zero for regular solutions if $\delta_1 = \delta_2$ and the components will be miscible in all proportions. In general $(\delta_1 - \delta_2)^2$ must be small for the components to be miscible.

This last equation gives the heat of mixing of regular solutions in which the components mix with no volume change on mixing at constant pressure, no reaction between the components, and no complex formation or special associations.

The solubility parameter of a mixture is often taken to be the sum of the products of the component solubility parameters with their volume fractions. For the case of two monomers A and B dissolved in a solvent S :

$$\delta_{mixture} = \phi_A^c \delta_A + \phi_B^c \delta_B + \phi_S^c \delta_S . \tag{1.19}$$

In order to determine the solubility parameter, δ_i, for a component i, the energy change, ΔE_i^v, must be related to the enthalpy of vaporization :

$$\Delta E_i^v = \Delta H_i^v - RT . \tag{1.20}$$

Indeed, the solubility parameters of solvents can generally be determined by measuring the enthalpy of vaporization (or using a correlation for ΔH_i^v) and using the following equation :

$$\delta_i = \left(\frac{\Delta H_i^v - RT}{V_i} \right)^{1/2} . \tag{1.21}$$

Nevertheless, the Hildebrand solubility parameter is a broad qualitative indicator, which can be quantitatively useful only for a limited number of hydrocarbons : it cannot be calculated for polymers from heat of vaporization data because of their non volatility. Paine (1990b) shown advantages to the three-dimensional Hansen scale, where the total cohesive energy density, δ_t, is given as a sum of terms representing the dispersion, δ_d, the polarity (permanent dipole-dipole interactions), δ_p, and the hydrogen bonding contributions, δ_h :

$$\delta_t^2 = \delta_d^2 + \delta_p^2 + \delta_h^2 . \tag{1.22}$$

The solubility parameters of a mixture (solvent + monomers) are then calculated as follows (Xu, 2000) :

$${}^m\delta_t^2 = {}^m\delta_d^2 + {}^m\delta_p^2 + {}^m\delta_h^2 , \tag{1.23}$$

$$\text{with } {}^m\delta_d = \sum_{i=1}^{n} \phi_i^c \delta_d^i , \quad {}^m\delta_p = \sum_{i=1}^{n} \phi_i^c \delta_p^i , \quad {}^m\delta_h = \sum_{i=1}^{n} \phi_i^c \delta_h^i , \tag{1.24}$$

where ${}^m\delta_t$ is the total cohesive energy density of the mixture, n the number of components, I, in the mixture and ϕ_i^c is the volume fraction of component i in the continuous medium.

Concerning the solubility parameters of a copolymer, it should also be suitable to define it as a function of its composition.

The domain of solubility of a polymer is characterized by the distance, R_{12}, between the continuous phase (1) and the polymer (2) coordinates :

$$R_{12} = \left((\delta_{1d} - \delta_{2d})^2 + (\delta_{1p} - \delta_{2p})^2 + (\delta_{1h} - \delta_{2h})^2 \right)^{1/2} . \tag{1.25}$$

Van Krevelen (1976) proposed that the polymer is soluble in the continuous phase if this distance is less than about 5 δ-units.

The present work deals with the copolymerization of styrene and acrylonitrile in a polyol media in the presence of a precursor stabilizer (S5200). Tables 1.3 and 1.4 present the solubility parameters of the different components of this system.

Table 1.3 : Hansen's parameters of monomers and polymers (Bandrup, 1989)

Solvent and Polymers	δ_d [(MPa)$^{1/2}$]	δ_p [(MPa)$^{1/2}$]	δ_h [(MPa)$^{1/2}$]	δ_t [(MPa)$^{1/2}$]
Styrene	18.6	1.0	4.1	19.0
Acrylonitrile	16.4	17.4	6.8	24.8
PolyStyrene	21.3	5.8	4.3	22.5
PolyAcrylonitrile	18.2	16.2	6.7	25.3

There is no data concerning poly(styrene-co-acrylonitrile), but a first approximation would be to calculate the parameters of the copolymer as a mixture of the two polymers using the same kind of relation than Eq. 1.36. Hansen's solubility parameters of the polyol and S5200 are predicted using the parameter component group contributions (Van Kravelen, 1976).

Table 1.4 : Hansen's parameters estimated by Van Kravelen method

Solvents	δ_d [(MPa)$^{1/2}$]	δ_p [(MPa)$^{1/2}$]	δ_h [(MPa)$^{1/2}$]	δ_t [(MPa)$^{1/2}$]
Polyether-polyol IP 3040	15	1	8.5	17.4
S5200	15	0.58	7.4	16.9

These predictions do not pretend to give more than rather rough estimates. They are predicted from group contributions using the following equations :

$$\delta_d = \frac{\sum F_{di}}{V},\ \delta_p = \frac{\sqrt{\sum F_{pi}^2}}{V} \text{ and } \delta_h = \sqrt{\frac{\sum E_{hi}}{V}}, \tag{1.26}$$

where F_d, F_p and E_h are given by tables for given groups.

The solubility parameters may be used qualitatively to predict the solubility of polymers in a given solvent. This method shows that polystyrene and polyacrylonitrile are not well soluble in polyol, but it does not take into account the size of the polymer chain and the copolymer composition, which may influence the solubility.

These parameters have mainly been used in dispersion polymerization in order to follow the influence of the solvent on the particles size (Paine, 1990b), (Xu, 2000).

b) Critical chain length

Different works have been realized in order to determine the chains length of polymers at which they precipitate in the continuous phase, the critical chain length, l_{crit}, assuming a self-nucleation model. In the following models it is assumed that the polymer molecules with chain length greater than or equal to l_{crit} are completely insoluble whereas the polymer molecules with chain length lower are completely soluble.

- Lu (1988) tried to determine l_{crit} of polystyrene in ethanol, although this system seems to follow aggregation nucleation. He selected the components of the mixture to simulate the initial conditions of the dispersion polymerization in batch of styrene in ethanol with 25.0 wt.% monomer and 1.0 wt.% initiator (AIBN) (based on styrene monomer) in ethanol. The reaction mixture was allowed to run for four minutes at 70°C during which the reaction mixture became milky. The polymerization was stopped by adding hydroquinone/ethanol solution to the reaction mixture. The precipitated polymer was isolated by centrifugation, the clear supernatant serum was mixed with water and styrene and ethanol were stripped out. The dissolved oligomers were precipitated by this way and their molecular weight distribution was determined by gel permeation chromatography (GPC). The maximum peak of the molecular weight distribution (MWD) was approximately 3400 g/mol that is to say 33 styrene units.

A polystyrene standard of $\bar{M}_w$ = 3550 g/mol and $\bar{M}_w / \bar{M}_n$ =1.05 was then mixed with a mixture containing 25 wt.% styrene and 75 wt.% ethanol and a small amount of hydroquinone : the standard was completely dissolved in the test medium at 70 °C.

Nevertheless, the critical chain length of styrene oligomers, l_{crit}, decreases if the medium contains a lower styrene concentration at the same temperature, showing the importance of the solvency of the dispersion medium. A curve expressing the critical chain length as a function of the mixture solvency has been obtained.

$$\ln(l_{crit}) = 28.498 - 2.085\,\delta_{mix} \text{ at } 70°C, \tag{1.27}$$

$$\text{with } \delta_{mix}^2 = \phi_{sc}\delta_s^2 + \phi_{ec}\delta_e^2, \tag{1.28}$$

where ϕ_{sc} and ϕ_{ec} are the volume fractions of styrene and ethanol in the continuous phase, respectively.

This curve was generated by placing a given amount of polystyrene standard of known molecular weight in ethanol with a small amount of hydroquinone at 70 °C. The styrene monomer was then gradually added to the ethanol medium until the polystyrene standard dissolved in the mixture.

- Ahmed & Poehlein (1997) carried out experiments to detect the monomer concentration at which polystyrene molecular weight standards of different chain lengths precipitated from styrene-ethanol solutions by measuring the turbidity of the solution. A small quantity (approximately 10 g/L) of the polystyrene standard was dissolved in fresh styrene. Ethanol was then added successively and the turbidity of the solution measured. Turbidity declined as the styrene concentration of the solution decreased as a result of ethanol addition. The polystyrene chains precipitated when the monomer concentration decreased below their solubility limit and the turbidity of the solution increased drastically. It allowed to draw the number-average chain length as a function of the monomer volume fraction at which this change occurred. Then, the critical chain length for homogeneous nucleation of primary particles, with δ_{mix}, the mixture solubility parameter of the continuous phase at different temperatures, were obtained from regression fitting of the plots :

$$\text{at } 60\ °C,\ \ln(l_{crit})(\pm 1.1) = 24.433(\pm 1.71) - 1.693(\pm 0.14)\delta_{mix}, \tag{1.29}$$

$$\text{at } 70\ °C,\ \ln(l_{crit})(\pm 1.1) = 21.772(\pm 2.30) - 1.460(\pm 0.19)\delta_{mix}, \tag{1.30}$$

$$\text{at } 80\ °C,\ \ln(l_{crit})(\pm 1.1) = 21.319(\pm 1.98) - 1.412(\pm 0.16)\delta_{mix}, \tag{1.31}$$

with δ_{mix} in $(cal/cm^3)^{1/2}$.

- Araujo & Pinto (2000) used a critical chain length of 200 for modeling dispersion polymerization of styrene in ethanol.

- Yasuda et al. (2001b) measured the molecular weight distribution of polymers in the ethanol phase at a reaction time of 1 hour using reaction conditions similar as for particle synthesis. The polymerization was stopped with hydroquinone and the solid particles were removed from the sample by centrifugation. The highest degree of polymerization in the ethanol phase was 120 when the monomer concentration and stirring speed were 20 wt. % and 30 rpm, respectively. Further they took 120 for the critical chain length irrespective of the monomer concentration and the stirring speed.

As a conclusion, the critical chain length, has been used to model the precipitation but it is quite complex to determine experimentally as it depends on many parameters as temperature, continuous phase composition, monomers concentrations, growing oligoradicals composition, etc...

4.4.2. Monomer Partitioning, locus of polymerization

The locus of polymerization depends on the way the monomers, the initiator and the chain transfer agent are partitioned between the continuous phase and the polymer particles. It is a key point of the process. Some works have been attempted to model the monomer partitioning.

Ober et al. (1986) studied the partitioning of styrene between the solvent and the growing particles. Dispersion polymerizations of styrene were carried out in a mixture of ethanol and 2-methoxy ethanol at different conversions and at 68 °C. Samples were centrifugated at 68 °C to separate solids from serum. The concentration of monomer contained in the solid phase was measured by gas chromatography (GC) and compared with the concentration of monomer determined for the whole system : here, most of the monomer was in the continuous phase. The partition coefficient ($[M]_p/[M]_c$) of styrene varied from 0.06 at 10% to 0.2 at 90% at 68°C.

Lu et al. (1988) studied the partitioning of styrene in dispersion polymerization of styrene in ethanol. He determined this partitioning experimentally and fitted the parameters of a theoretical model to the experimental results. The measurement of the partitioning was done by separating, at different conversions at 70°C, the solid from the serum by sedimentation at 4 °C (as sedimentation does not perturb the equilibrium between the two phases, contrary to centrifugation) and to measure the quantity of residual monomer in each phase by GC. The model used was based on Flory-Huggins' theory modified by Morton as exposed below. He fond that the partition coefficient ($[M]_p/[M]_c$) of styrene increased from 0.8 at 5% conversion to 1.1 at 95 % conversion at 70 °C.

Lacroix-Desmazes and Guillot (1997) studied the partitioning of styrene during dispersion polymerization of styrene in ethanol and in water/ethanol media at 70°C. They also developed a model issued from Flory-Huggins' and Morton's theory, which fits with experimental measurements. Samples were centifugated at 4-10°C and styrene concentration in solid and serum were measured by GC. They finally found that the partition coefficient ($[M]_p/[M]_c$) of styrene in an initial mixture composed of ethanol/water = 70/30 is about 4.8 at 70°C instead of about 1 in pure ethanol. Some experiments shown also that the higher the polymerization temperature, the lower the styrene concentration in the particles.

Ahmed and Poehlein (1997a) used the results of Lu et al. (1988) to model the partitioning of styrene in dispersion of polymerization of styrene in ethanol, and they assumed that the initiator (Azobis-isobutyronitrile) was equally distributed between the two phases.

Cao et al. (1999) applied the Flory-Huggins theory modified by Morton to simulate the monomer partition between the particles phase and the continuous phase in the dispersion polymerization of methyl methacrylate in methanol/water medium.

Saenz and Asua (1999) applied also the same theory for the monomers partitioning in the copolymerization of styrene and butyl acrylate in an ethanol/water medium, but they just introduced an unknown partitioning coefficient for the initiator equilibrium.

Araujo and Pinto (2000) used partitioning coefficient in their mathematical model of dispersion polymerization of styrene in ethanol, and they assumed that the initiator was completely dissolved in the continuous phase. Yasuda et al. (2001a, 2001b) used also the model presented below for dispersion polymerization of styrene in ethanol.

Thermodynamic equilibrium is attained when the partial molar free energies of mixing for the compounds i in the different phases are the same. Therefore, the following equilibrium equations can be written :

$$(\Delta G/RT)_i^p = (\Delta G/RT)_i^c . \tag{1.32}$$

Ugelstad et al. (Ugelstad, et al., 1983, 1992) proposed the following equilibrium equations based on the Flory-Huggins' theory, completed by Morton to take into account the interfacial free energy. Indeed, the classical Flory-Huggins' theory for the free energy of mixing of the component i is :

$$(\Delta G/RT)^l_{i_{mixing}} = \ln\phi_i^l + \sum_{\substack{j=1\\ j\neq i}}^{n}(1-m_{ij})\phi_j^l + \sum_{\substack{j=1\\ j\neq i}}^{n}\chi_{ij}(\phi_j^l)^2 + \sum_{\substack{j=1\\ j\neq i}}^{n-1}\sum_{\substack{k=j+1\\ k\neq i}}^{n}\phi_j^l\phi_k^l(\chi_{ij}+\chi_{ik}-\chi_{jk}m_{ij}), \tag{1.33}$$

where l = c (continuous phase) or p (particles), n is the total number of components,

ϕ_i^l is the volume fraction of the compound i in the phase l,

$$m_{ij} = \overline{V}_i/\overline{V}_j , \tag{1.34}$$

χ_{ij} is the interaction parameter per molecule of compound i with compound j.

The number of parameters describing the system is reduced because Flory's theory implies that:

$$m_{ji} = m_{ij}^{-1} , \tag{1.35}$$

$$\text{and } \chi_{ji} = \chi_{ij}\, m_{ji} . \tag{1.36}$$

The interfacial free energy is introduced by Morton :

$$(\Delta G/RT)^l_{i_{interfacial}} = 2\gamma\overline{V}_i/r_pRT , \tag{1.37}$$

$\overline{V}_i$ is the partial molar volume,

r_p is the radius of the swollen particles (dp/2 for the particles with dp the particle diameter)

γ is the interfacial tension, R is the gas constant, T is the temperature,

In first approximation, partial molar volumes are taken equal to the molar volumes of the pure compounds.

The interaction parameters may be expressed considering that χ_{ij} can be written as the sum of an entropic and an enthalpic component :

$$\chi_{ij} = \chi_{ij}^{S} + \chi_{ij}^{H}, \tag{1.38}$$

where χ_{ij}^{S} is the entropic term and χ_{ij}^{H} is the enthalpic term of the interaction parameter between the species i and j. The enthalpic component is related directly to the Hildebrand's parameters :

$$\chi_{ij} = \overline{V}_i(\delta_i - \delta_j)^2 / RT + k, \tag{1.39}$$

where δ_i and δ_j are the solubility parameters of the species i and j.

This allows to determine the interaction parameters knowing the solubility parameters.

χ_{ij}^{S} is usually considered to be a constant, k, between 0.3 and 0.4 for non polar systems (k=0.34 is often used). Hildebrand and Shinoda shown that the entropic term could be neglected when $\overline{V}_i \approx \overline{V}_j$.

Nevertheless, the use of solubility parameters does not allow to take into account hydrogen bonds.

In the case of copolymerization, the interaction parameter of the component i with the copolymer should be calculated (Saenz and Asua, 1999) as follows :

$$\chi_{iP} = Y_A \chi_{iP_A} + (1 - Y_A)\chi_{iP_B}, \tag{1.40}$$

where χ_{iP_k} is the interaction parameter of component i with homopolymer k and Y_A the copolymer composition.

4.5. Agglomeration and renucleation : Particle size distribution

Most of the works done on dispersion polymerization assumed monodisperse particle size. Paine (1990a) proposed a simple mechanistic model to predict particle size, which allows to discuss the conditions that lead to monodisperse particles and particularly the risks of secondary nucleation or of coalescence. From figure 1.4, which describes the different conformations that may have the steric stabilizer at the surface of the particles, Paine (1990a) exposed in a simple way how should happen the particle stabilization. The quantity of stabilizing moieties available in the system should be always between a minimum required quantity, corresponding to the surface of all the particles ("mushroom" conformation of figure 1.4.a), and a maximum required quantity, after which stabilizer cannot adsorb anymore onto the particle surface ("brush" conformation of figure 1.4.b).

This method needs models giving the quantity of stabilizing moieties available and the surface covered by the soluble moieties of the stabilizer. Paine (1990a) and further Yasuda et al. (2001b) considered that PVP get grafted to polystyrene chains by transfer reactions in dispersion of

styrene in ethanol and they estimated the coverage area of a soluble moiety from its radius of gyration that is assumed to be linked to its molecular weight.

The two types of breakdown of monodispersity that can be observed in dispersion polymerization are the stabilization of secondary particle populations and large particle coalescence. If the locus of polymerization is essentially the continuous phase, and if the stabilizer is produced *in situ*, then, an overproduction of stabilizer may occur. The quantity of soluble moieties of stabilizer exceeds the maximum quantity required and it will be able to stabilize a second crop of smaller particles growing from the dead chains formed in solution but not yet captured by the large particles. Therefore, the number of stabilized particles increases and the size distribution is broaden.

In the opposite way, if the polymerization inside the particles becomes dominant, the quantity of stabilizer produced in the continuous phase decreases until the quantity of stabilizer is less than the minimum quantity needed to stabilize the existing particles. In this case, there is coalescence of the particles, and therefore the number of particles decreases, the average diameter increases and the size distribution broadens.

4.6. Dispersion Copolymerization

Very few works have been realized on dispersion copolymerization (Saenz & Asua, 1999) (Kawaguchi et al., 1995), (Horak et al., 1995). As recalled by Walbridge (1989), the chemical composition of a copolymer formed by radical copolymerization of a homogeneous mixture of monomers depends on the relative reactivity of the individual monomers towards the propagating polymer radical. In dispersion polymerization, the overall reactivity is also influenced by the relative concentrations of the monomers at the site of polymerization, which depends on the partitioning coefficient of the two monomers between the two phases.

5. Main experimental parameters influencing dispersion polymerization

The different conditions that act on the properties of latex produced by dispersion polymerization are briefly overviewed below.

5.1. Diluent solvency

The diluent quality acts on the critical chain length of the oligomers (which increases as the polymer is more soluble in the diluent), the rate of adsorption of the stabilizer (which decreases with the solvency of the diluent) and the partitioning of the different species. This leads to an important effect on the particle size distribution, the polymerization kinetics and the molecular weights of polymer particles.

A general observation is that by increasing the solvency of the diluent, the particle size increases, the size distribution broadens, the polymerization kinetics decreases and the molecular weights decreases. Indeed, the locus of polymerization is directed to the continuous phase.

5.2. Monomers

According to Shen et al. (1994), the monomers concentration could influence the particle size in several ways : by changing the solubility parameter of the continuous phase (Eq. 1.23) it changes the solubility of the oligomer chains in the continuous phase (the critical chain length),

the solvency power of the *in situ* formed stabilizer and the rate of adsorption of this stabilizer ; by changing the polymerization rate, thereby changing the rate of nuclei formation.

Nevertheless, the last two points act in an opposing way on the particle size : increasing monomer concentration increases the solvency of the medium, which should reduce the rate of adsorption of the stabilizer but in the same time it increases the molecular weight of the polymer and therefore the molecular weight of the stabilizer that would increase its adsorption.

In the case of copolymerization, the ratio of the two monomers is also very important : it changes the grafting rate with the precursor stabilizer, the polymer composition and therefore its solubility in the continuous mixture.

5.3. Temperature

Temperature influences the kinetics, the viscosity and the thermodynamic equilibrium. An increase in temperature causes an increase in the initiator decomposition rate (and therefore in the number of radicals produced), in the propagation rate and in the solvency of the continuous medium. This results in an increase in the rate of growth of existing particles, a decrease of the viscosity, and a decrease in the adsorption of the stabilizer, which should be more soluble in the continuous phase.

Two opposite effects act on the length of the polymer chains : increasing radical concentration would result in shorter polymer segments, while the increase in the rate of propagation of the oligomer chains would result in longer segments.

Generally, an increase of the particle size is observed, even if more radicals are produced, which tends to justify an aggregative model for nucleation in these cases.

5.4. Initiator

An increase in the initiator concentration leads to an increase in the number of oligo-radicals that are produced. It increases therefore the quantity of stabilizer if it is produced *in situ* but should reduce the length of the polymer segments.

As explained in previously, if homogeneous nucleation happens, each oligoradical should provide a new particle and an increase of the initiator concentration will thus reduce the particle size. In an opposite way, if an aggregation nucleation mechanism happens, an increase of the initiator concentration should result in an increase of the particle size.

The type of initiator (characterized by its half-life time) is also important as it will be exposed in chapter 3 concerning the "natural grafting".

The effect of the initiator depends also of its partitioning between the continuous phase and the particles.

5.5. Chain Transfer Agent

An increase in the chain transfer agent concentration should result in a decrease in the polymer chain lengths. Its effect depends also of its partitioning between the two phases. If the chain lengths are lowered they may be more soluble in the continuous phase.

5.6. Stabilizer, Precursor stabilizer

When the quantity of stabilizer increases, the total surface of particles that can be covered also increases. Nevertheless, if the stabilizer is produced *in situ* by grafting with the growing oligoradicals, two opposite effects act on the particle size. Indeed, an increase of the precursor stabilizer concentration will increase the grafting and therefore the quantity of stabilizer, which

should decrease the particle size. However, an increase of the grafting may results in providing stabilizer molecules with several soluble moieties, that leads to an increase of the stabilizer solubility in the continuous phase and to a decrease of its adsorption rate onto the particle surface, finally leading to an increase of the particles sizes.

5.7. Agitation speed

The reactor (batch or continuous) must be well agitated in order to homogenize the continuous phase. Therefore the reactor and the agitation must be studied carefully. Nevertheless, some studies made on the type of agitation, reported by Saenz and Asua (1995), concluded that the type of agitation had a weak influence on the particle size. On the other hand, Hu et al. (1995), explained that the nucleation is determined by the local shear rate in the system. A high rotation speed leads to a high shear rate, which, in turn, results in a high rate of aggregation of the nuclei and therefore in large particle size.

6. Copolymer Polyols (CPP)

Copolymer polyol (CPP) has grown to be one of the major building blocks for the flexible polyurethane industry. The application of CPP in automotive high resilient (HR) molding formulations and in furniture improves processing and increases foam hardness. CPP's are produced within Dow in Freeport, Terneuzen and Zwijndrecht using both CSTR and batch reactor processes. The capacity of the CSTR plants present in Terneuzen and Freeport was respectively 50 million tones and 75 million tones per year in 2000.

Polyurethane chemistry will be firstly presented to understand the interest of polyols and copolymer polyols, which will be described further and finally, some examples of industrial CPP's produced by Dow will be shown.

6.1. Flexible polyurethane foams

Polyurethane chemistry is based on the reactions of isocyanates with active hydrogen-containing compounds. Isocyanates are compounds having one or more of the highly reactive isocyanate group (-N=C=O), which will readily react with hydrogen atoms that are attached to atoms more electronegative than carbon, like alcohols, as follows :

This is an addition process for which the heat (Δ) of reaction has been reported to be approximately 24 kcal/mole of urethane. Depending on the choice of starting materials, the R and R' groups may also contain isocyanate or isocyanate-reactive groups respectively. When extended to polyfunctional reactants, like toluene diisocyanate (TDI) and glycerine, this reaction provides a direct route to cross-linked polymers as shown in figure 1.6.

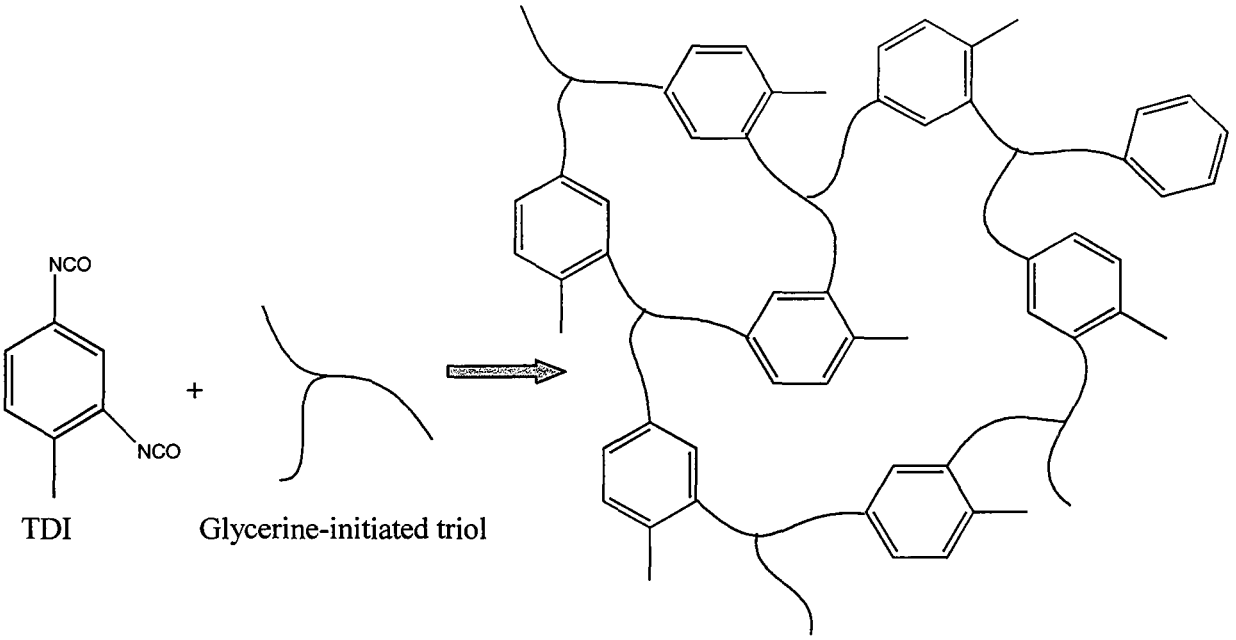

Figure 1.6: Cross-linking in polyurethane polymers

To make a foam, the polyurethane polymer must be expanded or blown by the introduction of bubbles and a gas. A convenient source of gas is the carbon dioxide produced from the reaction of an isocyanate group with water.

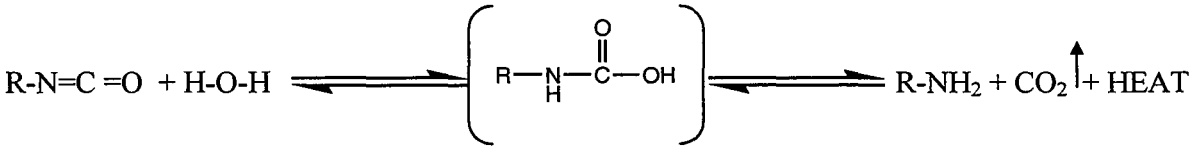

The intermediate product of this reaction is a thermally unstable carbamic acid, which spontaneously decomposes to an amine and carbon dioxide. Diffusion of the carbon dioxide into bubbles previously nucleated in the reacting medium causes expansion of the medium to make a foam. Further reaction of the amine with additional isocyanate gives a disubstituted urea.

The approximate total heat release per mole is 47 kcal.

Again if the isocyanate and amine molecules are polyfunctional, a cross-linked polymer will result. Another conceptual method of cross-linking the polymer is by reaction of a hydrogen atom from the disubstituted urea with a free isocyanate group to form a biuret linkage.

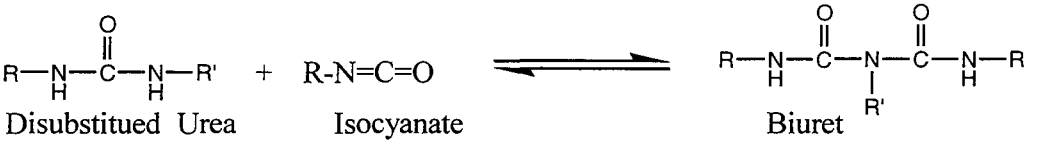

Disubstitued Urea Isocyanate Biuret

Blowing can also be achieved by the physical addition of a low-boiling nonreactive liquid to a foam formulation. Historically, the most commonly used physical blowing agents were the chlorofluorocarbons, urethane grade from methylene chloride and trichloroethane. Vaporization of these liquids by heat from exothermic reactions produces gas molecules, which diffuse into nucleated bubbles and contribute to foam expansion.

Flexible polyurethane foam recipes normally contain a host of ingredients selected to aid in achieving the desired grade of foam. Table 1.5 lists the most common ingredients and typical concentration ranges used in the production of flexible polyurethane foam.

Processing and properties of the resulting foam can be markedly influenced by the choice of the starting polyol structure (Casati and Herrington, 1998), (Kaushiva and Dounis, 2000). Copolymer polyol is a graft copolymer, which contains stable dispersions of a solid particulate polymeric phase in the liquid polyol phase.

Table 1.5 : Common recipes for flexible polyurethane foam production

Component	Parts by Weight
Polyol	100
Inorganic fillers	0-150
Water	1.5-7.5
Silicone surfactant	0.5-2.5
Amine catalyst	0.1-1.0
Tin catalyst	0.0-0.5
Chain-extender	0-10
Cross-linker	0-5
Additive	Variable
Auxiliary blowing agent	0-35
Isocyanate	25-85

6.2. Polyether polyol

A polyether polyol, also called "polyol" here for short, is the polymeric reaction product of an organic oxide and an initiator compound containing two or more active hydrogen atoms. The active hydrogen compound in the presence of a base catalyst initiates ring opening and oxide addition, which is continued until the desired molecular weight is obtained. If the initiator has two active hydrogens (type water, ethylene glycol...), a diol results. If a trifunctional initiator such as glycerin is used, oxide addition produces growth in three directions and a triol results. These reactions are exothermic.

The properties of the finished polyol depend largely on the oxide, or the mixture of oxides, used. Commercially, propylene oxide (PO) and ethylene oxide (EO) are the most widely used.

When the polymerization is carried out using propylene oxide, as illustrated below, secondary terminal hydroxyls result. For instance, "Flexstab" polyether polyols are produced with glycerine and propylene oxides :

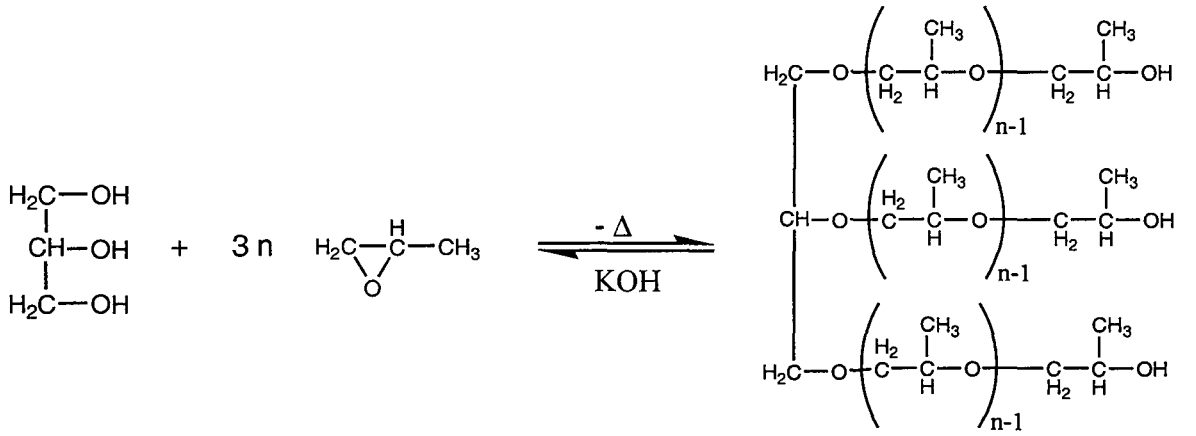

Glycerine Propylene Oxide "Flextab" polyether polyol

If the polymerization is carried out entirely with ethylene oxide or if propylene oxide polyol is capped with additional ethylene oxide, a primary hydroxyl group results.

Alcohol Ethylene oxide A Primary hydroxyl

Secondary Alcohol Ethylene oxide A Primary hydroxyl

Primary hydroxyl groups are generally stated to be three times more reactive with isocyanate than secondary hydroxyls. This increased reactivity is useful in the short production cycles needed for the various types of molded foam. Indeed "flexmold" polyether polyols, represented below, are produced by a sequential addition of propylene oxides on glycerine followed by addition of ethylene oxide :

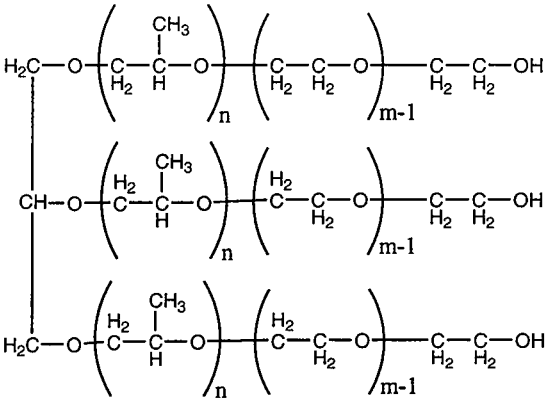

"Flexmold" polyether polyol

Two types of catalysis methods can be used to produce the polyols :

- "KOH-polyol", which means that the preparation of the polyol is catalysed by KOH, leading to significant amount of unsaturation or monol (typical 0.03 meq/g).

  This occurs when propylene oxide isomerizes at reactor conditions to form allyl alcohol, which then serves as an initiator site for the production of a monohydroxyl molecule.

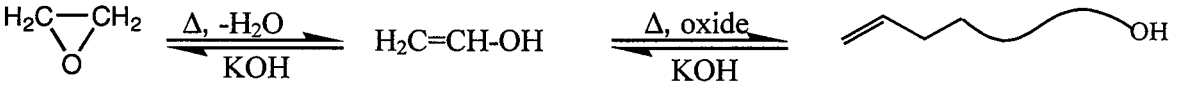

Oxide Allyl Alcohol Unsatured Monol

  This changes the polyol functionality and can generate "natural grafting" when these monols are present in a polyol used as a solvent for CPP preparation. The double bound of the monol can induce styrene and acrylonitrile copolymerization, which indeed becomes grafted SAN, but with a molecular weight of the graft lower than the stabilizer precursor.

- "DMC-polyol", which means that the preparation of the polyol is catalyzed by a neutral compound from the dimetal catalyst family. This catalyst leads to a polyol, which has very low unsaturation (< 0.001 meq/g)

An other side reaction than the formation of monols involves the formation of diols when oxide adds to water, which is usually present in small amounts in the incoming oxide feed. Even with care it contains up to twenty-five mole percent for some applications.

Water Ethylene Oxide (EO) Diol

6.3. Grafted copolymer polyol

Polyether polyols can be "filled" with other organic polymers to produce viscous, white to off-white, fluids that are useful in making foams of higher hardness than can be obtained using the unmodified polyols previously presented. Filled polyols also aid foam processing by improving cell-openness. The filler polymer is normally formed by *in situ* polymerization of monomers in a polyol base, through either free radical or step addition processes. The first use of non aqueous dispersion polymerization techniques to prepare polymer dispersions in the polyether polyols was reported in 1966 by Union Carbide researchers (Kuryla, 1966) and referred to a Belgium patent deposed by the Union Carbide Corp. in 1963 (Stamberger, 1963).

The successful preparation of stable, colloidal dispersions requires that the particle have some steric stabilization to prevent flocculation of the suspension. This stabilization is typically provided by a "grafting" process in which either the base polyol or a special added stabilizer molecule copolymerizes with the monomers to form a copolymer. They are typically synthesized via either free-radical or step-addition polymerization.

The polyether polyols, that are used in this work, are produced through chain-growth polymerization, where free radicals are generated from an initiator molecule. The first commercial copolymer polyols were based on the use of acrylonitrile as the sole monomer, and were first used for the production of cold-molded high-resiliency foams with increased hardness, strength, foam processing and cell-opening, which led them to commercial success. These dispersions contained 20% of poly(acrylonitrile) by weight and had viscosities of 3000-5000 mPa.s. The grafting of the polyol chains to the poly(acrylonitrile) was proven by separating the solid particles from the polyol serum-phase and demonstrating that the particles contained polyol, which could not be solvent-extracted. The grafting process was reported to have occurred by a transfer to poyol, that is to say by the abstraction of hydrogen from the polyol backbone to form radicals, which then initiated polymerization of the acrylonitrile. This so-called "natural" grafting to polyether polyols has been reported to occur when using reactive monomers such as acrylonitrile and vinyl acetate.

As copolymer polyol products continued to evolve and to be used in other areas such as slabstock foams, deficiencies in the 100 % acrylonitrile products were found. Among these were notable discoloration and lower flame resistance in slabstock foams. This led to the development of styrene-acrylonitrile mixtures as the preferred monomers for making copolymer polyols. The copolymer polyols require the use of a more efficient stabilizer molecule to form the grafted portion of the polymer. This is because the copolymerization of styrene and acrylonitrile is quite favorable, and the tendency for free radicals to be generated on the polyol molecule is reduced. The stabilizers used are called "macromers" or "macromolecular monomers". These are polyols that have been functionalized in some fashion with a vinyl moiety, which will readily undergo copolymerization with SAN monomers.

For high resiliency (HR) molded and slabstock foam applications, copolymer polyols which are 25-40% solids with viscosities of 2500-7000 mPa.s are commonly used. For conventional slabstock foam applications, 40-43% solids products with viscosities of 4000-6000 mPa.s are used. These latter products are used mainly for making prime carpet underlay.

In addition to the copolymer polyols made using free-radical polymerization processes, copolymer polyols can also be made using step-growth methods : PHD (polyharnstoff dispersion) polyols and PIPA (Poly Isocyanate Poly Addition) polyols are mainly known. PHD polyols are dispersions of polyurea particles in conventional polyols. They are prepared by the reaction of diamine with diisocyanate in the presence of a polyether polyol. Final molecular

weight of the polymer produced in this process is considerably lower than that found in SAN copolymer polyols. The viscosity of PHD polyols is higher than SAN CPP : around 20-28 % solids with viscosities of 3000-3500 mPa.s. PIPA polyols are similar to the PHD polyols, but contain instead, dispersed particles of polyurethane formed by the in situ reaction of an isocyanate and an alkanolamine.

6.4. Examples of Grafted Copolymer polyol produced by Dow Chemical and applications

Polyurethane foam is one of the most versatile materials available today, with use in a wide range of applications, primarily in the areas of insulation, packaging, and load-bearing such as cushioning. Therefore there is a broad range of automotive interior applications including seating, armrests, headrests, door panels, instrument panels, bolsters, etc.

As mentioned before, there are two types of polyurethane foams : conventional slab stock foams and molded foams. As presented by Kaushiva and Dounis. (2000), molded foams result from a relatively newer technology and are foams in which the formulation mix is either poured into a closed mould. It represents approximately one-fourth of all polyurethane foams produced industrially, as opposed to slab stock foams. The majority of molded foams are used in transportation seating and trim parts. They are also used in packaging, furniture and novelty items. The biggest advantage is that the foam is molded into the intricate shape desired and, hence, the need of cutting is eliminated. Also molded foams can be produced with inserts for reinforcement, multiple zones of hardness, or with a liner such as plastic or fabric skin, all of which reduce labor costs of final product assembly.

Molded foams do not differ from conventional slab stock foams in just that they are produced in moulds rather than in semi-continuous process, but in fact, are considerably more chemically complex. Usually, higher molecular weight, more reactive polyols are used for reasons of increased productivity (primary polyols preferred than secondary polyols). Along with a higher reactivity formulation, factors such assize of individual shot, release agents, mould temperature gradients, and curing times also contribute to the complication. Furthermore, the polyols are often modified with fillers to produce open-cell foams of higher hardness. Polymeric filler for foams can be copolymer polyols, which are grafted polyether polyol containing copolymerized styrene and acrylonitrile and filtered to 100 microns.

Below are presented some copolymer polyols produced industrially by the Dow Chemical Company.

Voralux® HL 430 Copolymer Polyol is commonly used in the full density range of high load-bearing flexible foams over the density range of 19 – 72 $kg.m^{-3}$. The typical properties of Voralux® HL 430 are :

Hydroxyl number : 29.3 – 32.8

Water, max. : 0.08 %

Viscosity at 25 °C : 5500 – 8000 mPa.s

Density at 25°C : 1.042 $kg.m^{-3}$

Solid content (typical): 43 %

Specflex® semi-flexible polyurethane foam systems are available for a broad range of applications requiring a plush, padded look and feel. These systems are currently used in instrument panels, consoles, headrests, armrests and door panels. New specialized formulations have been designed for air bag doors, foam for energy management, acoustical foam, and all-

water blown integral skin foam for steering wheels. Specflex® systems provide excellent flow, stain resistance, good adhesion properties, increased efficiency and productivity. For instance, Specflex® NC 700 is a high solids and high reactivity copolymer polyol used for high resilience moulded foam, whose typical properties are :

Hydroxyl number (typical) : 22

Water content : 0.07 %

Typical viscosity at 25 °C : 5500 mPa.s

Density at 25°C : 1.050 $kg.m^{-3}$

Solid content (typical) : 40 %

Approx. molecular weight : 5000 g/mol

Voranol® polyether polyols are provided with a wide range of properties needed to produce low to high density seating foams.

Conclusion

This literature overview shows that the dispersion polymerization process can be applied to various solvents (aliphatic, polar, mixtures, $scCO_2$), monomers (styrenics, acrylics, ...) and stabilizers (blocs, grafted, preformed or produced *in situ*).
Nevertheless, as a rather important diversity of systems have been studied, it is quite difficult to understand precisely the general mechanism of dispersion polymerization as each part of the mechanism (nucleation, steric stabilization, particle growth, monomer partitioning,...) depends on the specific system and the process conditions (temperature, pressure, agitation, reactor,...).
The works done for styrene or methyl methacrylate in polar medium gives ideas of what could happen in the dispersion copolymerization of styrene and acrylonitrile in polyol medium using S5200 pre-stabilizer, but an important study of the process parameters applied to this system is required in order to describe this particular process. Most of all, the grafting mechanism for this system needs to be better known.

CHAPTER 2
EXPERIMENTAL TECHNIQUES

INTRODUCTION **95**

1. PRODUCTION OF CPP LATEX **95**

1.1. PREMIX FORMULATION 95
1.1.1. Monomers : Styrene, Acrylonitrile *95*
1.1.2. Solvent : Polyether Polyol *96*
1.1.3. Initiator : Trigonox T27 ..... *96*
1.1.4. Chain transfer agent : NDM *96*
1.1.5. Precursor stabilizer : S5200 ..... *97*
1.1.6. Seed or Preformed stabilizer : SAN solid highly grafted copolymer *99*

1.2. CONTINUOUS PRIMARY REACTOR AND ITS ENVIRONMENT 99
1.2.1. Equipment *99*
1.2.2. The procedures *101*

2. ANALYTICAL METHODS TO FOLLOW CPP PROPERTIES **103**

2.1. ISOLATION OF THE SOLIDS FROM CPP : WASHING / CENTRIFUGATION WITH HEXANE-ETHYL ACETATE MIXTURES 104

2.2. HEADSPACE GAS CHROMATOGRAPHY (HSGC) / FLAME IONIZATION DETECTOR (FID) 104

2.3. GEL PERMEATION CHROMATOGRAPHY (GPC) – UV DETECTOR 105
2.3.1. Principles of Gel Permeation Chromatography *105*
2.3.2. SAN Molecular Weight Distribution of CPP samples *107*
2.3.3. Serum SAN average molecular weight and quantification *107*

2.4. PARTICLE SIZE DISTRIBUTION 108
2.4.1. Low Angle Laser Light Scattering (LALLS) *109*
2.4.2. Scanning Electron Microscopy (SEM) *111*

2.5. RHEOMETRY 112
2.5.1. Cone & cup sensors *113*
2.5.2. Cone & plate sensors *113*

2.6. NUCLEAR MAGNETIC RESONANCE (NMR) : ^{1}H AND ^{13}C 114
2.6.1. Proton (^{1}H)-NMR *114*
2.6.2. Carbon (^{13}C)-NMR *116*

2.7. MINIPULSED NUCLEAR MAGNETIC RESONANCE 116

2.8. NIC DERIVATIZATION FOLLOWED BY GPC – FLUORESCENCE 117

2.9. LIQUID CHROMATOGRAPHY ON SILICA GEL / UV DETECTOR..... 118

CONCLUSION..... 120

Introduction

The industrial continuous process of copolymer polyols production uses two successive reactors: a stirred tank reactor, where happens around 85 to 95 % of the monomer conversion (depending upon the acrylonitrile to styrene ratio), followed by a plug flow reactor, which goes on the conversion until 95 to 98 %. The objective of this work is to study the primary reactor and the influence of the process conditions on the physical properties of the CPP produced, in order to better understand the chemistry inside this reactor and to further provide a model and tools for numerical simulation of the process.

This chapter presents the different experimental techniques that was used to study the copolymerization of styrene and acrylonitrile in polyol medium at a laboratory scale. The first part deals with the reactants and the devices used to produce CPP while the second part presents the analytical techniques used to study the properties of CPP.

1. Production of CPP latex

1.1. Premix Formulation

The initial mixture of compounds, which is introduced continuously inside the stirred tank reactor, is called the "premix". For standard copolymer polyols, this premix is composed of :

- 40 wt-% of monomers with a wt-% ratio Sty/AN = 70/30,
- 1.5 wt-% of precursor stabilizer S5200,
- 0.2 wt-% of peroxide (initiator),
- 0.3 wt-% of chain transfer agent,
- 2 wt-% of seed,
- and the rest is the solvent : polyether polyol.

The characteristics and the properties of these compounds are exposed below.

1.1.1. Monomers : Styrene, Acrylonitrile

Styrene was provided by Aldrich and contained 10 to 15 ppm of 4-*tert*-butylcatechol (TBC) inhibitor. Acrylonitrile was also provided by Aldrich and contained 35 to 45 ppm of monomethyl ether hydroquinone inhibitor.

Table 2.1. Properties of Styrene and Acrylonitrile

Monomer properties	Styrene	Acrylonitrile
Molecular weight, $g.mol^{-1}$	$M_B = 104$	$M_A = 53$
Density, $kg.m^{-3}$	$\rho_B = 909$	$\rho_A = 806$
Glass transition temperature, K	$T_{gB} = 185$	$T_{gA} = 190.4$

The data concerning the glass transition temperature of styrene and acrylonitrile were given by Garcia-Rubio et al. (1985).

1.1.2. Solvent : Polyether Polyol

The solvent used was the polyether polyol IP3040 provided by Dow Benelux. It was a hetero fed PO/EO polyether, with 11% ethylene oxide (EO) and 89 % propylene oxyde (PO), that means that the both oxide were added together in the reactor and not one after the other. This polyether polyol was also produced by KOH catalysis, which means that it contained around 0.03 meq/g of monols (see paragraph 6 of chapter 1). The quantity of primary OH was less than 5 %. Its main use in industry is flexible slab stock foam for mattresses and furniture. Its molecular weight is around $M_S = 3040$ g/mol and its density is $\rho_s = 1020$ kg.m^{-3}.

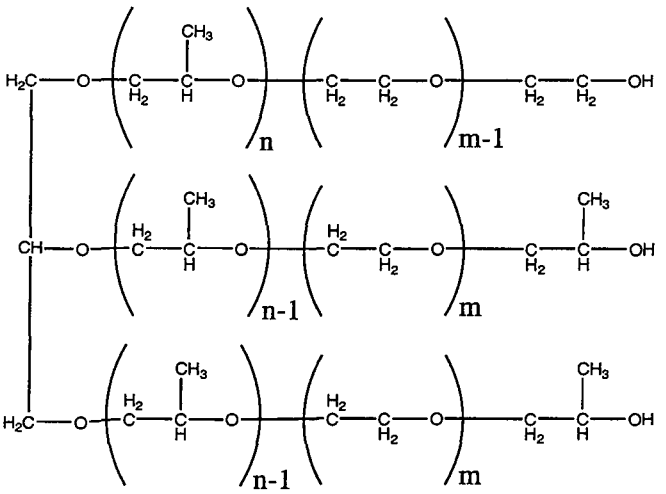

Figure 2.1. Polyether polyol

1.1.3. Initiator : Trigonox T27

The initiator used was a liquid peroxide : tert-Butyl peroxy-2-diethylacetate, called Trigonox 27 (T27), provided by Akzo Nobel Chemicals. Its molecular weight is $M_I = 188.3$ g/mol. The tertio-butyl radical is known to be very active decomposing into a methyl radical, which is also a strong hydrogen abstractor.

The kinetic constant of decomposition of T27, k_d, studied by Dow gives :

$$k_d = A\exp(-E/RT) \qquad (2.1)$$

with A= 2.45 10^{15} s^{-1}, E= -134 kJ mol^{-1} and R = 8.314 J mol^{-1} K^{-1}

This means that the half-life of T27 is 180 s at 120°C, 65 s at 130 °C and 25s at 140 °C.

1.1.4. Chain transfer agent : NDM

The chain transfer agent used was 1-Dodecanethiol (also called Normal-Dodecamethyl Mercaptan (NDM)). It was provided by Riedel-de-Haën.

It reacts with oligoradicals, R*, as follows :

$$CH_3\text{-}(CH_2)_{10}\text{-}CH_2\text{-}SH + R^* \rightleftharpoons CH_3\text{-}(CH_2)_{10}\text{-}CH_2\text{-}S^* + RH$$

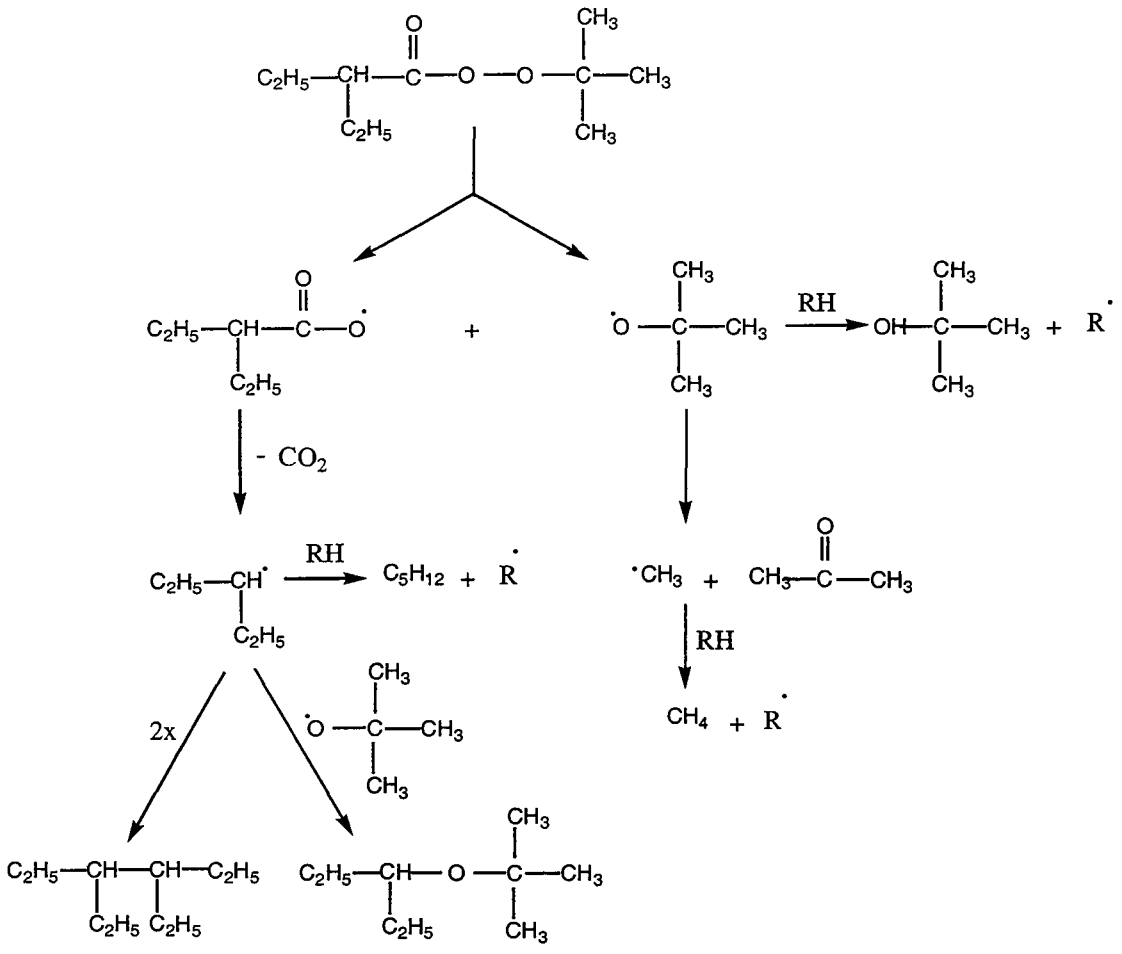

Figure 2.2 : Thermal dissociation of Trigonox 27 initiator

1.1.5. Precursor stabilizer : S5200

A small amount of vinyltrimethoxysilane (VTMS) is transetherified with a polyether triol (CP3320) resulting in the stabilizer precursor S5200 :

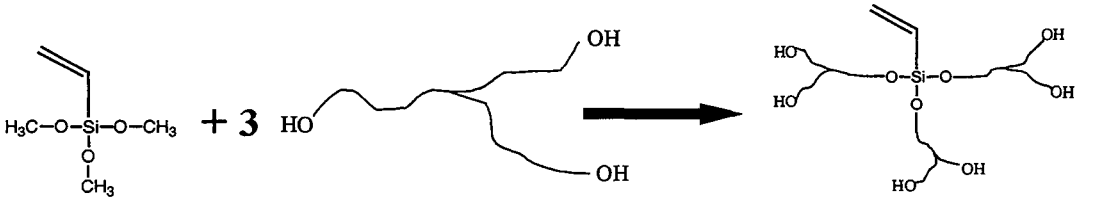

VTMS CP3320 (M=3300 g/mol) S5200 (M ≈ 10000 g/mol)

This is the main molecule that is produced during this reaction but some other species can be produced. As shown by gel permeation chromatography (figure 2.3), a sample of S5200 contains also the polyether triol (11.6 ; 13.5 mL). Moreover the peak of S5200 itself (10 ; 11.6 mL) is

composed of a main peak corresponding to the molecule described above, and of another peak corresponding to species of lower molecular weights (figure 2.4.a & b).

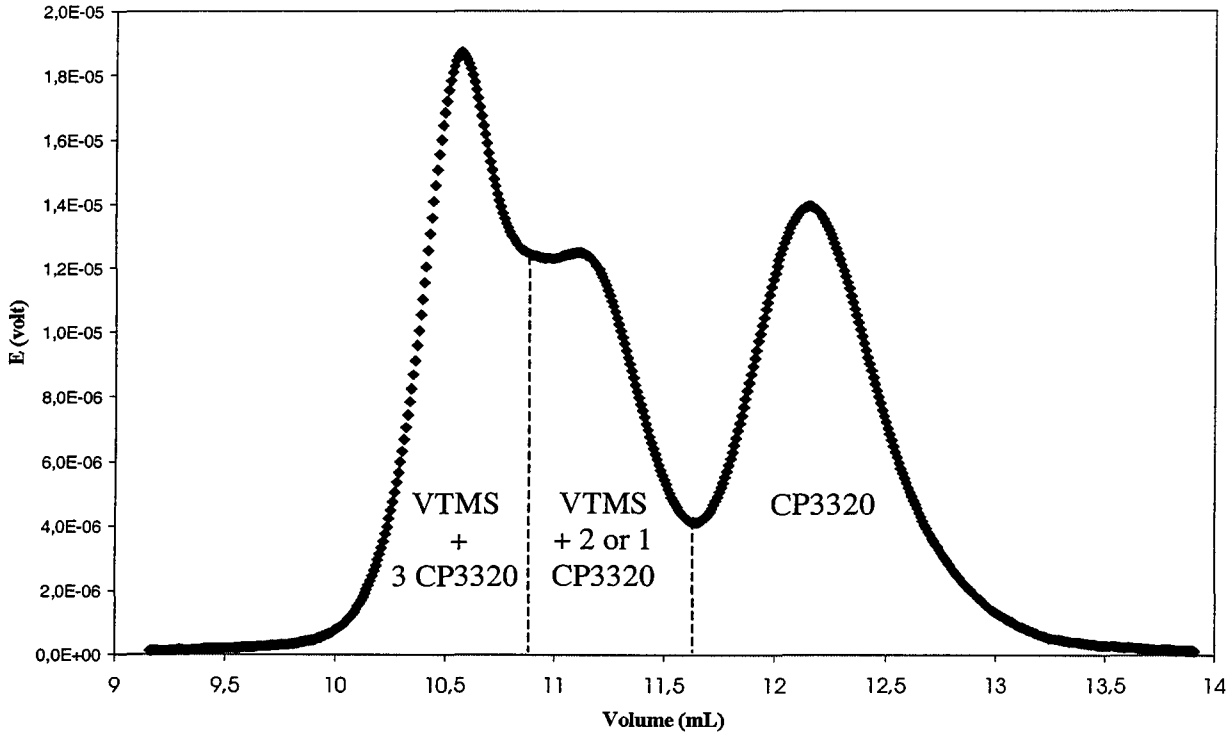

Figure 2.3 : GPC chromatogram of a sample of S5200

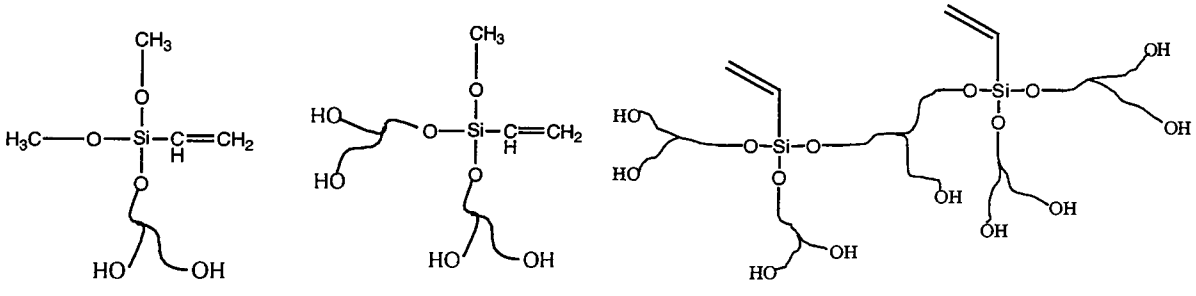

a) VTMS + 1 CP3320 b) VTMS + 2 CP3320 c) 2 VTMS + 5 CP3320

Figure 2.4 : Species that may also be present in S5200 samples

Species of higher molecular weights than S5200 may also be present if VTMS react with S5200 itself providing for instance the molecule drawn in figure 2.4.c. This indicates that the precursor stabilizer S5200 is therefore not a perfectly well defined molecule.

1.1.6. Seed or Preformed stabilizer : SAN solid highly grafted copolymer

In addition to the precursor stabilizer, a preformed stabilizer was also used. It was provided by Dow Benelux N.V. and produced by reaction between a small amount of styrene and acrylonitrile with a larger amount of stabilizer precursor. This preformed stabilizer contains both soluble and insoluble SAN polymeric material, which is called "seed".

Seed was produced using 8 wt-% of monomers with a wt-% ratio Sty / AN = 70/30, 35 wt-% of S5200, a molding polyol V4735, and a peroxide as initiator.

The same quantity of seed was used in all experiments : 2 wt-%.

1.2. Continuous primary reactor and its environment

The experiments were realized on a primary reactor at laboratory scale. The equipment was provided by Dow Benelux B.V. : the mechanical construction was realized by De Feyter Terneuzen B.V. and the process control and the software were realized by Camile Products.

1.2.1. Equipment

1.2.1.1.Experimental device

As shown in figure 2.5, the premix was introduced continuously in the reactor from a glass feed bowl, owing to a gear pump.

The reactor was constructed of thick-walled steel for carrying out chemical reactions under pressure and high temperatures. Its volume was 0.5 L. The agitation device was set in order to be exactly the same as the systems used by Dow : two impellers R200 and four baffles as shown in figure 2.6. The lower impeller was positioned in order to be above the inlet of the premix in the reactor.

A back pressure valve MITY MITE from Grove LTD was used at the reactor output in order to control the pressure inside the reactor. Indeed, it was necessary to maintain a pressure between 3 to 4 bars in the system in order that the styrene and the acrylonitrile never turn to gas at the temperatures of the experiments. The pressure was controlled by the pressure of air that blocks the valve : if the pressure in the system was greater than the air pressure, then, the latex could push the valve and go out.

1.2.1.2.Sensors

a) Temperature

A double PT100 temperature probe was inserted inside the reactor : platinum resistance thermometers offer excellent accuracy over a wide temperature range (from -75 to 250 °C). The principle of operation was to measure the resistance of a platinum element knowing that the most common type, PT100, has a resistance of 100 ohms at 0 °C and 138.4 ohms at 100 °C. One probe was connected to a digital display an the other to the computer and the Camile software.

b) Pressure

The pressure was given by a manometer connected on a pipe after the reactor, and by a pressure transmitter, which measured the pressure directly in the reactor and which was connected to the computer and the Camile software.

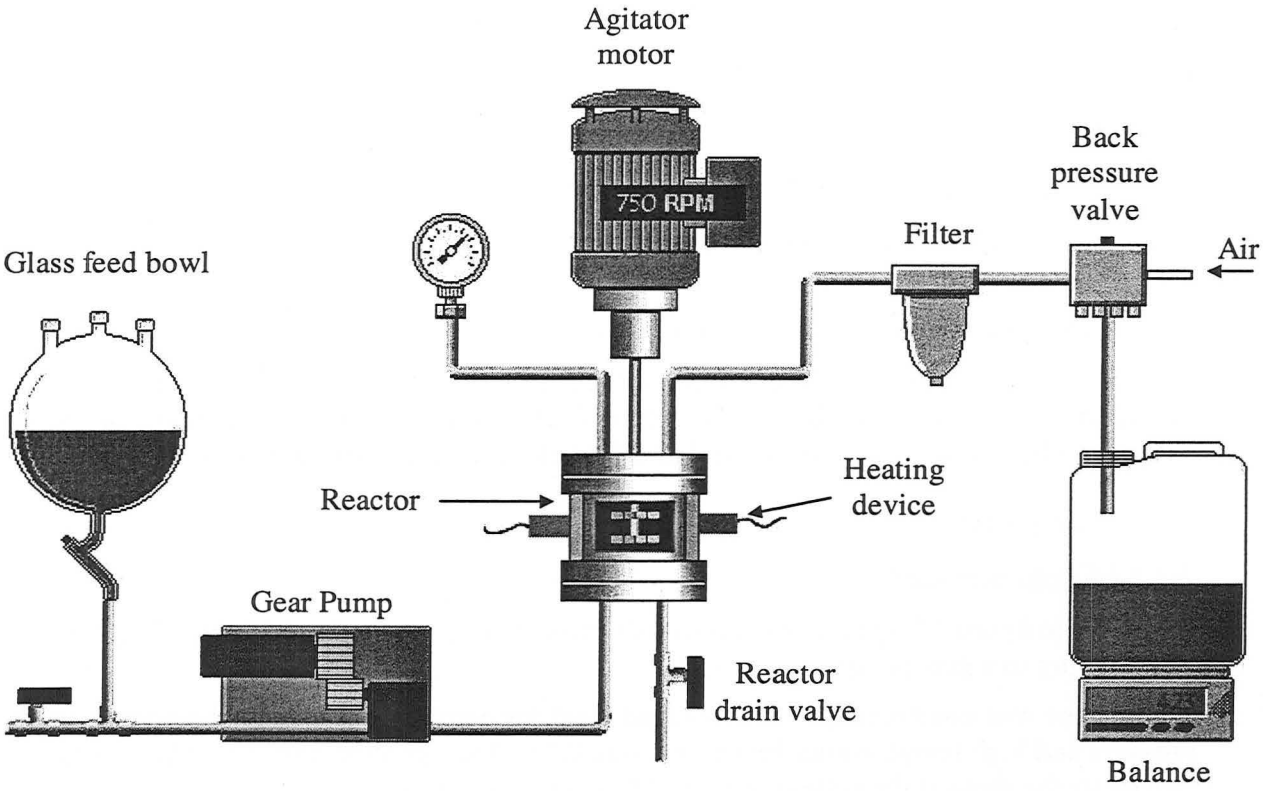

Figure 2.5. Scheme of the laboratory rig

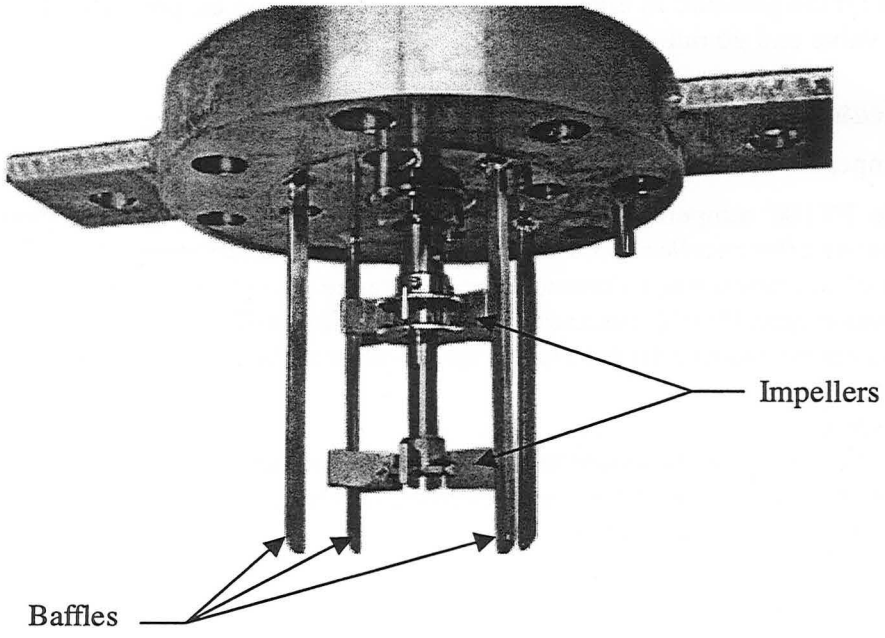

Figure 2.6. Agitation device of the reactor

c) Mass flow

The weight of material, which went out of the reactor outlet was measured by a Mettler Toledo SB8000 precision balance as a function of the time. This balance was linked to the computer owing to a RS 323 cable and the Camile software calculated the mass flow at each time.

d) Agitation speed

The agitation speed was controlled manually with the agitator power supply. An optical sensor communicated the number of rotations per minute of the agitator to the computer and the Camile software.

1.2.1.3.Process control

The Camile software controlled the pump and the heating device automatically in order to reach and maintain a given set-point of temperature in the reactor and of mass flow at the reactor outlet. A proportional-integral control was done on the gear pump and on the heater. With proportional band, the controller output was proportional to the error or a change in measurement, but an offset (deviation from set-point) may be present. Integral action was therefore included in controllers to eliminate this offset : the controller output was proportional to the amount of time there is a difference between the measurement and the set-point.

The gear pump speed was controlled by the following tuning constants :

Proportional action : Kc = 0.2
Integration action : T_I = 0.01

The answer of the mass flow was rather quick and its control was quite easy for the software.

The electrical heating device was controlled by the following tuning constants :

Proportional action : Kc = 0.53
Integration action : T_I = 0.001

The tuning factors of the temperature control were obtained using a software which measured them automatically by varying the action of the heater and by measuring the answer of the system. This measurement was made on polyol.
Nevertheless, the temperature was rather difficult to control automatically as it had long answer times. Therefore, it was necessary to adjust the temperature almost manually, or, in other words to forecast the exothermicity of styrene/acrylonitrile copolymerization, setting an initial set point of temperature 15 °C below the final desired set point and finally fixing the good set-point when the temperature reached its maximum.

In steady state, if there were not instabilities in the reactor (production of unstable particles, which collapse together and block the filter and the pipes), the mass flow and the temperature were well controlled.

1.2.2. The procedures

a) Premix :

6 kg + 3 kg of premix were prepared in two times in a 6 L jerrican. The liquid initiator (Trigonox 27), the stabilizer (S5200), the seed and the chain transfer agent (NDM) were added firstly in the jerrican. Then the styrene and the acrylonitrile were added and the jerrican was well shaken. Finally the polyol was added and the jerrican was again well shaken.

b) Starting up :

Before starting a run, the agitation was put on, the reactor was filled with polyol and the heater was put on until reaching a temperature 15°C below the final desired temperature. The air inlet was open in order to set a pressure of 3-4 bars in the system. Then the polyol was drained from the feed bowl, which was next filled with the premix.

When the system was ready to start a run the "Start Feed" button activated the following procedure :

Step 1 : Wait until the reactor temperature has reached a set temperature
Step 2 : Start pump at initial output of 6.8 % for minimum of 3 min. The reactor pressure must be minimum 1.8 bar to start ramping.
Step 3 : Ramp flow to 10 g/min over 2 min.
Step 4 : Ramp flow to final set point of 25 g/min over 30 min
Step 5 : Stay at 25 g/min

The starting procedure was very important for the stability of the CPP. Nevertheless, for particular premix recipes, this ramping procedure was not enough to stabilize the CPP that was produced. Therefore, for recipes that were forecasted to be unstable (Sty/AN =80/20, low temperature, low stabilizer...), the runs were started with 3 kg of a stable premix until reaching the steady state regime. Then, the 6 kg of the premix recipe, which was desired to be tested, were added in the feed bowl as soon as this one was emptied of the first premix.

c) Sampling :

Two samples of 100 g were taken after 5h of run with steady mass flow (about 15 residence times) and then 470 g of material were taken for the filtration test. The samples were directly put in a refrigerator to stop any reaction.

d) Cleaning :

After the run, the reactor was drained owing to the drain valve and N_2 pressure and washed by filling it with polyol until 500 g of material has come out of the outlet. The reactor was again emptied using the drain valve under N_2 pressure. The filter was cleaned every two runs.

A complete washing of the reactor was done every two runs by further filling it with KOH (50%) and NMP, and letting the reactor running during 30 min at 115 °C - 140 °C. The reactor was then drained and filled with water and drained 3 times, before letting it drying by flushing the rig with N_2 at high temperature. Finally, the complete rig was filled with polyol to be ready to start a new run.

e) Filtration test :

The sample (470 g) of CPP was mixed with isopropanol (940 g). This mixture was poured into a glass bowl of filtration with a metal mesh screen fixed at the outlet. The timer was started when the liquid starts to come out of the equipment. The time of passing through was noted and, if it blocks, the quantity which had passed. This gives indications concerning the stability of the CPP. A perfectly stable CPP passes through in less than 300 s.

2. Analytical methods to follow CPP properties

Figure 2.7. shows the different analytical methods that were used to study the properties of the samples of CPP produced in the laboratory rig. Most of these analyses were realized by the laboratories of Dow Chemical, Terneuzen. For safety reasons, the residual monomers (styrene and acrylonitrile) had to be removed before the analyses : the CPP samples were stripped in film evaporator at 130°C under vacuum for at least half an hour (a small nitrogen purge was also applied).

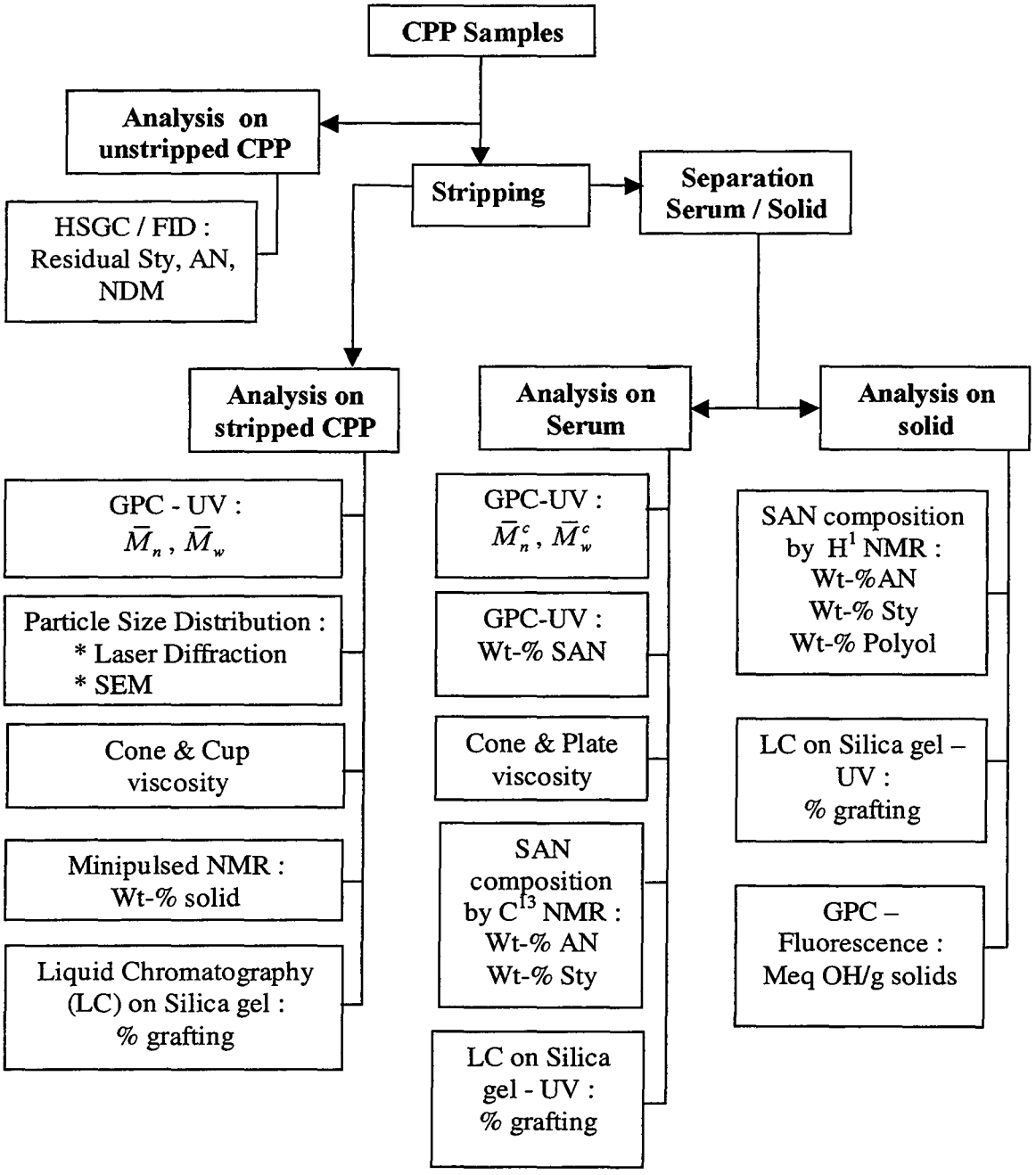

Figure 2.7 : Schema of all the analytical methods used

2.1. Isolation of the solids from CPP : washing / centrifugation with hexane-ethyl acetate mixtures

In order to separate the solids from the serum, the polyol and other low molecular weight serum-soluble components (SAN oligomers, residual S5200, highly grafted low molecular weight SAN, additives, etc) must be washed out of the solids. Different Hexane/ ethyl acetate (C6/EtOAc) mixtures were tested on a variety of commercial and experimental CPP samples at Dow, Terneuzen. Although this washing sounds easy, it is very difficult and labor intensive to obtain completely polyol-free solids and serum without small SAN particles.

The following general procedure was used to obtain polyol-free solids :

- Weight approximately 10 g of CPP in a polypropylene centrifugation tube (Falcon, 50 µL polypropylene conical tubes, 30*115 mm) and add 45 mL of an 80/20 (v/v) C6/EtOAc mixture,
- Shake the mixture manually until no longer any CPP is sticking to the bottom or wall of the tube,
- Shake overnight on a shaker,
- Centrifuge the samples at 3000 rpm during one and a half-hour,
- Collect the supernatant liquid with a disposable Pasteur pipette. Be very cautious not to disturb the top layer of the solids as this top layer can redisperse very easily (smallest particles) ; stop collecting the liquid when it is approximately standing 0.5 cm above the solids,
- Then pour again 50 mL of the 80/20 C6/EtOAc mixture on the solids and shake vigorously in order to redisperse the solids as well as possible. The solids are shaken again during one hour,
- Then repeat the centrifugation and collection of the serum phase one or more times until no polyol is longer washed out. After drying the solids in a fume hood, they are crushed in a mortar and put in a vacuum oven at 35°C and 50 mbar in order to remove absorbed solvents. If the polyol is completely washed out, the powder is generally very statically charged (polyol is a good antistatic agent). The solids are stored in a capped vial in order to prevent uptake and humidity,
- The final serum phase is obtained after removing solvent by distillation in a rotavapor.

The experience has learned that most CPP samples need three or four washes to remove all occluded non-bonded polyol.

2.2. Headspace Gas Chromatography (HSGC) / Flame Ionization Detector (FID)

Headspace gas chromatography makes use of the equilibrium between the volatile components of a liquid or solid sample and the surrounding gas phase in a sealed vessel, aliquots of the gas phase being injected into gas chromatography (GC) for analysis. The sample containing volatile components is placed in a sealed vial and conditioned until the volatile components partition into the vapor space above the sample reach equilibrium. As a result their concentration in the vapor phase is a function of the concentration in the original mixture. In this method, the sample is extracted by inert gas, carried through the GC column and its components undergo separation by interaction with the stationary phase inside the column. As the components exit the column,

they are mixed with hydrogen gas and enter an air-rich hydrogen flame where they are thermally ionized to produce an electrical signal proportional to their concentration.

It is better to use a gas as a solvent with its ideal solubility for every volatile component as well as the advantage that a gas is normally available in higher purity than any liquid solvent, which avoids problems with trace impurity interferences. In addition, a gas does not cause a peak with tailing in the chromatogram.

Here, the samples were shaken with methanol containing toluene as internal standard, subsequent the methanol was separated from the polymer by filtration over a 0.4 μm filter and analyzed by GC. The estimated relative precision (95 % CL) of the method was estimated to be ± 10 %.

2.3. Gel Permeation Chromatography (GPC) – UV detector

Gel permeation chromatography was used to determine the molecular weight distribution of the SAN copolymer in the whole CPP and of the SAN dissolved in the continuous phase. It was also used to quantify the quantity of SAN present in the serum. GPC was coupled with an UV detector, which detects styrene unsaturations.

2.3.1. Principles of Gel Permeation Chromatography

Gel permeation chromatography, also called size-exclusion chromatography, uses porous particles to separate molecules of different sizes in order to determine molecular weights and molecular distributions of polymers. Molecules that are smaller than the pore size can enter the particles and therefore have a longer path and longer transit time than larger particles that cannot enter the particles. All molecules larger than the pore size are unretained and elute together, whereas, molecules that can enter the pores will have an average residence time in the particles that depends on the hydrodynamic volume of the molecule.

The elution volume is equal to : $V_E = V_I + K_D V_P$ (2.2)

Where V_P is the volume of the pores and V_I is the interstitial volume inside the column (between the particles). For big molecules which are eluted with the solvent, $V_E = V_I$ that is to say that $K_D=0$ and for the smallest molecules $V_E = V_T$, that is to say that $K_D=1$.

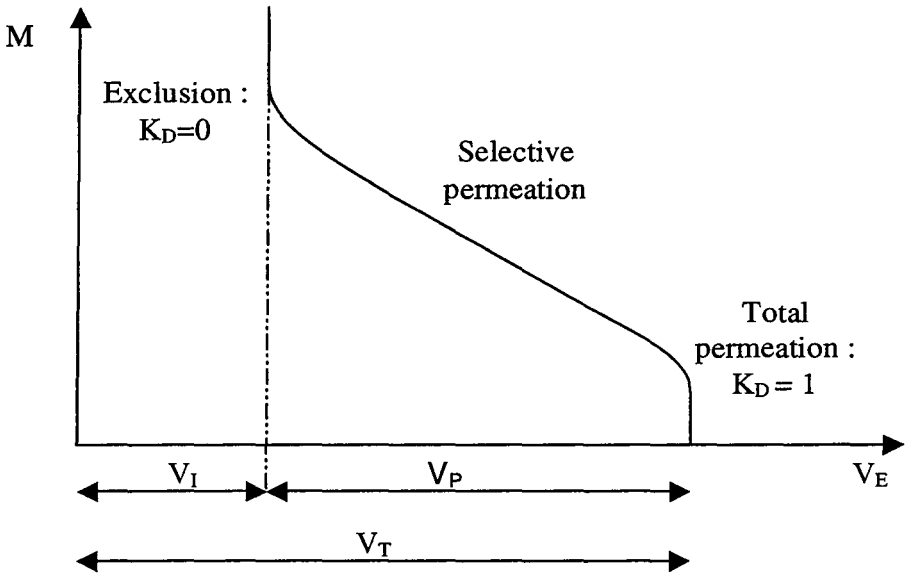

Figure 2.8. GPC calibration curve : molecular weight vs. elution volume

This calibration curve is obtained by injecting different samples of the same monodispersed standard polymer with well known molecular weights.

The GPC device that was used gave a signal proportional to $\frac{dW_F}{dLnM}$, defined in Eq. 2.4, as a function of the elution volume V (mL). Using known polystyrene standards, it was possible to translate elution volumes into polystyrene molecular weights, M (g/mol).

The number-average molecular weight, $\bar{M}_n$ and the weight-average molecular weight, $\bar{M}$, were calculated by integrating the distribution in number, φ(M), numerically by the method of the trapezes :

$$W_F = \int_0^M M\,\varphi(M)\,dM \ , \tag{2.3}$$

$$\text{then, } \frac{dW_F}{dLnM} = \frac{dW_F}{dM} M = M^2 \varphi(M). \tag{2.4}$$

However, the step between two different molecular weights, is equal in logarithm :

$$(\Delta LnM)_i = \frac{\Delta M_i}{M_i} = \Delta, \text{ is a constant.} \tag{2.5}$$

Therefore :

$$\bar{M}_n = \frac{\sum_i M_i\,\varphi_i\,\Delta M_i}{\sum_i \varphi_i\,\Delta M_i} = \frac{\sum_i M_i^2\,\varphi_i}{\sum_i M_i \varphi_i} = \frac{\sum_i \left(\frac{dW_F}{dLnM}\right)_i}{\sum_i \frac{1}{M_i}\left(\frac{dW_F}{dLnM}\right)_i}, \tag{2.6}$$

$$\bar{M}_w = \frac{\sum_i M_i^2\,\varphi_i\,\Delta M_i}{\sum_i M_i \varphi_i\,\Delta M_i} = \frac{\sum_i M_i^3\,\varphi_i}{\sum_i M_i^2 \varphi_i} = \frac{\sum_i M_i \left(\frac{dW_F}{dLnM}\right)_i}{\sum_i \left(\frac{dW_F}{dLnM}\right)_i}. \tag{2.7}$$

The molecular weight distribution in weight is $M\varphi(M)$ vs. M, but here the distribution that is given by the apparatus is $M^2\varphi(M)$ vs. M.

Various mathematical functions may be employed to describe theoretically the distribution of molecular weights : Gaussian, log-normal, Poisson or gamma (also called Flory-Schultz) functions. As experimental curves show a tail in the high molecular weights, a gamma function has been chosen to compare theoretical distributions to the experimental ones.

The gamma distribution is $\varphi(M) = \frac{M^n \exp(-M/\tau)}{\tau^{n+1}\,\Gamma(n+1)}$, (2.8)

$$\text{with } n = \frac{2\bar{M}_n - \bar{M}_w}{\bar{M}_w - \bar{M}_n}, \tag{2.9}$$

$$\text{and } \tau = \bar{M}_w - \bar{M}_n. \tag{2.10}$$

$\Gamma(x)$ is the gamma function (see Annex 4). It is assumed here that $\bar{M}_w/\bar{M}_n < 2$.

The curved that should be compared latter are therefore $\frac{dW_F}{dLnM}$ vs. M (experimental curve) and $M^2\varphi(M)$ vs. M (theoretical curve).

2.3.2. *SAN Molecular Weight Distribution of CPP samples*

The instrumental conditions were the following :

Column :	Three Mixed-B Plgel columns, 10-µm, 300 mm * 7.5 mm ID
Temperature :	35°C
Eluent :	THF/NMP (50/50 v/v)
Flow rate :	1 mL/min
Injection volume :	50 µL
Detector :	Shimadzu UV-Visible SPD-10 A with λ=258 nm ; sensitivity : 0.05 AUFS
Run time :	35 min

The estimated relative precision (95 % CL) of the method was estimated to be ± 5 %. Nevertheless, in order to determine the molecular weights of the SAN copolymers, the calibration again was made with an external polystyrene standard. This may induce an error on the measurement as the SAN copolymer produced contained 60, 70 or 80 wt-% of styrene.

2.3.3. *Serum SAN average molecular weight and quantification*

In order to quantify the amount of SAN that was dissolved in serum phase, the area of the peaks present in the GPC-UV chromatogram (> 3000 g/mol) was integrated.

The instrumental conditions were the following :

Column :	One Plgel 5-µm mixed-D column, 300 mm * 7.5 mm ID
Temperature :	30°C
Eluent :	THF/NMP (50/50 v/v) + 0,05% v/v triethyl amine
Flow rate :	1 mL / min
Injection volume :	25 µL
Detector :	Shimadzu UV-Visible SPD-10 A with λ=258 nm ; sensitivity : 0.2 AUFS
Run time :	20 min

In order to convert the peak area under the SAN distribution to a weight percentage of "soluble SAN" in the serum phase, a SAN copolymer standard (32 wt-% AN) was used as external calibration standard. A calibration line was then constructed by plotting the UV area counts of the SAN standard versus the amount of SAN (mg) of standard present in a 2,5 mL vial. The UV signal was cut at the retention time corresponding with 3000 g/mol in order to avoid that oligomers and antioxidant were being integrated as well. These however should give rise to too high values of SAN when integrated together with the high molecular weights.

Therefore, the amount of SAN in the serum phase was calculated using the following formula :

Wt-% serum SAN = 100((area counts-intercept)/ slope) / (mg of serum weighed in 2.5 mL vial) (2.11)

The UV signal of the serum SAN was caused by the styrene elements in the copolymer backbone. So if another Sty/ AN ratio was present in the sample instead of inside the SAN standard (32 wt-% AN), this procedure would give rise to biased data. Indeed, the samples analyzed contained 20 to 40 wt-% AN.

2.4. Particle Size Distribution

The basic problem of particle size analysis is that we generally want one value only to describe particles that are 3-dimensional objects. There is only one shape that can be described by one unique number and that is a sphere. If there is a technique that measures the weight of a particle, it is possible to convert this weight into the weight of a sphere remembering that

$$weight = \frac{4}{3}\pi r^3 \cdot \rho, \quad \text{with } \rho \text{ the particle density,} \tag{2.12}$$

and to calculate one unique number (d = 2r) for the diameter of the sphere of the same weight as the particle. This is the theory of equivalent sphere. A property of the particle is measured and it is assumed that this refers to a sphere, hence deriving one unique number (the diameter of this sphere) to describe the particle.

Each characterization technique will measure a different property of a particle (maximum length, minimum length, volume, surface area, weight, projected area, sedimentation rate,...) as it is shown on figure 2.9.

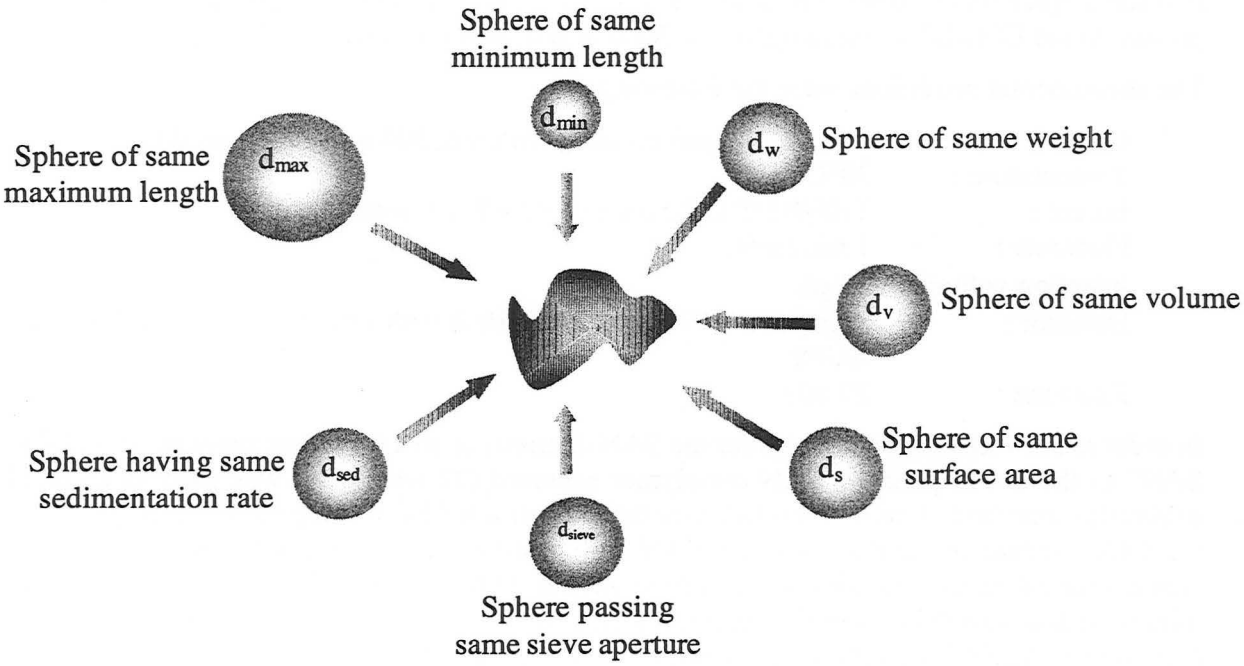

Figure 2.9 : Different possible descriptions for a particle

Depending on which bases it is necessary to compare these spheres, different expressions of average sizes are used :

$$Number-length\ mean=\frac{\sum d}{n}=D[1,0] \tag{2.13}$$

$$Number-surface\ mean=\sqrt{\frac{\sum d^2}{n}}=D[2,0] \tag{2.14}$$

$$Number-volume\ mean=\sqrt[3]{\frac{\sum d^3}{n}}=D[3,0] \tag{2.15}$$

The main problem with the simple means, D[1,0], D[2,0] and D[3,0], is that the number of particles, n, is inherent in the formulae, which requires to count large numbers of particles.

Hence, the concept of moment means needs to be introduced, as it is used to calculate average molecular weights. The two most important moment means are the following :

- the Surface Area Moment Mean (Sauter Mean Diameter) :

$$D[3,2]=\frac{\sum d^3}{\sum d^2} \tag{2.16}$$

- the Volume or Weight Moment Mean (De Brouckere Mean Diameter) :

$$D[4,3]=\frac{\sum d^4}{\sum d^3} \tag{2.17}$$

These formulae indicate around which central point of the frequency the (surface area or volume/weight) distribution would rotate, and they do not require knowledge of the number of particles involved.

As it will be explained latter, the model developed in this work provided D[3,2]. Therefore, it was necessary to calculate this term experimentally. Two methods were used to determine particle size distributions : laser diffraction and electron microscopy. Laser diffraction calculates a distribution based around volume terms and provides the D[4,3] in prominent manner. From this particle size distribution in volume it is also possible to calculate the other moment means. An electron microscope was used on some samples to check the particle size distribution given by laser diffraction and to observe the agglomeration phenomenon. This last method generates actually the D[2,0] as image analysis is processed and the area of each particle is measured and divided by the number of particles.

4 1 L ngle La er L ght atter ng (L LL)

This method has become the preferred standard in many industries for characterization and quality control. The applicable range according to ISO13320 is 0.1 – 3000 μm. Instrumentation has been developed in this field over the last twenty years or so. The method relies on the fact that diffraction angle is inversely proportional to particle size.

Instruments consist of :

- A laser as a source of coherent intense light of fixed wavelength. He-Ne gas lasers (λ = 0.63 μm) are the most common as they offer the best stability (especially with respect to temperature) and better signal to noise than the higher wavelength laser diodes.

- A suitable detector. Usually this is a slice of photosensitive silicon with a number of discrete detectors. It can be shown that there is an optimum number of detectors (16 - 32) – increased numbers do not mean increased resolution. For the photon correlation spectroscopy technique (PCS) used in the range 1 nm – 1 μm approximately, the intensity of light scattered is so low that a photomultiplier tube, together with a signal correlator is needed to make sense of the information.
- Some means of passing the sample through the laser beam. Particles in suspension can be measured by recirculating the sample in front of the laser beam.

For a specific material, the scattering pattern of a particle is unique for its size. Deconvolution of the sample scattering pattern with an optical model such as Mie or Fraunhofer results in the particle size distribution. Briefly, the Fraunhofer approximation assumes that :

- the particles are much larger than the wavelength of light employed (ISO13320 defines this as being greater than 10 μm when a He-Ne laser is used),
- all sizes of particles scatter with equal efficiencies,
- the particles are opaque and transmits no light.

These assumptions are never correct for many materials and for small material they can give rise to errors approaching 30% especially when the relative refractive index of the material and medium is close to unity. When the particle size approaches the wavelength of light the scattering becomes a complex function with maxima and minima. The full Mie theory completely solves the equations for interaction of light with matter. This allows completely accurate results over a large size range (0.02 – 2000 μm typically). The Mie theory assumes the volume of the particle as opposed to Fraunhofer, which is a projected area prediction. The "penalty" for this complete accuracy is that the refractive indices for the material and medium need to be known and the absorption part of the refractive index known or guessed.

As explained before, the laser light scattering provides the volume particle size distribution, g(L). The software shows [g(L) dL] vs. L, where $L_i = \sqrt{d_i \cdot d_{i+1}}$, with d_i the particle diameter associate to the detector i. The link with the number particle size distribution, n(L), is :

$$g(L)\,dL = L^3\, n(L)\,dL\;\phi_v / D[3,0]^2, \tag{2.18}$$

where ϕ_v is a shape factor ($\phi_v = 1$, if particles are perfect spheres).

Therefore, supposing spheres,

$$D[4,3] = \frac{\int_0^\infty L^4 n(L)\,dL}{\int_0^\infty L^3 n(L)\,dL} = \frac{\int_0^\infty L\, g(L)\,dL}{\int_0^\infty g(L)\,dL} = \frac{\sum_i L_i \left[g(L)\,\Delta L\right]_i}{\sum_i \left[g(L)\,\Delta L\right]_i}, \tag{2.19}$$

$$\text{and } D[3,2] = \frac{\int_0^\infty L^3 n(L)\,dL}{\int_0^\infty L^2 n(L)\,dL} = \frac{\int_0^\infty g(L)\,dL}{\int_0^\infty g(L)\,dL/L} = \frac{\sum_i \left[g(L)\,\Delta L\right]_i}{\sum_i \left[g(L)\,\Delta L\right]_i / L_i}. \tag{2.20}$$

The samples were prepared in methanol with 0.8 wt-% of CPP.

At LSGC, Nancy, the Malvern MS100 was used with a 300 mm Fourier lens (from 0.5 to 900 µm) and Fraunhofer theory as the refractive indices of CPP could not be measured.

At Dow, Terneuzen, the Coulter LS230 was used with the patented polarization intensity differential scattering (PIDS) technology and the small volume module, which allows to study

non aqueous lattices in the range 0.04 μm – 2000 μm. PIDS uses three wavelengths of light, filtered for polarization in the vertical and the horizontal planes. Six detectors (in addition to the 126 detectors used here for measuring scattered light) are positioned at around 90 degrees to the direction of the light path to measure the differential intensity between scattered light of vertical and horizontal polarizations. A total of 42 measurements are made at six scattering angles and three wavelengths, each at two polarizations. The combination of multiple wavelengths and two polarizations provides information that differentiates between sub-micron particle sizes and dramatically increases resolution.

2.4.2. Scanning Electron Microscopy (SEM)

The Scanning Electron Microscope (SEM) is a microscope that uses electrons rather than light to form an image. There are many advantages to use the SEM instead of a light microscope. It has a large depth of field, which allows a large amount of the sample to be in focus at one time, and it also produces images of high resolution, which means that closely spaced features can be examined at a high magnification.

As shown on Fig. 2.10 below, a beam of electrons is produced at the top of the microscope by heating of a metallic filament. The electron beam follows a vertical path through the column of the microscope. It makes its way through electromagnetic lenses, which focus and direct the beam down towards the sample. Once it hits the sample, other electrons (backscattered or secondary) are ejected from the sample. Indeed, when the electron beam strikes the sample some of the electrons will interact with the nucleus of the atom. The negatively-charged electron will be attracted to the positive nucleus but if the angle is just right instead of being captured by the gravitational pull of the nucleus it will circle the nucleus and come back out of the sample slowing done. These electrons are called backscattered electrons because they come back out of the sample. Moreover, sometimes beam electrons interact with the electrons present in the atom rather than the nucleus, repelling the electrons present in the sample. The repulsion is so great that the specimen electrons are pushed out of the atom and exit the surface of the sample : they are called secondary electrons. Then, detectors collect the secondary or backscattered electrons, and convert them to a signal that is sent to a viewing screen similar to the one in an ordinary television, producing an image.

Since the SEM uses electrons to produce an image, most conventional SEM's require that the samples be electrically conductive. All metals are conductive and require no preparation to be viewed using SEM. In order to view non-conductive samples such as ceramics or plastics, the sample must be covered with a thin layer of a conductive material.

At Dow, Terneuzen, the samples were diluted 100-fold in 2-propanol and filtered trough a 0.2 μm size filter pack. The pack was cut open and a pie-shaped section was cut out of the filter membrane. The specimen was mounted on an aluminum stub via double-sided conductive carbon tape and coated with a 2 nm Pd/Pt layer to make it conductive. Electron photomicrographs at magnifications of 1000 and 5000 were taken via Philips FEG-SEM XL 30 operating at an accelerating voltage of 5 kV. It uses a fine electron source of a Lathanum hexaboride single crystal system, which enables the attainment of much higher brightness source with a higher resolution images than a conventional tungsten filament SEM.

Images were imported in the software QWIN with a resolution of 0.0265 μm/pixel in auto contrast mode in which the white level was adjusted first to give full-scale output on the whitest part of the image then black level was adjusted to give zero output on the darkest part of the image. Unwanted artifacts in the background were removed by convolution. A specific routine

was used to detect the particles. The equivalent diameter of and the area occupied by the detected copolymer particles, with an area larger than 9 pixels and a diameter smaller than 4 μm, were used to construct a histogram from 0 to 4 μm in 20 intervals. The obtained histograms were used in an Excel program to calculate D[1,0], D[2,1], D[3,2] and D[4,3].

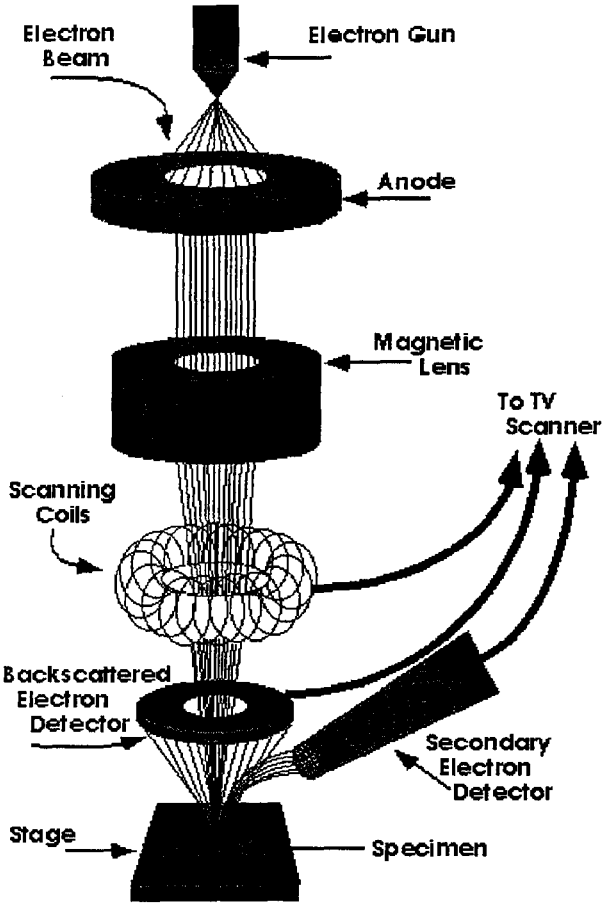

Figure 2.10 : General principle of Scanning Electron Microscope

2.5. Rheometry

The viscosity of two different products was investigated : the stripped CPP latex with a cone and cup device and the serum with a cone and plate device.

Rotational viscometers generally consist of two basic parts separated by the fluid being tested. The principle of the measurements is the following : the shear stress, τ (Pa), on the sensor is measured while the apparatus controls the shear rate, $\dot{\gamma}$, which varies linearly from 1 to 100 s^{-1} at 25°C. If τ vs. $\dot{\gamma}$ is linear, it can be assumed that the fluid is Newtonian, and the slope gives the viscosity, η (Pa.s) :

$$\tau = \eta \cdot \dot{\gamma} \qquad (2.21)$$

The two different devices used are described below.

2.5.1. Cone & cup sensors

The cone and cup device is a coaxial-cylinder system : the inner cylinder is here a cone and the external one is called a cup. Figure 2.11 shows a typical cone & cup system that has a fluid confined within a narrow gap ($R_i/R_o \geq 0.99$).

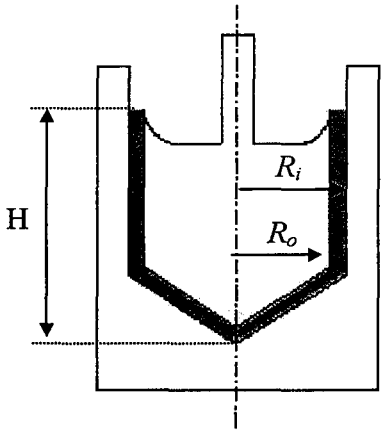

Figure 2.11 : Cone & Cup sensor

The shear rate is determined by geometrical dimensions and the shear stress is calculated from the torque and the geometrical dimensions :

$$\dot{\gamma}(R_i) \cong \dot{\gamma}(R_o) = \frac{\Omega \overline{R}}{R_o - R_i}, \tag{2.22}$$

$$\tau(R_i) = \frac{M_i}{2\pi R_i^2 H} \text{ or } \tau(R_o) = \frac{M_o}{2\pi R_o^2 H}, \tag{2.23}$$

where R_i and R_o are the radii of inner and outer cylinder, respectively,
$\overline{R} = (R_o + R_i)/2$,
M_i and M_o are the torques exerting on inner and outer cylinders, respectively
H is the height of inner cone,
Ω is the angular velocity (rad.s^{-1}).

The common feature of a cone-and-plate viscometer is that the fluid is sheared between a flat plate and a cone with a low angle as seen on figure 2.12.

The cone-and-plate system produces a flow in which the shear rate is very nearly uniform. Let's consider a fluid, which is contained in the gap between a plate and a cone with a very small gap angle, • (≤ 4°). The shear rate of the fluid depends on the gap angle and the linear speed of the plate. Assuming that the cone is stationary and the plate rotates with a constant angular velocity of Ω, the shear rate and the shear stress can be calculated from experimentally measured torque, M, and given geometric dimensions as follows :

$$\dot{\gamma} = \Omega/\beta, \tag{2.24}$$

$$\tau = \frac{3M}{2\pi R^3}, \qquad (2.25)$$

where R is the radius of the cone and Ω is the angular velocity (rad.s^{-1}).

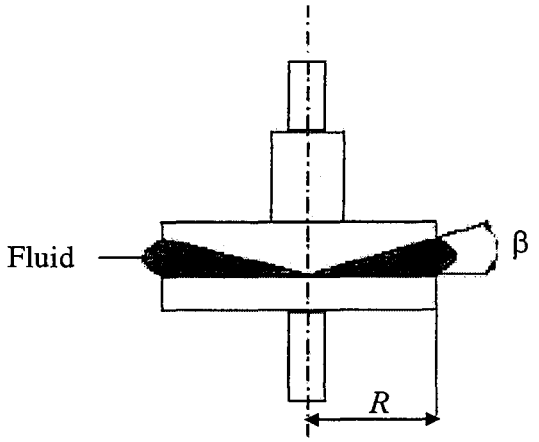

Figure 2.12 : Cone & Plate sensor

2.6. Nuclear Magnetic Resonance (NMR) : ^{1}H and ^{13}C

Proton (^{1}H)-NMR and carbon (^{13}C)-NMR allowed to reach the global composition in styrene and acrylonitrile of the SAN copolymer. It allowed also to determine the overall polyol bonded to the total SAN solid, assuming that all polyol was washed out of the solids and that all measured polyol was covalently bonded.

2.6.1. Proton (^{1}H)-NMR

The ^{1}H-NMR spectrum of the isolated solids can be used for a quick comparison of the types of polyols used in the grafting compounds.

Sample handling : Approximately 0.1 g of CPP solids were weighed in a 2-mL vial and 1 mL of CD_2Cl_2 was added. Using a roller mixer the vials were rotated until a clear solution formed. The solution was then transferred into a 5-mm NMR tube.

Apparatus : Bruker Advance 400 equipped with a 5-mm dedicated ^{1}H probe. Frequency was 400.13 MHz for ^{1}H-NMR. ^{1}H flip angle used was 30° (30° pulse is 5 µs) and repetition delay (time between two consecutive pulses) was 4.9 s. Total number of scans was 2048. Temperature was controlled at 303 K. TD was 64000 points. The spectra were used for quantification after a Fourier transform with exponential multiplication smoothing equivalent to a line broadening of 0.3 Hz.
An example of ^{1}H-NMR chromatogram is shown in figure A3.51 in annex 3. Based upon reference spectra, all peaks could be assigned. By means of the areas of relevant regions in the spectra, the composition was calculated. Despite the efforts to remove residual solvents used in the solids separation procedure, the ^{1}H-NMR spectra showed that all of the solid phase samples contained residual ethylacetate and n-hexane, the total amount ranging from 1 to 7.7 wt-% (for the sum of both compounds).

The area PfTtl is the total area developed by non-aromatic and non-solvent protons of the sample. AromTtl is the total area developed by the 5 protons of the aromatic group of styrene. HexMethl is the area developed by the 6 protons of the two methyl groups of n-Hexane. POMethl is the area developed by the 3 protons of the methyl group of PO in polyol. EAMethl is the area developed by the 3 protons of the methyl group of ethyl acetate. EACH2 is the area developed by the 2 protons of the methylene group of ethyl acetate. EO_PO is the area developed by all the protons due to –CH2O- or –CHO- in EO and PO in polyol. EAMethx is the area developed by the protons of the methoxy group of ethyl acetate.

Table 2.2 : ^{1}H-NMR spectrum analysis

Region (ppm)	Name
0.19 – 4.61	PfTtl
5.84 – 8.92	AromTtl
0.85 –0.95	HexMethl
1.06 – 1.18	POMethl
1.25 – 1.36	EAMethl
2.00 – 2.03	EACH2O
3.21 – 3.96	EO_PO
4.00 – 4.20	EAMethx

Therefore, the composition in terms of the number of moles (or units) present in the sample was calculated in the following way :

Styrene = AromTtl/5 (2.26)

Ethylacetate (EA) = EAMethx/3 (2.27)

Hexane = HexMethl/6 (2.28)

Polyol PO = POMethl/3 (2.29)

Polyol EO = (EO_PO – POMethl)/4 (2.30)

AN = (PfTtl – 3 Styrene – 8 EA – 14 Hexane – 6 PolyolPO – 4 PolyolEO) / 3 (2.31)

Finally, based upon the above compositions and the molecular weight of the various units, the wt-% of styrene, acrylonitrile and poyol in solid SAN are :

wt-% Styrene in SAN = Styrene*M_{Sty} / (Styrene *M_{Sty} +AN*M_{AN}), (2.32)

wt-% AN in SAN = AN / (Styrene *M_{Sty} +AN*M_{AN}), (2.33)

wt-% Polyol = (PolyolPO + PolyolEO) / (Styrene*M_{Sty} +AN*M_{AN} + PolyolPO*M_{PO} + PolyolEO*M_{EO}), (2.34)

with M_{Sty} =104 g/mol, M_{AN} = 53 g/mol, M_{PO} = 58 g/mol and M_{EO} = 44 g/L.

The relative precision (95% CL) is estimated to be 30 %.

2.6.2. Carbon (^{13}C)-NMR

The ^{13}C-NMR spectrum allows better characterization of the type of polyol that is present in the solid phase as well as a quantitative characterization of the solids. The drawback of this way of quantification is that it takes approximately 50 hours of instrument time while ^{1}H-NMR experiments could be run within 1 hour. This method was used to check ^{1}H-NMR results.

Sample handling : Approximately 0.9 g of CPP solids were weighed in a 5-mL vial and 2.5 mL of CD_2Cl_2 were added. Using a roller mixer the vials were rotated until a clear solution formed. The solution was then transferred into a 10-mm NMR tube.

Apparatus : Bruker Avance 400 equipped with a 10-mm multinuclear probe. Frequency was 100.62 MHz for ^{13}C-NMR. ^{13}C flip angle used was 90° (90° pulse is 16 μs) and repetition delay (time between two consecutive pulses) was 25 s. Total number of scans was 8192(8K). Temperature was controlled at 303 K. TD was 64000 points. The spectra were used for quantification after a Fourier transform with exponential multiplication smoothing equivalent to a line broadening of 1 Hz.

2.7. Minipulsed Nuclear Magnetic Resonance

This analytical method was used to measure the solid content of stripped copolymer polyols having a solid content between 20 and 45 wt-%. The procedure is based upon the fact that the magnitude of the NMR signal immediately sampled after a so called 90° pulse is directly proportional to the amount of magnetic nuclei (protons) located within the detection system of the instrument. The shape of the NMR signal after a so called 90° pulse (free induction decay, FID) is approached by the following expression :

$$S_\tau = S_0 \exp\left(-\tau/T_2^*\right), \qquad (2.35)$$

where τ = time after the pulse,
S_τ = signal at time is τ,
S_0 = original signal,
T_2^* = apparent relaxation time which is mainly influenced by the T_2 relaxation time.

For solids, this time constant is relatively short (10 – 100 μs), while in liquids relaxation times between 1ms and several seconds have been observed. In a two phases system like copolymer polyol the sampling time has to be chosen in such a way that the NMR signal is composed of one of the two components. The linearity of the NMR is proven to be excellent in the region of interest and therefore one calibration point is sufficient. In these cases where no absolute standards are available the NMR reading can be calibrated using a sample containing 100 % liquid e.g. the pure base polyol.

The instrument used at Dow, Terneuzen, was a Bruker PC 100 Minispec equipped with a PCPH 20/10 VTS probe and a LIST PROM. The measurements were performed as follows : the sample tube was preheated in a oven for at least 30 min at the temperature equal to magnet temperature (40°C). Two sample tubes of the calibration standard (base polyol) and each of the copolymer polyols were prepared. The NMR signal of these products was measured in the following sequence :

Polyol tube 1 = a Volt
Sample tube 1 = b Volt
Sample tube 2 = c Volt
Polyol tube 2 = d Volt

The figures were corrected for a offset value : it was obtained by at least 6 different measurements and subtracted from the NMR figures.

Then, the date directly obtained from the NMR measurements are expressed in weight/ volume units :

$$\text{NMR} = \text{wt/vol \% Solids} = 100\left(1-\frac{b'+c'}{a'+d'}\right), \tag{2.36}$$

with a',b', c' and d' corrected for offset.

However, as the density of copolymer polyol samples differ from the density of the polyol standard a correction should be made :

$$\text{Solids (wt\%/ wt\%)} = 100-\frac{(100-NMR)x}{y} \tag{2.37}$$

Where x is the density of the polyol at 40°C and y is the density of the copolymer polyol at 40°C.

For solids levels between 20 and 45 wt-% an absolute precision of ± 5 % (95% confidence level) was proven to be attainable.

2.8. NIC Derivatization followed by GPC – Fluorescence

This procedure determines the quantity of OH groups grafted to solids (meq OH/ g solids) and provides the molecular weight distribution of grafted SAN chains. It is based upon the isolation of the solids from the CPP (making sure that non-bonded polyol and stabilizer is washed out) followed by the fluorescent tagging of the polyol OH groups bonded to the SAN with Naphthyl Isocyanate (NIC). Subsequent analysis of the NIC-derivatized solids by GPC followed by fluorimetric detection allows to selectively quantify the number of OH end groups bonded to the solids without interference with by the SAN backbone. The molecular weight distribution of SAN grafted with polyol is also obtained.

The derivatization reaction is the following :

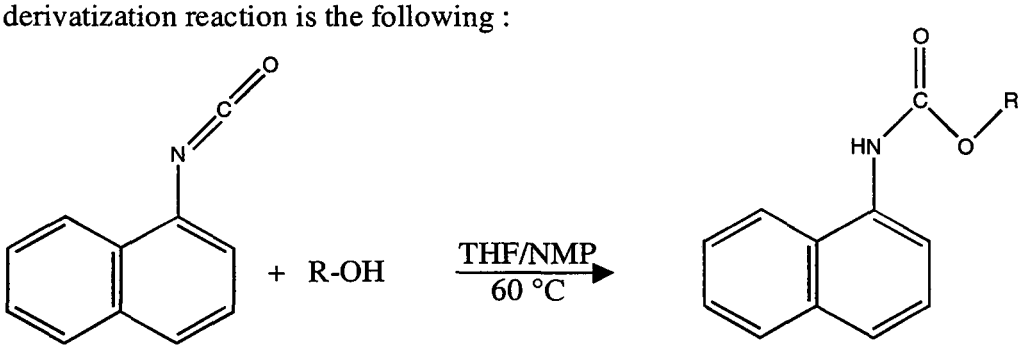

Approximately 40 mg of CPP solids were weighed in a 4-mL Waters autosampler vial (to the nearest 0.1 mg). The solids were dissolved by adding 2.5 mL of dried THF/NMP (50/50 v/v) solution and by putting the closed vials in ultrasonic bath for 15 min. After this, 25 L of dibutyltin dilaurate (DABCO T12) solution (50 % in dried THF) was added, followed by 25 L of NIC. The vials were closed with a plastic screw cap using a self-sealing septum and shaken. The vials were then injected into the GPC system without further filtration.

The instrumental parameters are :

Column : one Plgel 5- m mixed-D column, 300 mm * 7.5 mm ID
Temperature : 30 °C

Eluent :	THF + 0.005% v/v triethyl amine
Flowrate :	1 mL/min
Injection :	25 L
Detector :	Waters 470 Fluorescent detector with λexcitation = 232 nm and λemission = 358 nm; sensitivity 0.16 AUFS
Run time :	20 min

In order to convert the peak area under the graft distribution in the GPC chromatogram to meq OH/g solids, it was necessary to use an external calibration standard. Several researches led to use a commercial P2000 polypropylene glycol sample with known %OH (1.64 %). The polyol standards of different concentrations were derivatized and injected into GPC-Fluo providing a calibration curve Fluorescent area counts versus meq OH in 2.5 mL THF/NMP (50/50 v/v).

Nevertheless, this method is very time consuming (solids isolation, derivatization,...) and rather complex to do as it is necessary to take care of the aging of the reagent solutions and to the adsorption of polymer on the GPC column. Moreover, NIC is a toxic volatile isocyanate, which much be handle with care.

2.9. Liquid Chromatography on Silica gel / UV detector

This method was developed by Dow, Terneuzen, in order to separate quickly and to quantify the ratio of grafted SAN in CPP. Gradient liquid chromatography with a Chromspher silica gel column as stationary phase was used to optimize the separation between the different polymeric constituents of CPP. The very polar silanol functionality of silica gel is essential in separating the SAN from grafted SAN by a polar interaction mechanism. Other silica gel columns (e.g. Zorbax-Sil or Zorbax-Rx-Sil) from different manufacturers were tested, giving very similar results. The separation developed seemed to be quite robust and did not depend upon one specific column from one specific manufacturer.

The liquid mobile phase was dichloromethane (DCM). Solids were dissolved in DCM in a concentration of approximately 100 mg/ 5 mL DCM. CPP samples were dissolved in DCM at a concentration of 200 –250 mg / 5 mL DCM. Most of the studied CPP samples were fully soluble in DCM. In case the solutions appeared somewhat hazy, the solutions were filtered trough Millex® LCR filter (Millipore corp., 0.45 m pore size diameter). In case the filtration was very difficult, autosampler vial inserts were used to collect a couple of drops of filtered solution sufficient for analysis : this therefore only showed the grafting in the soluble portion.

Before each series of samples were injected into the LC apparatus, two blank DCM injections were performed and run under identical instrumental conditions as applied for the samples (see Fig. 2.13).

On figure 2.15, two main peaks are clearly observable : a peak in the retention time window 10.8 – 12.8 min corresponding to ungrafted SAN and a last broad peak in the retention time window 15–22 min corresponding to grafted SAN (Graft). Indeed, the more the SAN chains are grafted the higher is the retention time, as polyol interacts with the silica gel column.

The broad peak, depending of samples was composed of two fractions : a fraction in the range 15 –18 min which corresponds to high molecular weight (HMW) SAN with a small quantity of grafts and a fraction at around 19 min which is composed of low molecular weight (LMW) SAN highly grafted with polyol. The nature of the species corresponding to the different peaks was determined using ^{1}H NMR, ^{13}C NMR and Infrared (IR) analyses.

The areas of the SAN peak (after subtraction of the blank DCM peak area) and of the grafted SAN peak (after baseline subtraction) were determined. The molecular percentage of the all SAN chains, which were grafted is therefore :

$$\% \text{ Graft} = 100 \text{ area Graft} / (\text{area SAN} + \text{area Graft}) \quad (2.38)$$

Assuming an equal molecular weight, and a same composition in styrene for SAN and SAN grafted with polyol, this also expresses the wt-% of SAN that is grafted.

This method has this advantage to be quick, easy and quantitative. The precision is better than the derivatization – GPC procedure. Moreover, LC method gives an indication about the broadness of graft distribution but it does not provide information about the wt-% of polyol present in the grafts. Finally, this method can be used to study the whole CPP, the serum and the solids and it is the first method of choice of Dow to study the grafting of CPP materials.

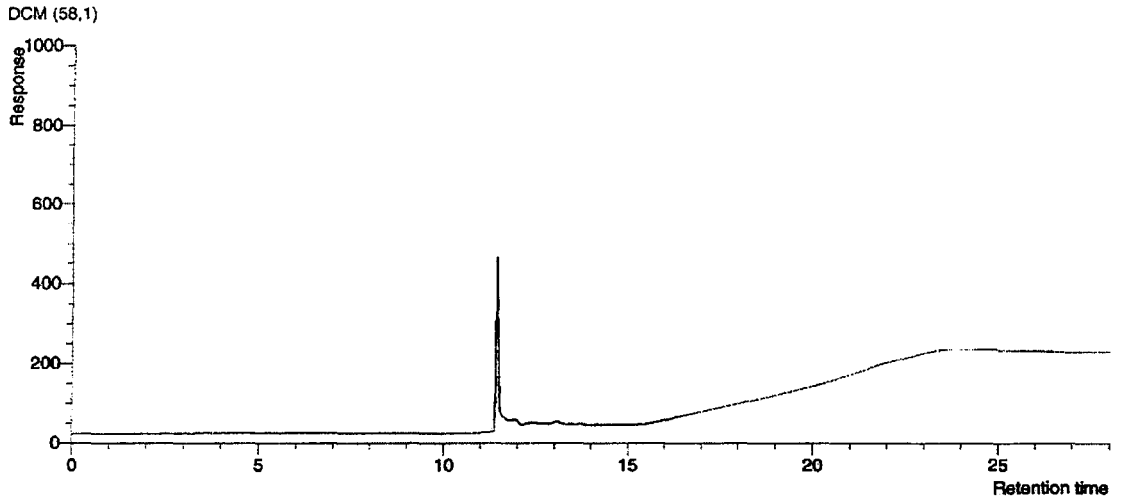

Figure 2.13 : Chromatogram of the DCM blank

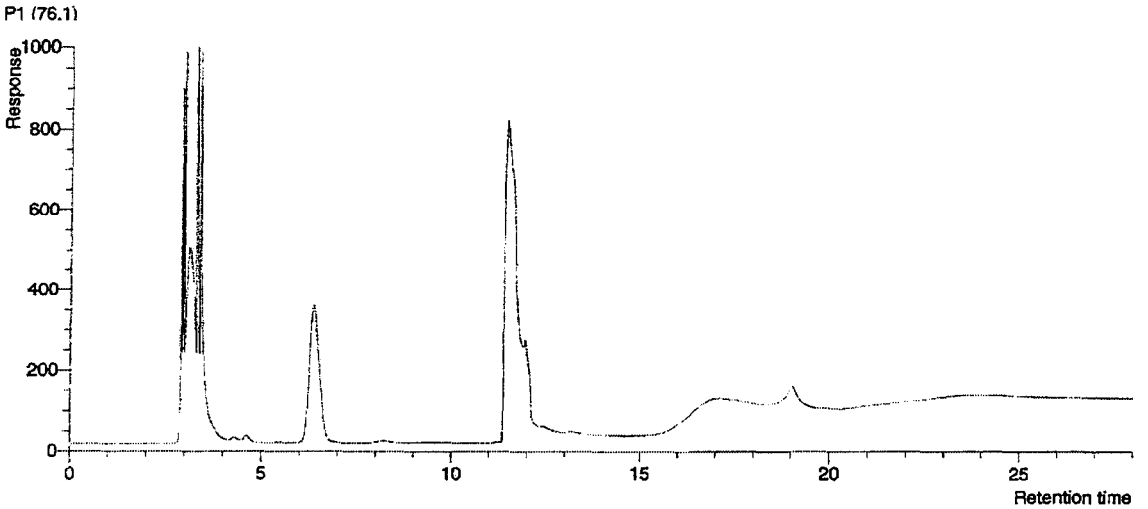

Figure 2.14 : HL400 chromatogram without baseline subtraction

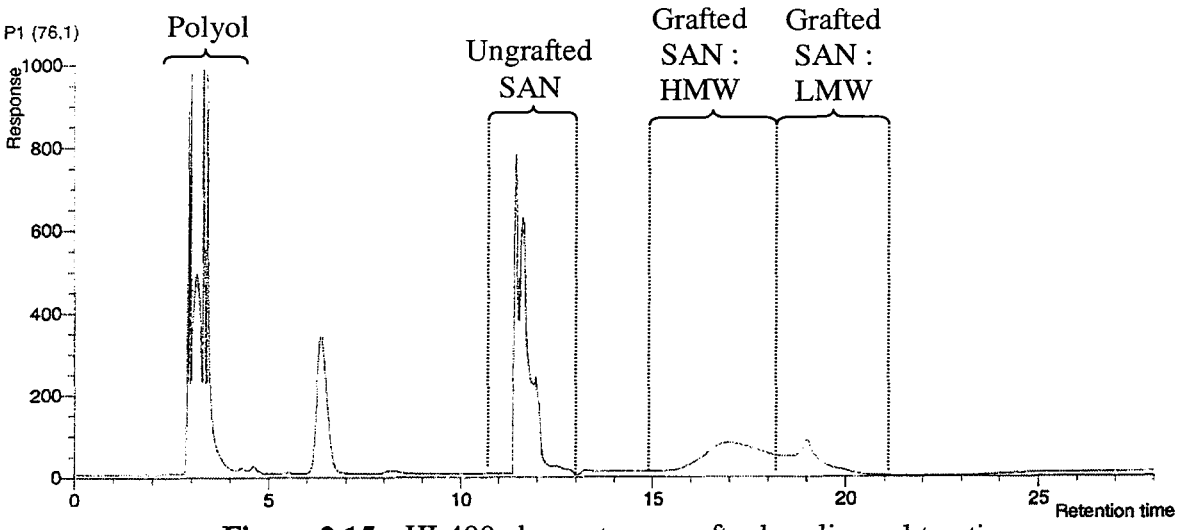

Figure 2.15 : HL400 chromatogram after baseline subtraction

Conclusion

This chapter presented the reactants used, the experimental device used at the laboratory and the several analytical methods that were required to study the best as possible the physical properties of the copolymer polyol produced in the purpose to better understand the chemistry inside the continuous stirred tank reactor and in order to further provide a model.

Nevertheless, some of these methods are rather time consuming, expensive and difficult to realize. One of the difficulties came from the separation of the solid phase from the serum, which is a long work as the process need to be repeated several times. That is why the analytical department of Dow Chemical tried to develop methods in order to quantify the grafting using the whole CPP.

CHAPTER 3
EXPERIMENTAL STUDY OF THE PROCESS

INTRODUCTION **123**

1. PRELIMINARY STUDIES **123**

1.1. NDM AND MONOMER PARTITIONING 123

1.2. "NATURAL" GRAFTING 124

1.2.1. Mechanisms leading to "Natural Grafting" *124*

1.2.2. Summary of the study and conclusions *125*

1.3. RELATIONSHIP BETWEEN GRAFTING AND VISCOSITY 126

2. EXPERIMENTAL RESULTS **127**

2.1 EXPERIMENTAL DESIGN 127

2.2. STUDY OF THE STEADY STATE REGIME 128

2.3. RESULTS 129

2.3.1. Molecular weight distributions *129*

2.3.2. Consumption of reactants and solids production *139*

2.3.3. Viscosities of the stripped CPP and the serum *140*

2.3.4. Particle Size Distributions *142*

2.3.5. Grafting *144*

2.3.6. Polymer composition *148*

2.3.7. SAN dissolved in serum : amounts and molecular weights *149*

2.4. RELATIONSHIPS BETWEEN THE DIFFERENT CPP PROPERTIES 150

2.4.1. Estimation of the number of S5200 grafts per grafted SAN chain *150*

2.4.2. Relationships between grafting, viscosity and molecular weights *152*

2.4.3. Depletion stabilization *152*

CONCLUSION **153**

Introduction

In order to better understand the phenomena that act in the continuous process of dispersion copolymerization of styrene and acrylonitrile in polyol medium, different experiments were realized. In the first part of this chapter will be presented some preliminary results, obtained by the Dow Chemical Company, and investigated in order to help the modeling and to better explain the process. In a second part, will be presented the experimental design used to study the influence of the process conditions, i.e. : the styrene/acrylonitrile ratio, the concentrations of the precursor stabilizer S5200, the initiator T27, the chain transfer agent NDM and the temperature. Then, the different physical properties of the copolymer polyol produced will be described by observing the influence of the process conditions on them. Finally, the different conclusions concerning this experimental study will be explained.

1. Preliminary studies

In this first part are exposed the principal results obtained in order to help the modeling : the monomer partitioning, the presence of natural grafting and the link that could be found between the grafting and the viscosity.

1.1. NDM and Monomer Partitioning

The analytical department of Dow Chemical Company investigated the partitioning of NDM, styrene, and acrylonitrile between the two phases system of polyol (liquid) and poly(styrene-co-acrylonitrile) particles.

Head Space Gas Chromatography with FID detector was used under the following conditions:

Temperature :	120 °C
Equilibration time :	90 min
Pressure :	200 kPa
Injection time :	0.03 min
Column :	CP-Wax 52 CB, 50m * 0.53 mm * 1.2 µm

The partitioning of the chain transfer agent, NDM, was investigated in HL 400 copolymer polyol. Several dilutions of HL400 with polyol IP3040 were prepared. A known amount of NDM was spiked to the CPP/polyol mixtures and the samples were mixed over night to ensure optimal homogeneity. 1.0 g of each sample was weighed into headspace vials for subsequent HS-GC analysis.

The detected peak areas of NDM of the respective samples were a measure for volatile NDM. In order to quantify the quantity of NDM immersed in the sample (SAN/polyol mixture), the %-absorbance was calculated. It gave therefore a linear relationship between the %-absorbance and the solids content in polyol from 40 wt-% to 20 wt-%. An extrapolation allowed to predict theoretically the absorption of NDM in pure SAN solid (100 wt-%) and in pure polyol (0 wt-%). The ratio of these both absorbencies gave the partitioning coefficient of NDM at 120 °C :

$$H_{CTA} = \frac{[CTA]_p}{[CTA]_c} = 0.98 \cdot \qquad (3.1)$$

The partitioning of the monomers was investigated in two different CPPs : HL400L and NC700. Dilution of HL400L (composed of 60 wt-% styrene) with polyol IP3040 and NC700 (composed

of 70 wt-% styrene) with polyol V4735 were prepared in order to obtain different mixtures with solid content from 10 to 40 wt-%. 200 mg of each solid concentration were spiked with 17 mg of stock solution. The stock solution was composed of 60 wt-% styrene and 40 wt-% acrylonitrile for measurements with HL400L and of 70 wt-% styrene and 30 wt-% acrylonitrile for measurements with NC700.

In the same way, the absorbance was then measured and extrapolations gave the following partitioning coefficients for the both CPPs :

$$\text{Acrylonitrile at 120 °C} : H_A = \frac{[A]_p}{[A]_c} \approx 1, \tag{3.2}$$

$$\text{Styrene at 120 °C} : H_B = \frac{[B]_p}{[B]_c} \approx 0.90, \tag{3.3}$$

that is to say that styrene has a slight preference for polyol.

1.2. "Natural" Grafting

As presented in chapter 1, the grafting of the polymer particles with a precursor stabilizer is an important key of the dispersion polymerization process. The stabilizer precursor used in this study was the S5200 macromere presented in chapter 2. The grafting was supposed to happen through the copolymerization of its Si-C=C bond with the styrene/acrylonitrile system. Nevertheless it is believed that other mechanisms, so called "natural grafting", occurred during the polymerization. Dow Chemical realized a study (TNV-3706) of this phenomenon in order to quantify the degree on natural grafting in CPP production.

1.2.1. Mechanisms leading to "Natural Grafting"

Two main mechanisms are identified :

a) Copolymerization of the monol vinyl group with styrene and acrylonitrile

As exposed in chapter 1, the polyether polyol is produced by the polymerization of propylene oxide and ethylene oxide using a polyhydric initiator. During this polymerization carried out in alkaline medium, the oxide can also be transformed into allyl alcohol by isomerization. This latter then reacts further with propylene oxide (PO) and/or ethylene oxide (EO) leading to an unsaturated monol. During the production of CPP, this terminal vinyl double bond can be initiated by any classical initiator or can be polymerized into a growing SAN chain leading to a monol-SAN block copolymer or a graft copolymer respectively :

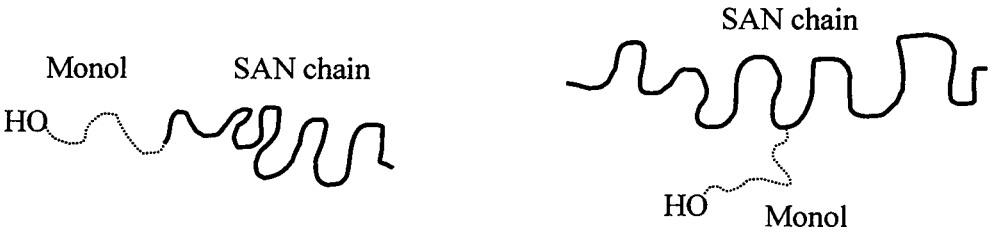

Figure 3.1. : Monol-SAN diblock and monol-g-SAN copolymers

b) Reaction leading to the abstraction of a hydrogen atom on the polyol

As seen in chapter 1, the polyol used as solvent for CPPs is a mixed feed EO/PO triol or an EO capped PO triol. In both cases, the polyol chains contain single hydrogens carried by a carbon atom (tert. C-H bonds from the PO repeating unit). Therefore, an initiator radical or any other polymeric radical can abstract this hydrogen from the polyol backbone creating a radical on the polyol. Thus, the polyol backbone is able to behave as a chain transfer agent, initiating a new polymerization of present monomers. This kind of mechanisms leads to *in situ* formation of a polyol-SAN stabilizer macromolecule :

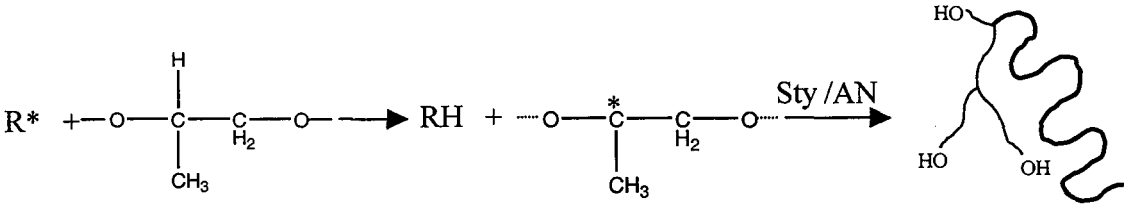

1.2.2. Summary of the study and conclusions

In order to quantify the importance and the type of the natural grafting that happens during the production of CPP, two different polyols were used : a "KOH-polyol" supposed to contain a significant amount of monols (typical 0.08 meq/g) and a "DMC-polyol", with a very low amount of unsaturations (< 0.008 meq/g).

Two different initiators were also used in order to study the importance of hydrogen abstraction : Trigonox 27 (T27), a peroxyester molecule, yelding to t.butoxy radicals that are strong H-abstractors, and Azo(bis-methylbutyronitrile) (AMBN), which has a very low hydrogen abstraction capacity that is typical for azo-type initiators.

Experiments were realized with and without S5200. The influence of the different constituents is summarized below :

Influence of initiators :

- The T27 initiator led to a significant higher grafting level, a higher low molecular weight (LMW) grafting level and higher high molecular weight (HMW) grafting level.
- The system T27 / "KOH-polyol" in the absence of S5200 led to very high viscosity product and threat-like agglomeration of the SAN particles with a very broad particle size distribution.
- The system AMBN / "DMC-polyol" with S5200 led to the best particle size distribution without agglomeration.
- The T27 initiator led to higher molecular weight SAN structures in the serum phase and to higher wt-% of SAN in the serum.

Influence of the polyols :

- The "KOH-polyol" gave higher HMW grafting but similar LMW grafting and higher mean particle size.
- The viscosity was lower with the "DMC-polyol".

Influence of the S5200 macromere :

- Adding S5200 led to a significant decrease of the mean particle size and to somewhat higher viscosities, but the effect is not strongly pronounced.
- S5200 increased the average molecular weights (most visible with T27) of the SAN copolymer inside the particles and dissolved in the continuous phase. It increased also the quantity of SAN copolymer dissolved in the medium.
- Without S5200, the grafting was less efficient leading to particle agglomerations.
- The presence of S5200 in the reaction medium increased only slightly the weight percentage of polyol in the solids.
-

This study showed that the degree of natural grafting in CPP production was significant in comparison with grafting obtained through copolymerization of the Si-C=C bond of S5200 with styrene and acrylonitrile.

With the peroxyester T27, the resulting alkoxy radicals are strong H-abstractors and lead to polyol-SAN diblock structures. This reaction was significant as about 50 % of the SAN-grafted polyol was obtained through this mechanism with T27. The effect of vinyl unsaturations (KOH polyol) and monol incorporation in SAN chains was small in comparison with this mechanism.

Moreover, the natural grafting levels obtained with both initiators arose from transfers of SAN oligoradicals to carrier polyol, again leading to block polyol-SAN structures.

The incorporation of carrier polyol (3040 g/mol) and unsaturated monols (1000 g/mol) in the graft structures was unfavorable, as the resulting polyol-SAN stabilizer was not enough effective: the molecular weight of the polyol part was too low and the steric layer was too thin. Furthermore, the presence of high molecular weight polyols such as S5200 (10000 g/mol) had a significant positive influence on the CPP properties. Especially the AMBN/DMC-polyol/S5200 combination lead to improved CPP properties : lower viscosity, better particle size distribution, less particle agglomerations and lower natural grafting. Therefore, this showed that the nature of the grafted polyol was more important than the amount of total grafting.

The viscosity seemed to increase when natural grafting and particularly H-abstraction happened. This could be explained by the fact that as the polyol radical formed could initiate a SAN chain, the resulting growing grafted SAN chain was more polyol-soluble and less mobile, which favored terminations or transfers, giving rise to LMW grafting, which increased the viscosity of the final product.

For these reasons, it was suggested to focus on azo-type initiators, low monol polyols using reactive vinyl groups in the polyol macromer in order to minimize natural grafting reactions and to control better the CPP stabilization. Nevertheless, as the system presented in this study was a T27/KOH-polyol/S5200 combination, it will be necessary to take into account the natural grafting to explain the results.

1.3. Relationship between grafting and viscosity

The viscosity of the copolymer polyols is one of the key points for the customers. It depends obviously on two factors : the viscosity of the based polyol and the volume fraction of the polymer particles.

Some experiments done by replacing the serum phase of a CPP sample by pure polyol showed that the viscosity of the new sample decreased. Therefore, the grafted SAN that was soluble in the continuous phase seemed to act directly on the viscosity of the whole product. The question was to know what was the influence onto the viscosity of both grafted SAN soluble in the serum and grafted SAN at the particles surface.

Dow Chemical investigated this subject and in order to study the influence of the SAN grafted in the serum phase, samples with the same solid phase but with different amounts of grafted SAN in the serum phase were prepared. Indeed, some "synthetic" samples were obtained by extracting the solid phase of a given CPP and by replacing it by pure polyol. Then, different ratios were prepared by mixing the original product with the synthetic one.

In the same way, to study the influence of the SAN grafted in the solid phase, samples with the same serum phase but with different amounts of grafted SAN in the solid phase were prepared. Two CPP samples were used : HL400, which is highly grafted as compared to the second sample, HS100. The serum phase and the solid phase of both samples were isolated. The serum phases of both samples were mixed together and this new serum phase was added to the solids to form two synthetic samples, which were mixed at different ratios.

The isolations were conducted as described in chapter 2 with both a Theta solvent of the polyol and the usual solvent of extraction Hexane/EtOAc (80/20, v/v), which extracts more soluble SAN than the first one.

It was observed that, compared to pure polyols, the serum viscosities were higher if the medium contained soluble SAN. Moreover, when the quantity of grafted SAN in the serum decreased, the viscosity of the whole product decreased also but much more than the viscosity of the serum. It was also noticed that when the quantity of grafted SAN in the serum decreased, the resulting chromatograms obtained by liquid chromatography showed a decrease of the shoulder corresponding to the LMW grafted SAN.

Furthermore, the grafted SAN in the solids influenced also the viscosity of the whole CPP but this influence appeared to be greater than the grafted SAN of the continuous phase.

Finally, this study showed the influence of the grafted SAN on the CPP viscosity but it did not explain how this influence worked. However, the previous study about natural grafting showed clearly that it was more the nature of the grafted polyol than the quantity of grafted SAN that seemed to be the most important concerning the stabilization of particles.

2. Experimental Results

2.1 Experimental design

The influence of different process parameters on the resulting CPP properties was studied in order to better understand the process chemistry and to provide a model.

We went from the standard process conditions of production of NC700 copolymer polyol, which is obtained using 43 wt-% of monomers with a Sty/AN ratio of 70/30 wt-%, 0.30 wt-% of NDM, 0.15 wt-% of T27, 2 wt-% of S5200 and 2 wt-% of seed at a temperature of 130 °C with a mass flow fixed to 25 g/min and a mixing speed of 750 rpm.

It is forecasted that when the chain transfer agent, the initiator and the temperature increases, the length of the polymer chains decreases and therefore the grafting level should decrease. When the concentration of S5200 increases, the grafting level should increases. When the

styrene/acrylonitrile ratio increases, the grafting level should decreases as acrylonitrile drives grafting in the case of vinyl alkoxy silane stabilization. The viscosity should increase when the grafting level increases as well.

These five parameters (wt-% NDM, wt-% T27, T, wt-% S5200 and Sty/AN ratio) were chosen to be investigated and varied while keeping constant the quantity of seed (2 wt-%), the mass flow (25g/min) and the agitation speed (750 rpm). These last two parameters act actually on the residence time and on the mixing inside the reactor.

The experimental design used to study the influence on the CPP properties is exposed in table 3.1. The limits of the experimental design were studied, that is to say the combinations of the conditions presented with the codes "–1" and "1", which provided $2^5 = 32$ experiments, and also some experiments in the center of the design (code "0"), that is to say with standard conditions. An other notation will also be used in this work : for instance low NDM means the smallest concentration in NDM of the experimental design corresponding to "-1", i.e. 0.15 wt-% and high NDM means the highest concentration of NDM of the experimental design corresponding to "1", i.e., 0.45 wt-%.

Table 3.1. : Experimental design for CPP process study

Code	**-1**	**0**	**1**
(CTA) **NDM** (weight %)	0.15	0.30	0.45
(I) **T27** (weight %)	0.10	0.15	0.20
T (°c)	120	130	140
S5200 (weight %)	1	2	3
Sty/AN (weight %)	60/40	70/30	80/20

In practice three experiments of the experimental design were not ran until the end as these conditions gave too unstable CPPs, which blocked the pipes. The first of these unstable recipes was low NDM, low T27, low T, low S5200 and low Sty/AN. The two others were high Sty/AN ratio, low T27, low T, low S5200 and low and high NDM.

2.2. Study of the steady state regime

Without seeds, an oscillating phenomena (as observed in many continuous emulsion/dispersion polymerization processes) appeared. This was an indication of excessive renucleations / agglomerations as a result of stabilizer imbalances.

A first part of the work was to check the stabilization effect of the seeds by studying the evolution of the particle size distribution and the molecular weight versus the reaction time, after 100 min of run (5 residence times).

Figure A3.1 of annex 3 shows the evolution of the molecular weights for two standard runs (runs n°33 and n° 34) and for a run particularly unstable (run n°36). For the standard runs, the average molecular weights are stable (variations less than 5% relative). However, a slight variation of less than 10 % (relative) of the average molecular weights is observed for the run n°36.

The particle size distributions determined using the Malvern MS100 instrument on samples resulting from the standard runs n° 33, 34 and 35 are stable and monodisperse, corresponding to a gamma distribution (figures A3.5.a and b of Annex 3). Figure A3.2 shows that the Sauter diameter is around 1.2 μm for all standard runs.

Figures A3.3 and A3.4 of Annex 3 show the Sauter diameters versus reaction time for the runs carried out with low styrene (Sty/AN = 60/40) and high S5200 (3 wt-%). Only the mean diameter of the run n°36, done with low NDM (0.15 wt-%), low T27 (0.10 wt-%) and low temperature (120°C) is not stable. All other runs seemed to reach a stable mean diameter around 1.1-1.3 μm after 9 residence times (180 min).

Indeed, for instance for run n° 42 done with low NDM, high T27 (0.20 wt-%) and low T (120°C), the volume particle size distributions at different times presented in figure A3.6.a and b shows that after a reaction time of 180 min, the distribution is monodisperse and stable.

However, for run n° 36, the particle size distribution shows clearly a competition between roughly two distributions (figure A3.7.a and b) : a first one with almost the same particles sizes that for the other runs with mean diameters around 1.2 μm and a second one with higher particle sizes with mean diameters around 10-15 μm. The oscillations of the mean particle diameter are probably due to the cycles of renucleations, which provide small particles, and agglomerations that provide large particles.

All the results that will be presented in the following study were obtained from samples collected after 13 residence times (5h runs) in order to have the most stable CPPs.

2.3. Results

2.3.1. Molecular weight distributions

2.3.1.1. Average Molecular weights

As explained in chapter 2, the average molecular weights were calculated after calibration of the GPC columns with standard polystyrene fractions. Nevertheless, the SAN copolymer studied contained 40 wt-% (57 mol-%), 30 wt-% (46 mol-%) or 20 wt-% (33 mol-%) of acrylonitrile, which may give rise to biased data. Moreover, the polyol or S5200 grafts may have an important hydrodynamic volume, which was counted as styrene, and which may also give inaccurate molecular weights.

One can notice that the samples resulting from runs 2, 4 and 6 (with Sty/AN = 60/40, S5200 = 1 wt-% and NDM = 0.15 wt-%) are not completely soluble in THF/NMP. Hence, the resulting chromatograms correspond only to the soluble part.

According to the results presented in the tables A3.1 to A3.5 of Annex 3, the two main process parameters that influence the average molecular weights are the amount of chain transfer agent (NDM) and the Styrene/Acrylonitrile ratio. Indeed, high NDM concentration and Sty/AN = 80/20 reduced significantly the molecular weights.

The standard runs (table A3.5) give $\bar{M}_n$ around 30600 g/mol and $\bar{M}_w$ around 85400 g/mol with a polydispersity index of 2.8. The relative error between the average molecular weights of these five runs is about less than 10%.

With Sty/AN = 60/40 (tables A3.1 and A3.2.a and b) and low NDM (0.15 wt-%), the weight-average molecular weights, $\bar{M}_w$, reach values from 150000 g/mol to 300000 g/mol, whereas they reach values from 70000 g/mol to 96000 g/mol for high NDM (0.45 wt-%). With Sty/AN = 80/20 (tables 3.4 and 3.5), $\bar{M}_w$ is in a range 90000 - 126000 g/mol at low NDM (0.15 wt-%), whereas $\bar{M}_w$ is in a range 33000 - 43000 g/mol at high NDM (0.45 wt-%).

Concerning $\bar{M}_n$, the number-average molecular weight, the results show that with Sty/AN = 60/40 (tables A3.1 and A3.2.a and b) the values are in the range 32000 - 60000 g/mol for low NDM and in the range 24000 - 28000 g/mol for high NDM. With Sty/AN = 80/20 (tables A3.3 and A3.4) they are in the range 30000 - 44000 g/mol for low NDM and in the range 13000 - 18000 g/mol for high NDM.

The influence of styrene/acrylonitrile ratio is firstly due to the propagation kinetic constant of styrene that is lower than the propagation kinetic constant of acrylonitrile (see Eq. 4.1 to 4.3 of chapter 4). Secondly, as the proportion of styrene is increased, the polymer looses its crystalline nature due to polyacrylonitrile, but it is still compact and not significantly swollen by the monomers up to at least 60 wt-% of styrene. This compactness is a result of the insolubility of the polymer in the monomers and polyol. Nevertheless, for high styrene levels, above 80 wt-%, the polymer becomes soluble in styrene and therefore is swollen. Therefore for 80 wt-% styrene, the resulting SAN copolymer is more soluble in the continuous phase than at 60 wt-% styrene, which means that the polymerization happens more in the continuous phase. This favors a solution polymerization in front of bulk polymerization, providing shorter SAN chains.

For Sty/AN = 60/40, high NDM allowed a better stabilization of the particles whereas for Sty/AN = 80/20, high NDM destabilized the particles, as with these conditions, the resulting polymer chains are too short and too much soluble in the medium. Indeed, at low styrene (Sty/AN = 60/40) / high NDM and high styrene (Sty/AN = 80/20) / low NDM, the molecular weights are closer to those obtained in the standard stable runs.

The effect of initiator concentration and temperature on molecular weights is not as obvious as forecasted if one considers the average molecular weights. The molecular weights should decrease when the initiator concentration increases, as it is shown comparing runs 4 and 6, runs 8 and 10 or runs 12 and 14 (decrease of 20 to 30 % relative). Nevertheless, as shown for instance in table A3.1, comparing runs 1 and 3 and comparing runs 5 and 7, an increase of the peroxide concentration induces a small decrease (5 %) of $\bar{M}_n$, and an increase (5 % and 15%) of $\bar{M}_w$. The same phenomenon appears comparing runs 9 and 11, runs 13 and 15 at 60 % styrene (table A3.2) and comparing runs 18 and 20, runs 19 and 21, runs 22 and 24, runs 26 and 28, at 80 % styrene, where the increase of $\bar{M}_w$ is of about 10 to 20 %.

The effect of temperature on molecular weights is also not very pronounced. The number-average molecular weight decreases slightly when the temperature increases but the effect on the weight-average molecular weights is more complex. With Sty/AN = 60/40 and low NDM, $\bar{M}_w$ decreased (20 to 50 %) when the temperature increases, whereas with high NDM, $\bar{M}_w$ increases (10 to 25 %) with the temperature. With Sty/AN = 80/20, only runs16 and 20 show a decrease (15%) of $\bar{M}_w$ when the temperature increases. The explanation that can be given is that the temperature increases the number of radicals in the continuous phase, providing more and shorter SAN chains in the serum, but it increased also the kinetics of propagation inside the

particles providing less but longer SAN chains. These are two antagonist effects on average molecular weights.

Increasing the concentration of the S5200 macromere, increases slightly the average molecular weights, $\bar{M}_n$ and $\bar{M}_w$, from 5 to 15 %.

Therefore, considering the accuracy of the measurement (5%), the polystyrene GPC calibration method used and of the experimental conditions reproducibility, temperature, initiator and S5200 concentrations have a relatively small influence on the average molecular weights of CPP. Indeed, the comparison of runs n° 8 to 15 to runs n° 37 to 44 of table A3.2.a and b, done with the same experimental conditions, shows that the relative error between these measurements is about 20 %.

2.2.2.2. Molecular weights distributions of whole CPP

The weight and number molecular weight distributions of runs n°1 to 32 are presented in figures A3.8 to A3.25 of annex 3. As shown on figures 3.2 and 3.3, these distributions do not follow simple gamma distributions and it was attempted to deconvoluate these curves in order to identify the different populations of macromolecules.

Indeed, as observed on figures 3.4 to 3.11, the deconvolution shows clearly the presence of at least three gamma distributions in the molecular weight distributions as if the SAN copolymer is present in CPP under roughly three different populations of macromolecules. This explains that the polydispersity ($\bar{M}_w / \bar{M}_n$) is higher than two.

The influence of the styrene/acrylonitrile ratio and the quantity of NDM is clearly observable on these three populations. For instance, if we consider run n° 9, done with Sty/AN = 60/40, S5200 = 3 wt-%, NDM = 0.45 wt-% and T27 = 0.10 wt-% at T = 120 °C, the deconvolutions presented on figure 3.4 and 3.5 give the values of $\bar{M}_n$ and $\bar{M}_w$ corresponding to these three populations (table 3.2).

Table 3.2 : Deconvolution of the molecular weight distribution of run n°9

Population	**1**	**2**	**3**	**Total population**
$\bar{M}_n$ **(g/mol)**	3000	13800	57300	28500
$\bar{M}_w$ **(g/mol)**	3930	18660	88600	73600
Mol-%	21	37	42	100
Wt-%	2	17	81	100

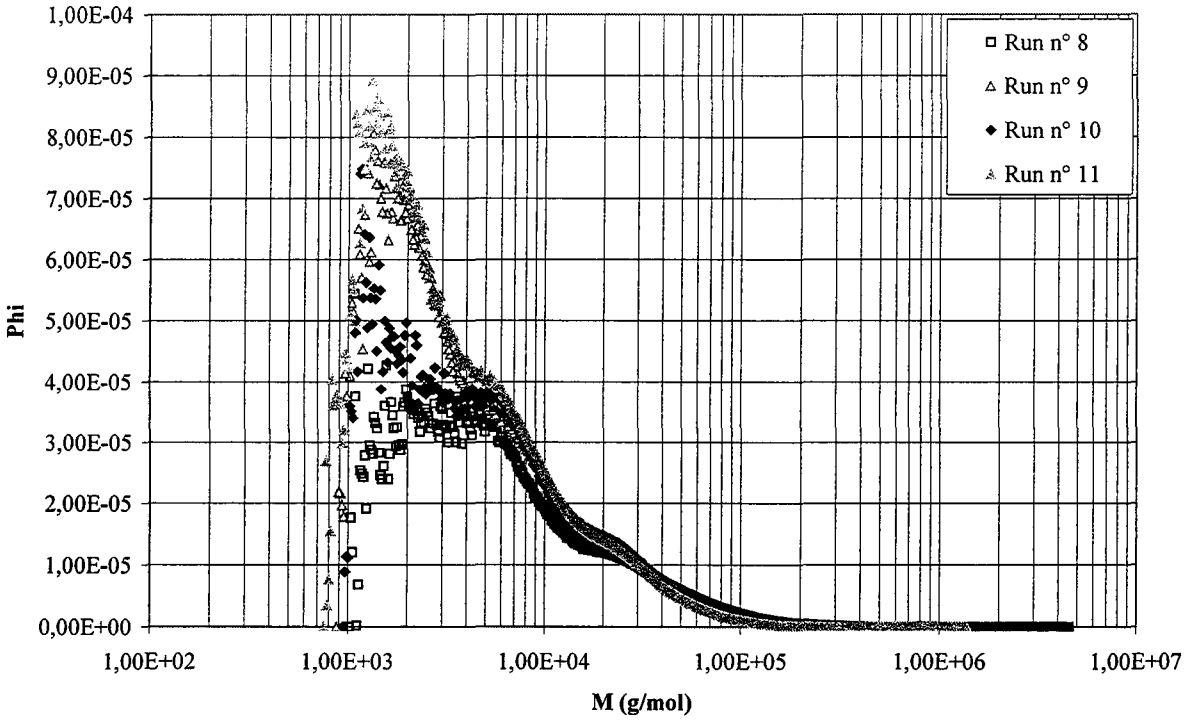

Figure 3.2 : Number molecular weight distribution of the runs n° 8 (low NDM, low T27), n° 9 (high NDM, low T27), n° 10 (low NDM, high T27) and n° 11 (high NDM, high T27) done with low styrene (Sty/AN=60/40), high S5200 (3 wt-%) and low T (120 °C)

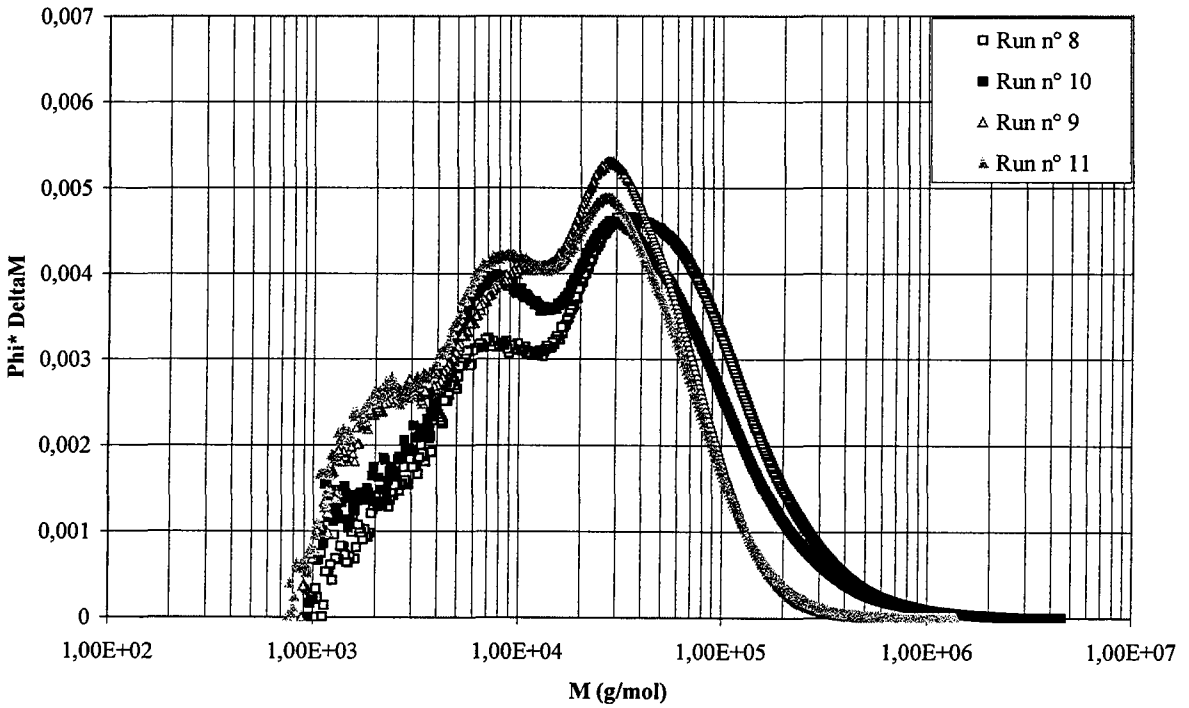

Figure 3.3 : Weight molecular weight distribution of the runs n° 8 (low NDM, low T27), n° 9 (high NDM, low T27), n° 10 (low NDM, high T27) and n° 10 (high NDM, high T27) done with low styrene (Sty/AN=60/40), high S5200 (3 wt-%) and low T (120 °C)

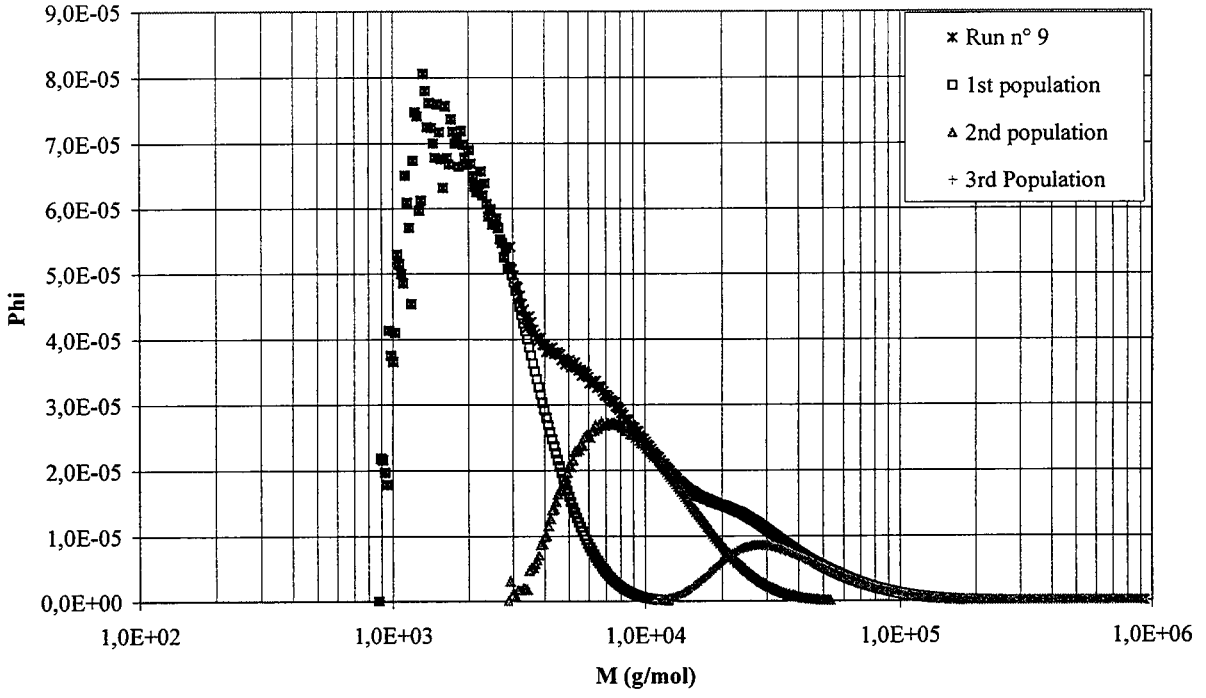

Figure 3.4 : Deconvolution of the number molecular weight distribution of the run n° 9 done with Sty/AN=60/40, S5200 =3 wt-%, NDM = 0.45 wt-%, T27 = 0.10 wt-% and T=120 °C

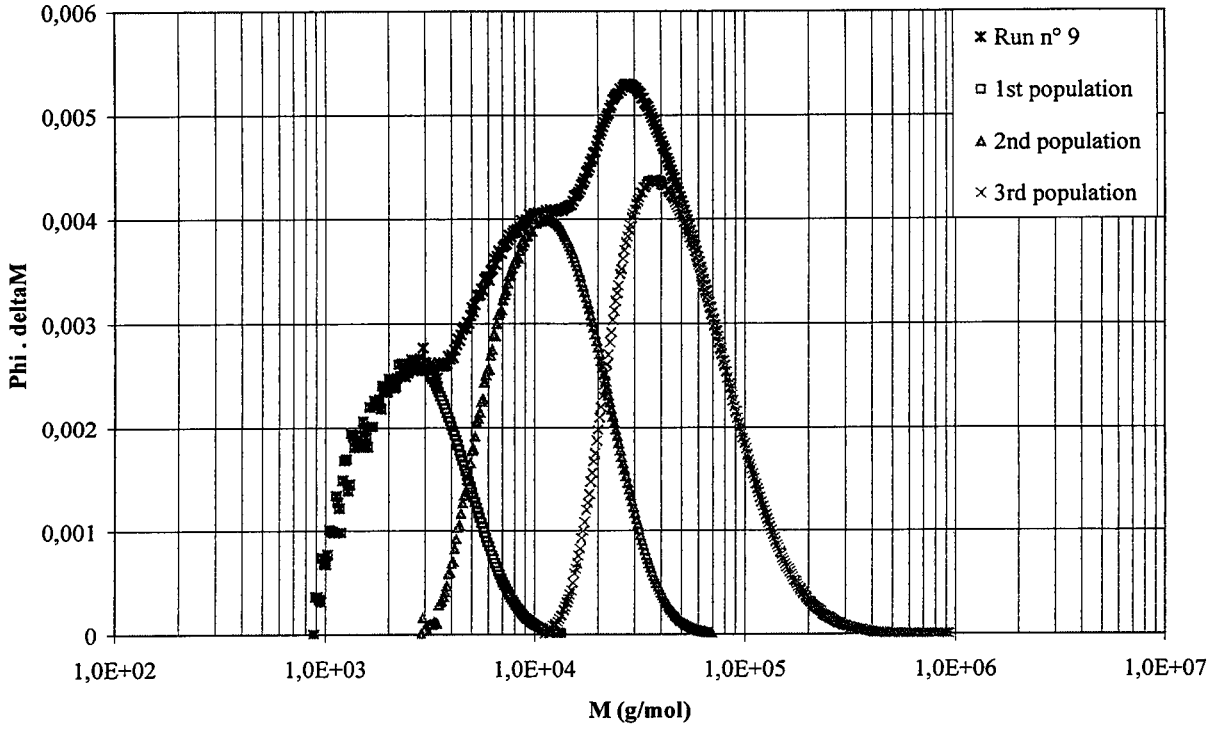

Figure 3.5 : Deconvolution of the weight molecular weight distribution of the run n° 9 done with Sty/AN=60/40, S5200 =3 wt-%, NDM = 0.45 wt-%, T27 = 0.10 wt-% and T=120 °C

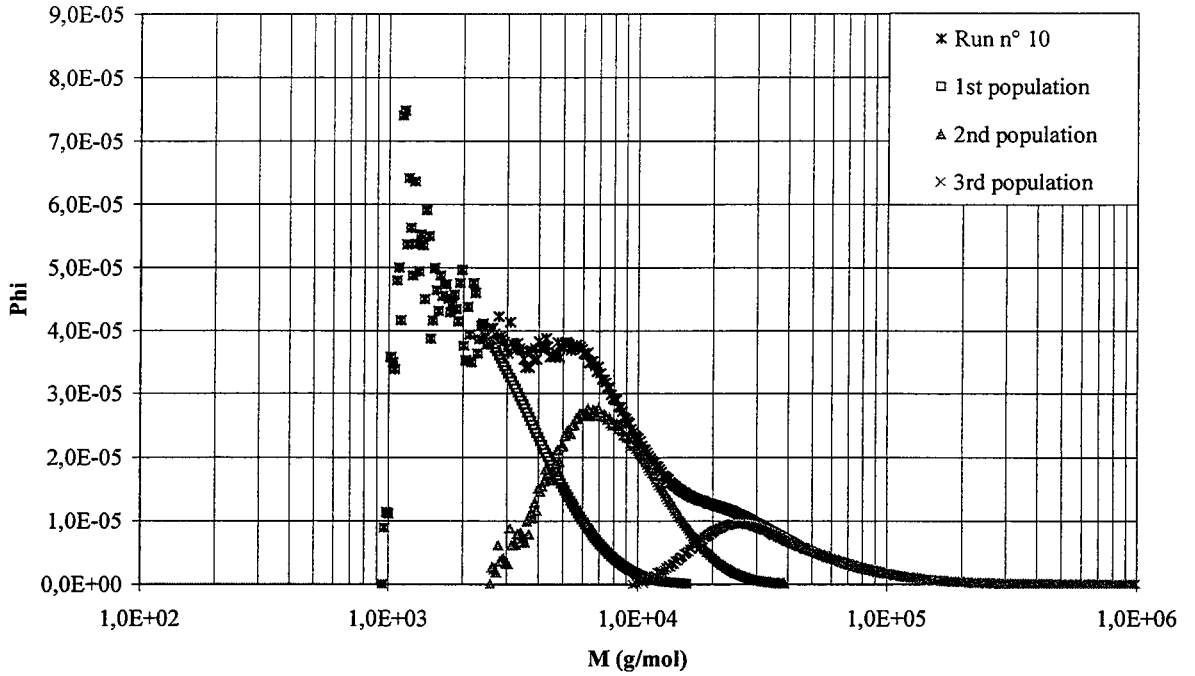

Figure 3.6 : Deconvolution of the number molecular weight distribution of the run n° 10 done with Sty/AN=60/40, S5200 =3 wt-%, NDM = 0.15 wt-%, T27 = 0.2 wt-% and T = 120 °C

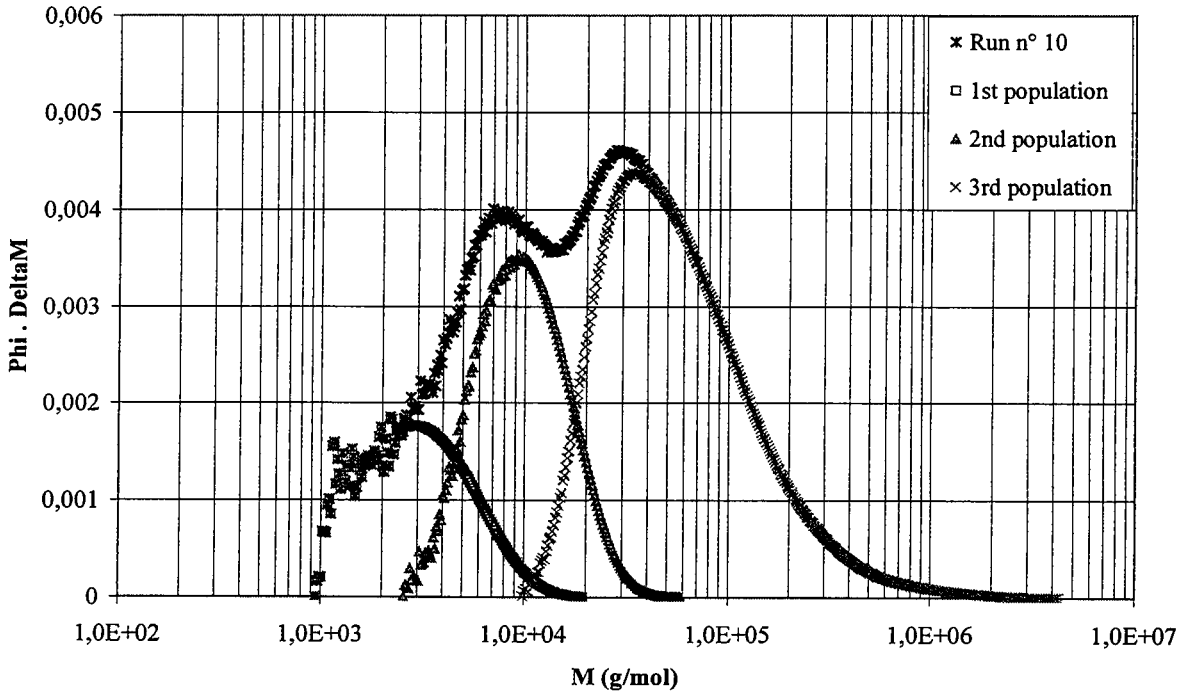

Figure 3.7 : Deconvolution of the weight molecular weight distribution of the run n° 10 done with Sty/AN=60/40, S5200 =3 wt-%, NDM = 0.15 wt-%, T27 = 0.20 wt-% and T=120 °C

Table 3.3 : Deconvolution of the molecular weight distribution of run n°10

Population	1	2	3	Total population
$\bar{M}_n$ (g/mol)	3550	10980	83700	49310
$\bar{M}_w$ (g/mol)	5030	14130	206230	191600
Mol-%	17	28.5	54.5	100
Wt-%	1.2	6.3	92.5	100

Comparing figures 3.6 to 3.4 and 3.7 to 3.5 showed that the first population of run n°10 has almost the same average molecular weights than the one of run n°9 but its quantity was less important with run 10, obtained for low NDM. The second population of run 10 has lower molecular weights, but its quantity has decreased slightly.

The main difference concerns the third population where the distribution reaches higher molecular weights with low NDM (run n° 10), and actually this last population could also be deconvoluate in at least two gamma distributions. Finally, with low NDM there seemed to be less short soluble SAN chains, and a higher number of longer SAN chains inside particles.

Therefore, with Sty/AN = 60/40, decreasing the NDM concentration decreases the quantity of soluble SAN and increases the quantity of long SAN chains. Nevertheless, the quantity of the second population do not change, which would indicate that this population is rather composed of SAN grafted with S5200 rather than of SAN macromolecules resulting from transfers.

The first population ($\bar{M}_n$ = 3000 g/mol), which represents 21 % in number but only 2 % in weight of the total population may be the population of small SAN macromolecules dissolved in the continuous phase, whereas the third population ($\bar{M}_n$ = 57300 g/mol), which represents 42 % in number and 81 % in weight of the total population, may correspond to the polymer produced in bulk inside of the particles and terminated by combination reactions. The second population may correspond to the polymer chains terminated by transfers to NDM or to polyol. It may also correspond to the SAN macromolecules grafted with S5200.

Now, if we consider run n° 10, always done with Sty/AN = 60/40 at T = 120°C, with S5200 = 3 wt-% but with T27 = 0.20 wt-% and NDM = 0.15 wt-% (distribution closed to run n° 11). $\bar{M}_n$ and $\bar{M}_w$ of the three populations together with those of the global sample are given in table 3.3.

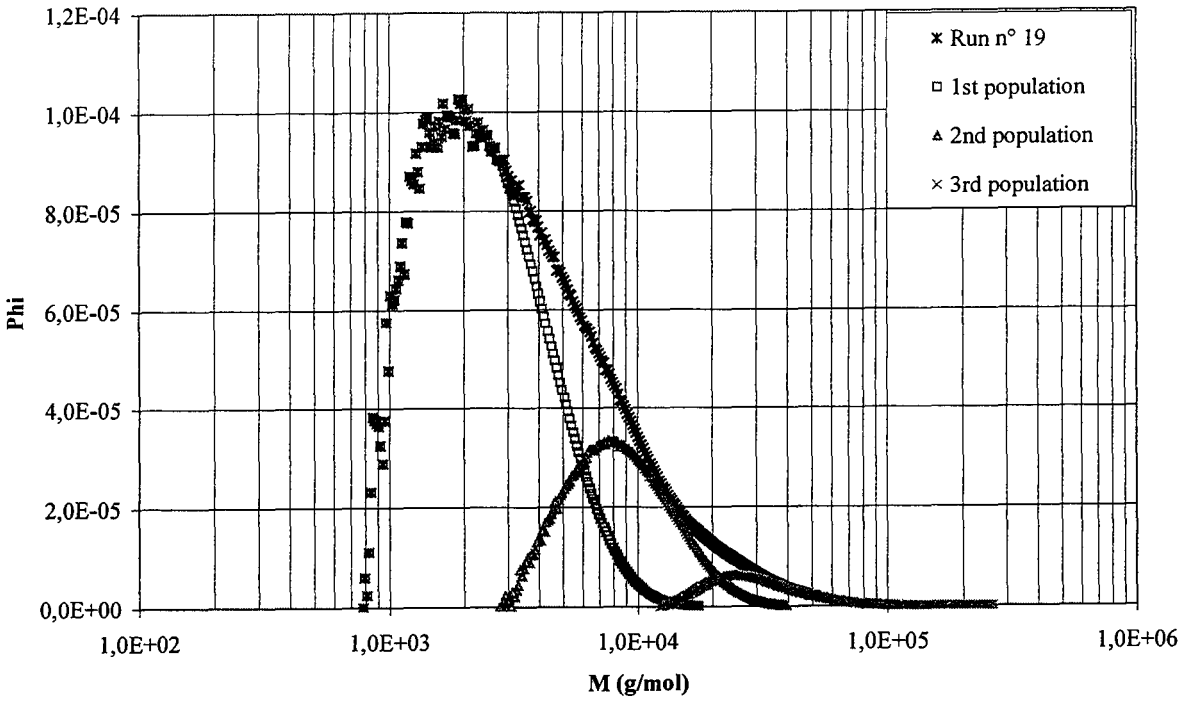

Figure 3.8 : Deconvolution of the number molecular weight distribution of the run n° 19 done with Sty/AN=80/20, S5200 =1 wt-%, NDM = 0.45 wt-%, T27 = 0.10 wt-% and T=140 °C

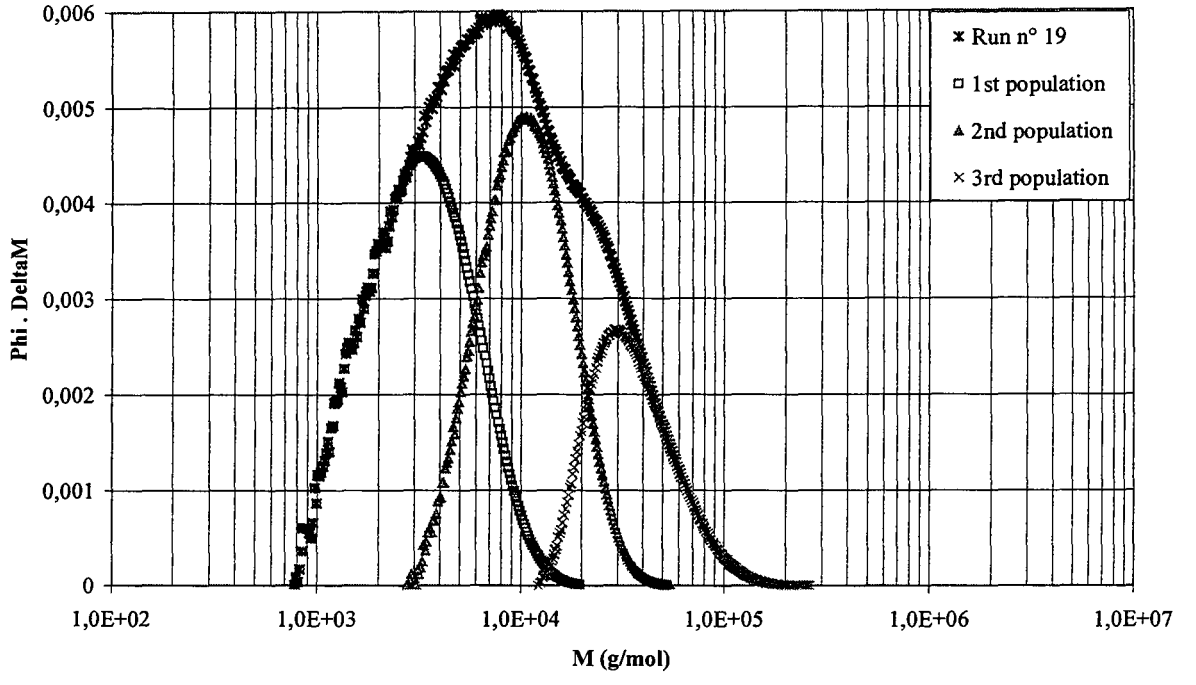

Figure 3.9 : Deconvolution of the weight molecular weight distribution of the run n° 19 done with Sty/AN=80/20, S5200 =1 wt-%, NDM = 0.45 wt-%, T27 = 0.10 wt-% and T=140 °C

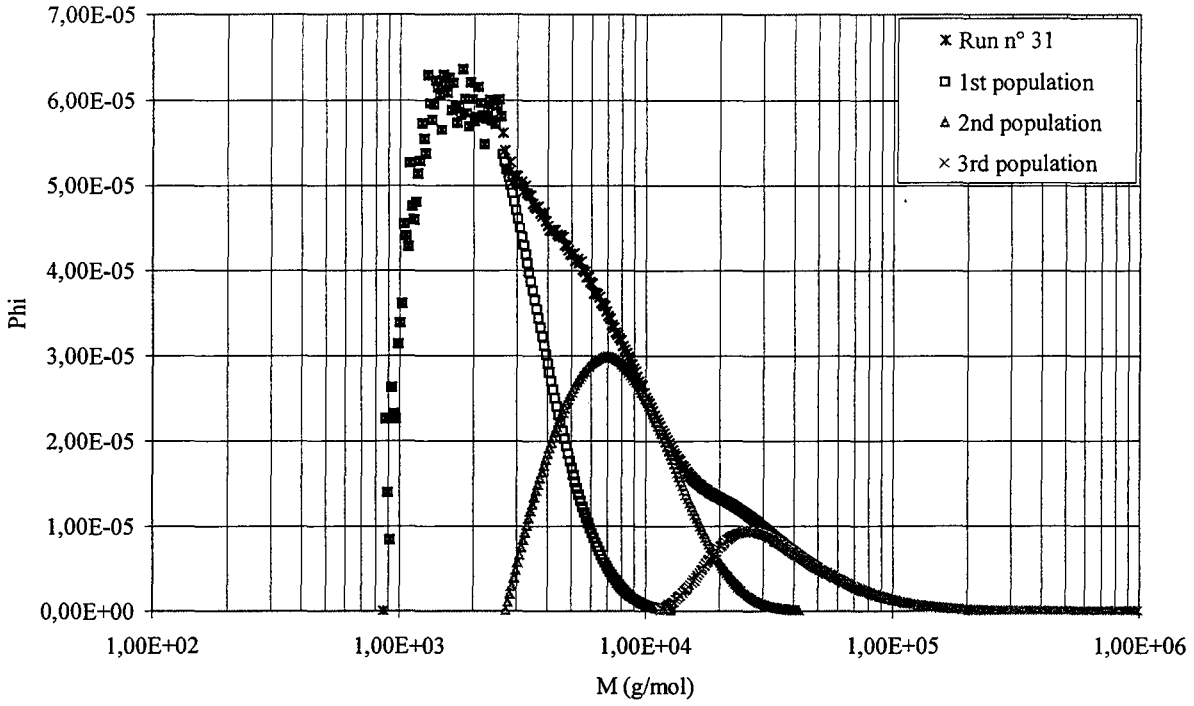

Figure 3.10 : Deconvolution of the number molecular weight distribution of the standard run n° 31 done with Sty/AN=70/30, S5200 =2 wt-%, NDM = 0.30 wt-%, T27 = 0.15 wt-% and T=130 °C

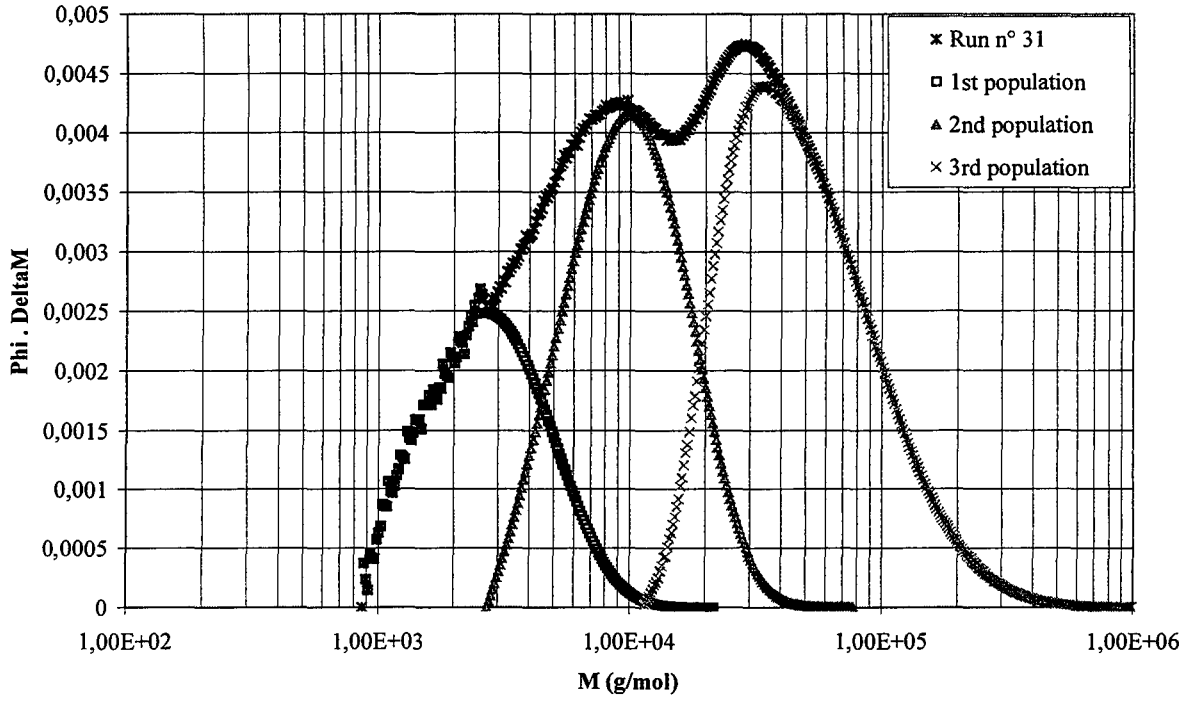

Figure 3.11 : Deconvolution of the weight molecular weight distribution of the standard run n° 31 done with Sty/AN=70/30, S5200 =2 wt-%, NDM = 0.30 wt-%, T27 = 0.15 wt-% and T=130 °C

The difference between 60% and 80 % styrene appears also clearly in the molecular weight distributions. The example is given by run n° 19 done with 80 % styrene at 140°C, with S5200 = 1 wt-%, T27 = 0.10 wt-% and NDM = 0.45 wt-%. Indeed looking at figures A3.30 and A3.31 of annex 3 and at table 3.4 below, the third population is less important at 80 % styrene than at 60 % styrene and there is more short SAN chains that may be soluble in the continuous phase : with Sty/AN = 80/20, the first population represents about 40 % in number and 10% in weight of the total distribution whereas it is around 20 % in number and 2 % in weight with 60 % styrene. The proportion of the second population increases also, and it can be noticed that the chains obtained have the same order of size. The third population decreases considerably as it becomes the smallest population in number of macromolecules (from about 45-55 mol-% at 60 % styrene to 20 mol-% at 80 % styrene). The proportion in weight is still the most important but it decreases from about 80-93 wt-% at 60 % styrene to 55 wt-% at 80 % styrene.

Table 3.4. Deconvolution of the molecular weight distribution of run n°19

Population	**1**	**2**	**3**	**Total population**
$\bar{M}_n$ **(g/mol)**	3800	11900	39700	13400
$\bar{M}_w$ **(g/mol)**	5200	15100	51300	33300
Mol-%	41.2	39.2	19.6	100
Wt-%	11.1	33.3	55.6	100

It can be observed on the molecular weight distributions of standard run n° 31 (figures 3.10 and 3.11), done with Sty/AN =70/30, S5200 = 2 wt-%, T27= 0.15 wt-%, NDM = 0.30 wt% and T = 130 °C, that the three populations are present and almost in the same proportions that with Sty/AN = 60/40.

Table 3.5. Deconvolution of the molecular weight distribution of standard run n°31

Population	**1**	**2**	**3**	**Total population**
$\bar{M}_n$ **(g/mol)**	3160	11280	61580	31200
$\bar{M}_w$ **(g/mol)**	4160	14580	108380	93500
Mol-%	20.1	34.4	45.5	100
Wt-%	1.9	11.9	86.2	100

It can be noticed however on figures A3.22 and A3.23 (annex 3) showing the distributions of both the standard runs n° 31 and 32 that these distributions are almost similar, except a small peak at 1000 g/mol for run n° 32. Indeed another population of very short SAN macromolecules is present at around 1000 g/mol.

For all runs realized with high NDM there is no influence of temperature and of T27 concentration on the average molecular weights. However, at low NDM, increasing the concentration of T27 increases slightly the first and second populations and decreases the third one, decreasing slightly the average molecular weights. This can be observed for instance comparing runs n° 8 and 10 on figures 3.2 and 3.3, and in annex 3 comparing runs n° 4 and 6 on figures A3.10 and A3.11, runs 12 and 14 on figures A3.12 and A3.13, runs n° 18 and 20 on figures A3.16 and A3.17 and runs n° 26 and 28 on figures A3.20 and A3.21. Increasing the temperature has the same effect for low NDM concentrations, increasing the first and the second population and decreasing the third one, decreasing slightly the average molecular weights. This phenomenon can be observed for instance comparing runs 2 and 6 on figures A3.8 to A3.11, runs n° 8 and 12 and runs n° 10 and 14 on figures 3.2 and A3.13, runs n° 16 and 20 on figures A3.14 to A3.17 and runs n° 22 and 26 and runs n° 25 and 29 on figures A3.18 to A3.21.

Moreover, there is no significant influence of the concentration of the precursor stabilizer S5200 on the molecular weight distributions except a slight increase of the average molecular weights.

As a conclusion, the molecular weight distributions shows the presence of around three types of sizes of SAN macromolecules, which help to understand the influence of the different experimental conditions on the composition of the CPPs produced. High styrene ratio and high NDM increases the first and the second population of macromolecules and reduces the third one, in the same way these molecular weights are also reduced. For high NDM, the influence of temperature and T27 concentration is not obvious, whereas at low NDM, increasing these parameters has the effect to decrease slightly the average molecular weights by increasing the first and the second population and reducing the third one.

2.3.2. Consumption of reactants and solids production

The quantity of residual reactants (Res.), in weight-%, and their conversions (conv.) for styrene, acrylonitrile and NDM, as well as the quantity of solids in stripped CPP, in weight-%, are presented in tables A3.6 to A3.10 of Annex 3.

According to these measurements the chain transfer agent reacts with a conversion from 90 to 100 %. Such a small amount of residual NDM in the medium does not allowed identifying clearly the effect of the different parameters on its conversion.

The main process parameter that influences the conversions of styrene and acrylonitrile was the styrene/acrylonitrile ratio (Sty/AN) : with 60 % styrene the styrene conversion evolves from 90 to 95 %, while that of acrylonitrile varies from 85 to 90 %, whereas with 80 % styrene the styrene conversion is in the range 54-96% and that of acrylonitrile in the range 54-83%. For the standard runs the conversions are around 86 % for styrene and 85% for acrylonitrile, has showed in table A3.10.

The quantity of solids in the stripped CPP results directly from the conversions in monomers. It would be equal to 43 wt-% if the conversions of the monomers were complete as there is 43 wt-% of monomers in the premix. With 60 % styrene, the quantity of solids is in the range 35.5 - 41.6 wt-%, whereas with 80 % styrene it is dispersed between 30.8 and 39.9 wt-%.

The fact that the conversions were lower at 80% styrene may be explained as following : solution polymerization was more important at this ratio as the SAN copolymer was more soluble in the continuous medium and therefore, as the molecular weights that were reached were lower, a lower quantity of monomer was consumed. For instance, considering the run n°19 in table A3.8 seen before, the conversions were rather low : 54% for styrene and 64 % for

acrylonitrile, that explains also the low molecular weights obtained ($\overline{M}_n$ =13400 g/mol and $\overline{M}_w$ = 33300 g/mol, see table A3.3).

Nevertheless, there is no clear influence of the other process parameters than the styrene/acrylonitrile ratio on the conversions.

2.3.3. Viscosities of the stripped CPP and the serum

The viscosities measured at 25 °C of both the stripped CPP and the serum are given in annex 3 (tables A3.11 to A3.15). The sample resulting from run n°17 has not been analyzed as it is too unstable.

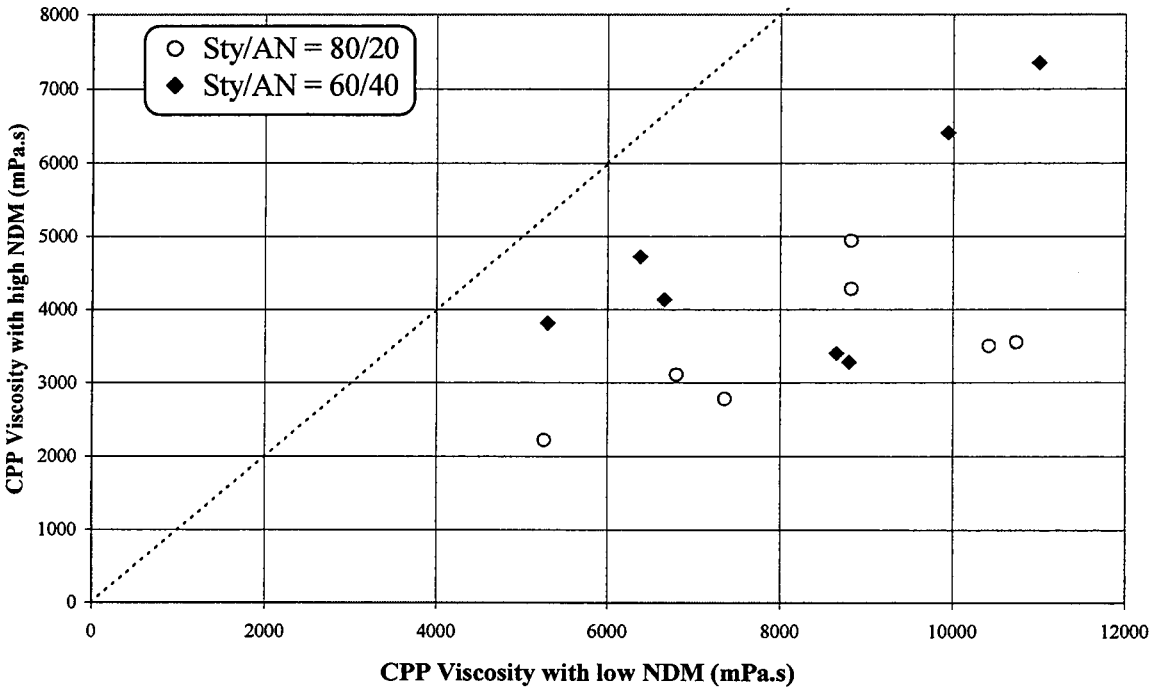

Figure 3.12 : Influence of NDM and Sty/AN ratio on the viscosity of stripped CPP

The viscosity of the stripped CPP is highly influenced by the quantity of chain transfer agent. As shown in figure 3.12 below, which gives the viscosity of CPP at high NDM as a function of the viscosity obtained under the same experimental conditions but at low NDM, the viscosity decreases when NDM concentration increases, which implies that there is a strong relationship between the SAN molecular weights and the CPP viscosity.

Moreover, the CPP viscosity seems to increase as the initiator concentration increases as shown in the figure 3.13 below and it can also be noticed that the highest viscosities are obtained with recipes combining low NDM and high T27. Indeed, high T27 produces more primary radicals in the medium and therefore more polymer chains, and low NDM gives longer SAN chains : the viscosities are higher when the SAN chains are longer and in higher number. In the same way, the lowest viscosities are almost always obtained with high NDM and low T27.

With Sty/AN = 80/20, the molecular weights are smaller than with Sty/AN = 60/40 and the viscosities are also smaller. Indeed, this time, combining Sty/AN = 80/20, high NDM and low T27 gives the lowest viscosities.

Nevertheless, low viscosity does not seem to be linked with CPP stability, and for the Sty/AN = 80/20, this low viscosity is also due to the fact that the monomers conversion is lower : less solids produced and more residual monomers in the medium.

Conclusions cannot be given concerning the temperature and the S5200 concentration influences as viscosities increases or decreases, not systematically with the other conditions.

Some measurements have been made on the serum viscosity as it is forecasted that the differences of CPP viscosities result from the SAN chains soluble in the serum and increasing its viscosity. Nevertheless, as it can be seen in table A3.11, the serum viscosity does not vary with the NDM concentration as much as the CPP viscosity does. For instance, between runs 2 and 3 CPP viscosity varies from 8650 mPa.s to 3400 mPa.s whereas the serum viscosity varies from 484 mPa.s to 477 mPa.s.

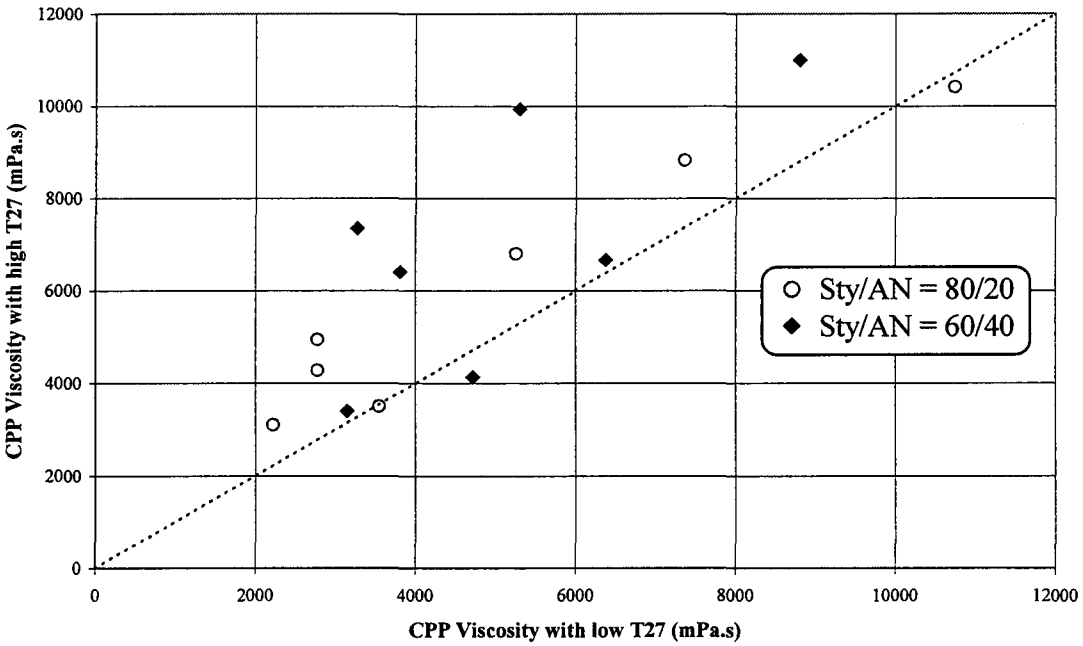

Figure 3.13 : Influence of the T27 concentration on the CPP viscosity

It is not either significantly modified by the temperature, the initiator concentration and the Sty/AN ratio. However, high S5200 seems to increase slightly the serum viscosity comparing runs 1 and 9 (343 to 561 mPa.s), runs 2 and 10 (484 to 571 mPa.s) and runs 3 to 11 (477 to 546 mPa.s). This would mean that at high S5200, more SAN chains are soluble in the continuous phase, as it is concluded by the other study presented in paragraph 1.2.2 of this chapter.

The serum viscosity does not appear to be directly responsible of the CPP viscosity, even it shows that it increases with the presence of soluble SAN chains.

It can be noticed that the standard runs (table A3.15) gives the lowest serum viscosities and CPP viscosities.

As a conclusion, the length and the number of SAN chains seems to act on the viscosity of the resulting CPP product, whereas the majority of these polymer chains are inside the particles.

2.3.4. Particle Size Distributions

The volume particle size distributions measured with the Coulter LS230 device are presented in figures A3.24 to A3.31 of Annex 3. The Sauter mean diameters (D[3, 2]) calculated from these distributions are presented in tables A3.11 to A3.15.

Figure 3.14 shows the volume particle size distribution of the standard sample n°31. The Sauter diameter is found to be equal to 0.9 µm (table A3.15) but the size distribution shows clearly a bimodal distribution : a main population with sizes between 0.5 and 5 µm with a maximum at 1.8 µm, and a second population of small sizes from 0.05 to 0.5 µm with a maximum at 0.2 µm. These small particles are the primary particles produced in the system and the particles coming from the seed. Nevertheless, the seed particles represent only 0.4 wt-% of the particles produced in the reactor. It must also be noticed that the drawback of laser light scattering is that big particles are hiding the smaller ones and therefore the information on small particles is less accurate. Nevertheless, the data are more accurate with the Coulter LS320 than with the Malvern MS100, which besides does not detect these small particles (see figures A3.5.a and b).

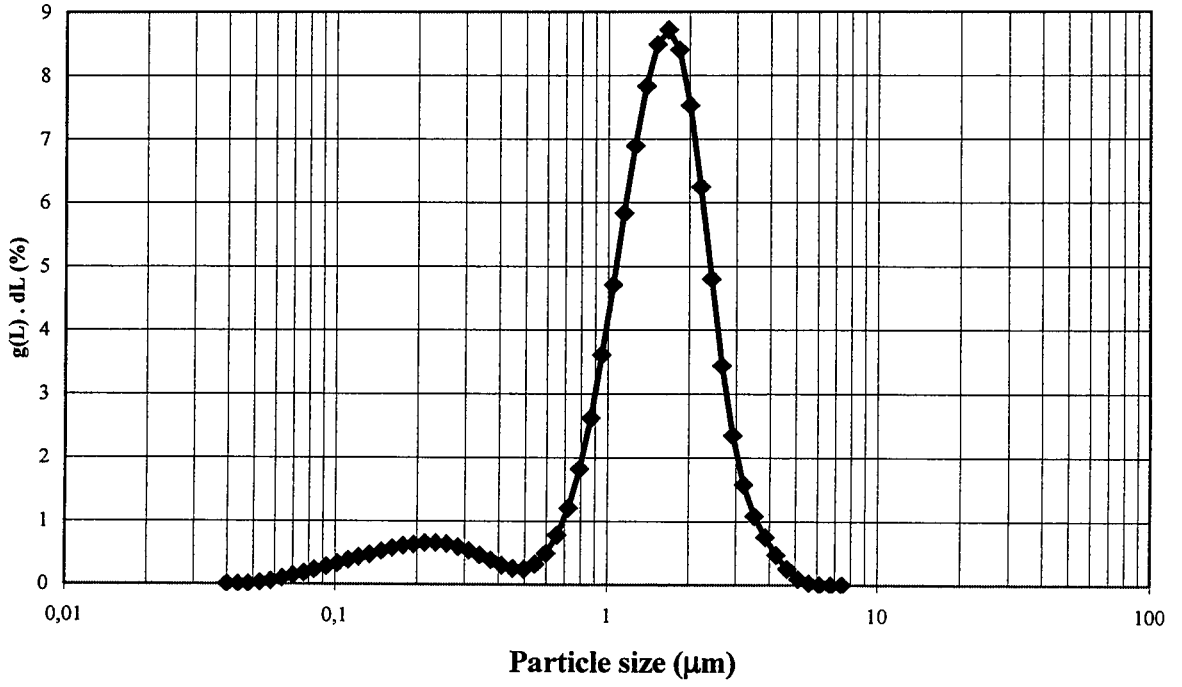

Figure 3.14 : Volume particle size distributions of run n° 31 done with standard conditions (0.30 wt-% NDM, 0.15 wt-% T27, T=130°C, 2 wt-% S5200 and Sty/AN = 70/30

The most important point noticed concerning the influence of the experimental conditions is the major effect of Sty/AN ratio on the particle size and on particles stability.

The recipes containing low styrene (Sty/AN = 60/40) give quite stable copolymer polyol lattices. The Sauter diameters are in a range 0.5 –1.6 µm (tables A3.11 and A3.12). Nevertheless, as

shown on figures A3.24 to A3.31 of annex 3, the volume particle size distributions were not monodisperse, as actually, the two distributions seen in the standard run are present with particles of larger sizes. Indeed, the majority of particle volumes is between 0.6 and 5 µm with a maximum at around 1.7-2 µm and a small population was in the range 0.05-0.6 µm. Nevertheless an irregular population appears on particular samples from 5 to 70 µm. These high particular sizes were observable on samples that were less stable than the others. For instance, in figure A3.24 of Annex 3, presenting three runs obtained with low S5200 and low NDM, a hazy population appears from 5 to 40 µm. These samples are noticed to be poorly soluble in the different solvents used to analyze the samples (THF/NMP and DCM). Moreover, the sample coming from run n° 8 have a thin layer of solid at the bottom of the vessel and as shown on figure A3.26, the particle sizes reach 70 µm. It can be noticed that all these samples had the particularity to present high viscosities and high molecular weights.

However, these high particle sizes were suspected to result from some artifacts given by the apparatus, that is to say, actually, from smaller particles that are agglomerate. SEM pictures allow to answer to this question and to observe the shapes of the particles.

There is a clear difference between the pictures of sample n° 11 and pictures of samples n° 4, 5 and 10. Indeed, on the SEM picture of sample n° 11 (figure A3.35 of annex 3), for which there is only a very small population from 4 to 6 µm on figure A3.37, the particles were quite perfectly spherical, and all the particles appeared to be smaller than 1.2 µm.

On pictures from samples n° 4, 5 and 10 (figures A3.32 to A3.40) however, the particles are not spherical, but look like agglomeration of smaller particles, and particularly for both runs n°4 and n°10, done with low NDM : the particles look like to be stuck with each other. Concerning the picture of sample n°5 (figure A3.44), at high NDM, it is observable that the particles grow by absorbing smaller particles but the resulting particles had clear spherical shapes, compared to the two previous samples. Nevertheless, the population of particles that appears between 10 and 20 µm on the distribution of figure A3.25 may also result from agglomeration.

The recipes containing high styrene (Sty/AN=80/20) give mostly unstable copolymer polyols. The Sauter diameters are in the range 1.3 – 6.4 µm (tables A3.13 and A3.14). However, as it can be seen on figures A3.28 to A3.31, the volume particle size distributions are also polydisperse.

A small population of particles between 0.05 and 1 µm is observable only on runs n° 19, 21 and 22 (figures A3.29 and A3.30). All the other distributions do not show the presence of small particles, but as it can be observable on the SEM pictures from samples 18, 19, 26 and 27 (figures A3.36 to A3.39), there is a wide variety of particle sizes and particularly big particles reaching sizes of 20 µm for instance on figure A3.36 (run n° 18) and on figure A3.37 (run n°19). These large particles hide the smaller ones that could not be observable by laser light scattering. Nevertheless, the particle shapes are quite spherical and do not look like the particles produced by runs n° 4 and n° 10.

The sizes larger than 30 µm on volume particle size distributions may be due to particle agglomerations. Furthermore, the fact that big layer of solids are observable at the bottom of the vessels containing samples n°18 and 19 may be due to the instability of the particles, which agglomerate with each other, but also to the sedimentation of these big particles.

The samples that are the most stable, and whose volume particle size distributions are similar to the one of the standard sample, are realized with low styrene, high NDM and high temperature.

Increasing the precursor stabilizer concentration seems also to stabilize the particles of runs done with low styrene as it can be seen comparing figures A3.24 and A3.25, and figures A3.26 and A3.27, as it reduces the quantity of high particle sizes and slightly the values of the Sauter mean diameters (Tables A3.11 and A3.12). Nevertheless, with high styrene, increasing S5200 concentration is not enough to stabilize the particles even if a small decrease of the Sauter mean diameter is observable (tables A3.13 and A3.14).

With low styrene content, increasing the chain transfer agent concentration decreases the quantity of unstable big particles as it can be seen for instance comparing figures A3.24 and A3.25, and figures A3.26 and A3.27. Nevertheless, with high styrene content, the effect of NDM concentration seemed to be slightly the opposite as the Sauter diameters are lower for low NDM (tables A3.13 and A3.14). Indeed, the stabilizer (grafted SAN chains) is more soluble in the continuous phase in these conditions and therefore does not stabilize enough the particles.

The temperature and the initiator concentration do not seem to have a significant influence on the particle size distributions. Nevertheless, the three runs that were not done, as they were too unstable, were run with low T27, low temperature and low NDM.

Moreover, as it was seen in the preliminary studies part, the volume particle size distributions of unstable samples have variations as a function of the time showing a succession of agglomerations and nucleations of particles.

Furthermore, the Sauter mean diameter does not allow describing the particle sizes as these distributions are at least bimodal, but it gives an order of magnitude for the particle sizes.

2.3.5. Grafting

The results concerning the measurement using LC-UV of the weight percentage of SAN grafted in whole CPP, in solids and in SAN chains soluble in the serum are presented in tables A3.16 to A3.20 of annex 3. Some chosen LC-UV chromatograms of grafted SAN are presented in figures A3.41 to A3.49 of Annex 3.

On the chromatograms, the % Graft is split into high molecular weights portion (HMW) in the range 15 –18.45 min and low molecular weights portion (LMW) in the range 18.45-21 min. The LMW is very similar to that of seed, i.e. low styrene containing with a lot of grafting. The HMW graft is considered to be the real graft formed during the process.

It is noticed that the samples resulting from runs 2, 4, 6 and 22 are not completely soluble in DCM. Therefore, some very long chains are not represented in the resulting LC chromatograms and the grafting is therefore over evaluated.

The % graft measured in the solids and in the whole CPP are similar as the quantity of SAN in the serum phase is very low compared to the quantity of SAN inside particles.

The major influence of the process conditions results from the NDM concentration. As shown on figure 3.15 below, with the same experimental conditions, high NDM gives lower grafting with relative decreases from 16 to 63 %.

This phenomenon is easily observable in figures A3.41 between runs 2 and 3 : the LMW portions of run 2 (LMW = 5.8 %) is almost twofold greater than the one of run 3 (LMW = 2.3 %). But the HMW portion is threefold greater (38 % vs. 13.6 %).

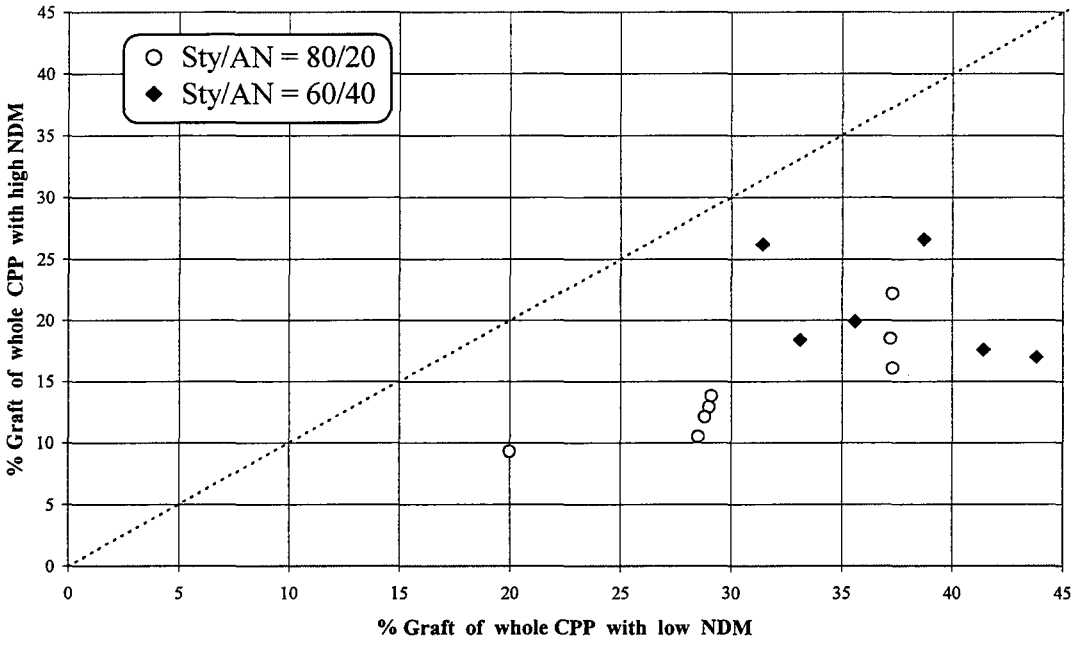

Figure 3.15 : Influence of the NDM concentration on % graft of whole CPP

The same phenomenon appears on figures A3.42 to A3.49. It is observed that the stability of the produced CPP is related to the quantity of HMW SAN grafts. Indeed, runs n°23, 25, 27, 29 and 30 seen on figures A3.45, A3.46, A3.48 and A3.49, made with high styrene and high NDM are all unstable with a more or less important layer of solid in the bottom of the vessels, that is to say, particle agglomeration and sedimentation. On these chromatograms, the HMW portion is less than for runs 22, 24, 26 and 28 done with low NDM. In unstable runs, there is not enough grafted SAN produced to stabilize properly the particles. Besides, a comparison of runs 29 and 30, made under the same conditions, gives both unstable CPPs but with slight differences. Indeed, run n°30 seems more stable with a thinner layer of solid in the bottom of the vessel than run n°29. It appears (figures A3.48 and A3.49) that a slightly bigger peak of HMW was present on the chromatogram of run n°30.

The Sty/AN ratio has also an important influence. Figure 3.16 shows that when the styrene ratio increased, the %Graft decreased from 3 to 47 % relative. There is only one couple of runs which does not follow this evolution : runs n° 6 and 20.

Figure A3.47 of Annex 3 shows the chromatograms of run n°10 (Sty/AN=60/40) and run n°24 (Sty/AN=80/20) done under the same conditions (low NDM, high T27, low T and high S5200). It appears clearly that the HMW portion of run 10 is greater than the one of run 24, but the LMW portions are quite similar. Both curves are compared with a standard HL400 run, which has an important but smaller HMW peak.

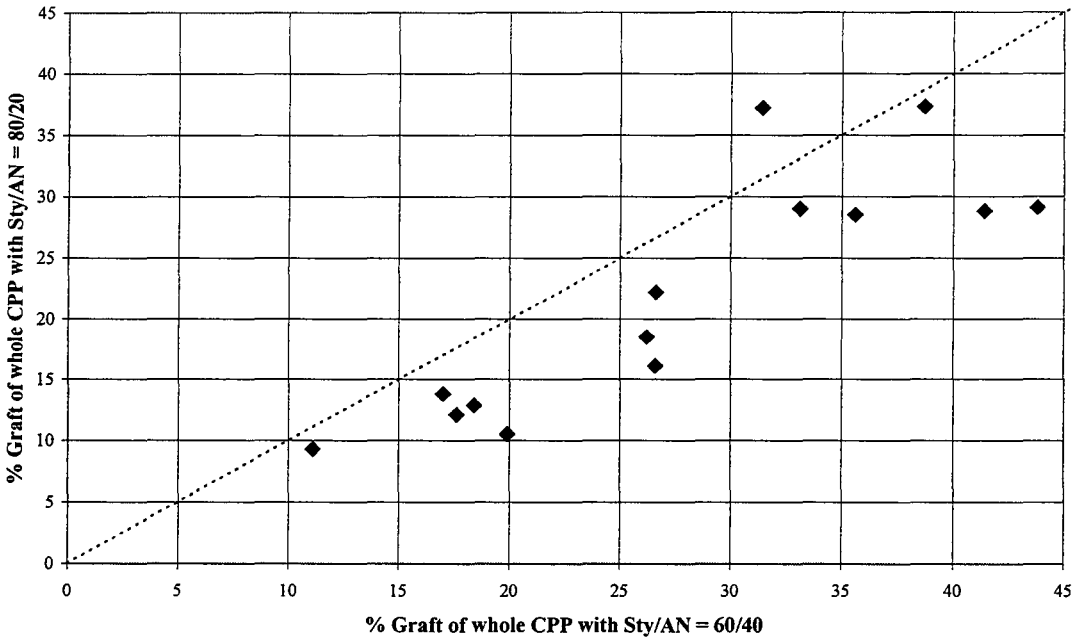

Figure 3.16 : Influence of the Sty/AN ratio on the % Graft of whole CPP

Moreover, figure 3.17 shows that increasing the T27 concentration provides a relative increase of the %Graft of the whole CPP from 8 to 100 %. For instance, the figure A3.44 of Annex 3 shows the chromatograms of runs 9 and 11. The HMW and the LMW areas of run 11 (high T27) are clearly greater than the ones of run 9 (low T27).

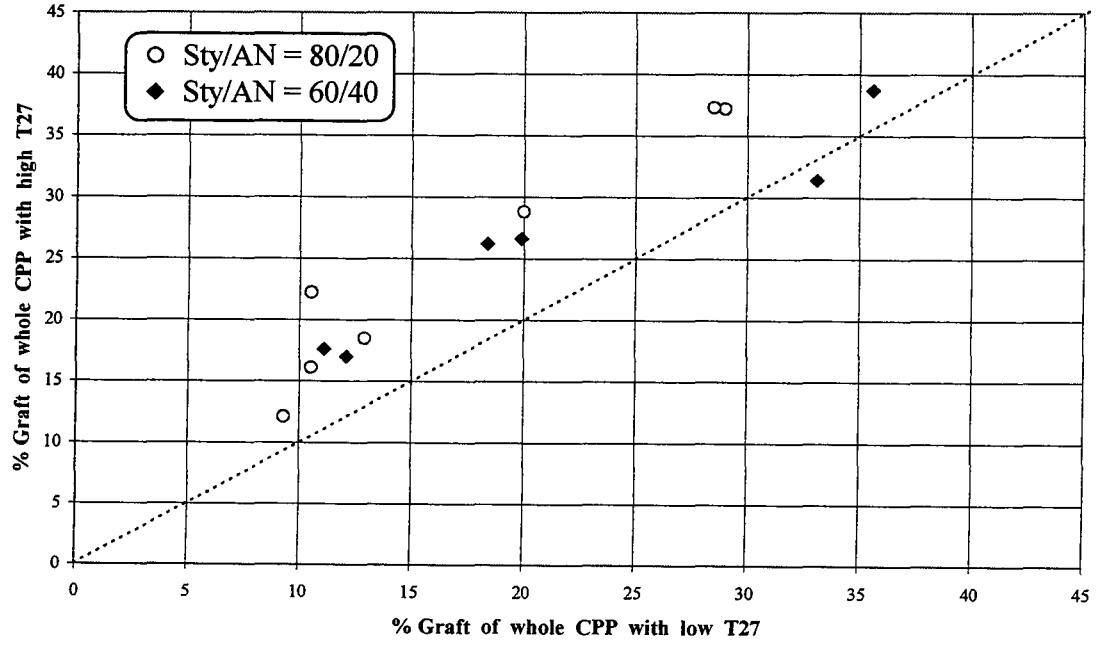

Figure 3.17 : Influence of the T27 concentration on % graft of whole CPP

Furthermore, figure 3.18 presents the influence of the temperature : an increase of temperature increases the grafting level in most cases. Only two points do not follow this evolution. These are the couples of runs 2-6 and 10-14. Anyway, as said before, for runs 2 and 4, the samples analyzed are hardly dissolved in DMC, which may introduce inaccuracy in the measurements.

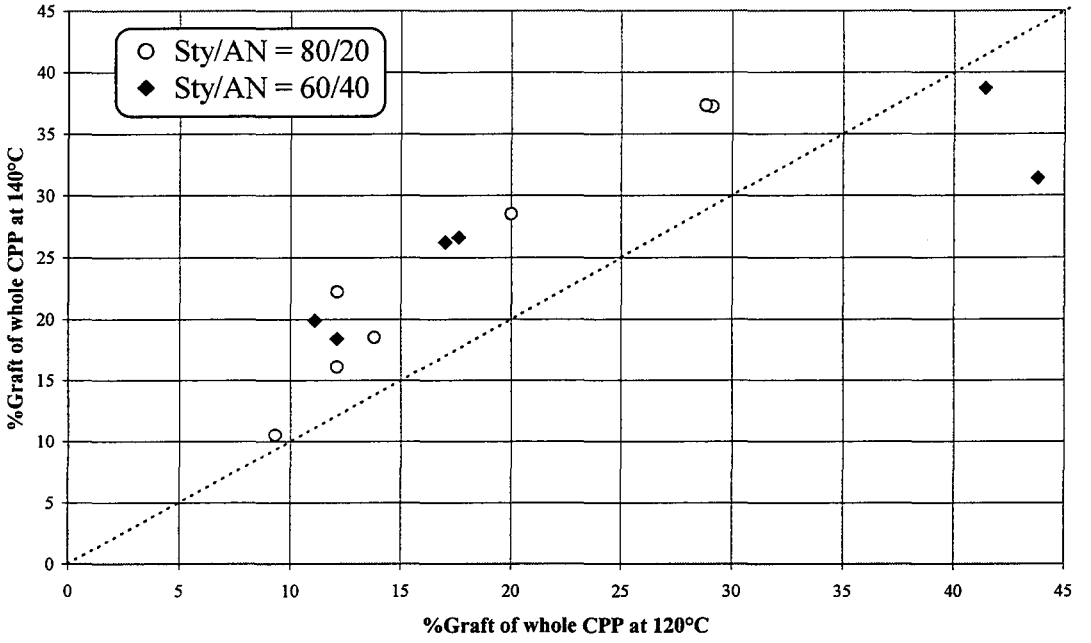

Figure 3.18 : Influence of the temperature on % graft of whole CPP

Nevertheless, the important remark that can be made is that the concentration of S5200 has no influence on the grafting level, as shown on figure 3.19. However, it is clear that for high S5200 contents the resulting CPPs are more stable as observed studying the particle size distributions.

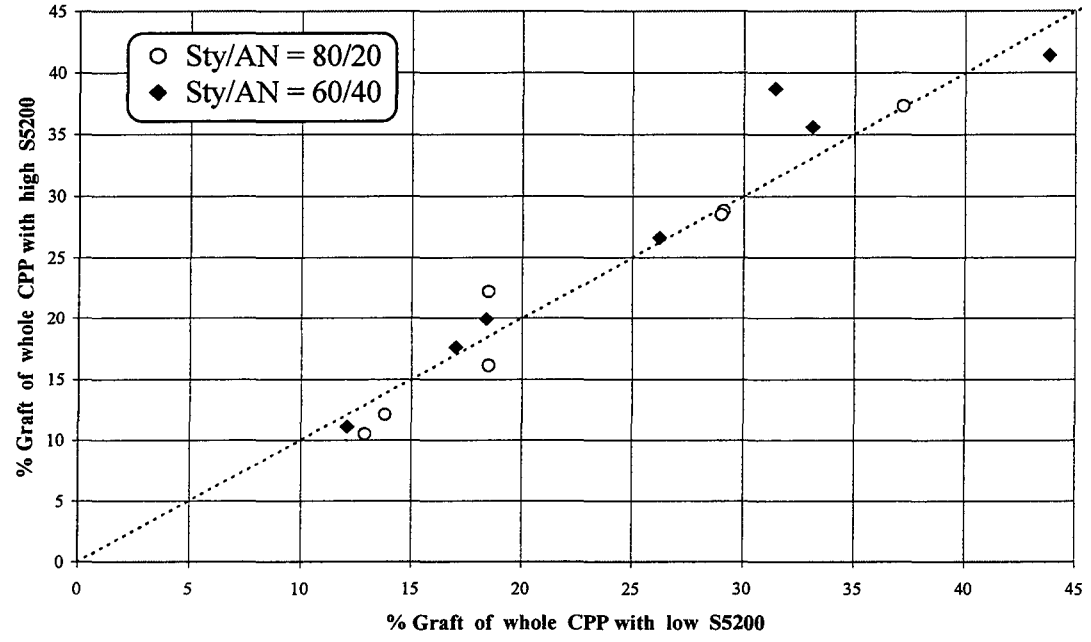

Figure 3.19 : Influence of the S5200 concentration on % graft of whole CPP

The error on the measurement of the percentage of grafted SAN chains soluble in the serum is estimated to be ± 20 % relative. A greater proportion of SAN chains are grafted in SAN chains soluble in the serum phase (from 45 % to 85 %). The fact that they are grafted with polyol or S5200 increases their solubility in the continuous medium. The soluble grafted SAN corresponds actually to the LMW highly grafted SAN, which contains grafted chains from the seed.

The %graft in the serum evolves in the same way that the %graft of whole CPP versus the quantity of NDM and T27. Nevertheless, considering the rather important inaccuracy on the measurement (due to the solid/serum separation) it is not possible to conclude on the influence of Sty/AN ratio and the temperature. However, the concentration of S5200 does not have remarkable influence on the %graft of soluble SAN.

As a conclusion, low NDM, low styrene, high T27, and high temperature increase the quantity of HMW grafts and provide better stabilized copolymer polyols. The second important point deals with the precursor stabilizer S5200 that does not influence the percentage of grafted species.

2.3.6. Polymer composition

Styrene/Acrylonitrile composition

The composition of SAN poly(styrene-co-acrylonitrile) of the solid phase was determined by ^{1}H NMR while that of the chains dissolved in the serum was determined by ^{13}C NMR. The results are presented in Annex 3 (tables A3.21 to A3.25). Some examples of the chromatograms, which provided these data, are shown in figures A3.50 to A3.52. The compositions of the two types of SAN macromolecules are almost similar, and therefore, some measurements were not done using both the methods. Besides, this composition must be fixed by the composition of the premix.

Considering that the accuracy of the method is estimated to be ± 30 %, the measurements obtained for recipes using a ratio Sty/AN = 60/40 give the results that were forecasted, as the measurements deviates from the 60/40 reference of 5 % maximum in the solids and of 10 % in the serum. Nevertheless, three measurements done in the serum deviates from 20 to 30 % from the 60/40 reference (runs 9, 10 and 11 of table A3.22). It is still in the range of the accuracy of the method but these measurements may be suspicious as the other series are better. With recipes containing Sty/AN =80/20, the deviations with the reference are bigger but less than 10 %.

Polyol grafted to solid SAN

The results concerning the weight percentage of polyol in the solid CPP measured by ^{1}H NMR are presented in tables A3.21 to A3.25 of annex 3. The values are in a range from 1.7 wt-% to 4 wt-% with an accuracy of ± 30 %.

As shown in table A3.26, the results obtained by ^{1}H NMR are in agreement with those obtained by the NIC-derivatization method followed by GPC-fluorescence analysis.

Actually, the GPC-fluorescence method gives meq OH/g solids, which are converted into wt-% polyol by multiplying it by the equivalent weight of the alcohol branch of S5200 that is to say by

1500 g/mol, as S5200 is composed of three polyol chains of 3000 g/mol and contains 6 OH groups.

Some examples of chromatograms are given in figure A3.64 of annex3. They may be compared to the chromatograms obtained with the LC-UV method (figures A3.42, A3.43 and A3.45). The first macromolecules that come out of the column are the biggest ones. The peak observed after 6.75 min of retention time corresponds to free polyol, which is not removed from the solids in spite of the several washes. It can be noticed, comparing runs n° 22 and n° 23 done with Sty/AN=80/20 that for high NDM the high molecular weights (HMW) (4-6 min) are considerably reduced and the low molecular weights (LMW) (6 – 7 min) are rather important. However, for Sty/AN=60/40 (runs n° 5, 6 and 7), the HMW % are bigger with longer chains and particularly for run n°6 obtained with low NDM. For runs n° 6 and n° 7 the increase of the NDM concentration reduces the HMW grafted macromolecules.

The GPC-fluorescence results are higher than the ^{1}H NMR ones; nevertheless, due to competitive grafting mechanisms (allyl monol grafting and polyol H-abstraction) the real value must be lower bringing the fluorescence data closer to NMR data. But, this can also be due to the fact that some free polyol solvent may be still present in the solids (see runs n° 6, 7 and 22 of figure A3.53). This was the reason why the measurement of the quantity of OH groups grafted to solids by NIC-derivatization and GPC-fluorescence was abandoned, as it took a lot of time and effort to make solids really polyol free.

Moreover an increase of the S5200 concentration, or of the quantity of acrylonitrile in the premix should increase the grafting and therefore the wt-% of polyol in the solid phase, but there is not significant effect of these process conditions. Two possibilities can be proposed : the method is not enough accurate and reliable or S5200 is not grafted on the particle surface.

2.3.7. SAN dissolved in serum : amounts and molecular weights

The number and weight molecular weight distributions of SAN chains soluble in the serum were obtained by GPC-UV. As explained in chapter 2, the UV signal was cut at the retention time corresponding to 3000 g/mol in order to avoid integration of oligomers and antioxidant. However as shown in figures A3.54 to A3.59, this cuts the molecular weight distributions almost at the middle of the SAN peaks. Therefore, the average molecular weights presented in tables A3.27 to A3.31 of annex 3 are overestimated because they are calculated considering only the area of the peak corresponding to molecular weights higher than 3000 g/mol. Besides, a relative error of ± 50 % was estimated on the measurement of the number and weight average molecular weights.

Furthermore, as the amount of SAN dissolved in serum phase is calculated by integrating the area of these peaks using an external SAN standard (32 wt-% AN), this quantity is underestimated. Moreover this method is much more dependant on the way the serum was isolated than on the fact that the GPC-UV chromatograms were calibrated on SAN (32 wt-% AN). With a pure polyol theta solvent, there are concentrations of 0.2-0.5 wt-% SAN in serum whereas with the classically used 80/20 hexane/EtOAc mixture, concentrations of 1-1.5 wt-% are measured.

Here, the measurements are made with 80/20 hexane/EtOAc. The results presented in tables A3.27 to A2.31 of Annex 3 show that the quantity of soluble SAN varies from 0.7 to 2 wt-% and the relative error is estimated to be ± 20 %. The only points that could be noted, are those corresponding to the influence of the Sty/AN ratio and the temperature : more SAN is dissolved

in the serum phase with 80% styrene than with 60 % styrene, and more at 140°C than at 120°C. It follows the fact that with high styrene and at high temperature, the SAN copolymer is more soluble in the continuous phase.

Nevertheless, these distributions confirm that the first population of molecular weights observed in the MWDs of whole CPPs corresponded to SAN soluble in the continuous phase. Indeed the molecular weights of the SAN peak that are cut are in the estimated range of 1000-10000 g/mol with a maximum around 2000-4000 g/mol.

Comparing figures A3.56 and A3.57 to figure A3.59 showed that with high styrene (Sty/AN = 80/20) the SAN chains that are soluble in the continuous phase are longer than with low styrene (Sty/AN = 60/40). Between samples n° 22 and n° 23 (figure A3.58 and A3.59), an increase of the NDM concentration reduces the molecular weights. Besides on the weight molecular weight distribution of the sample n° 23, it is observed that this distribution may be composed of at least two populations of molecular weights : a peak with a maximum at around 3000 g/mol and a smaller peak at around 10000 g/mol corresponding to the second population observed on whole CPP molecular weight distributions.

2.4. Relationships between the different CPP properties

2.4.1. Estimation of the number of S5200 grafts per grafted SAN chain

In order to determine roughly the number of grafts S5200 per grafted SAN chain, it is possible to find a relationship between the percentage of SAN chain grafted, obtained by LC-UV, to the wt-% of polyol grafted to the solids, obtained by ^{1}H NMR.

Let us consider the SAN chains of molecular weight M_{SAN} and the grafted SAN chains of molecular weight (M_{SAN} + n M_G) with n the number of grafts of weight M_G = 10 000 g/mol (assuming that the SAN chains have the same length).

The percentage of high molecular weight grafted SAN macromolecules can be defined as follows:

$$\%HMW = HMW / (HMW + LMW + Ungrafted\ SAN), \tag{3.4}$$

which is measured by LC-UV. Only the HMW part of the grafting is considered here as the LMW part is mostly soluble in the continuous phase.

Then, the wt-% of polyol is approximately equal to :

$$wt\%\ \ polyol \approx (\%HMW) \cdot n \cdot M_G / \bar{M}_n \,. \tag{3.5}$$

This allows to calculate the average number of grafts S5200 per grafted chain, assuming that there is no natural grafting :

$$n \approx \frac{(wt\%\ \ Polyol)}{\%\ HMW} \cdot \frac{M_G}{\bar{M}_n} \tag{3.6}$$

Therefore, table 3.6 shows that there would be less than one graft S5200 per grafted SAN chain.

It should be noticed that if actually 50 % of the grafting is coming from the natural grafting, these numbers might be doubled providing a mean of 1-2 grafts per grafted SAN chain.

Nevertheless, the measurements of the wt-% polyol and the grafting level are not enough accurate to be sure of these results. It gives just a rough indication. Moreover, the wt-% polyol,

as seen before, does not vary significantly for different experimental conditions. This does not allow giving conclusions concerning this data.

Table 3.6. Estimation of the number, n, of grafts S5200 by grafted SAN chain from experimental data

Run	NDM	T27	T	S5200	Sty/AN	Mn g/mol	wt-% polyol	% HMW	n
1	1	-1	-1	-1	-1	27100	1,59	9,8	0,44
2	-1	1	-1	-1	-1	51600	1,77	38	0,24
3	1	1	-1	-1	-1	25500	2,03	13,6	0,38
4	-1	-1	1	-1	-1	48000	3,14	26,9	0,56
5	1	-1	1	-1	-1	25800	2,01	14,8	0,35
6	-1	1	1	-1	-1	32000	4,25	21,9	0,62
7	1	1	1	-1	-1	24500	3,08	20,7	0,36
9	1	-1	-1	1	-1	28500	1,7	9	0,54
10	-1	1	-1	1	-1	51000	3,1	34,7	0,46
11	1	1	-1	1	-1	27600	2,4	14	0,47
12	-1	-1	1	1	-1	41500	2,9	31,5	0,38
13	1	-1	1	1	-1	26200	2,3	17,2	0,35
14	-1	1	1	1	-1	32300	4,1	32,7	0,40
15	1	1	1	1	-1	24500	3,5	22,8	0,38
16	-1	1	-1	-1	1	38000	2,8	26,2	0,41
17	1	1	-1	-1	1	14500	2,7	10,8	0,36
18	-1	-1	1	-1	1	35300	2,8	26,2	0,38
19	1	-1	1	-1	1	13400	2,5	10,1	0,33
20	-1	1	1	-1	1	30200	3,5	32,9	0,32
21	1	1	1	-1	1	15000	3,4	14,6	0,35
22	-1	-1	-1	1	1	43800	2,01	16,8	0,52
23	1	-1	-1	1	1	14000	2,37	5,8	0,57
24	-1	1	-1	1	1	42700	2,5	23,4	0,46
25	1	1	-1	1	1	17500	2,5	7,1	0,62
26	-1	-1	1	1	1	40000	2,5	23,5	0,43
27	1	-1	1	1	1	16800	2,2	6	0,62
28	-1	1	1	1	1	36500	3,1	30,3	0,37
29	1	1	1	1	1	17600	2,8	9,2	0,54
30	1	1	1	1	1	16300	3,7	17,3	0,35
31	0	0	0	0	0	31200	2,50	16,1	0,48

2.4.2. Relationships between grafting, viscosity and molecular weights

The viscosity of CPP increases with an increase of the T27 concentration, a decrease of the NDM concentration and with an increase of the acrylonitrile content. The influence of the temperature is not clear and there is no effect from the precursor stabilizer concentration.

The same conditions (low NDM, high T27, Sty/AN = 60/40) produced the longer SAN chains and give the highest average molecular weights.

The main effect on the grafting results also from the NDM concentration : low NDM gave the highest grafting levels. Increasing the T27 concentration increases also the HMW and the LMW grafting. Nevertheless, the grafting level increases slightly also by increasing the acrylonitrile content and by increasing the temperature.

Therefore, increasing the molecular weight increases the percentage of grafting. Indeed, if, for instance, the molecular weight is infinite it would mean that there is only one chain and automatically this would mean 100 % grafting.

High T27 and high temperature increases the number of primary radicals and therefore the number of SAN chains. With natural grafting, the polyol grafts initiate the polymerization with styrene and acrylonitrile. Therefore, SAN chains grafted with polyol start with low molecular weight but, by recombination and chain transfer to polymer, the percentage of grafted chains grows as these terminations reduce the number of chains and increase the number of grafted species. Nevertheless, transfers to NDM reduce the chain lengths and do not decrease the number of SAN chains and therefore decrease the percentage of grafted SAN chains.

Moreover, the styrene/acrylonitrile ratio has an influence on the monomer conversion, on the solubility of the SAN copolymer and therefore on the locus of polymerization. The more there is styrene, the more the polymerization is shifted into solution rather than inside of the particles and thus the molecular weights and the monomer conversions are lower.

Furthermore, as seen in the preliminary studies, the more there are grafted SAN chains in the solid, that is to say that the percentage of grafted SAN chains increases, the more the viscosity of CPP increases too.

The most stable CPPs, considering the stability of particle size distributions, are also obtained at Sty/AN = 60/40, high temperature and high T27 concentration, but for high NDM concentration. Too long SAN chains (at low NDM, Sty/AN =60/40) or too short SAN chains (at high NDM and Sty/AN = 80/20) give the less stable particle dispersions with a lot of agglomerations.

2.4.3. Depletion stabilization

The analysis of the CPP properties clearly shows that the precursor stabilizer S5200 concentration does not act as much as it was forecasted, even if its presence improves the stability of the resulting product.

Indeed, as observed in this chapter, increasing the S5200 concentration or the styrene/acrylonitrile ratio, that should increase the grafting, have not any influence on the wt-% polyol. The same observation is made concerning the influence of the S5200 concentration on the grafting percentage. However, it may slightly increase the average molecular weights.

A possibility is that the SAN chains grafted by S5200 stabilize more the particles by depletion stabilization than by steric stabilization. Indeed, Napper (1983) noticed that depletion stabilization differs from steric stabilization in that stability is imparted not by attached polymer

but rather by macromolecules that are free in solution. According to Feigin & Napper (1980), this stabilization may be generated simply by dissolving non-ionic polymer into the dispersion medium. Stability arises from the depletion of the concentration of free polymer between the surfaces of the particles when they are in close proximity. Closer approach of the particles can only be achieved by a further depletion of the segment concentration between particles. In a good solvent, this is energetically unfavorable. Even closer approach of the particles, however, results in the almost complete exclusion of polymer molecules from between the surface. Almost pure solvent thus occupies the interparticle space. Closer approach is now favored energetically because it results in mixing of almost pure solvent with polymer solution. This can result in depletion flocculation.

Actually, according to Fleer et al. (1988), the depletion attraction increases with the polymer concentration, but passes through a maximum. In very concentrated solutions the depletion attraction may again become too small to induce flocculation and the system is again stable. This phenomenon was called depletion stabilization but as the stability is not a consequence of some repulsive barrier but simply of too weak an attraction, the term depletion restabilization would be more appropriate.

Nevertheless, in all these experiments, as a "KOH-polyol" was used with T27 initiator, an important part of the grafting may come from natural grafting. In order to study very specifically the influence of S5200 it would be necessary to be sure that there is the less natural grafting as possible. Using "DMC-polyol" and azo(bis-methylbutyronitrile) (AMBN) as initiator would be therefore a way to study more specifically whether S5200 acts by depletion stabilization.

Conclusion

This experimental study shows the great importance of the ratio of monomers (styrene/acrylonitrile), and the concentration of the chain transfer agent, NDM, in the process. These two experimental conditions, by acting on the length of the polymer chains and their solubility in the continuous phase, control the stability of the resulting particles and the viscosity of the resulting copolymer polyol lattices. It appears that the viscosity is linked to the size of the polymer chains and to the grafted species inside the particles and to the stability of the particles.

The measurements on the serum give important information on the process but a lot of inaccuracy on the measurements results from the method used to separate the solids from the continuous phase.

This study shows also the complexity of the system that is needed to elaborate a representative model of the whole process. The multimodal molecular weight and particle size distributions and the presence of natural grafting are also important limitations.

Moreover, the presence of natural grafting does not allow to study correctly the influence of S5200, which seems to stabilize the particles by depletion stabilization either than by steric stabilization.

CHAPTER 4 : MODELING

INTRODUCTION **157**

1. MAIN ASSUMPTIONS **157**

1.1. STYRENE-ACRYLONITRILE COPOLYMERIZATION 157
1.1.1. Initiation on styrene and acrylonitrile *157*
1.1.2. Homo-polymerizations of styrene and acrylonitrile *157*
1.1.3. Styrene / Acrylonitrile Copolymerization *157*
1.1.3. Transfers *161*

1.2. MONOMER UNITS 162

1.3. GRAFTING 163
1.3.1. Copolymerization of styrene and acrylonitrile with the vinyl bond of S5200 ..... *163*
1.3.2. Natural Grafting of S5200 and Polyol *164*
1.3.3. Terminations with grafted species *165*
1.3.4. Notations for Grafting Modeling *165*

1.4. THERMODYNAMICS 166

1.5. CAPTURE BY PARTICLES 167
1.5.1. Absorption *167*
1.5.2. Precipitation *167*

1.6. PARTICLE STABILIZATION : MODEL FOR AVERAGE PARTICLE SIZE 168

1.7. KINETIC SCHEME 170
1.7.1. Polymerization in the continuous phase *170*
1.7.2. Polymerization inside the particles *172*

2. THE DEFINITION OF THE SYSTEM **173**

2.1. BALANCE ON THE TOTAL CONCENTRATIONS OF THE SPECIES IN THE REACTOR ... 173

2.2. BALANCE ON THE CONCENTRATIONS OF FREE SPECIES IN THE REACTOR 174
2.2.1. Definition of the concentrations in the continuous phase and inside the swollen particles *174*
2.2.2. Balance on free acrylonitrile in the reactor *174*
2.2.3. Balance on free styrene in the reactor *175*
2.2.4. Balance on free G (the precursor stabilizer S5200) in the reactor *175*
2.2.5. Balance on free solvent (polyol) in the reactor *175*

2.2.6. Balance on Chain Transfer Agent *176*
2.2.7. Balance on Initiator in the reactor *176*
2.2.8. Global composition of the dead polymer *176*

2.3. BALANCE ON RADICALS, DEAD POLYMER CHAINS AND MOMENTS IN THE REACTOR 177

2.4. CALCULATION OF DATA TO BE COMPARED TO THE MEASUREMENTS 179
2.4.1. Average molecular weights *179*
2.4.2. Weight % of solids in stripped CPP and residual quantities of reactants *182*
2.4.3. Composition of the SAN copolymer *183*
2.4.4. Quantity of SAN copolymer dissolved in the continuous phase *183*
2.4.5. Grafting quantification *183*

3. ESTIMATION OF THE STEADY STATE REGIME 185

CONCLUSION 187

Introduction

This chapter presents the model that is chosen in order to predict the different physical properties of copolymer polyols that can be measured as a function of the process conditions presented in the experimental study shown in chapter 3.

The first part will be devoted to the different assumptions used to elaborate the model. These assumptions will concern the styrene-acrylonitrile copolymerization, the grafting mechanisms, the thermodynamics, the absorption, the precipitation and the particle stabilization. They will lead to a kinetic scheme. Then, the second part will present the system of equations describing the reactor state resulting from these hypotheses. Finally, the third part will describe how the system will be solved in order to simulate the whole process.

1. Main Assumptions

1.1. Styrene-Acrylonitrile copolymerization

1.1.1. Initiation on styrene and acrylonitrile

The kinetic constants of initiation of the primary radicals on styrene and acrylonitrile monomers cannot be identified as the consumption of monomers following these reactions is negligible in front of the consumption due to the propagation reactions. Therefore, arbitrary values are chosen and these kinetic constants are assumed to be equal to the propagation ones of the respective homopolymers :

$k^c_{RA} = k^c_{pAA}$ and $k^c_{RB} = k^c_{pBB}$ in the continuous phase,

and $k^p_R = k^p_p$ and $k^p_{RB} = k^p_{pBB}$ inside the particles.

1.1.2. Homo-polymerizations of styrene and acrylonitrile

Different data related to the kinetics of propagation of acrylonitrile (A) and styrene (B) are given in the literature. k_{pAA} and k_{pBB} are the kinetic rate constants for the homo-propagation of acrylonitrile and styrene respectively. According to Odian (1981), styrene and acrylonitrile undergo termination almost exclusively by coupling. k_{tcAA} and k_{tcBB} are respectively the kinetic rate constants for the homo-termination by combination of acrylonitrile and styrene. These data are summed up in table 4.1.

Poly(styrene-co-acrylonitrile) (SAN) is one of the largest volume copolymers of styrene and has physical properties adapted to many thermoplastic applications. SAN are characteristically hard, rigid, and dimensionally stable with load bearing capabilities. Indeed, poly-acrylonitrile imparts chemical resistance, better heat distortion, and improved mechanical properties. High acrylonitrile contents tend to produce a yellow polymer, and this is one of the reasons why styrene is used with acrylonitrile in the production of copolymer polyols.

Table 4.1 : Kinetic constants of homopropagation and homotermination of styrene and acrylonitrile at 120 °C and 140 °C from the literature.

Kinetic constant	Arrhenius parameters (T in K)	T = 120 °C	T = 140 °C	Unit	Reference
k_{pAA}	$1.047\ 10^5\ Exp(-3663/T)$	9.4	14.8	$m^3\ mol^{-1}\ s^{-1}$	Garcio-Rubia et al., 1985
k_{pBB}	$1.051\ 10^4\ Exp(-3557/T)$	1.2	1.9	$m^3\ mol^{-1}\ s^{-1}$	Hui & Hamielec, 1972
K_{pBB}	$1.09\ 10^5\ Exp(-3545/T)$	1.3	2.0	$m^3\ mol^{-1}\ s^{-1}$	Keramopoulos & Kiparissides, 2002
k_{tcAA}	$1.98\ 10^{11}\ Exp(-2715/T)$	$1.98\ 10^8$	$2.77\ 10^8$	$m^3\ mol^{-1}\ s^{-1}$	Keramopoulos & Kiparissides, 2002
k_{tcBB}	$1.255\ 10^6\ Exp(-838/T)$	$1.49\ 10^5$	$1.65\ 10^5$	$m^3\ mol^{-1}\ s^{-1}$	Keramopoulos & Kiparissides, 2002
k_{tcBB}	$1.255\ 10^6\ Exp(-844/T)$	$1.47\ 10^5$	$1.63\ 10^5$	$m^3\ mol^{-1}\ s^{-1}$	Hui & Hamielec, 1972

a) Reactivity ratios and propagation rate constants

This system is one of the major examples better described by the penultimate than by the terminal model of copolymerization. However the terminal model was used in our model as, according to Hill et al. (1982), there is only a small difference separating terminal and penultimate model for SAN.

Assuming a terminal mode means that the reactivity of the propagating species depends only on the terminal monomer unit. Four propagation reactions are therefore possible :

Homo-propagations :

$$A^* + A \xrightarrow{k_{pAA}} A^*$$

$$B^* + B \xrightarrow{k_{pBB}} B^*$$

Cross-propagations :

$$A^* + B \xrightarrow{k_{pAB}} B^*$$

$$B^* + A \xrightarrow{k_{pBA}} A^*$$

A and B are respectively acrylonitrile and styrene monomers and A* and B* symbolize oligoradicals terminated by acrylonitrile or styrene respectively.

Cross-propagation kinetics are generally defined in comparison with the homo-propagation ones. Two reactivity ratios are then defined :

$$r_A = k_{pAA}/k_{pAB} \tag{4.1}$$

$$r_B = k_{pBB}/k_{pBA} \tag{4.2}$$

The values of these reactivity ratios, r_A and r_B, are smaller than one and their product is closed to zero therefore SAN polymers are considered as random linear copolymers (Odian, 1981).

In most cases the copolymer composition is different from that of the copolymer feed from which it is produced as the monomers have different tendencies to undergo copolymerisation as seen in table 4.2. If f_A and f_B are the molar fractions of monomers A and B in the feed, and F_A and F_B the molar fractions of A and B in the copolymer, then (Odian, 1981) :

$$F_B = \frac{r_B f_B^2 + f_B f_A}{r_B f_B^2 + 2 f_B f_A + r_A f_A^2}, \tag{4.3}$$

$$F_A = 1 - F_B. \tag{4.4}$$

If c_A and c_B are the weight fractions of monomers A and B in the feed, and C_A and C_B are the weight fractions of A and B in the copolymer, then

$$c_B = \frac{f_B M_B}{f_B M_B + (1 - f_B) M_A}, \tag{4.5}$$

$$c_A = 1 - c_B, \tag{4.6}$$

$$C_B = \frac{F_B M_B}{F_B M_B + (1 - F_B) M_A}, \tag{4.7}$$

$$C_A = 1 - C_B. \tag{4.8}$$

Figure 4.1 shows an azeotropic point for $f_B = 0.62$ ($c_B = 75$ wt-%) for styrene with $r_A = 0.33$ and $r_B = 0.05$. A composition drift in SAN copolymers is undesirable because of the incompatibility between SAN copolymers with different compositions. Copolymer compositions other than this azeotropic point are possible by using continuous, well-mixed, stirred-tank reactors or highly recirculating loop reactors that keep the comonomer concentrations nearly constant through the reactor.

The glass transition temperature of CPP being around 80 °C, the temperatures of copolymerisation will be between 120°C and 140°C. It is therefore assumed in this model that there is no glass effect.

Table 4.2: Reactivity ratios between acrylonitrile (A) and styrene (B) in bulk and in solution polymerizations

Polymerization Process	T (°C)	r_B	r_A	$r_B . r_A$	References
Bulk	70	0.41	0.04	0.016	Arita et al., 1981
Bulk	-	0.33	0.05	0.016	Hill et al., 1982
Bulk	50	0.34	0.06	0.020	Thompson & Raines, 1959
In DMSO	60	0.30	0.17	0.051	Asakura et al., 1981
In DMSO	80	0.33	0.17	0.056	Asakura et al., 1981
In CH_3CN	60	0.33	0.15	0.049	Asakura et al., 1981
In CH_3CN	80	0.36	0.17	0.061	Asakura et al., 1981
In EtOH	60	0.46	0.07	0.032	Asakura et al., 1981
In EtOH	80	0.41	0.06	0.025	Asakura et al., 1981
In Benzene	60	0.43	0.03	0.013	Asakura et al., 1981
In Benzene	80	0.55	0.06	0.033	Asakura et al., 1981

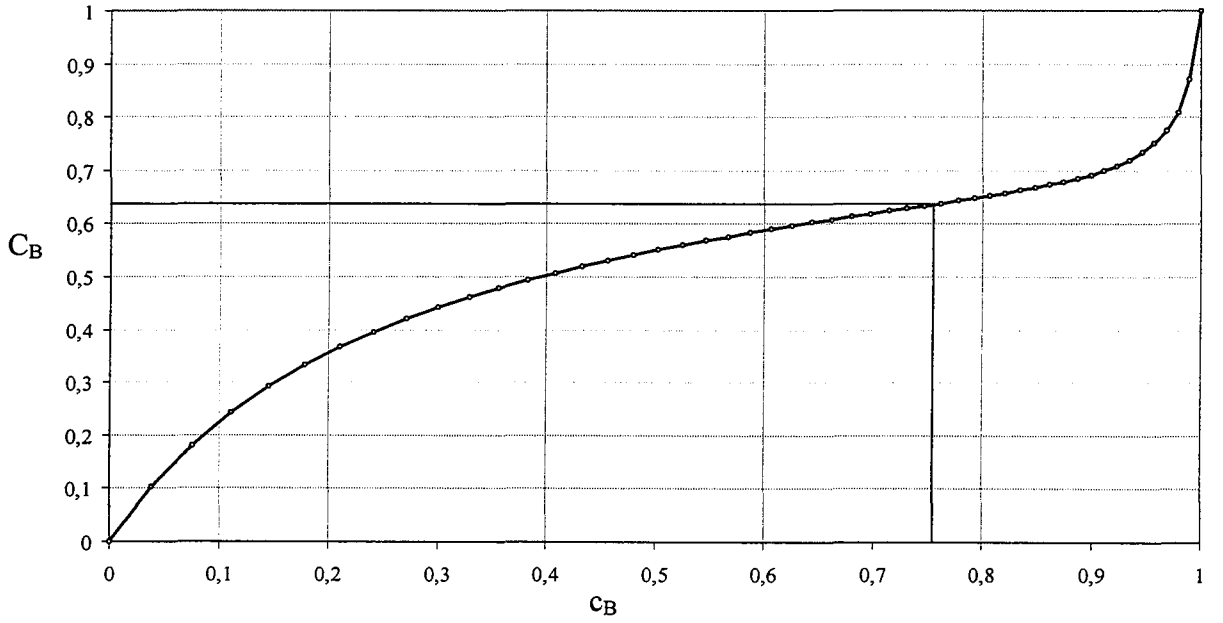

Figure 4.1 : Dependence of the instantaneous copolymer weight composition C_B on the comonomer feed c_B for radical copolymerisation of acrylonitrile- styrene system.

b) Cross-termination and gel effect

The cross-termination in the continuous phase (c) is expressed by the following relationship (Odian, 1981) :

$$k^c_{tcAB} = \phi_c \sqrt{k^c_{tcAA} k^c_{tcBB}} \tag{4.9}$$

ϕ <1 means that cross-termination is not favored, while ϕ >1 means that cross-termination is favored. The tendency towards cross-termination is parallel to the tendency toward cross-propagation in that ϕ increases as the product of reactivity ratios approaches zero, which is the case for the styrene-acrylonitrile system. Mendizabal et al. (1995) found values of ϕ in the range 10 – 70 at 60°C for this system.

The decrease of the termination rate constant due to the gel effect inside the particles has been accounted for by using an empirical expression as done by Plessis et al. (2001a, 2001b) :

$$k^p_{tcAA} = k^c_{tcAA} \cdot g \ , \tag{4.10}$$

$$\text{and } k^p_{tcBB} = k^c_{tcBB} \cdot g \ , \tag{4.11}$$

$$\text{with } g = Exp\left[-\left(gel_1 \cdot Y_B + gel_2 \cdot (1 - Y_B)\right) x_p\right]. \tag{4.12}$$

When Y_B is the weight fraction of styrene in the SAN copolymer, x_p the copolymer fraction in weight in particles swollen by the monomers and gel_1 and gel_2 are adjustable parameters of the model.

The cross-termination inside the particles was expressed by the same kind of relationship as Eq. 4.9 :

$$k^p_{tcAB} = \phi_p \sqrt{k^p_{tcAA} k^p_{tcBB}} \tag{4.13}$$

In order to simplify the model, and as cross-termination may happen in the same way in the both phases, it is considered that :

$$\phi_p = \phi_c . \tag{4.14}$$

1.1.3. Transfers

The transfers to the chain transfer agent (NDM) happen in the both phases, depending on the partitioning. The Polymer Handbook (Brandrup & Immergut, 1989) gives the following transfer reactivities :

1-Dodecanethiol (NDM) with Acrylonitrile at 50 °C :

$$R_{TA} = k_{tr,A} / k_{pAA} = 0.73 , \tag{4.15}$$

1-Dodecanethiol (NDM) with Styrene at 110 °C :

$$R_{TB} = k_{tr,B} / k_{pBB} = 26 . \tag{4.16}$$

$k_{tr,A}$ and $k_{tr,B}$ are the kinetic constants of transfer to NDM of radical chains terminated by acrylonitrile and styrene units respectively

In this model, it was assumed that the transfer reactivities were the same in the both phases in order to reduce the number of parameters to identify :

$$R_{TA}^{c} = R_{TA}^{p} \tag{4.17}$$

$$R_{TB}^{c} = R_{TB}^{p} \tag{4.18}$$

Some transfers to the polyol may happen, allowing to the polyol chains of the solvent to be grafted on SAN chains, as it will be exposed below in the grafting part.

1.2. Monomer units

The modeling of copolymerization processes uses the notion of monomeric unit in order to simplify the average molecular weights calculation. This method is applied when the two monomers have molecular weights of the same order of magnitude. Saenz and Asua (1999) used this approximation to model the copolymerization of styrene (M = 104 g/mol) and butyl acrylate (M = 128 g/mol).

Actually, in the purpose to determine the copolymer composition, the oligoradicals and the dead polymer will be noticed as follows : $A^{*}_{k,l,j}$, $B^{*}_{k,l,j}$ and $P_{k,l,j}$ are respectively oligoradicals terminated by an acrylonitrile (A) unit, a styrene unit (B) and dead polymers, having k acrylonitrile, l styrene and j polyol grafts units. However, the composition of the polymer may be simply approximated by the quantity of monomers incorporated, but it does not allow to reach the weight average molecular weights.

Nevertheless, the use of three indices requires too long computing times. Here, $M_A = 53$ g.mol^{-1} and $M_B = 104$ g.mol^{-1}. Therefore, we consider that the weight of the monomer unit is between 52 g.mol^{-1} and 53 g.mol^{-1}. Then, we assume that when one unit A is added, a single monomeric unit is added to the growing chain and when one unit B is added, two monomeric units are added to the growing chain. This means that both indices of styrene, l, and acrylonitrile, k, can be taken globally as only one, i, representing the weight of the both monomers inside the polymer chains. This corresponds to a simple variable change :

$$i = k + 2\,l. \tag{4.19}$$

Indeed, $^{*}_{k,l,j}$, $B^{*}_{k,l,j}$ and $P_{k,l,j}$ become respectively $A^{*}_{i,j}$, $B^{*}_{i,j}$ and $P_{i,j}$, where i is the number of monomeric units and j is the number of graft units. Only this notation will be used further.

This assumption can be used as the copolymerization of acrylonitrile with styrene gives random linear amorphous copolymers, which means that the units A and B are statistically alternate.

The average molecular weight of the monomeric unit is therefore :

$$M_u = \frac{[A_P]M_A + 2[B_P]M_B/2}{[A_P] + 2[B_P]}, \tag{4.20}$$

where $M_B/2 < M_u < M_A$, that is to say that M_u is in the range of 52-53 g/mol depending on the copolymer composition.

The average molar volume of the corresponding monomeric unit is :

$$V_u = \frac{[A_P]\frac{M_A}{\rho_{PA}} + 2[B_P]\frac{M_B}{2\rho_{PB}}}{[A_P] + 2[B_P]}, \tag{4.21}$$

where $[A_P]$ and $[B_P]$ are the concentration of monomers A and B incorporated in the polymer chains and ρ_{PA} and ρ_{PB} the densities of the monomers A and B once they are incorporated in the polymer. The densities are actually the densities of the homopolymers :

$\rho_{PA} = 1170$ kg m^{-3} and $\rho_{PB} = 1040$ kg m^{-3} (Brandrup & Immergut, 1989).

As an element of comparison, the densities of the free monomers are :

$\rho_A = 806$ kg m^{-3} and $\rho_B = 909$ kg m^{-3}.

The details leading to equations 4.20 and 4.21 are exposed in annex 4.

1.3. Grafting

1.3.1. o olym iz ion of s y n nd c yloni il wi vinyl bond of S5200

The grafting of the precursor stabilizer, S5200, on SAN polymer chains is considered to result mainly from the reaction of growing oligoradicals on the vinyl bond of the silane group. Indeed, S5200 results from the reaction of vinyltrimethoxysilane (VTMS) with a polyether triol (CP3320) as seen in chapter 2.

The different reactivity ratios found in the literature for the reaction of styrene and acrylonitrile with different silanes are presented in table 4.3.

Table 4.3 : Reactivity ratios from literature for styrene and acrylonitrile reacting with silanes

Monomer	Silane	Conditions	R_{iG}	R_{Gi}	Reference
Styrene	VTES	Unknown	20.86	0	Brandrup & Immergut (1989)
Styrene	VMDAS	In bulk at 60°C	10.4 ± 0.3	0	Bajaj & Gupta (1979)
Styrene	VMDAS	In toluene at 60°C	4.03 ± 0.03	0	Bajaj & Gupta (1979)
Styrene	VMDAS	In toluene at 60°C	5.7 ± 0.02	0.13 ± 0.06	Bajaj & Gupta (1979)
Styrene	VMDES	In bulk at 60°C	11.7 ± 0.01	0	Bajaj & Gupta (1979)
Acrylonitrile	VTES	Unknown	26.83	2.69	Brandrup & Immergut (1989)
Acrylonitrile	VTES	Unknown	6.59	0.41	Brandrup & Immergut (1989)
Acrylonitrile	VTMS	Unknown	9.09	0.45	Brandrup & Immergut (1989)
Acrylonitrile	VMDAS	In bulk at 50°C	2.26 ± 0.25	0	Bajaj & Gupta (1979)

Let us define the following reactivity ratios where i is A for acrylonitrile or B for styrene :

$$R_{iG} = k_{piG}/k_{pii}\ , \tag{4.22}$$

$$R_{Gi} = k_{pGi}/k_{pGG}\ . \tag{4.23}$$

For steric reasons it is assumed that the propagation between two S5200 macromeres is negligible : $k_{pGG} \approx 0$. Moreover, as shown in table 4.3, R_{Gi} is closed to zero with relatively small silane groups like VTES, VMDAS and VMTMS. It is then assumed in this model that $k_{pGA} \approx 0$ and $k_{pGB} \approx 0$ as the size of the S5200 macromere may tend to reduce the reactivity of the grafts S5200 with the monomers. This mean that, once the SAN chain is grafted with S5200 there is no more propagation possible. It is assumed that there is only one graft per SAN chain as the experimental data suggested it.

1.3.2. N u l G fing of S5200 nd Polyol

The other different grafting mechanisms are called "natural grafting" mechanisms and are described in chapter 3. The copolymerization of the monol vinyl groups with styrene and acrylonitrile is not considered here. Indeed the abstraction of an hydrogen atom on the polyol by the primary radicals appears to be the main reaction :

$$R^* + S \xrightarrow{k^c_{RS,ng}} S^*,$$

where R* is a primary radical, S the polyol solvent and S* the solvent radicals.

Hydrogen abstraction may also happen on the precursor stabilizer :

$$R^* + G \xrightarrow{k^c_{RG,ng}} G^*.$$

It is assumed that $k^c_{RS,ng} = k^c_{RG,ng}$, as it is a similar mechanism.

Transfers to polyol may be also a way to produce "natural grafts" :

$$A^* + S \xrightarrow{k^c_{tr,AS}} P + S^*$$

$$B^* + S \xrightarrow{k^c_{tr,BS}} P + S^*$$

Transfers to S5200 may also occur :

$$A^* + G \xrightarrow{k^c_{tr,AG}} P + G^*$$

$$B^* + G \xrightarrow{k^c_{tr,BG}} P + G^*$$

Here, for steric reasons, it is assumed that there is no transfers of G* with G. Transfers to polyol and transfers to S5200 obey to the same mechanisms, therefore $k^c_{tr,AS} = k^c_{tr,AG}$ and $k^c_{tr,BS} = k^c_{tr,BG}$. Nevertheless, transfers to S5200 may be neglected as the concentration of S5200 in the continuous phase may be very less than the concentration of the solvent : $[G]_c \square [S]_c$.

Then, "natural grafts" could initiate polymerization with styrene and acrylonitrile.

$$S^* + A \xrightarrow{k^c_{SA}} A^*$$

$$S^* + B \xrightarrow{k^c_{SB}} B^*$$

$$G^* + A \xrightarrow{k^c_{GA}} A^*$$

$$G^* + B \xrightarrow{k^c_{GB}} B^*$$

It is also assumed that the species that are grafted by "natural grafting" will not be grafted by S5200 molecules by propagation on their vinyl bonds : the probability that it happens is considered to be too low and the concentration of the resulting species will be neglected.

Therefore, this model considers that the grafted SAN chains contains only one graft S5200 or one graft polyol. Species containing more grafts are not predicted here.

1.3.3. Terminations with grafted species

The oligoradicals terminated by acrylonitrile or styrene undergo termination almost exclusively by coupling. It is assumed that the quantity of grafted species is small compared to the quantity of ungrafted SAN chains and the probability for two grafted species to undergo termination is too small to be considered. Otherwise the model will predict the production of SAN chains grafted at their both ends.

Concerning oligoradicals terminated by a graft G (S5200), as further propagation with styrene or acrylonitrile ars neglected, only disproportionation is taken into account. The disproportionation between two species terminated by G is neglected for statistical reasons.

1.3.4. Notations for Grafting Modeling

In order to model the grafting, it is assumed that there will be only one graft per SAN chain. In order to differentiate the two types of grafts, S5200 and polyol, contained in the growing chains, an index, j, will be used :

j = 0 means that the SAN chain is not grafted,

j = 1 means that there is one graft polyol on a SAN chain,

j = 3 means that there is one graft S5200 on a SAN chain (as $M_{S5200} \approx 3\ M_{Polyol}$).

The index j is actually the equivalent of the number of graft units as the index i is the number of monomeric units. Therefore, the use of two indices allows to know for each SAN chain the number of monomeric units it contained and the way it is grafted. Below are presented the different notations corresponding to the concentrations of SAN chains depending on the terminations of the radicals, the type of graft and the phase considered :

$\left[G^*_{0,3}\right]_c$ is the concentration of S5200 molecules activated by action of primary radicals on the vinyl bonds or by H-abstraction on PO groups.

$\left[S^*_{0,1}\right]_c$ is the concentration of polyol molecules (solvent) activated by H-abstraction on PO groups by primary radicals issued from T27 (peroxide).

$\left[A^*_{i,0}\right]_c$, $\left[A^*_{i,1}\right]_c$, $\left[A^*_{i,3}\right]_c$, $\left[A^*_{i,0}\right]_p$, $\left[A^*_{i,1}\right]_p$ and $\left[A^*_{i,3}\right]_p$ are the concentrations of oligoradicals having i monomeric units, terminated by an acrylonitrile unit and having 0 graft (j=0), 1 graft

unit (polyol : j = 1) or 3 graft units (S5200 : j = 3) in the continuous phase (c) and inside the particles (p).

$[B^*_{i,0}]_c$, $[B^*_{i,1}]_c$, $[B^*_{i,3}]_c$, $[B^*_{i,0}]_p$, $[B^*_{i,1}]_p$ and $[B^*_{i,3}]_p$ are the concentrations of oligoradicals having i monomeric units, terminated by styrene and having 0 graft (j=0), 1 graft unit (polyol : j = 1) or 3 graft units (S5200 : j = 3) in the continuous phase (c) and inside the particles (p).

$[G^*_{i,3}]_c$ is the concentration of oligoradicals having i monomeric units and terminated by 3 graft units (S5200) in the continuous phase.

$[G^*_{i,3}]$, the concentration of oligoradicals having i monomeric units and terminated by 3 graft units (S5200) adsorbed at the particles surface is neglected.

$[P_{i,0}]_c$, $[P_{i,1}]_c$, $[P_{i,3}]_c$, $[P_{i,0}]_p$, $[P_{i,1}]_p$ and $[P_{i,3}]_p$ are the concentrations of dead polymer having i monomeric units and having 0 graft (j=0), 1 graft unit (polyol : j = 1) or 3 graft units (S5200 : j = 3), in the continuous phase (c) and inside the particles (p).

$[A^*_{T,0}]_c$, $[A^*_{T,1}]_c$, $[A^*_{T,3}]_c$, $[A^*_{T,0}]_p$, $[A^*_{T,1}]_p$, $[A^*_{T,3}]_p$, $[B^*_{T,0}]$, $[B^*_{T,1}]$, $[B^*_{T,3}]$, $[B^*_{T,0}]_p$, $[B^*_{T,1}]_p$, $[B^*_{T,3}]_p$, $[G^*_{T,3}]_c$, $[G^*_{T,3}]_p$, $[P^*_{T,0}]_c$, $[P^*_{T,1}]_c$, $[P^*_{T,3}]_c$, $[P^*_{T,0}]_p$, $[P^*_{T,1}]_p$ and $[P^*_{T,3}]_p$ are the total concentrations of each species.

$[R^*]_c$ and $[R^*]_p$ are the concentrations of primary radicals resulting from initiator decomposition and transfers to chain transfer agent, in the continuous phase and inside the particles.

1.4.Thermodynamics

The concentrations in the continuous phase and in the particles of the monomers (acrylonitrile and styrene), the initiator and the chain transfer agent are considered to be in thermodynamic equilibrium. The partitioning coefficients are then defined as follows :

$$H_A = \frac{[A]_p}{[A]_c} = \frac{A_p/V_p}{A_c/V_c} \tag{4.24}$$

$$H_B = \frac{[B]_p}{[B]_c} = \frac{B_p/V_p}{B_c/V_c} \tag{4.25}$$

$$H_{CTA} = \frac{[CTA]_p}{[CTA]_c} = \frac{CTA_p/V_p}{CTA_c/V_c} \tag{4.26}$$

$$H_I = \frac{[I]_p}{[I]_c} = \frac{I_p/V_p}{I_c/V_c} \tag{4.27}$$

A_p, A_c, B_p, B_c, CTA_p, CTA_c, I_p and I_c are the quantity of acrylonitrile, styrene, NDM and T27 in the particles and in the continuous phase respectively. V_p and V_c are the volumes of the particle phase and the continuous phase respectively.

It is assumed that there is no free polyol or free S5200 inside particles, but only grafted onto their surfaces.

1.5. Capture by particles

1.5.1. Absorption

It is assumed that the ungrafted SAN chains may be differently absorbed by the polymer particles depending on the way they are grafted.

The rate of absorption of ungrafted species is (see paragraph 4.3.1 of chapter 1):

$$\bar{J}_a^0 = \bar{k}_a^0 \pi d_p^2 N_p \left(\left[A_{T,0}^* \right]_c + \left[B_{T,0}^* \right]_c + \left[P_{T,0} \right]_c \right), \tag{4.28}$$

$$\text{with } \bar{k}_a^0 = 2\bar{D}_0 / d_p \text{ (see Eq. 1.8).} \tag{4.29}$$

N_p is the number of particles in the reactor and d_p is the average particle diameter.

The rate of absorption of species grafted with polyol solvent is :

$$\bar{J}_a^1 = \bar{k}_a^1 \pi d_p^2 N_p \left(\left[A_{T,1}^* \right]_c + \left[B_{T,1}^* \right]_c + \left[P_{T,1} \right]_c \right), \tag{4.30}$$

$$\text{with } \bar{k}_a^1 = 2\bar{D}_1 / d_p . \tag{4.31}$$

The rate of absorption of species grafted with S5200 is :

$$\bar{J}_a^3 = \bar{k}_a^3 \pi d_p^2 N_p \left(\left[A_{T,3}^* \right]_c + \left[B_{T,3}^* \right]_c + \left[P_{T,3} \right]_c \right), \tag{4.32}$$

$$\text{with } \bar{k}_a^3 = 2\bar{D}_3 / d_p . \tag{4.33}$$

The desorption of the radicals from the particles is neglected.

The concentration of species terminated by G* in the continuous phase, $\left[G_{T,3}^* \right]_c$, may be neglected compared to $\left[A_{T,3}^* \right]_c$, $\left[B_{T,3}^* \right]_c$ and $\left[P_{T,3} \right]_c$. Therefore, the adsorption of these oligoradicals is neglected and as a consequence, $\left[G_{T,3}^* \right]_p \approx 0$.

The more the species are grafted, the more they will be soluble in the continuous phase. Therefore there will be the following relationship between the average diffusion coefficients :

$$\bar{D}_3 \leq \bar{D}_1 \leq \bar{D}_0 . \tag{4.34}$$

1.5.2. Precipitation

Let us consider that homogeneous nucleation is, in a first attempt, the simplest way to model the precipitation i.e. that at a given critical number of monomeric units, i_{crit}, the oligoradicals precipitate. Nevertheless, there are two important difficulties : firstly, it is be necessary to evaluate this critical length, which depends on the solvency of the medium, of the composition in styrene/acrylonitrile, and of the temperature, and secondly, the combination terminations may induce precipitation if the degree of polymerization of the resulting dead polymer is greater than i_{crit}. Considering all the possible combinations that induce precipitation provide too heavy computational calculations and this will not allow a further parameter identification in acceptable times.

Aggregative nucleation (which may be closer to the reality than the homogeneous one) is therefore considered : the oligomer chains formed by solution polymerization associate with each other increasingly as their molecular weight and concentration rise.

If $\bar{J}_p$ is the precipitation rate of all the species that are in solution (in mol.s^{-1}), the following relationship is proposed :

$$\bar{J}_p = \bar{K}_p \left(\begin{array}{l} \left[A^*_{T,0}\right]_c + \left[A^*_{T,1}\right]_c + \left[A^*_{T,3}\right]_c + \left[B^*_{T,0}\right]_c + \left[B^*_{T,1}\right]_c \\ + \left[B^*_{T,3}\right]_c + \left[G^*_{T,3}\right]_c + \left[P_{T,0}\right]_c + \left[P_{T,1}\right]_c + \left[P_{T,3}\right]_c \end{array} \right) V_c \, \bar{M}^c_n / M_u \ . \tag{4.35}$$

$\bar{K}_p$ (in s^{-1}) is a constant of precipitation, which is an adjustable parameter of the model and $\bar{M}^c_n$ is the number – average molecular weight in the continuous phase.

This means that in this model, the rate of precipitation of a given species depends on its quantity in the continuous phase and on the average size of the SAN chains that are in the medium, with which each oligoradical or dead polymer may precipitate.

1.6.Particle Stabilization : model for average particle size

It is assumed (i) that all the particles were covered by the grafts, which are firmly attached, and (i.i) that the particles are monodisperse. The average particle diameter is calculated from the total volume and the total surface of the particles.

This total volume of the particles, V_p, is assumed to be linked to the quantity of monomers that are incorporated into the polymer. Indeed, neglecting the amount of polymer dissolved in the continuous phase as compared to the amount of polymer inside the solid phase, it is possible to express the total volume of particles swollen by the monomers from $\left[A_p\right]$ and $\left[B_p\right]$, the concentrations of monomers A and B incorporated in the polymer :

$$V_p \approx \underbrace{\left(\left[A_p\right]M_A/\rho_{PA} + \left[B_p\right]M_B/\rho_{PB}\right)V}_{\text{Volume of polymer}} + \underbrace{\left(\left[A\right]_p M_A/\rho_{PA} + \left[B\right]_p M_B/\rho_{PB}\right)V_p}_{\text{Volume of free monomers inside particles}} \tag{4.36}$$

$$V_p \approx \left(\frac{\left[A_p\right]V M_A/\rho_{PA} + \left[B_p\right]V M_B/\rho_{PB}}{1 - \left[A\right]_p V_p M_A/\rho_{PA} - \left[B\right]_p V_p M_B/\rho_{PB}} \right) V \tag{4.37}$$

Actually, the weight of monomers incorporated in the polymer is equal (neglecting the radicals) to the weight of the dead polymer in the both phases :

$$\begin{aligned} \left(\left[A_p\right]M_A + \left[B_p\right]M_B\right)V &= \left(\left[A_p\right] + 2\left[B_p\right]\right)M_u V \\ &= \left\{\left[P_{T,0}\right]_p \mu^p_{1,0} + \left[P_{T,1}\right]_p \mu^p_{1,1} + \left[P_{T,3}\right]_p \mu^p_{1,3}\right\} M_u V_p \\ &+ \left\{\left[P_{T,0}\right]_c \mu^c_{1,0} + \left[P_{T,1}\right]_c \mu^c_{1,1} + \left[P_{T,3}\right]_c \mu^c_{1,3}\right\} M_u V_c \end{aligned} \tag{4.38}$$

where, $\mu^p_{1,0}$, $\mu^p_{1,1}$, $\mu^p_{1,3}$, $\mu^c_{1,0}$, $\mu^c_{1,1}$ and $\mu^c_{1,3}$ are the moments of order one of the distributions corresponding to the respective species and are defined in annex 4.

Knowing that $V_c = V - V_p$, Eq. 4.39 gives the exact volume of the swollen polymer phase :

$$V_p = \left(\frac{\left[A_p\right] + 2\left[B_p\right] - \left[P_{T,0}\right]_c \mu^c_{1,0} - \left[P_{T,1}\right]_c \mu^c_{1,1} - \left[P_{T,3}\right]_c \mu^c_{1,3}}{\left[P_{T,0}\right]_p \mu^p_{1,0} + \left[P_{T,1}\right]_p \mu^p_{1,1} + \left[P_{T,3}\right]_p \mu^p_{1,3} - \left[P_{T,0}\right]_c \mu^c_{1,0} - \left[P_{T,1}\right]_c \mu^c_{1,1} - \left[P_{T,3}\right]_c \mu^c_{1,3}} \right) V . \tag{4.39}$$

Eq. (4.37) is easier to calculate V_p but must be compared to Eq. (4.39) to be validate.

The total surface of particles is assumed to be equal to the total surface covered by the grafts. It is therefore necessary to know the number of grafts present at the particles surface and the area covered by one graft. The number of S5200 grafts is equal to the number of SAN chains containing one S5200 graft, that is to say, the sum of all the species with one S5200 graft :

$$N_G = \left\{ \left[A^*_{T,3}\right]_p + \left[B^*_{T,3}\right]_p + \left[G^*_{T,3}\right]_p + \left[P_{T,3}\right]_p \right\} V_p N_A \tag{4.40}$$

The number of polyol grafts is equal to the number of SAN chains with one polyol graft :

$$N_S = \left\{ \left[A^*_{T,1}\right]_p + \left[B^*_{T,1}\right]_p + \left[P_{T,1}\right]_p \right\} V_p N_A \tag{4.41}$$

The area covered by each type of graft depends on their radii of gyrations. It can be seen on figure 4.2, that when polyol is grafted, only the 2/3rd of M_{polyol} may covers the particle and when S5200 is grafted only the 4/9th of M_{S5200} may cover the particle.

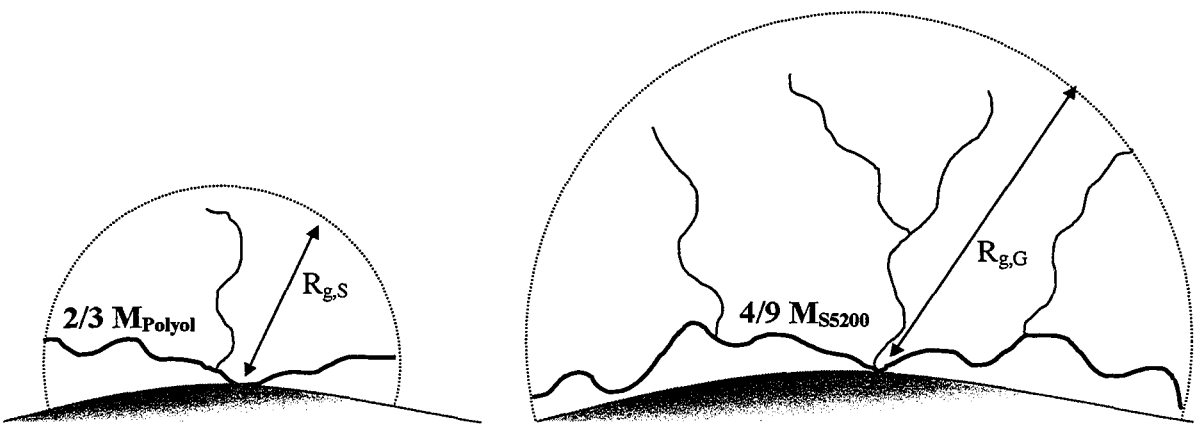

Figure 4.2 : Radii of gyrations of polyol and S5200

In order to estimate the radii of gyrations it is necessary to take into account the average length of the long chain from the grafting point, which is assumed to be meanly 75% of the maximum length that can cover the particle, as suggested by Yasuda et al. (2001a).

The average radius of gyration of the S5200 grafts is therefore :

$$R_{g,G} = a \left(0.75 \cdot 4/9 \cdot M_{S5200}\right)^{1/3}, \tag{4.42}$$

and the average radius of the polyol grafts is therefore :

$$R_{g,S} = a \left(0.75 \cdot 2/3 \cdot M_{Polyol}\right)^{1/3}. \tag{4.43}$$

Yasuda et al. (2001a) found a = 5.3 10^{-7} m.(mol.kg^{-1})$^{1/3}$ for PVP.

Therefore the total surface of the particles is equal to :

$$S_p = \pi\left(N_G R_{g,G}^2 + N_S R_{g,S}^2\right) \tag{4.44}$$

Finally, the mean particle diameter, which actually can be connected to the surface area moment mean (see Eq. 2.16), is :

$$d_p = d_{32} = 6\frac{V_p}{S_p} = \frac{6}{\pi}\frac{V_p}{\left(N_G R_{g,G}^2 + N_S R_{g,S}^2\right)} \tag{4.45}$$

The number of particles can be therefore deduced :

$$N_p = \frac{6}{\pi} V_p d_p^{-3} \tag{4.46}$$

However, this model does not forecast the particle size distribution, which require a more complex model as the real system presents multimodal distributions.

1.7.Kinetic Scheme

Below are summed up all the kinetics involved in the model using the notations previously mentioned.

1.7.1. Polymerization in the continuous phase

(1) Initiator decomposition

$$I \xrightarrow{f_c, k_d^c} 2\,R^*$$

(2) Initiation

$$R^* + A \xrightarrow{k_{RA}^c} A_{1,0}^*$$

$$R^* + B \xrightarrow{k_{RB}^c} B_{2,0}^*$$

$$R^* + G \xrightarrow{k_{RG}^c} G_{0,3}^*$$

$$R^* + G \xrightarrow{k_{RG,ng}^c} G_{0,3}^* \qquad \text{(H abstraction on PO groups)}$$

$$R^* + S \xrightarrow{k_{RS,ng}^c} S_{0,1}^* \qquad \text{(H abstraction on PO groups)}$$

$$G_{0,3}^* + A \xrightarrow{k_{GA}^c} A_{1,3}^*$$

$$G_{0,3}^* + B \xrightarrow{k_{GB}^c} B_{2,3}^*$$

$$S_{0,1}^* + A \xrightarrow{k_{SA}^c} A_{1,1}^*$$

$$S_{0,1}^{*} + B \xrightarrow{k_{SB}^{c}} B_{2,1}^{*}$$

(3) Propagation (j = 0, 1 or 3)

$$A_{i,j}^{*} + A \xrightarrow{k_{pAA}^{c}} A_{i+1,j}^{*}$$

$$A_{i,j}^{*} + B \xrightarrow{k_{pAB}^{c}} B_{i+2,j}^{*}$$

$$B_{i,j}^{*} + A \xrightarrow{k_{pBA}^{c}} A_{i+1,j}^{*}$$

$$B_{i,j}^{*} + B \xrightarrow{k_{pBB}^{c}} B_{i+2,j}^{*}$$

(4) Grafting

$$A_{i,0}^{*} + G \xrightarrow{k_{pAG}^{c}} G_{i,3}^{*}$$

$$B_{i,0}^{*} + G \xrightarrow{k_{pBG}^{c}} G_{i,3}^{*}$$

(5) Termination by combination (j = 0, 1 or 3)

$$A_{i-u,j}^{*} + A_{u,0}^{*} \xrightarrow{k_{tcAA}^{c}} P_{i,j}$$

$$B_{i-u,j}^{*} + B_{u,0}^{*} \xrightarrow{k_{tcBB}^{c}} P_{i,j}$$

$$A_{i-u,j}^{*} + B_{u,0}^{*} \xrightarrow{k_{tcAB}^{c}} P_{i,j}$$

$$B_{i-u,j}^{*} + A_{u,0}^{*} \xrightarrow{k_{tcAB}^{c}} P_{i,j}$$

(6) Termination by disproportionation (j = 0, 1 or 3)

$$G_{u,3}^{*} + A_{i,j}^{*} \xrightarrow{k_{tdGA}^{c}} P_{u,3} + P_{i,j}$$

$$G_{u,3}^{*} + B_{i,j}^{*} \xrightarrow{k_{tdGB}^{c}} P_{u,3} + P_{i,j}$$

(7) Transfer to NDM (j = 0, 1 or 3)

$$A_{i,j}^{*} + CTA \xrightarrow{k_{tr,A}^{c}} P_{i,j} + R^{*}$$

$$B_{i,j}^{*} + CTA \xrightarrow{k_{tr,B}^{c}} P_{i,j} + R^{*}$$

$$G_{i,3}^{*} + CTA \xrightarrow{k_{tr,G}^{c}} P_{i,3} + R^{*}$$

(8) Transfer to Polyol (j = 0, 1 or 3)

$$A_{i,j}^{*} + S \xrightarrow{k_{tr,AS}^{c}} P_{i,j} + S_{0,1}^{*}$$

$$B_{i,j}^{*} + S \xrightarrow{k_{tr,BS}^{c}} P_{i,j} + S_{0,1}^{*}$$

(9) Transfer to S5200 (j = 0,1 or 3)

$$A^*_{i,j} + G \xrightarrow{k^c_{tr,AG}} P_{i,j} + G^*_{0,3}$$

$$B^*_{i,j} + G \xrightarrow{k^c_{tr,BG}} P_{i,j} + G^*_{0,3}$$

1.7.2. Polymerization inside the particles

(1) Initiator decomposition

$$I \xrightarrow{f_p, k^p_d} 2\ R^*$$

(2) Initiation

$$R^* + A \xrightarrow{k^p_{RA}} A^*_{1,0}$$

$$R^* + B \xrightarrow{k^p_{RB}} B^*_{2,0}$$

(3) Propagation (j = 0, 1, 3)

$$A^*_{i,j} + A \xrightarrow{k^p_{pAA}} A^*_{i+1,j}$$

$$A^*_{i,j} + B \xrightarrow{k^p_{pAB}} B^*_{i+2,j}$$

$$B^*_{k,l,j} + A \xrightarrow{k^p_{pBA}} A^*_{k+1,l,j}$$

$$B^*_{i,j} + B \xrightarrow{k^p_{pBB}} B^*_{i+2,j}$$

(4) Termination by combination (j = 0, 1, 3)

$$A^*_{i-u,j} + A^*_{u,0} \xrightarrow{k^p_{tcAA}} P_{i,j}$$

$$B^*_{i-u,j} + B^*_{u,0} \xrightarrow{k^p_{tcBB}} P_{i,j}$$

$$A^*_{i-u,j} + B^*_{u,0} \xrightarrow{k^p_{tcAB}} P_{i,j}$$

$$B^*_{i-u,j} + A^*_{u,0} \xrightarrow{k^p_{tcAB}} P_{i,j}$$

(5) Transfer to NDM (CTA) (j = 0, 1, 3)

$$A^*_{i,j} + CTA \xrightarrow{k^p_{tr,A}} P_{i,j} + R^*$$

$$B^*_{i,j} + CTA \xrightarrow{k^p_{tr,B}} P_{i,j} + R^*$$

2. The definition of the system

It is assumed that the reactor used is a perfectly mixed reactor that is to say that the concentrations were homogeneous inside the reactor.

Below are presented the different balances made using the different hypotheses previously presented. The balances will define the system of equations that describes the state of the reactor. Then, from this system state, theoretical data will be calculated, which will be then compared to the results obtained from polymerisations carried out under different experimental conditions.

2.1. Balance on the total concentrations of the species in the reactor

The volume flow at the reactor inlet and outlet were equal, $Q_e = Q_s$ (in $m^3.s^{-1}$), as the volume of the reactor, V, is a constant. The mass flow at the outlet of the reactor, Q_{sm}, will be maintained constant by the process control, then, it is necessary to link the mass flow to the volume flow:

$$Q_{sm}/m_{CPP} = Q_s/V = Q_e/V . \tag{4.47}$$

A general balance on the different species present in the reactor is done firstly in order to determine the weight inside the reactor, m_{CPP}.

If $[A_T]$, $[B_T]$, $[G_T]$, $[S_T]$, $[CTA_T]$ and $[I_T]$ are the total concentrations of the different species (free or incorporated in the polymer) and $[A]_e$, $[B]_e$, $[G]_e$, $[S]_e$, $[CTA]_e$ and $[I]_e$ are the concentrations of the different species in the premix, the following balances can be done, using Eq. 4.47 :

Balance on the total acrylonitrile concentration :

$$d([A_T])/dt = \frac{Q_{sm}}{m_{CPP}} \left([A]_e - [A_T]\right) \tag{4.48}$$

Balance on the total styrene concentration :

$$d([B_T])/dt = \frac{Q_{sm}}{m_{CPP}} \left([B]_e - [B_T]\right) \tag{4.49}$$

Balance on the total S5200 concentration :

$$d([G_T])/dt = \frac{Q_{sm}}{m_{CPP}} \left([G]_e - [G_T]\right) \tag{4.50}$$

Balance on the total polyol concentration :

$$d([S_T])/dt = \frac{Q_{sm}}{m_{CPP}} \left([S]_e - [S_T]\right) \tag{4.51}$$

Balance on the total NDM concentration :

$$d([CTA_T])/dt = \frac{Q_{sm}}{m_{CPP}} \left([CTA]_e - [CTA_T]\right) \tag{4.52}$$

Balance on the total T27 concentration :

$$d([I_T])/dt = \frac{Q_{sm}}{m_{CPP}} \left([I]_e - [I_T]\right) \tag{4.53}$$

Obviously, these simple balances show that in the steady state regime, the total concentrations are equal to the concentrations in the premix mixture.

Assuming that the volume change during the incorporation of monomers is negligible, the weight inside the reactor is the sum of all the weights present inside the reactor :

$$m_{CPP} = \left\{[A_T]M_A + [B_T]M_B + [S_T]M_S + [G_T]M_G + [CTA_T]M_{CTA} + [I_T]M_I\right\}V \tag{4.54}$$

2.2. Balance on the concentrations of free species in the reactor

2.2.1. Definition of the concentrations in the continuous phase and inside the swollen particles

Using the partitioning coefficients defined by Eq 4.30 to Eq 4.33, the concentrations of the different species in the continuous phase can be expressed as a function of their global concentration in the reactor :

$$[A]_c = [A]V/\left(H_A V_p + V_c\right) \tag{4.55}$$

$$[B]_c = [B]V/\left(H_B V_p + V_c\right) \tag{4.56}$$

$$[CTA]_c = [CTA]V/\left(H_{CTA} V_p + V_c\right) \tag{4.57}$$

$$[I]_c = [I]V/\left(H_I V_p + V_c\right) \tag{4.58}$$

$[A]_p$, $[B]_p$, $[CTA]_p$ and $[I]_p$ are then calculated from equations 4.24 to 4.27.

2.2.2. Balance on free acrylonitrile in the reactor

The accumulation of acrylonitrile versus the reaction time is equal to :

$$d([A])/dt = \frac{Q_{sm}}{m_{CPP}} \left([A]_e - [A]\right)$$

(balance between input and output)

$$-k_{RA}^c \left[R^*\right]_c [A]_c V_c/V - k_{RA}^p \left[R^*\right]_p [A]_p V_p/V$$

(initiations in the both phases with primary radicals)

$$-\left(k_{GA}^c \left[G_{0,3}^*\right]_c + k_{SA}^c \left[S_{0,1}^*\right]_c\right)[A]_c V_c/V$$

(initiations in the continuous phase by activated S5200 and polyol grafts)

$$-\left(k_{pAA}^c \left(\left[A_{T,0}^*\right]_c + \left[A_{T,1}^*\right]_c + \left[A_{T,3}^*\right]_c\right) + k_{pBA}^c \left(\left[B_{T,0}^*\right]_c + \left[B_{T,1}^*\right]_c + \left[B_{T,3}^*\right]_c\right)\right)[A]_c V_c/V$$

(propagation with oligoradicals in the continuous phase)

$$-\left(k_{pAA}^{p}\left(\left[A_{T,0}^{*}\right]_{p}+\left[A_{T,1}^{*}\right]_{p}+\left[A_{T,3}^{*}\right]_{p}\right)+k_{pBA}^{p}\left(\left[B_{T,0}^{*}\right]_{p}+\left[B_{T,1}^{*}\right]_{p}+\left[B_{T,3}^{*}\right]_{p}\right)\right)[A]_{p}V_{p}/V \quad (4.59)$$

(propagation with oligoradicals inside the particles)

2.2.3. Balance on free styrene in the reactor

$$d[B]/dt=\frac{Q_{sm}}{m_{CPP}}\left([B]_{e}-[B]\right)$$

(balance between input and output)

$$-k_{RB}^{c}\left[R^{*}\right]_{c}[B]_{c}V_{c}/V-k_{RB}^{p}\left[R^{*}\right]_{p}[B]_{p}V_{p}/V$$

(initiations in the both phases with primary radicals)

$$-\left(k_{GB}^{c}\left[G_{0,3}^{*}\right]_{c}+k_{pSB}^{c}\left[S_{0,1}^{*}\right]_{c}\right)[B]_{c}V_{c}/V$$

(initiations in the continuous phase by activated S5200 and polyol grafts)

$$-\left(k_{pBB}^{c}\left(\left[B_{T,0}^{*}\right]_{c}+\left[B_{T,1}^{*}\right]_{c}+\left[B_{T,3}^{*}\right]_{c}\right)+k_{pAB}^{c}\left(\left[A_{T,0}^{*}\right]_{c}+\left[A_{T,1}^{*}\right]_{c}+\left[A_{T,3}^{*}\right]_{c}\right)\right)[B]_{c}V_{c}/V$$

(propagation with oligoradicals in the continuous phase)

$$-\left(k_{pBB}^{p}\left(\left[B_{T,0}^{*}\right]_{p}+\left[B_{T,1}^{*}\right]_{p}+\left[B_{T,3}^{*}\right]_{p}\right)+k_{pAB}^{c}\left(\left[A_{T,0}^{*}\right]_{p}+\left[A_{T,1}^{*}\right]_{p}+\left[A_{T,3}^{*}\right]_{p}\right)\right)[B]_{p}V_{p}/V$$

(propagation with oligoradicals inside particles) (4.60)

2.2.4. Balance on free G (the precursor stabilizer S5200) in the reactor

$$d([G])/dt=\frac{Q_{sm}}{m_{CPP}}\left([G]_{e}-[G]\right)$$

(balance between input and output)

$$-\left(k_{RG}^{c}+k_{RG,ng}^{c}\right)\left[R^{*}\right]_{c}[G]$$

(initiation of S5200 with primary radicals

$$-\left(k_{pAG}^{c}\left[A_{T,0}^{*}\right]_{c}+k_{pBG}^{c}\left[B_{T,0}^{*}\right]_{c}\right)[G] \quad (4.61)$$

(Grafting on the vinyl bond of S5200)

2.2.5. Balance on free solvent (polyol) in the reactor

$$d[S]/dt=\frac{Q_{sm}}{m_{CPP}}\left([S]_{e}-[S]\right)$$

(balance between input and output)

$$-k_{RS}^{c}\left[R^{*}\right]_{c}[S]$$

(initiation in the medium with primary radicals)

$$-\left\{k_{tr,AS}^{c}\left(\left[A_{T,0}^{*}\right]_{c}+\left[A_{T,1}^{*}\right]_{c}+\left[A_{T,3}^{*}\right]_{c}\right)+k_{tr,BS}^{c}\left(\left[B_{T,0}^{*}\right]_{c}+\left[B_{T,1}^{*}\right]_{c}+\left[B_{T,3}^{*}\right]_{c}\right)+k_{tr,GS}^{c}\left[G_{T,3}^{*}\right]_{c}\right\}[S]$$

(transfers to solvent of the different oligoradicals in the continuous phase)

(4.62)

2.2.6. *Balance on Chain Transfer Agent*

$$d\left([CTA]\right)/dt=\frac{Q_{sm}}{m_{CPP}}\left([CTA]_{e}-[CTA]\right)$$

(balance between input and output)

$$-\left(k_{tr,A}^{p}\left(\left[A_{T,0}^{*}\right]_{p}+\left[A_{T,1}^{*}\right]_{p}+\left[A_{T,3}^{*}\right]_{p}\right)+k_{tr,B}^{p}\left(\left[B_{T,0}^{*}\right]_{p}+\left[B_{T,1}^{*}\right]_{p}+\left[B_{T,3}^{*}\right]_{p}\right)+k_{tr,G}^{p}\left[G_{T,3}^{*}\right]_{p}\right)[CTA]_{p}V_{p}/V$$

(transfers to chain transfer agent of all the oligoradicals inside the particles)

$$-\left(k_{tr,A}^{c}\left(\left[A_{T,0}^{*}\right]_{c}+\left[A_{T,1}^{*}\right]_{c}+\left[A_{T,3}^{*}\right]_{c}\right)+k_{tr,B}^{c}\left(\left[B_{T,0}^{*}\right]_{c}+\left[B_{T,1}^{*}\right]_{c}+\left[B_{T,3}^{*}\right]_{c}\right)+k_{tr,G}^{c}\left[G_{T,3}^{*}\right]_{c}\right)[CTA]_{c}V_{c}/V$$

(transfers to chain transfer agent of all the oligoradicals in the continuous phase)

(4.63)

2.2.7. *Balance on Initiator in the reactor*

$$d[I]/dt=\frac{Q_{sm}}{m_{CPP}}\left([I]_{e}-[I]\right)$$

(balance between input and output)

$$-k_{d}^{c}[I]_{c}V_{c}/V-k_{d}^{p}[I]_{p}V_{p}/V \qquad (4.64)$$

(initiator dissociation in both phases)

2.2.8. *Global composition of the dead polymer*

The concentration of monomers incorporated in the polymer can be calculated from the total concentration inside the reactor and the concentration of free monomers :

$$\left[A_{p}\right]=\left[A_{T}\right]-[A] \qquad (4.65)$$

$$\left[B_{p}\right]=\left[B_{T}\right]-[B] \qquad (4.66)$$

$$\left[G_{p}\right]=\left[G_{T}\right]-[G] \qquad (4.67)$$

$$\left[S_{p}\right]=\left[S_{T}\right]-[S] \qquad (4.68)$$

The molecular weight of the monomeric units is deduced from this global composition ($52 < Mu < 53$ g/mol) using Eq. 4.20.

2.3. Balance on radicals, dead polymer chains and moments in the reactor

In order to determine the concentrations of all the radicals, the dead polymer chains and their moments of order one and two, the balance between their creation and their consumption is made. Below, only one example is explained for legibility reasons. All the balances are however presented in annex 4.

Here is presented how is calculated the quantity of radicals $A^*_{T,0}$ in the continuous phase and their moments of order one and two.

Firstly, a balance on radicals having only one monomeric unit, $[A^*_{1,0}]_c$, is done giving the differential equation 4.77, where $\Delta^c_{1,0} = \left[A^*_{1,0}\right]_c / \left[A^*_{T,0}\right]_c$ as defined in Annex 4 :

$$d\left(V_c\left[A^*_{T,0}\right]_c \Delta^c_{1,0}\right)/dt = k^c_{RA}\left[R^*\right]_c [A]_c V_c - \frac{Q_{sm}}{m_{CPP}} V_c \left[A^*_{T,0}\right]_c \Delta^c_{1,0}$$

(production of radicals by initiation and output of radicals)

$$-\left\{k^c_{pAA}[A]_c + k^c_{pAB}[B]_c + k^c_{pAG}[G]_c\right\} V_c \left[A^*_{T,0}\right]_c \Delta^c_{1,0}$$

(propagation with all the monomers in the medium)

$$-\left\{k^c_{tcAA}\left(2\left[A^*_{T,0}\right]_c + \left[A^*_{T,1}\right]_c + \left[A^*_{T,3}\right]_c\right) + k^c_{tcBA}\left(\left[B^*_{T,0}\right]_c + \left[B^*_{T,1}\right]_c + \left[B^*_{T,3}\right]_c\right) + k^c_{tdGA}\left[G^*_{T,3}\right]_c\right\} V_c \left[A^*_{T,0}\right]_c \Delta^c_{1,0}$$

(termination reactions with all the oligoradicals in the medium)

$$-\left\{k^c_{tr,A}[CTA]_c + k^c_{tr,SA}[S]_c + k^c_{tr,GA}[G]_c\right\} V_c \left[A^*_{T,0}\right]_c \Delta^c_{1,0}$$

(transfers to NDM, to solvent and to S5200)

$$-\left(2\pi d_p N_p \bar{D}_0 + K_p \bar{M}^c_n / M_u\right) V_c \left[A^*_{T,0}\right]_c \Delta^c_{1,0} \qquad (4.69)$$

(absorption and precipitation of the radicals)

Then, a balance on radicals having more monomeric units than one ($[A^*_{i,0}]$ for $i \geq 2$) provides the following relationship, where $\Delta^c_{i,0} = \left[A^*_{i,0}\right]_c / \left[A^*_{T,0}\right]_c$ as defined in Annex 4 :

$$d\left(V_c\left[A^*_{T,0}\right]_c \Delta^c_{i,0}\right)/dt = \left\{k^c_{pAA}\left[A^*_{T,0}\right]_c \Delta^c_{i-1,0}[A]_c + k^c_{pBA}\left[B^*_{T,0}\right]_c \Gamma^c_{i-1,0}[A]_c\right\} V_c$$

(production of oligoradicals $A^*_{i,0}$ by propagation with oligoradicals of lower size)

$$-\left\{\frac{Q_{sm}}{m_{CPP}} + k^c_{pAB}[B]_c + k^c_{pAA}[A]_c + k^c_{pAG}[G]_c\right\} V_c \left[A^*_{T,0}\right]_c \Delta^c_{i,0}$$

(output and disappearance of oligoradicals $A^*_{i,0}$ by propagation with monomers)

$$-\left\{k_{tcAA}^{c}\left(2\left[A_{T,0}^{*}\right]_{c}+\left[A_{T,1}^{*}\right]_{c}+\left[A_{T,3}^{*}\right]_{c}\right)+k_{tcBA}^{c}\left(\left[B_{T,0}^{*}\right]_{c}+\left[B_{T,1}^{*}\right]_{c}+\left[B_{T,3}^{*}\right]_{c}\right)+k_{tdGA}^{c}\left[G_{T,3}^{*}\right]_{c}\right\}V_{c}\left[A_{T,0}^{*}\right]_{c}\Delta_{i,0}^{c}$$

(termination reactions with all the oligoradicals in the medium)

$$-\left\{k_{tr,A}^{c}\left[CTA\right]_{c}+k_{tr,SA}^{c}\left[S\right]_{c}+k_{tr,GA}^{c}\left[G\right]_{c}\right\}V_{c}\left[A_{T,0}^{*}\right]_{c}\Delta_{i,0}^{c}$$

(transfers to NDM, to solvent and to S5200)

$$-\left(2\pi d_{p}N_{p}\bar{D}_{0}+K_{p}\bar{M}_{n}^{c}/M_{u}\right)V_{c}\left[A_{T,0}^{*}\right]_{c}\Delta_{i,0}^{c} \qquad (4.70)$$

(absorption and precipitation of the radicals)

Finally, the sum of all the species gives the total differential equation for the quantity of radicals $A_{T,0}^{*}$ in the continuous phase :

$$d\left(V_{c}\left[A_{T,0}^{*}\right]_{c}\right)/dt=\left(k_{RA}^{c}\left[R^{*}\right]_{c}+k_{pBA}^{c}\left[B_{T,0}^{*}\right]_{c}\right)\left[A\right]_{c}V_{c}-\left(\frac{Q_{sm}}{m_{CPP}}+k_{pAB}^{c}\left[B\right]_{c}+k_{pAG}^{c}\left[G\right]_{c}\right)V_{c}\left[A_{T,0}^{*}\right]_{c}$$

$$-\left\{k_{tcAA}^{c}\left(2\left[A_{T,0}^{*}\right]_{c}+\left[A_{T,1}^{*}\right]_{c}+\left[A_{T,3}^{*}\right]_{c}\right)+k_{tcBA}^{c}\left(\left[B_{T,0}^{*}\right]_{c}+\left[B_{T,1}^{*}\right]_{c}+\left[B_{T,3}^{*}\right]_{c}\right)+k_{tdGA}^{c}\left[G_{T,3}^{*}\right]_{c}\right\}V_{c}\left[A_{T,0}^{*}\right]_{c}$$

$$-\left\{k_{tr,A}^{c}\left[CTA\right]_{c}+k_{tr,SA}^{c}\left[S\right]_{c}+k_{tr,GA}^{c}\left[G\right]_{c}\right\}V_{c}\left[A_{T,0}^{*}\right]_{c}$$

$$-2\pi d_{p}N_{p}\bar{D}_{0}V_{c}\left[A_{T,0}^{*}\right]_{c}-K_{p}V_{c}\left[A_{T,0}^{*}\right]_{c}\bar{M}_{n}^{c}/M_{u} \qquad (4.71)$$

The sum of $d\left(V_{c}\left[A_{T,0}^{*}\right]_{c}\Delta_{i,0}^{c}\,i\right)/dt$ for i ≥1 gives a relationship between $\left(V_{c}\left[A_{T,0}^{*}\right]_{c}\right)$ and $\lambda_{1,0}^{c}$, the moment of order one (see its definition in annex 4) :

$$d\left(V_{c}\left[A_{T,0}^{*}\right]_{c}\lambda_{1,0}^{c}\right)/dt=\left\{k_{RA}^{c}\left[R^{*}\right]_{c}\left[A\right]_{c}+k_{pAA}^{c}\left[A_{T,0}^{*}\right]_{c}\left[A\right]_{c}+k_{pBA}^{c}\left[B_{T,0}^{*}\right]_{c}\left[A\right]_{c}\left(\eta_{1,0}^{c}+1\right)\right\}V_{c}$$

$$-\left\{\frac{Q_{sm}}{m_{CPP}}+k_{pAB}^{c}\left[B\right]_{c}+k_{pAG}^{c}\left[G\right]_{c}+k_{tcAA}^{c}\left(2\left[A_{T,0}^{*}\right]_{c}+\left[A_{T,1}^{*}\right]_{c}+\left[A_{T,3}^{*}\right]_{c}\right)\right\}V_{c}\left[A_{T,0}^{*}\right]_{c}\lambda_{1,0}^{c}$$

$$-\left\{k_{tcBA}^{c}\left(\left[B_{T,0}^{*}\right]_{c}+\left[B_{T,1}^{*}\right]_{c}+\left[B_{T,3}^{*}\right]_{c}\right)+k_{tdGA}^{c}\left[G_{T,3}^{*}\right]_{c}+k_{tr,A}^{c}\left[CTA\right]_{c}+k_{tr,SA}^{c}\left[S\right]_{c}+k_{tr,GA}^{c}\left[G\right]_{c}\right\}V_{c}\left[A_{T,0}^{*}\right]_{c}\lambda_{1,0}^{c}$$

$$-\left(2\pi d_{p}N_{p}\bar{D}_{0}+K_{p}\bar{M}_{n}^{c}/M_{u}\right)V_{c}\left[A_{T,0}^{*}\right]_{c}\lambda_{1,0}^{c}, \qquad (4.72)$$

using $\sum_{i=1}^{\infty}\left(\left(i+1\right)\Gamma_{i,0}^{c}\right)=\eta_{1,0}^{c}+1$.

The sum of $d\left(V_{c}\left[A_{T,0}^{*}\right]_{c}\Delta_{i,0}^{c}\,i^{2}\right)/dt$ for i ≥1 gives a relationship between $\left(V_{c}\left[A_{T,0}^{*}\right]_{c}\right)$ and $\lambda_{2,0}^{c}$, the moment of order two:

$$d\left(V_{c}\left[A_{T,0}^{*}\right]_{c}\lambda_{2,0}^{c}\right)/dt=\left\{k_{RA}^{c}\left[R^{*}\right]_{c}\left[A\right]_{c}+k_{pAA}^{c}\left[A_{T,0}^{*}\right]_{c}\left[A\right]_{c}\left(2\lambda_{1,0}^{c}+1\right)+k_{pBA}^{c}\left[B_{T,0}^{*}\right]_{c}\left[A\right]_{c}\left(\eta_{2,0}^{c}+2\eta_{1,0}^{c}+1\right)\right\}V_{c}$$

$$-\left\{\frac{Q_{sm}}{m_{CPP}}+k^c_{pAB}[B]_c+k^c_{pAG}[G]_c+k^c_{tcAA}\left(2\left[A^*_{T,0}\right]_c+\left[A^*_{T,1}\right]_c+\left[A^*_{T,3}\right]_c\right)\right\}V_c\left[A^*_{T,0}\right]_c\lambda^c_{2,0}$$

$$-\left\{k^c_{tcBA}\left(\left[B^*_{T,0}\right]_c+\left[B^*_{T,1}\right]_c+\left[B^*_{T,3}\right]_c\right)+k^c_{tcGA}\left[G^*_{T,3}\right]_c+k^c_{tr,A}[CTA]_c+k^c_{tr,SA}[S]_c+k^c_{tr,GA}[G]_c\right\}V_c\left[A^*_{T,0}\right]_c\lambda^c_{2,0}$$

$$-\left(2\pi d_p N_p \bar{D}_0+K_p\bar{M}^c_n/M_u\right)V_c\left[A^*_{T,0}\right]_c\lambda^c_{2,0}, \tag{4.73}$$

using $\sum_{i=1}^{\infty}\left((i+1)^2\Gamma^c_{i,0}\right)=\eta^c_{2,0}+2\eta^c_{1,0}+1$.

2.4. Calculation of data to be compared to the measurements

The state of the reactor being known it is possible to deduce several data that can be compared to those determined from measurements. Fifteen data can then be calculated but only twelve have been used further for the parameters identification.

2.4.1. Average molecular weights

2.4.1.1 Oligoradicals

In order to understand how the number-average molecular weight $\bar{M}_N$ and the weight-average molecular weight, $\bar{M}_W$, of whole CPP were calculated, it is necessary to explain on some examples how the moments of order one and two were used.

For instance, the number-average and the weight-average molecular weights of ungrafted oligoradicals (j = 0) terminated by A* in the continuous phase are calculated as follows :

$$\bar{M}_N\left(A^*_{T,0_c}\right)=\frac{V_c\left[A^*_{T,0}\right]_c\lambda^c_{1,0}M_u}{V_c\left[A^*_{T,0}\right]_c}=\lambda^c_{1,0}M_u, \tag{4.74}$$

$$\bar{M}_W\left(A^*_{T,0_c}\right)=\frac{V_c\left[A^*_{T,0}\right]_c\lambda^c_{2,0}M_u^2}{V_c\left[A^*_{T,0}\right]_c\lambda^c_{1,0}M_u}=\frac{\lambda^c_{2,0}}{\lambda^c_{1,0}}M_u. \tag{4.75}$$

This last equation can also be written as follows :

$$\bar{M}_W\left(A^*_{T,0_c}\right)=\bar{M}_N\left(A^*_{T,0_c}\right)+\frac{\left(\lambda^c_{2,0}-\lambda^{c\,2}_{1,0}\right)}{\bar{M}_N\left(A^*_{T,0_c}\right)}M_u^2. \tag{4.76}$$

In the same way, the number-average and the weight-average molecular weights of oligoradicals terminated by A* and grafted with the polyol in the continuous phase are calculated as follows :

$$\bar{M}_N\left(A^*_{T,1_c}\right)=\frac{V_c\left[A^*_{T,1}\right]_c\left(\lambda^c_{1,1}M_u+M_S\right)}{V_c\left[A^*_{T,1}\right]_c}=\lambda^c_{1,1}M_u+M_S \tag{4.77}$$

$$\bar{M}_W\left(A^*_{T,1_c}\right)=\frac{V_c\left[A^*_{T,1}\right]_c\left(\lambda^c_{2,1}M_u^2+M_S^2+2\lambda^c_{1,1}M_uM_S\right)}{V_c\left[A^*_{T,1}\right]_c\left(\lambda^c_{1,1}M_u+M_S\right)}=\frac{\lambda^c_{2,1}M_u^2+M_S^2+2\lambda^c_{1,1}M_uM_S}{\lambda^c_{1,1}M_u+M_S} \tag{4.78}$$

This last equation can also be written as follows :

$$\bar{M}_W\left(A^*_{T,1_c}\right)=\bar{M}_N\left(A^*_{T,1_c}\right)+\frac{\left(\lambda^c_{2,1}-\lambda^{c\,2}_{1,1}\right)}{\bar{M}_N\left(A^*_{T,1_c}\right)}M_u^2 \tag{4.79}$$

And finally, the number-average and the weight-average molecular weights of oligoradicals terminated by A* and grafted with S5200 in the continuous phase are calculated as follows :

$$\bar{M}_N\left(A^*_{T,3_c}\right)=\frac{V_c\left[A^*_{T,3}\right]_c\left(\lambda^c_{1,3}M_u+M_G\right)}{V_c\left[A^*_{T,3}\right]_c}=\lambda^c_{1,3}M_u+M_G \tag{4.80}$$

$$\bar{M}_W\left(A^*_{T,3_c}\right)=\frac{V_c\left[A^*_{T,3}\right]_c\left(\lambda^c_{2,3}M_u^2+M_G^2+2\lambda^c_{1,3}M_uM_G\right)}{V_c\left[A^*_{T,3}\right]_c\left(\lambda^c_{1,3}M_u+M_G\right)}=\frac{\lambda^c_{2,3}M_u^2+M_G^2+2\lambda^c_{1,3}M_uM_G}{\lambda^c_{1,3}M_u+M_G} \tag{4.81}$$

This last equation can also be written as follows :

$$\bar{M}_W\left(A^*_{T,3_c}\right)=\bar{M}_N\left(A^*_{T,3_c}\right)+\frac{\left(\lambda^c_{2,3}-\lambda^{c\,2}_{1,3}\right)}{\bar{M}_N\left(A^*_{T,3_c}\right)}M_u^2 \tag{4.82}$$

2.4.1.2. Whole CPP

The number-average molecular weight of whole CPP, $\bar{M}_N$, concerns all the species (oligoradicals or dead polymer) present in both phases. This leads to the following relationship:

$$\bar{M}_N=\frac{\begin{pmatrix}\left[A^*_{T,0}\right]_c\lambda^c_{1,0}M_u+\left[A^*_{T,1}\right]_c\left(\lambda^c_{1,1}M_u+M_S\right)+\left[A^*_{T,3}\right]_c\left(\lambda^c_{1,3}M_u+M_G\right)\\+\left[B^*_{T,0}\right]_c\eta^c_{1,0}M_u+\left[B^*_{T,1}\right]_c\left(\eta^c_{1,1}M_u+M_S\right)+\left[B^*_{T,3}\right]_c\left(\eta^c_{1,3}M_u+M_G\right)\\+\left[G^*_{T,3}\right]_c\left(\nu^c_{1,3}M_u+M_G\right)\\+\left[P_{T,0}\right]_c\mu^c_{1,0}M_u+\left[P_{T,1}\right]_c\left(\mu^c_{1,1}M_u+M_S\right)+\left[P_{T,3}\right]_c\left(\mu^c_{1,3}M_u+M_G\right)\end{pmatrix}V_c+\begin{pmatrix}\left[A^*_{T,0}\right]_p\lambda^p_{1,0}M_u+\left[A^*_{T,1}\right]_p\left(\lambda^p_{1,1}M_u+M_S\right)+\left[A^*_{T,3}\right]_p\left(\lambda^p_{1,3}M_u+M_G\right)\\+\left[B^*_{T,0}\right]_p\eta^p_{1,0}M_u+\left[B^*_{T,1}\right]_p\left(\eta^p_{1,1}M_u+M_S\right)+\left[B^*_{T,3}\right]_p\left(\eta^p_{1,3}M_u+M_G\right)\\+\left[G^*_{T,3}\right]_p\left(\nu^p_{1,3}M_u+M_G\right)\\+\left[P_{T,0}\right]_p\mu^p_{1,0}M_u+\left[P_{T,1}\right]_p\left(\mu^p_{1,1}M_u+M_S\right)+\left[P_{T,3}\right]_p\left(\mu^p_{1,3}M_u+M_G\right)\end{pmatrix}V_p}{\left(\left[A^*_{T,0}\right]_c+\left[A^*_{T,1}\right]_c+\left[A^*_{T,3}\right]_c+\left[B^*_{T,0}\right]_c+\left[B^*_{T,1}\right]_c+\left[B^*_{T,3}\right]_c+\left[G^*_{T,3}\right]_c+\left[P_{T,0}\right]_c+\left[P_{T,1}\right]_c+\left[P_{T,3}\right]_c\right)V_c+\left(\left[A^*_{T,0}\right]_p+\left[A^*_{T,1}\right]_p+\left[A^*_{T,3}\right]_p+\left[B^*_{T,0}\right]_p+\left[B^*_{T,1}\right]_p+\left[B^*_{T,3}\right]_p+\left[G^*_{T,1}\right]_p+\left[P_{T,0}\right]_p+\left[P_{T,1}\right]_p+\left[P_{T,3}\right]_p\right)V_p} \tag{4.83}$$

It must be noticed that the quantity of ungrafted dead polymer inside particles should be very greater than that of the other species, therefore the number-average molecular weight of CPP can be roughly estimated by :

$$\overline{M}_N \approx \frac{\left[P_{T,0}\right]_p \mu_{1,0}^p M_u V_p}{\left[P_{T,0}\right]_p V_p} = \mu_{1,0}^p M_u \tag{4.84}$$

In the same way, the weight-average molecular weight of whole CPP, $\overline{M}_W$, concerns all the species (oligoradicals or dead polymer) present in both phases. This leads to the following relationship (Eq. 4.90) :

$$\overline{M}_N\overline{M}_W = \frac{\begin{pmatrix} \left[A_{T,0}^*\right]_c \lambda_{2,0}^c M_u^2 + \left[A_{T,1}^*\right]_c \left(\lambda_{2,1}^c M_u^2 + M_S^2 + 2\lambda_{1,1}^c M_u M_S\right) + \left[A_{T,3}^*\right]_c \left(\lambda_{2,3}^c M_u^2 + M_G^2 + 2\lambda_{1,3}^c M_u M_G\right) \\ + \left[B_{T,0}^*\right]_c \eta_{2,0}^c M_u + \left[B_{T,1}^*\right]_c \left(\eta_{2,1}^c M_u^2 + M_S^2 + 2\eta_{1,1}^c M_u M_S\right) + \left[B_{T,3}^*\right]_c \left(\eta_{2,1}^c M_u^2 + M_G^2 + 2\eta_{1,3}^c M_u M_G\right) \\ + \left[G_{T,3}^*\right]_c \left(\nu_{2,3}^c M_u^2 + M_G^2 + 2\nu_{1,3}^c M_u M_G\right) \\ + \left[P_{T,0}\right]_c \mu_{2,0}^c M_u^2 + \left[P_{T,1}\right]_c \left(\mu_{2,1}^c M_u^2 + M_S^2 + 2\mu_{1,1}^c M_u M_S\right) + \left[P_{T,3}\right]_c \left(\mu_{2,3}^c M_u^2 + M_G^2 + 2\mu_{1,3}^c M_u M_G\right) \end{pmatrix} V_c}{\left(\left[A_{T,0}^*\right]_c + \left[A_{T,1}^*\right]_c + \left[A_{T,3}^*\right]_c + \left[B_{T,0}^*\right]_c + \left[B_{T,1}^*\right]_c + \left[B_{T,3}^*\right]_c + \left[G_{T,3}^*\right]_c + \left[P_{T,0}\right]_c + \left[P_{T,1}\right]_c + \left[P_{T,3}\right]_c\right) V_c}$$
$$+ \frac{\begin{pmatrix} \left[A_{T,0}^*\right]_p \lambda_{2,0}^p M_u^2 + \left[A_{T,1}^*\right]_p \left(\lambda_{2,1}^p M_u^2 + M_S^2 + 2\lambda_{1,1}^p M_u M_S\right) + \left[A_{T,3}^*\right]_p \left(\lambda_{2,3}^p M_u^2 + M_G^2 + 2\lambda_{1,3}^p M_u M_G\right) \\ + \left[B_{T,0}^*\right]_p \eta_{2,0}^p M_u + \left[B_{T,1}^*\right]_p \left(\eta_{2,1}^p M_u^2 + M_S^2 + 2\eta_{1,1}^p M_u M_S\right) + \left[B_{T,3}^*\right]_p \left(\eta_{2,3}^p M_u^2 + M_G^2 + 2\eta_{1,3}^p M_u M_G\right) \\ + \left[G_{T,3}^*\right]_p \left(\nu_{2,3}^p M_u^2 + M_G^2 + 2\nu_{1,3}^p M_u M_G\right) \\ + \left[P_{T,0}\right]_p \mu_{2,0}^p M_u^2 + \left[P_{T,1}\right]_p \left(\mu_{2,1}^p M_u^2 + M_S^2 + 2\mu_{1,1}^p M_u M_S\right) + \left[P_{T,3}\right]_p \left(\mu_{2,3}^p M_u^2 + M_G^2 + 2\mu_{1,3}^p M_u M_G\right) \end{pmatrix} V_p}{+\left(\left[A_{T,0}^*\right]_p + \left[A_{T,1}^*\right]_p + \left[A_{T,3}^*\right]_p + \left[B_{T,0}^*\right]_p + \left[B_{T,1}^*\right]_p + \left[B_{T,3}^*\right]_p + \left[G_{T,3}^*\right]_p + \left[P_{T,0}\right]_p + \left[P_{T,1}\right]_p + \left[P_{T,3}\right]_p\right) V_p} \tag{4.85}$$

Again, if we consider that ungrafted dead polymer in the particles may be the majority of the species, $\overline{M}_W$ can be roughly approximated to :

$$\overline{M}_W \approx \frac{\mu_{2,0}^p}{\mu_{1,0}^p} M_u \tag{4.86}$$

2.4.1.3. <u>SAN dissolved in the continuous phase</u>

The number-average molecular weight of SAN in the serum, $\overline{M}_N^c$, is calculated as follows :

$$\overline{M}_N^c = \frac{\begin{pmatrix} \left[A_{T,0}^*\right]_c \lambda_{1,0}^c M_u + \left[A_{T,1}^*\right]_c \left(\lambda_{1,1}^c M_u + M_S\right) + \left[A_{T,3}^*\right]_c \left(\lambda_{1,3}^c M_u + M_G\right) \\ + \left[B_{T,0}^*\right]_c \eta_{1,0}^c M_u + \left[B_{T,1}^*\right]_c \left(\eta_{1,1}^c M_u + M_S\right) + \left[B_{T,3}^*\right]_c \left(\eta_{1,3}^c M_u + M_G\right) \\ + \left[G_{T,3}^*\right]_c \left(\nu_{1,3}^c M_u + M_G\right) \\ + \left[P_{T,0}\right]_c \mu_{1,0}^c M_u + \left[P_{T,1}\right]_c \left(\mu_{1,1}^c M_u + M_S\right) + \left[P_{T,3}\right]_c \left(\mu_{1,3}^c M_u + M_G\right) \end{pmatrix} V_c}{\left(\left[A_{T,0}^*\right]_c + \left[A_{T,1}^*\right]_c + \left[A_{T,3}^*\right]_c + \left[B_{T,0}^*\right]_c + \left[B_{T,1}^*\right]_c + \left[B_{T,3}^*\right]_c + \left[G_{T,3}^*\right]_c + \left[P_{T,0}\right]_c + \left[P_{T,1}\right]_c + \left[P_{T,3}\right]_c\right) V_c} \tag{4.87}$$

The weight-average molecular weight of SAN in the serum, $\overline{M}_W^c$, is expressed as follows :

$$\overline{M}_N^c\overline{M}_W^c = \frac{\left(\begin{array}{l}\left[A_{T,0}^*\right]_c \lambda_{2,0}^c M_u^2 + \left[A_{T,1}^*\right]_c \left(\lambda_{2,1}^c M_u^2 + M_S^2 + 2\lambda_{1,1}^c M_u M_S\right) + \left[A_{T,3}^*\right]_c \left(\lambda_{2,3}^c M_u^2 + M_G^2 + 2\lambda_{1,3}^c M_u M_G\right) \\ + \left[B_{T,0}^*\right]_c \eta_{2,0}^c M_u + \left[B_{T,1}^*\right]_c \left(\eta_{2,1}^c M_u^2 + M_S^2 + 2\eta_{1,1}^c M_u M_S\right) + \left[B_{T,3}^*\right]_c \left(\eta_{2,1}^c M_u^2 + M_G^2 + 2\eta_{1,3}^c M_u M_G\right) \\ + \left[G_{T,3}^*\right]_c \left(\nu_{2,3}^c M_u^2 + M_G^2 + 2\nu_{1,3}^c M_u M_G\right) \\ + \left[P_{T,0}\right]_c \mu_{2,0}^c M_u^2 + \left[P_{T,1}\right]_c \left(\mu_{2,1}^c M_u^2 + M_S^2 + 2\mu_{1,1}^c M_u M_S\right) + \left[P_{T,3}\right]_c \left(\mu_{2,3}^c M_u^2 + M_G^2 + 2\mu_{1,3}^c M_u M_G\right)\end{array}\right) V_c}{\left(\left[A_{T,0}^*\right]_c + \left[A_{T,1}^*\right]_c + \left[A_{T,3}^*\right]_c + \left[B_{T,0}^*\right]_c + \left[B_{T,1}^*\right]_c + \left[B_{T,3}^*\right]_c + \left[G_{T,3}^*\right]_c + \left[P_{T,0}\right]_c + \left[P_{T,1}\right]_c + \left[P_{T,3}\right]_c\right) V_c} \tag{4.88}$$

2.4.2. Weight % of solids in stripped CPP and residual quantities of reactants

From the state of the system it is possible to calculate the weight-% of solids in stripped CPP and the weight-% of residual acrylonitrile, styrene and NDM in the whole CPP :

$$\text{Wt-\% solids in stripped CPP} = 100\frac{m_{solids}}{m_{CPP} - m_A - m_B} \tag{4.89}$$

With : $m_A = V[A]M_A$ (4.90)

$$m_B = V[B]M_B \tag{4.91}$$

$$m_{CTA} = V[CTA]M_{CTA} \tag{4.92}$$

The weight of CPP in the reactor, m_{CPP}, is given by Eq. 4.54.

The weight of the stripped solid phase is :

$$m_{solids} = \left(\begin{array}{l}\left[A_{T,0}^*\right]_p \lambda_{1,0}^p M_u + \left[A_{T,1}^*\right]_p \left(\lambda_{1,1}^p M_u + M_S\right) + \left[A_{T,3}^*\right]_p \left(\lambda_{1,3}^p M_u + M_G\right) \\ + \left[B_{T,0}^*\right]_p \eta_{1,0}^p M_u + \left[B_{T,1}^*\right]_p \left(\eta_{1,1}^p M_u + M_S\right) + \left[B_{T,3}^*\right]_p \left(\eta_{1,3}^p M_u + M_G\right) \\ + \left[G_{T,3}^*\right]_p \left(\nu_{1,3}^p M_u + M_G\right) \\ + \left[P_{T,0}\right]_p \mu_{1,0}^p M_u + \left[P_{T,1}\right]_p \left(\mu_{1,1}^p M_u + M_S\right) + \left[P_{T,3}\right]_p \left(\mu_{1,3}^p M_u + M_G\right)\end{array}\right) V_p . \tag{4.93}$$

Nevertheless, for the calculations, the weight of solid has been approximated by the total weight of monomers incorporated in the polymer, neglecting the quantity of polymer dissolved in the continuous phase in front of that in the solid polymer :

$$m_{solids} \approx \left[A_p\right] V M_A + \left[B_p\right] V M_B \tag{4.94}$$

Then, the quantities of residual reactants is given by :

$$\text{Residual AN (wgt-\%)} = 100\frac{m_A}{m_{CPP}}, \tag{4.95}$$

$$\text{Residual Sty (wgt-\%)} = 100\frac{m_B}{m_{CPP}}, \tag{4.96}$$

$$\text{Residual NDM (ppm)} = 10^6\frac{m_{CTA}}{m_{CPP}}, \tag{4.97}$$

where the weight of CPP inside the reactor, m_{CPP}, is calculated using Eq. 4.60.

2.4.3. Composition of the SAN copolymer

As all the experiments are made in a continuous reactor, the composition of the polymer is ruled by the composition of the medium in steady state regime. Nevertheless, as the partitioning coefficients of styrene and acrylonitrile may be different, the ratio of monomers may be different in the continuous phase and inside particles and therefore the composition of SAN copolymer also. However, as the great majority of the polymer is inside the particles, we have considered that the composition of the polymers is directly linked to the quantity of each monomer incorporated :

$$\text{Wt-\% Sty in SAN} = Y_B = 100\frac{[B_p]M_B}{[A_p]M_A + [B_p]M_B} \tag{4.98}$$

2.4.4. Quantity of SAN copolymer dissolved in the continuous phase

The quantity of SAN copolymer dissolved in the serum can be calculated from the system state as follows :

$$\text{Wt-\% SAN/ solvent} = 100\frac{m^c_{SAN}}{m_{serum}} \tag{4.99}$$

Where the weight of SAN dissolved in the serum is :

$$m^c_{SAN} = \begin{pmatrix} [A^*_{T,0}]_c \lambda^c_{1,0} M_u + [A^*_{T,1}]_c (\lambda^c_{1,1} M_u + M_S) + [A^*_{T,3}]_c (\lambda^c_{1,3} M_u + M_S) \\ + [B^*_{T,0}]_c \eta^c_{1,0} M_u + [B^*_{T,1}]_c (\eta^c_{1,1} M_u + M_S) + [B^*_{T,3}]_c (\eta^c_{1,3} M_u + M_G) \\ + [G^*_{T,3}]_c (\nu^c_{1,3} M_u + M_G) \\ + [P_{T,0}]_c \mu^c_{1,0} M_u + [P_{T,1}]_c (\mu^c_{1,1} M_u + M_S) + [P_{T,3}]_c (\mu^c_{1,3} M_u + M_G) \end{pmatrix} V_c, \tag{4.100}$$

and where the weight of the serum phase (unstripped) is

$$m_{serum} = [S]VM_S + [G]VM_G + [A]_c V_c M_A + [B]_c V_c M_B + m^c_{SAN}.$$

Obviously the other species (I, CTA) are negligible.

2.4.5. Grafting quantification

The liquid chromatography followed by UV detector allows separating the grafted SAN chains from the ungrafted ones. Nevertheless the observed signal that is proportional to the quantity of styrene present in the polymer chains. The weight % of graft present in a given phase is the ratio of the weight of styrene in grafted SAN chains over the total weight of styrene incorporated in this phase.

Therefore, in the serum phase :

$$\text{Wt-\% SAN grafted in serum} = 100\, m^{c}_{B_{SAN-grafted}} \Big/ m^{c}_{B_{SAN}} \tag{4.101}$$

where,

$$m^{c}_{B_{SAN-grafted}} = \begin{pmatrix} \lambda^{c}_{1,1}\left[A^{*}_{T,1}\right]_c + \lambda^{c}_{1,3}\left[A^{*}_{T,3}\right]_c + \eta^{c}_{1,1}\left[B^{*}_{T,1}\right]_c + \eta^{c}_{1,3}\left[B^{*}_{T,3}\right]_c + \nu^{c}_{1,3}\left[G^{*}_{T,3}\right]_c \\ + \mu^{c}_{1,1}\left[P_{T,1}\right]_c + \mu^{c}_{1,3}\left[P_{T,3}\right]_c \end{pmatrix} V_c M_u Y_B , \tag{4.102}$$

and,

$$m^{c}_{B_{SAN}} = \left(\lambda^{c}_{1,0}\left[A^{*}_{T,0}\right]_c + \eta^{c}_{1,0}\left[B^{*}_{T,0}\right]_c + \mu^{c}_{1,0}\left[P_{T,0}\right]_c\right) V_c M_u B_{ratio} + m^{c}_{SAN-grafted} . \tag{4.103}$$

In the solid phase :

$$\text{Wt-\% SAN grafted in solid} = 100 \cdot m^{p}_{B_{SAN-grafted}} \Big/ m^{p}_{B_{SAN}} , \tag{4.104}$$

where,

$$m^{p}_{B_{SAN-grafted}} = \begin{pmatrix} \lambda^{p}_{1,1}\left[A^{*}_{T,1}\right]_p + \lambda^{p}_{1,3}\left[A^{*}_{T,3}\right]_p + \eta^{p}_{1,1}\left[B^{*}_{T,1}\right]_p + \eta^{p}_{1,3}\left[B^{*}_{T,3}\right]_p + \nu^{p}_{1,3}\left[G^{*}_{T,3}\right]_p \\ + \mu^{p}_{1,1}\left[P_{T,1}\right]_p + \mu^{p}_{1,3}\left[P_{T,3}\right]_p \end{pmatrix} V_p M_u Y_B , \tag{4.105}$$

and,

$$m^{p}_{B_{SAN}} = \left(\lambda^{p}_{1,0}\left[A^{*}_{T,0}\right]_p + \eta^{p}_{1,0}\left[B^{*}_{T,0}\right]_p + \mu^{p}_{1,0}\left[P_{T,0}\right]_p\right) V_p M_u Y_B + m^{p}_{SAN-grafted} . \tag{4.106}$$

Therefore, in whole CPP :

$$\text{Wt-\% SAN grafted in whole CPP} = 100 \frac{m^{c}_{B_{SAN-grafted}} + m^{p}_{B_{SAN-grafted}}}{m^{c}_{B_{SAN}} + m^{p}_{B_{SAN}}} . \tag{4.107}$$

The weight-% of polyol present in the solid phase is measured by ^{1}H RMN. It is the weight of the grafts over the total weight of all SAN chains in the particles :

$$\text{Wt-\% polyol} = 100\ \frac{m^{p}_{Graft}}{m^{p}_{SAN}} , \tag{4.108}$$

where,

$$m^{p}_{Graft} = \left(\left[A^{*}_{T,1}\right]_p + \left[B^{*}_{T,1}\right]_p + \left[P_{T,1}\right]_p\right) V_p M_S + \left(\left[A^{*}_{T,3}\right]_p + \left[B^{*}_{T,3}\right]_p + \left[G^{*}_{T,3}\right]_p + \left[P_{T,3}\right]_p\right) V_p M_G , \tag{4.109}$$

and,

$$m_{SAN}^{p} = \begin{pmatrix} \left[A_{T,0}^{*}\right]_p \lambda_{1,0}^{p} M_u + \left[A_{T,1}^{*}\right]_p \left(\lambda_{1,1}^{p} M_u + M_S\right) + \left[A_{T,3}^{*}\right]_p \left(\lambda_{1,3}^{p} M_u + M_G\right) \\ + \left[B_{T,0}^{*}\right]_p \eta_{1,0}^{p} M_u + \left[B_{T,1}^{*}\right]_p \left(\eta_{1,1}^{p} M_u + M_S\right) + \left[B_{T,3}^{*}\right]_p \left(\eta_{1,3}^{p} M_u + M_G\right) \\ + \left[G_{T,3}^{*}\right]_p \left(\nu_{1,3}^{p} M_u + M_G\right) \\ + \left[P_{T,0}\right]_p \mu_{1,0}^{p} M_u + \left[P_{T,1}\right]_p \left(\mu_{1,1}^{p} M_u + M_S\right) + \left[P_{T,3}\right]_p \left(\mu_{1,3}^{p} M_u + M_G\right) \end{pmatrix} V_p . \qquad (4.110)$$

3. Estimation of the steady state regime

The steady state regime of this system is needed to be calculated, nevertheless as the system described previously is non-linear, we decided to solve it by dynamic resolution. The system is initiated by considering that there is only polyol inside the reactor as it is done experimentally at the beginning of each run. Nevertheless, the simulation may be valid only in steady state regime and does not pretend to represent the transient regime.

In order to avoid numerical instabilities during the system resolution, we have decided to use the quasi-steady state approximation in order to stabilize the integration. Therefore, all the production rates of radicals are considered to be equal to zero. Only the differential equations concerning the monomers, the initiator, the chains transfer agent, the precursor stabilizer S5200, the polyol, the dead polymer and their moment were considered.

The simulation is made using given parameters of the model (kinetic constants, reactivities, partitioning coefficients, ...) and process conditions (premix composition, temperature and mass flow).

The system has been resolved dynamically, that is to say, through a numerical integration of the differential equations with a Runge-Kutta method from t = 0 to t = 10 000 s (almost 8 residence times) with a step of integration of $\Delta t = 0.1$ s. A longer step gives inaccurate integrations and smaller ones takes too long integration times and creates numerical instabilities. The choice of these two values is a compromise between the necessity to have the best accuracy and the smallest computing times as possible. It defines a kind of standard for the simulations that will have to be realized with these conditions to take into account the parameters identification.

At a given time of integration, t, two systems are integrated successively : the global concentrations firstly, and secondly, the concentrations of the free species and of the dead polymer concentrations with their moments of order one and two.

* Global system at t :

The system is initiated by (at t = 0) :

$$[A_T] = [B_T] = [G_T] = [CTA_T] = [I_T] = 0$$

$$[S_T] = \rho_S / M_S$$

and $m_{CPP} = V \cdot \rho_S$

Then equations 4.48 to 4.53 are integrated giving new values for these global concentrations at t + Δt, allowing to calculate m_{CPP} at this new time using equation 4.54.

* Detailed system at t :

This system is composed of 16 equations, which are the derivative equations of the concentration of free species in the reactor (Eq. 4.59 to 4.64), of the quantities of dead polymer in both phases (Eq. A4.88, A4.91, A4.94, A4.128, A4.131 and A4.134).

The moments of order one and two of the dead polymer are calculated using equations A4.89, A4.90, A4.129 and A4.130 of Annex 4. For instance, the moment of order 1 of the ungrafted dead polymers in the continuous phase is calculated using equations A4.88 and A4.89 of annex 4 as follows, in order to avoid the numerical instabilities :

$$\frac{d\mu_{1,0}^c}{dt} = \frac{1}{V_c\left[P_{T,0}\right]_c}\left\{\frac{d\left(V_c\left[P_{T,0}\right]_c\mu_{1,0}^c\right)}{dt} - \mu_{1,0}^c\frac{d\left(V_c\left[P_{T,0}\right]_c\right)}{dt}\right\}. \tag{4.111}$$

This leads to equation 4.112 below:

$$\begin{aligned} V_c\left[P_{T,0}\right]_c d\mu_{1,0}^c/dt = &+\left(k_{tcAA}^c\left[A_{T,0}^*\right]_c^2\left(2\lambda_{1,0}^c-\mu_{1,0}^c\right)+k_{tcBB}^c\left[B_{T,0}^*\right]_c^2\left(2\eta_{1,0}^c-\mu_{1,0}^c\right)\right)V_c \\ &+k_{tcAB}^c\left[A_{T,0}^*\right]_c\left[B_{T,0}^*\right]_c\left(\lambda_{1,0}^c+\eta_{1,0}^c-\mu_{1,0}^c\right)V_c \\ &+k_{tdGA}^c\left[G_{T,3}^*\right]_c\left[A_{T,0}^*\right]_c\left(\nu_{1,3}^c+\lambda_{1,0}^c-\mu_{1,0}^c\right)V_c+k_{tdGB}^c\left[G_{T,3}^*\right]_c\left[B_{T,0}^*\right]_c\left(\nu_{1,3}^c+\eta_{1,0}^c-\mu_{1,0}^c\right)V_c \\ &+\left\{k_{t,A}^c\left[CTA\right]_c+k_{tr,AG}^c\left[G\right]_c+k_{tr,AS}^c\left[S\right]_c\right\}V_c\left[A_{T,0}^*\right]_c\left(\lambda_{1,0}^c-\mu_{1,0}^c\right) \\ &+\left\{k_{t,B}^c\left[CTA\right]_c+k_{tr,BG}^c\left[G\right]_c+k_{tr,BS}^c\left[S\right]_c\right\}V_c\left[B_{T,0}^*\right]_c\left(\eta_{1,0}^c-\mu_{1,0}^c\right) \end{aligned} \tag{4.112}$$

$\mu_{1,0}^c$, $\mu_{1,0}^p$, $\mu_{2,0}^c$ and $\mu_{2,0}^p$ are therefore calculated by this way.

It is then supposed that :

$$\mu_{1,0}^c = \mu_{1,1}^c = \mu_{1,3}^c, \tag{4.113}$$

$$\mu_{1,0}^p = \mu_{1,1}^p = \mu_{1,3}^p, \tag{4.114}$$

$$\mu_{2,0}^c = \mu_{2,1}^c = \mu_{2,3}^c, \tag{4.115}$$

$$\mu_{2,0}^p = \mu_{2,1}^p = \mu_{2,3}^p. \tag{4.116}$$

That is to say that the moments of the dead polymer grafted are supposed to be equal to the moments of the ungrafted polymer chains. This has been further checked by simulation.

The system is initiated by considering all the concentrations equal to zero except the concentration of solvent in the reactor,

$$\left[S\right] = \rho_S/M_S \text{ at t} = 0, \tag{4.117}$$

and the moments are initiated to unity.

When all these concentrations are known at t + Δt, it is possible to calculate the volume of the polymer phase using equation 4.37 and equations below giving the concentration of monomers incorporated in the polymer :

$$\left[A_p\right]=\left[A_T\right]-\left[A\right], \tag{4.118}$$

$$\left[B_p\right]=\left[B_T\right]-\left[B\right]. \tag{4.119}$$

Then the composition in styrene, Y_B, of the produced SAN copolymer is approximated and the molecular weight of the monomeric unit, M_u, is calculated using equation 4.20.

Further, the concentrations of the monomers, chain transfer agent and initiator can be calculated in each phase (Eq. 4.55 to 4.58).

The concentrations of all the radicals in the medium are then calculated by using the quasi-steady state approximation, assuming that all the production rates of radicals and moments are equal to zero. Moreover, the new concentrations calculated at t + Δt, are calculated using the previous values at t. For instance, the square of a given radical concentration x at t + Δt, $\left(x(t+\Delta t)\right)^2$, becomes $x(t+\Delta t)\cdot x(t)$, the concentration at t + Δt times the concentration at t, in order to simplify the calculation and to avoid the resolution of equations of the second degree, but most of all, in order to stabilize the integration and to avoid the numerical instabilities. The mathematical justification of this assumption is presented at the end of annex 4.

Finally, all the data that can be compared to the measurements and which are presented in paragraph 2.4 of this chapter, the weight proportion of polymer inside swollen particles, x_p, and the new value of the gel effect constant, g (Eq. 4.12), are calculated at t + Δt.

Conclusion

This model has been realized taking into account the experimental knowledge about the process. The purpose was to define a model able to calculate the data provided by analytical methods and which describe the properties of copolymer polyols. The objective was also to better understand the grafting mechanisms and to forecast the grafting level from the experimental conditions.

Nevertheless, it was necessary to make assumptions and simplifications in order to obtain a model with the lowest number of parameters to identify and which provided times of simulation sufficiently short.

It must be remember anyway, that this model is a tendency model. The parameters defined here are not the real constant kinetics, for instance, but contains a larger number of kinetic constants, which are simplified in a smaller number of constants to simplify the model, but with the aim to forecast the same data with an acceptable accuracy.

CHAPTER 5
PARAMETER IDENTIFICATION

INTRODUCTION **191**

1. PRINCIPLES OF EVOLUTIONARY ALGORITHM AND PARAMETER IDENTIFICATION **191**

1.1. INTRODUCTION AND VOCABULARY 191

1.2. PRINCIPLE 192

1.3. DESCRIPTION OF THE COMPONENTS OF THE GENETIC OR EVOLUTIONARY ALGORITHM 192

1.3.1. Coding *192*
1.3.2. Generation of the initial population *192*
1.3.3. Evaluation *192*
1.3.4. End criteria *193*
1.3.5. Selection *193*
1.3.6. Mutation *194*
1.3.7. Cross over *194*
1.3.8. Replacement *194*

1.4. PARAMETER IDENTIFICATION 194

2. DEFINITION OF THE PARAMETERS TO IDENTIFY **195**

2.1. FIXED PARAMETERS 195

2.2. IDENTIFIED PARAMETERS 195

2.3. EXPERIMENTAL DATA CONSIDERED 197

3. RESULTS AND DISCUSSION **198**

3.1. RESULTS 198

3.2. AVERAGE MOLECULAR WEIGHTS 201

3.3. SOLIDS AND RESIDUAL CONCENTRATIONS OF ACRYLONITRILE, STYRENE AND NDM. 205

3.4. SAN COPOLYMER COMPOSITION 205

3.5. SERUM : WT-% OF SAN DISSOLVED AND % OF GRAFTED SAN 211

3.6. % OF GRAFTED SAN IN WHOLE CPP (HMW) AND WT-% OF POLYOL IN SOLIDS 214

3.7. SAUTER MEAN DIAMETER 217

4. VALIDATION AND DISCUSSION 219

4.1. VALIDATION ON STANDARD RUNS CARRIED OUT AT T = 130°C 219

4.2. CONFIDENCE INTERVAL OF THE IDENTIFIED PARAMETERS 221

4.3. GRAFTING MODELING AND PATH FORWARD 222

CONCLUSION 223

Introduction

The model presented in chapter 4 will be now used in order to forecast the experimental results shown in chapter 3. Considering the lack of accuracy of some of the measurements combined with the instability of some of the recipes used, a perfect appropriateness between the model and the experiments is not foreseen, but the number of measurements done may be sufficient to foresee the orders of magnitude and to check the different hypotheses chosen for the model.

For this study we will use adapted mathematical tools such as evolutionary algorithms. Therefore, the different principles of the algorithm used here for the parameter identification will be exposed in the first part. Then, the different parameters chosen to be identified will be presented. In the third part, the results of the identifications at 120 °C and 140 °C will be developed. Finally, the validation of the model on the standard recipes will be shown with a discussion of the results, and the different possibilities to go on with this work will be approached.

1. Principles of Evolutionary Algorithm and Parameter Identification

1.1. Introduction and vocabulary

In the seventies, a new approach appeared in order to treat issues of optimization, called genetic algorithms (Holland, 1975) or evolution strategy algorithm (Rechenberg, 1973), and get famous since fifteen years (Goldberg, 1989). Actually, evolutionary algorithms (Bäck, 1996) have been constructed by analogy with models of natural evolution of the biological population. Indeed, the optimization methods are based on the Darwin's concept of the theory of evolution and on the principle that species are issued one from the others following the law of natural selection, effect of the fight for the life (Darwin, 1859). Therefore, only the best species of a population can prevail in a given environment.

First of all, it is necessary to define specific terms of vocabulary that are used in this domain, knowing that the terminology of genetic algorithm will be the same that of genetics:

- individual : element or point of the solution space
- chromosome : individual's code
- performance : value of a function F or evaluation of an individual
- population : gathering of the individuals
- generation : crossing from a population to the other
- parents : individuals that are selected to form a new generation
- children : individuals coming from the cross-over of the parents

Under the pressure of the medium, the individuals of a population mutate and reproduce themselves by the way of genetic operators, which allow them to stay alive and to adapt themselves to the constraints given by their environment. After a given number of generations, the best individuals, or the ones that are the best adapted to their environment, appear in the population, that is to say the optima of the function F. The biological evolution does not provide a "super unique individual" but to some species which interact with and adapt to each other. The

probability that these methods get trapped in local minima is lower than the classical algorithm (Newtonian methods,...), because they explore in parallel a set of possible solutions. In theory however, even if the solutions are better from generations to generations, there is no certitude that the algorithm will find the optimum solution. Moreover, the particularity of these methods is that they only use the evaluation functions and they do not need to calculate furthermore the partial derivatives and the Jacobian matrix. Finally, it is possible to work with variables, which are mixed, integers and reals. This is why these algorithms have been used in several applications as, for instance, in mechanics (Schoenauer et al., 1996), chemical engineering (Leboreiro & Acevedo, 2004), and in parameter identification (Perrin et al, 1993).

1.2. Principle

An evolutionary (or genetic) algorithm is an iterative process of optimization, which principle can be described as follows : an initial population is generated and each individual is generated from the knowledge of the research domain. This population represents the potential solutions of the problem. One performance is associated to each possible solution by the way of an evaluation function which is deduced from the optimization criteria. As long as the population is not good enough or the criteria of convergence is not respected, a selection process, which favors the survival of the best adapted individuals to the detriment of the worst ones, is done and a renewal of the population using genetic operators (cross over, mutation). This iterative approach allows to make evolve the individuals from generations to generations until obtaining the best population possible.

1.3. Description of the components of the genetic or evolutionary algorithm

The figure 5.1 presents the general principle of the evolutionary algorithm, that has been developed by Bicking et al. (1994), and Fonteix et al. (1995), and that was used to solve the system presented in chapter 4. The different steps of this algorithm are described below.

1.3.1. Coding

One of the most important phase consists in giving a code under the form of a chromosome to the variables of the problem of optimization. There are two types of code : binary code which allows to describe the variables with series of bits 0 or 1 (characteristic of genetic algorithms), and real code where the variables have directly their values (characteristic of evolutionary algorithms). But other types of codings may exist depending on the problem, which is treated.

1.3.2. Generation of the initial population

The initial population is generated randomly or among a specific distribution of the research space. It is also possible to take into account the *a priori* knowledge by adding manually good solutions. But in this case, one should be careful to the lost of diversity. Finally, the initial population can be the result of a previous evolution or take into account several populations.

1.3.3. Evaluation

It is the most time consuming operation as the evaluation function (also called fitness), F, can be very complex to determine. It can be necessary for instance to use a numerical resolution for solving systems of differential equations for instance. This function should not be calculated needlessly (it is possible to replace the calculation by an experimental result).

1.3.4. End criteria

As explained by Schoenauer et al. (1994), the process stops when a target value for the best fitness, or some a priori maximal number of generations is run, or the best fitness value in the population does not improve during a user-defined number of generations, which ever comes first. If the end criteria is not fulfilled, another generation starts.

1.3.5. Selection

The aim of this step is to select the individuals, which reproduce with each other, trying to favors the best ones. A compromise should be done to avoid a lost of diversity if the best elements are excessively selected, and to avoid the non-convergence of the algorithm due to the deficiency in the selection of the best ones.

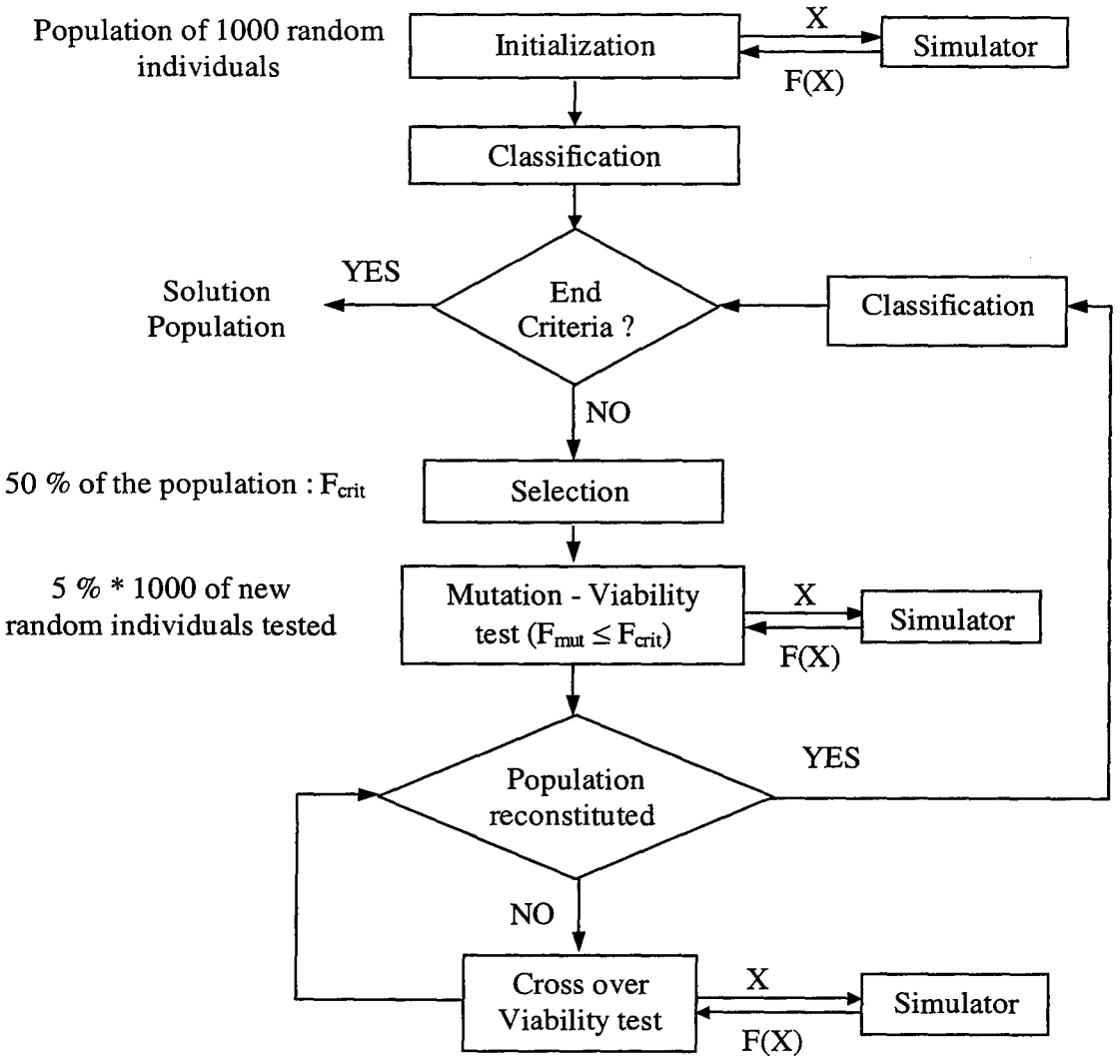

Figure 5.1 : Scheme of the genetic algorithm

1.3.6. Mutation

Mutation corresponds to the asexual reproduction and allows to give a counterbalance for the children with respect to the parents. It is an exploration operator used to check that the algorithm does not miss the absolute maximum. Actually it is a new individual randomly chosen in the space of solutions.

1.3.7. Cross over

The cross over corresponds to a sexual reproduction between selected parents. Therefore, the children inherit of the qualities of the both parents. It is an operator of exploitation, which regulates the algorithm convergence. There are different type of cross overs but in real coding the cross over that is usually used is generally barycentric between the two parents in order to provide a new child. A weight is given to each parent, and it can be negative to enlarge the exploration of the space (Michalewicz, 1992).

1.3.8. Replacement

After the creation of the children by the use of different genetic operators, a new generation leads to the new population.

1.4. Parameter identification

An evolutionary algorithm is used in order to identify the parameters of the model presented in chapter 4 : the purpose is to find the acceptable set of solutions such as theoretical and experimental data may be the closer as possible.

The individuals, vectors X, contain the possible values of the parameters. The performance of each individual X is calculated by the method of maximum likelihood estimator (Walter & Pronzato, 1997). This leads to minimize the function F :

$$F(X)=\sum_{k=1}^{nm} n_{ek} Log\left[J(k,X)\right], \tag{5.1}$$

where nm is the number of different types of measurements used for the identification, and n_{ek} is the number of experiments taken into account for the measurement of the data k.

J(k,X) is the sum of squared discrepancies (the most straightforward way to measure the fitness between the model, Z_{theo}, and the measurements, Z_{exp}) for each type, k, of data Z measured ($\bar{M}_n$, $\bar{M}_w$,...) :

$$J(k,X)=\sum_{i=1}^{ne} k\left[Z_{theo}(i,k,X)-Z_{\exp}(i,k)\right]^2, \tag{5.2}$$

where i corresponds to the different experiments (experimental design) and ne is the total number of experiments taken into consideration.

The number of individuals per generation (the population size) should be around 45 times the number of parameters : for 24 parameters, a population of 1000 individuals, is chosen.

50 % of the population is replaced at each generation. Actually, the individuals of each generation are classified from the best to the worst. The performance of the last individual selected is used to test the new children : their performances have to be better to replace the bad individuals otherwise, they are rejected, and new cross-over or mutations are processed, until the population is finally complete.

A given number of attempts (5 % of the number of individuals to reconstitute) are done to find new individuals coming from mutation. They are chosen randomly in the space of solutions and their viability was tested : only the new individuals whose performances are better than the critical performance are kept ($F_{mut} \leq F_{crit}$) in the new population. F_{crit} is the value of the best parent.

The crossovers are done between two different parents selected randomly from the best parents, that is to say from the population whose performances are better than the critical performance ($F_{parent} \leq F_{crit}$). The characteristics of the child are obtained as following classifying the parents such as "parent1" is better than "parent2" :

$$X^{child} = Coef \cdot X^{parent1} + (1 - Coef) \cdot X^{parent2}, \tag{5.3}$$

$$\text{where } Coef = 1.2 \cdot Ran^{0.5} - 0.1, \tag{5.4}$$

and Ran is a random number from 0 to 1. A different value of Ran is calculated for each element of vector X.

By this way the best parent is favored as the square root of Ran gives some values of Coef more closed to 1.1 than to -0.1, and the exploration is a bit enlarged.

2. Definition of the parameters to identify

2.1. Fixed parameters

Some parameters of the model presented in chapter 4 were fixed as they were supposed to be close to the values that were measured.

The partitioning of acrylonitrile (A) and styrene (B) in thermodynamic equilibrium were fixed to the data obtained experimentally and presented in the preliminary studies in chapter 3 :

$H_A = 1$

$H_B = 0.9$

Concerning the initiator, it was supposed that, as its half-life time is very short (180 s at 120 °C and 25 s at 140 °C) compared to the residence time inside the reactor (20 min at Q_{sm}=25 g/min), it is decomposed almost completely as soon as it enters in the reactor, in the continuous phase, and therefore the quantity of free initiator inside the particles is negligible :

$H_I = 0.$

The kinetic constant used for initiator dissociation is :

$$k_d^c = 2,45.10^{15} Exp\left(-\frac{134000}{8,314 \ . \ T}\right) (s^{-1}).$$

The coefficients of absorption are considered to be equal to simplify the system to solve :

$D_0 = D_1 = D_3.$

2.2. Identified parameters

The different identified parameters are presented in table 5.1. In a first step, this system does not take into account the natural grafting.

Table 5.1. : Parameters of the model identified using the genetic algorithm

Parameter n°	Name	Range of research	Unit
1	k_{pAA}^{c}	1 ; 3000	$m^3.mol^{-1}.s^{-1}$
2	k_{pBB}^{c}	1 ; 1000	$m^3.mol^{-1}.s^{-1}$
3	k_{tcAA}^{c}	10^7, 7 10^8	$m^3.mol^{-1}.s^{-1}$
4	k_{tcBB}^{c}	10^5 ; 6 10^6	$m^3.mol^{-1}.s^{-1}$
5	R_{AB}^{c}	0.05 ; 0.9	-
6	R_{BA}^{c}	0.05 ; 0.9	-
7	$R_{t,A}^{c}$	0 ; 15	-
8	$R_{t,B}^{c}$	0 ; 15	-
9	ϕ_c	1 ; 120	-
10	k_{pAA}^{p}	1 ; 15000	$m^3.mol^{-1}.s^{-1}$
11	k_{pBB}^{p}	1 ; 3000	$m^3.mol^{-1}.s^{-1}$
12	Gel1	1 ; 10	-
13	R_{AB}^{p}	0.05 ; 0.9	-
14	R_{BA}^{p}	0.05 ; 0.9	-
15	K_p	0 ; 10^{-4}	s^{-1}
16	R_{AG}^{c}	0.01 ; 10	-
17	R_{BG}^{c}	1 ; 60	-
18	$k_{tr,G}^{c}$	1 ; 3000	$m^3.mol^{-1}.s^{-1}$
19	k_{tdG}^{c}	5 10^6 ; 4 10^8	$m^3.mol^{-1}.s^{-1}$
20	k_{tdG}^{p}	5 10^5 ; 10^8	$m^3.mol^{-1}.s^{-1}$
21	a	10^{-11} ; 5 10^{-9}	$m.(mol.kg^{-1})^{1/3}$
22	Gel2	1 ; 20	-
23	f_c	0 ; 0.6	-
24	H_{CTA}	0.5 ; 2.5	

By attempting to include the natural grafting in the model, six other parameters to identify are added, as shown in table 5.2.

Table 5.2. : Parameters of the model concerning natural grafting

Parameter n°	Name	Range of research	Unit
25	k_{RG}^{c}	0 ; 100	$m^3.mol^{-1}.s^{-1}$
26	$k_{GA}^{c} = k_{SA}^{c}$	0 ; 100	$m^3.mol^{-1}.s^{-1}$
27	$k_{GB}^{c} = k_{SB}^{c}$	0 ; 100	$m^3.mol^{-1}.s^{-1}$
28	$k_{RG,ng}^{c} = k_{RS,ng}^{c}$	0 ; 100	$m^3.mol^{-1}.s^{-2}$
29	$k_{tr,AG}^{c} = k_{tr,AS}^{c}$	0 ; 100	$m^3.mol^{-1}.s^{-1}$
30	$k_{tr,BG}^{c} = k_{tr,BS}^{c}$	0 ; 100	$m^3.mol^{-1}.s^{-1}$

The coefficient of absorption, D_0, is considered to be zero in a first attempt.

In order to use the evolutionary algorithm, it is necessary to define the range of research of the different parameters. The order of magnitude of some particular parameters can be given by the literature, as shown in chapter 4. Nevertheless it is necessary to consider larger ranges of research as the kinetic constants that are identified do not correspond exactly to the real kinetic constants as the model is a tendency model. For the other parameters, for which no indicative data are available, the ranges of research are estimated and tested, knowing that the final way to identify the parameters is to minimize the maximum likelihood estimator, F(X).

2.3. Experimental data considered

Twelve different physical properties of the CPP samples are used to identify the parameters of the model :

- The average molecular weights in the whole CPP : $\bar{M}_n$ and $\bar{M}_w$ (g/mol),
- The weight percentage of solids in stripped CPP (wt-% solid),
- The residual acrylonitrile quantity (wt-%),
- The residual styrene quantity (wt-%),
- The residual NDM quantity (ppm),
- The quantity of SAN copolymer present in the continuous phase (wt-%),
- The acrylonitrile composition of the SAN copolymer (wt-%),
- The percentage of grafted SAN chains in the serum phase, (%)
- The percentage of grafted high molecular weight SAN in the whole CPP, (%)
- The weight percentage of polyol in the solids, (wt-%)
- The surface area moment mean diameter (μm).

The average molecular weights of SAN copolymer in the serum are not used as they are not enough accurate, as shown in chapter 3. The wt-% grafting in solids is also not considered as

actually it is redundant with the wt-% grafting in whole CPP as the quantity of SAN in the continuous phase is negligible as compared to the quantity of SAN inside the particles.

Concerning the Sauter mean diameter, D[3,2], only the values obtained with recipes containing low styrene (Sty/AN = 60/40) are considered to identify the parameters. Indeed, at high styrene (Sty/AN = 80/20), as shown in chapter 3, the particle size distributions are too complex to be able to consider that they are monodisperse.

3. Results and discussion

The parameters were identified with data obtained at 140 °C, which were the most accurate, and then with data obtained at 120 °C. This allowed to frame the values of the parameters and then to estimate the parameters at 130 °C and to validate the model on measurements done on standards recipes produced at 130 °C.

Identifications were firstly done neglecting the natural grafting and the absorption. Then, attempts were done to test these models in order to obtain lower values of the maximum likelihood estimator. In a first part, the results of the identification at 120°C and 140°C will be presented and then, the theoretical data given by the model will be compared to experimental ones in order to evaluate the model.

3.1. Results

At 140 °C, 17 polymerizations were considered with 12 measurements per experiment. 9 of those measurements concerning the mean particle size were not taken into account to identify the parameters, as they were not enough accurate. Therefore 195 data were used to identify the 24 parameters of the model neglecting natural grafting.

At 120 °C, 13 polymerizations were considered with 12 measurements per experiment. Nevertheless, among these data only some were used to identify the parameters, the others appearing to be erroneous. Therefore, 145 data were used to identify the parameters.

The values of the parameters corresponding to the lowest maximum likelihood estimator, F(X), for each temperature, are exposed in table 5.3. It can be noticed that the values obtained at both temperatures are rather close. Estimation and validation of these parameters at 130 °C will be presented in part 4.

As shown in chapter 4, the literature gives $k_{pAA} = 9.4$ m^3 mol^{-1} s^{-1} at 120 °C and $k_{pAA} = 14.8$ m^3 mol^{-1} s^{-1} at 140 °C for bulk polymerization of acrylonitrile (Garcia-Rubio et al., 1985). The identification provided values of homopolymerization of acrylonitrile around $k^c_{pAA} \approx 2300$ m^3 mol^{-1} s^{-1} in the continuous phase and around $k^p_{pAA} \approx 8800$-9840 m^3 mol^{-1} s^{-1} inside the particles that is to say thousand fold higher. It can be noticed that the kinetic constants identified are fourfold higher inside particles than in the serum.

Concerning the homopolymerization of styrene, Keramopoulos & Kiparissides (2002) gives for bulk polymerisation of styrene $k_{pBB} = 1.3$ m^3 mol^{-1} s^{-1} at 120 °C and $k_{pBB} = 2.0$ m^3 mol^{-1} s^{-1} at 140 °C, whereas the parameters obtained were $k^c_{pBB} \approx 28$ m^3 mol^{-1} s^{-1} in the continuous phase and $k^p_{pBB} \approx 490$ m^3 mol^{-1} s^{-1} inside the particles at 140 °C and $k^p_{pBB} \approx 265$ m^3 mol^{-1} s^{-1} inside the particles at 120°C, that is to say around hundred to two hundred fold higher.

Table 5.3. Results of parameter identification at 140°C and 120°C

Parameter n°	Name	T = 140°C	T = 120 °C	Unit
1	k_p^c	2380	2200	$m^3.mol^{-1}.s^{-1}$
2	k_{pBB}^c	48.1	48	$m^3.mol^{-1}.s^{-1}$
3	k_{tcAA}^c	$1.27\ 10^8$	$1.67\ 10^8$	$m^3.mol^{-1}.s^{-1}$
4	k_{tcBB}^c	$3.40\ 10^6$	$2.43\ 10^6$	$m^3.mol^{-1}.s^{-1}$
5	R_{AB}^c	0.42	0.43	-
6	R_{BA}^c	0.30	0.29	-
7	$R_{t,A}^c$	3.9	2.7	-
8	$R_{t,B}^c$	8.1	9.0	-
9	ϕ	27	28	-
10	$_{AA}$	9840	8800	$m^3.mol^{-1}.s^{-1}$
11	$_{BB}$	490	265	$m^3.mol^{-1}.s^{-1}$
12	Gel1	1.0	1.3	-
13	R_{AB}^p	0.50	0.45	-
14	R_{BA}^p	0.48	0.28	-
15	K_p	$5.95\ 10^{-5}$	$8.85\ 10^{-5}$	s^{-1}
16	R_{AG}^c	0.32	0.77	-
17	R_{BG}^c	29.3	36.3	-
18	$k_{tr,G}^c$	1900	1810	$m^3.mol^{-1}.s^{-1}$
19	k_{tdAG}^c	$1.72\ 10^8$	$1.57\ 10^8$	$m^3.mol^{-1}.s^{-1}$
20	k_{tdBG}^p	$1.01\ 10^7$	$1.57\ 10^7$	$m^3.mol^{-1}.s^{-1}$
21	a	$2.50\ 10^{-9}$	$3.65\ 10^{-9}$	$m.(mol.kg^{-1})^{1/3}$
22	Gel2	11.0	11.9	-
23	f_c	0.27	0.28	-
24	H_{CTA}	0.64	0.55	-
	F(x)	322.60	384.98	-

Concerning the homo-termination by combination of acrylonitrile, Keramopoulos & Kiparissides (2002) gives $_{tcAA}$ = 1.98 10^8 $m^3 mol^{-1} s^{-1}$ at 120 °C and $_{tcAA}$ = 2.77 10^8 $m^3 mol^{-1} s^{-1}$ at 140°C. The parameter identification lead to k^c_{tcAA} ≈ 1.5 10^8 m^3 mol^{-1} s^{-1} that is in the same order of magnitude. The value obtained at 120°C is higher than the one obtained at 140 °C, but these values are rather close and considering the accuracy of the experimental data, it can just be noticed that they are in the same order of magnitude.

Concerning the homo-termination by combination of styrene, Keramopoulos & Kiparissides (2002) gave $_{tcBB}$ = 1.49 10^5 $m^3 mol^{-1} s^{-1}$ at 120 °C and $_{tcBB}$ = 1.65 10^5 $m^3 mol^{-1} s^{-1}$ at 140°C. The parameter identification lead to k^c_{tcBB} ≈ 2.43 10^6 m^3 mol^{-1} s^{-1} at 120°C and k^c_{tcBB} ≈ 3.4 10^6 m^3 mol^{-1} s^{-1} at 140°C that is in a tenfold order of magnitude.

The reactivity ratios R^c_{BA}, in the serum, and R_{BA}, inside particles, are closed and in a range [0.3 ; 0.5], which corresponds to data coming from the literature (see r_B in Table 4.2 of chapter 4). Nevertheless, the reactivity ratios R^c_{AB}, in the serum, and R^p_{AB}, inside particles, are around 0,45 that is greater than the ones given by the literature (see r_A in Table 4.2 of chapter 4) obtained at temperatures in the range [50 ; 80] °C. It could be explained by the fact that the reactivity ratios may increase with temperature.

The cross-termination coefficient is identified to be equal to $\phi \approx 27$, that is in the range [10 ; 70] found by Mendizabal et al. (1995) at 60°C for the styrene-acrylonitrile system.

The gel effect is given by the parameters Gel1, linked to the gel effect due to styrene, and Gel2, linked to the gel effect due to acrylonitrile. Gel1 is found to be around [1 ; 1.3] and Gel2 around [11 ; 11.9]. It means that acrylonitrile provides more gel effect than styrene. Assuming that the proportion in weight of polymer inside the particles is about $x_p = 0.96$, the gel effect coefficient, g, can be calculated using equation 4.16 in chapter 4 :

$g = 5.6\ 10^{-2}$ for Sty/AN = 80/20,

and $g = 8.2\ 10^{-3}$ for Sty/AN = 60/40.

The transfer reactivities to the chain transfer agent, NDM, $^c_{,A}$ in the range [2.7 ; 3.9] and $^c_{,B}$ in the range [8.1 ; 9] are in the order of magnitude of the data given by the literature (Eq. 4.19 and 4.20) even if they are quite different. Indeed, the literature gives data of reactivities at 50°C and does not precise in which solvent.

Concerning the grafting, the reactivity coefficient related to the grafting of oligoradicals terminated by acrylonitrile on the vinyl bond of S5200, R^c_{AG}, is identified to be in a range [0.32 ; 0.77], whereas the literature (see table 4.3 of chapter 4) gives values of reactivity coefficients of acrylonitrile with different silanes in a range [2 ; 27]. The reactivity coefficient concerning the grafting of oligoradicals terminated by styrene on the vinyl bond of S5200, R^c_G , is identified to be in a range [29 ; 36], whereas the literature (see table 4.3 of chapter 4) gives values of reactivity coefficients of styrene with different silanes in a range [4 ; 21]. Therefore, the model forecast an important grafting with acrylonitrile and a small grafting with styrene.

The transfer of oligoradicals terminated by S5200 with the chain transfer agent NDM, $k^c_{t,G}$, is identified to be in the range [1800 ; 1900] $m^3.mol^{-1}.s^{-2}$.

The dismutation termination reactions of oligoradicals terminated by acrylonitrile or styrene with oligoradicals terminated by S5200, k^c_{tdAG} and $k^c_{td\ G}$, were identified to be k^c_{tdAG} = 1.7 10^8

$m^3.mol^{-1}.s^{-1}$ at 140°C and k^c_{tdAG} = 1.6 10^8 $m^3.mol^{-1}.s^{-1}$ at 120°C, and $k^c_{td\ G}$ = 1.0 10^7 $m^3.mol^{-1}.s^{-1}$ at 140 °C and $k^c_{td\ G}$ = 1.6 10^7 $m^3.mol^{-1}.s^{-1}$ at 120 °C. There are no data in the literature concerning these kinetic constants but the range of research of the combination terminations was considered as reference.

The kinetic constant of transfer of the oligoradicals terminated by a graft S5200, is estimated to be around $k^c_{tr,G}$ = 1800-1900 $m^3.mol^{-1}.s^{-1}$. The range of research of this parameter was considered in the range of research of the both other kinetic constant of transfers.

The efficiency of the primary radicals in the continuous phase, f_c, is identified to be in the range [0.27 ; 0.28]. This value is rather low as compared to values of 0.7 that was forecasted but this difference can be explained as only half of the primary radicals produced from the initiator (T27) decomposition is efficient, as shown in paragraph 1.1.3 of chapter 2.

The identification of the partitioning coefficient of the chain transfer agent, H_{CTA}, gave values lower than the measurement. Indeed, the measurements shown in chapter 3 provided H_{CTA} = 0.98, whereas the identification gave H_{CTA} = 0.55 at 120°C and H_{CTA} = 0.64 at 140°C. This would mean that the concentration of NDM is greater in the continuous phase than inside the particles.

The parameter calculating the radii of gyrations is found to be a = 2.50 10^{-9} $m.(mol.kg^{-1})^{1/3}$ at 140 °C and a = 3.65 10^{-9} $m.(mol.kg^{-1})^{1/3}$ at 120 °C. Yasuda et al. (2001a) found a = 5.3 10^{-7} $m.(mol.kg^{-1})^{1/3}$ for PVP in ethanol.

The constant of precipitation is found to be K_p = 5.95 10^{-5} s^{-1} at 140 °C and K_p = 8.85 10^{-5} s^{-1} at 120 °C. The fact that this parameter decreases when the temperature increases could be explained by the fact that the higher is the temperature the longer are the polymer chains soluble in the medium.

The identification procedures was also used to identify the coefficient of absorption D_0, and the kinetics corresponding to the natural grafting of table 5.2, nevertheless, the values obtained which minimized the maximum likelihood estimator were very closed to zero. Therefore, at this state of the research the extension of the model to the natural grafting phenomena does not allow to obtain better simulations.

3.2. Average molecular weights

Recent studies done by Dow have shown the error on the determinations of the average molecular weights due to the fact that the GPC measurements used polystyrene standards for the calibration of the systems. Indeed, the average molecular weights of a standard SAN copolymer sample, composed of 25 wt-% of acrylonitrile (azeotropic point), were measured by two different methods : on one hand by GPC using polystyrene standards (as it was done in all the measurements presented in this work) and on the other hand using an absolute technique without calibration of the system and using directly the data collected from the light scattering sensor.

As shown in table 5.4, the absolute values of the average molecular weights were 0.8 times the values obtained by GPC, which is more important than forecasted. This difference should increase with the quantity of acrylonitrile. For instance, the average molecular weights of samples done with Sty/AN = 60/40 may be lower than the values measured by GPC.

Table 5.4. : Broad and absolute measurement

SAN copolymer	$\bar{M}_n$ (g/mol)	$\bar{M}_w$ (g/mol)	$\bar{M}_w/\bar{M}_n$
GPC (standards PS)	83000	178000	2.14
Absolute : via LS	67410	144600	2.15

Nevertheless, the system identified the parameters of the model using these values of the average molecular weights (GPC with polystyrene standards calibration). Therefore, the underestimation of the average molecular weights that will be shown below can be explained by the measurements inaccuracy.

Figures 5.2 and 5.3 present the comparison between the number-average molecular weights measured and these forecasted by the model at 140 °C and 120 °C. Tables A5.1 and A5.2 of annex 5 allow to compare the values. The experimental values presented were the ones that were used to identify the parameters. The median line (dotted line) represents the theoretical equality between data from measurements and data given by the model. An experimental error of ± 20 % is also represented on the figures to give an indication, as the exact accuracy is not known considering the problem of using the GPC calibration polystyrene standard. Actually, an accuracy of ± 5 % on the measurement itself is given, but it does not take into account additional inaccuracy on the experimental conditions and the deviation to the absolute value.

At 140 °C (figure 5.2), $\bar{M}_n$ is rather well estimated by the model. The points that are the less close to the median correspond to experiments done with Sty/AN = 60/40. The experimental values should be lower than the ones that are measured. At 120°C (figure 5.3), the model underestimates also the measurements.

Figures 5.4 and 5.5 present the comparison between the weight-average molecular weights measured and forecasted by the model at 140 °C and 120 °C. Tables A5.3 and A5.4 of annex 5 allow to compare the values. The experimental values presented were the ones that were used to identify the parameters. At both temperatures, $\bar{M}_w$ are rather well estimated by the model for samples done at Sty/AN = 80/20. However, the recipes done with Sty/AN = 60/40 give underestimate theoretical values for $\bar{M}_w$.

Actually, the system identified the parameters in order to reach these average molecular weights. This could explain the fact that the order of magnitude of the kinetics of propagation of styrene and acrylonitrile that are identified is greater than forecasted by the literature.

Generally, it could be noticed that the theory and the measurements show a small increase of the average molecular weights by increasing the quantity of precursor stabilizer, S5200.

Moreover, the attempts to introduce theoretically the natural grafting in the model showed that the consequences were to reduce the theoretical average molecular weights. Indeed, the initiation and the transfers to the polyol solvent increased the number of polymer chains produced and therefore decreased the degree of polymerization. Therefore, it gave worst maximum likelihood estimator values.

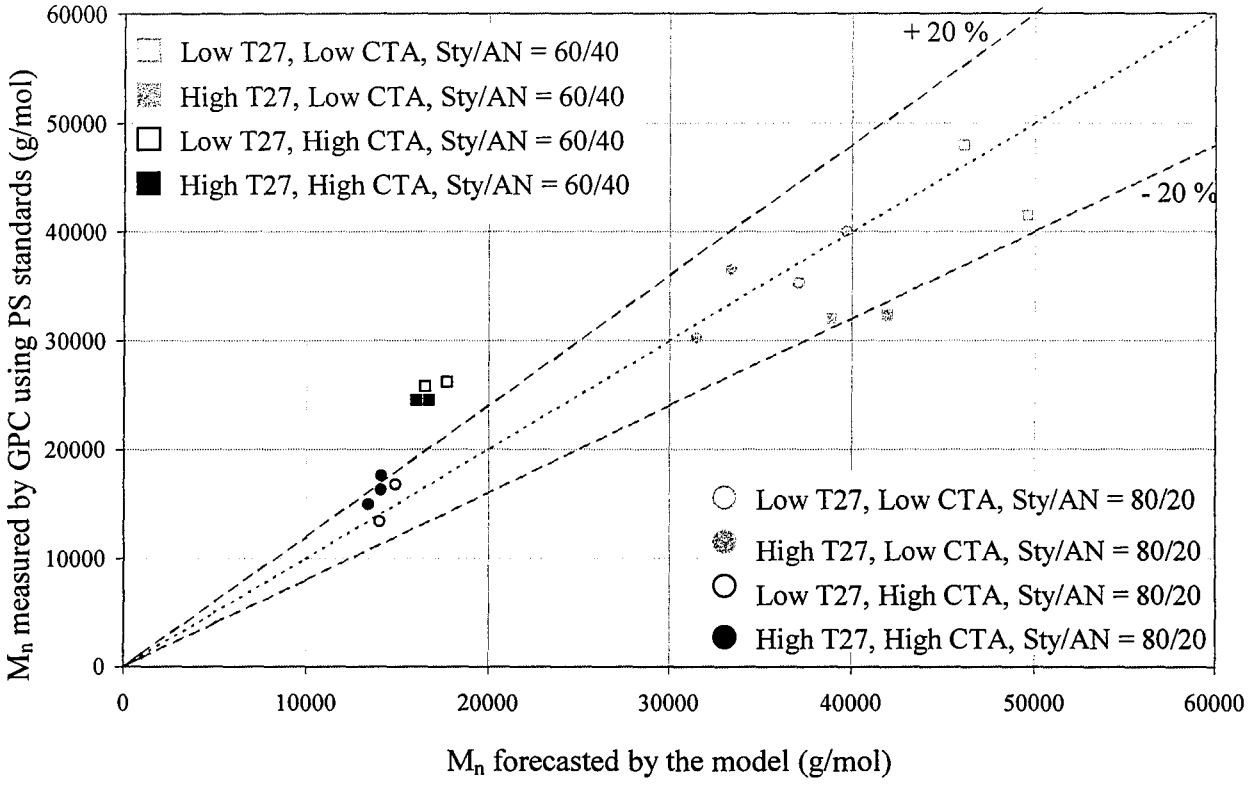

Figure 5.2 : Number-average molecular weights ; Measurements vs. modeling using the parameters identified at 140 °C

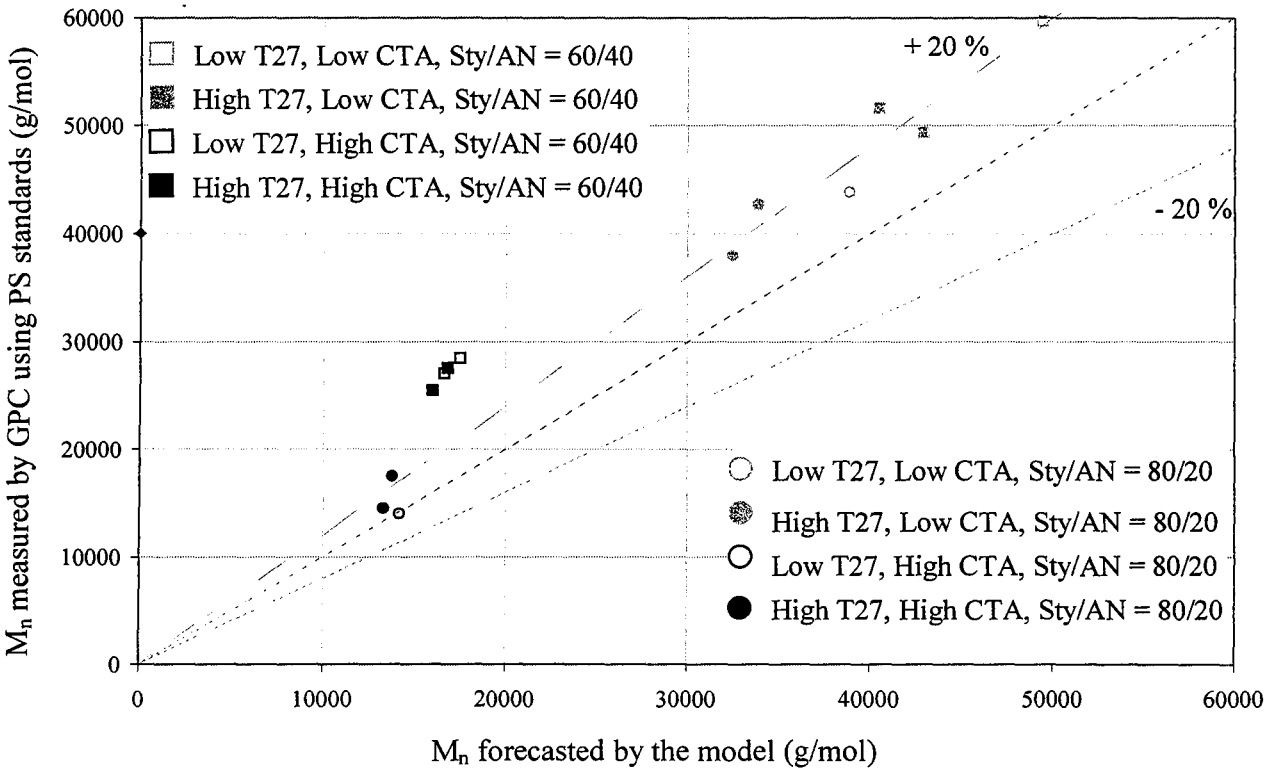

Figure 5.3 : Number-average molecular weights ; Measurements vs. modeling using the parameters identified at 120 °C

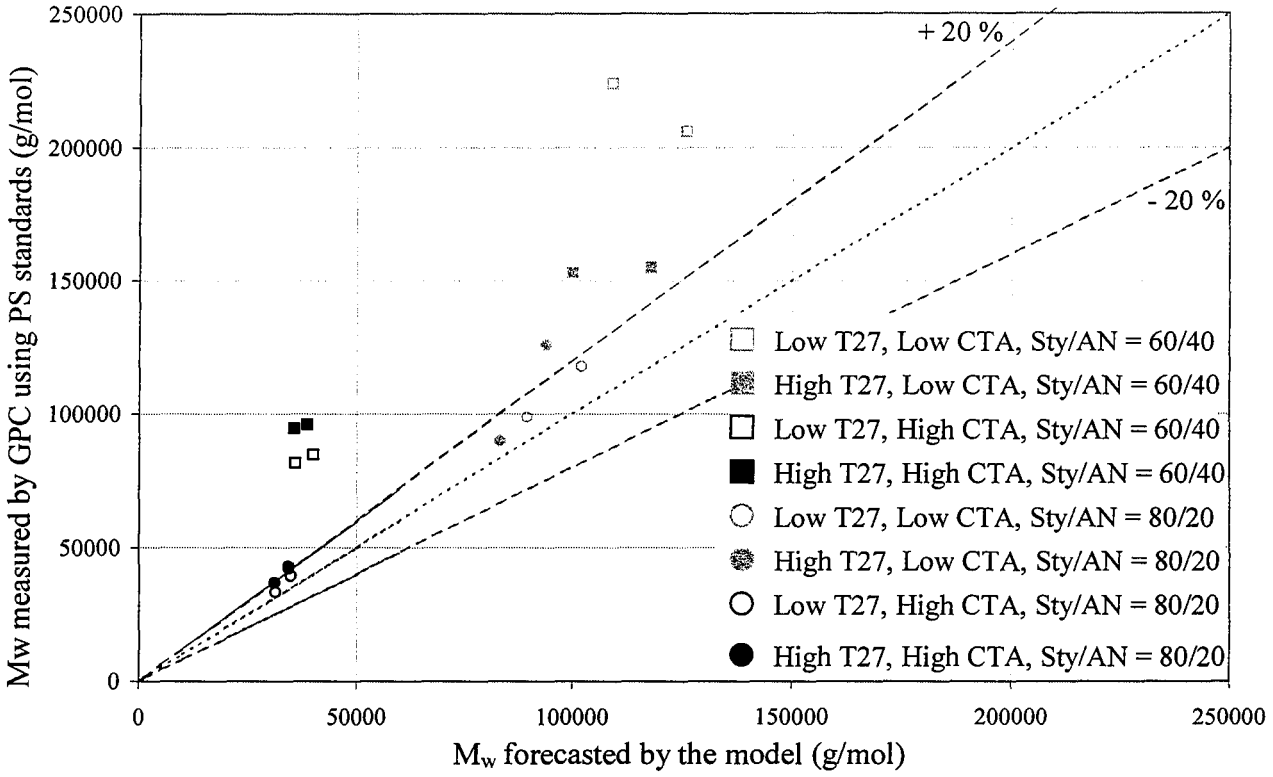

Figure 5.4 : Weight-average molecular weights ; Measurements vs. modeling using the parameters identified at 140 °C

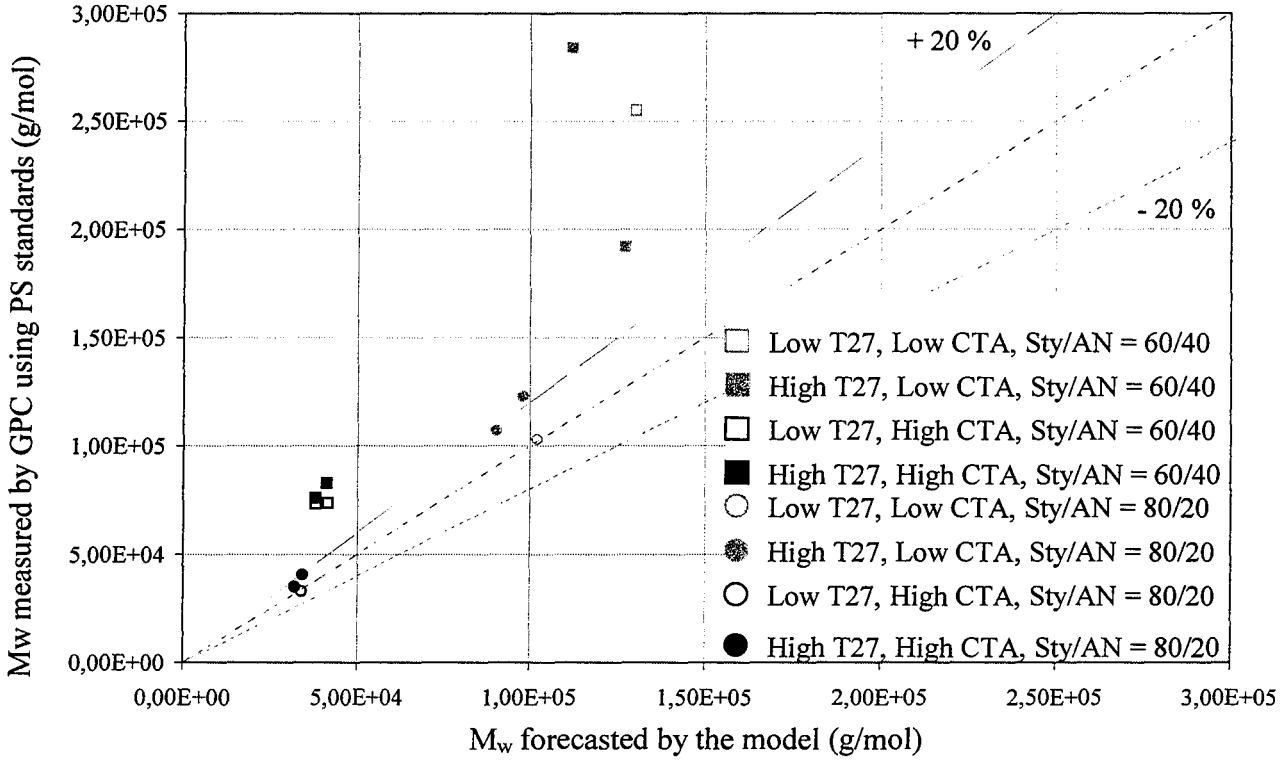

Figure 5.5 : Weight-average molecular weights ; Measurements vs. modeling using the parameters identified at 120 °C

3.3. Solids and residual concentrations of acrylonitrile, styrene and NDM

As shown in figures 5.6 and 5.7, the wt-% of solids is rather well estimated by the model at both temperatures with a relative experimental error of ± 10 % (tables A5.5 and A5.6 in annex 5). The ± 5 % lines correspond to the estimated accuracy of the method. The values that are out of the ± 5 % experimental error region correspond actually to the less stable samples done with high styrene content (Sty/AN = 80/20).

The results presenting the residual concentrations of acrylonitrile, styrene and NDM are shown in figures A5.1 to A5.6 in annex 5. Their conversions are presented in figures 5.8 to 5.13 below. Tables A5.7 to A5.18 in annex 5 compare the values resulting from the measurements and from the theory.

The conversions of acrylonitrile at 140°C and 120°C (figures 5.8 and 5.9) are predicted by the model with an accuracy of ± 5 % for the recipes done with Sty/AN = 60/40. Nevertheless, for unstable experiments done with Sty/AN = 80/20, the measurements are more dispersed and the theory forecast the measurements with a relative error less than ± 20% (but up to 40 % for the particularly unstable run n°27 done with low initiator, T27, and high chain transfer agent (NDM) contents).

The conversions of styrene at 140°C and 120°C (figures 5.10 and 5.11) are slightly underestimated for Sty/AN = 60/40 and are overestimated for Sty/AN = 80/20. The evolutionary algorithm tried to find the best set of parameters, which suits to both populations. It can be observable that the model forecasts a smaller difference of conversions between the different experiments done at Sty/AN = 80/20 than does the measurements.

The conversions of the chain transfer agent, NDM, at 140°C and 120°C (figures 5.12 and 5.13) are rather well predicted by the model with an accuracy of ± 5 % even if the residual concentrations of NDM seemed not to be accurate as shown on figures A5.6 and A5.7 in annex 5. Actually, these conversions are greater than 90 % and there are very small quantities of NDM in the samples.

Finally, the conversions of the stable samples are rather well in agreement with the experimental values used for the identification.

3.4. SAN copolymer composition

The composition of the SAN copolymer is fixed by the composition of the premix as the reaction is processed in a continuous reactor and therefore the model forecasts easily the measurements. Nevertheless, figures 5.14 and 5.15 (corresponding to tables A5.19 and A5.20 of Annex 5), obtained respectively at 140°C and 120°C, show clearly the experimental discrepancies, which stay in the ± 20 % relative error of the measurement method.

It can be noticed that with recipes containing Sty/AN= 80/20, the model forecasts 22.5 to 22.9 wt-% of acrylonitrile in the polymer. This is explained by the fact that the partitioning coefficient of styrene was fixed to $H_B = 0.9$, which means that styrene was preferably soluble in the polyol than inside particles, changing the composition of the monomers in the particles. With recipes containing Sty/AN = 60/40, the final copolymer composition is however less modified as the model forecast 40.1 wt-% of acrylonitrile.

Actually, the SAN copolymer composition does not provide enough information to identify the parameters of the model as it depends on only one process condition, and it would be not necessary to measure it for further studies.

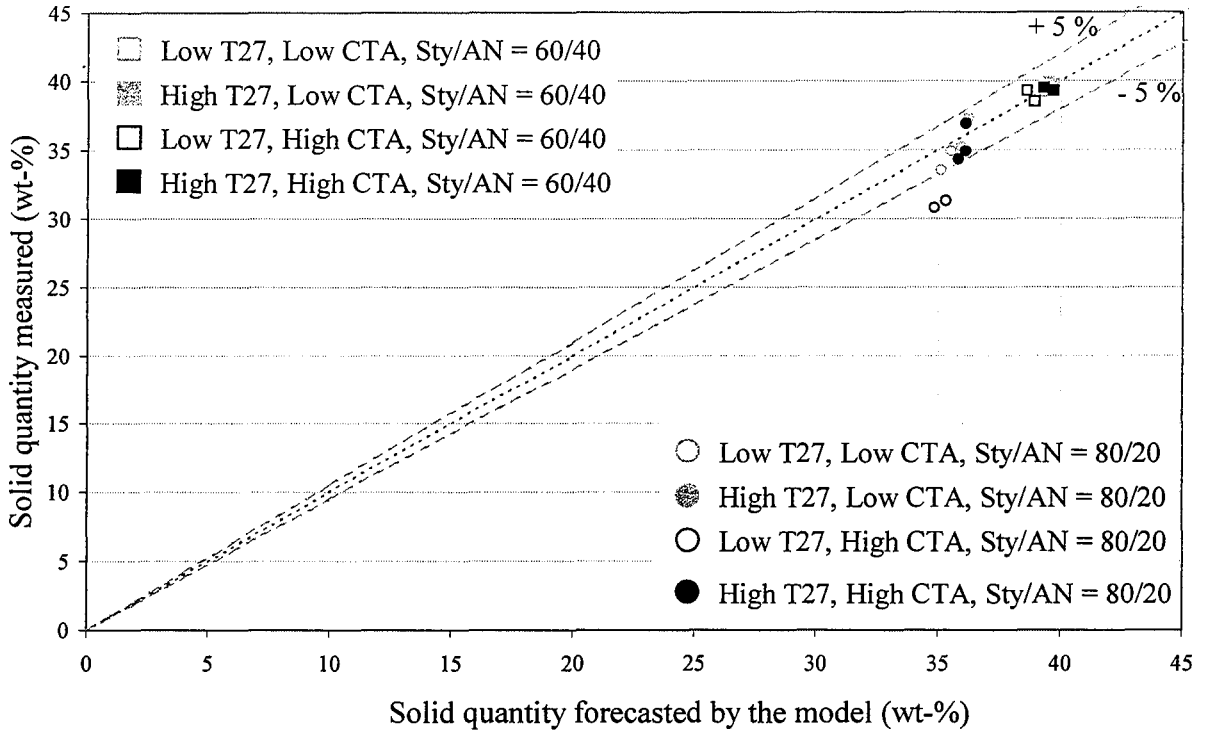

Figure 5.6 : Solids quantities ; Measurements vs. modeling, using the parameters identified at 140 °C

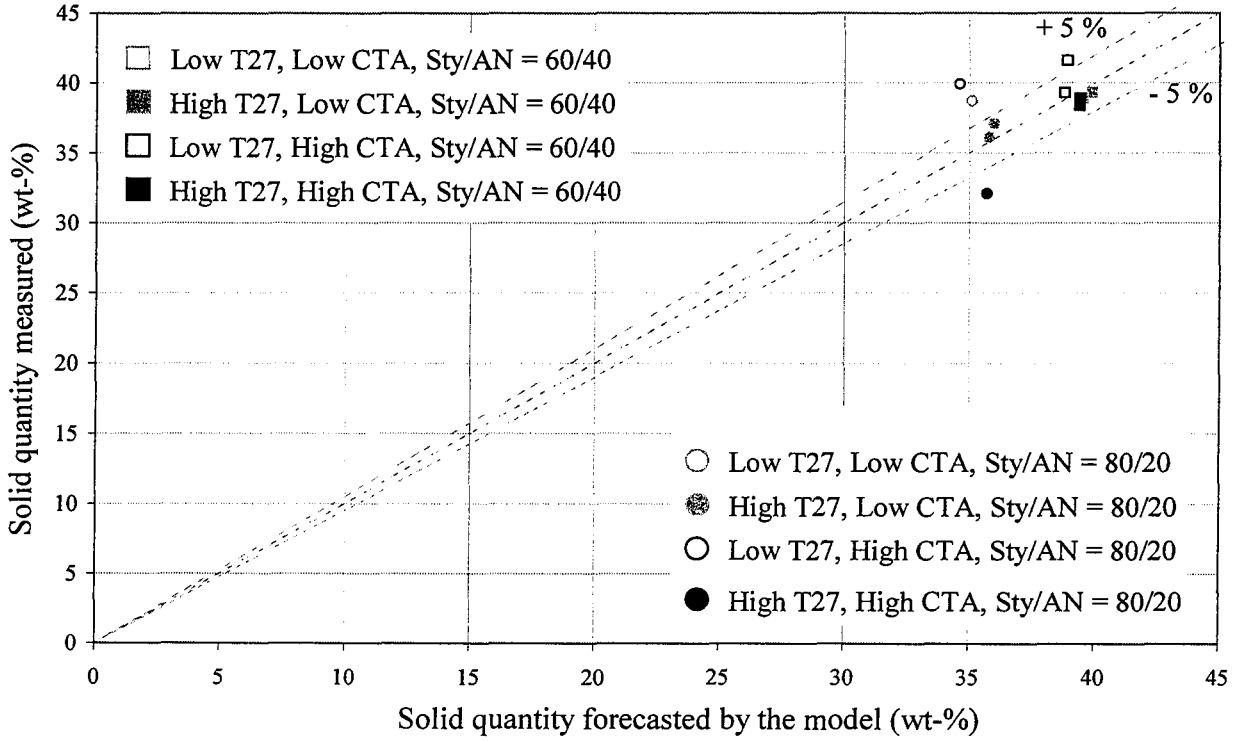

Figure 5.7 : Solids quantities ; Measurements vs. modeling, using the parameters identified at 120 °C

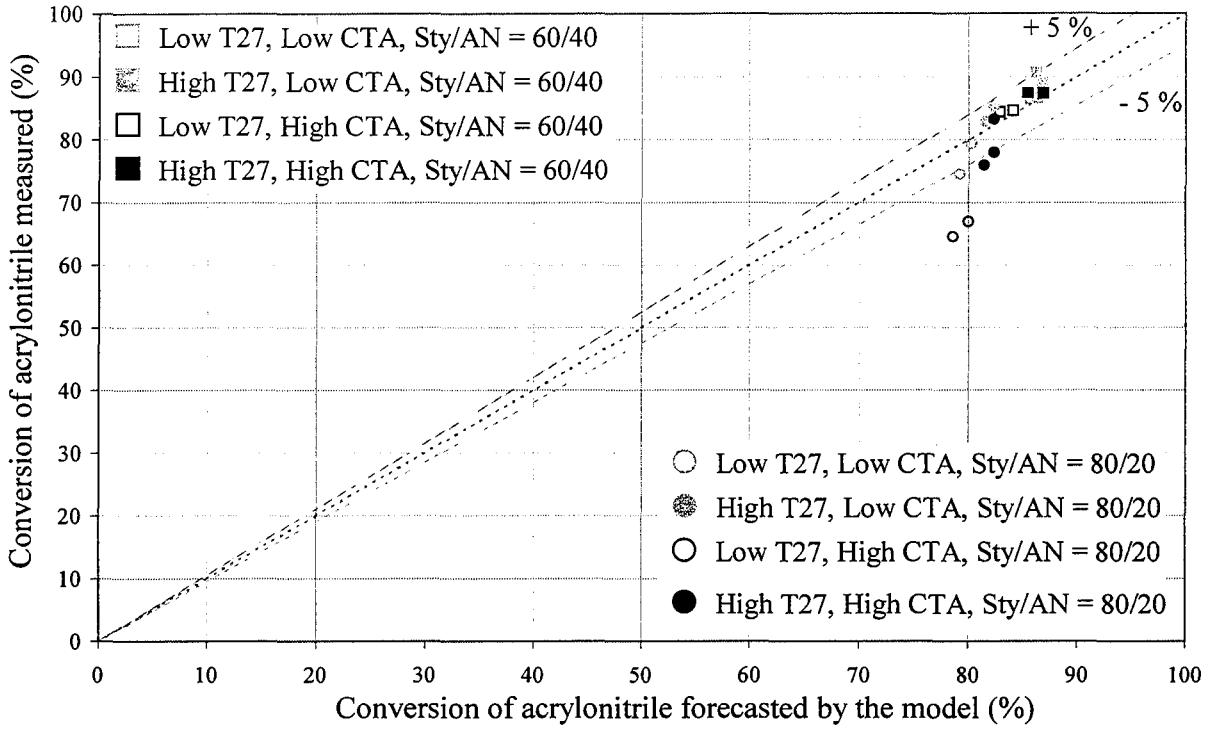

Figure 5.8 : Conversions of acrylonitrile ; Measurements vs. modeling using the parameters identified at 140 °C

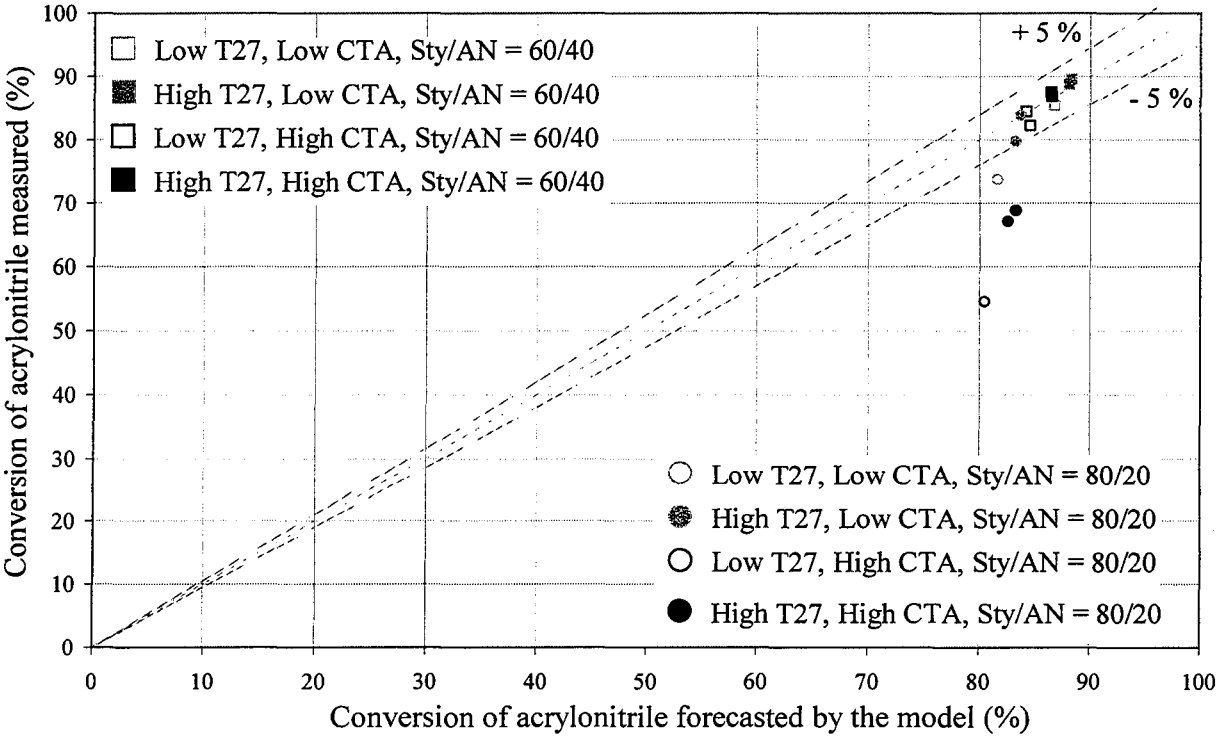

Figure 5.9 : Conversions of acrylonitrile ; Measurements vs. modeling using the parameters identified at 120 °C

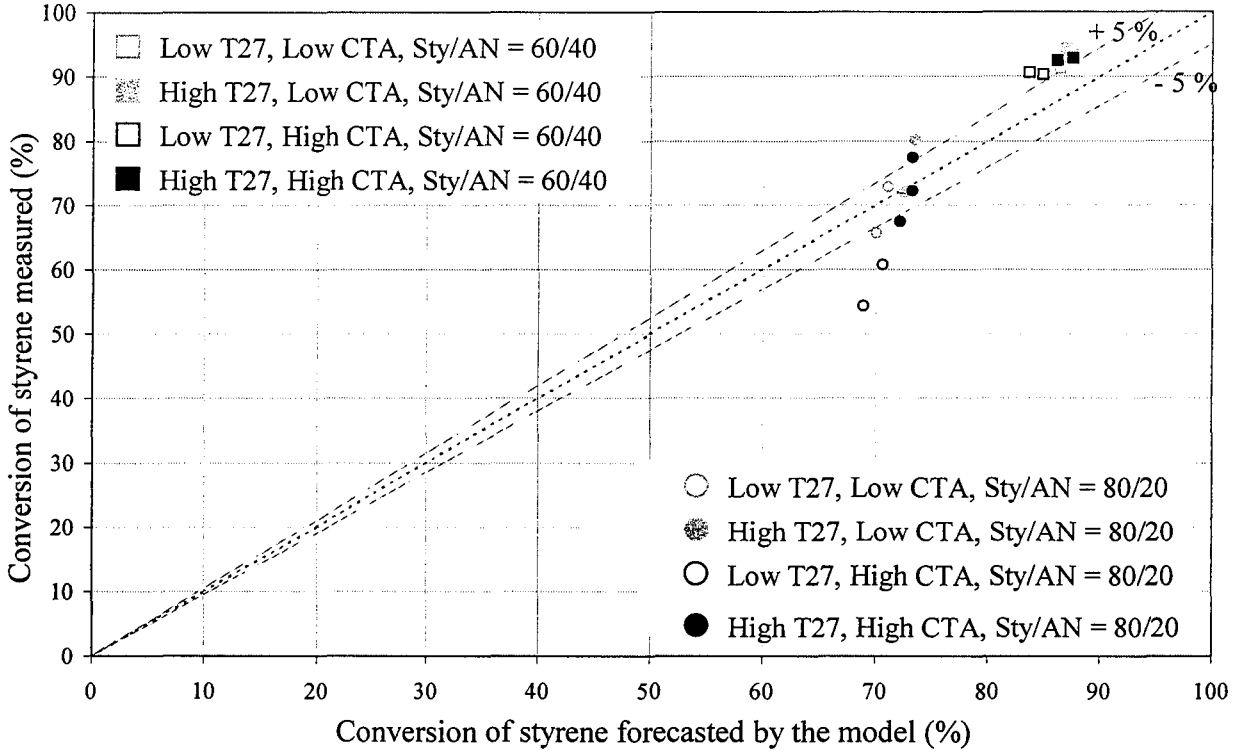

Figure 5.10 : Conversions of styrene ; Measurements vs. modeling using the parameters identified at 140 °C

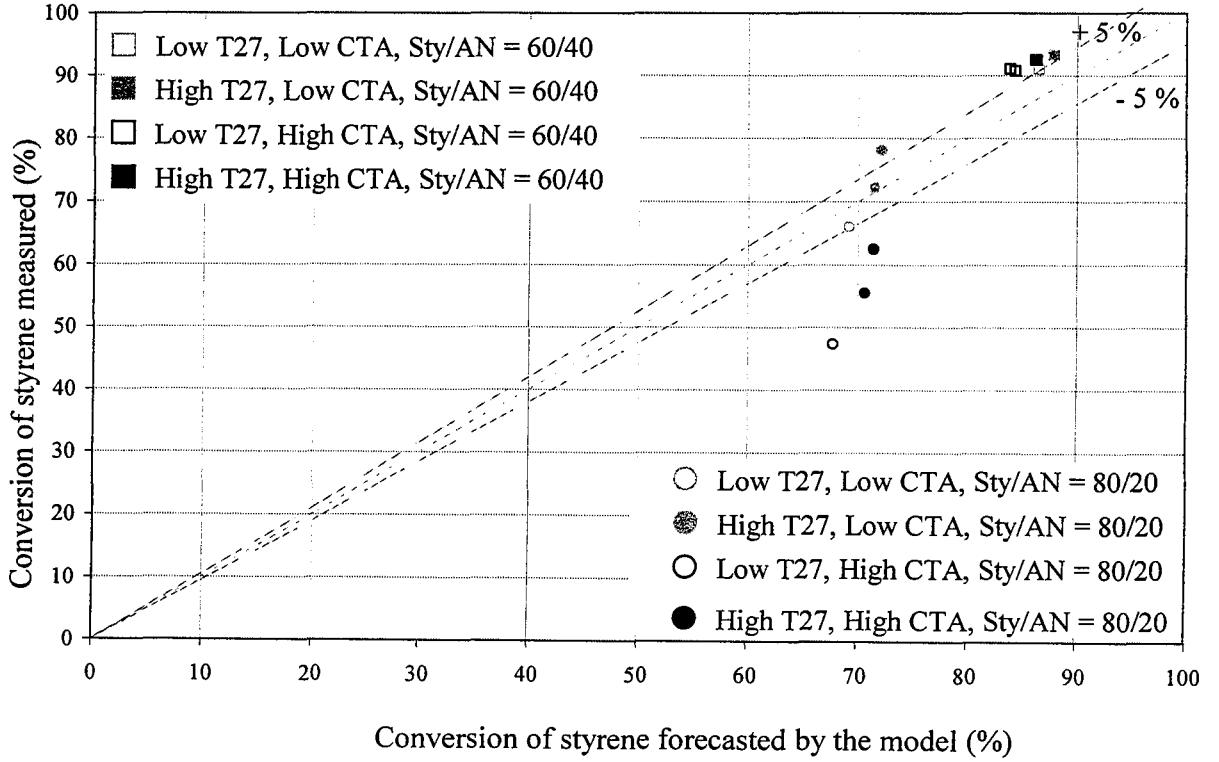

Figure 5.11 : Conversions of styrene ; Measurements vs. modeling using the parameters identified at 120 °C

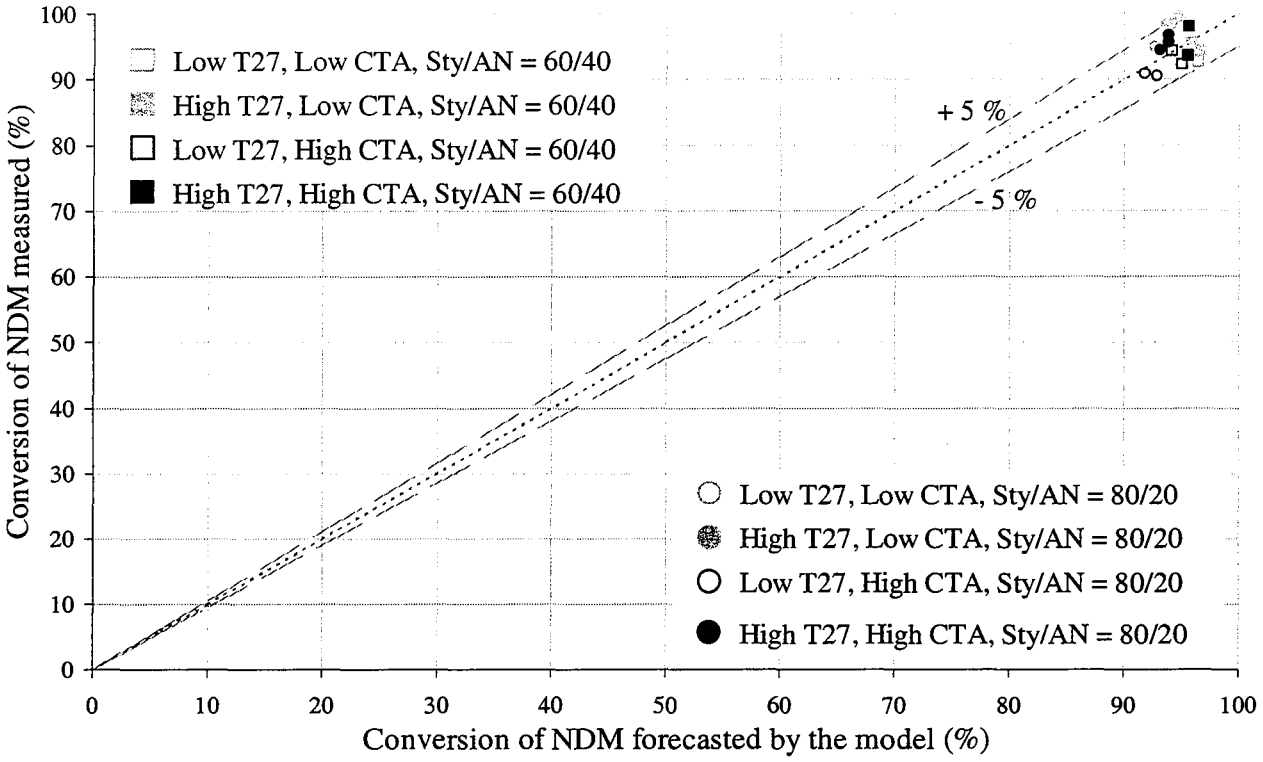

Figure 5.12 : Conversions of NDM ; Measurements vs. modeling using the parameters identified at 140 °C

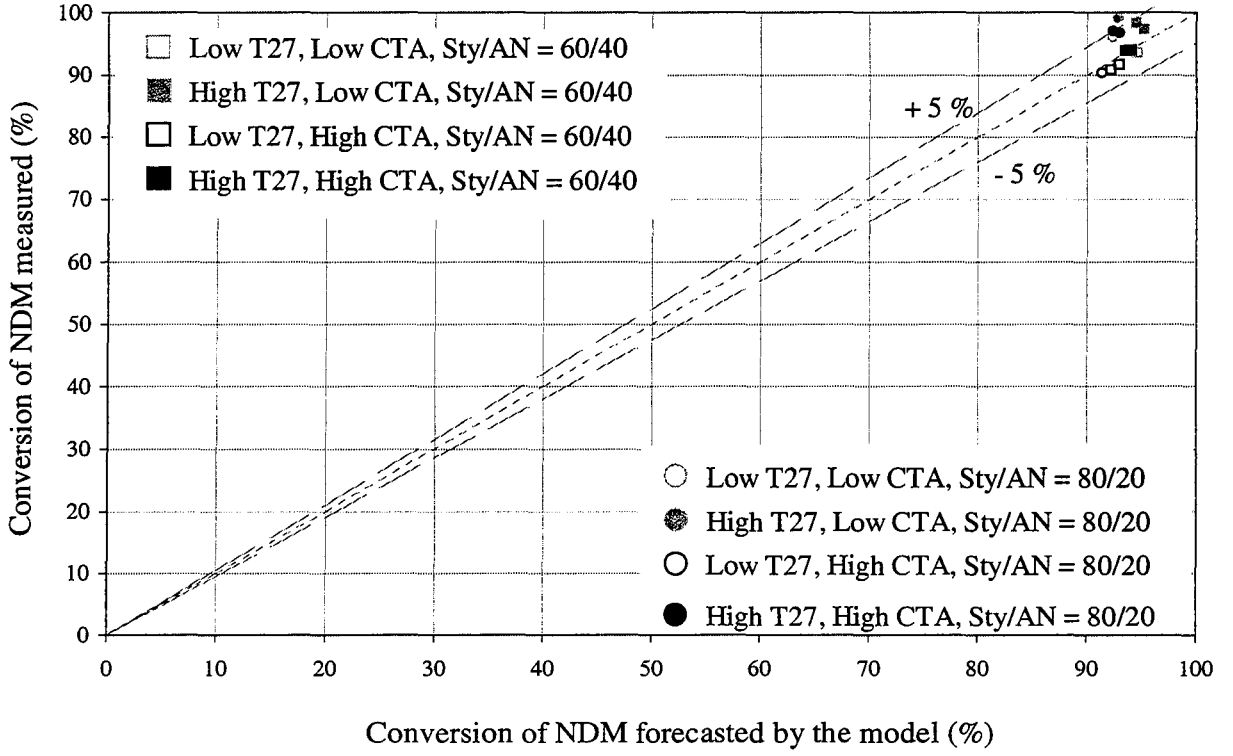

Figure 5.13 : Conversions of NDM ; Measurements vs. modeling using the parameters identified at 120 °C

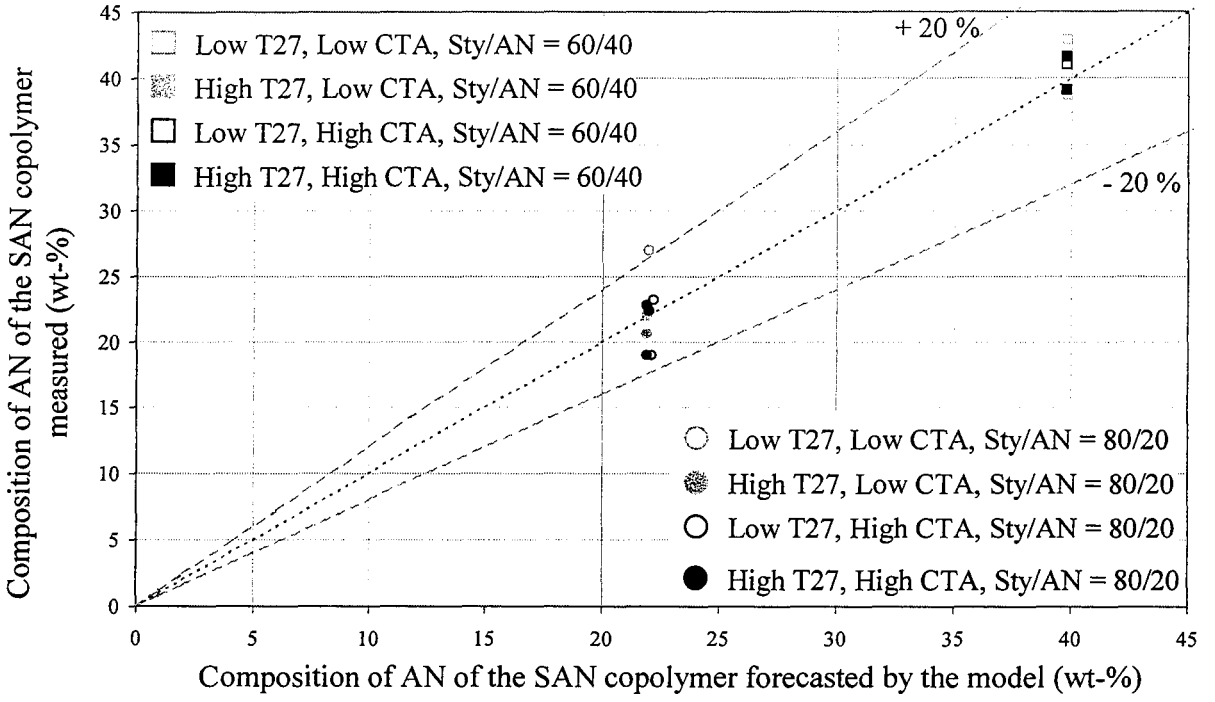

Figure 5.14 : Composition of AN of the SAN copolymer : Measurements vs. modeling using the parameters identified at 140 °C

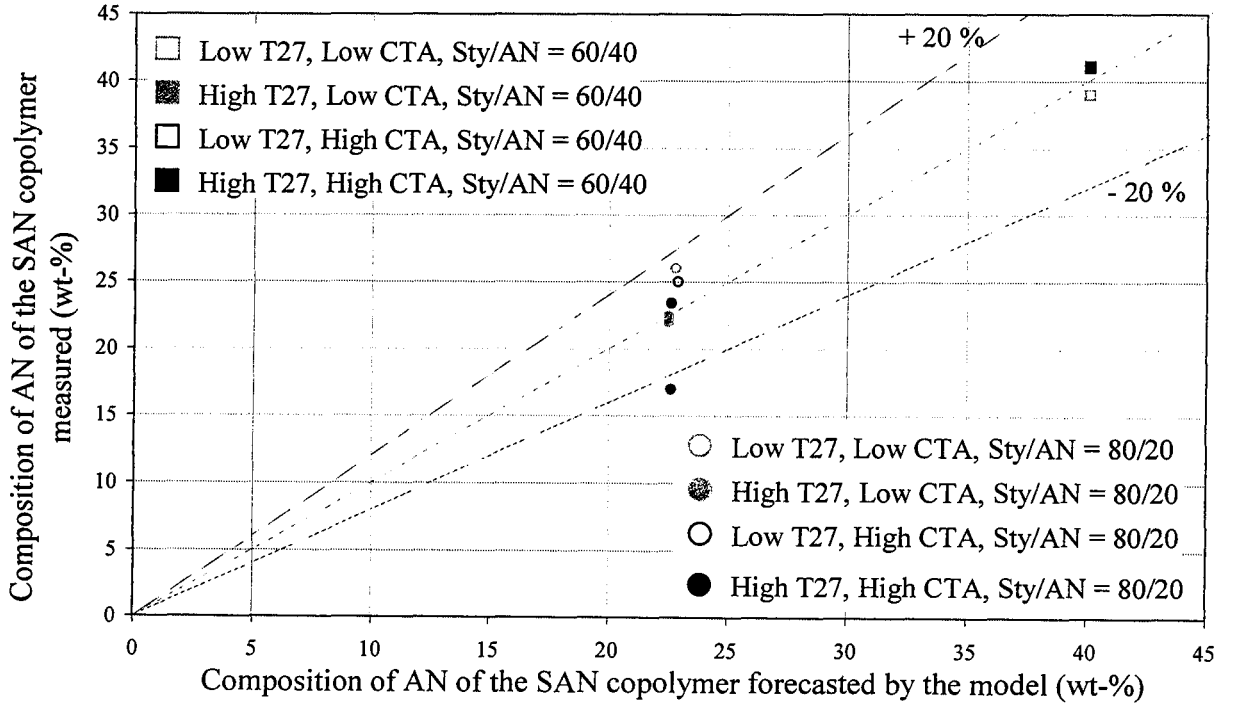

Figure 5.15 : Composition of AN of the SAN copolymer: Measurements vs. modeling using the parameters identified at 120 °C

3.5. Serum : wt-% of SAN dissolved and % of grafted SAN

As explained in previous chapters, the accuracy on the measurements concerning the serum phase depends mostly on the separation of the two phases. Indeed, depending on the solvent used to extract the serum, some variations in the quantity of SAN copolymer dissolved in the continuous phase were observed.

Figures 5.16 and 5.17 below, present the quantity of SAN copolymer dissolved in the serum at 140 °C and 120 °C. The corresponding values are reported in tables A5.21 and A5.22 in annex 5).

Samples 16 and 17 (black points) show the high discrepancy on the measurements. Considering the accuracy of the measurements used to identify the parameters, the model gives relatively good estimations of the order of magnitude of the quantity of polymer in the continuous phase.

It can be observed that increasing the S5200 concentration, increases also theoretically and experimentally the quantity of SAN dissolved in the medium. The influence of the chain transfer agent concentration appears clearly theoretically but very slightly experimentally : the model forecasts that the quantity of SAN copolymer is lower at low NDM concentrations, whereas the measurements show only a small decrease. Indeed, theoretically, the more there are short polymer chains, the more they are soluble in the continuous phase. The long polymer chains obtained with low T27, low NDM and low styrene (gray squares) are the less soluble whereas the short polymer chains obtained with high T27, high NDM and high styrene (black points) are forecasted to be the more soluble, which is actually observed experimentally.

However, the percentage of grafted SAN in the continuous phase is not reached by the model, as shown by figures 5.18 and 5.19, and corresponding tables A5.23 and A5.24 in annex 5. The measurements gave values between 45 % to 85 % of the SAN chains grafted in the serum whereas, the model forecast values between 2 to 32 %. The model using the parameters of table 5.3 cannot forecast the grafting level in the continuous phase. This could be due to the fact that the model does not take into account the grafting introduced in the reactor from the seed in the premix, but most of all it does not take into account the grafting with the solvent, polyol. The results obtained with the natural grafting hypotheses will be exposed further. Nevertheless, theoretically, it can be noticed that the highest level of grafting obtained are realized with experimental conditions combining low T27, low NDM and low styrene, which provided the longer SAN chains, whereas the lowest level of grafting obtained are with high T27, high CTA and high styrene, which provides the smallest SAN chains. Increasing the S5200 concentration increases also theoretically the grafting level. These variations are however not clearly observed experimentally and this can be due to the inaccuracy of the method.

Moreover, the attempt to consider the natural grafting appeared to be not efficient. Indeed, it reduced the grafting levels instead of increasing them. This phenomenon could be explained by the fact that the natural grafting, such as it is introduced in the model, reduces the average molecular weights, which are linked to the grafting level.

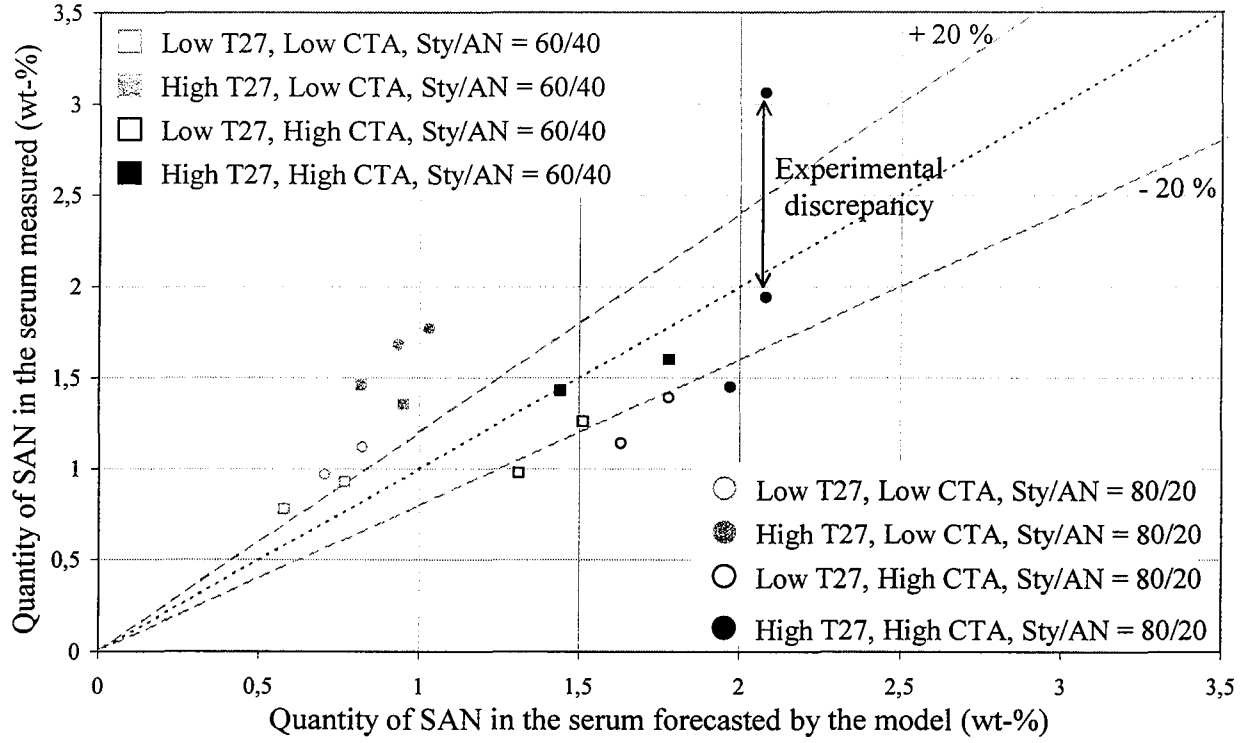

Figure 5.16 : Quantity of SAN copolymer dissolved in the serum : Measurements vs. modeling using the parameters identified at 140 °C

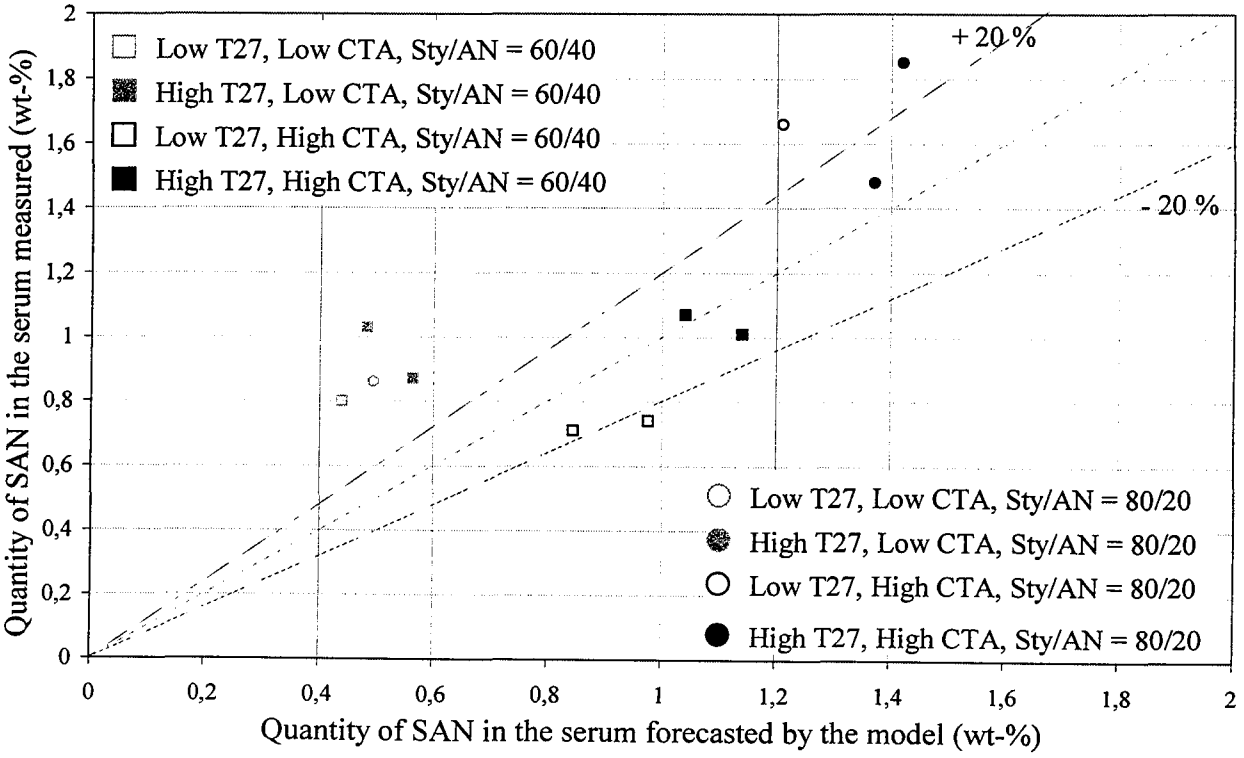

Figure 5.17 : Quantity of SAN copolymer dissolved in the serum : Measurements vs. modeling using the parameters identified at 120 °C

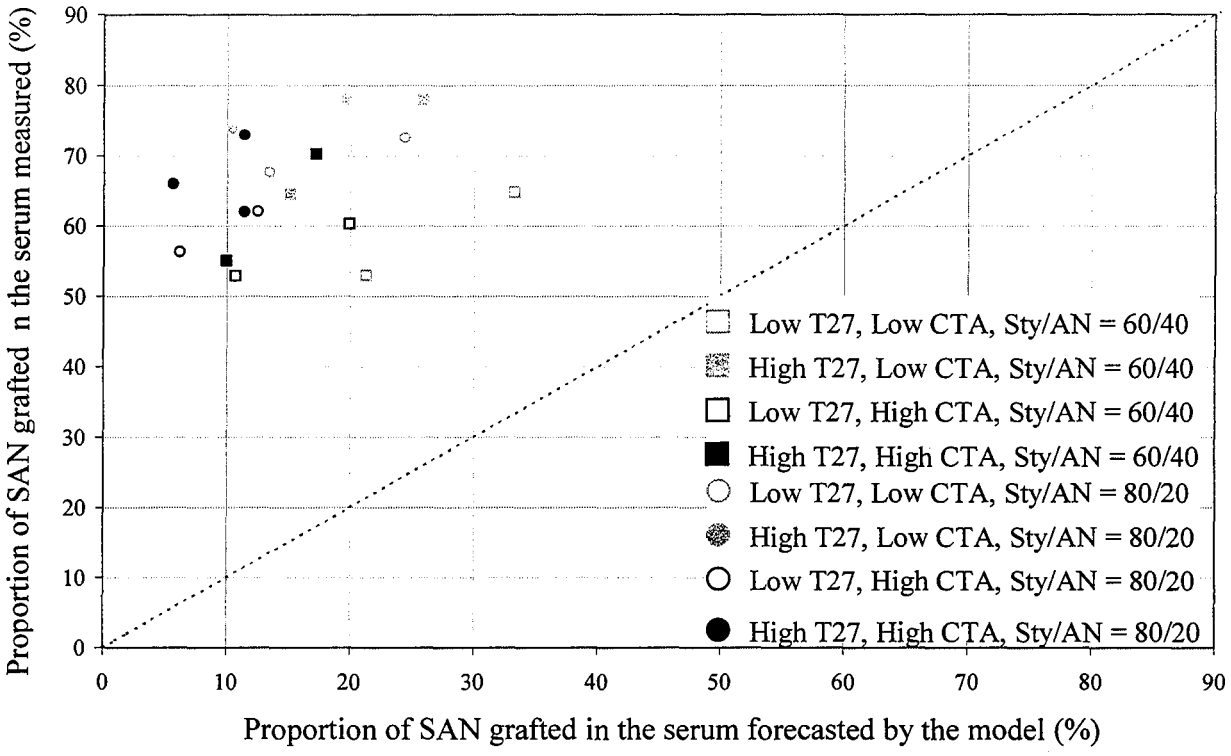

Figure 5.18 : Proportion of SAN grafted dissolved in the serum : Measurements vs. modeling using the parameters identified at 140 °C

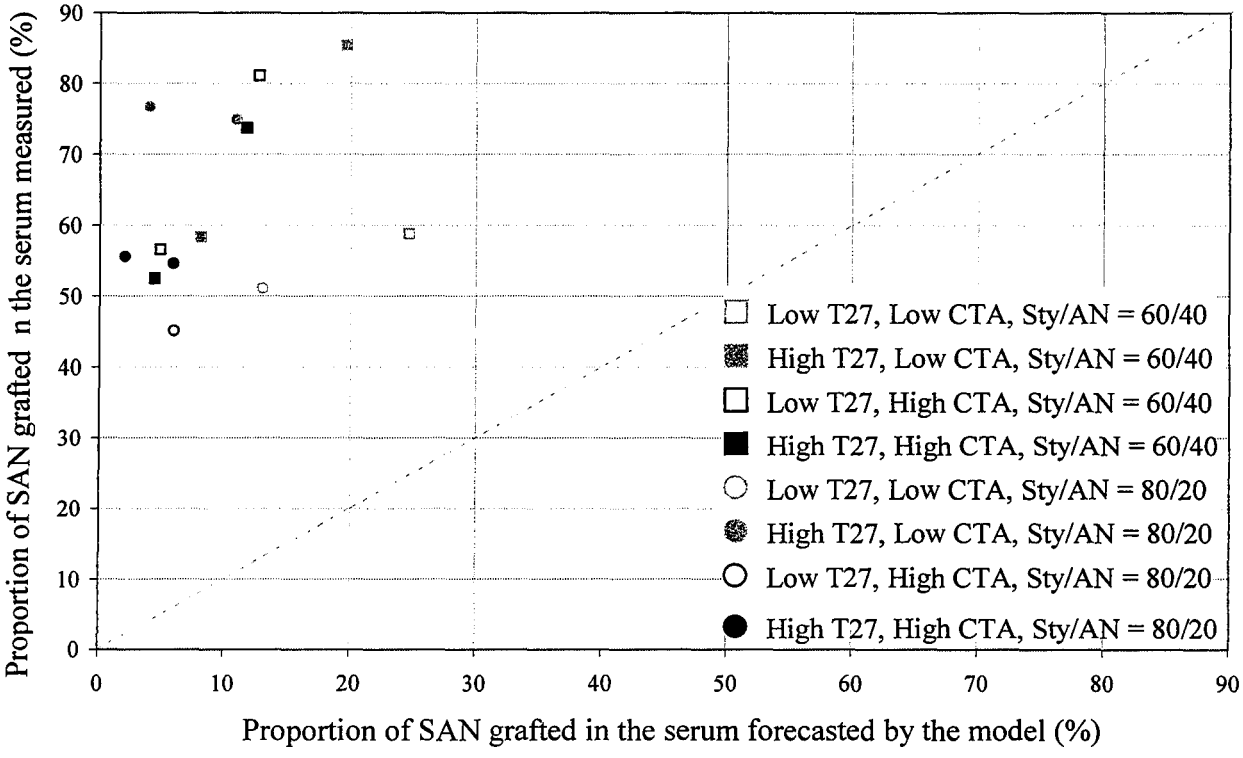

Figure 5.19 : Proportion of SAN grafted dissolved in the serum : Measurements vs. modeling using the parameters identified at 120 °C

3.6. % of grafted SAN in whole CPP (HMW) and wt-% of polyol in solids

A purpose of the study is to experiment some models which could forecast the measurements concerning the grafting. The first of these measurements is the percentage of SAN copolymer grafted in whole copolymer polyol. Figures 5.20 and 5.21, corresponding to tables A5.25 and A5.26 of annex 5, show that the model underestimates this grafting level. Indeed, the experiments provide values from 5 to 38 % whereas the simulations gives values from 2 to 22 % of SAN chains grafted in CPP. Only the high molecular weight grafted SAN chains are considered here.

Increasing the S5200 concentration from 1 wt-% to 3 wt-%, increases around twofold the values of the grafting level given by the simulator at 140 °C, and around 2.8 - 3 times at 120 °C. Nevertheless, as it was noticed in the chapter 3, this increase of the precursor stabilizer concentration does not increase significantly the grafting levels that are measured, and besides, for some cases there is a decrease of the grafting level. It should be however taken into account that there seems to be an important discrepancy on these measurements as it can be seen for the two black points on the figure 5.20 at 9 % of theoretical grafting level corresponding to the samples n° 16 and n° 17, which varies from 9 to 17 %, whereas the experiments were made under the same conditions. The problem could be seen in the other way : reducing the S5200 concentration reduces theoretically the grafting level but not experimentally.

However, it can be noticed that experimentally and theoretically, the grafting level increases when the quantity of acrylonitrile in the SAN copolymer increases, comparing circles and squares of the same color. The influence of the chain transfer agent is also important both theoretically and experimentally : the grafting level increases with low NDM. Nevertheless, there is a very small influence of the initiator on the grafting level in the model whereas the experimental values are rather sensible.

Therefore, the simulator forecast that the grafting level increases when the average molecular weight of the polymer increase, as it is observed experimentally. Nevertheless, this model does not take into account all the grafting mechanisms.

The simulator forecast also the weight percentage of polyol that is grafted in the solid. The comparison between the measurements and the values given by the model are presented below in the figures 5.22 and 5.23, and in the tables A5.27 and A5.28 in annex 5. As shown on these figures, the points do not follow the median line. Indeed, experimentally, there is no influence of the S5200 concentration, whereas the model forecasts an increase of the quantity of polyol grafted in the solids when the quantity of S5200 increases. When the S5200 concentration increases from 1 wt-% to 3 wt-%, the theoretical values increase around twofold at 140 °C and between 2.8 - 3 fold at 120 °C, as increases the grafting level.

Moreover, increasing the chain transfer agent concentration increases theoretically the quantity of polyol grafted in the solid whereas the grafting level decreases. Experimentally, the only significant influence comes from the initiator concentration, that increased the quantity of polyol grafted while increasing from 0.10 wt-% to 0.20 wt-%. Nevertheless, this variation does not influence significantly the theoretical values.

The natural grafting assumptions made the grafting levels decreasing, instead of increasing them, as it decreased the theoretical degrees of polymerization.

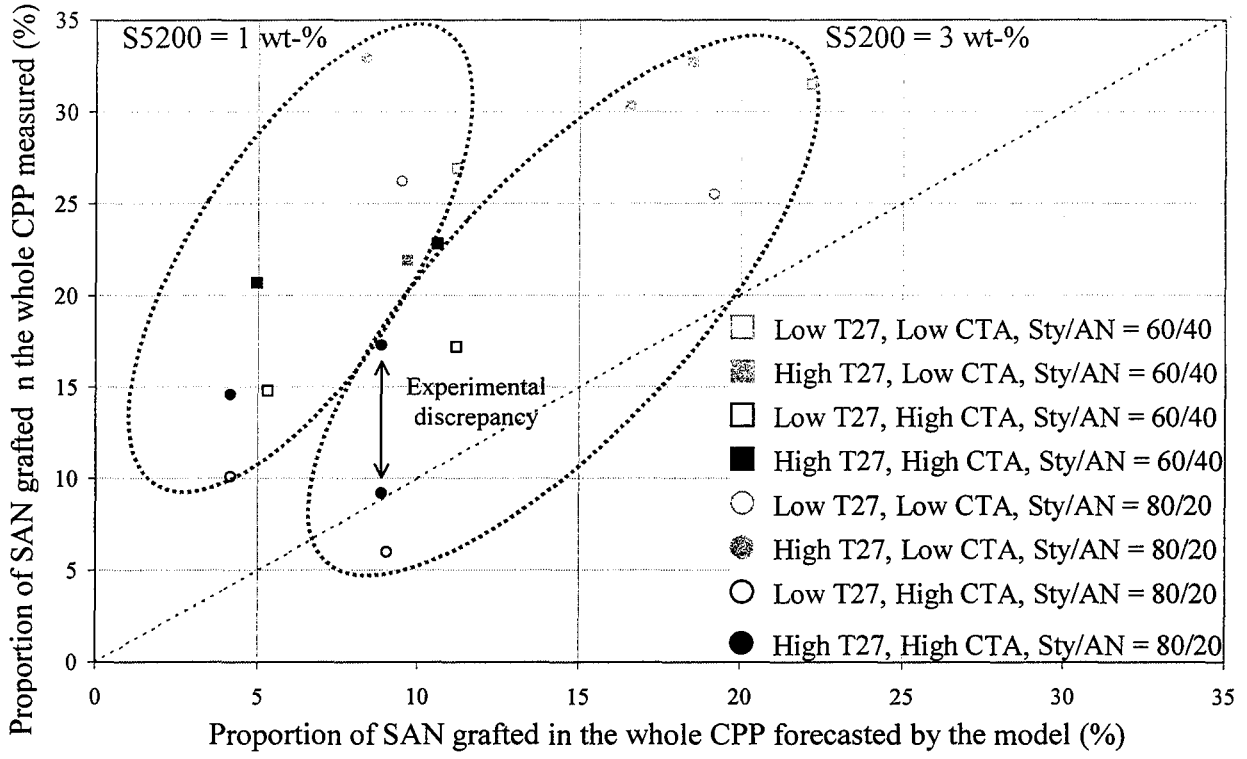

Figure 5.20 : Proportion of SAN grafted in the whole CPP : Measurements vs. modeling using the parameters identified at 140 °C

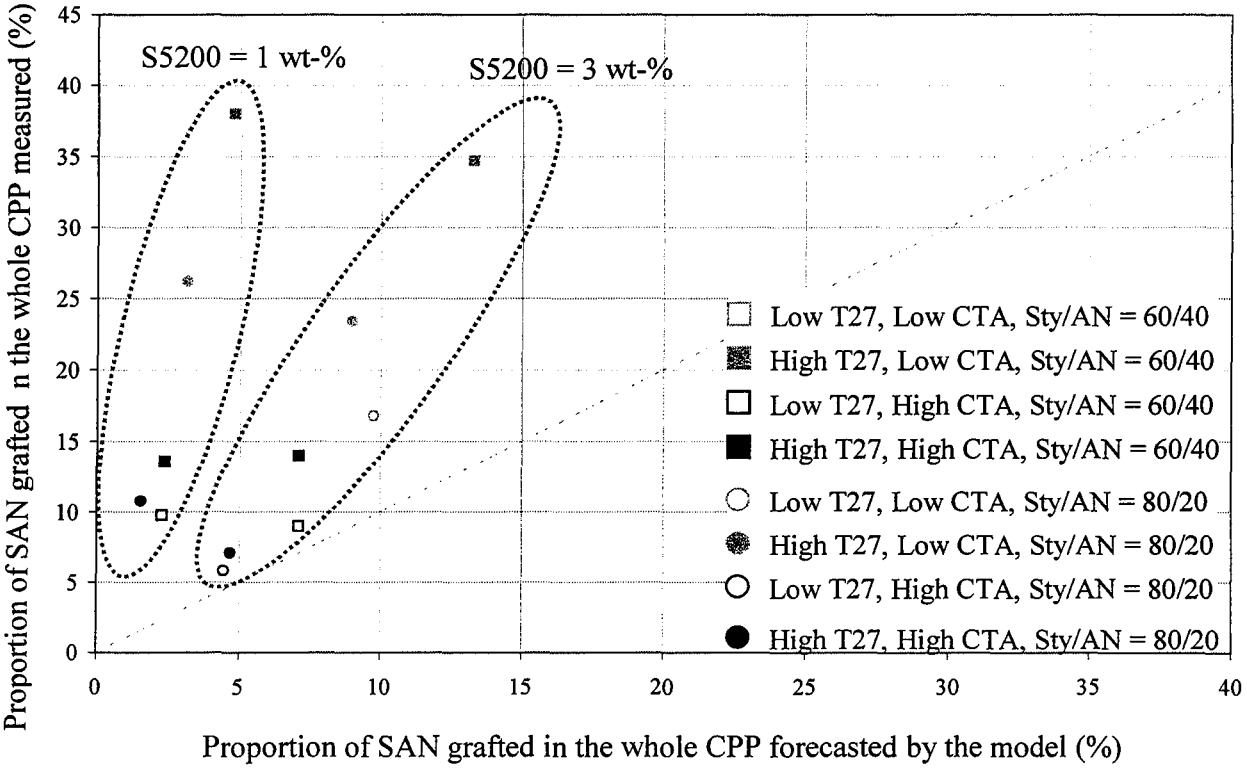

Figure 5.21 : Proportion of SAN grafted in the whole CPP: Measurements vs. modeling using the parameters identified at 120 °C

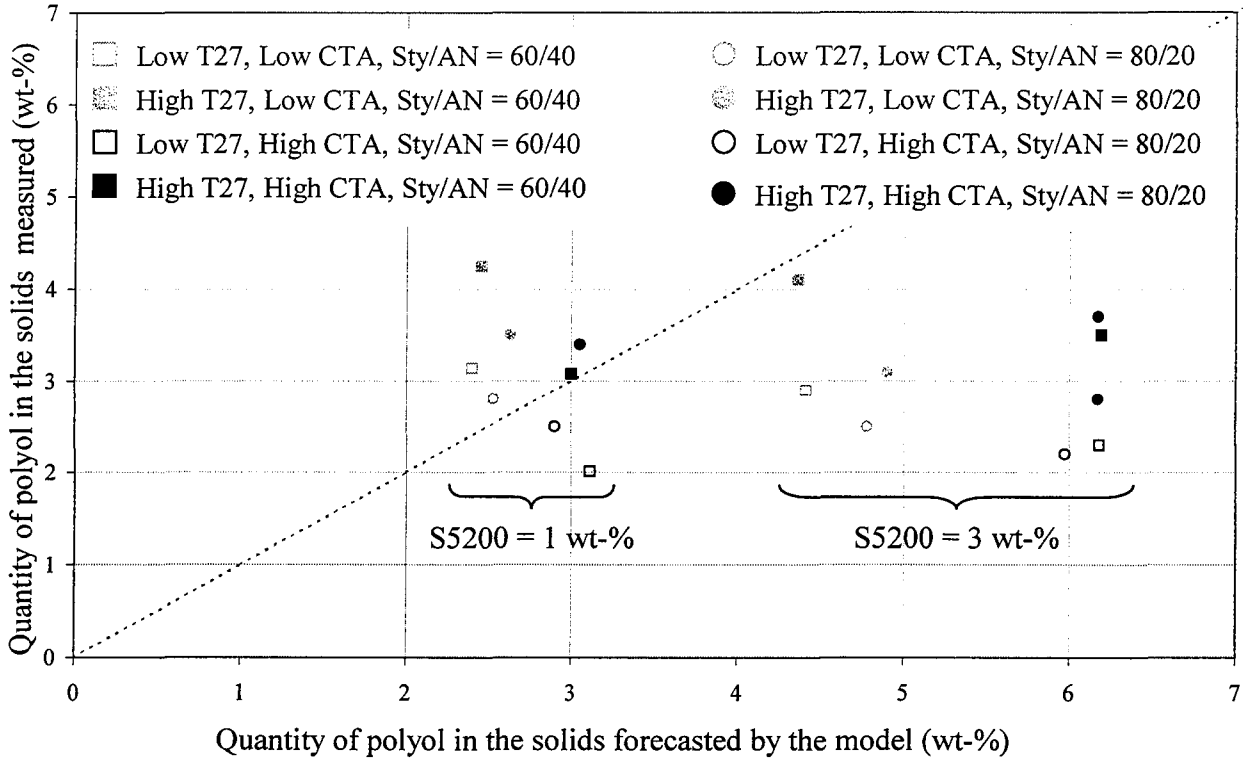

Figure 5.22 : Quantity of polyol in the solids: Measurements vs. modeling using the parameters identified at 140 °C

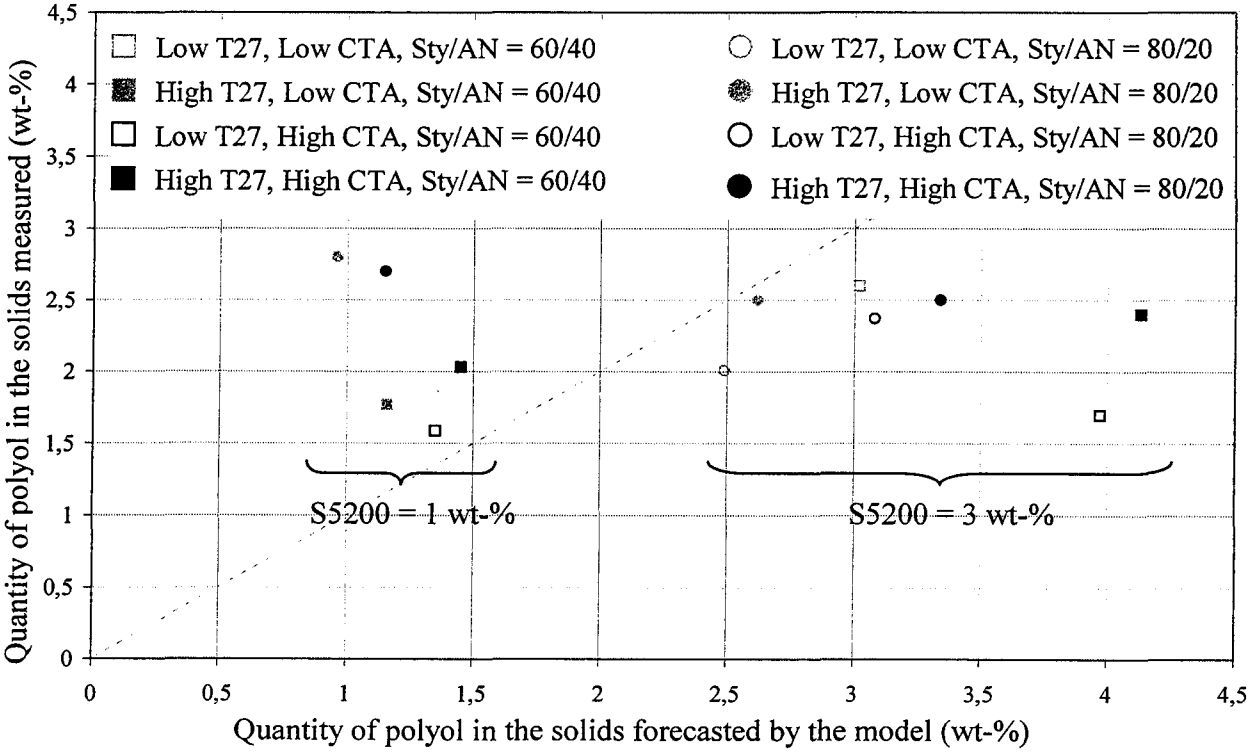

Figure 5.23 : Quantity of polyol in the solids : Measurements vs. modeling using the parameters identified at 120 °C

3.7. Sauter mean diameter

In order to identify the parameters of the model, only the Sauter mean diameters, D[3, 2], measured on samples done with low styrene content (Sty/AN = 60/40) were used, as these samples were more stable. As shown on figures 5.24 and 5.25, corresponding to the values of tables A5.29 and A5.30 of annex 5, the order of magnitude of the simulated values are in good agreement with the experimental ones at 140 °C. At 120° C however, the order of magnitude around 0.4 – 1.4 μm is correct but the points does not follow the median line. Actually, at 120 °C, the samples were less stable and some particles were agglomerate together, which may explain the difficulty to forecast the mean particle size.

Particularly, the grey square on figure 5.25, corresponds to a polymerization done with low T27, low NDM, high S5200 and low styrene at 120°C (run n° 8). The particle size distribution corresponding to this sample showed agglomerations of particles, which explain why this point is so far from the median line. Indeed, the model cannot predict the agglomeration of the particles and multimodal distributions.

When the S5200 concentration increases from 1 wt-% to 3 wt-%, the theoretical average particle size, D[3, 2], decreases twofold at 140 °C and around threefold at 120 °C. Experimentally, a small decrease of D[3, 2] is observable at 140 °C but there is no significant variation at 120 °C. The precursor stabilizer and the temperature stabilize experimentally the particles by preventing their agglomeration but the stable particles have almost the same size.

The initiator concentration does not act significantly on the theoretical particle size whereas some variations appear experimentally, but that should be due to the discrepancy on the measurements. Moreover, the higher the NDM concentration, the lower the theoretical particle size. This phenomenon is also slightly observed experimentally (figures 5.24 and 5.25).

Therefore, considering the fact that the experimental particle size distribution is not monodisperse, the simulator gives acceptable estimations of the Sauter mean diameters.

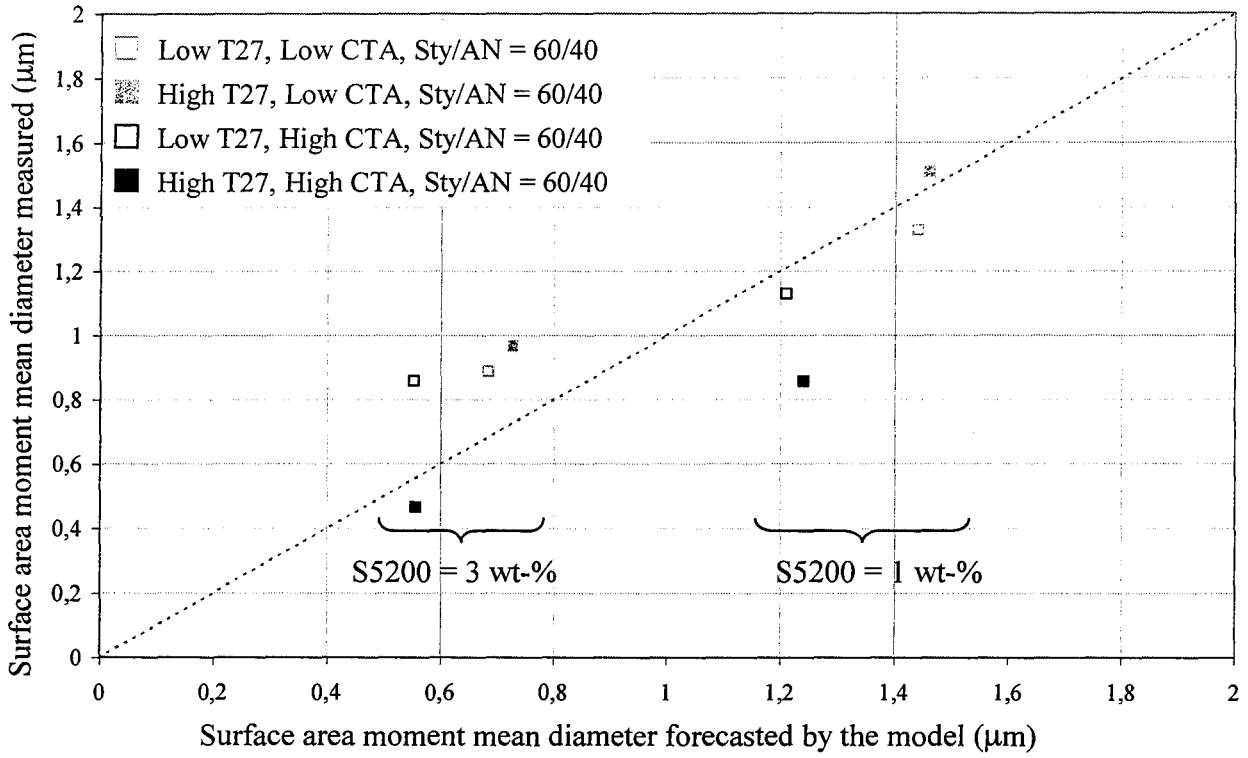

Figure 5.24 : Quantity of SAN copolymer dissolved in the serum: Measurements vs. modeling using the parameters identified at 140 °C

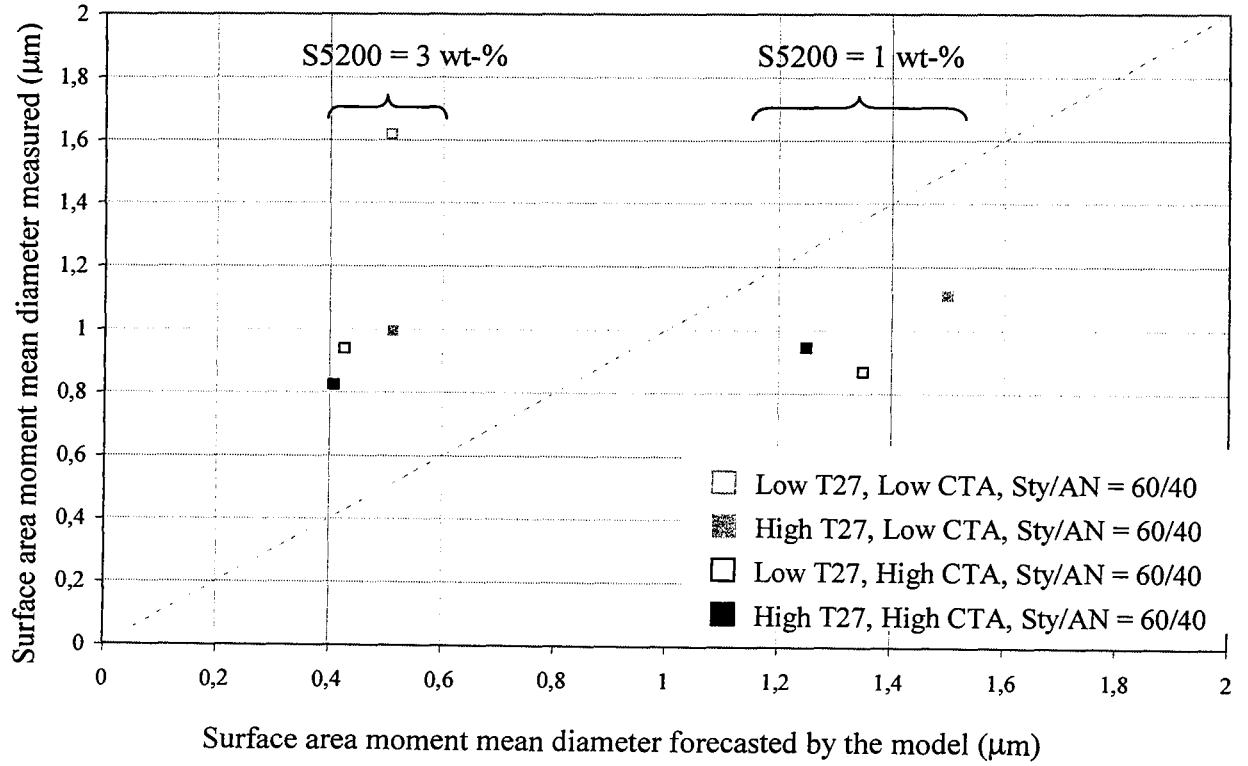

Figure 5.25 : Quantity of SAN copolymer dissolved in the serum: Measurements vs. modeling using the parameters identified at 120 °C

4. Validation and discussion

4.1. Validation on standard runs carried out at T = 130°C

The parameters of the model at 130°C are determined from the parameters identified at 120°C and 140°C. Indeed, as these values are close to each other (table 5.3) at these both temperatures, the values of the parameters at 130 °C (table 5.6) are considered to be the arithmetic mean values between 120 °C and 140 °C.

Table 5.5 shows the results of the simulation with the standard conditions and the experimental intervals established with the standard runs n° 31 to n° 35. For each data the number of measurements realized is indicated and in which table of annex 3 they can be found. Then, the experimental intervals take into account the estimated accuracy (given by Dow) on each measurement.

Table 5.5. : Data simulated with the standard conditions

Data	Theoretical values	Experimental interval	Unit	Measurements in table	Number of measurements done
$\bar{M}_n$	25300	26000 - 37900	g mol^{-1}	A3.5	5
$\bar{M}_w$	59800	64100 - 98200	g mol^{-1}	A3.5	5
Solids	38.5	32.1 – 40.3	wt-%	A3.10	2
Residual AN	1.85	1.58 – 2.17	wt-%	A3.10	2
AN conversion	85.7	83.2 – 87.7	%	A3.10	2
Residual Sty	5.42	3.61 – 4.57	wt-%	A3.10	2
Sty conversion	82.0	84.8 – 88.0	%	A3.10	2
Residual NDM	140	96.3 - 118	ppm	A3.10	1
NDM conversion	95.3	96.1 – 96.8	%	A3.10	1
SAN composition in AN	30.9	19.2 – 34.8	wt-%	A3.25	2
SAN in serum	0.56	0.84 – 1.28	wt-%	A3.31	2
SAN grafted in serum	24.2	42.1 – 93.2	%	A3.20	2
SAN grafted in CPP	16.2	12.9 – 19.3	%	A3.20	1
Polyol in solid	5.98	1.54 – 3.25	wt-%	A3.25	2
D[3, 2]	0.346	0.71 – 1.06	µm	A3.15	1

Table 5.6. Values of the parameters at 130 °C

Parameter n°	Name	T = 130 °C	Unit
1	k^c_{pAA}	2290	$m^3.mol^{-1}.s^{-1}$
2	k^c_{pBB}	48	$m^3.mol^{-1}.s^{-1}$
3	k^c_{tcAA}	$1.47\ 10^8$	$m^3.mol^{-1}.s^{-1}$
4	k^c_{tcBB}	$2.92\ 10^6$	$m^3.mol^{-1}.s^{-1}$
5	R^c_{AB}	0.43	-
6	R^c_{BA}	0.29	-
7	$R^c_{t,A}$	3.3	-
8	$R^c_{t,B}$	8.6	-
9	ϕ	27.3	-
10	k^p_{pAA}	9320	$m^3.mol^{-1}.s^{-1}$
11	k^p_{pBB}	377	$m^3.mol^{-1}.s^{-1}$
12	Gel1	1.15	-
13	R^p_{AB}	0.48	-
14	R^p_{BA}	0.38	-
15	K_p	$7.4\ 10^{-5}$	s^{-1}
16	R^c_{AG}	0.54	-
17	R^c_{BG}	32.8	-
18	$k^c_{t,G}$	1855	$m^3.mol^{-1}.s^{-1}$
19	k^c_{tdAG}	$1.64\ 10^8$	$m^3.mol^{-1}.s^{-1}$
20	k^p_{tdBG}	$1.29\ 10^7$	$m^3.mol^{-1}.s^{-1}$
21	a	$3.08\ 10^{-9}$	$m.(mol.kg^{-1})^{1/3}$
22	Gel2	11.4	-
23	f_c	0.28	-
24	H_{CTA}	0.60	-

The average molecular weights, $\bar{M}_n$ and $\bar{M}_w$, are underestimated by the model, but the experimental confidence interval does not take into account the fact that the values measured are not the absolute values. The absolute values should indeed be around 0.8 times the values obtained using polystyrene standards as reference considering that the SAN copolymer composition of the standard premix (Sty/AN = 70/30) is closed to the composition of the azeotropic point (Sty/AN = 75/25).

The solid quantity forecasted, 38.5 wt-%, corresponds well to the measurements. The acrylonitrile conversion is also well foreseen, 85.7 %, but the styrene and the NDM conversions are slightly underestimated (82 % and 95.3 % respectively). Nevertheless, globally the order of magnitude of the conversions is rather well foreseen with this model.

The SAN copolymer composition in AN is predicted to be 30.9 wt-%, that is in the range observed experimentally.

Nevertheless, concerning the serum, as already observed with experiments done at 120°C and 140 °C, the model underestimates the quantity of SAN copolymer in the medium and underestimates largely the percentage of SAN chains that are grafted. Although, it should be recalled that the measurements on the serum phase are not accurate due to the method of separation of the two phases.

Concerning the grafting in the whole CPP and in the solid, the percentage of SAN grafted in CPP that is forecasted is in the range of the measurements, but it would need more measurements to confirm this. However, the quantity of polyol in the solid is overestimated. This means that the relationship in the model between the percentage of grafted SAN chains and the quantity of polyol in the solid is not correct. This relationship is indeed based on the fact that all the grafts are S5200 molecules. Nevertheless, it is shown in chapter 2 that the S5200 samples are not purely molecules with 6 OH, and some experiments showed that the solvent (polyether triol) can also be grafted.

The mean particle size forecasted is underestimated. Nevertheless, the order of magnitude is correct and the experimental particle size distribution is actually bimodal that cannot foresee this model.

4.2. Confidence interval of the identified parameters

The accuracy on the parameter may be estimated considering the populations of results given by the evolutionary algorithm. Nevertheless, there are too many limitations due to the lake of accuracy of the measurements to give an accurate confidence interval of the parameters.

- The average molecular weights of SAN copolymer are measured using polystyrene standards which provide overestimated values. It would be necessary to use SAN copolymers of the desired composition as standards but the easier SAN standards that can be produced have the composition of the azeotrope, that is to say 24-25 wt-% of acrylonitrile. Moreover, it was observed experimentally that the molecular weight distributions are polydisperse, that does not forecast the model.
- The residual concentrations of the monomers determined by HS-GC presented some discrepancy for a ratio Sty/AN = 80/20, particularly for the most unstable samples.
- The data concerning the serum phase cannot be accurate because of the serum/solid separation, which depends on the solvent used to extract the serum. Moreover the

grafting of the serum phase depends on the low molecular weight grafted SAN chains that may contain the seed that goes inside the reactor. Nevertheless, the presence of the seed was not introduced in the model. Furthermore, the inaccuracy concerning the serum may also come from the simplified precipitation model.

- The particle size distributions showed polydisperse populations of particles for each sample and a lot of agglomeration for the unstable samples. Besides, the experimental results obtained with Sty/AN = 80/20 could not be used to identify the parameters. This model cannot forecast these distributions but can just give the orders of magnitude of the average particle sizes.
- The quantity of polyol in the solid is obtained through a method that takes too long time to wash the solids to be sure that there is not free polyol left onto the particles. This method is estimated to be accurate at ± 30 % and it cannot be used to identify the parameters.

Moreover, it would be necessary to study further the influence on the chosen ranges of research on the values of the identified parameters, and to determine the sensitivity of each parameter.

The accuracy of the identification depends also on the dynamic integration of the differential equation and particularly on the step of time and on the final time. A step of 0.1 s until 10000 s was chosen as a compromise between a sufficient accuracy and an acceptable computing time. The identification was realized with these conditions, and therefore the simulation can be used to forecast the transient regime but only to give some orders of magnitude as there was no data available for the identification in the transient regime.

4.3. Grafting modeling and path forward

As explained before, introducing the natural grafting in the model as it was explained in chapter 4 did not allow to obtain better maximum likelihood estimators than without natural grafting. Indeed, as this model forecasts more primary radicals coming from the solvent, the number of polymer chains increases and the average molecular weights decrease. However, as observed experimentally, when the degree of polymerization decreases, the percentage of species grafted decreases also.

The model seemed to provide correct values of the grafting level for standard recipes, nevertheless it would need more measurements on standard samples to confirm these tendencies.

In order to validate the model, it would be necessary to do the studies at 120°C, 130 °C and 140°C but with some systems, which provide the less natural grafting as possible ("DMC-polyol" and an azo-type initiator like azo(bis-methylbutyronitrile (AMBN)). This would allow to study more precisely the influence of the precursor stabilizer S5200 on the grafting and on the stability of the copolymer polyol. Indeed, the S5200 molecule may act in a depletion stabilization mechanism, as the experiments and the model have shown that the grafting on its vinyl bound is not sufficient to explain the results.

Nevertheless, in order to run the parameter identification it would be necessary to use more accurate measurements and stable samples. Particularly, the monomer composition Sty/AN = 80/20 has been shown to provide mostly unstable lattices and should not be studied further. It would be recommended however to study the ratios Sty/AN= 60/40 and Sty/AN = 70/30, which give stable CPPs.

In order to be efficient the serum analysis should not be taken into account in the calculations as it is too much time consuming and not enough accurate. The copolymer composition in acrylonitrile and in polyol may also not be investigated as the composition in acrylonitrile does not give important information for the parameter identification and because the measurement of the quantity of polyol in the solid is not enough accurate. Therefore, only the average molecular weight distributions, the conversions and the quantity of solid, the proportion of grafted species in the whole CPP and the mean particle size may be required to be calculated. These analyses are relatively rapid and it would allow to run an important number of experiments.

With these conditions, better reproducible data may be provided, which should allow to estimate more precisely the parameters of this model. Moreover, the residence time inside the reactor (that is to say the mass flow) and the agitation speed may be further enter in the experimental conditions to study.

When the results given by the simulation will reach an acceptable level of prediction, a study may be done in order to control the process.

Conclusion

The purpose was to study the CPP process on the widest range of experimental conditions, even using the less stable experimental conditions. It allowed to understand better the process and to establish a model. Due to the complexity of the system, many parameters were required to be identified. Several simplifications had to be done to reduce as far as possible their number, to solve the system and to identify these parameters.

Considering the lack of accuracy and the instability of several of the samples, the identification method tried to forecast as well as possible the experimental data. The final model obtained gives acceptable orders of magnitude for the average molecular weights, the solid composition and the conversions. The prediction of the grafting level in the whole CPP may be improved by reducing the possibilities of natural grafting during the experiments.

CONCLUSIONS AND RECOMMENDATIONS

1. Recall of the objectives

The objectives of this work were to answer to the different questions concerning the dispersion copolymerization process of styrene and acrylonitrile in polyol medium, and particularly to better understand the stabilizer technology and the influence of the process conditions on the final copolymer polyol properties. Indeed, the stabilizing system is the most important component of the copolymer polyol production. Nevertheless, many important information were not known concerning the action of the precursor stabilizer S5200. Particularly, it was required to know the exact structure of the stabilizer molecule produced *in situ*. The majority of the different kinetics involved in the process were also unknown and particularly the kinetics of the stabilizer precursor – styrene – acrylonitrile system reactions together with the adsorption kinetics onto the SAN particles surface. The effect of grafting on the CPP stability and viscosity had also to be better known. The second important aspect was the partitioning of monomers over the two phases and where did the radical reaction take place (polyol or solids phase) and how the splitting occurred.

The main goal was to try to answer to these different questions. Therefore, the influence of the process conditions on the physical properties of the copolymer polyols produced were studied in order to better understand the different mechanisms involved and to develop a tendency model for the overall process.

2. Conclusions

In the first chapter, a literature overview showed that the dispersion polymerization process could be applied to various solvents, monomers and stabilizers. This presented the important diversity of studied systems and the difficulty to understand precisely the general mechanism of dispersion polymerization as each part of the mechanism (nucleation, steric stabilization, particle growth, monomer partitioning,...) depends on the specific system studied and the process conditions (temperature, pressure, agitation, concentrations, reactor, residence time...). A quick overview of the use of copolymer polyols in polyurethane industry allowed to present the CPP properties targeted.

Chapter 2 presents the reactants and the experimental device used, and the several analytical methods required to study the physical properties of the copolymer polyol produced. Indeed, different analytical methods have been developed and tested, particularly in order to study the serum phase and the grafting level. Nevertheless, some of these methods are time consuming, expensive and difficult to realize. One of the difficulties comes particularly from the separation of the solid phase from the serum, which is a long work, as the process needs to be repeated several times.

Then, in order to better understand the phenomena that act in the continuous process of dispersion copolymerization of styrene and acrylonitrile in polyol medium, an experimental design has been elaborated and the results have been presented in chapter 3. A first part exposed some preliminary results obtained by Dow Chemical concerning the determination of the partitioning of the monomers, and the chain transfer agent (NDM) between the continuous polyol phase and the SAN polymer particles. Then, a report dealing with "natural" grafting mechanisms revealed that the nature of the grafted polyol is more important to stabilize the particles than the total amount of grafting. Indeed, the presence of high molecular weight polyol grafts such as S5200 has a significant positive influence on the CPP properties. Moreover, it

appeared that using the peroxyester T27 as initiator, almost 50 % of the SAN-grafted polyol was obtained through "natural" grafting of the polyol diluent itself. Finally, a study showed the major influence of the grafted SAN in the solids, which is correlated with an increase of the CPP viscosity. Actually, the influence of the grafted SAN in the solids appeared to be much more important than the grafted SAN species dissolved in the continuous phase.

A second part exposed the experimental design used to study the influence of the process conditions, i.e. : the styrene to acrylonitrile ratio, the concentrations of the precursor stabilizer S5200, the initiator T27, the chain transfer agent NDM and the temperature. Then, the different physical properties of the copolymer polyol produced have been described by observing the influence of the process conditions on them.

The main conclusions are exposed below. The study of the molecular weight distributions has shown the presence of three types of sizes of SAN macromolecules. The smallest average molecular weights seemed to be related to the SAN chains soluble in the continuous phase while the longest appeared to be the SAN chains produced by bulk polymerization inside the particles. The medium size population may correspond to the SAN chains grafted by the precursor stabilizer, S5200. The main parameters that influence the average molecular weights are the styrene to acrylonitrile ratio and the NDM concentration. An increase of the quantities of this chain transfer agent and of styrene increases the two populations containing the smallest SAN chains and decreases the population containing the longest SAN chains, decreasing the average molecular weights and the conversions. Therefore, it appeared that the higher the styrene and NDM level, the more the polymerization is shifted into solution rather than inside of the particles.

Moreover, the viscosity of the whole CPP and the percentage of grafted SAN chains are directly related to the SAN molecular weights. The styrene to acrylonitrile ratio and the NDM content have the major effect on these three characteristics. With high acrylonitrile and low NDM contents, the degrees of polymerization are high, while with high T27 initiator content and high temperature the number of SAN chains increases. This increases also the viscosity of the whole CPP and the grafting level.

The particle size distributions obtained using the laser diffraction technique are polydispersed. A bimodal distribution appears on the more stable samples with a population of small particles centered at around 0.2 µm and a second population centered at around 1.7 – 2 µm. Moreover, an irregular population is visible from 5 to 70 µm, depending on the degree of instability of the dispersion. Scanning electron microscopy images confirmed that it corresponds to particle agglomerations. The styrene to acrylonitrile ratio has a major influence on the particle size and on particle stability. Indeed, the most stable samples have been obtained with low styrene content, high temperature and high NDM content. Therefore, this shows that the stabilization does not depend only of the grafting level, but firstly on the average molecular weights and on the locus of polymerization.

Nevertheless, a high content of precursor stabilizer, S5200, seems to better stabilize the particles, according to the particle size distributions, even if the quantity of S5200 does not seem to have any influence on the grafting level and on the percentage of polyol grafted in the solids. It has been suggested to further study the possibility that S5200 acts by depletion stabilization rather than by steric stabilization, which would explain these results.

As a conclusion, the major process conditions that influence the CPP properties, are the ones that act directly on the SAN molecular weights, that is to say the styrene to acrylonitrile ratio and the NDM content, and then in smaller degree the initiator quantity and the temperature. The

degree of polymerization of the SAN chains is then directly related to the CPP viscosity and the grafting level. These results have also shown the complexity of the problem, the ambiguous role of the precursor stabilizer, S5200, and the lack of accuracy of some of the measurements.

The second part of the work concerned the whole process modeling, which has been developed in chapters 4 and 5. Indeed, chapter 4 presents the different assumptions taking into account the experimental knowledge of the process in order to provide a model able to calculate the data describing the CPP properties that are collected by analytical methods. In order to reduce as much as possible the computing times it has been necessary to reduce the number of unknown parameters and to make simplifications concerning, in particular, the precipitation, the thermodynamics, the particle size and the grafting. Moreover, some assumptions have been made in order to test theories concerning the grafting, i.e. : preference to acrylonitrile, grafting on the double bond of S5200 and "natural" grafting. Then, balances and quasi-steady state approximation provided a system of equations, which has been solved in order to simulate the reactor state versus the reaction time.

Further, the chapter 5 has presented the mathematical tools used in order to identify the unknown parameters of the model through the use of an evolutionary algorithm. Identifications at the two experimental temperatures allowed to give the better parameters, which allow to fit the best as possible the theory with the experimental results. Nevertheless, as the discrepancy and the inaccuracy on the measurements are rather high, the final model can only give estimated orders of magnitude. A validation on the standard recipes has shown that the model gives acceptable orders of magnitude for the average molecular weights, the solids composition and the conversions.

Concerning the grafting, the model used cannot reach the values measured and particularly in the serum. The introduction of "natural" grafting did not help to increase theoretically the grafting levels as desired as actually it reduced the average molecular weights, reducing the percentage of grafted SAN chains. Moreover, considering a classical grafting of S5200 on its vinyl bond, the variations of the S5200 concentrations have a theoretical effect on the grafting level and on the particle size but this was not observed experimentally. This would mean that the grafting mechanisms are different from the ones taken into account. Particularly, it has been suggested to explain these phenomena that S5200 acts by depletion stabilization rather than by steric stabilization.

3. Recommendations

Finally, different recommendations can be made to go further in this work. Despite the complexity of the problem, it has been shown that it is possible to define a model, which forecasts the main properties of copolymer polyols with acceptable orders of magnitude. In order to improve this model different points may be investigated.

(1) Firstly, the experimental design and the process conditions must be adapted in order to obtain more accurate measurements and stable samples, that would make easier the parameter identification. Particularly, the monomer composition Sty/AN = 80/20 has been shown to provide mostly unstable lattices and should not be studied further. It would be recommended however to study the ratios Sty/AN = 60/40 and Sty/AN = 70/30, which give stable CPPs. Furthermore, it would be necessary to do the studies at 120°C, 130 °C and 140°C but with some systems, which provide the less "natural" grafting as possible ("DMC-polyol" and an azo-type initiator like azo(bis-methylbutyronitrile (AMBN)). This would allow to study more precisely

the influence of the precursor stabilizer S5200 on the grafting and on the stability of the copolymer polyol.

(2) Secondly, it is required to improve accuracy on the analytical measurements. Indeed, it is needed to establish the relationship between the absolute average molecular weights and the molecular weights measured by GPC using a calibration with polystyrene standards for the different SAN compositions used. Moreover, the study of the serum, which cannot be accurate enough to help the parameter identification, may be avoided. It appeared, indeed, that some of the data measured cannot help for the identification, for instance, the composition of the SAN copolymer in styrene, acrylonitrile and polyol. Therefore, a higher number of experiments will be required.

(3) Moreover, as soon as the results of the parameter identification will be improved, it will be necessary to estimate more precisely the accuracy of the method and to study the influence of the characteristics of the evolutionary algorithm (population size, number of mutations, number of individuals replaced) and the conditions of integration (the step of integration and the final time) on the final results.

(4) Furthermore, the residence time inside the reactor, i.e. the mass flow, and the agitation speed may further be part of the experimental conditions to study.

(5) The next step will be then to reduce the tendency model, that is to simplify the model in order to forecast some specific properties, with the final purpose to run multicriteria optimization, after having defined fixed objectives, and to develop the control of the process.

LIST OF REFERENCES

The list of the 131 references quoted in this work is presented below.

Abad, C., et al. (1995). Modeling Nucleation and Particle Growth in Emulsion Copolymerization in Continuous Loop Reactors. *Macromol. Symp.*, **92**, 195-204.

Ahmed, S. F. & Poehlein, G. W. (1997a). Kinetics of Dispersion Polymerization of Styrene in Ethanol. 1. Model Development. *Ind. Eng. Chem. Res.*, **36**, 2597-2604.

Ahmed, S. F. & Poehlein, G. W. (1997b). Kinetics of Dispersion Polymerization of Styrene in Ethanol. 2. Model Validation. *Ind. Eng. Chem. Res.*, **36**, 2605-2615.

Almog, Y., et al. (1982). Monodisperse Polymeric Spheres in the Micron Size Range by a Single Step Process. *British Polymer Journal*, **14**, 131-136.

Araujo, P. H. H. & Pinto, J. C. (2000). Mathematical Modeling of Dispersion Polymerizations. Study of the Styrene Polymerization in Ethanol. *Brazilian Journal of Chemical Engineering*, **17**, 383-393.

Arita, K., et al. (1981). Analysis of the Monomer Sequence Distribution in Alternating Acrylonitrile-Styrene Copolymers by ^{13}C-NMR. *Journal of Polymer Science : Polymer Letters Edition*, **19**, 211-216.

Arshady, R. (1992). Suspension, Emulsion and Dispersion Polymerization: A Methodological Survey. *Colloid & Polymer Science*, **270**, 717-732.

Arshady, R. (1999). In the Name of Particle Formation. *Colloid and Surfaces A : Physiochemical and Engineering Aspects*, **153**, 325-333.

Asakura, J. I., et al. (1981). Effect of Solvent on the Radical Copolymerizability of Styrene with Acrylonitrile. *J. Macromol. Sci.-Chem.*, **A15(8)**, 1473-1478.

Bäck, Th. (1996), Evolutionary Algorithms in Theory and Practice, Oxford University Press, New York

Baines, F. L., et al. (1996). Use of Block Copolymer Stabilizers for the Dispersion Polymerization of Styrene in Alcoholic Media. *Macromolecules*, **29**, 3096-3102.

Bajaj, P. & Gupta, D. C. (1979). Copolymerization of Styrene and Acrylonitriles with Functional Silanes. *European Polymer Journal*, **15**, 271-275.

Barret, K. E. J. (1975). Dispersion Polymerization in Organic Media. London, Wiley.

Barrett, K. E. J. (1973). Dispersion Polymerization in Organic Media. *Br. Polym. J.*, **5**, 259-271.

Bicking, F., et al. (1994). Global Optimization by Artificial Life : a New Technique Using Genetic Population Evolution. *RAIRO-Operation Research*, **28**(1), 23-36.

Brandrup, J. & Immergut, E. H. (1989). Polymer Handbook. New York, Wiley Interscience Publication.

Canelas, D. A., et al. (1996). Dispersion Polymerization of Styrene in Supercritical Carbon Dioxide : Importance of Effective Surfactants. *Macromolecule*, **29**, 2818-2821.

Cao, K., et al. (1999). Micron-Size Uniform Poly(Methyl Methacrylate) Particles by Dispersion Polymerization in Polar Media. 4. Monomer Partition and Locus Polymerization. *Colloids and Surfaces A: Physiochemical and Engineering Aspects*, **153**, 179-187.

Cao, K., et al. (2000a). Micron-Size Uniform Poly(Methyl Methacrylate) Particles by Dispersion Polymerization in Polar Media. 1. Particle Size and Particle Size Distribution. *Chemical Engineering Journal*, **78**, 211-215.

Cao, K., et al. (2000b). Micron-Size Functional Uniform PMMA Particles by Dispersion Copolymerization in Polar Media. *Macromol. Symp.*, **150**, 195-200.

Cao, K., et al. (2000c). Mechanism and Model of Dispersion Polymerization Using Homopolymer as Dispersant in Polar Media. *Macromol. Symp.*, **150**, 187-194.

Casati, E. M. & Herrington, R. M. (1998). Tailoring the Performance of Molded Flexible Polyurethane Foams for Car Seats. *Journal of Cellular Plastics*, **34**(5), 430-466.

Cawse, J. L. (1997). Dispersion Polymerization. Emulsion Polymerization and Emulsion Polymers, London, Wiley.

Chatzidoukas, C., et al. (2003). Mathematical Modeling of Dispersion Polymerization of Methyl Methacrylate in Supercritical Carbon Dioxide. *Ind. Eng. Chem. Res.*, **42**, 743-751.

Chen, Y. & Yang, H.-W. (1992). Hydroxypropyl Cellulose (HPC) - Stabilized Dispersion Polymerization of Styrene in Polar Solvents: Effect of Reaction Parameters. *Journal of Polymer Science: Part A: Polymer Chemistry*, **30**, 2765-2772.

Chernyshev, A. V., et al. (1997). A Mathematical Model of Dispersion Radical Polymerization Kinetics. *J. Polym. Sci. A: Polym. Chem.*, **35**, 1799-1807.

Corner, T. (1981). Polyelectrolyte Stabilised Latices. Part 1, Preparation. *Colloids and Surfaces*, **3**, 119-129.

Croucher, M. D. & Winnik, M. A. (1987). Control of Particle Size in the Dispersion Polymerization of Sterically Stabilised Polymer Colloids. *NATO ASI Applied Sciences; future directions in Polymer Colloids*, **138**, 209-227.

Croucher, M. D. & Winnik, M. A. (1990). Preparation of Polymer Particles by Dispersion Polymerization. *NATO ASI Series C: Mathematical and Physical Sciences; Scientific Methods for the study of Polymeric Colloids and their Applications*, **303**, 35-72.

Dai, Q., et al. (2003). Preparation of Monodisperse Poly(Methyl Methacrylate) Particles by Radiation-Induced Dispersion Using Vinyl Terminus Polysiloxane Macromonomer as a Polymerizable Stabilizer. *Polymer*, **44**, 73-77.

Darwin, C. (1859). On the Origin of Species.

de Gennes, P. G. (1987). Polymers at an Interface; a Simplified View. *Advances in Colloid and Interface Science*, **27**, 189-209.

DeSimone, J. M., et al. (1992). Synthesis of Fluoropolymers in Supercritical Carbon Dioxide. *Science*, **257**, 945.

DeSimone, J. M., et al. (1994). Dispersion Polymerizations in Supercritical Carbon Dioxide. *Science*, **265**, 356-359.

Feigin, R. I. & Napper, D. H. (1980). Depletion Stabilization and Depletion Flocculation. *Journal of Colloid and Interface Science*, **75**(2), 525-541.

Fitch, R. M. & Tsai, C. H. (1971). Homogenous Nucleation of Polymer Colloids, IV: The Role of Soluble Oligomeric Radicals. *Polymer Colloids*, 103.

Fitch, R. M. & Tsai, C. H. (1971). Particle Formation in Polymer Colloids, III: Prediction of the Number of Particles by a Homogeneous Nucleation Theory. *Polymer Colloids*, 73.

Fleer, G. J., et al. (1988). Theoretical Progress in Polymer Adsorption, Steric Stabilization and Flocculation. *Colloids and Surfaces*, **31**, 1-29.

Fonteix, C., et al. (1995). Haploïd and Diploïd algorithms, a New Approach for Global Optimization : Compared Performances. *Int. Jour. of Systems Science,* **26**(10), 1919-1933.

Gabaston, L., et al. (1998). Living Free-Radical Dispersion Polymerization of Styrene. *Macromolecules*, **31**(9), 2883-2888.

Galia, A., et al. (2003). Dispersion Copolymerization of Vinyl Monomers in Supercritical Carbon Dioxide. *Ind. Eng. Chem. Res.*, **42**, 448-455.

Garcia-Rubio, L. H., et al. (1985). Bulk Copolymerization of Styrene and Acrylonitrile: Experimental Kinetics and Mathematical Modeling. *Polymer*, **26**(13), 2001-2013.

Goldberg, D. E. (1989). Genetic Algorithms in Search, Optimization and Machine Learning, Addison-Wesley Publishing company.

Guyot, A. (1999). Recent Advances and Challenges in the Synthesis of Polymer Colloids. *Colloids and Surfaces A: Physiochemical and Engineering Aspects*, **153**, 11-21.

Guyot, A., et al. (1999). Reactive Surfactants in Heterophase Polymerization. *Acta. Polym.*, **50**, 57-66.

Hansen, F. K. & Ugelstad, J. (1982). Emulsion Polymerization. New York, Academic Press.

Harkins, W. D. (1947). A General Theory of the Mechanism of Emulsion Polymerization. *J. Amer. Chem. Soc.*, **69**, 1428-1444.

Hattori, M., et al. (1993). Highly Crosslinked Polymer Particles by Dispersion Polymerization. *Journal of Applied Polymer Science*, **50**, 2027-2037.

Hildebrand, J. H. & Scott, R. L. (1949). The Solubility of Non-Electrolytes. New York, Reinhold.

Hill, D. J. T., et al. (1982). Analysis of the Mechanism of Copolymerization of Styrene and Acrylonitrile. *Macromolecules*, **15**, 960-966.

Holland, J. H. (1975). Adaptation in Natural and Artificial Systems, Ann Arbor : University of Michigan Press.

Horak, D., et al. (1995). Preparation and Control of Surface Properties of Monodisperse Micrometer Size Beads by Dispersion Copolymerization of Styrene and Butyl Methacrylate in Polar Media. *Journal of Polymer Science: Part A: Polymer Chemistry*, **33**, 2329-2338.

Hsiao, Y.-L., et al. (1995). Dispersion Polymerization of Methylacrylate Stabilized with Poly(1,1-Dihydroperfluorooctyl Acrylate) in Supercritical Carbon Dioxide. *Macromolecules*, **28**, 8159-8166.

Hu, R., et al. (1995). Monodisperse Poly(Butadiene/Styrene) Particles by Dispersion Polymerization. *Applied Polymer Science*, **55**, 1411-1415.

Hui, A. W. & Hamielec, A. E. (1972). Thermal Polymerization of Styrene at High Conversions and Temperatures. An Experimental Study. *Journal of Applied Polymer Science*, **16**, 749-769.

Kaim, A. & Oracz, P. (1998). Terminal and Penultimate Models of Copolymerization in the Styrene-Acrylonitrile System in Bulk According to Unifac. *Polymer*, **39**(17), 3901-3904.

Kaushiva, B. D. & Dounis, D. V. (2000). Influences of Copolymer Polyol on Structural and Viscoelastic Properties in Molded Flexible Polyurethane Foam. *Journal of Applied Polymer Science*, **78**(4), 766 - 786.

Kawaguchi, H. (2000). Dispersion Polymerization. *Surfactant Science Series*, **92**, 609-623.

Kawaguchi, S., et al. (1995). Dispersion Copolymerization of N-Butyl Methacrylate with Poly(Ethylene Oxide) Macromonomers in Methanol-Water. Comparison of Experiment with Theory. *Macromolecules*, **28**, 1159-1169.

Kawaguchi, S., et al. (1996). ^{1}H NMR Study of Dispersion Copolymerization of N-Butyl Methacrylate with Poly(Ethylene Oxide) Macromonomer in Deuterated Methanol-Water. *Macromolecules*, **29**, 4465-4472.

Keramopoulos, A. & Kiparissides, C. (2002). Development of a Comprehensive Model for Diffusion-Controlled Free-Radical Copolymerization Reactions. *Macromolecules*, **35**, 4155-4166.

Kiatkamjornwong, S. & Kongsupapsiri, C. (2000). Control of Monodisperse Particle Size of Styrenic-Acrylate Copolymers in Dispersion Copolymerization. *Polymer International*, **49**, 1395-1408.

Kim, J. W., et al. (2000). Monodisperse Micron-Sized Cross-Linked Polystyrene Particles. VI. Understanding of Nucleated Particle Formation and Particle Growth. *Colloid Polym. Sci.*, **278**, 591-594.

Kobayashi, S., et al. (1990). Preparation of Monodispersed Poly(Methyl Methacrylate) Particle in the Size of Micron Range. *Polymer Journal*, **22**(8), 759-761.

Kobayashi, S., et al. (1992). Size Control of Poly(Methyl Methacrylate) Particles by Dispersion Polymerization in Polar Media. *Macromol. Chem.*, **193**, 2355-2362.

Kuryla, W. C., et al. (1966). Polymer/Polyols, a New Class of Polyurethane Intermediates. *Journal of Cellular Plastics*, **March**, 84-96.

Lacroix-Desmazes, P. & Guillot, J. (1997). Dispersion Polymerization of Styrene in Ethanol-Water Media: Monomer Partioning Behavior and Locus of Polymerization. *Polymer Science*, **36**, 325-335.

Lacroix-Desmazes, P. & Guyot, A. (1995). Reactive Surfactants in Heterophase Polymerization. 2. Maleate Based Poly(Ethylene Oxide) Macromonomers as Steric Stabilizer Precursors in the Dispersion Polymerization of Styrene in Ethanol - Water Media. *Macromolecules*, **29**, 4508-4515.

Lacroix-Desmazes, P. & Guyot, A. (1996a). Reactive Surfactants in Heterophase Polymerization. 3. Poly(Ethylene Oxide) Macromonomers and Polymerizable

Surfactants (Surfmers) as Stabilizers in Styrene Dispersion Polymerization. *Polymer Bulletin*, **37**, 183-189.

Lacroix-Desmazes, P. & Guyot, A. (1996b). Reactive Surfactants in Heterophase Polymerization. 4. Dispersion Polymerization of Styrene and Methyl Methacrylate : Particle and Prediction of Final Size. *Colloid Polym. Sci.*, **274**, 1129-1136.

Leboreiro, J. & Acevedo, J. (2004). Processes Synthesis and Design of Distillation Sequences Using Modular Simulators : a Genetic Framework. *Computers and Chemical Engineering*, **28**, 1223-1236.

Lee, K. C., et al. (1994). Hydrocarbon Dispersions of Acrylic Microspheres with Polar Surface Functionality. *J. Polym. Sci.:Part A : Chem. Ed.*, **32**, 2333-2344.

Lee, K. C., et al. (1995). Copolymerization of Styrene and Acrylonitrile in Ternary Oil-in-Water Microemulsions. *Polymer*, **36**(19), 3719-3725.

Liu, J., et al. (1998). Dispersion Polymerization of Styrene in Aqueous Ethanol Media Using Poly(Ethylene Oxide) Macromonomer as a Polymerizable Stabilizer. *Polymer*, **39**(2), 283-289.

Lok, K. P. & Ober, C. K. (1985). Particle Size Control in Dispersion Polymerization of Polystyrene. *Can. J. Chem.*, **63**, 209.

Lu, Y. Y. (1988). Dispersion Polymerization of Styrene in Ethanol, 179p, Ph.D. : Polymer Science and Engineering, Lehigh University, n° 8901879.

Lu, Y. Y., et al. (1988). Dispersion Polymerization of Styrene in Ethanol: Monomer Partitioning Behavior and Locus of Polymerization. *Journal of Polymer Science: Part B: Polymer Physics*, **26**, 1187-1203.

Marten, F. L. & Hamielec, A. E. (1978). High Conversion Diffusion-Controlled Polymerization. *ACS. Symp. Ser.*, **104**, 43-70.

Marten, F. L. & Hamielec, A. E. (1982). High-Conversion Diffusion-Controlled Polymerization of Styrene. I. *Journal of Applied Polymer Science*, **27**, 489-505.

Mendizabal, E., et al. (1995). Monomer Chain Cross-Transfer Contants and Cross Termination Factor Evaluations on Styrene-Acrylonitrile Copolymerization. *Polym. Eng. Sci.*, **35**(2), 195-201.

Michalewicz, Z. (1992). Genetic Algorithms + Data Structures = Evolution Programs, Springer-Verlag.

Napper, D. H. (1977). Steric Stabilization. *Journal of Colloid and Interface Science*, **58**(2), 390-407.

Napper, D. H. (1983). Polymeric Stabilization of Colloidal Dispersions. London, Academic Press.

Ober, C. K. (1990). Dispersion Copolymerization in Non-Aqueous Media. *Makromol. Chem., Macromol. Symp.*, **35/36**, 87-104.

Ober, C. K. & Hair, M. L. (1987). The Effect of Temperature and Initiator Levels on the Dispersion Polymerization of Polystyrene. *Journal of Polymer Science: Part A: Polymer Chemistry*, **25**, 1395-1407.

Ober, C. K. & Lok, K. P. (1987). Formation of Large Monodisperse Copolymer Particles by Dispersion Polymerization. *Macromolecules*, **20**, 268-273.

Ober, C. K., et al. (1985). Monodispersed, Micron-Sized Polystyrene Particles by Dispersion Polymerization. *Journal of Polymer Science: Polymer Letters Edition*, **23**, 103-108.

Ober, C. K., et al. (1986). Partioning of Monomer During Dispersion Polymerization. *Colloids and Surfaces*, **21**, 355-369.

Odian, G. (1981). Principles of Polymerization. New York, John Wiley & Sons.

Okubo, M., et al. (1989). Preparation of Micron-Size Monodisperse Polymer Microspheres Having Chloromethyl Group. *Colloid Polym. Sci.*, **267**(3), 193-200.

Okubo, M. & Izumi, J. (1999). Synthesis of Micron-Sized Monodispersed, Core-Shell Composite Polymer Particles by Seeded Dispersion Polymerization. *Colloids and Surfaces A: Physiochemical and Engineering Aspects*, **153**, 297-304.

O'Neil, M., et al. (1998a). Dispersion Polymerization in Supercritical CO_2 with Siloxane-Based Macromonomer. 1. The Particle Growth Regime. *Macromolecules*, **31**(9), 2838-2847.

O'Neil, M., et al. (1998b). Dispersion Polymerization in Supercritical CO_2 with Siloxane-Based Macromonomer. 2. The Particle Formation Regime. *Macromolecules*, **31**(9), 2848-2856.

Osmond, D. W., et al. (1962). Brit. Patent 893429, Imperial Chemical Industries

Paine, A. J. (1990a). Dispersion Polymerization of Styrene in Polar Solvents. 1. Grafting Mechanism of Stabilization by Hydroxypropyl Cellulose. *Journal of Colloid and Interface Science*, **138**(1), 157-169.

Paine, A. J. (1990b). Dispersion Polymerization of Styrene in Polar Solvents. 4. Solvency Control of Particle Size from Hydroxypropyl Cellulose Stabilized Polymerizations. *Journal of Polymer Science: Part A: Polymer Chemistry*, **28**, 2485-1990.

Paine, A. J. (1990c). Dispersion Polymerization of Styrene in Polar Solvents. 7. A Simple Mechanistic Model to Predict Particle Size. *Macromolecules*, **23**, 3109-3117.

Paine, A. J., et al. (1990a). Dispersion Polymerization in Polar Solvents. 2. Visualization of Surface Layers of Steric Stabilizer on Dispersion-Polymerized and Precipitated Polystyrene Latex Particles by Transmission Electron Microscopy. *Journal of Colloid and Interface Science*, **138**(1), 170-181.

Paine, A. J., et al. (1990b). Dispersion Polymerization of Styrene in Polar Solvents. 6. Influence of Reaction Parameters on Particle Size and Molecular Weight in Poly(N-Vinylpyrrolidone)-Stabilized Reactions. *Macromolecules*, **23**, 3104-3109.

Perrin, E., et al. (1993). Identification paramétrique d'un modèle hydrodynamique d'un bioréacteur à l'aide d'un algorithme de type génétique. Récents progrès en génie des procédés, Conduite et commande des procédés, 4ème Congrès de Génie des Procédés, 21-23 septembre 1993, Grenoble, **7**(29), 57-62

Plessis, C., et al. (2001a). Modeling of Seeded Semibatch Emulsion Polymerization of N-Ba. *Ind. Eng. Chem. Res.*, **40**, 3883-3894.

Plessis, C., et al. (2001b). Kinetics and Polymer Microstructure of the Seeded Semi-batch Emulsion Copolymerization of N-Butyl Acrylate and Styrene. *Macromolecules*, **34**, 5147-5157.

Rechenberg, I. (1973). Evolutionstrategie : Optimierung Technisher Systeme nach Prinzipien des Biologischen Evolution. Fromman-Holzboog Verlag, Stuttgart.

Saenz, J. M. & Asua, J. M. (1995). Dispersion Polymerization in Polar Solvents. *Journal of Polymer Science: Part A: Polymer Chemistry*, **33**, 1511-1521.

Saenz, J. M. & Asua, J. M. (1998). Kinetics of the Dispersion Copolymerization of Styrene and Butyl Acrylate. *Macromolecules*, **31**, 5215-5222.

Saenz, J. M. & Asua, J. M. (1999). Mathematical Modeling of Dispersion Copolymerization. *Colloids and Surfaces, A: Physiochemical and Engineering Aspects*, **153**, 61-74.

Shaffer, K. A., et al. (1996). Dispersion Polymerizations in Carbon Dioxide Using Siloxane-Based Stabilizers. *Macromolecules*, **29**, 2704-2706.

Shay, J. S., et al. (2000). Dispersion Polymerization of Polystyrene Latex Stabilized with Novel Grafted Poly(Ethylene Glycol) Macromers in 1-Propanol/Water. *Macromolecules*, **33**, 6664-6671.

Schoenauer, M., et al. (1996). Mechanical Inclusions Identifications by Evolutionary Computation. *Revue européenne des éléments finis*, **5**(5-6), 619-648.

Shen, S., et al. (1993). Control of Particle Size in Dispersion Polymerization of Methyl Methacrylate. *Polymer Science*, **31**, 1393-1402.

Shen, S., et al. (1994). Dispersion Polymerization of Methyl Methacrylate: Mechanism of Particle Formation. *Polymer Science*, **32**, 1087-1100.

Simroth, D. W. (1991). Improved Polymer/Polyol and Preformed Stabilizer Systems. EP 0 461 800 A1, Arco Chemical Technology Inc.

Stamberger, P. (1963). Belg. Patent 625351, to the Union Carbide Corp.

Takahashi, K., et al. (1996). Preparation of Micron-Size Monodisperse Poly(2-Hydroxyethyl Methacrylate) Particles by Dispersion Polymerization. *Journal of Polymer Science : Part A : Polymer Chemistry*, **34**, 175-182.

Thompson, B. R. & Raines, R. H. (1959). A Revised Q-E Diagram. *Journal of Polymer Science*, **41**, 265-274.

Tseng, C. M., et al. (1986). Uniform Polymer Particles by Dispersion Polymerization in Alcohol. *Journal of Polymer Science: Part A : Polymer Chemistry Edition*, **24**, 2995-3007.

Tuncel, A., et al. (1993). Monosize Polystyrene Microbeads by Dispersion Polymerization. *Journal of Applied Polymer Science*, **50**, 303-319.

Tuncel, A., et al. (1994). Monosize Polystyrene Latices Carying Functional Groups on Their Surfaces. *Journal of Applied Polymer Science*, **51**, 1485-1498.

Ugelstad, J., et al. (1983). Thermodynamics of Swelling of Polymer, Oligomer and Polymer-Oligomer Particles. Preparation and Application of Monodisperse Polymer Particles. Science and Technology of Polymer Colloids, 51.

Ugelstad, J., et al. (1992). Preparation and Application of New Monosized Polymer Particles. *Prog. Polym. Sci.*, **17**, 87-161.

Van Krevelen, D. W. (1976). Chapter 7. Cohesive Properties and Solubility. Properties of Polymers. Their Estimation and Correlation with Chemical Structure. Amsterdam-Oxford- New York, Elsevier Scientific Publishing Company, 129-159.

Walbridge, D. J. (1989). Polymerization in Non-Aqueous Dispersions. *Comprehensive Polymer Science*, **4**(15), 243-260.

Walter, E., & Pronzato, L. (1997). Identification of Parametric Models from Experimental Data, Springer, Communications and Control Engineering Series, Londres.

Wang, W., et al. (2003). Monitoring Dispersion Polymerizations of Methyl Methacrylate in Supercritical Carbon Dioxyde. *European Polymer Journal*, **39**, 423-428.

Winnik, F. M. & Ober, C. K. (1987). Colored Particles by Dispersion Polymerization. *Eur. Polym. J.*, **23**(8), 617-622.

Xu, Z. (2000). Study of Kinetics of Dispersion Polymerization of Styrene in Organic Media. *J. Dispersion and Technology*, **21**(7), 869-882.

Yang, W., et al. (2000). Morphological Investigations of Polymer Microspheres Prepared by Dispersion Copolymerization. *Macromol. Symp.*, **150**, 211-217.

Yang, W., et al. (2001). Dispersion Copolymerization of Styrene and Other Vinyl Monomers in Polar Solvents. *Journal of Polymer Science: Part A: Polymer Chemistry*, **39**, 555-561.

Yasuda, M., et al. (2001a). Simulation of a Particle Formation Stage in the Dispersion Polymerization of Styrene. *Macromolecules*, **34**(10), 3261-3270.

Yasuda, M., et al. (2001b). Simulation of Particle Growth in the Dispersion Polymerization of Styrene : The Termination Rate Constant in Particles. *Macromolecular Theory and Simulations*, **10**, 54-62.

Ye, Q., et al. (2003). Formation of Monodisperse PMMA Particles by Radiation-Induced Dispersion Polymerization - I. Synthesis and Polymerization Kinetics. *Radiation Physics and Chemistry*, **11**, 11-16.

ANNEXES

ANNEX 1
MAIN WORKS DONE ON DISPERSION PRECIPITATION FROM THE 1980S TO NOW

Table A1.1 : Bibliography list on dispersion polymerization from the 1980s to now

Monomers	Solvent	Precursor Stabilizer	Reference
Styrene	Ethanol / H_2O	PAA	Corner, 1981
Styrene, MMA	Methanol, Ethanol, Isopropanol, t-Butanol, n-Propanol, sec-Butanol	PEI, PVME, PVP, PAA, PVPAc	Almog et al., 1982
Styrene	Ethanol / Methyl cellosolve	HPC	Ober et al., 1985
Vinyl Acetate	isooctane	Poly(2-ethylhexyl methacrylate)	Lok, 1985
Styrene	Ethanol / Methyl cellosolve Methanol / H_2O Ethanol / H_2O	HPC	Lok & Ober, 1985
Styrene	Ethanol	PVP	Tseng et al., 1986
Styrene	Methyl cellosolve / alcohol mixture	HPC	Ober et al., 1986
Styrene	Ethanol / Methyl cellosolve	HPC	Ober & Hair, 1987
Styrene n-butylmethacrylate	Ethanol / H_2O	PAA	Ober & Lock, 1987
Styrene	Ethanol	PVP	Lu, 1988
Styrene	Ethanol	PVP	Lu et al., 1988
Styrene	Polar solvents	HPC	Paine, 1990a
Styrene	Polar solvents	HPC, PVP, PAA	Paine et al., 1990a
Styrene	Polar solvents	HPC, PVP, PAA	Paine, 1990b
Styrene	Polar solvents	PVP	Paine et al., 1990b
Styrene	Polar solvents	HPC, PVP, PAA, poly(vinylbutyral), poly(N-vinylpyridine)	Paine, 1990c
MMA	Methanol / H_2O	PEtOZO PEI	Kobayashi et al., 1990
MMA	Methanol / H_2O	PPIE PEI	Kobayashi et al., 1992a
Styrene	Polar solvents	HPC	Chen & Yang, 1992
MMA	Methanol	PVP	Shen et al., 1993
Divinylbenzene Styrene / Divinylbenzene	Methanol Methanol / co-solvents	PVP	Hattori et al., 1993
Styrene	Isopropanol / H_2O 1-Butanol / H_2O 2-Butanol / H_2O	PAA	Tuncel et al., 1993
Sty functionnalized	Isopropanol / H_2O	PAA	Tuncel et al., 1994

MMA Styrene	Methanol Ethanol	PVP	Shen et al., 1994
MMA	$ScCO_2$	Fluorinated and organosiloxane polymers	DeSimone et al., 1994
n- Butylmethacrylate	Methanol / H_2O	PEO	Kawaguchi et al., 1995
Styrene / Butyl Methacrylate	Ethanol / H_2O	HPC, PAA, PVP	Horak et al., 1995
Styrene / Butylacrylate Styrene	Ethanol / H_2O Ethanol	PVP	Saenz & Asua, 1995
Butadiene / Styrene	Ethanol	PVP	Hu et al., 1995
MMA	$ScCO_2$	PFOA	Hsiao et al., 1995
MMA	$ScCO_2$	PDMS	Shaffer et al., 1996
Styrene	$ScCO_2$	PFOA	Canelas et al., 1996
n- Butylmethacrylate	Deuterated Methanol / H_2O	PEO	Kawaguchi et al., 1996
2-hydroxyethyl methacrylate	Good and poor solvents	PMMA, PS, methacryloyl-terminated PMMA, poly(MMA-co-MA-graft-Sty), PolyButadiene derivatives containing reactive vinyl groups	Takahashi et al., 1996
Styrene	Isopropanol	PVP	Chernyshev et al., 1997
Styrene	Ethanol / H_2O	PVP	Lacroix-Desmazes & Guillot, 1997
Styrene	Ethanol	PVP	Ahmed & Poehlein, 1997a, 1997b
Styrene	Ethanol / H_2O	PEO	Liu et al., 1998
Styrene	Alcoholic medium / H_2O	PVP	Gabaston et al., 1998
Styrene / Butylacrylate Styrene	Ethanol / H_2O Ethanol	PVP	Saenz & Asua, 1998
MMA	$ScCO_2$	PDMS-co-mMA	O'Neil et al., 1998a, 1998b
PMMA core Polystyrene shell	Methanol / H_2O		Okubo & Izumi, 1999
Styrene / Butyl acrylate	Ethanol / H_2O	PVP	Saenz & Asua, 1999
MMA	Methanol / H_2O	PVP	Cao et al, 1999
Styrene / n Butylacrylate Styrene / 2-EHA	Ethanol / H_2O	PVP	Kiatkamjornwong & Kongsupapsiri, 2000

Styrene	Propanol / H_2O	PEG	Shay et al., 2000
MMA	Methanol / H_2O	PAA, PVP, PVA	Cao et al., 2000a
MMA / Acrylic monomers with different functional groups (AA, GMA, HEMA, DMAEMA, EGDMA)	Methanol / H_2O	PVP	Cao et al., 2000b
MMA	Methanol / H_2O	PVP	Cao et al., 2000c
Styrene / GMA Styrene / Acrylamide Styrene / NVC	Ethanol	PVP	Yang et al., 2000
Styrene	Alcohol / methyl or butyl cellosolve	HPMC	Xu, 2000
Styrene	Ethanol	PVP	Araujo & Pinto, 2000
Styrene	Ethanol	PVP	Yasuda et al., 2001a, 2001b
Styrene / Acrylamide Styrene / AA Styrene / GMA Styrene / MMA Styrene / EMA Styrene / NVC Styrene / TMSPMA	Ethanol / H_2O	PVP	Yang et al., 2001
MMA	$ScCO_2$	PDMS	Wang et al., 2003
MMA	Hexane / ethanol	Vinyl terminus polysiloxane	Dai et al., 2003
MMA	Methanol / H_2O	PVP	Ye et al., 2003
MMA / DMA	$ScCO_2$	Polysiloxane surfactants	Galia et al., 2003
MMA	$ScCO_2$	PHEMA-g-PFOA, PDMS-mMA	Chatzidoukas et al., 2003

ANNEX 2

EXPERIMENTAL PROCEDURES

A2.1. PROCEDURES TO RUN THE LABORATORY RIG..... 253

A2.2. FILTERABILITY TEST ON COPOLYMER POLYOLS 255

A2.3. WASTE DISPOSAL PROCEDURE 257

A2.4. HANDLING OF ACRYLONITRILE & STYRENE SPILLS 258

A2.5. EXPOSURE TO ACRYLONITRILE AND STYRENE..... 258

A2.1. Procedures to run the laboratory rig

Start up of the equipment.	The extraction of the fume hood is always on. - Turn main power switch on the main power control cabinet. - Switch on the agitator of the rig by pushing on the button. - Switch on the computer, start 'CAMILE' program - Click on temperature control : put the heater on, in manual mode with output fixed on 60%, Setting the SP value as desired.
Preparation of the premix	Always prepare premix inside the fume hood, according to the run sheet **Use protective clothing, gloves and goggles.** - Start with adding the initiator, Trigonox 27 (**be careful, peroxides**). - After use of the initiator(s) place the initiators back inside the refrigerator - Add stabilizer(s), seed and additive(s) like NDM. Shake well - Add the required amount of monomer(s) and shake well, till the initiator is solved - Then the correct amount of polyol is added and again shake well
Start up reaction	As the desired temperature of the reactor is reached - Start up the pump using the pump control panel. Put it on manual mode fixing the output value from 10% to 30%. - Wait until the feed bowl is empty and fill the feed bowl with the prepared premix (use a funnel). - When the rig is under pressure and material comes out of the outlet of the rig then stop the pump - On the Camile, click on the 'Start Feed' button on the screen - Fill in or adjust to the desired level; run number, first set point and ramp time of the first ramp up maximum feed deviation (A tolerance of ± 10% is allowed) minimum start temperature, initial pump speed and its hold time final set point (of flow speed) and ramp up time - Click 'close' to close off and if the correct temperature of the reactor is reached the run will start.
Collecting of product	When the feed is on full solids: Waste the first 5 kg (≈ 10 residence times) of product Change the waste container for a glass vacuum bottle and start collecting product Sample: - See item **Sampling.**
Sampling	- Collect at least 800 g of product into a glass vacuum bottle. - From this amount a 25 ml glass vial is filled. Label this as unstripped material. - Take 470 ± 10 g of material out and use this for the filtration test.

Emptying the rig	• Drain the reactor using the drain valve and N2 pressure, • Drain the premix vessel using the drain valve of the pump, • Fill the feed bowl with polyol • Switch on the pump and flush the pump with polyol letting open the reactor drain valve, • Stop the pump, drain the reactor with N2 and close the reactor drain valve, • Switch on the pump, and pump until 200-500 g of polyol has come out of the outlet, • Empty the filter unit using the drain valve and N2 pressure, • Close the drain valve, • If complete washing: ➢ Bypass the filter, ➢ Close the valve at the reactor entrance, ➢ Remove the bolt from the top of the reactor, ➢ Fill the reactor with 30 mL KOH (50%) and 4 bottles of NMP and put back the bolt, ➢ Let the reactor running 30 min and maintain temperature at 115°C-140°C ➢ Drain the reactor with its drain valve, ➢ Fix the water pipe at the reactor entrance, ➢ Fill the rig with water, drain the reactor and the exit pipe with N2 : this 3 times, ➢ Flush all the rig with N2 keeping high temperature (5 min), in order to be sure there is no more water in the pipes ➢ Fix the pump pipe at the reactor entrance, and turn the bypass valve • Fill up the complete rig with polyol • Bring temperature back to 25°C during pumping, and when the reactor is full, switch off equipment.
	Clean all spillage of premix and polyol

A2.2. Filterability test on Copolymer Polyols

Objective	The filtration value indicates the stability of the copolymer and the fouling of the Copolymer polyol unit. Because no calibration is done the results of the test must be regarded as relative.
Equipment	Filtration apparatus 3 L cans for collecting the filtered material Mesh screen (stainless steel, 700 threads per inch, 30 µm) 5 L container for mixing IPA (= Isopropanol, Isopropyl alcohol or 2-propanol)
Execution of the test	- The bowl of the filtration equipment must be free of water. *See notes.* - Weigh 470 ± 5 g of copolymer product into a 5 L container - Add 940 ± 5 g isopropanol to it and shake well for at least 1 min. - Place a clean mesh screen into the filtration apparatus. *(See Figure A2.1.b)* For each test a new (clean) mesh screen has to be used. - Pour CPP/IPA mixture into the bowl of the filtration apparatus and when material starts coming out of outlet of the equipment, start timer - Measure the amount of cc of mixture that passes the mesh screen over 150 s and 300 s - 100% filtration is when the liquid level reaches the division between neck and cone at the lower end of the bowl. *(See Figure A2.1.c)* - Calculate the percentage of passed mixture using the following formulation : (cc mix collected / 1700) * 100 % = % product passed Note down the results after 150 s and 300 s in percentages If all the CPP/IPA mix passes in less than 300 s then note down 100 % together with the time to pass. (e.g. 100%/240 sec) If the material blocks before the 300 s time limit than the amount of material which passed the filter is measured and the percentage is calculated and noted down as percentage blocked. (e.g. 84% Block) After use the filtration equipment is rinsed out with Isopropyl alcohol and dried on the air. When the equipment will not be used for a longer time then the equipment must be cleaned out with water and dried on the air. Product, IPA and water used for rinsing the equipment are regarded as chemical waste and must be treated like so.

Safety	Some percentages of free monomers and or other volatiles can be left in the Copolymer polyol. This test has to be done in a fume hood or in a cabinet with air extraction The use of gloves (i.e. Latex) is recommended because IPA dries out the skin Take care, when mixing hot CPP with IPA. Boiling point of IPA is 82°C! IPA vapors easily mix with air. **See a recent safety sheet for Isopropyl alcohol.**
Calibration, check of equipment	No calibration is performed.
Notes	Presence, in the test set-up, of materials other than IPA and Copolymer Polyol even in tiny amounts can have a negative influence on the result of the test. Materials like acetone, water, hydrocarbons, aromatic and (poly-)cyclic compounds can lead to gelling or polymerization of the sample material. Also the sample container and mix container should be clean and dry. It is advisable to use unused and clean containers. Only the 3 liter waste container *(See Figure A2.1.a)* may be 'fouled' but only if this is not interfering with a correct read-off of the result. It is imperative that the time between preparation of the CPP/IPA mixture and the execution of the test will be as least as possible and will never be longer than 15 min. A fresh mix gives the most reliable results. A deviation, between results of the same material, which not exceeds the 30 seconds is acceptable. The residue left on the filter screen can give an indication on the type and amount of fouling. In some cases another type of mesh screen can be used. (i.e.17 µm screen) If so, reporting results must always be done in connection with the type of screen. Temperature of the IPA/CPP material mix during the test is, in general, not of great influence on the test result.

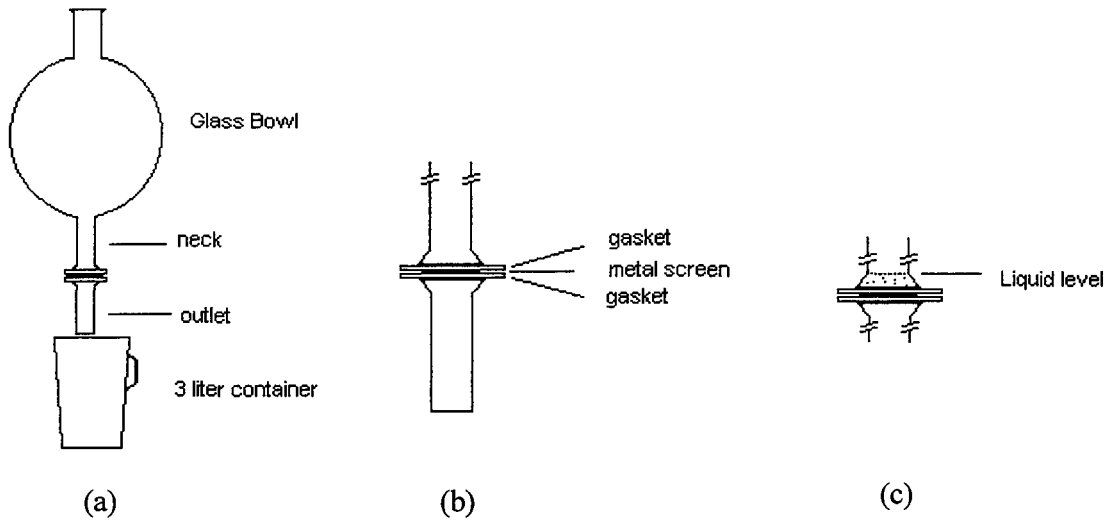

Figure A2.1 : Equipment for the filterability test

A2.3. Waste disposal procedure

Purpose	1. Waste from CPP production on the laboratory rigs 2. Waste from cleaning the laboratory rigs
1. Waste from CPP production on the lab rigs	Waste from the rigs is poured into a 10 kg waste pail Before CPP waste is put into a 10 kg waste pail a few drops of **DEHA** (Diethyl Hydroxylamine 85%), or another auto polymerization inhibitor, are added in every pail to prevent or inhibit auto-polymerization of possible (unreacted) monomers. When the 10 kg waste pail is full, it is emptied into the 200 kg waste drums outside the building. The full labeled drums will be removed by a truck of Environmental services.
2. Waste from cleaning the lab rigs	The lab rigs are cleaned with a NMP/KOH (45% KOH in water) mixture and after this flushed with water. After use the water and the NMP/KOH waste mixture is poured in a separate 200 kg (closed lid) drum. The full drum will be collected by Environmental services. NMP = N-Methyl Pyrrolidone KOH = Potassium Hydroxide

A2.4. Handling of Acrylonitrile & Styrene spills

Cleaning up small spills *Spills and/or emissions < 50 kg (air, water or contained) or spills < 10kg to the soil*	- Use PBM's (personal protection equipment) as rubber, neoprene or nitrilbutadiene gloves and wear breathing equipment (especially in case of a spill outside an air extraction area like a fume hood or when insufficient or no ventilation is available). - Fire and explosion hazardous so shut off all sources of ignition. - Prevent ground water contamination - Dike significant spills in with sand or other non absorbing material. - Spillage's should be contained by and covered with large quantities adsorbent, sand, earth or similar material which is then brushed in vigorously to assist adsorption. - The use of absorbent **Rench rapid Absorbent** (CAN & Styrene) and **Power sorb** (ACN) towels is advisable. - The mixture can then be collected with a rubber or plastic shovel into 'open top' drums with a plastic bag as lining and removed outdoor for disposal. Use water for dilution and cooling of the mixture. - Ventilate area and wash spill site after material pick up is complete. - Seek medical immediate advice for people who were (or suspected to be) exposed to Styrene and/or ACN by way of inhalation / eyes / ingestion or skin. Leak through time ACN • for Neoprene gloves : 20 minutes • for Nitrilbutadiene gloves : 150 minutes

A2.5. Exposure to acrylonitrile and styrene

First Aid in case of exposure to AN		**Always wear PBM's when giving first aid !** **<u>NEVER</u> do mouth to mouth resuscitation.**
Exposure of AN to :		**Always expect an exposure to skin and inhalation !**
Eyes	*Symptoms*	Red eyes, due to irritation. Chance on exposure to skin and inhalation!
	First aid	Flush eyes for at least 15 minutes. Protect the intact eye.
Skin	*Symptoms*	Red discoloration of the skin, sometimes blisters, chance on suffocation!
	First aid	Flush thoroughly with water (Emergency shower). During flushing remove clothes, shoes, gloves etc. Bring victim into the open air immediately

Ingestion	*Symptoms*	Chance of suffocation. Also chance on exposure to skin and inhalation!
	First aid	If victim is still conscience, give 10 gram N-acetylcysteïne (ACN first aid case in the laboratory / (pilot) plant area) diluted in 50 ml (drinking) water to drink. Bring victim into the open air immediately.
Inhalation	*Symptoms*	Chance on suffocation, coughing, gasping
	First aid	Bring victim into the open air immediately. If victim is still conscience, give 10 gram N-acetylcysteïne (ACN first aid case in the laboratory) diluted in 50 ml (drinking) water to drink.

First Aid in case of exposure to Styrene		**Never give fluids or induce vomiting if patient is unconscious or is having convulsions.** **Always wear PBM's when giving first aid!** **<u>Be very careful</u> in doing mouth to mouth resuscitation.**
Exposure of Styrene to :		**Always expect an exposure to skin and inhalation!**
Eyes	*Symptoms*	Red eyes, due to irritation. Chance on exposure to skin and inhalation!
	First aid	Flush eyes for at least 15 minutes. Protect the intact eye. Consult medical personnel
Skin	*Symptoms*	Red discoloration of the skin, sometimes blisters, chance on suffocation!
	First aid	Flush thoroughly with water (Emergency shower). During flushing remove clothes, shoes, gloves etc. Bring victim then into the open air immediately
Ingestion	*Symptoms*	Chance of suffocation, coughing. Also chance on exposure to skin and inhalation !
	First aid	Bring victim into the open air immediately. If victim is still conscience, do not induce vomiting. Call a physician and/or transport to emergency facility immediately.
Inhalation	*Symptoms*	Chance on suffocation, coughing, gasping.
	First aid	Remove victim into the open air immediately. If not breathing, give artificial respiration. If breathing is difficult, oxygen should be administered by qualified personnel. Call a physician or transport to a medical facility.

ANNEX 3

TABLES AND FIGURES OF CHAPTER 3

A3.1. TABLES OF CHAPTER 3 263

A3.1.1 AVERAGE MOLECULAR WEIGHTS OF WHOLE CPP 263

A3.1.2. RESIDUAL CONCENTRATION AND CONVERSIONS OF MONOMERS AND NDM, WT-% SOLIDS 265

A3.1.3. VISCOSITY OF STRIPPED CPP AND SERUM, AND SAUTER MEAN PARTICLE DIAMETER 267

A3.1.4. GRAFTING FROM LC-UV IN SOLIDS, WHOLE CPP AND SERUM 269

A3.1.5. COMPOSITION OF SOLIDS (WT-% OF POLYOL, STY, AN), COMPOSITION OF SOLUBLE SAN AND QUANTITY OF SOLUBLE SAN IN THE SERUM PHASE 270

A3.1.6. SAN IN SERUM 272

A3.2. FIGURES OF CHAPTER 3 274

A3.2.1. EVOLUTION OF PARTICLES SIZES AND AVERAGE MOLECULAR WEIGHTS WITH TIME ... 274

A3.2.2. MOLECULAR WEIGHT DISTRIBUTIONS OF WHOLE CPP 279

A3.2.3. PARTICLE SIZE DISTRIBUTIONS 287

A3.2.4. SCANNING ELECTRON MICROSCOPY ANALYSES 291

A3.2.5. CHROMATOGRAMS FROM LC-UV 294

A3.2.6. CHROMATOGRAMS FROM NMR 297

A3.2.7. CHROMATOGRAMS FROM NIC-DERIVATIZATION FOLLOWED BY GPC-FLUO 300

A3.2.8. MOLECULAR WEIGHT DISTRIBUTIONS OF THE SERUM PHASE 301

A3.1. Tables of Chapter 3

A3.1.1 Average Molecular Weights of whole CPP

Table A3.1 : Average molecular weights of whole CPP of runs done with Sty/AN = 60/40 (-1) and S5200 = 1 wt-% (-1)

Run	NDM	T27	T	Mn (g/mol)	Mw (g/mol)	Mw/Mn
1	1	-1	-1	27100	73200	2,7
2	-1	1	-1	51600	283800	5,5
3	1	1	-1	25500	76100	3,0
4	-1	-1	1	48000	224300	4,7
5	1	-1	1	25800	81600	3,2
6	-1	1	1	32000	152800	4,8
7	1	1	1	24500	94500	3,9

Table A3.2.a. : Average molecular weights of whole CPP of runs done with Sty/AN = 60/40 (-1) and S5200 = 3 wt-% (1)

Run	NDM	T27	T	Mn (g/mol)	Mw (g/mol)	Mw/Mn
8	-1	-1	-1	59700	255200	4,27
9	1	-1	-1	28500	73600	2,58
10	-1	1	-1	49300	191600	3,89
11	1	1	-1	27600	82800	3,00
12	-1	-1	1	41500	205700	4,96
13	1	-1	1	26200	84900	3,24
14	-1	1	1	32300	155200	4,80
15	1	1	1	24500	96000	3,92

Table A3.2.b. : Average molecular weights of whole CPP of runs done with Sty/AN = 60/40 (-1) and S5200 = 3 wt-% (1)

Run	NDM	T27	T	Mn (g/mol)	Mw (g/mol)	Mw/Mn
37	-1	-1	-1	60000	260000	4,3
38	1	-1	-1	32562	70615	2,2
39	-1	1	-1	52000	278500	5,4
40	1	1	-1	26000	75100	2,9
41	-1	-1	1	45700	228500	5,0
42	1	-1	1	25600	85000	3,3
43	-1	1	1	unsoluble sample		-
44	1	1	1	23900	102600	4,3

Table A3.3 : Average molecular weights of whole CPP of runs done with Sty/AN = 80/20 (1) and S5200 = 1 wt-% (-1)

Run	NDM	T27	T	Mn (g/mol)	Mw (g/mol)	Mw/Mn
16	-1	1	-1	38000	106600	2,8
17	1	1	-1	14500	34900	2,4
18	-1	-1	1	35300	98800	2,8
19	1	-1	1	13400	33300	2,5
20	-1	1	1	30200	90000	3,0
21	1	1	1	15000	36800	2,5

Table A3.4 : Average molecular weights of whole CPP of runs done with Sty/AN = 80/20 (1) and S5200 = 3 wt-% (1)

Run	NDM	T27	T	Mn (g/mol)	Mw (g/mol)	Mw/Mn
22	-1	-1	-1	43800	103000	2,4
23	1	-1	-1	14000	33000	2,4
24	-1	1	-1	42700	122700	2,9
25	1	1	-1	17500	40500	2,3
26	-1	-1	1	40000	118100	3,0
27	1	-1	1	16800	39300	2,3
28	-1	1	1	36500	126400	3,5
29	1	1	1	17600	42900	2,4
30	1	1	1	16300	42000	2,6

Table A3.5 : Average molecular weights of whole CPP of runs done with Sty/AN = 70/30 (0) and S5200 = 2 wt-% (0)

Run	NDM	T27	T	Mn (g/mol)	Mw (g/mol)	Mw/Mn
31	0	0	0	31200	93500	3,0
32	0	0	0	28700	88400	3,1
33	0	0	0	30800	89400	2,9
34	0	0	0	27400	67500	2,5
35	0	0	0	35100	87420	2,5

A3.1.2. Residual concentration and conversions of monomers and NDM, Wt-% Solids

Table A3.6 : Residual concentrations and conversions of monomers and NDM and Wt-% solids of runs done with Sty/AN = 60/40 (-1) and S5200 = 1 wt-% (-1)

				Styrene		Acrylo nitrile		NDM		Solid
Run	NDM	T27	T	Res. (wt-%)	Conv.	Res. (wt-%)	Conv.	Res. (ppm)	Conv.	wt-%
1	1	-1	-1	2,29	0,911	2,67	0,844	414	0,908	39,3
2	-1	1	-1	1,73	0,933	1,80	0,895	25	0,983	39,3
3	1	1	-1	1,92	0,925	2,15	0,874	277	0,938	38,4
4	-1	-1	1	1,8	0,930	2,31	0,866	78	0,948	39,9
5	1	-1	1	2,42	0,906	2,68	0,843	258	0,943	39,8
6	-1	1	1	1,46	0,943	1,62	0,906	68	0,955	39,3
7	1	1	1	1,85	0,928	2,18	0,873	90	0,980	39,8

Table A3.7.a : Residual concentrations and conversions of monomers and NDM and Wt-% solids of runs done with Sty/AN = 60/40 (-1) and S5200 = 3 wt-% (1)

				Styrene		Acrylo nitrile		NDM		Solid
Run	NDM	T27	T	Res. (wt-%)	Conv.	Res. (wt-%)	Conv.	Res. (ppm)	Conv.	wt-%
8	-1	-1	-1	2,31	0,910	2,51	0,854	96	0,936	38,9
9	1	-1	-1	2,37	0,908	3,05	0,822	375	0,917	41,6
10	-1	1	-1	1,72	0,933	1,93	0,888	40	0,973	39,3
11	1	1	-1	1,94	0,924	2,26	0,868	270	0,940	38,9
12	-1	-1	1	2,24	0,949	2,33	0,864	111	0,926	39,2
13	1	-1	1	2,5	0,904	2,64	0,846	347	0,923	38,5
14	-1	1	1	1,73	0,942	1,9	0,889	84	0,944	39,8
15	1	1	1	1,94	0,947	2,17	0,873	289	0,936	39,5

Table A3.7.b : Residual concentrations and conversions of monomers and NDM and Wt-% solids of runs done with Sty/AN = 60/40 (-1) and S5200 = 3 wt-% (1)

Run	NDM	T27	T	Solid (wt-%)
39	-1	1	-1	37,8
40	1	1	-1	38,1
41	-1	-1	1	37
42	1	-1	1	37
44	1	1	1	37

Table A3.8 : Residual concentrations and conversions of monomers and NDM and Wt-% solids of runs done with Sty/AN = 80/20 (1) and S5200 = 1 wt-% (-1)

				Styrene		Acrylo nitrile		NDM		Solid
Run	NDM	T27	T	Res. (wt-%)	Conv.	Res. (wt-%)	Conv.	Res. (ppm)	Conv.	wt-%
16	-1	1	-1	9,57	0,733	1,74	0,797	14	0,991	36,1
17	1	1	-1	15,33	0,552	2,83	0,669	135	0,970	nd
18	-1	-1	1	11,79	0,657	2,2	0,744	77	0,949	33,5
19	1	-1	1	15,66	0,543	3,05	0,644	412	0,908	30,8
20	-1	1	1	9,62	0,72	1,47	0,829	26	0,983	35,2
21	1	1	1	11,22	0,675	2,07	0,758	250	0,944	34,3

Table A3.9 : Residual concentrations and conversions of monomers and NDM and Wt-% solids of runs done with Sty/AN = 80/20 (1) and S5200 = 3 wt-% (1)

				Styrene		Acrylo nitrile		NDM		Solid
Run	NDM	T27	T	Res. (wt-%)	Conv.	Res. (wt-%)	Conv.	Res. (ppm)	Conv.	wt-%
22	-1	-1	-1	1,17	0,966	2,26	0,737	60	0,960	38,7
23	1	-1	-1	1,81	0,947	3,91	0,543	435	0,903	39,9
24	-1	1	-1	7,51	0,781	1,39	0,838	1	0,999	37,1
25	1	1	-1	12,9	0,623	2,68	0,687	149	0,967	32,1
26	-1	-1	1	9,34	0,728	1,78	0,793	26	0,983	34,9
27	1	-1	1	13,5	0,606	2,84	0,668	429	0,905	31,3
28	-1	1	1	6,83	0,801	1,27	0,825	9	0,994	37,3
29	1	1	1	9,55	0,721	1,90	0,778	201	0,955	34,9
30	1	1	1	7,78	0,773	1,44	0,832	153	0,966	36,9

Table A3.10 : Residual concentrations and conversions of monomers and NDM and Wt-% solids of runs done with Sty/AN = 70/30 (0) and S5200 = 2 wt-% (0)

				Styrene		Acrylo nitrile		NDM		Solid
Run	NDM	T27	T	Res. (wt-%)	Conv.	Res. (wt-%)	Conv.	Res. (ppm)	Conv.	wt-%
31	0	0	0	4,15	0,862	1,97	0,847	107	0,964	33,8
32	0	0	0	4,01	0,866	1,76	0,863	nd	nd	33,8

A3.1.3. Viscosity of stripped CPP and serum, and Sauter mean particle diameter

Table A3.11 : Viscosities of stripped CPP and serum, and Sauter mean particle diameters of runs done with Sty/AN = 60/40 (-1) and S5200 = 1 wt-% (-1)

				Viscosity (mPa.s)		D[3,2]	Notes done by the operators
Run	NDM	2		Stripped CPP	seru	icrons	
1	1	-1	-1	3150	343	0,87	-
2	-1	1	-1	8650	484	1,11	-
3	1	1	-1	3400	477	0,95	-
4	-1	-1	1	8800	481	1,33	Porely soluble in DCM
5	1	-1	1	3280	484	1,13	-
6	-1	1	1	11000	480	1,51	Porely soluble in DCM
7	1	1	1	7350	491	0,86	-

Table A3.12.a : Viscosities of stripped CPP and serum, and Sauter mean particle diameters of runs done with Sty/AN = 60/40 (-1) and S5200 = 3 wt-% (1)

				Viscosity (mPa.s)		D[3,2]	Notes done by the operators
Run	NDM	T27	T	Stripped CPP	serum	microns	
8	-1	-1	-1	6380	nd	1,62	Thin layer of solid
9	1	-1	-1	4720	561	0,94	-
10	-1	1	-1	6660	571	1,00	-
11	1	1	-1	4130	546	0,82	-
12	-1	-1	1	5300	nd	0,89	Completely stable, no particles in the bottom
13	1	-1	1	3810	nd	0,86	Completely stable, no particles in the bottom
14	-1	1	1	9940	nd	0,97	Stable but more viscous
15	1	1	1	6410	nd	0,47	Stable but more viscous

Table A3.12.b : Viscosities of stripped CPP and serum, and Sauter mean particle diameters of runs done with Sty/AN = 60/40 (-1) and S5200 = 3 wt-% (1)

				Viscosity (mPa.s)
Run	NDM	T27	T	Stripped CPP
39	-1	1	-1	5828
40	1	1	-1	4069
41	-1	-1	1	5209
42	1	-1	1	3594
44	1	1	1	6244

Table A3.13 : Viscosities of stripped CPP and serum, and Sauter mean particle diameters of runs done with Sty/AN = 80/20 (1) and S5200 = 1 wt-% (-1)

				Viscosity (mPa.s)		D[3,2]	Notes done by the operators
Run	**NDM**	**T27**	**T**	**Stripped CPP**	**serum**	**microns**	
16	-1	1	-1	10010	nd	4,24	Very viscous
17	1	1	-1	nd	nd	nd	Huge quantity of solid, completely unstable
18	-1	-1	1	5260	nd	5,21	Thin layer of solid
19	1	-1	1	2220	nd	6,13	Big layer of solid, lumps
20	-1	1	1	6800	nd	4,14	Layer of solid, lumps
21	1	1	1	3110	nd	6,38	Layer of solid, lumps

Table A3.14 : Viscosities of stripped CPP and serum, and Sauter mean particle diameters of runs done with Sty/AN = 80/20 (1) and S5200 = 3 wt-% (1)

				Viscosity (mPa.s)		D[3,2]	Notes done by the operators
Run	**NDM**	**T27**	**T**	**Stripped CPP**	**serum**	**microns**	
22	-1	-1	-1	10740	426	1,38	Not completely soluble in DCM
23	1	-1	-1	3550	412	2,80	Unstable sample, precipitate on bottom
24	-1	1	-1	10420	503	2,82	-
25	1	1	-1	3500	599	3,89	Unstable sample, precipitate on bottom
26	-1	-1	1	7360	462	3,08	-
27	1	-1	1	2780	514	4,62	Unstable sample, precipitate on bottom
28	-1	1	1	8820	501	2,50	-
29	1	1	1	4280	447	3,05	Unstable sample, precipitate on bottom
30	1	1	1	4940	nd	2,56	Very thin layer of solid in the bottom

Table A3.15 : Viscosities of stripped CPP and serum, and Sauter mean particle diameters of runs done with Sty/AN = 70/30 (0) and S5200 = 2 wt-% (0)

				Viscosity (mPa.s)		D[3,2]
Run	**NDM**	**T27**	**T**	**Stripped CPP**	**serum**	**microns**
31	0	0	0	3530	371	0,885
32	0	0	0	2810	363	nd

A3.1.4. Grafting from LC-UV in solids, whole CPP and serum

Table A3.16 : Grafting from LC-UV in solids, whole CPP and serum of runs done with Sty/AN = 60/40 (-1) and S5200 = 1 wt-% (-1)

				Solids	Whole CPP			Serum
Run	NDM	T27	T	% Graft	% HMW	%LMW	% Graft	% Graft
1	1	-1	-1	12,8	9,8	2,3	12,1	56,6
2	-1	1	-1	42,6	38	5,8	43,8	58,4
3	1	1	-1	17,8	13,6	3,4	17	52,5
4	-1	-1	1	38,5	26,9	6,2	33,1	53
5	1	-1	1	19,2	14,8	3,6	18,4	52,9
6	-1	1	1	39,6	21,9	9,5	31,4	64,6
7	1	1	1	26	20,7	5,5	26,2	55,1

Table A3.17 : Grafting from LC-UV in solids, whole CPP and serum of runs done with Sty/AN = 60/40 (-1) and S5200 = 3 wt-% (1)

				Solids	Whole CPP			Serum
Run	NDM	T27	T	% Graft	% HMW	%LMW	% Graft	% Graft
8	-1	-1	-1	33,6	nd	nd	nd	58,8
9	1	-1	-1	10	9	2,2	11,1	81,1
10	-1	1	-1	41,6	34,7	6,7	41,4	85,4
11	1	1	-1	16,9	14	3,6	17,6	73,7
12	-1	-1	1	35,6	31,5	4,1	35,6	64,8
13	1	-1	1	19,9	17,2	2,7	19,9	60,3
14	-1	1	1	38,7	32,7	6	38,7	78
15	1	1	1	26,6	22,8	3,8	26,6	70,3

Table A3.18 : Grafting from LC-UV in solids, whole CPP and serum of runs done with Sty/AN = 80/20 (1) and S5200 = 1 wt-% (-1)

				Solids	Whole CPP			Serum
Run	NDM	T27	T	% Graft	% HMW	%LMW	% Graft	% Graft
16	-1	1	-1	29,1	26,2	3	29,1	76,7
17	1	1	-1	13,8	10,8	3	13,8	55,6
18	-1	-1	1	29	26,2	2,8	29	67,6
19	1	-1	1	12,9	10,1	2,8	12,9	56,3
20	-1	1	1	37,2	32,9	4,3	37,2	73,9
21	1	1	1	18,5	14,6	3,9	18,5	66

Table A3.19 : Grafting from LC-UV in solids, whole CPP and serum of runs done with Sty/AN = 80/20 (1) and S5200 = 3 wt-% (1)

				Solids	Whole CPP			Serum
Run	NDM	T27	T	% Graft	% HMW	%LMW	% Graft	% Graft
22	-1	-1	-1	19,1	16,8	3,2	20	51,1
23	1	-1	-1	19,8	5,8	3,5	9,3	45,1
24	-1	1	-1	28,1	23,4	5,4	28,8	74,9
25	1	1	-1	13,3	7,1	5	12,1	54,6
26	-1	-1	1	29,1	23,5	5	28,5	72,6
27	1	-1	1	11,4	6	4,5	10,5	62,1
28	-1	1	1	37,6	30,3	7	37,3	78
29	1	1	1	16,4	9,2	6,9	16,1	62
30	1	1	1	22,2	17,3	4,9	22,2	73

Table A3.20 : Grafting from LC-UV in solids, whole CPP and serum of runs done with Sty/AN = 70/30 (0) and S5200 = 2 wt-% (0)

				Solids	Whole CPP			Serum
Run	NDM	T27	T	% Graft	% HMW	%LMW	% Graft	% Graft
31	0	0	0	21,4	16,1	4,1	20,2	77,7
32	0	0	0	25,6	nd	nd	nd	52,6

A3.1.5. Composition of solids (wt-% of polyol, Sty, AN), composition of soluble SAN and quantity of soluble SAN in the serum phase

Table A3.21 : Composition of solids (wt-% of polyol, Sty, AN), composition of soluble SAN and quantity of soluble SAN in the serum phase of runs done with Sty/AN = 60/40 (-1) and S5200 = 1 wt-% (-1)

				Solids H NMR			Serum C NMR	
Run	NDM	T27	T	Wt-% polyol	Wt-% Sty	Wt-% AN	Wt-% Sty	Wt-% AN
1	1	-1	-1	1,59	59,0	41,0	61	39
2	-1	1	-1	1,77	58,8	41,2	64	36
3	1	1	-1	2,03	58,9	41,1	69	31
4	-1	-1	1	3,14	57,1	42,9	68	32
5	1	-1	1	2,01	59,0	41,0	67	33
6	-1	1	1	4,25	58,2	41,8	64	36
7	1	1	1	3,08	58,4	41,6	67	33

Table A3.22 : Composition of solids (wt-% of polyol, Sty, AN), composition of soluble SAN and quantity of soluble SAN in the serum phase of runs done with Sty/AN = 60/40 (-1) and S5200 = 3 wt-% (1)

				Solids H NMR			Serum C NMR	
Run	NDM	T27	T	Wt-% polyol	Wt-% Sty	Wt-% AN	Wt-% Sty	Wt-% AN
8	-1	-1	-1	2,6	61	39	nd	nd
9	1	-1	-1	1,7	nd	nd	74	26
10	-1	1	-1	3,1	nd	nd	75	25
11	1	1	-1	2,4	nd	nd	77	23
12	-1	-1	1	2,9	61,3	38,7	nd	nd
13	1	-1	1	2,3	60,9	39,1	nd	nd
14	-1	1	1	4,1	61	39	nd	nd
15	1	1	1	3,5	60,9	39,1	nd	nd

Table A3.23 : Composition of solids (wt-% of polyol, Sty, AN), composition of soluble SAN and quantity of soluble SAN in the serum phase of runs done with Sty/AN = 80/20 (1) and S5200 = 1 wt-% (-1)

				Solids H NMR			Serum C NMR	
Run	NDM	T27	T	Wt-% polyol	Wt-% Sty	Wt-% AN	Wt-% Sty	Wt-% AN
16	-1	1	-1	2,8	77,6	22,4	nd	nd
17	1	1	-1	2,7	76,6	23,4	nd	nd
18	-1	-1	1	2,8	77,7	22,3	nd	nd
19	1	-1	1	2,5	76,8	23,2	nd	nd
20	-1	1	1	3,5	79,4	20,6	nd	nd
21	1	1	1	3,4	77,6	22,4	nd	nd

Table A3.24 : Composition of solids (wt-% of polyol, Sty, AN), composition of soluble SAN and quantity of soluble SAN in the serum phase of runs done with Sty/AN = 80/20 (1) and S5200 = 3 wt-% (1)

				Solids H NMR			Serum C NMR	
Run	NDM	T27	T	Wt-% polyol	Wt-% Sty	Wt-% AN	Wt-% Sty	Wt-% AN
22	-1	-1	-1	2,01	72,7	27,3	74	26
23	1	-1	-1	2,37	72,0	28,0	75	25
24	-1	1	-1	2,5	nd	nd	78	22
25	1	1	-1	2,5	nd	nd	83	17
26	-1	-1	1	2,5	nd	nd	73	27
27	1	-1	1	2,2	nd	nd	81	19
28	-1	1	1	3,1	nd	nd	78	22
29	1	1	1	2,8	nd	nd	81	19
30	1	1	1	3,7	77,2	22,8	nd	nd

Table A3.25 : Composition of solids (wt-% of polyol, Sty, AN), composition of soluble SAN and quantity of soluble SAN in the serum phase of runs done with Sty/AN = 70/30 (0) and S5200 = 2 wt-% (0)

				Solids H NMR			Serum C NMR	
Run	**NDM**	**T27**	**T**	**Wt-% polyol**	**Wt-% Sty**	**Wt-% AN**	**Wt-% Sty**	**Wt-% AN**
31	0	0	0	2,50	nd	nd	71	29
32	0	0	0	2,20	nd	nd	76	24

Table A3.26 : Comparison between two methods used to measure the polyol content

						wt-% Polyol	
Runs	NDM	T27	T	S5200	Sty/AN	**H NMR**	**GPC-fluo**
1	1	-1	-1	-1	-1	1,59	2,5
2	-1	1	-1	-1	-1	1,77	3,9
3	1	1	-1	-1	-1	2,03	2,9
4	-1	-1	1	-1	-1	3,14	2,9
5	1	-1	1	-1	-1	2,01	3,0
6	-1	1	1	-1	-1	4,25	4,0
7	1	1	1	-1	-1	3,08	3,8
22	-1	-1	-1	1	1	2,01	2,5
23	1	-1	-1	1	1	2,37	2,7
32	0	0	0	0	0	2,20	3,3

A3.1.6. SAN in serum

Table A3.27. : SAN in serum of runs done with Sty/AN = 60/40 (-1) and S5200 = 1 wt-% (-1)

Run	**NDM**	**T27**	**T**	**Mn (g/mol)**	**Mw (g/mol)**	**Mw/Mn**	**Wt-% SAN in serum**
1	1	-1	-1	6080	17500	2,9	0,71
2	-1	1	-1	6680	33100	5,0	1,03
3	1	1	-1	6370	17400	2,7	1,07
4	-1	-1	1	6910	46000	6,7	0,78
5	1	-1	1	6420	16300	2,5	0,98
6	-1	1	1	6410	24400	3,8	1,46
7	1	1	1	6150	13100	2,1	1,43

Table A3.28. : SAN in serum of runs done with Sty/AN = 60/40 (-1) and S5200 = 3 wt-% (1)

Run	NDM	T27	T	Mn (g/mol)	Mw (g/mol)	Mw/Mn	Wt-% SAN in serum
8	-1	-1	-1	9130	78250	8,6	0,8
9	1	-1	-1	7850	28200	3,6	0,74
10	-1	1	-1	8170	52400	6,4	0,87
11	1	1	-1	7280	23200	3,2	1,01
12	-1	-1	1	8335	85100	10,2	0,93
13	1	-1	1	7685	30100	3,9	1,26
14	-1	1	1	7060	47200	6,7	1,35
15	1	1	1	6940	25850	3,7	1,6

Table A3.29. : SAN in serum of runs done with Sty/AN = 80/20 (1) and S5200 = 1 wt-% (-1)

Run	NDM	T27	T	Mn (g/mol)	Mw (g/mol)	Mw/Mn	Wt-% SAN in serum
16	-1	1	-1	7100	20900	2,9	1,45
17	1	1	-1	5885	13200	2,3	1,48
18	-1	-1	1	7005	22150	3,2	0,97
19	1	-1	1	5785	13100	2,3	1,14
20	-1	1	1	7435	24250	3,3	1,68
21	1	1	1	5810	12950	2,2	1,45

Table A3.30. : SAN in serum of runs done with Sty/AN = 80/20 (1) and S5200 = 3 wt-% (1)

Run	NDM	T27	T	Mn (g/mol)	Mw (g/mol)	Mw/Mn	Wt-% SAN in serum
22	-1	-1	-1	8160	30700	3,8	0,86
23	1	-1	-1	6090	14200	2,3	1,66
24	-1	1	-1	8840	31400	3,6	1,53
25	1	1	-1	7300	18900	2,6	1,85
26	-1	-1	1	9010	35700	4,0	1,12
27	1	-1	1	7230	19200	2,7	1,39
28	-1	1	1	8840	26800	3,0	1,77
29	1	1	1	7600	19900	2,6	1,94
30	1	1	1	72945	18300	2,5	3,06

Table A3.31. : SAN in serum of runs done with Sty/AN = 70/30 (0) and S5200 = 2 wt-% (0)

Run	NDM	T27	T	Mn (g/mol)	Mw (g/mol)	Mw/Mn	Wt-% SAN in serum
31	0	0	0	7420	24400	3,3	1,05
32	0	0	0	6920	16800	2,4	1,07

A3.2. Figures of Chapter 3

A3.2.1. Evolution of particles sizes and average molecular weights with time

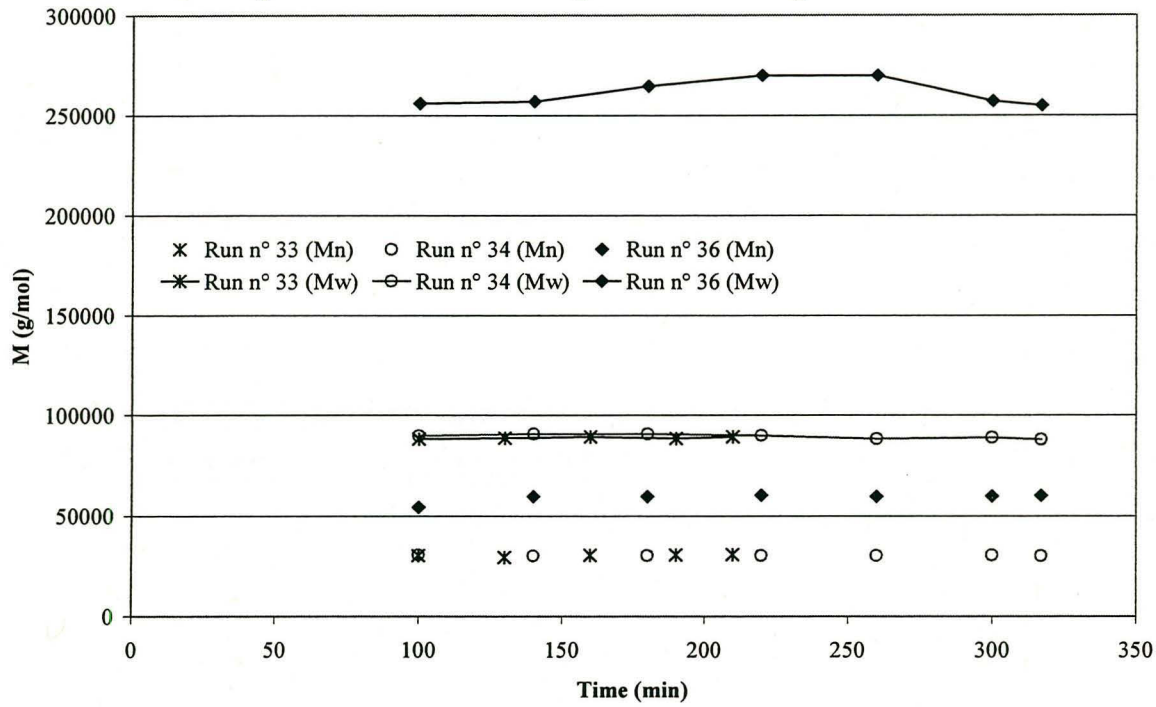

Figure A3.1. : Evolution of Mn and Mw versus time during the production of different CPP samples : standard runs n° 33 and n° 34 (Sty/AN = 70/30, S5200 = 2 wt-%, NDM = 0.30 wt-%, T27 = 0.15 wt-%, T = 130 °C) and the unstable run n° 36 (Sty/AN = 60/40, S5200 = 3 wt-%, NDM = 0.15 wt-%, T27 = 0.10 wt-%, T = 120 °C)

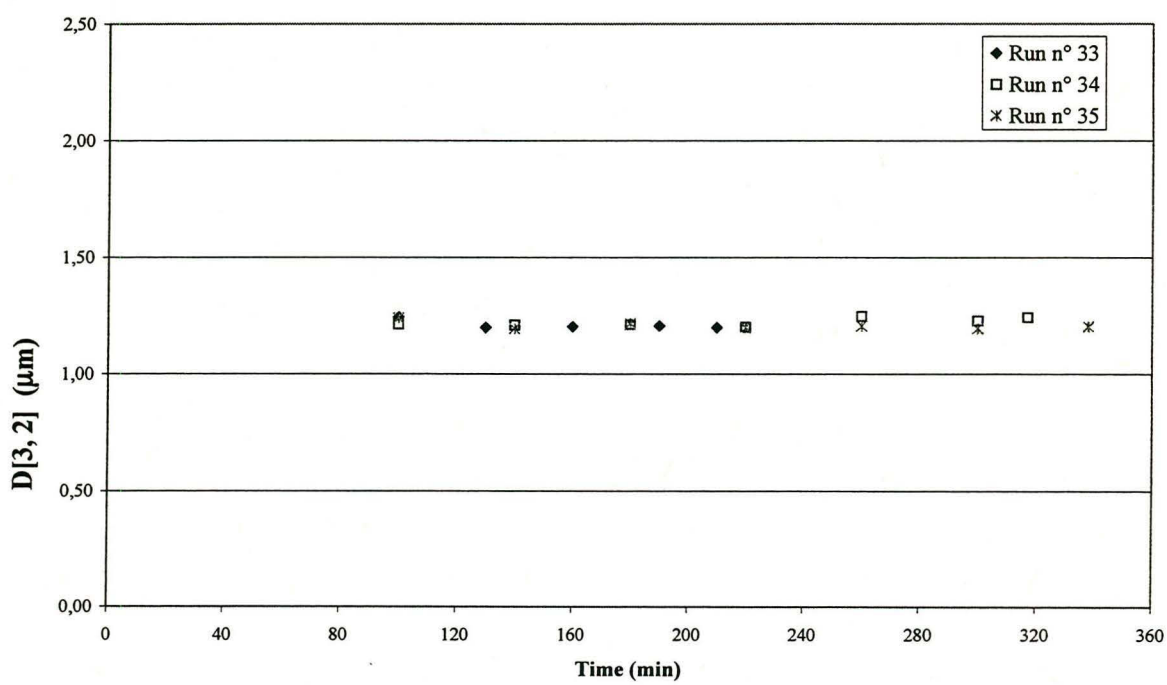

Figure A3.2. : Evolution of the surface area moment mean diameter versus time during the production of standard CPP samples (Sty/AN = 70/30, S5200 = 2 wt-%, NDM = 0.30 wt-%, T27 = 0.15 wt-%, T = 130 °C)

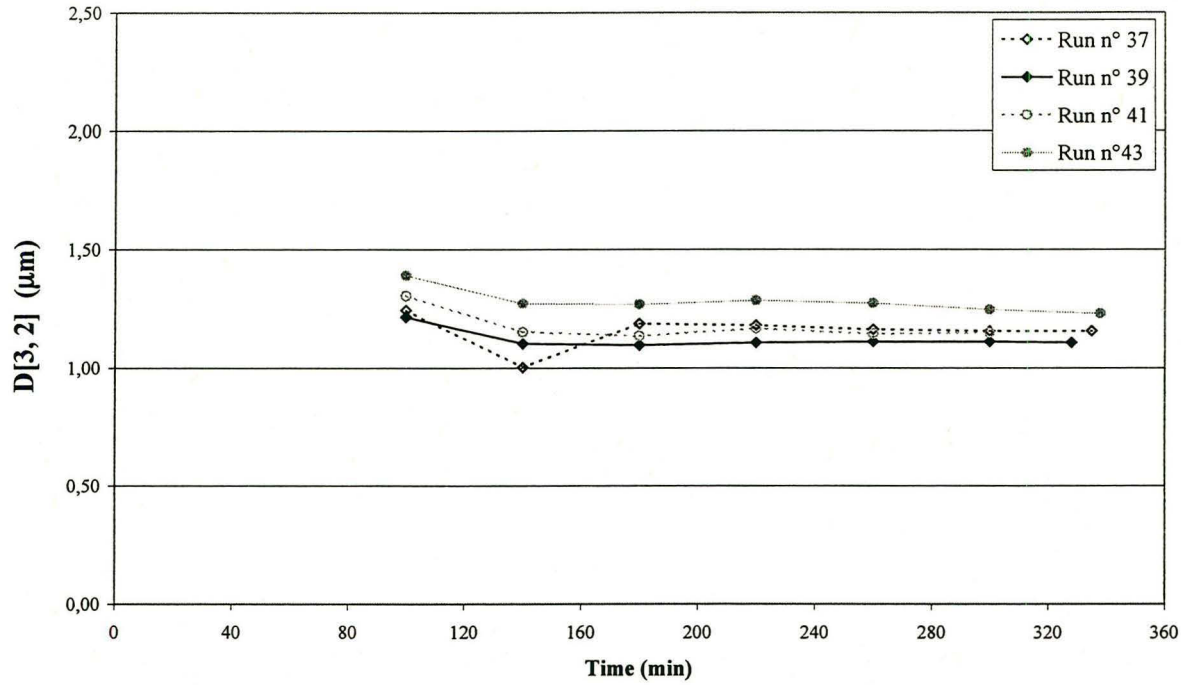

Figure A3.3. : Evolution of the surface area moment mean diameter versus time during the production of CPP during the runs n° 37 (low T27, low T), n° 39 (high T27, low T), n° 41 (low T27, low T) and n° 43 (high T27, low T) done with high NDM (0.45 wt-%), low styrene (Sty/AN = 60/40) and high S5200 (3 wt-%)

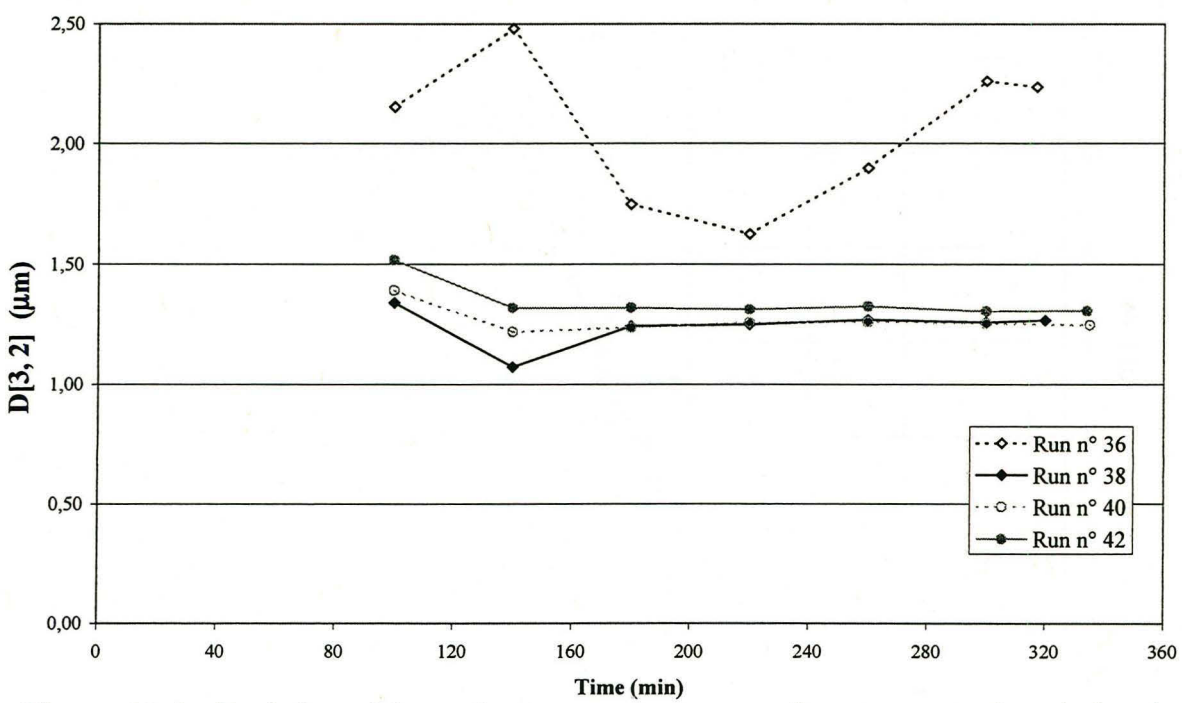

Figure A3.4. : Evolution of the surface area moment mean diameter versus time during the production of CPP during the runs n° 36 (low T27, low T), n° 38 (high T27, low T), n° 40 (low T27, low T) and n° 42 (high T27, low T) done with low NDM (0.15 wt-%), low styrene (Sty/AN = 60/40) and high S5200 (3 wt-%)

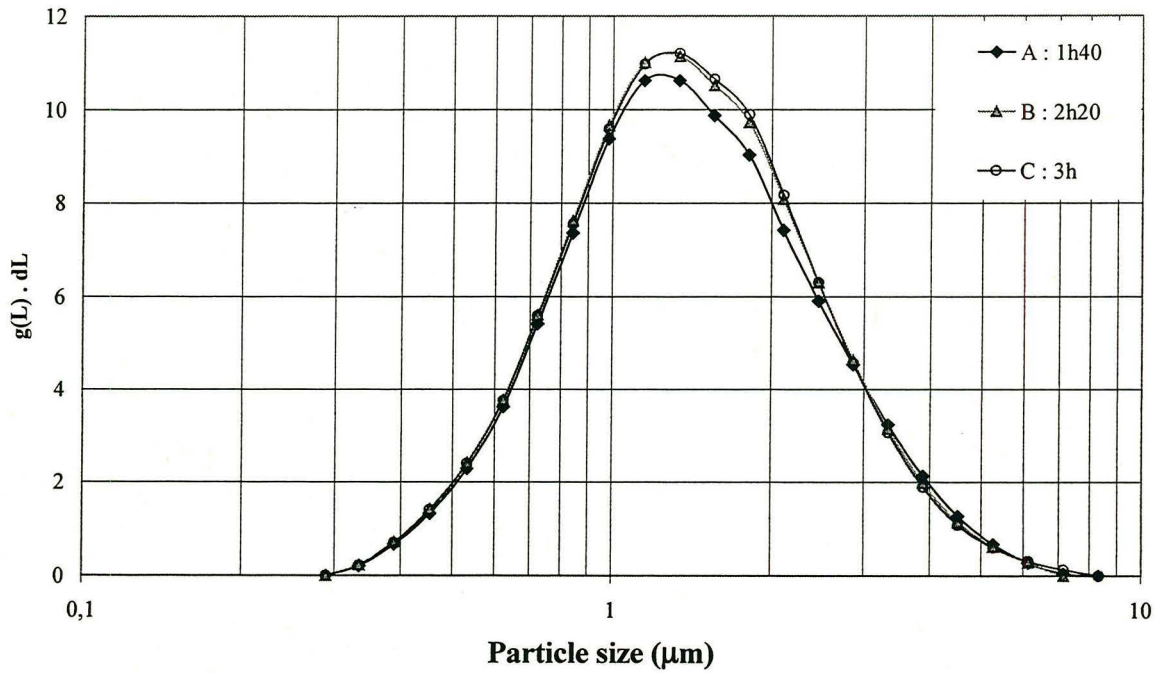

Figure A3.5.a : Evolution of the volume particle size distributions with time of the run n° 34 done with a standard recipe (Sty/AN=70/30, S5200 = 2 wt-%, NDM = 0.30 wt-%, T27 = 0.15 wt-% and T = 130 °C)

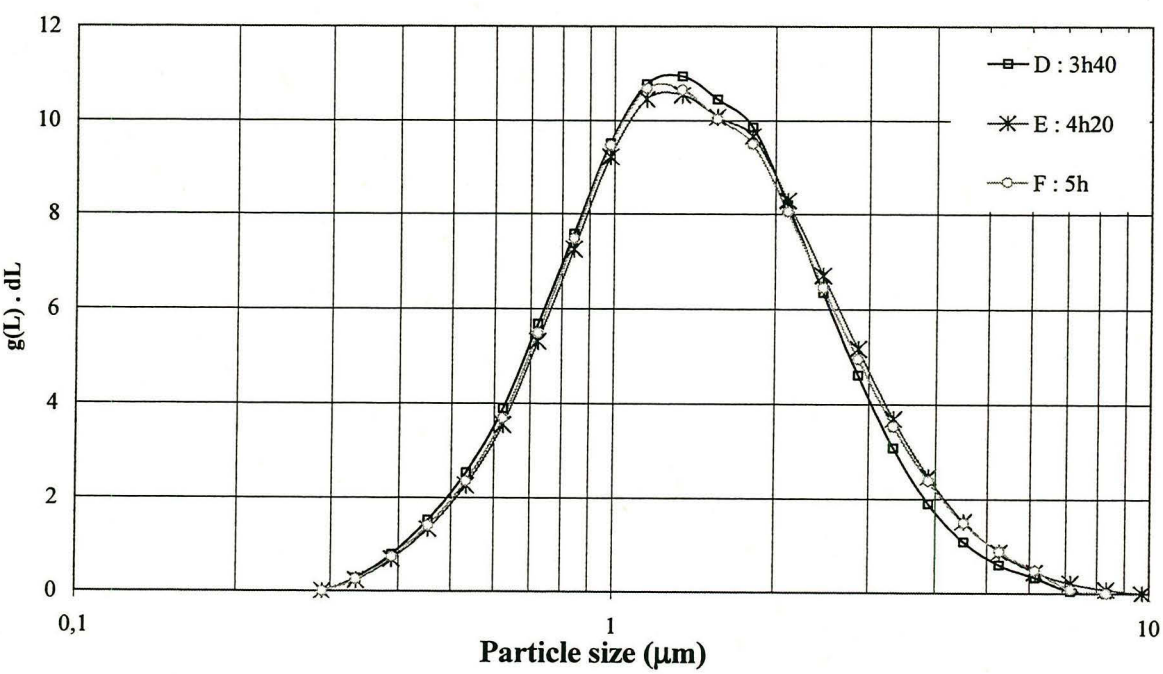

Figure A3.5.b : Evolution of the volume particle size distributions with time of the run n° 34 done with a standard recipe (Sty/AN=70/30, S5200 = 2 wt-%, NDM = 0.30 wt-%, T27 = 0.15 wt-% and T = 130 °C)

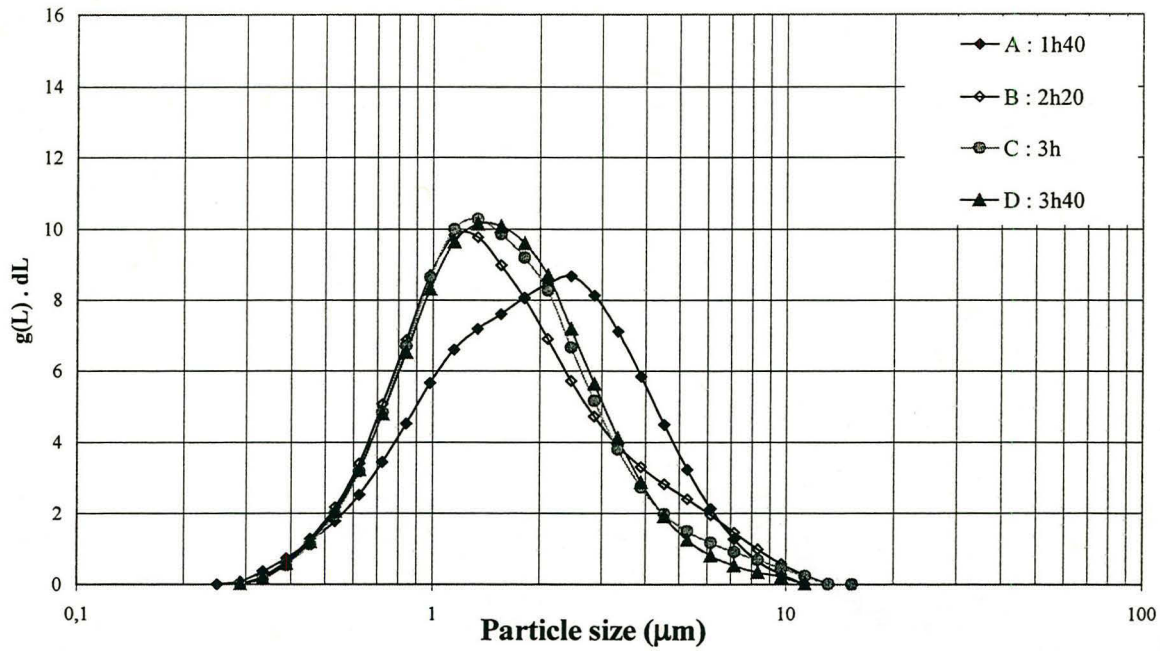

Figure A3.6.a : Evolution of the volume particle size distributions with time of the run n° 42 done with low styrene (Sty/AN=60/40), high S5200 (3 wt-%), low NDM (0.15 wt-%), high T27 (0.20 wt-%) and high T (140 °C)

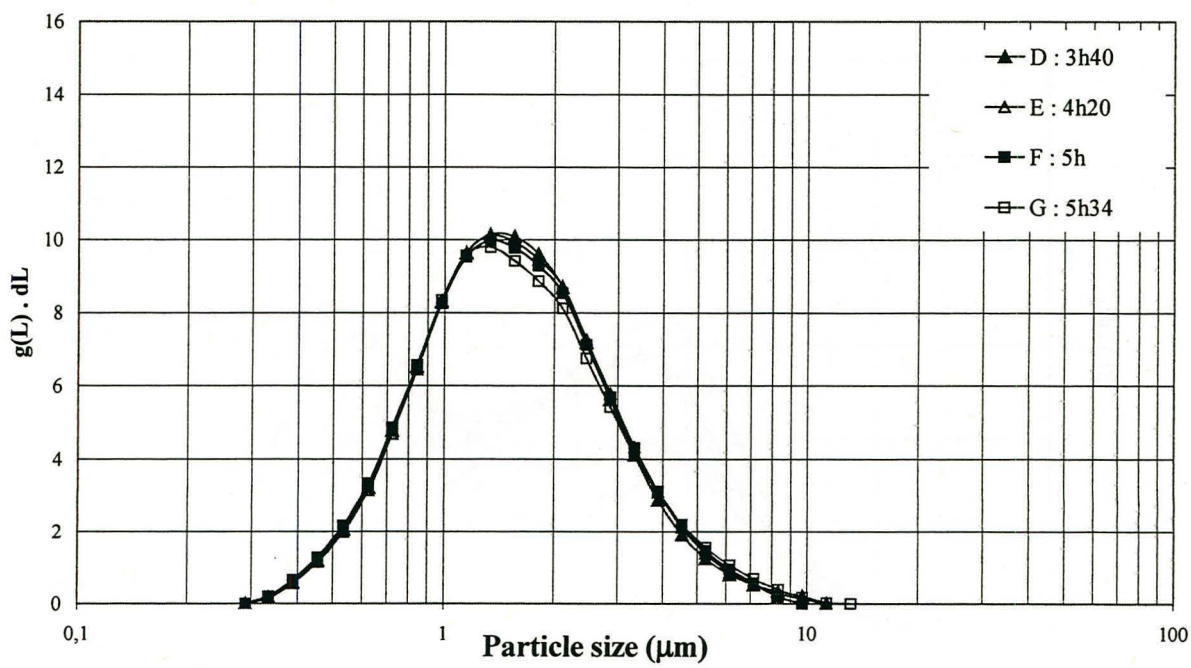

Figure A3.6.b : Evolution of the volume particle size distributions with time of the run n° 42 done with low styrene (Sty/AN=60/40), high S5200 (3 wt-%), low NDM (0.15 wt-%), high T27 (0.20 wt-%) and high T (140 °C)

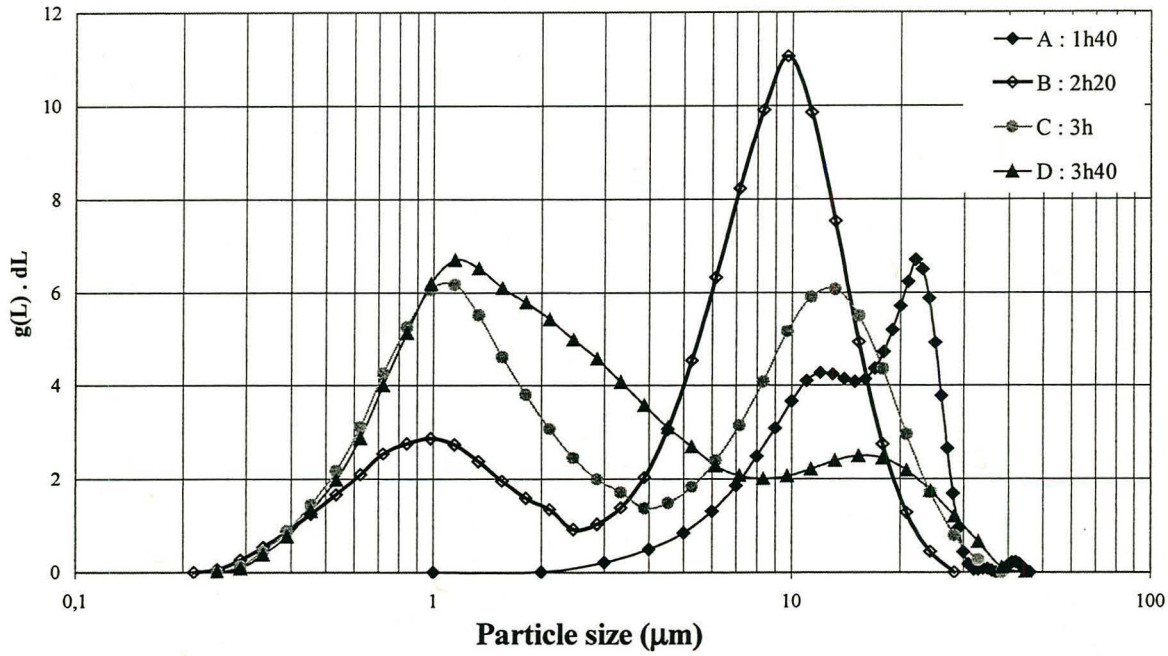

Figure A3.7.a : Evolution of the volume particle size distributions with time of the run n° 36 done with low styrene (Sty/AN=60/40), high S5200 (3 wt-%), low NDM (0.15 wt-%), low T27 (0.10 wt-%) and low T (120 °C)

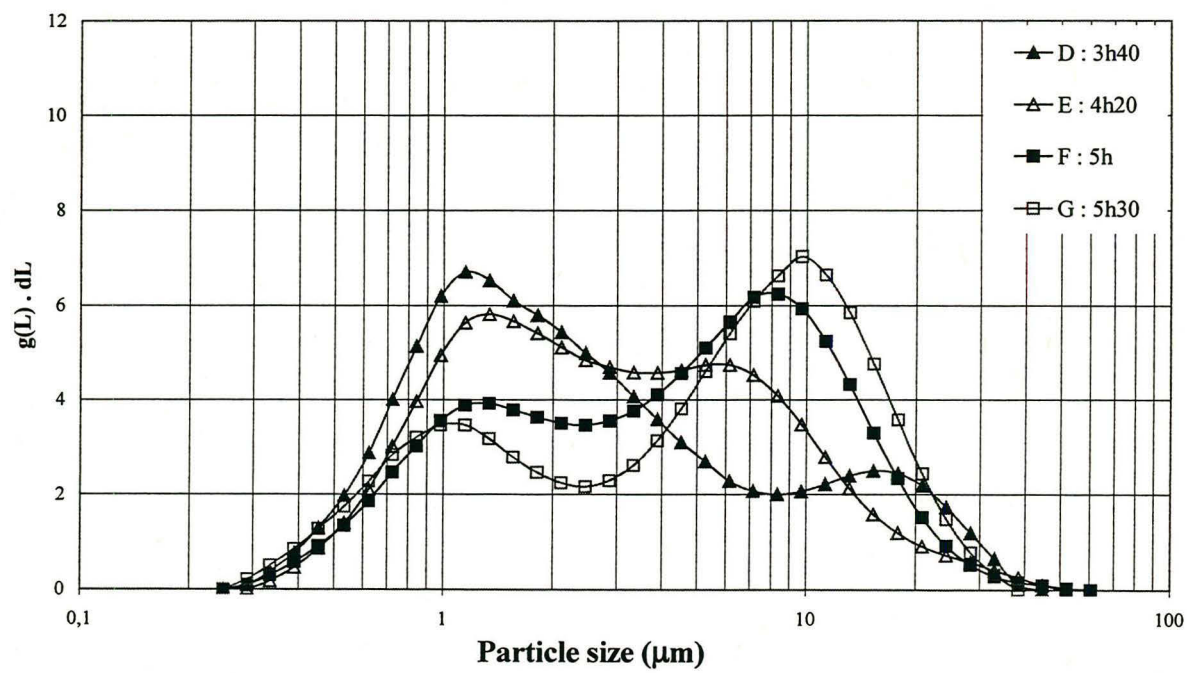

Figure A3.7.b : Evolution of the volume particle size distributions with time of the run n° 36 done with low styrene (Sty/AN=60/40), high S5200 (3 wt-%), low NDM (0.15 wt-%), low T27 (0.10 wt-%) and low T (120 °C)

A3.2.2. Molecular weight distributions of whole CPP

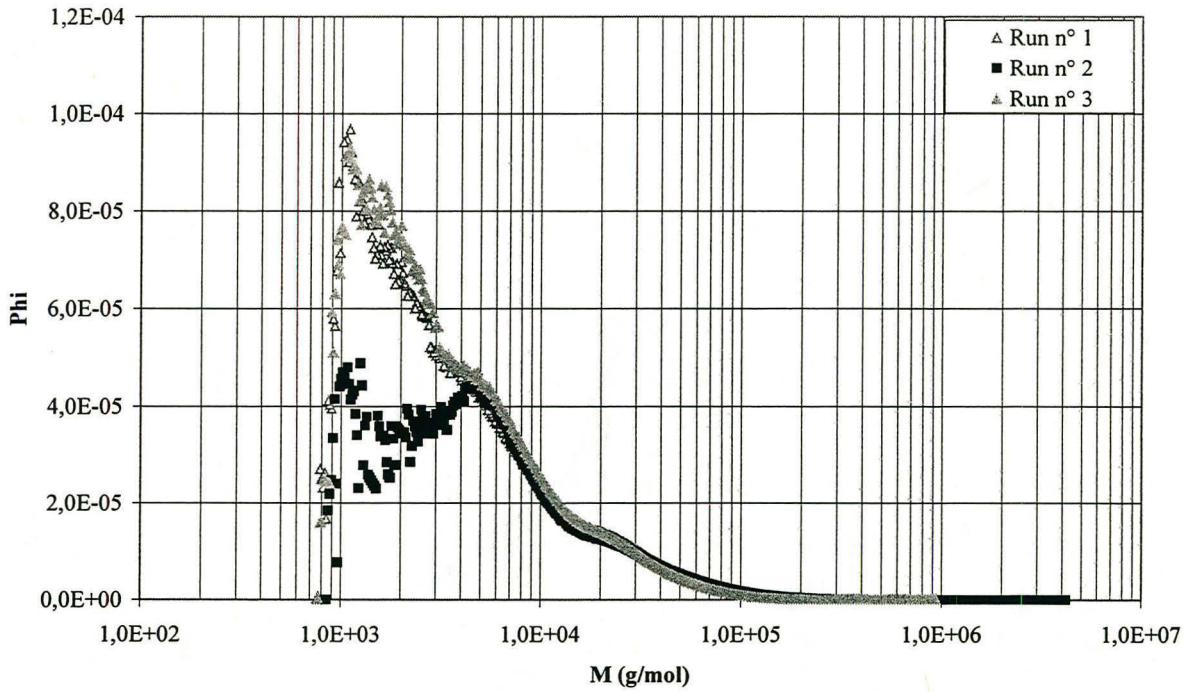

Figure A3.8. : Numbre molecular weight distribution of the runs n° 1 (high NDM, low T27), n° 2 (low NDM, high T27) and n° 3 (high NDM, high T27) done with low styrene (Sty/AN=60/40), low S5200 (1 wt-%) and low T (120 °C)

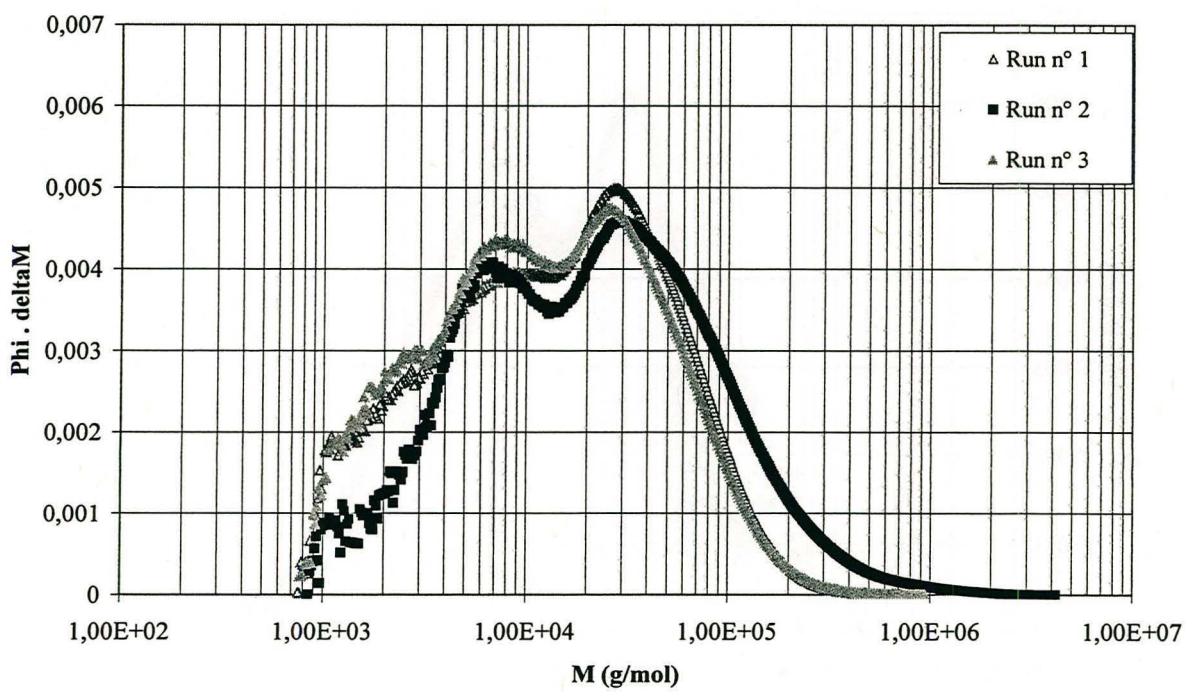

Figure A3.9. : Weight molecular weight distribution of the runs n° 1 (high NDM, low T27), n° 2 (low NDM, high T27) and n° 3 (high NDM, high T27) done with low styrene (Sty/AN=60/40), low S5200 (1 wt-%) and low T (120 °C)

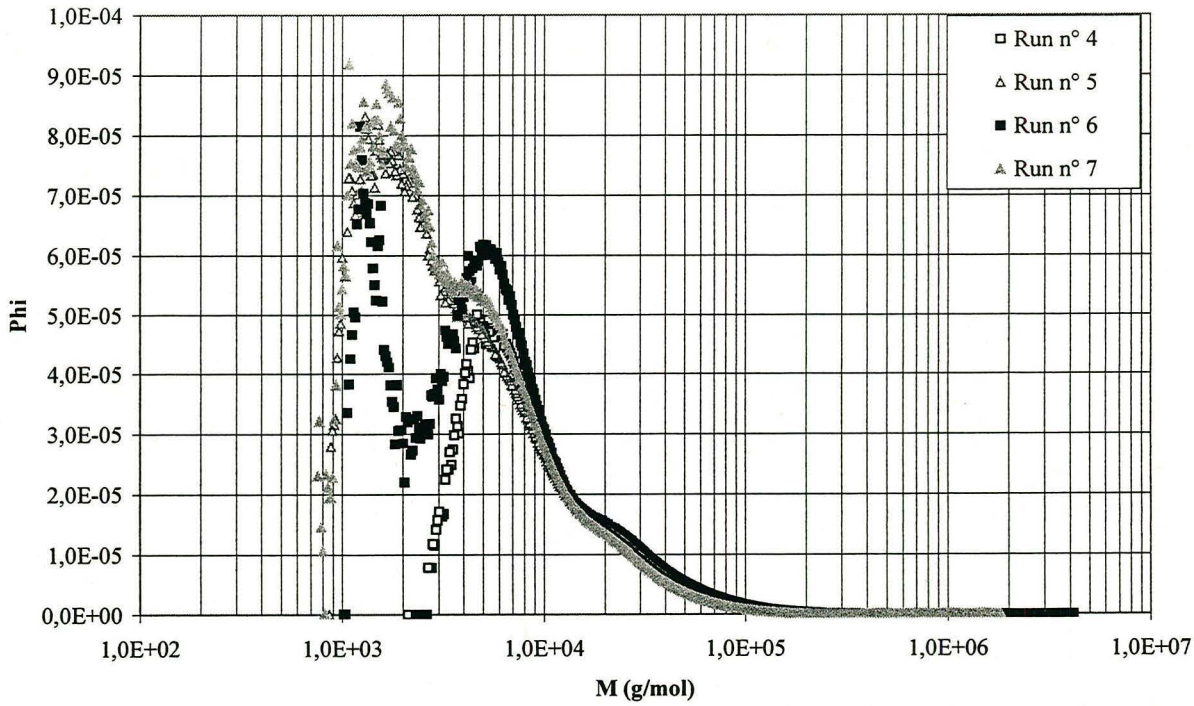

Figure A3.10. : Numbre molecular weight distribution of the runs n° 4 (low NDM, low T27), n° 5 (high NDM, low T27), n° 6 (low NDM, high T27) and n° 7 (high NDM, high T27) done with low styrene (Sty/AN=60/40), low S5200 (1 wt-%) and high T (140 °C)

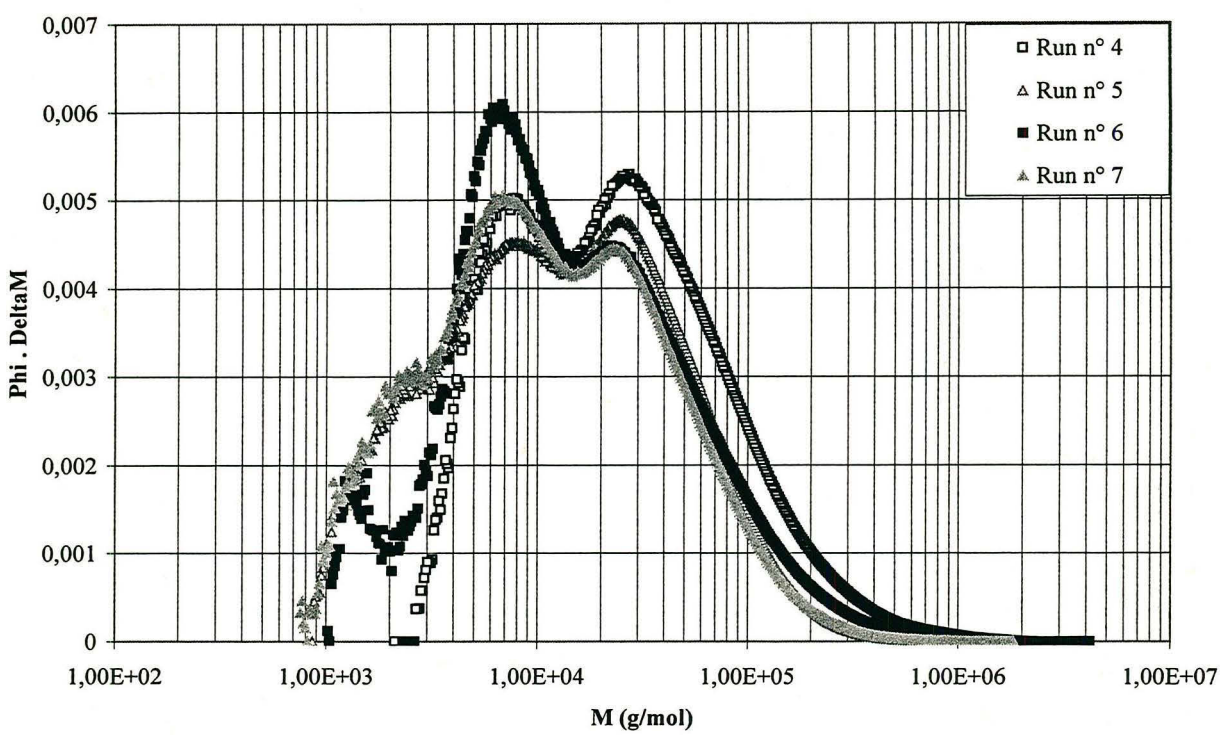

Figure A3.11. : Weight molecular weight distribution of the runs n° 4 (low NDM, low T27), n° 5 (high NDM, low T27), n° 6 (low NDM, high T27) and n° 7 (high NDM, high T27) done with low styrene (Sty/AN=60/40), low S5200 (1 wt-%) and high T (140 °C)

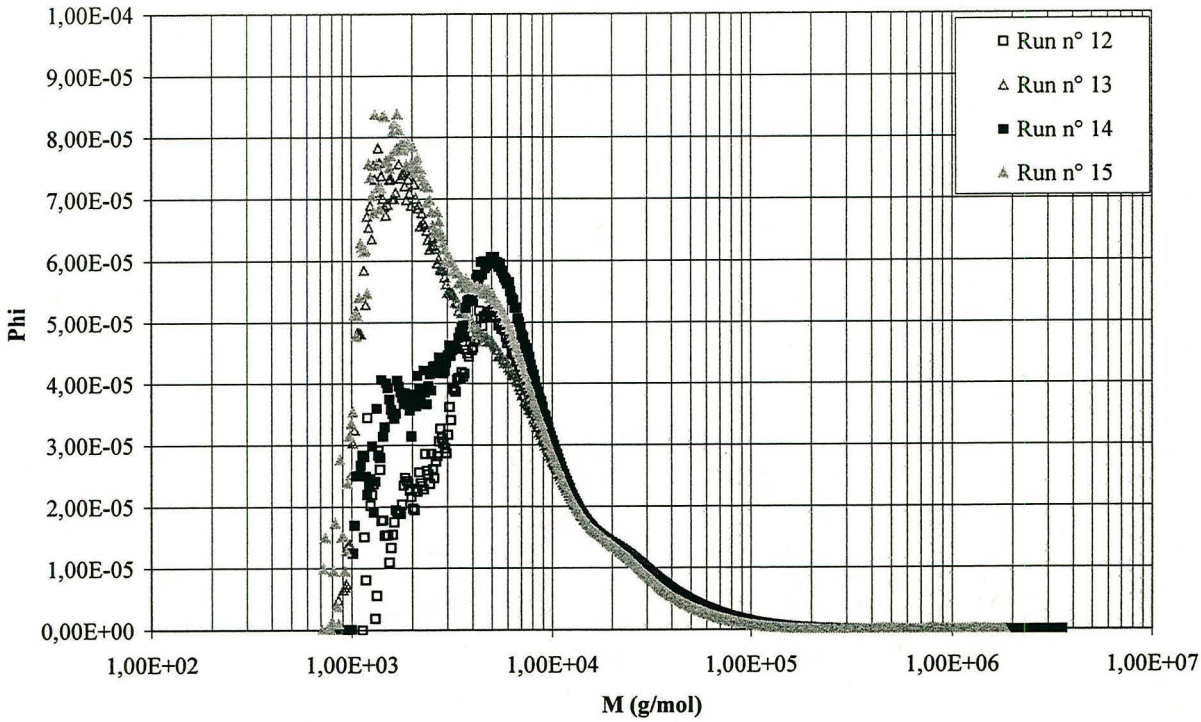

Figure A3.12. : Numbre molecular weight distribution of the runs n° 12 (low NDM, low T27), n° 13 (high NDM, low T27), n° 14 (low NDM, high T27) and n° 15 (high NDM, high T27) done with low styrene (Sty/AN=60/40), high S5200 (3 wt-%) and high T (140 °C)

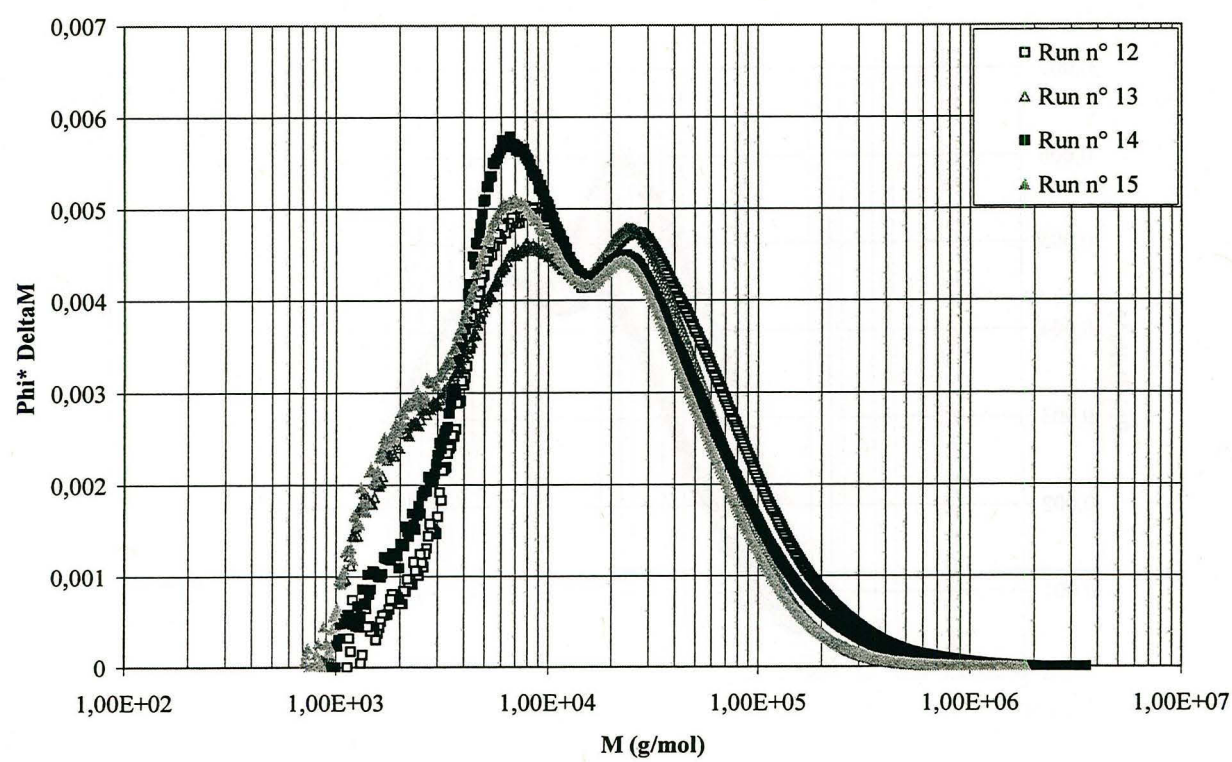

Figure A3.13. : Weight molecular weight distribution of the runs n° 12 (low NDM, low T27), n° 13 (high NDM, low T27), n° 14 (low NDM, high T27) and n° 15 (high NDM, high T27) done with low styrene (Sty/AN=60/40), high S5200 (3 wt-%) and high T (140 °C)

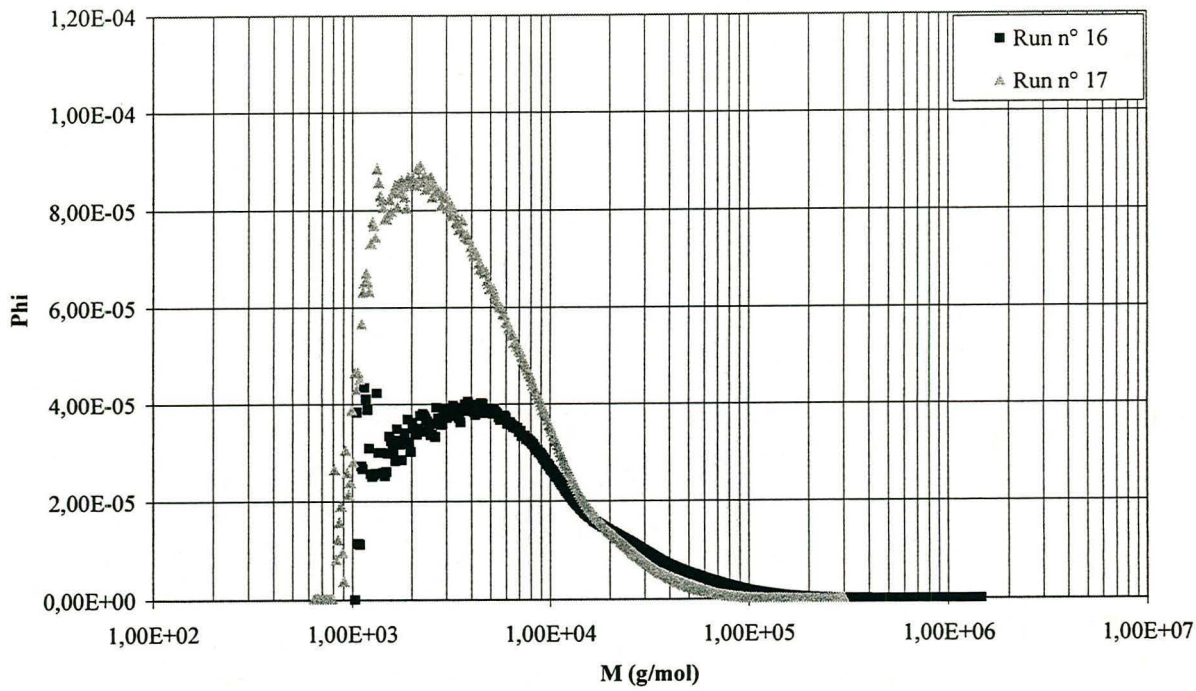

Figure A3.14. : Numbre molecular weight distribution of the runs n° 16 (low NDM, high T27) and n° 17 (high NDM, high T27) done with high styrene (Sty/AN=80/20), low S5200 (1 wt-%) and low T (120 °C)

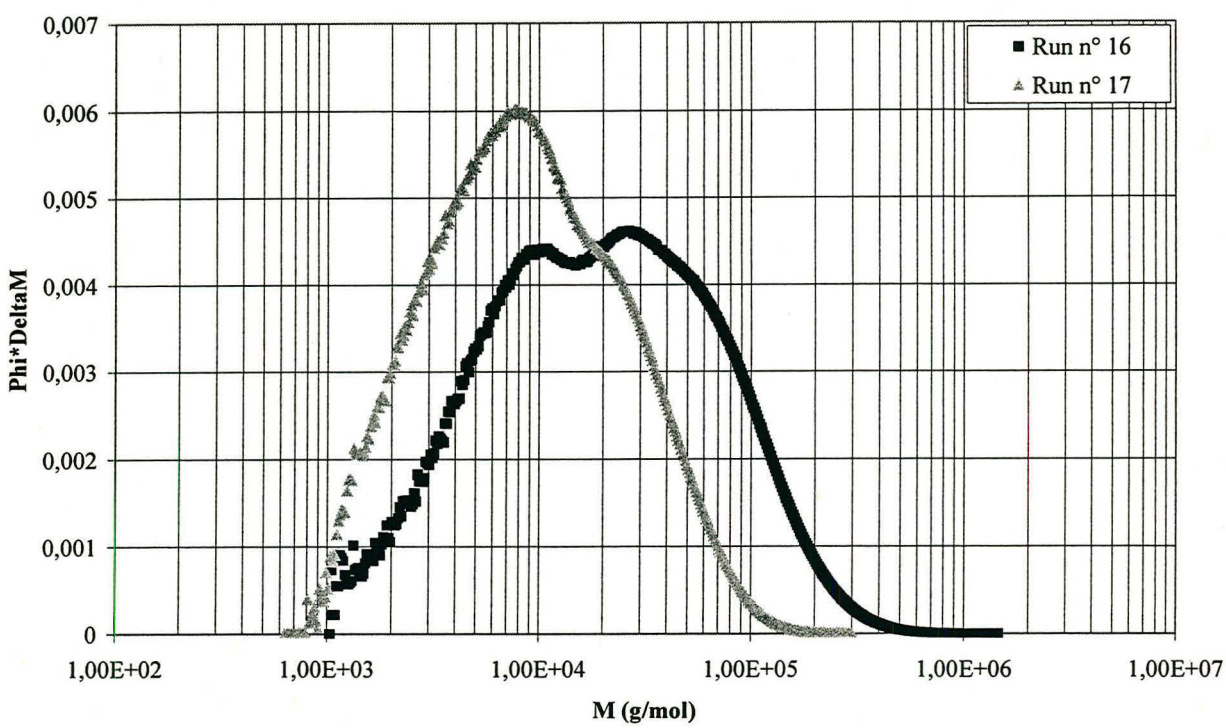

Figure A3.15. : Weight molecular weight distribution of the runs n° 16 (low NDM, high T27) and n° 17 (high NDM, high T27) done with high styrene (Sty/AN=80/20), low S5200 (1 wt-%) and low T (120 °C)

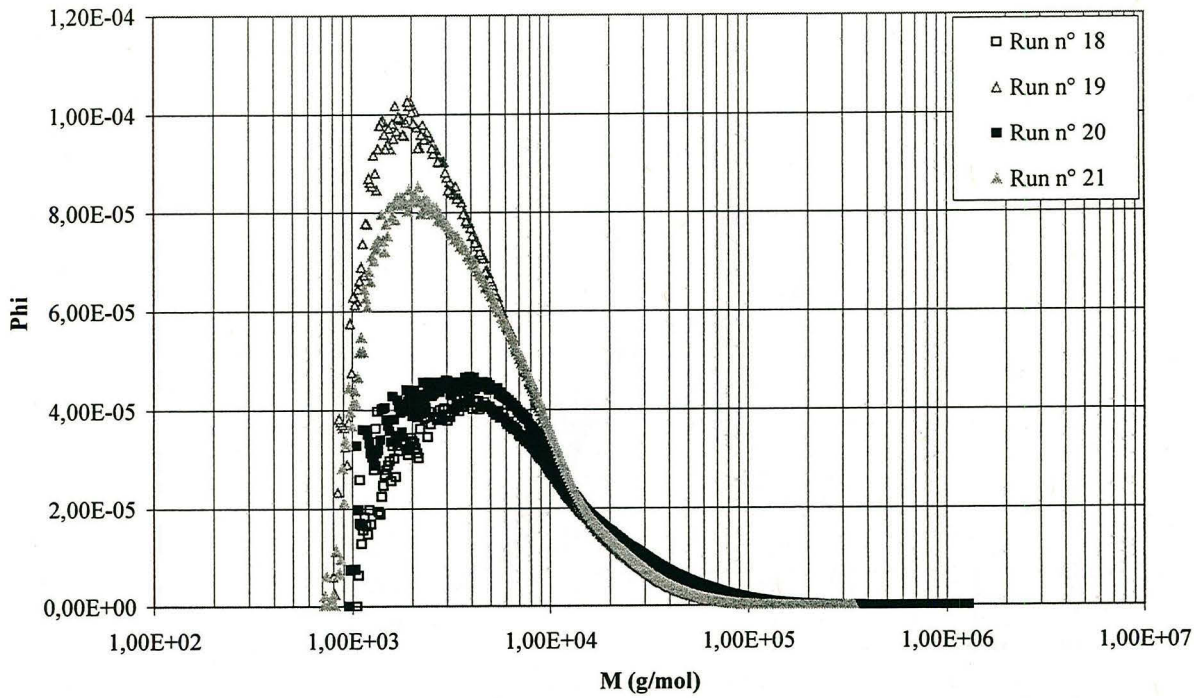

Figure A3.16. : Numbre molecular weight distribution of the runs n° 18 (low NDM, low T27), n° 19 (high NDM, low T27), n° 20 (low NDM, high T27) and n° 21 (high NDM, high T27) done with high styrene (Sty/AN=80/20), low S5200 (1 wt-%) and high T (140 °C)

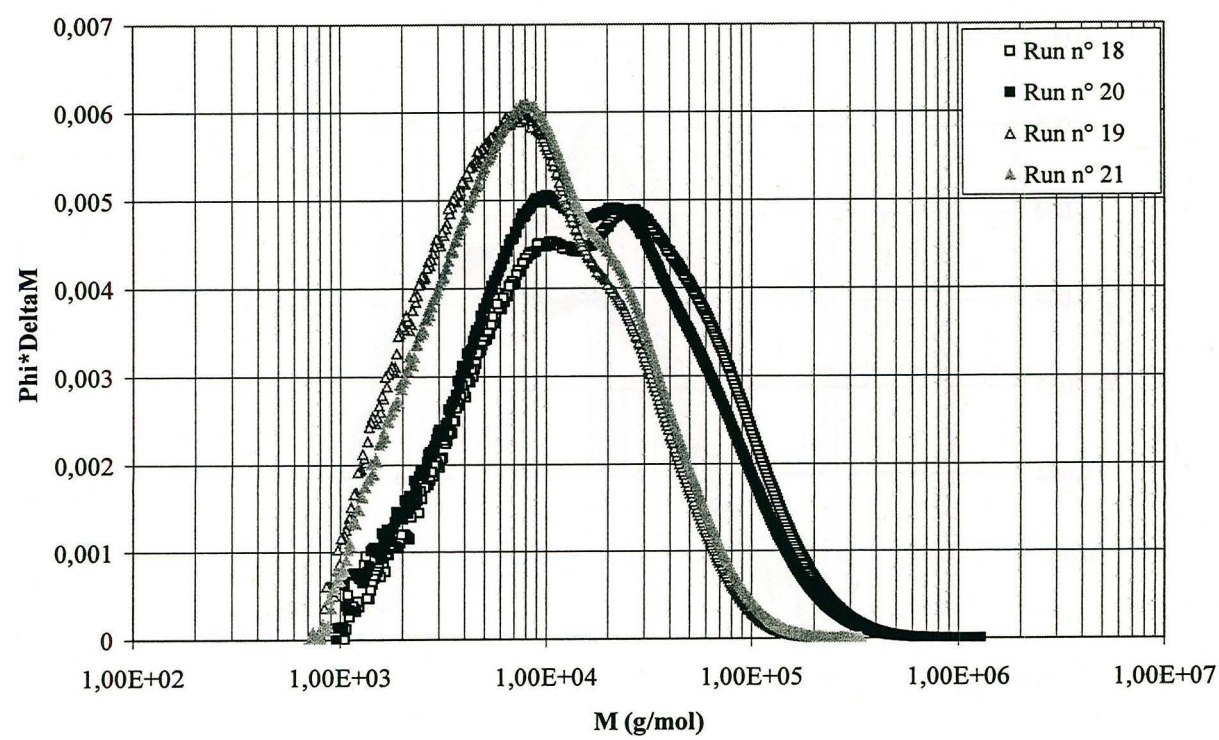

Figure A3.17. : Weight molecular weight distribution of the runs n° 18 (low NDM, low T27), n° 19 (high NDM, low T27), n° 20 (low NDM, high T27) and n° 21 (high NDM, high T27) done with high styrene (Sty/AN=80/20), low S5200 (1 wt-%) and high T (140 °C)

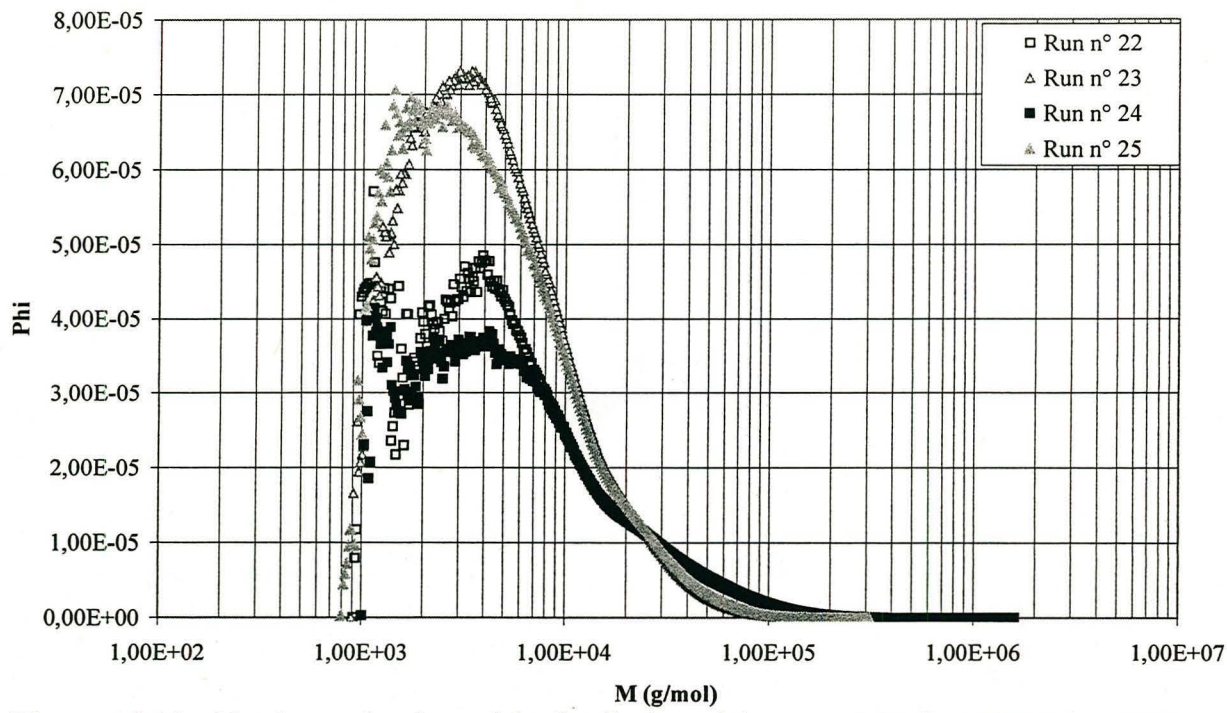

Figure A3.18. : Numbre molecular weight distribution of the runs n° 22 (low NDM, low T27), n° 23 (high NDM, low T27), n° 24 (low NDM, high T27) and n° 25 (high NDM, high T27) done with high styrene (Sty/AN=80/20), high S5200 (3 wt-%) and low T (120 °C)

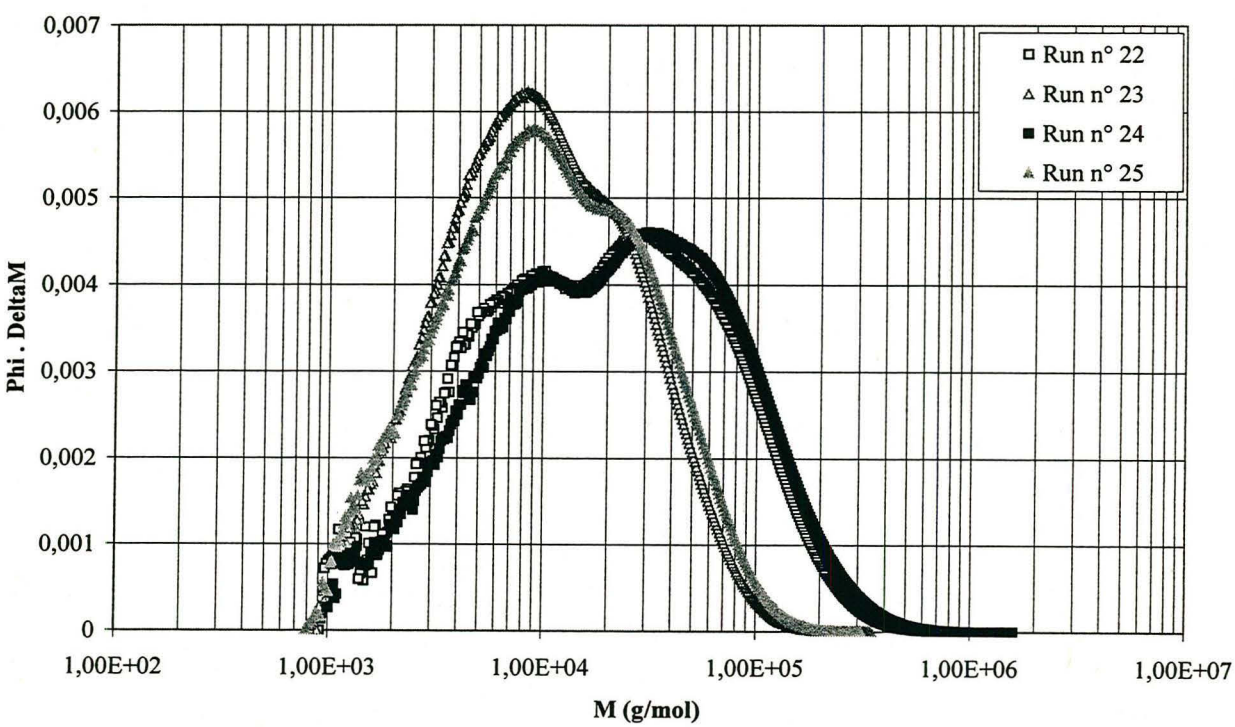

Figure A3.19. : Weight molecular weight distribution of the runs n° 22 (low NDM, low T27), n° 23 (high NDM, low T27), n° 24 (low NDM, high T27) and n° 25 (high NDM, high T27) done with high styrene (Sty/AN=80/20), high S5200 (3 wt-%) and low T (120 °C)

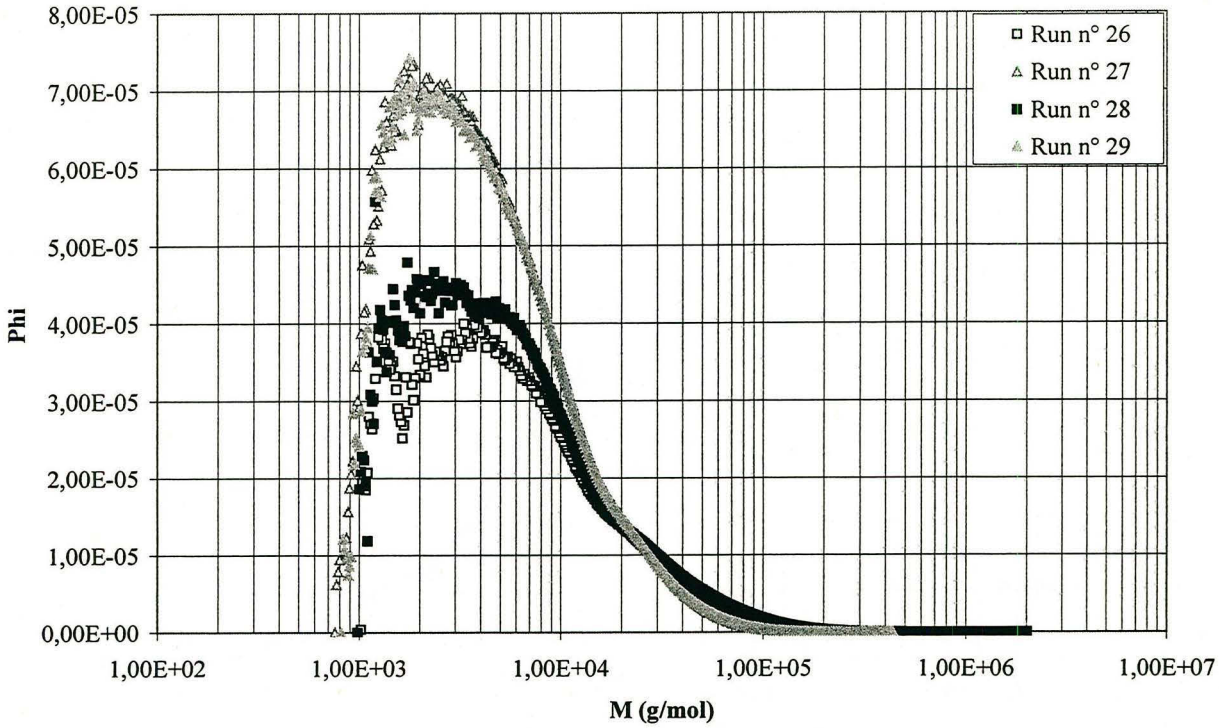

Figure A3.20. : Numbre molecular weight distribution of the runs n° 26 (low NDM, low T27), n° 27 (high NDM, low T27), n° 28 (low NDM, high T27) and n° 29 (high NDM, high T27) done with high styrene (Sty/AN=80/20), high S5200 (3 wt-%) and high T (140 °C)

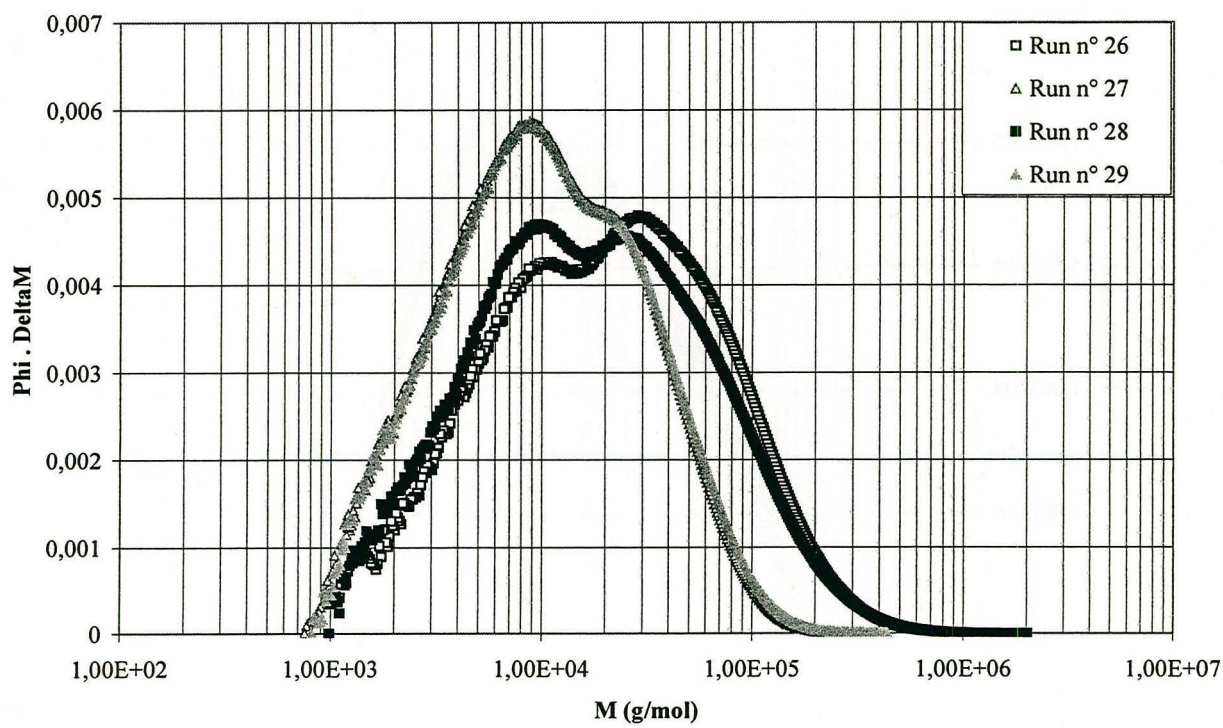

Figure A3.21. : Weight molecular weight distribution of the runs n° 26 (low NDM, low T27), n° 27 (high NDM, low T27), n° 28 (low NDM, high T27) and n° 29 (high NDM, high T27) done with high styrene (Sty/AN=80/20), high S5200 (3 wt-%) and high T (140 °C)

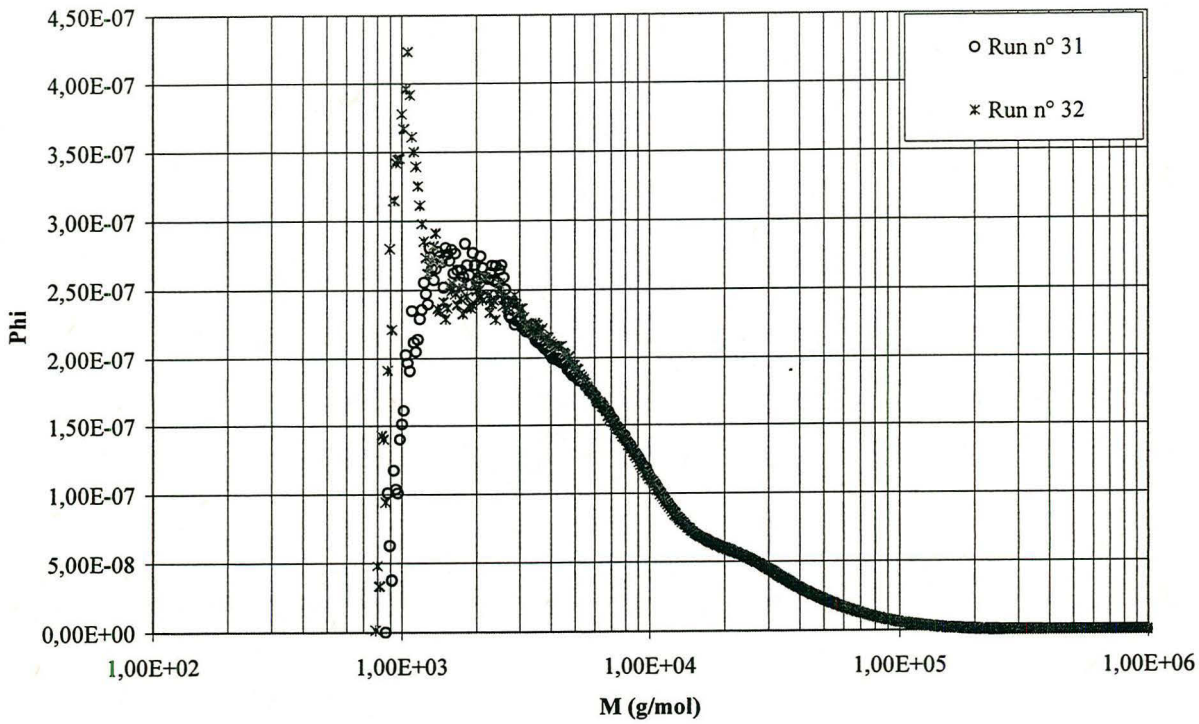

Figure A3.22. : Numbre molecular weight distribution of the standard runs n° 31 and n° 32 done with Sty/AN=70/30, S5200 =2 wt-%, NDM = 0.30 wt-%, T27 = 0.15 wt-% and T=130 °C

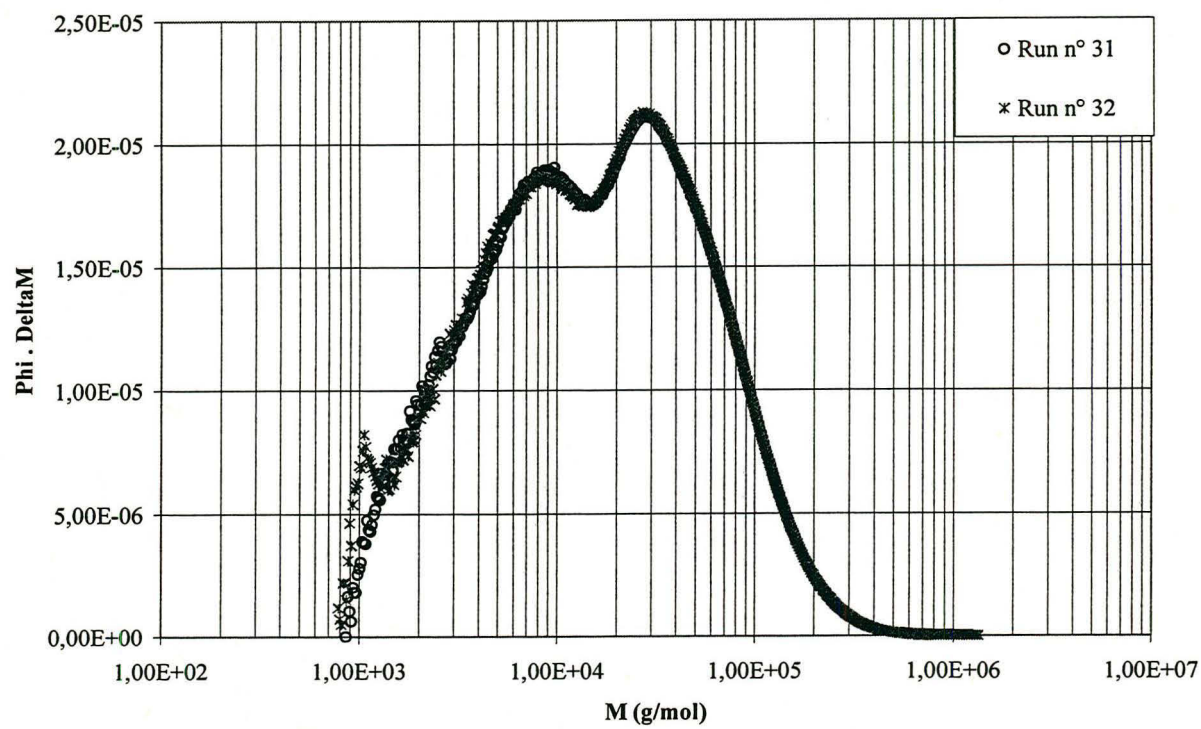

Figure A3.23. : Weight molecular weight distribution of the standard runs n° 31 and n° 32 done with Sty/AN=70/30, S5200 =2 wt-%, NDM = 0.30 wt-%, T27 = 0.15 wt-% and T=130 °C

A3.2.3. Particle size distributions

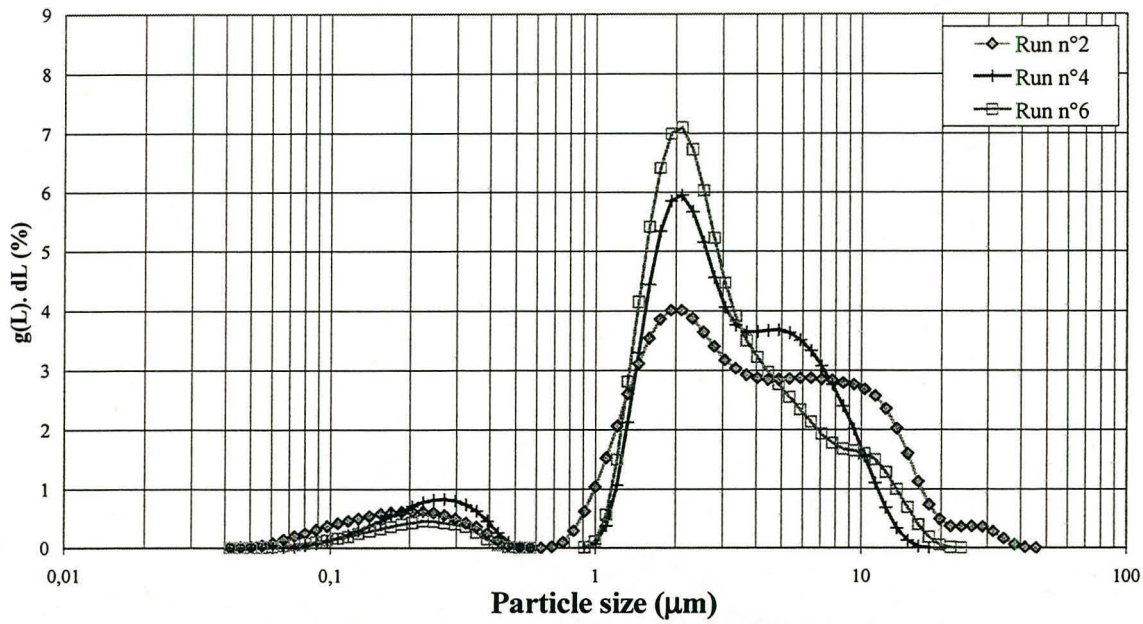

Figure A3.24 : Volume particle size distributions of runs n° 2 (high T27 and low T), n°4 (low T27 and high T) and n°6 (high T27 and high T) done with Sty/AN=60/40, low S5200 (1 wt-%) and low NDM (0.15 wt-%).

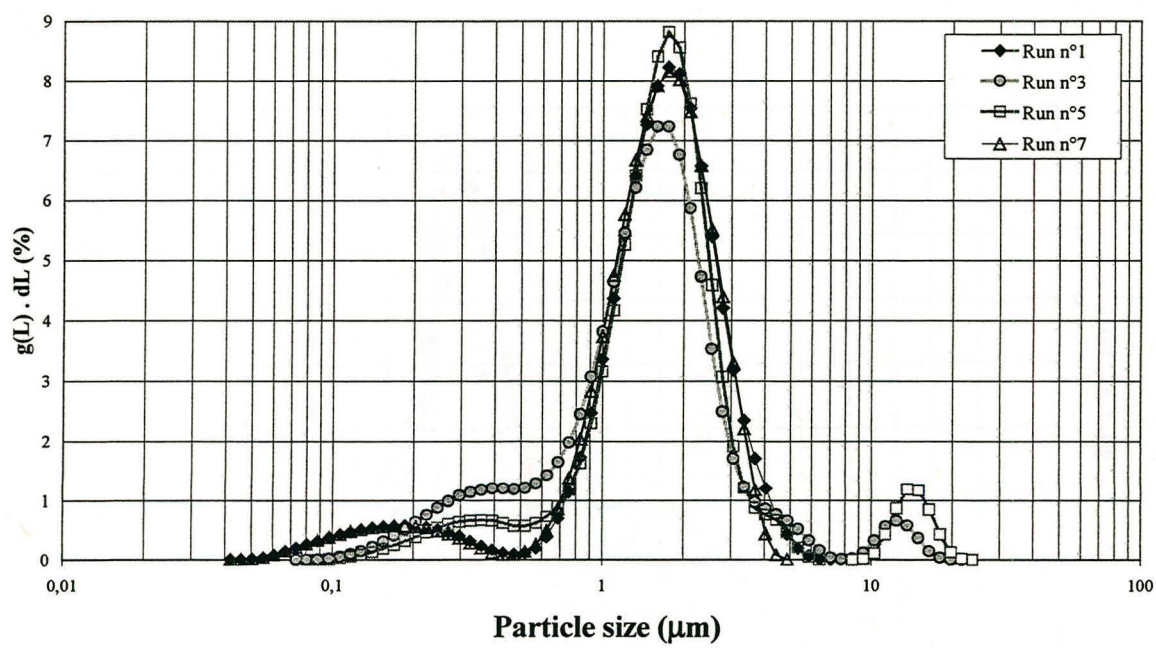

Figure A3.25 : Volume particle size distributions of runs n° 1 (low T27 and low T), n°3 (high T27 and high T), n°5 (low T27 and high T) and n°7 (high T27 and high T) done with Sty/AN=60/40, low S5200 (1 wt-%) and high NDM (0.45 wt-%)

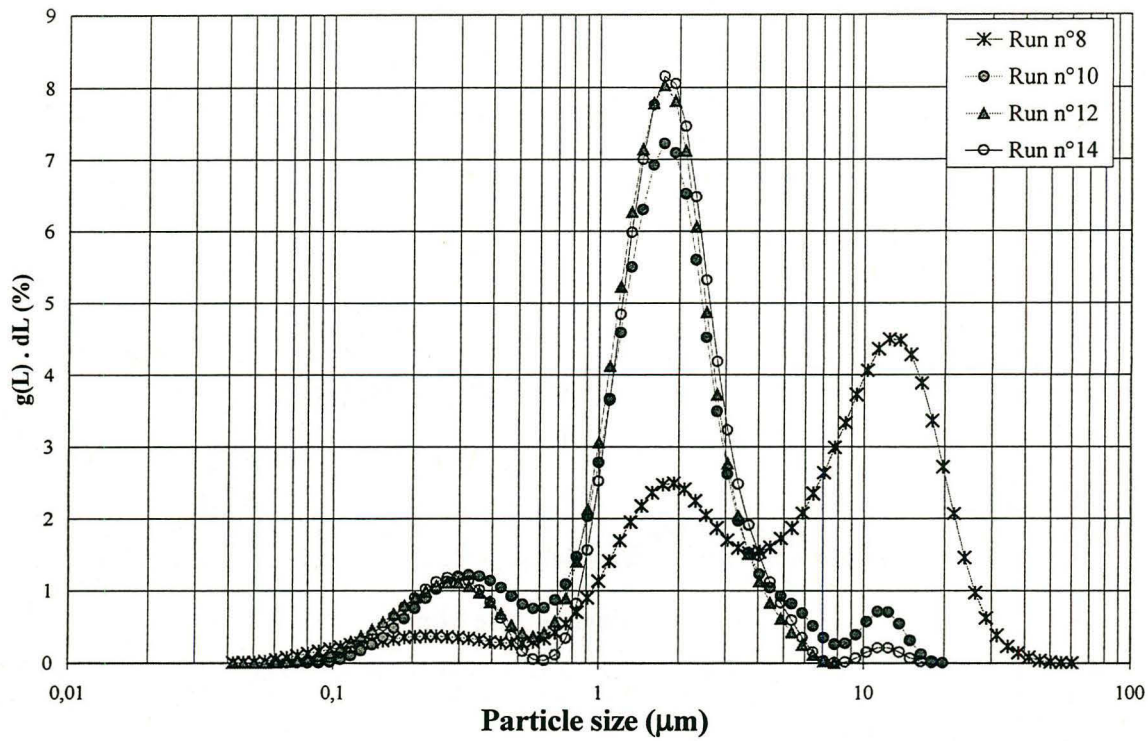

Figure A3.26 : Volume particle size distributions of runs n° 8 (low T27 and low T), n°10 (high T27 and low T), n°12 (low T27 and high T) and n°14 (high T27 and high T) done with Sty/AN=60/40, S5200 = 3 wt-% and low NDM

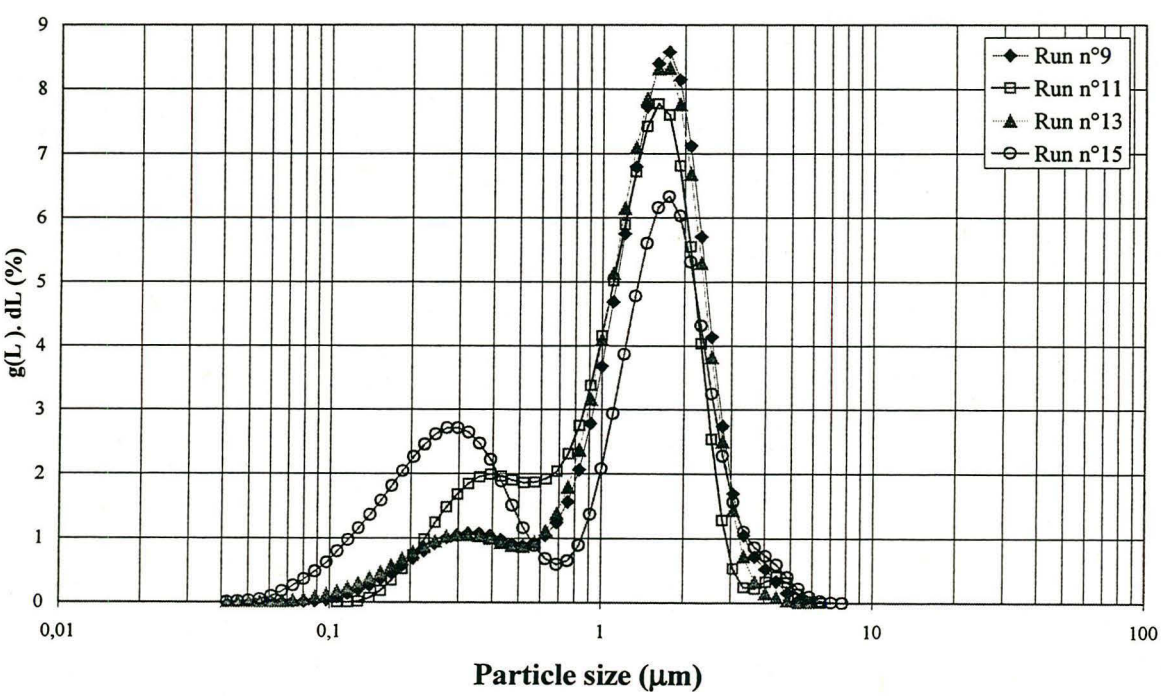

Figure A3.27 : Volume particle size distributions of runs n° 9 (low T27 and low T), n°11 (high T27 and high T), 13 (low T27 and high T) and n°15 (high T27 and high T) done with Sty/AN=60/40, S5200 = 3 wt-% and high NDM

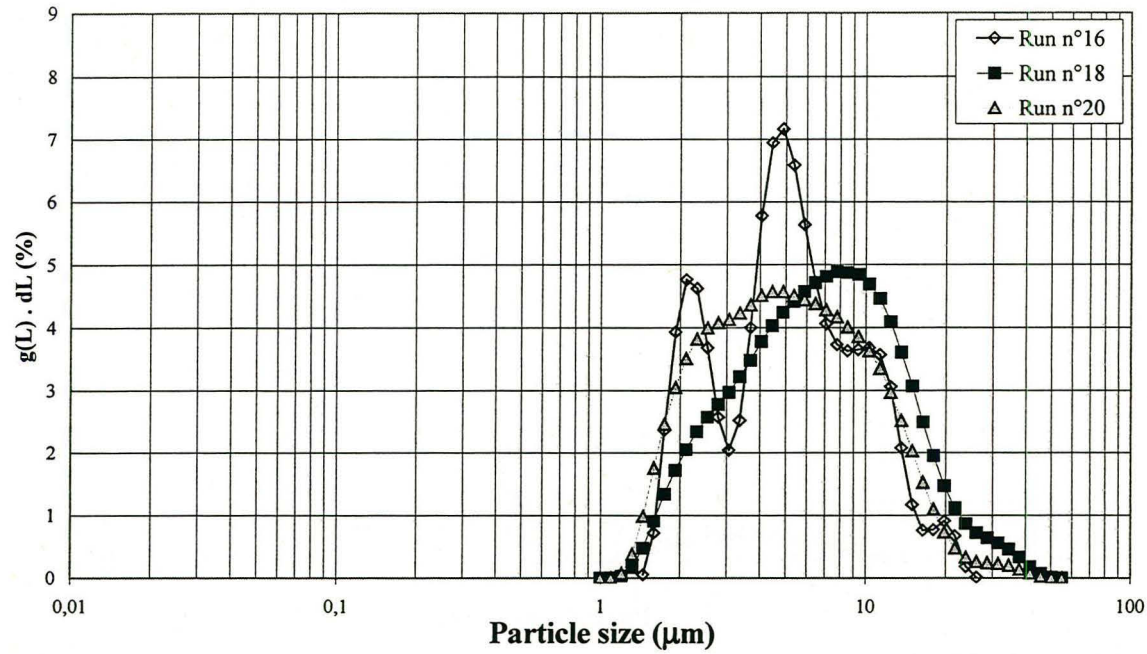

Figure A3.28 : Volume particle size distributions of runs n° 16 (high T27 and high T), n°18 (low T27 and high T) and n°20 (high T27 and high T) done with Sty/AN=80/20, S5200 = 1 wt-% and low NDM

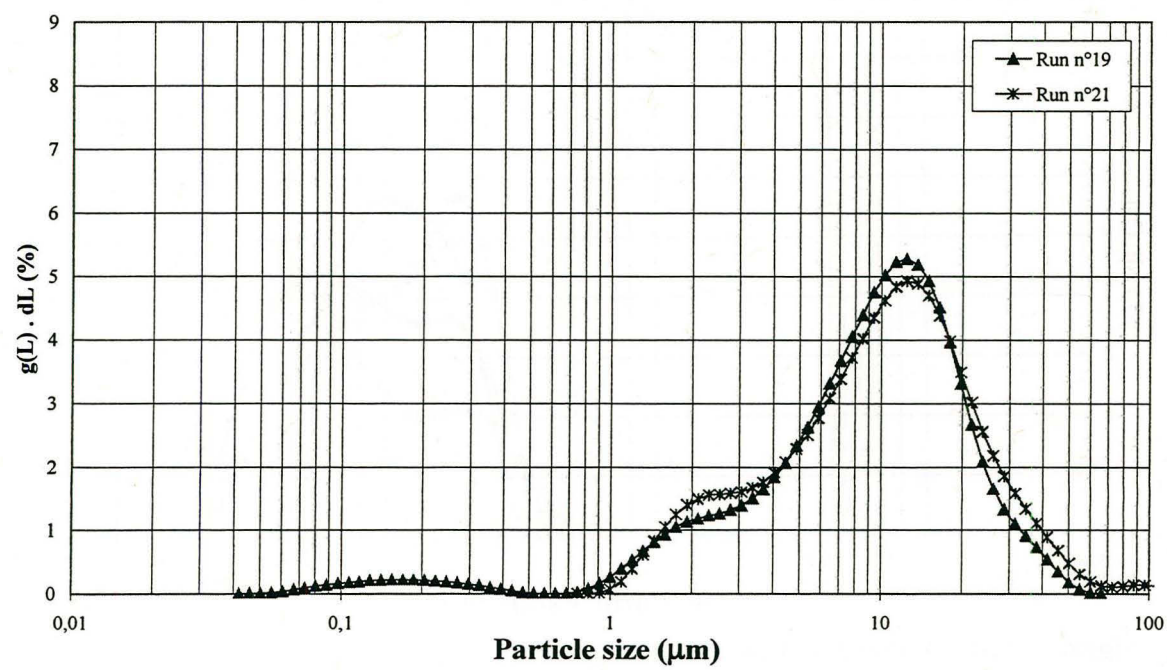

Figure A3.29 : Volume particle size distributions of runs n°19 (low T27 and high T) and n°21 (high T27 and high T) done with Sty/AN=80/20, S5200 = 1 wt-% and high NDM

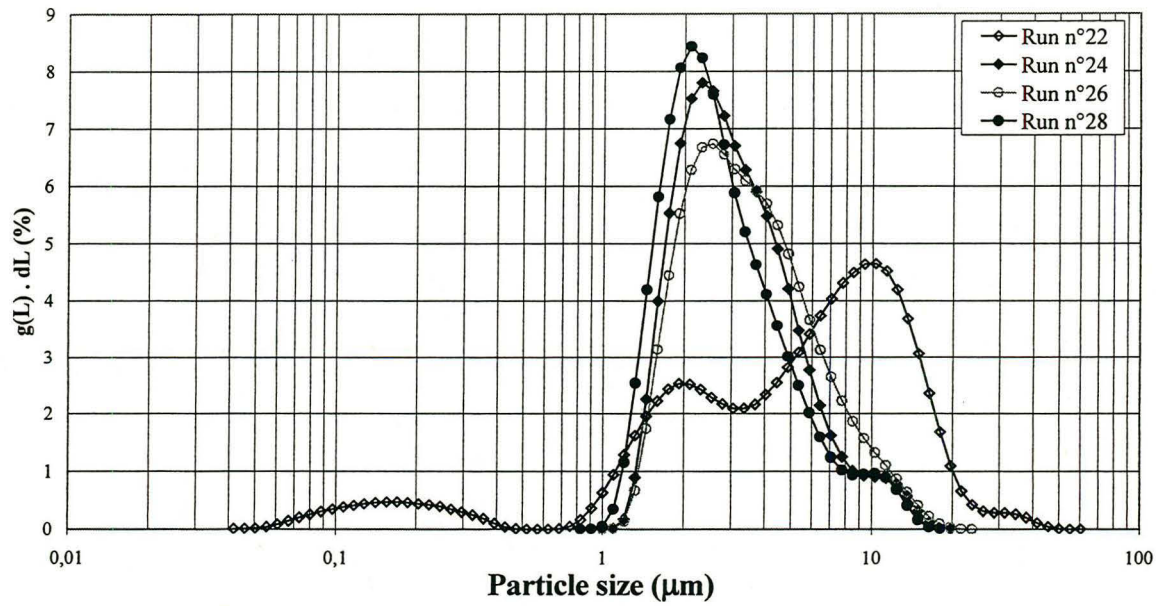

Figure A3.30 : Volume particle size distributions of runs n° 22 (low T27 and low T), n°24 (high T27 and low T), n°26 (low T27 and high T) and n°28 (high T27 and high T) done with Sty/AN=80/20, S5200 = 3 wt-% and low NDM

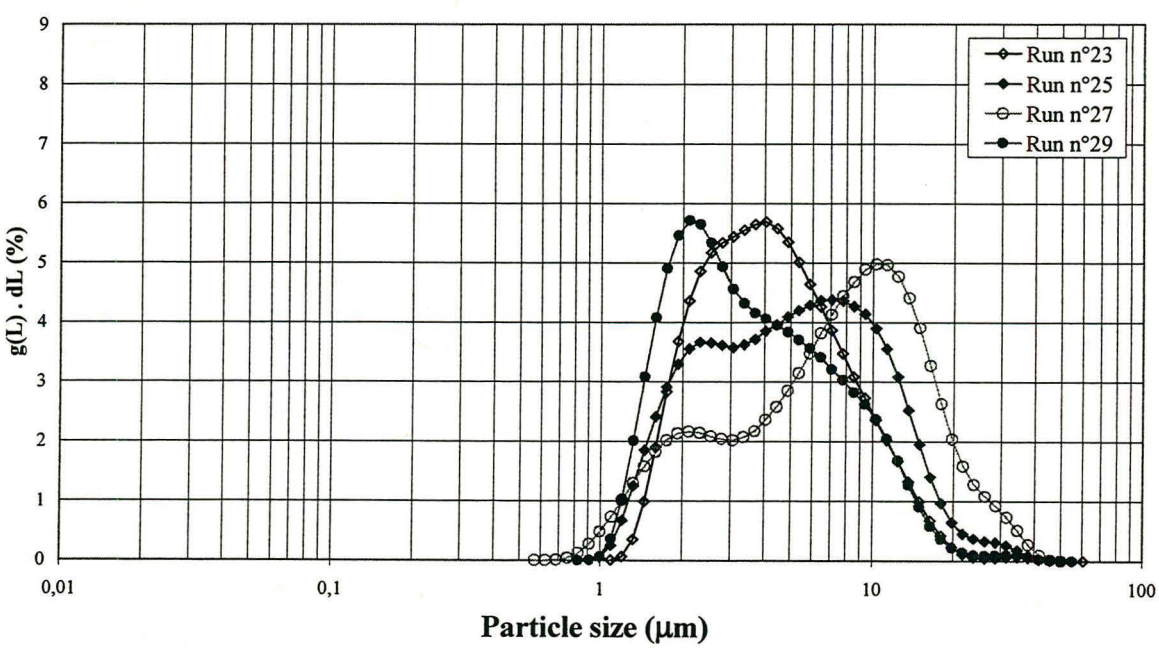

Figure A3.31 : Volume particle size distributions of runs n° 23 (low T27 and low T), n°25 (high T27 and low T), n°27 (low T27 and high T) and n°29 (high T27 and high T) done with Sty/AN=80/20, S5200 = 3 wt-% and high NDM

A3.2.4. Scanning Electron Microscopy analyses

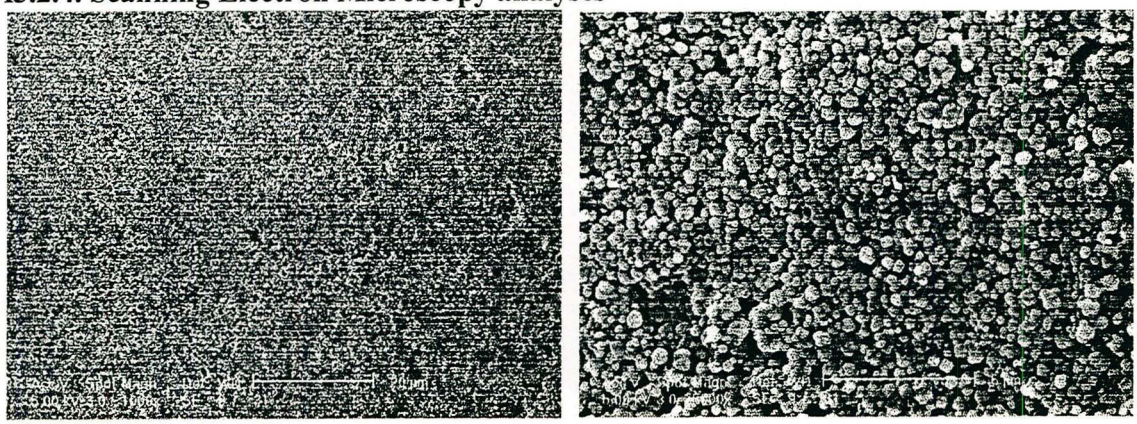

Figure A3.32 : SEM pictures and particle sizes distributions of the **run n° 4** done with low NDM (0.15 wt-%), low T27 (0.10 wt-%), high temperature (140°C), low styrene (Sty/AN = 60/40) and low S5200 (1 wt-%).

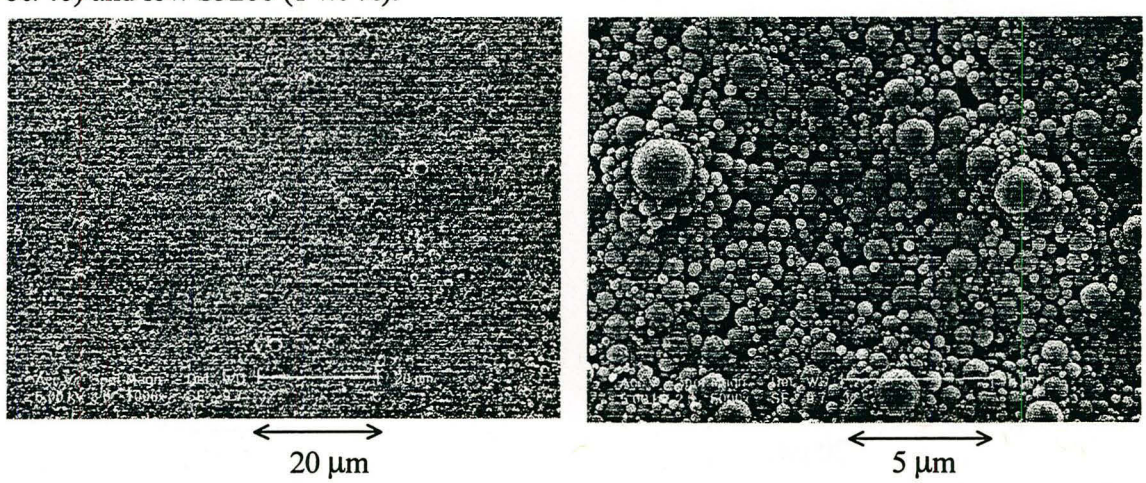

Figure A3.33 : SEM pictures and particle sizes distributions of the **run n° 5** done with high NDM (0.45 wt-%), low T27 (0.10 wt-%), high temperature (140°C), low styrene (Sty/AN = 60/40) and low S5200 (1 wt-%).

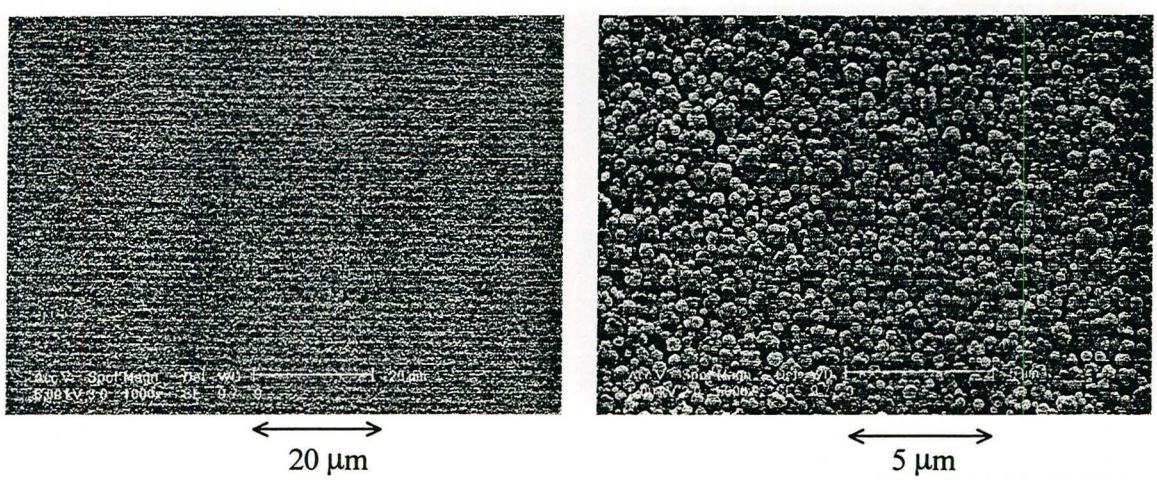

Figure A3.34 : SEM pictures and particle sizes distributions of the **run n° 10** done with low NDM (0.15 wt-%), high T27 (0.20 wt-%), low temperature (120°C), low styrene (Sty/AN = 60/40) and high S5200 (3 wt-%).

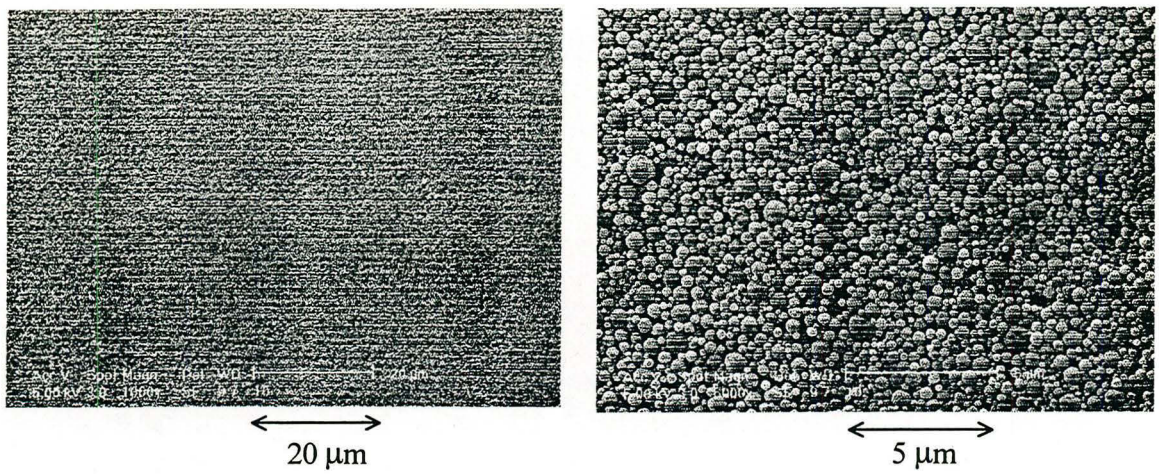

Figure A3.35 : SEM pictures and particle sizes distributions of the **run n° 11** done with high NDM (0.45 wt-%), high T27 (0.20 wt-%), low temperature (120°C), low styrene (Sty/AN = 60/40) and high S5200 (3 wt-%).

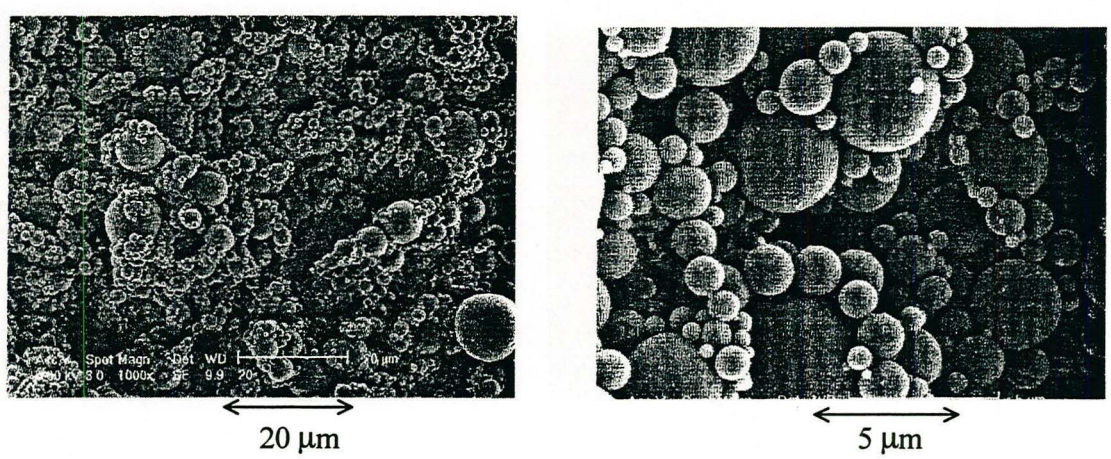

Figure A3.36 : SEM pictures and particle sizes distributions of the **run n° 18** done with low NDM (0.15 wt-%), low T27 (0.10 wt-%), high temperature (140°C), high styrene (Sty/AN = 80/20) and low S5200 (1 wt-%).

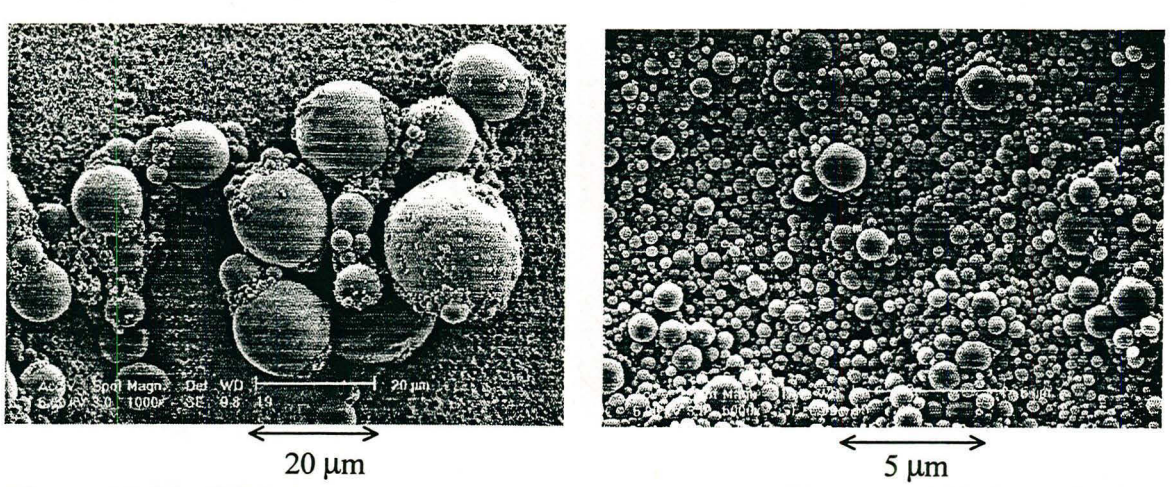

Figure A3.37 : SEM pictures and particle sizes distributions of the **run n° 19** done with high NDM (0.45 wt-%), low T27 (0.10 wt-%), high temperature (140°C), high styrene (Sty/AN = 80/20) and low S5200 (1 wt-%).

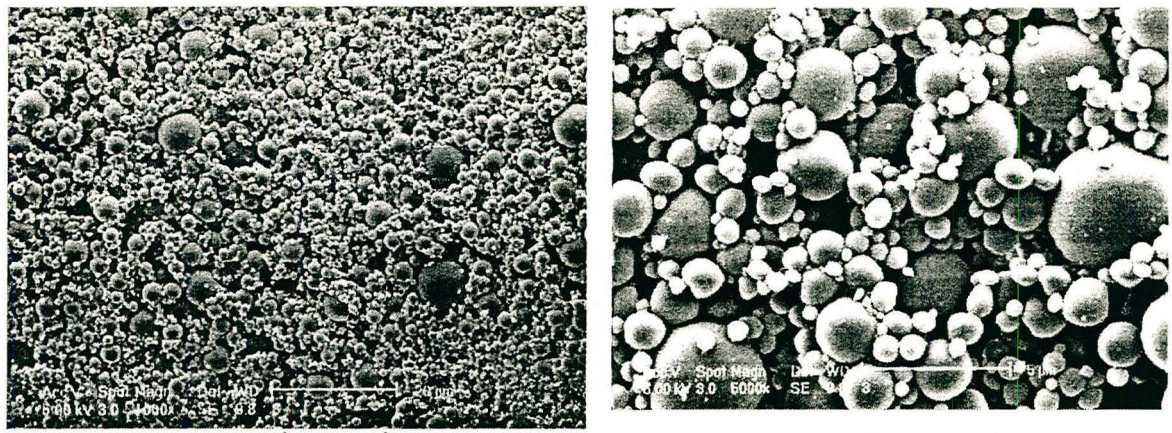

20 µm 5 µm

Figure A3.38 : SEM pictures and particle sizes distributions of the **run n° 26** done with low NDM (0.15 wt-%), low T27 (0.10 wt-%), high temperature (140°C), high styrene (Sty/AN = 80/20) and high S5200 (3 wt-%).

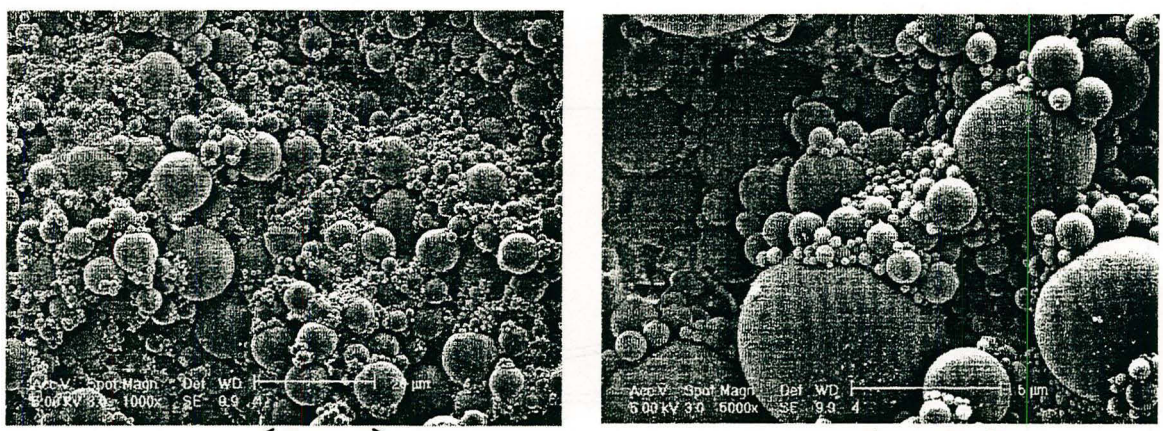

20 µm 5 µm

Figure A3.39 : SEM pictures and particle sizes distributions of the **run n° 27** done with high NDM (0.45 wt-%), low T27 (0.10 wt-%), high temperature (140°C), high styrene (Sty/AN = 80/20) and high S5200 (3 wt-%).

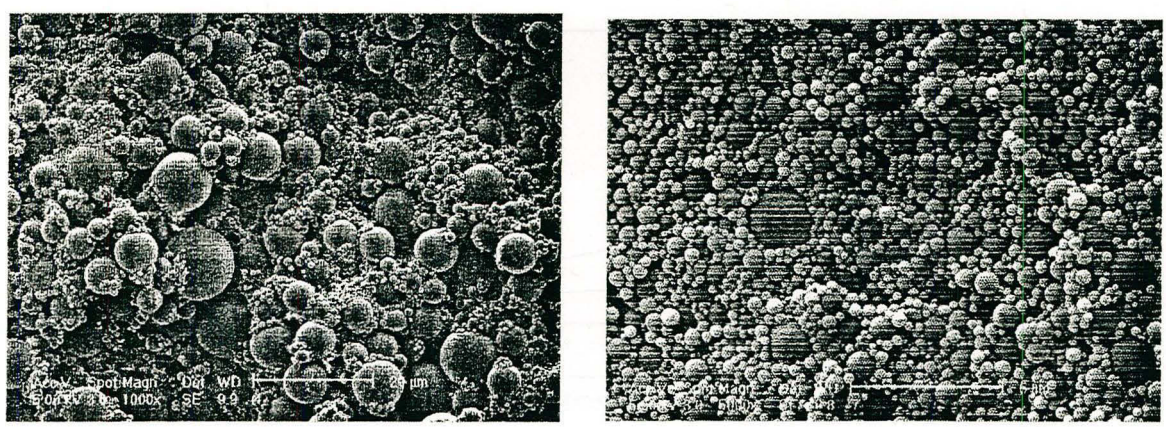

20 µm 5 µm

Figure A3.40 : SEM pictures and particle sizes distributions of the standard **run n° 31** done with high NDM = 0.30 wt-%, T27 = 0.15 wt-%, T = 130°C, Sty/AN = 70/30) and S5200 = 2 wt-%).

A3.2.5. Chromatograms from LC-UV

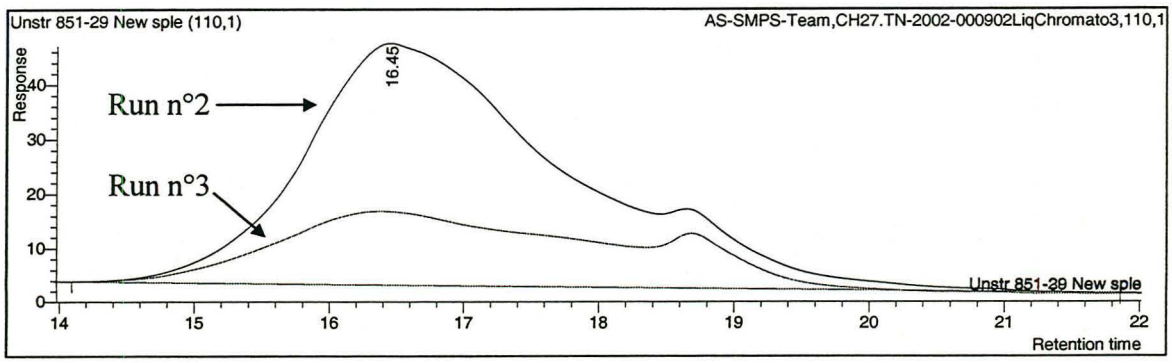

Figure A3.41 : LC-UV chromatograms of grafted SAN from samples n° 2 (low NDM) and 3 (high NDM), both at high T27, low T, low styrene and low S5200.

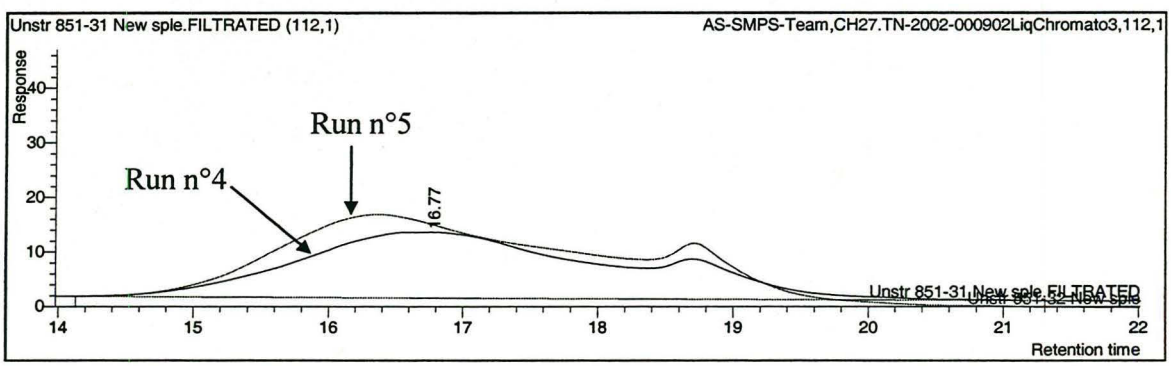

Figure A3.42 : LC-UV chromatograms of grafted SAN from samples n° 4 (low NDM) and 5 (high NDM), both at low T27, high T, low styrene and low S5200.

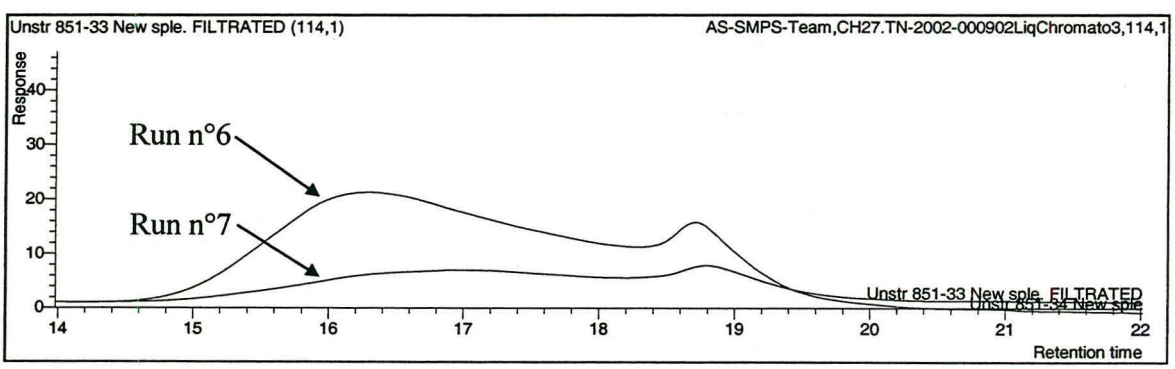

Figure A3.43 : LC-UV chromatograms of grafted SAN from samples n° 6 (low NDM) and 7 (high NDM), both at high T27, high T, low styrene and low S5200.

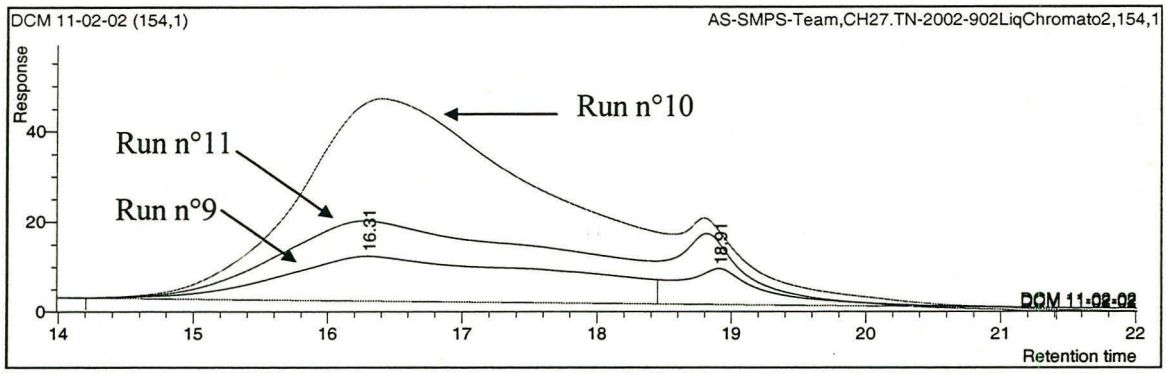

Figure A3.44 : LC-UV chromatograms of grafted SAN from samples n° 10 (low NDM, high T27), 9 (high NDM, low T27), and 11 (high NDM, high T27), all at low T, low styrene and high S5200.

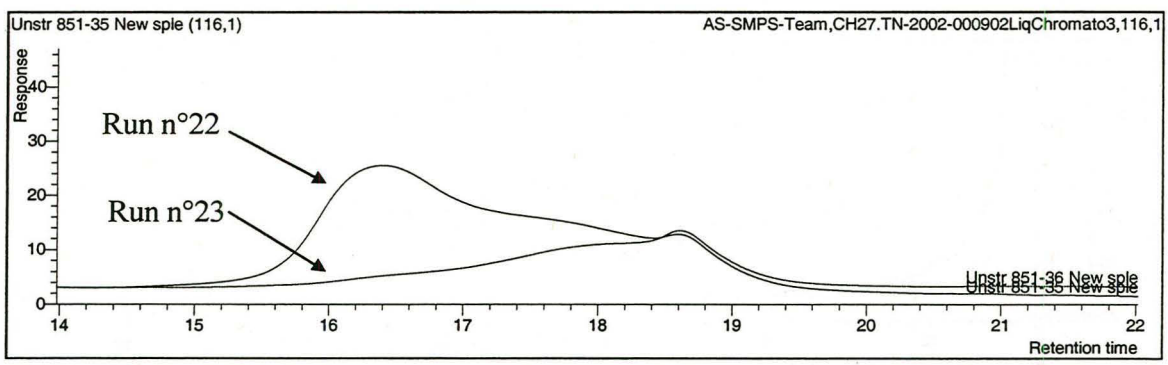

Figure A3.45 : LC-UV chromatograms of grafted SAN from samples n° 22 (low NDM) and 23 (high NDM), both at low T27, low T, high styrene and high S5200.

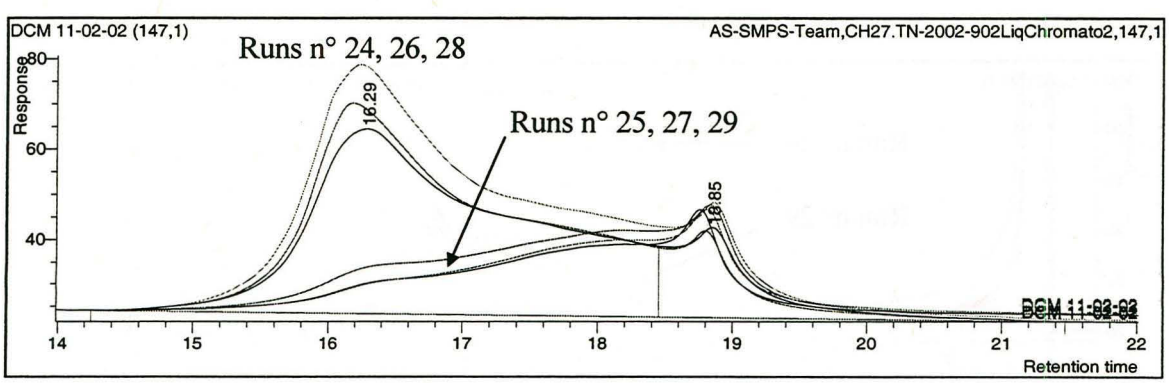

Figure A3.46 : LC-UV chromatograms of grafted SAN from samples n° 24, 26 and 28 (low NDM) and 25, 27 and 29 (high NDM), all at high styrene and high S5200.

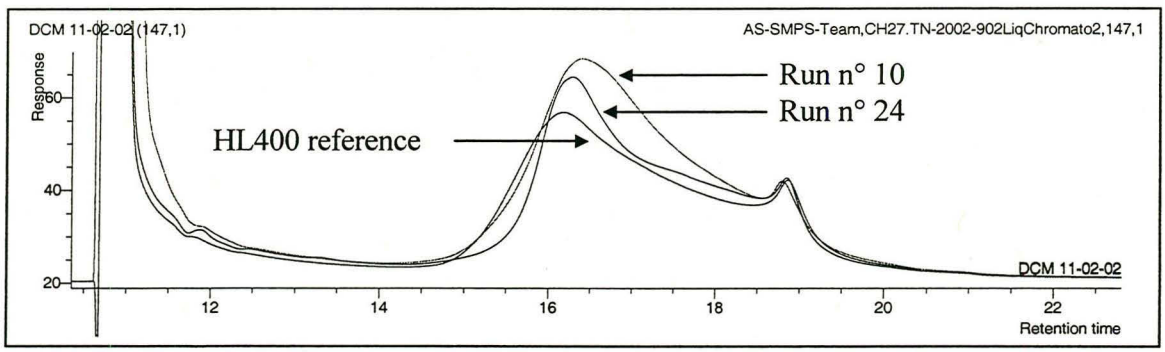

Figure A3.47 : LC-UV chromatograms of grafted SAN from samples n° 10 (low styrene) and 23 (high styrene), both at low NDM, high T27, low T and high S5200, and a sample of HL400 (Sty/AN= 60/40).

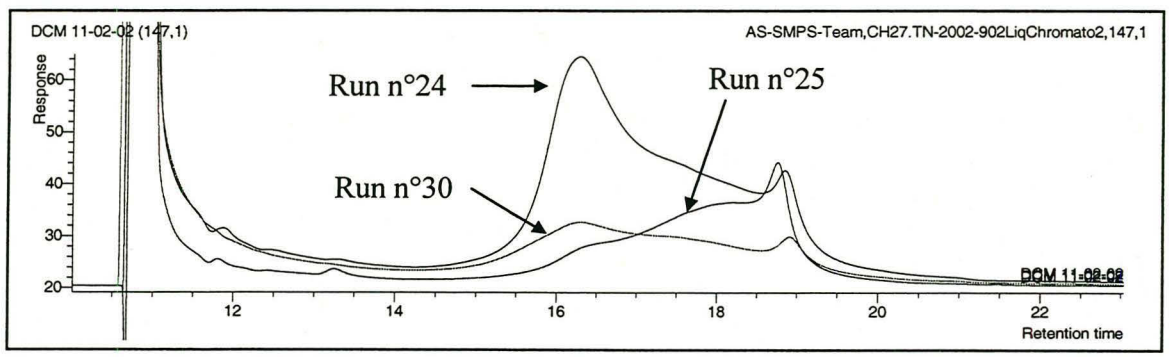

Figure A3.48 : LC-UV chromatograms of grafted SAN from samples n° 24 (low NDM, high T27, low T), 25 (high NDM, high T27, low T) and 30 (high NDM, high T27, high T), all at high styrene and high S5200.

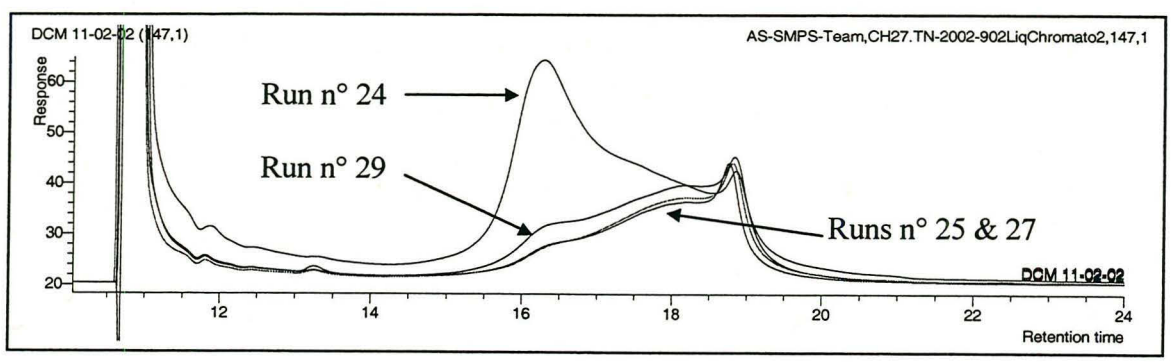

Figure A3.49 : LC-UV chromatograms of grafted SAN from samples n° 24 (low NDM, high T27, low T), 25 (high NDM, high T27, low T), 27 (high NDM, low T27, high T) and 29 (high NDM, high T27, high T), all at high styrene and high S5200.

A3.2.6. Chromatograms from NMR

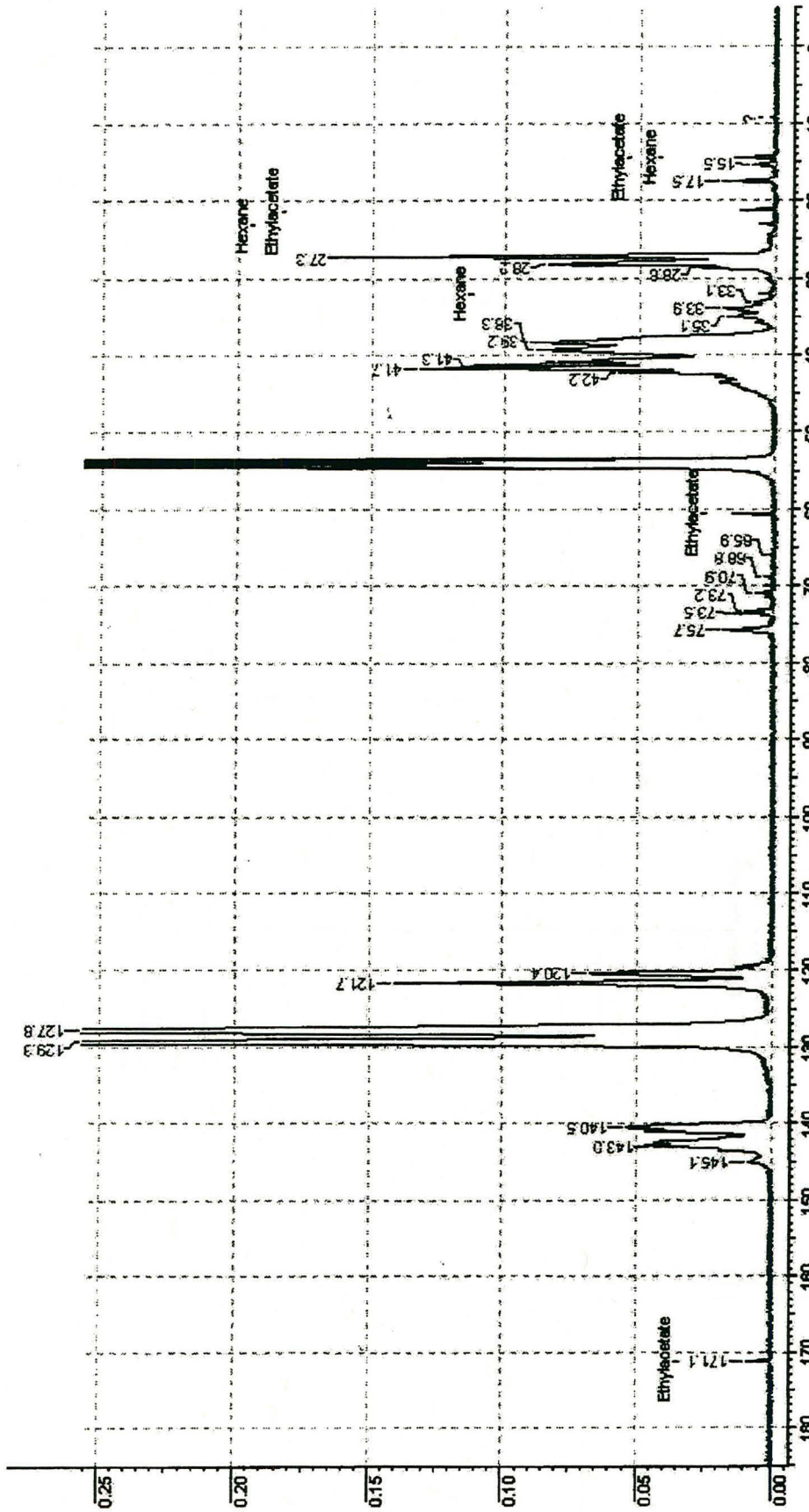

Figure A3.50 : Example of ^{13}C NMR chromatogram of solids from a sample of standard HL 400 copolymer polyol

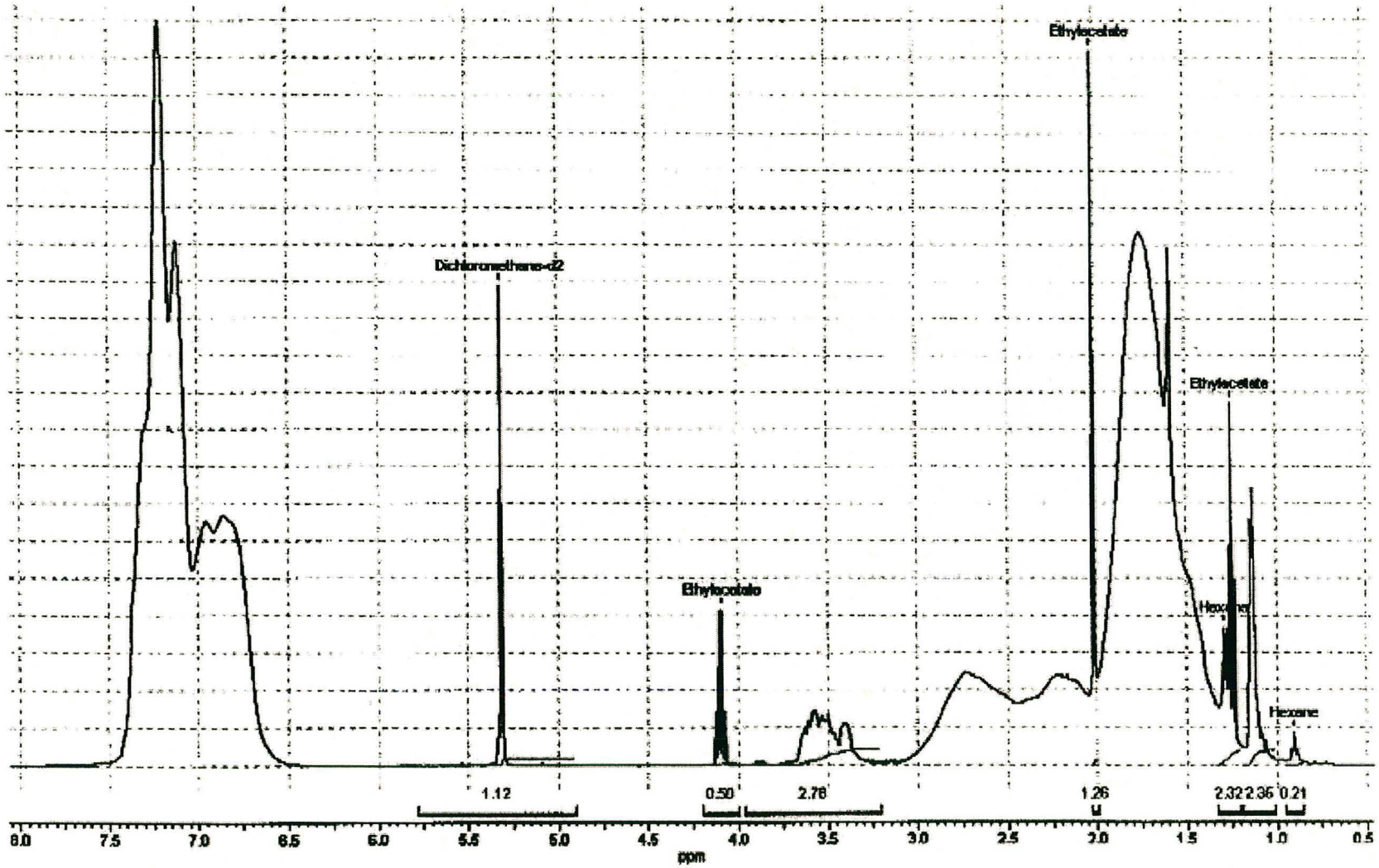

Figure A3.51 : Example of ^{1}H NMR chromatogram of solids from a sample of standard HL 400 copolymer polyol

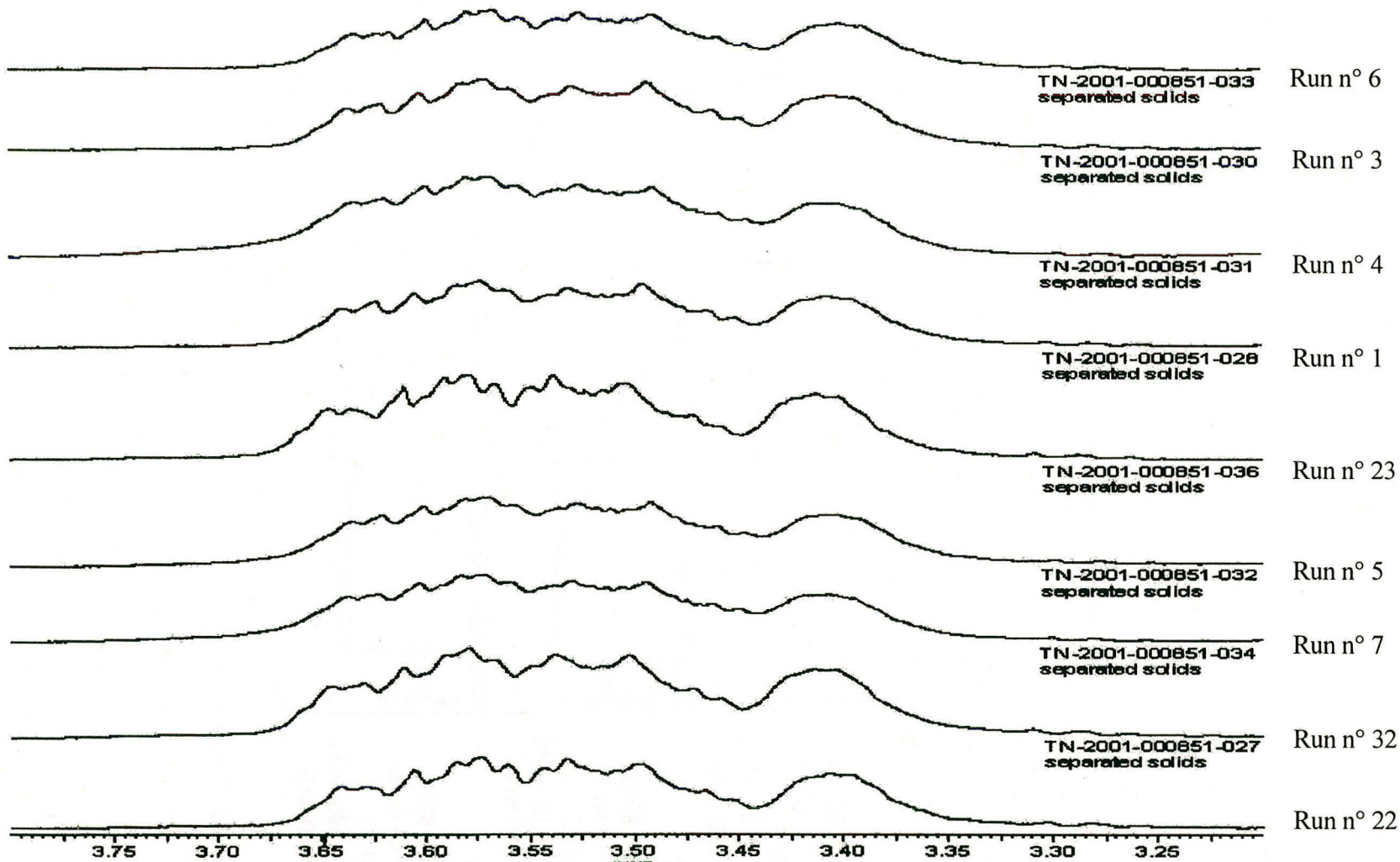

Figure A3.52 : Examples of ^{1}H NMR chromatograms of solids from CPP samples : expansion in the 3.2-3.8 ppm region of the polyol

A3.2.7. Chromatograms from NIC-derivatization followed by GPC-Fluo

Run n° 5

Sty/AN = 60/40
S5200 = 1 wt-%
T = 140 °C
NDM = 0.45 wt-%
T27 = 0.10 wt%

Run n° 6

Sty/AN = 60/40
S5200 = 1 wt-%
T = 140 °C
NDM = 0.15 wt-%
T27 = 0.20 wt%

Run n° 7

Sty/AN = 60/40
S5200 = 1 wt-%
T = 140 °C
NDM = 0.45 wt-%
T27 = 0.20 wt%

Run n° 22

Sty/AN = 80/20
S5200 = 3 wt-%
T = 120 °C
NDM = 0.15 wt-%
T27 = 0.10 wt%

Run n° 23

Sty/AN = 80/20
S5200 = 3 wt-%
T = 120 °C
NDM = 0.45 wt-%
T27 = 0.10 wt%

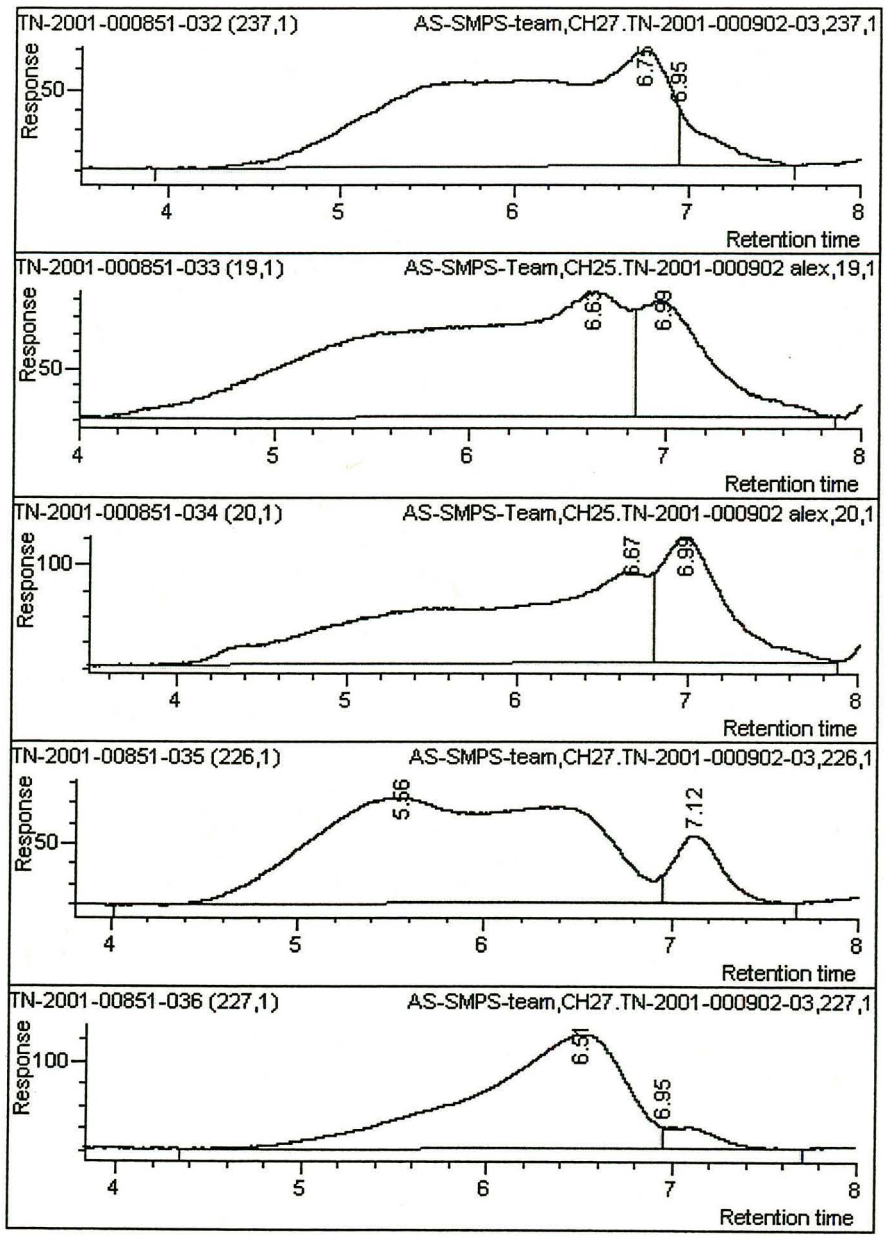

Figure A3.53 : Examples of chromatograms obtained by NIC-derivatization of solids followed by GPC-Fluorescence

A3.2.8. Molecular weight distributions of the serum phase

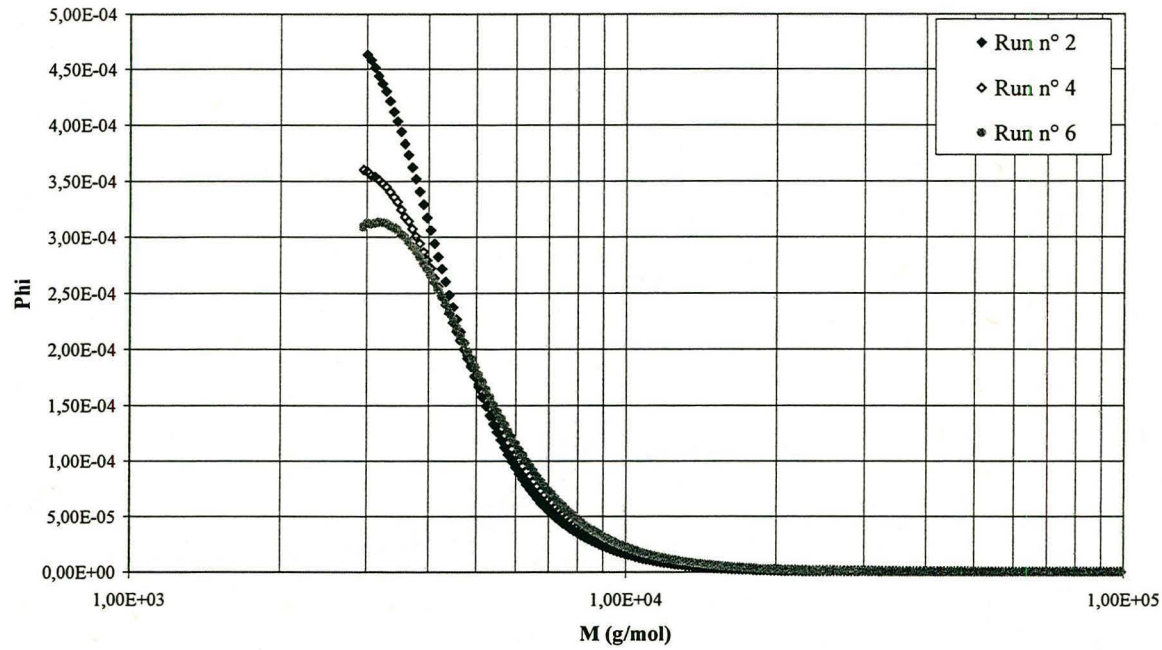

Figure A3.54 : Number molecular weight distribution of SAN polymer dissolved in serum coming from samples n°2 (high T27, low T), n° 4 (low T27, high T) and n° 6 (high T27, high T) done with Sty/AN = 60/40, S5200=1 wt-% and NDM=0.15 wt-%

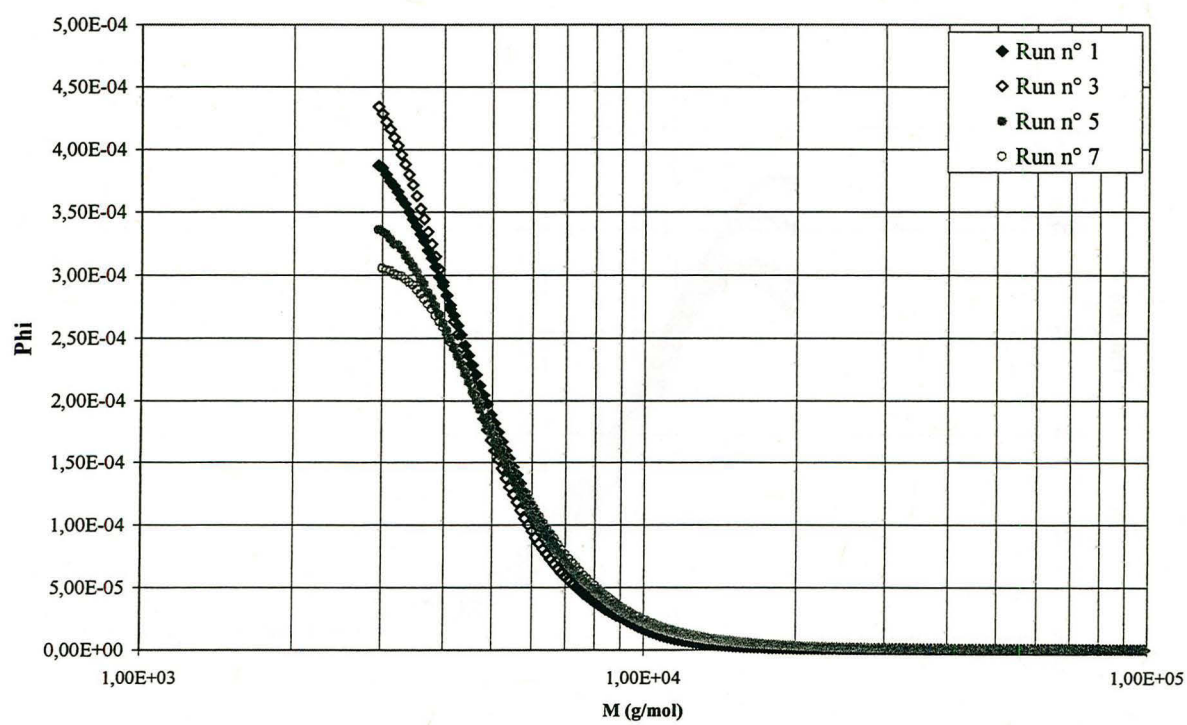

Figure A3.55 : Number molecular weight distribution of SAN polymer dissolved in serum coming from samples n°1 (low T27, low T), n°3 (high T27, low T), n° 5 (low T27, high T) and n° 7 (high T27, high T) done with Sty/AN = 60/40, S5200=1 wt-% and NDM=0.45 wt-%

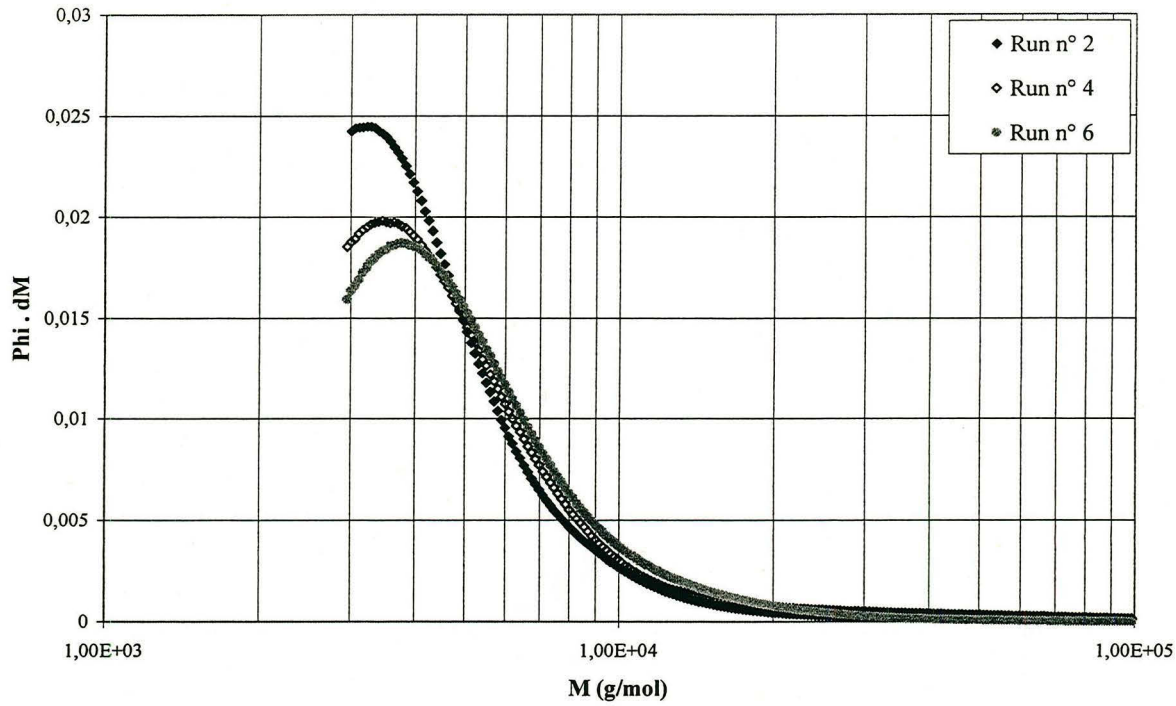

Figure A3.56 : Weight molecular weight distribution of SAN polymer dissolved in serum coming from samples n°2 (high T27, low T), n° 4 (low T27, high T) and n° 6 (high T27, high T) done with Sty/AN = 60/40, S5200=1 wt-% and NDM=0.15 wt-%

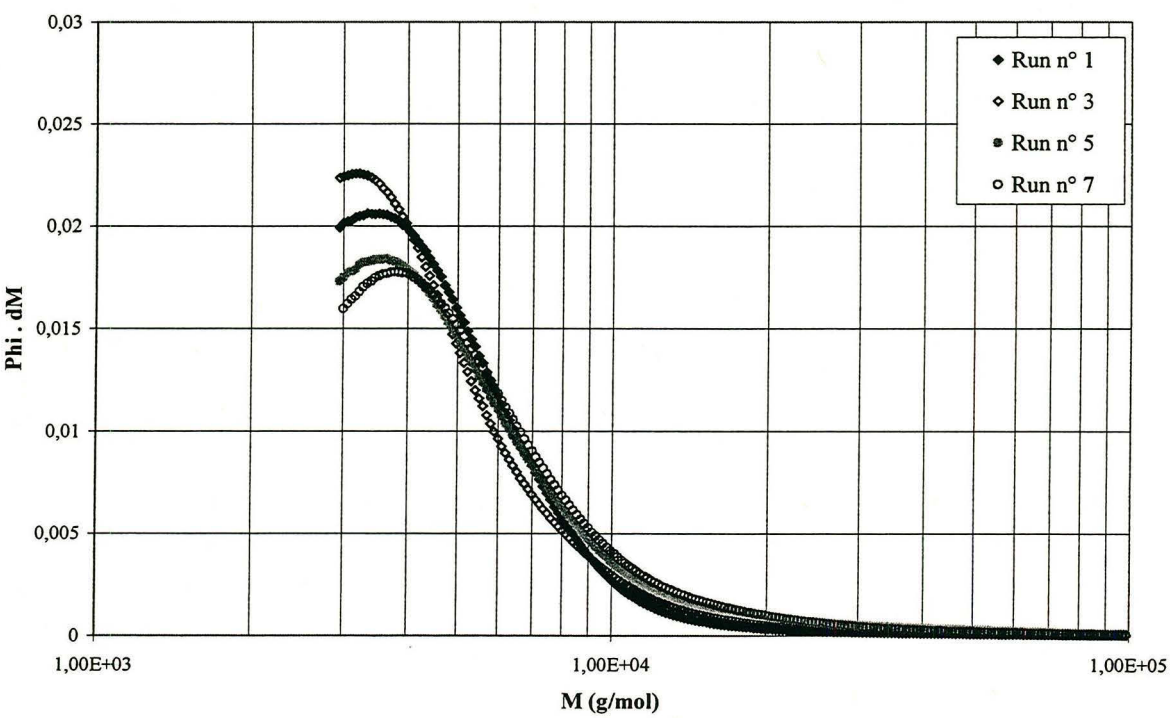

Figure A3.57 : Weight molecular weight distribution of SAN polymer dissolved in serum coming from samples n°1 (low T27, low T), n°3 (high T27, low T), n° 5 (low T27, high T) and n° 7 (high T27, high T) done with Sty/AN = 60/40, S5200=1 wt-% and NDM=0.45 wt-%

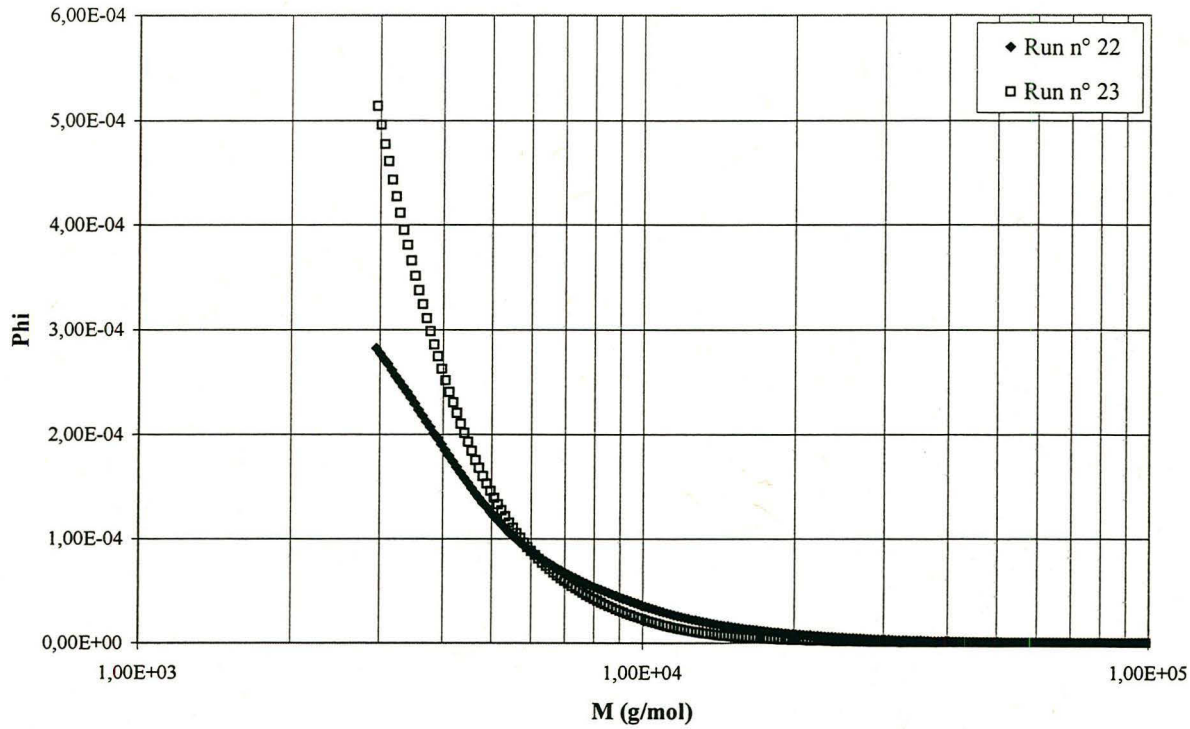

Figure A3.58 : Number molecular weight distribution of SAN polymer dissolved in serum coming from samples n°22 (low NDM), and n° 23 (high NDM) done with Sty/AN = 80/20, S5200 = 1 wt-% and T27 = 0.10 wt-%

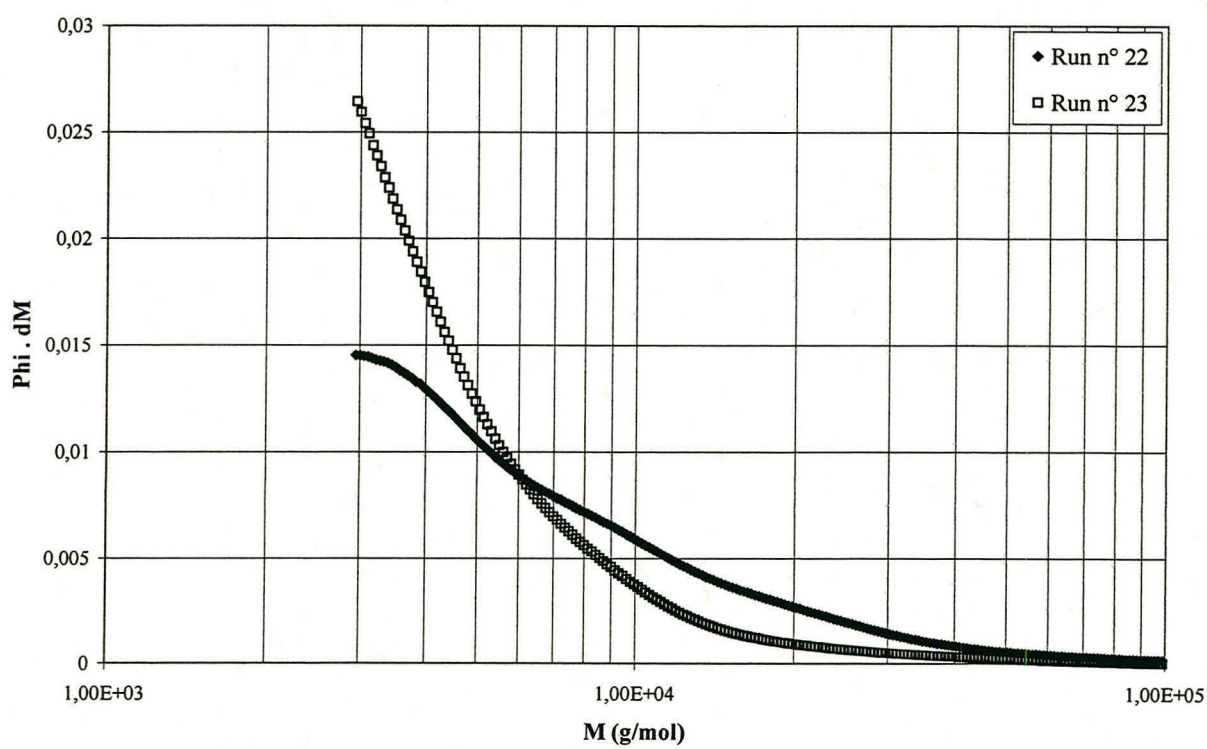

Figure A3.59 : Weight molecular weight distribution of SAN polymer dissolved in serum coming from samples n°22 (low NDM), and n° 23 (high NDM) done with Sty/AN = 80/20, S5200 = 1 wt-% and T27 = 0.10 wt-%

ANNEX 4

CALCULATIONS

A4.1 COMPLETE BALANCES DESCRIBING THE MODEL 307

A4.1.1. MONOMERIC UNITS 307
A4.1.2. DEFINITION OF DISTRIBUTIONS AND MOMENTS 310
A4.1.2.1. Distributions 310
A4.1.2.2. Moments of order one 312
A4.1.3.3. Moments of order two 313

A4.1.3 BALANCES ON RADICALS, DEAD POLYMER AND MOMENTS IN THE CONTINUOUS PHASE 313
A4.1.3.1 Balance on primary radicals R coming from initiator decomposition and transfers to NDM 313*
A4.1.3.2. Balance on activated Polyol 314
A4.1.3.3. Radicals with a terminal A and having 0 graft 314*
A4.1.3.4. Radicals with a terminal A and having one polyol graft 314*
A4.1.3.5. Radicals with a terminal A and having one S5200 graft 315*
A4.1.3.6. Radicals with a terminal B and having 0 graft 316*
A4.1.3.7. Radicals with a terminal B and having one polyol graft 317*
A4.1.3.8. Radicals with a terminal B and having one S5200 graft 318*
A4.1.3.9. Radicals with a terminal G 320*
A4.1.3.10. Balance on polymer having 0 graft 321
A4.1.3.11. Balance on polymer having one polyol graft 321
A4.1.3.12. Balance on Polymer having one S5200 graft 322

A4.1.4. BALANCE ON OLIGORADICALS, DEAD POLYMER AND MOMENTS WITHIN PARTICLES .. 323
A4.1.4.1. Balance on radicals R coming from initiator decomposition and transfers: ... 323*
A4.1.4.2. Radicals with a terminal A and having 0 graft 324*
A4.1.4.3. Radicals with a terminal A and having one polyol graft 325*
A4.1.4.4. Radicals with a terminal A and having one S5200 graft 326*
A4.1.4.5. Radicals with a terminal B and having 0 graft 327*
A4.1.4.6. Radicals with a terminal B and having one polyol graft 329*
A4.1.4.7. Radicals with a terminal B and having one S5200 graft 330*
A4.1.4.9. Balance on polymer having 0 Graft 331
A4.1.4.10. Balance on polymer having one polyol graft 332
A4.1.4.11. Balance on polymer having one S5200 graft 333

A4.2. THE GAMMA FUNCTION 334

A4.3. APPROXIMATION TO INTEGRATE DERIVATIVE EQUATIONS BETWEEN T AND T + ΔT 336

A4.1 Complete Balances describing the model

A4.1.1. Monomeric Units

The objective of using monomeric units is to estimate quickly the average molecular weights.

Indeed, let us consider $\left[A^*_{k,l,j}\right]$, the concentration of oligoradicals with a terminal A* and having k acrylonitrile units, l styrene units and j graft units, and $\left[A^*_T\right]$, the total concentration of oligoradicals with a terminal A*, the following ratio is therefore defined :

$$\Delta_{k,l,j} = \left[A^*_{k,l,j}\right] / \left[A^*_T\right], \tag{A4.1}$$

$$\text{where } \left[A^*_T\right] = \sum_{k,l,j} \left[A^*_{k,l,j}\right]. \tag{A4.2}$$

For instance, if we consider the oligoradicals with a terminal A*, the molecular weight of the species having k acrylonitrile units, l styrene units, and j graft units is the following :

$$M\left(A^*_{k,l,j}\right) = k\,M_A + l\,M_B + j\,M_S. \tag{A4.3}$$

Therefore, the number-average molecular weight of all the oligoradicals with a terminal A* is :

$$\bar{M}_n\left(A^*_T\right) = \sum_{k,l,j} \left(k\,M_A + l\,M_B + j\,M_S\right)\Delta_{k,l,j}. \tag{A4.4}$$

Then, the weight-average molecular weight of all the oligoradicals with a terminal A* is :

$$\bar{M}_w\left(A^*_T\right) = \sum_{k,l,j} \left(k\,M_A + l\,M_B + j\,M_S\right)^2 \Delta_{k,l,j} \Big/ \bar{M}_n\left(A^*_T\right). \tag{A4.5}$$

It will be shown below that $\bar{M}_n$ and $\bar{M}_w$ can be estimated using monomeric units. Indeed, it has been seen in chapter 4 (paragraph 1.2) that it is possible to write the molecular weight of the monomeric unit as follows :

$$M_u = \frac{[A_P]M_A + [B_P]M_B}{[A_P] + 2[B_P]}. \tag{A4.6}$$

$$\text{with } \left[A_P\right] = \sum_{k,l,j} k\left(\left[A^*_T\right]\Delta_{k,l,j} + \left[B^*_T\right]\Gamma_{k,l,j} + \left[G^*_T\right]\Pi_{k,l,j} + \left[P_T\right]\Omega_{k,l,j}\right), \tag{A4.7}$$

$$\text{and } \left[B_P\right] = \sum_{k,l,j} l\left(\left[A^*_T\right]\Delta_{k,l,j} + \left[B^*_T\right]\Gamma_{k,l,j} + \left[G^*_T\right]\Pi_{k,l,j} + \left[P_T\right]\Omega_{k,l,j}\right). \tag{A4.8}$$

Γ, Π and Ω have the same definition as Δ (Eq. A4.1 and A4.2) replacing A by B, G and P (respectively oligoradicals with a terminal B*, and G* and the dead polymer).

Lemma I demonstrates that this definition is usable.

Lemma I : $M_B/2 \le M_u \le M_A$ (A4.9)

Proof :

$$M_A - M_u = \frac{[A_P]M_A + 2M_A[B_P] - [A_P]M_A - [B_P]M_B}{[A_P] + 2[B_P]} = \frac{(2M_A - M_B)[B_P]}{[A_P] + 2[B_P]} \ge 0 \quad \text{(A4.10)}$$

$$M_u - M_B/2 = \frac{[A_P]M_A + M_B[B_P] - [A_P]M_B/2 - [B_P]M_B}{[A_P] + 2[B_P]} = \frac{(2M_A - M_B)[A_P]}{2([A_P] + 2[B_P])} \ge 0 \quad \text{(A4.11)}$$

The approximated number-average molecular weight of the oligoradicals with a terminal A* is defined by :

$$\bar{M}_n(A_T^*) = \sum_{k,l,j} ((k+2l)M_u + jM_S)\Delta_{k,l,j} \quad \text{(A4.12)}$$

Therefore the error is :

$$e_\Delta = \sum_{k,l,j} [k(M_A - M_u) + l(M_B - 2M_u)]\Delta_{k,l,j} . \quad \text{(A4.13)}$$

Lemma II allows to neglect this error on all the species.

Lemma II : $[A_T^*]e_\Delta + [B_T^*]e_\Gamma + [G_T^*]e_\Pi + [P_T]e_\Omega = 0$ (A4.14)

Proof :

$[A_T^*], [B_T^*], [G_T^*]$ and $[P_T]$ are the total concentrations of oligoradicals with a terminal A*, B*, G* and of dead polymers respectively, and e_Δ, e_Γ, e_Π and e_Ω are the respective corresponding errors related to the use of the monomeric unit.

Using Eq. A4.7 and A4.8 in the definition of M_u (Eq. A4.6), we can write :

$$\sum_{k,l,j} (kM_A + lM_B)([A_T^*]\Delta_{k,l,j} + [B_T^*]\Gamma_{k,l,j} + [G_T^*]\Pi_{k,l,j} + [P_T]\Omega_{k,l,j}) = M_u \sum_{k,l,j} (k+2l)([A_T^*]\Delta_{k,l,j} + [B_T^*]\Gamma_{k,l,j} + [G_T^*]\Pi_{k,l,j} + [P_T]\Omega_{k,l,j}) . \quad \text{(A4.15)}$$

$$\sum_{k,l,j} (k(M_A - M_u) + l(M_B - 2M_u))([A_T^*]\Delta_{k,l,j} + [B_T^*]\Gamma_{k,l,j} + [G_T^*]\Pi_{k,l,j} + [P_T]\Omega_{k,l,j}) = 0 \quad \text{(A4.16)}$$

Using Eq. A4.13, Eq. A4.16 gives Eq. A4.14.

Now, it is necessary to check that the error on the approximation of the weight-average molecular weight is also negligible.

Lemma III : It is possible to calculate the weight-average molecular weight of oligoradicals with a terminal A* using M_u with a small error.

Proof :

$$\bar{M}_w\left(A_T^*\right)=\sum_{k,l,j}\left(kM_A+lM_B+jM_S\right)^2\Delta_{k,l,j}\Big/\bar{M}_n\left(A_T^*\right)$$

$$\bar{M}_w\left(A_T^*\right)\bar{M}_n\left(A_T^*\right)=\sum_{k,l,j}\left(kM_A+lM_B\right)^2\Delta_{k,l,j}+\sum_{k,l,j}2jM_S\left(kM_A+lM_B\right)\Delta_{k,l,j}+\sum_{k,l,j}j^2M_S^2\Delta_{k,l,j}$$

$$=\sum_{k,l,j}\left(kM_A+lM_B-(k+2l)M_u\right)^2\Delta_{k,l,j}+\sum_{k,l,j}2jM_S\left(kM_A+lM_B-(k+2l)M_u\right)\Delta_{k,l,j}$$

$$+\sum_{k,l,j}j^2M_S^2\Delta_{k,l,j}-\sum_{k,l,j}(k+2l)^2M_u^2\Delta_{k,l,j}+2\sum_{k,l,j}\left(kM_A+lM_B\right)(k+2l)M_u\Delta_{k,l,j}$$

$$+\sum_{k,l,j}2jM_S(k+2l)M_u\Delta_{k,l,j}$$

$$=\sum_{k,l,j}\left(k(M_A-M_u)+l(M_B-2M_u)\right)^2\Delta_{k,l,j}+2M_S\sum_{k,l,j}j\left(k(M_A-M_u)+l(M_B-2M_u)\right)\Delta_{k,l,j}$$

$$+M_S^2\sum_{k,l,j}j^2\Delta_{k,l,j}+M_u^2\sum_{k,l,j}(k+2l)^2\Delta_{k,l,j}+2M_u\sum_{k,l,j}\left(kM_A+lM_B-(k+2l)M_u\right)(k+2l)\Delta_{k,l,j}$$

$$+2M_SM_u\sum_{k,l,j}j(k+2l)\Delta_{k,l,j}$$

$$=M_S^2\sum_{k,l,j}j^2\Delta_{k,l,j}+M_u^2\sum_{k,l,j}(k+2l)^2\Delta_{k,l,j}+2M_SM_u\sum_{k,l,j}j(k+2l)\Delta_{k,l,j}$$

$$+\sum_{k,l,j}\left(k(M_A-M_u)+l(M_B-2M_u)\right)^2\Delta_{k,l,j}+2M_S\sum_{k,l,j}j\left(k(M_A-M_u)+l(M_B-2M_u)\right)\Delta_{k,l,j}$$

$$+2M_u\sum_{k,l,j}(k+2l)\left(k(M_A-M_u)+l(M_B-2M_u)\right)\Delta_{k,l,j}\qquad\text{(A4.17)}$$

The estimated weight-average molecular weight of oligoradicals with a terminal A* is :

$$\bar{M}_w\left(A_T^*\right)=\left(M_S^2\sum_{k,l,j}j^2\Delta_{k,l,j}+M_u^2\sum_{k,l,j}(k+2l)^2\Delta_{k,l,j}+2M_SM_u\sum_{k,l,j}j(k+2l)\Delta_{k,l,j}\right)\Big/\bar{M}_n\left(A_T^*\right)\qquad\text{(A4.18)}$$

The error is related to :

$$k(M_A-M_u)+l(M_B-2M_u),\qquad\text{(A4.19)}$$

which is considered to be small considering lemma II.

The variable change defined by Eq. 4.19 of chapter 4 (paragraph 1.2) is therefore possible :

$$\Delta_{i,j}=\sum_{\substack{k,l\\ i=k+2l}}\Delta_{k,l,j}\qquad\text{(A4.20)}$$

A4.1.2. Definition of Distributions and Moments

A4.1.2.1. Distributions

We define, considering the variable change, $\Delta_{i,j}$, the ratio of the number of oligoradicals with a terminal A* containing i monomeric units and j graft units over the total number of oligoradicals with a terminal A* and the same number of graft units. These oligoradicals can have 0, 1 or 3 graft units, depending of the grafting.

In the continuous phase :

$$\left[A^*_{i,0}\right]_c = \left[A^*_{T,0}\right]_c \Delta^c_{i,0}, \tag{A4.21}$$

$$\left[A^*_{i,3}\right]_c = \left[A^*_{T,3}\right]_c \Delta^c_{i,3} \tag{A4.22}$$

$$\text{and } \left[A^*_{i,1}\right]_c = \left[A^*_{T,1}\right]_c \Delta^c_{i,1} \tag{A4.23}$$

where $\left[A^*_{T,0}\right]_c$, $\left[A^*_{T,3}\right]_c$ and $\left[A^*_{T,1}\right]_c$ are the total concentrations of oligoradicals with a terminal A* having zero, one S5200 graft or one polyol graft in the continuous phase, and where :

$$\sum_{i=1}^{\infty} \Delta^c_{i,0} = 1, \sum_{i=1}^{\infty} \Delta^c_{i,3} = 1 \text{ and } \sum_{i=1}^{\infty} \Delta^c_{i,1} = 1. \tag{A4.24}$$

Within particles :

$$\left[A^*_{i,0}\right]_p = \left[A^*_{T,0}\right]_p \Delta^p_{i,0}, \tag{A4.25}$$

$$\left[A^*_{i,3}\right]_p = \left[A^*_{T,3}\right]_p \Delta^p_{i,3} \tag{A4.26}$$

$$\text{and } \left[A^*_{i,1}\right]_p = \left[A^*_{T,1}\right]_p \Delta^p_{i,1} \tag{A4.27}$$

where $\left[A^*_{T,0}\right]_p$, $\left[A^*_{T,3}\right]_p$ and $\left[A^*_{T,1}\right]_p$ are the total concentrations of oligoradicals with a terminal A* having zero graft, one graft S5200 or one graft polyol within particles, and where

$$\sum_{i=1}^{\infty} \Delta^p_{i,0} = 1, \sum_{i=1}^{\infty} \Delta^p_{i,3} = 1 \text{ and } \sum_{i=1}^{\infty} \Delta^p_{i,1} = 1. \tag{A4.28}$$

We define $\Gamma_{i,j}$, the ratio of the number of oligoradicals with a terminal B* containing i monomeric units and j graft units over the total number of oligoradicals with a terminal B* termination and the same number of graft units :

In the continuous phase :

$$\left[B^*_{i,0}\right]_c = \left[B^*_{T,0}\right]_c \Gamma^c_{i,0}, \tag{A4.29}$$

$$\left[B^*_{i,3}\right]_c = \left[B^*_{T,3}\right]_c \Gamma^c_{i,3} \tag{A4.30}$$

$$\text{and } \left[B^*_{i,1}\right]_c = \left[B^*_{T,1}\right]_c \Gamma^c_{i,1} \tag{A4.31}$$

where $\left[B^*_{T,0}\right]_c$, $\left[B^*_{T,3}\right]_c$ and $\left[B^*_{T,1}\right]_c$ are the total concentrations of oligoradicals with a terminal B* having zero graft, one graft S5200 or one graft polyol, and where

$$\sum_{i=2}^{\infty}\Gamma_{i,0}^{c}=1,\ \sum_{i=2}^{\infty}\Gamma_{i,3}^{c}=1 \text{ and } \sum_{i=2}^{\infty}\Gamma_{i,1}^{c}=1. \tag{A4.32}$$

Within particles :

$$\left[B_{i,0}^{*}\right]_{p}=\left[B_{T,0}^{*}\right]_{p}\ \Gamma_{i,0}^{p}, \tag{A4.33}$$

$$\left[B_{i,3}^{*}\right]_{p}=\left[B_{T,3}^{*}\right]_{p}\ \Gamma_{i,3}^{p} \tag{A4.34}$$

$$\text{and } \left[B_{i,1}^{*}\right]_{p}=\left[B_{T,1}^{*}\right]_{p}\ \Gamma_{i,1}^{p} \tag{A4.35}$$

where $\left[B_{T,0}^{*}\right]_{p}$, $\left[B_{T,3}^{*}\right]_{p}$ and $\left[B_{T,1}^{*}\right]_{p}$ are the total concentrations of oligoradicals with a terminal B* having zero graft, one graft S5200 or one graft polyol, and where

$$\sum_{i=2}^{\infty}\Gamma_{i,0}^{p}=1,\ \sum_{i=2}^{\infty}\Gamma_{i,3}^{p}=1 \text{ and } \sum_{i=2}^{\infty}\Gamma_{i,1}^{p}=1. \tag{A4.36}$$

We define $\Pi_{i,j}$, the ratio of the number of oligoradicals with a terminal G* and containing i monomeric units and j graft units over the total number of oligoradicals with a terminal G* and the same number of graft units :

In the continuous phase :

$$\left[G_{i,3}^{*}\right]_{c}=\left[G_{T,3}^{*}\right]_{c}\ \Pi_{i,3}^{c} \tag{A4.37}$$

where $\left[G_{T,3}^{*}\right]_{c}$ is the total concentration of oligoradicals with a terminal G* and having one S5200 graft, and where

$$\sum_{i=0}^{\infty}\Pi_{i,3}^{c}=1\ . \tag{A4.38}$$

Within particles :

$$\left[G_{i,3}^{*}\right]_{p}=\left[G_{T,3}^{*}\right]_{p}\ \Pi_{i,3}^{p} \tag{A4.39}$$

where $\left[G_{T,3}^{*}\right]_{p}$ is the total concentrations of oligoradicals with a terminal G* having one S5200 graft, and where

$$\sum_{i=0}^{\infty}\Pi_{i,3}^{p}=1. \tag{A4.40}$$

We define $\Omega_{i,j}$, the ratio of the number of dead polymer chains containing i monomeric units and j graft units over the total number of dead polymer chains and the same number of graft units :

In the continuous phase :

$$\left[P_{i,0}\right]_{c}=\left[P_{T,0}\right]_{c}\ \Omega_{i,0}^{c}, \tag{A4.41}$$

$$\left[P_{i,1}\right]_c = \left[P_{T,1}\right]_c \, \Omega^c_{i,1} \tag{A4.42}$$

$$\text{and } \left[P_{i,3}\right]_c = \left[P_{T,3}\right]_c \, \Omega^c_{i,3} \tag{A4.43}$$

where $\left[P_{T,0}\right]_c$, $\left[P_{T,1}\right]_c$ and $\left[P_{T,3}\right]_c$ are the total concentrations of polymers having zero graft, one S5200 graft or one polyol graft, and where

$$\sum_{i=1}^{\infty} \Omega^c_{i,0} = 1, \; \sum_{i=1}^{\infty} \Omega^c_{i,1} = 1 \text{ and } \sum_{i=1}^{\infty} \Omega^c_{i,3} = 1. \tag{A4.44}$$

Within particles :

$$\left[P_{i,0}\right]_p = \left[P_{T,0}\right]_p \, \Omega^p_{i,0}, \tag{A4.45}$$

$$\left[P_{i,1}\right]_p = \left[P_{T,1}\right]_p \, \Omega^p_{i,1} \tag{A4.46}$$

$$\text{and } \left[P_{i,3}\right]_p = \left[P_{T,3}\right]_p \, \Omega^p_{i,3} \tag{A4.47}$$

where $\left[P_{T,0}\right]_p$, $\left[P_{T,1}\right]_p$ and $\left[P_{T,3}\right]_p$ are the total concentrations of polymers having zero graft, one S5200 graft or one polyol graft, and where

$$\sum_{i=1}^{\infty} \Omega^c_{i,0} = 1, \; \sum_{i=1}^{\infty} \Omega^c_{i,1} = 1 \text{ and } \sum_{i=1}^{\infty} \Omega^c_{i,3} = 1. \tag{A4.48}$$

A4.1.2.2. Moments of order one

The moments of order one are the mean number of monomeric units in the oligoradicals with a terminal A*, B*, G* and in the dead polymer chains (all classified as a function of their type of grafts) and they were then defined below, respectively :

In the continuous phase,

$$\lambda^c_{1,0} = \sum_{i=1}^{\infty} \left(i\Delta^c_{1,0}\right), \; \lambda^c_{1,3} = \sum_{i=1}^{\infty} \left(i\Delta^c_{1,3}\right) \text{ and } \lambda^c_{1,1} = \sum_{i=1}^{\infty} \left(i\Delta^c_{1,1}\right), \tag{A4.49}$$

$$\eta^c_{1,0} = \sum_{i=2}^{\infty} \left(i \; \Gamma^c_{1,0}\right), \; \eta^c_{1,3} = \sum_{i=2}^{\infty} \left(i \; \Gamma^c_{1,3}\right) \text{ and } \eta^c_{1,1} = \sum_{i=2}^{\infty} \left(i \; \Gamma^c_{1,1}\right), \tag{A4.50}$$

$$\nu^c_{1,3} = \sum_{i=0}^{\infty} \left(i \; \Pi^c_{1,3}\right), \tag{A4.51}$$

$$\mu^c_{1,0} = \sum_{i=1}^{\infty} \left(i \; \Omega^c_{1,0}\right), \; \mu^c_{1,1} = \sum_{i=0}^{\infty} \left(i \; \Omega^c_{1,1}\right) \text{ and } \mu^c_{1,3} = \sum_{i=0}^{\infty} \left(i \; \Omega^c_{1,3}\right). \tag{A4.52}$$

Within particles,

$$\lambda^p_{1,0} = \sum_{i=1}^{\infty} \left(i \, \Delta^p_{i,0}\right), \; \lambda^p_{1,3} = \sum_{i=1}^{\infty} \left(i \; \Delta^p_{i,3}\right) \text{ and } \lambda^p_{1,1} = \sum_{i=1}^{\infty} \left(i \, \Delta^p_{i,1}\right), \tag{A4.53}$$

$$\eta^p_{1,0} = \sum_{i=2}^{\infty} \left(i \, \Gamma^p_{1,0}\right), \; \eta^p_{1,3} = \sum_{i=2}^{\infty} \left(i \; \Gamma^p_{1,3}\right) \text{ and } \eta^p_{1,1} = \sum_{i=2}^{\infty} \left(i \, \Gamma^p_{1,1}\right), \tag{A4.54}$$

$$\nu_{1,3}^{p} = \sum_{i=0}^{\infty}\left(i\ \Pi_{1,3}^{p}\right), \tag{A4.55}$$

$$\mu_{1,0}^{p} = \sum_{i=1}^{\infty}\left(i\ \Omega_{1,0}^{p}\right),\ \mu_{1,1}^{p} = \sum_{i=0}^{\infty}\left(i\ \Omega_{1,1}^{c}\right) \text{ and } \mu_{1,3}^{p} = \sum_{i=0}^{\infty}\left(i\ \Omega_{1,3}^{p}\right). \tag{A4.56}$$

For instance, $\lambda_{1,0}^{c}$ is the mean number of monomeric units in oligoradicals of the continuous phase with a terminal A* and having 0 graft.

A4.1.3.3. Moments of order two

The moments of order two of the distributions were defined as follows :

In the continuous phase,

$$\lambda_{2,0}^{c} = \sum_{i=1}^{\infty}\left(i^2\ \Delta_{2,0}^{c}\right),\ \lambda_{2,3}^{c} = \sum_{i=1}^{\infty}\left(i^2\ \Delta_{2,3}^{c}\right) \text{ and } \lambda_{2,1}^{c} = \sum_{i=1}^{\infty}\left(i^2\ \Delta_{2,1}^{c}\right), \tag{A4.57}$$

$$\eta_{2,0}^{c} = \sum_{i=2}^{\infty}\left(i^2\ \Gamma_{2,0}^{c}\right),\ \eta_{2,3}^{c} = \sum_{i=2}^{\infty}\left(i^2\ \Gamma_{2,3}^{c}\right) \text{ and } \eta_{2,1}^{c} = \sum_{i=2}^{\infty}\left(i^2\ \Gamma_{2,1}^{c}\right), \tag{A4.58}$$

$$\nu_{2,3}^{c} = \sum_{i=0}^{\infty}\left(i^2\ \Pi_{2,3}^{c}\right), \tag{A4.59}$$

$$\mu_{2,0}^{c} = \sum_{i=0}^{\infty}\left(i^2\ \Omega_{2,0}^{c}\right),\ \mu_{2,1}^{c} = \sum_{i=0}^{\infty}\left(i^2\ \Omega_{2,1}^{c}\right) \text{ and } \mu_{2,3}^{c} = \sum_{i=0}^{\infty}\left(i^2\ \Omega_{2,3}^{c}\right). \tag{A4.60}$$

Within particles,

$$\lambda_{2,0}^{p} = \sum_{i=1}^{\infty}\left(i^2\ \Delta_{2,0}^{p}\right),\ \lambda_{2,3}^{p} = \sum_{i=1}^{\infty}\left(i^2\ \Delta_{2,3}^{p}\right) \text{ and } \lambda_{2,1}^{p} = \sum_{i=1}^{\infty}\left(i^2\ \Delta_{2,1}^{p}\right), \tag{A4.61}$$

$$\eta_{2,0}^{p} = \sum_{i=2}^{\infty}\left(i^2\ \Gamma_{2,0}^{p}\right),\ \eta_{2,3}^{p} = \sum_{i=2}^{\infty}\left(i^2\ \Gamma_{2,3}^{p}\right) \text{ and } \eta_{2,1}^{p} = \sum_{i=2}^{\infty}\left(i^2\ \Gamma_{2,1}^{p}\right), \tag{A4.62}$$

$$\nu_{2,3}^{p} = \sum_{i=0}^{\infty}\left(i^2\ \Pi_{2,3}^{p}\right), \tag{A4.63}$$

$$\mu_{2,0}^{p} = \sum_{i=0}^{\infty}\left(i^2\ \Omega_{2,0}^{p}\right),\ \mu_{2,1}^{p} = \sum_{i=0}^{\infty}\left(i^2\ \Omega_{2,1}^{p}\right) \text{ and } \mu_{2,3}^{p} = \sum_{i=0}^{\infty}\left(i^2\ \Omega_{2,3}^{p}\right). \tag{A4.64}$$

A4.1.3 Balances on radicals, dead polymer and moments in the continuous phase

A4.1.3.1 Balance on primary radicals R coming from initiator decomposition and transfers to NDM*

$$d\left(V_c\left[R^*\right]_c\right)/dt = 2 f_c k_d^c [I]_c V_c - \frac{Q_{sm}}{m_{CPP}}\left[R^*\right]_c V_c$$

$$-\left\{k_{RA}^{c}\left[A\right]_{c}+k_{RB}^{c}\left[B\right]_{c}+\left(k_{RG}^{c}+k_{RG,ng}^{c}\right)\left[G\right]_{c}+k_{RS,ng}^{c}\left[S\right]_{c}\right\}\left[R^{*}\right]_{c}V_{c}$$
$$+\left(k_{tr,A}^{c}\left(\left[A_{T,0}^{*}\right]_{c}+\left[A_{T,1}^{*}\right]_{c}+\left[A_{T,3}^{*}\right]_{c}\right)+k_{tr,B}^{c}\left(\left[B_{T,0}^{*}\right]_{c}+\left[B_{T,1}^{*}\right]_{c}+\left[B_{T,3}^{*}\right]_{c}\right)+k_{tr,G}^{c}\left[G_{T,3}^{*}\right]_{c}\right)\left[CTA\right]_{c}V_{c}$$

(A4.65)

A4.1.3.2. Balance on activated Polyol

$$d\left(V_{c}\left[S_{0,1}^{*}\right]_{c}\right)/dt=-\left\{Q_{sm}/m_{CPP}+k_{SA}^{c}\ \left[A\right]_{c}+k_{SB}^{c}\ \left[B\right]_{c}\right\}V_{c}\left[S_{0,1}^{*}\right]_{c}$$
$$+\left\{k_{RS,ng}^{c}\left[R^{*}\right]_{c}+k_{trAS}^{c}\left(\left[A_{T,0}^{*}\right]_{c}+\left[A_{T,1}^{*}\right]_{c}+\left[A_{T,3}^{*}\right]_{c}\right)+k_{trBS}^{c}\left(\left[B_{T,0}^{*}\right]_{c}+\left[B_{T,1}^{*}\right]_{c}+\left[B_{T,3}^{*}\right]_{c}\right)+k_{trGS}^{c}\left[G_{T,3}^{*}\right]_{c}\right\}\left[S\right]_{c}V_{c}$$

(A4.66)

A4.1.3.3. Radicals with a terminal A and having 0 graft*

These balances are described in detail in chapter 4 (paragraph 2.3).

A4.1.3.4. Radicals with a terminal A and having one polyol graft*

Balance on $[A^{*}_{1,1}]_c$:

$$d\left(V_{c}\left[A_{T,1}^{*}\right]_{c}\Delta_{1,1}^{c}\right)/dt=k_{GA}^{c}\left[S_{0,1}^{*}\right]_{c}\left[A\right]_{c}V_{c}-\left\{\frac{Q_{sm}}{m_{CPP}}+k_{pAA}^{c}\left[A\right]_{c}+k_{pAG}^{c}\left[G\right]_{c}+k_{pAB}^{c}\left[B\right]_{c}\right\}V_{c}\left[A_{T,1}^{*}\right]_{c}\Delta_{1,1}^{c}$$
$$-\left\{k_{tcAA}^{c}\left(\left[A_{T,0}^{*}\right]_{c}+2\left[A_{T,1}^{*}\right]_{c}+\left[A_{T,3}^{*}\right]_{c}\right)+k_{tcBA}^{c}\left(\left[B_{T,0}^{*}\right]_{c}+\left[B_{T,1}^{*}\right]_{c}+\left[B_{T,3}^{*}\right]_{c}\right)\right\}V_{c}\left[A_{T,1}^{*}\right]_{c}\Delta_{1,1}^{c}$$
$$-\left\{k_{tdGA}^{c}\left[G_{T,1}^{*}\right]_{c}+k_{t,A}^{c}\left[CTA\right]_{c}+k_{tr,SA}^{c}\left[S\right]_{c}+k_{tr,GA}^{c}\left[G\right]_{c}+2\pi d_{p}N_{p}\bar{D}_{3}+K_{p}\bar{M}_{n}^{c}/M_{u}\right\}V_{c}\left[A_{T,1}^{*}\right]_{c}\Delta_{1,1}^{c}$$

(A4.67)

Balance on $[A^{*}_{i,1}]$ for $i\geq 2$:

$$d\left(V_{c}\left[A_{T,1}^{*}\right]_{c}\ \Delta_{i,1}^{c}\right)/dt=\left\{k_{pAA}^{c}\left[A_{T,1}^{*}\right]_{c}\ \Delta_{i-1,1}^{c}\ \left[A\right]_{c}+k_{pBA}^{c}\left[B_{T,1}^{*}\right]_{c}\ \Gamma_{i-1,1}^{c}\left[A\right]_{c}\right\}\ V_{c}$$
$$-\left\{\frac{Q_{sm}}{m_{CPP}}+k_{pAB}^{c}\left[B\right]_{c}+k_{pAA}^{c}\left[A\right]_{c}+k_{pAG}^{c}\left[G\right]_{c}+k_{tcAA}^{c}\left(\left[A_{T,0}^{*}\right]_{c}+2\left[A_{T,1}^{*}\right]_{c}+\left[A_{T,3}^{*}\right]_{c}\right)\right\}V_{c}\left[A_{T,1}^{*}\right]_{c}\Delta_{1,1}^{c}$$
$$-\left\{k_{tcBA}^{c}\left(\left[B_{T,0}^{*}\right]_{c}+\left[B_{T,1}^{*}\right]_{c}+\left[B_{T,3}^{*}\right]_{c}\right)+k_{tdGA}^{c}\left[G_{T,3}^{*}\right]_{c}\right\}V_{c}\left[A_{T,1}^{*}\right]_{c}\Delta_{1,1}^{c}$$
$$-\left\{k_{t,A}^{c}\left[CTA\right]_{c}+k_{tr,SA}^{c}\left[S\right]_{c}+k_{tr,GA}^{c}\left[G\right]_{c}+2\pi d_{p}N_{p}\bar{D}_{3}+K_{p}\bar{M}_{n}^{c}/M_{u}\right\}V_{c}\left[A_{T,1}^{*}\right]_{c}\Delta_{1,1}^{c}\quad\text{(A4.68)}$$

The global sum on all the species gives:

$$d\left(V_{c}\left[A_{T,1}^{*}\right]_{c}\right)/dt=\left(k_{GA}^{c}\left[S_{0,1}^{*}\right]_{c}+k_{pBA}^{c}\left[B_{T,1}^{*}\right]_{c}\right)\left[A\right]_{c}V_{c}-\left\{\frac{Q_{sm}}{m_{CPP}}+k_{pAG}^{c}\left[G\right]_{c}+k_{pAB}^{c}\left[B\right]_{c}\right\}V_{c}\left[A_{T,1}^{*}\right]_{c}$$
$$-\left\{k_{tcAA}^{c}\left(\left[A_{T,0}^{*}\right]_{c}+2\left[A_{T,1}^{*}\right]_{c}+\left[A_{T,3}^{*}\right]_{c}\right)+k_{tcBA}^{c}\left(\left[B_{T,0}^{*}\right]_{c}+\left[B_{T,1}^{*}\right]_{c}+\left[B_{T,3}^{*}\right]_{c}\right)\right\}V_{c}\left[A_{T,1}^{*}\right]_{c}$$
$$-\left\{k_{tdGA}^{c}\left[G_{T,3}^{*}\right]_{c}+k_{t,A}^{c}\left[CTA\right]_{c}+k_{tr,SA}^{c}\left[S\right]_{c}+k_{tr,GA}^{c}\left[G\right]_{c}+2\pi d_{p}N_{p}\bar{D}_{1}+K_{p}\bar{M}_{n}^{c}/M_{u}\right\}V_{c}\left[A_{T,1}^{*}\right]_{c}$$

(A4.69)

$$d\left(V_c\left[A^*_{T,1}\right]_c \lambda^c_{1,1}\right)/dt = \left\{k^c_{GA}\left[S^*_{0,1}\right]_c + k^c_{pAA}\left[A^*_{T,1}\right]_c + k^c_{pBA}\left[B^*_{T,1}\right]_c\left(\eta^c_{1,1}+1\right)\right\}V_c[A]_c$$
$$-\left\{\frac{Q_{sm}}{m_{CPP}} + k^c_{pAB}[B]_c + k^c_{pAG}[G]_c + k^c_{tcAA}\left(\left[A^*_{T,0}\right]_c + 2\left[A^*_{T,1}\right]_c + \left[A^*_{T,3}\right]_c\right)\right\}V_c\left[A^*_{T,1}\right]_c \lambda^c_{1,1}$$
$$-\left\{k^c_{tcBA}\left(\left[B^*_{T,0}\right]_c + \left[B^*_{T,1}\right]_c + \left[B^*_{T,3}\right]_c\right) + k^c_{tdGA}\left[G^*_{T,3}\right]_c\right\}V_c\left[A^*_{T,1}\right]_c \lambda^c_{1,1}$$
$$-\left\{k^c_{t,A}[CTA]_c + k^c_{tr,SA}[S]_c + k^c_{tr,GA}[G]_c + 2\pi d_p N_p \bar{D}_3 + K_p \bar{M}^c_n/M_u\right\}V_c\left[A^*_{T,1}\right]_c \lambda^c_{1,1} \qquad \text{(A4.70)}$$

$$d\left(V_c\left[A^*_{T,1}\right]_c \lambda^c_{2,1}\right)/dt = \left\{k^c_{GA}\left[S^*_{0,1}\right]_c + k^c_{pAA}\left[A^*_{T,1}\right]_c\left(2\lambda^c_{1,1}+1\right) + k^c_{pBA}\left[B^*_{T,1}\right]_c\left(\eta^c_{2,1}+2\eta^c_{1,1}+1\right)\right\}V_c[A]_c$$
$$-\left\{\frac{Q_{sm}}{m_{CPP}} + k^c_{pAB}[B]_c + k^c_{pAG}[G]_c + k^c_{tcAA}\left(\left[A^*_{T,0}\right]_c + 2\left[A^*_{T,1}\right]_c + \left[A^*_{T,3}\right]_c\right)\right\}V_c\left[A^*_{T,1}\right]_c \lambda^c_{2,1}$$
$$-\left\{k^c_{tcBA}\left(\left[B^*_{T,0}\right]_c + \left[B^*_{T,1}\right]_c + \left[B^*_{T,3}\right]_c\right) + k^c_{tdGA}\left[G^*_{T,3}\right]_c\right\}V_c\left[A^*_{T,1}\right]_c \lambda^c_{2,1}$$
$$-\left\{k^c_{t,A}[CTA]_c + k^c_{tr,SA}[S]_c + k^c_{tr,GA}[G]_c + 2\pi d_p N_p \bar{D}_3 + K_p \bar{M}^c_n/M_u\right\}V_c\left[A^*_{T,1}\right]_c \lambda^c_{2,1} \qquad \text{(A4.71)}$$

A4.1.3.5. Radicals with a terminal A and having one S5200 graft*

Balance on $[A^*_{1,3}]_c$:

$$d\left(V_c\left[A^*_{T,3}\right]_c \Delta^c_{1,3}\right)/dt = k^c_{GA}\left[G^*_{0,3}\right]_c[A]_c V_c - \left\{\frac{Q_{sm}}{m_{CPP}} + k^c_{pAA}[A]_c + k^c_{pAG}[G]_c + k^c_{pAB}[B]_c\right\}V_c\left[A^*_{T,3}\right]_c \Delta^c_{1,3}$$
$$-\left\{k^c_{tcAA}\left(\left[A^*_{T,0}\right]_c + \left[A^*_{T,1}\right]_c + 2\left[A^*_{T,3}\right]_c\right) + k^c_{tcBA}\left(\left[B^*_{T,0}\right]_c + \left[B^*_{T,1}\right]_c + \left[B^*_{T,3}\right]_c\right)\right\}V_c\left[A^*_{T,3}\right]_c \Delta^c_{1,3}$$
$$-\left\{k^c_{tdGA}\left[G^*_{T,3}\right]_c + k^c_{t,A}[CTA]_c + k^c_{tr,SA}[S]_c + k^c_{tr,GA}[G]_c + 2\pi d_p N_p \bar{D}_3 + K_p \bar{M}^c_n/M_u\right\}V_c\left[A^*_{T,3}\right]_c \Delta^c_{1,3}$$
(A4.72)

Balance on $[A^*_{i,3}]$ for $i \geq 2$:

$$d\left(V_c\left[A^*_{T,3}\right]_c \Delta^c_{i,3}\right)/dt = \left\{k^c_{pAA}\left[A^*_{T,3}\right]_c \Delta^c_{i-1,3}\ [A]_c + k^c_{pBA}\left[B^*_{T,3}\right]_c \Gamma^c_{i-1,3}[A]_c\right\}\ V_c$$
$$-\left\{\frac{Q_{sm}}{m_{CPP}} + k^c_{pAB}[B]_c + k^c_{pAA}[A]_c + k^c_{pAG}[G]_c + k^c_{tcAA}\left(\left[A^*_{T,0}\right]_c + \left[A^*_{T,1}\right]_c + 2\left[A^*_{T,3}\right]_c\right)\right\}V_c\left[A^*_{T,3}\right]_c \Delta^c_{1,3}$$
$$-\left\{k^c_{tcBA}\left(\left[B^*_{T,0}\right]_c + \left[B^*_{T,1}\right]_c + \left[B^*_{T,3}\right]_c\right) + k^c_{tdGA}\left[G^*_{T,3}\right]_c\right\}V_c\left[A^*_{T,3}\right]_c \Delta^c_{1,3}$$
$$-\left\{k^c_{tr,SA}[S]_c + k^c_{tr,GA}[G]_c + k^c_{t,A}[CTA]_c + 2\pi d_p N_p \bar{D}_3 + K_p \bar{M}^c_n/M_u\right\}V_c\left[A^*_{T,3}\right]_c \Delta^c_{1,3} \qquad \text{(A4.73)}$$

The global sum on all the species gives:

$$d\left(V_c\left[A^*_{T,3}\right]_c\right)/dt = \left(k^c_{GA}\left[G^*_{0,3}\right]_c + k^c_{pBA}\left[B^*_{T,3}\right]_c\right)[A]_c V_c - \left\{\frac{Q_{sm}}{m_{CPP}} + k^c_{pAG}[G]_c + k^c_{pAB}[B]_c\right\} V_c\left[A^*_{T,3}\right]_c$$
$$-\left\{k^c_{tcAA}\left(\left[A^*_{T,0}\right]_c + \left[A^*_{T,1}\right]_c + 2\left[A^*_{T,3}\right]_c\right) + k^c_{tcBA}\left(\left[B^*_{T,0}\right]_c + \left[B^*_{T,1}\right]_c + \left[B^*_{T,3}\right]_c\right)\right\} V_c\left[A^*_{T,3}\right]_c$$
$$-\left\{k^c_{tdGA}\left[G^*_{T,3}\right]_c + k^c_{t,A}[CTA]_c + k^c_{tr,SA}[S]_c + k^c_{tr,GA}[G]_c + 2\pi d_p N_p \bar{D}_3 + K_p \bar{M}^c_n / M_u\right\} V_c\left[A^*_{T,3}\right]_c$$

(A4.74)

$$d\left(V_c\left[A^*_{T,3}\right]_c \lambda^c_{1,3}\right)/dt = \left\{k^c_{GA}\left[G^*_{0,3}\right]_c + k^c_{pAA}\left[A^*_{T,3}\right]_c + k^c_{pBA}\left[B^*_{T,3}\right]_c\left(\eta^c_{1,3}+1\right)\right\} V_c[A]_c$$
$$-\left\{\frac{Q_{sm}}{m_{CPP}} + k^c_{pAB}[B]_c + k^c_{pAG}[G]_c + k^c_{tcAA}\left(\left[A^*_{T,0}\right]_c + \left[A^*_{T,1}\right]_c + 2\left[A^*_{T,3}\right]_c\right)\right\} V_c\left[A^*_{T,3}\right]_c \lambda^c_{1,3}$$
$$-\left\{k^c_{tcBA}\left(\left[B^*_{T,0}\right]_c + \left[B^*_{T,1}\right]_c + \left[B^*_{T,3}\right]_c\right) + k^c_{tdGA}\left[G^*_{T,3}\right]_c\right\} V_c\left[A^*_{T,3}\right]_c \lambda^c_{1,3}$$
$$-\left\{k^c_{t,A}[CTA]_c + k^c_{tr,SA}[S]_c + k^c_{tr,GA}[G]_c + 2\pi d_p N_p \bar{D}_3 + K_p \bar{M}^c_n / M_u\right\} V_c\left[A^*_{T,3}\right]_c \lambda^c_{1,3} \qquad \text{(A4.75)}$$

$$d\left(V_c\left[A^*_{T,3}\right]_c \lambda^c_{2,3}\right)/dt = \left\{k^c_{GA}\left[G^*_{0,3}\right]_c + k^c_{pAA}\left[A^*_{T,3}\right]_c\left(2\lambda^c_{1,3}+1\right) + k^c_{pBA}\left[B^*_{T,3}\right]_c\left(\eta^c_{2,3} + 2\eta^c_{1,3} + 1\right)\right\} V_c[A]_c$$
$$-\left\{\frac{Q_{sm}}{m_{CPP}} + k^c_{pAB}[B]_c + k^c_{pAG}[G]_c + k^c_{tcAA}\left(\left[A^*_{T,0}\right]_c + \left[A^*_{T,1}\right]_c + 2\left[A^*_{T,3}\right]_c\right)\right\} V_c\left[A^*_{T,3}\right]_c \lambda^c_{2,3}$$
$$-\left\{k^c_{tcBA}\left(\left[B^*_{T,0}\right]_c + \left[B^*_{T,1}\right]_c + \left[B^*_{T,3}\right]_c\right) + k^c_{tdGA}\left[G^*_{T,3}\right]_c\right\} V_c\left[A^*_{T,3}\right]_c \lambda^c_{2,3}$$
$$-\left\{k^c_{t,A}[CTA]_c + k^c_{tr,SA}[S]_c + k^c_{tr,GA}[G]_c + 2\pi d_p N_p \bar{D}_3 + K_p \bar{M}^c_n / M_u\right\} V_c\left[A^*_{T,3}\right]_c \lambda^c_{2,3}$$

(A4.76)

A4.1.3.6. Radicals with a terminal B and having 0 graft*

Balance on $[B^*_{2,0}]_c$:

$$d\left(V_c\ \left[B^*_{T,0}\right]_c \Gamma^c_{2,0}\right)/dt = k^c_{RB}\left[R^*\right]_c[B]_c V_c - \left\{\frac{Q_{sm}}{m_{CPP}} + k^c_{pBA}[A]_c + k^c_{pBG}[G]_c + k^c_{pBB}[B]_c\right\} V_c\left[B^*_{T,0}\right]_c \Gamma^c_{2,0}$$
$$-\left\{2k^c_{tcBB}\left(\left[B^*_{T,0}\right]_c + \left[B^*_{T,1}\right]_c + \left[B^*_{T,3}\right]_c\right) + k^c_{tcBA}\left(\left[A^*_{T,0}\right]_c + \left[A^*_{T,1}\right]_c + \left[A^*_{T,3}\right]_c\right)\right\} V_c\left[B^*_{T,0}\right]_c \Gamma^c_{2,0}$$
$$-\left\{k^c_{tdGB}\left[G^*_{T,3}\right]_c + k^c_{t,B}[CTA]_c + k^c_{tr,SB}[S]_c + k^c_{tr,GB}[G]_c + 2\pi d_p N_p \bar{D}_0 + K_p \bar{M}^c_n / M_u\right\} V_c\left[B^*_{T,0}\right]_c \Gamma^c_{2,0}$$

(A4.77)

Balance on $[B^*_{i,0}]$ for $i \geq 3$:

$$d\left(V_c\ \left[B^*_{T,0}\right]_c \Gamma^c_{i,0}\right)/dt = \left\{k^c_{pBB}\left[B^*_{i-2,0}\right]_c + k^c_{pAB}\left[A^*_{i-2,0}\right]_c\right\}[B]_c V_c - \left\{\frac{Q_{sm}}{m_{CPP}} + k^c_{pBA}\ [A]_c + k^c_{pBG}[G]_c\right\} V_c\left[B^*_{T,0}\right]_c \Gamma^c_{i,0}$$
$$-\left\{k^c_{pBB}\ [B]_c + 2k^c_{tcBB}\left(\left[B^*_{T,0}\right]_c + \left[B^*_{T,1}\right]_c + \left[B^*_{T,3}\right]_c\right) + k^c_{tcBA}\left(\left[A^*_{T,0}\right]_c + \left[A^*_{T,1}\right]_c + \left[A^*_{T,3}\right]_c\right)\right\} V_c\left[B^*_{T,0}\right]_c \Gamma^c_{i,0}$$

$$-\left\{k^c_{tdGB}\left[G^*_{T,3}\right]_c + k^c_{t,B}\left[CTA\right]_c + k^c_{tr,SB}\left[S\right]_c + k^c_{tr,GB}\left[G\right]_c + 2\pi d_p N_p \bar{D}_0 + K_p \bar{M}^c_n / M_u\right\} V_c \left[B^*_{T,0}\right]_c \Gamma^c_{i,0} \quad \text{(A4.78)}$$

The global sum on all the species gives:

$$\begin{aligned} d\left(V_c\left[B^*_{T,0}\right]_c\right)/dt &= k^c_{pAB}\left[B\right]_c V_c\left[A^*_{T,0}\right]_c + k^c_{RB}\left[R^*\right]_c\left[B\right]_c V_c \\ &-\left\{\frac{Q_{sm}}{m_{CPP}} + k^c_{pBA}\left[A\right]_c + k^c_{pBG}\left[G\right]_c + 2k^c_{tcBB}\left(\left[B^*_{T,0}\right]_c + \left[B^*_{T,1}\right]_c + \left[B^*_{T,3}\right]_c\right)\right\} V_c\left[B^*_{T,0}\right]_c \\ &-\left\{k^c_{tcBA}\left(\left[A^*_{T,0}\right]_c + \left[A^*_{T,1}\right]_c + \left[A^*_{T,3}\right]_c\right) + k^c_{tdGB}\left[G^*_{T,3}\right]_c\right\} V_c\left[B^*_{T,0}\right]_c \\ &-\left\{k^c_{t,B}\left[CTA\right]_c + k^c_{tr,SB}\left[S\right]_c + k^c_{tr,GB}\left[G\right]_c + 2\pi d_p N_p \bar{D}_0 + K_p \bar{M}^c_n / M_u\right\} V_c\left[B^*_{T,0}\right]_c \end{aligned} \quad \text{(A4.79)}$$

$$\begin{aligned} d\left(V_c\left[B^*_{T,0}\right]_c \eta^c_{1,0}\right)/dt &= 2k^c_{pBB}\left[B\right]_c V_c\left[B^*_{T,0}\right]_c + k^c_{pAB}\left[B\right]_c V_c\left[A^*_{T,0}\right]_c\left(\lambda^c_{1,0} + 2\right) + 2k^c_{RB}\left[R^*\right]_c\left[B\right]_c V_c \\ &-\left\{\frac{Q_{sm}}{m_{CPP}} + k^c_{pBA}\left[A\right]_c + k^c_{pBG}\left[G\right]_c + 2k^c_{tcBB}\left(\left[B^*_{T,0}\right]_c + \left[B^*_{T,1}\right]_c + \left[B^*_{T,3}\right]_c\right)\right\} V_c\left[B^*_{T,0}\right]_c \eta^c_{1,0} \\ &-\left\{k^c_{tcBA}\left(\left[A^*_{T,0}\right]_c + \left[A^*_{T,1}\right]_c + \left[A^*_{T,3}\right]_c\right) + k^c_{tdGB}\left[G^*_{T,3}\right]_c\right\} V_c\left[B^*_{T,0}\right]_c \eta^c_{1,0} \\ &-\left\{k^c_{t,B}\left[CTA\right]_c + k^c_{tr,SB}\left[S\right]_c + k^c_{tr,GB}\left[G\right]_c + 2\pi d_p N_p \bar{D}_0 + K_p \bar{M}^c_n / M_u\right\} V_c\left[B^*_{T,0}\right]_c \eta^c_{1,0} \end{aligned} \quad \text{(A4.80)}$$

$$\begin{aligned} d\left(V_c\left[B^*_{T,0}\right]_c \eta^c_{2,0}\right)/dt &= \left\{k^c_{pBB}\left[B^*_{T,0}\right]_c\left(4\eta^c_{1,0} + 4\right) + k^c_{pAB}\left[A^*_{T,0}\right]_c\left(\lambda^c_{2,0} + 4\lambda^c_{1,0} + 4\right) + 4k^c_{RB}\left[R^*\right]_c\right\}\left[B\right]_c V_c \\ &-\left\{\frac{Q_{sm}}{m_{CPP}} + k^c_{pBA}\left[A\right]_c + k^c_{pBG}\left[G\right]_c + 2k^c_{tcBB}\left(\left[B^*_{T,0}\right]_c + \left[B^*_{T,1}\right]_c + \left[B^*_{T,3}\right]_c\right)\right\} V_c\left[B^*_{T,0}\right]_c \eta^c_{2,0} \\ &-\left\{k^c_{tcBA}\left(\left[A^*_{T,0}\right]_c + \left[A^*_{T,1}\right]_c + \left[A^*_{T,3}\right]_c\right) + k^c_{tdGB}\left[G^*_{T,3}\right]_c\right\} V_c\left[B^*_{T,0}\right]_c \eta^c_{2,0} \\ &-\left\{k^c_{t,B}\left[CTA\right]_c + k^c_{tr,SB}\left[S\right]_c + k^c_{tr,GB}\left[G\right]_c + 2\pi d_p N_p \bar{D}_0 + K_p \bar{M}^c_n / M_u\right\} V_c\left[B^*_{T,0}\right]_c \eta^c_{2,0} \end{aligned} \quad \text{(A4.81)}$$

A4.1.3.7. Radicals with a terminal B and having one polyol graft*

Balance on $[B^*_{2,1}]_c$:

$$\begin{aligned} d\left(V_c\left[B^*_{T,1}\right]_c \Gamma^c_{2,1}\right)/dt &= k^c_{sB}\left[S^*_{0,1}\right]_c\left[B\right]_c V_c - \left\{\frac{Q_{sm}}{m_{CPP}} + k^c_{pBA}\left[A\right]_c + k^c_{pBG}\left[G\right]_c + k^c_{pBB}\left[B\right]_c\right\} V_c\left[B^*_{T,1}\right]_c \Gamma^c_{2,1} \\ &-\left\{2k^c_{tcBB}\left(\left[B^*_{T,0}\right]_c + \left[B^*_{T,1}\right]_c + \left[B^*_{T,3}\right]_c\right) + k^c_{tcBA}\left(\left[A^*_{T,0}\right]_c + \left[A^*_{T,1}\right]_c + \left[A^*_{T,3}\right]_c\right)\right\} V_c\left[B^*_{T,1}\right]_c \Gamma^c_{2,1} \\ &-\left\{k^c_{tdGB}\left[G^*_{T,3}\right]_c + k^c_{t,B}\left[CTA\right]_c + k^c_{tr,SB}\left[S\right]_c + k^c_{tr,GB}\left[G\right]_c + 2\pi d_p N_p \bar{D}_3 + K_p \bar{M}^c_n / M_u\right\} V_c\left[B^*_{T,1}\right]_c \Gamma^c_{2,1} \end{aligned} \quad \text{(A4.82)}$$

Balance on $[B^*_{i,1}]$ for $i \geq 3$:

$$d\left(V_c\left[B^*_{T,1}\right]_c \Gamma^c_{i,1}\right)/dt = \left\{k^c_{pBB}\left[B^*_{i-2,1}\right]_c + k^c_{pAB}\left[A^*_{i-2,1}\right]_c\right\}[B]_c V_c - \left\{\frac{Q_{sm}}{m_{CPP}} + k^c_{pBA}[A]_c + k^c_{pBG}[G]_c\right\} V_c\left[B^*_{T,1}\right]_c \Gamma^c_{i,1}$$
$$-\left\{k^c_{pBB}\ [B]_c + 2k^c_{tcBB}\left(\left[B^*_{T,0}\right]_c + \left[B^*_{T,1}\right]_c + \left[B^*_{T,3}\right]_c\right) + k^c_{tcBA}\left(\left[A^*_{T,0}\right]_c + \left[A^*_{T,1}\right]_c + \left[A^*_{T,3}\right]_c\right)\right\} V_c\left[B^*_{T,1}\right]_c \Gamma^c_{i,1}$$
$$-\left\{k^c_{tdGB}\left[G^*_{T,3}\right]_c + k^c_{t,B}[CTA]_c + k^c_{tr,SB}[S]_c + k^c_{tr,GB}[G]_c + 2\pi d_p N_p \bar{D}_3 + K_p \bar{M}^c_n / M_u\right\} V_c\left[B^*_{T,1}\right]_c \Gamma^c_{i,1} \quad \text{(A4.83)}$$

The global sum on all the species gives:

$$d\left(V_c\left[B^*_{T,1}\right]_c\right)/dt = \left\{k^c_{SB}\left[S^*_{0,1}\right]_c + k^c_{pAB}\left[A^*_{T,1}\right]_c\right\}[B]_c V_c - \left\{\frac{Q_{sm}}{m_{CPP}} + k^c_{pBA}[A]_c + k^c_{pBG}[G]_c\right\} V_c\left[B^*_{T,1}\right]_c$$
$$-\left\{2k^c_{tcBB}\left(\left[B^*_{T,0}\right]_c + \left[B^*_{T,1}\right]_c + \left[B^*_{T,3}\right]_c\right) + k^c_{tcBA}\left(\left[A^*_{T,0}\right]_c + \left[A^*_{T,1}\right]_c + \left[A^*_{T,3}\right]_c\right)\right\} V_c\left[B^*_{T,1}\right]_c$$
$$-\left\{k^c_{tdGB}\left[G^*_{T,3}\right]_c + k^c_{t,B}[CTA]_c + k^c_{tr,SB}[S]_c + k^c_{tr,GB}[G]_c + 2\pi d_p N_p \bar{D}_1 + K_p \bar{M}^c_n / M_u\right\} V_c\left[B^*_{T,1}\right]_c \quad \text{(A4.84)}$$

$$d\left(V_c\left[B^*_{T,1}\right]_c \eta^c_{1,1}\right)/dt = \left\{2k^c_{pBB}\left[B^*_{T,1}\right]_c + k^c_{pAB}\left[A^*_{T,1}\right]_c\left(\lambda^c_{1,1} + 2\right) + 2k^c_{SB}\left[S^*_{0,1}\right]_c\right\}[B]_c V_c$$
$$-\left\{\frac{Q_{sm}}{m_{CPP}} + k^c_{pBA}[A]_c + k^c_{pBG}[G]_c + 2k^c_{tcBB}\left(\left[B^*_{T,0}\right]_c + \left[B^*_{T,1}\right]_c + \left[B^*_{T,3}\right]_c\right)\right\} V_c\left[B^*_{T,1}\right]_c \eta^c_{1,1}$$
$$-\left\{k^c_{tcBA}\left(\left[A^*_{T,0}\right]_c + \left[A^*_{T,1}\right]_c + \left[A^*_{T,3}\right]_c\right) + k^c_{tdGB}\left[G^*_{T,3}\right]_c\right\} V_c\left[B^*_{T,1}\right]_c \eta^c_{1,1}$$
$$-\left\{k^c_{t,B}[CTA]_c + k^c_{tr,SB}[S]_c + k^c_{tr,GB}[G]_c + 2\pi d_p N_p \bar{D}_1 + K_p \bar{M}^c_n / M_u\right\} V_c\left[B^*_{T,1}\right]_c \eta^c_{1,1} \quad \text{(A4.85)}$$

$$d\left(V_c\left[B^*_{T,1}\right]_c \eta^c_{2,1}\right)/dt = \left\{k^c_{pBB}\left[B^*_{T,1}\right]_c\left(4\eta^c_{1,1} + 4\right) + k^c_{pAB}\left[A^*_{T,1}\right]_c\left(\lambda^c_{2,1} + 4\lambda^c_{1,1} + 4\right) + 4k^c_{SB}\left[S^*_{0,1}\right]\right\}[B]_c V_c$$
$$-\left\{\frac{Q_{sm}}{m_{CPP}} + k^c_{pBA}[A]_c + k^c_{pBG}[G]_c + 2k^c_{tcBB}\left(\left[B^*_{T,0}\right]_c + \left[B^*_{T,1}\right]_c + \left[B^*_{T,3}\right]_c\right)\right\} V_c\left[B^*_{T,1}\right]_c \eta^c_{2,1}$$
$$-\left\{k^c_{tcBA}\left(\left[A^*_{T,0}\right]_c + \left[A^*_{T,1}\right]_c + \left[A^*_{T,3}\right]_c\right) + k^c_{tdGB}\left[G^*_{T,3}\right]_c\right\} V_c\left[B^*_{T,1}\right]_c \eta^c_{2,1}$$
$$-\left\{k^c_{t,B}[CTA]_c + k^c_{tr,SB}[S]_c + k^c_{tr,GB}[G]_c + 2\pi d_p N_p \bar{D}_1 + K_p \bar{M}^c_n / M_u\right\} V_c\left[B^*_{T,1}\right]_c \eta^c_{2,1}$$

(A4.86)

A4.1.3.8. Radicals with a terminal B and having one S5200 graft*

Balance on $[B^*_{2,3}]_c$:

$$d\left(V_c\left[B^*_{T,3}\right]_c \Gamma^c_{2,3}\right)/dt = k^c_{GB}\left[G^*_{0,3}\right]_c [B]_c V_c - \left\{\frac{Q_{sm}}{m_{CPP}} + k^c_{pBA}[A]_c + k^c_{pBG}[G]_c + k^c_{pBB}[B]_c\right\} V_c\left[B^*_{T,3}\right]_c \Gamma^c_{2,3}$$
$$-\left\{2k^c_{tcBB}\left(\left[B^*_{T,0}\right]_c + \left[B^*_{T,1}\right]_c + \left[B^*_{T,3}\right]_c\right) + k^c_{tcBA}\left(\left[A^*_{T,0}\right]_c + \left[A^*_{T,1}\right]_c + \left[A^*_{T,3}\right]_c\right)\right\} V_c\left[B^*_{T,3}\right]_c \Gamma^c_{2,3}$$

$$-\left\{k^c_{tdGB}\left[G^*_{T,3}\right]_c + k^c_{t,B}\left[CTA\right]_c + k^c_{tr,SB}\left[S\right]_c + k^c_{tr,GB}\left[G\right]_c + 2\pi d_p N_p \bar{D}_3 + K_p \bar{M}^c_n / M_u\right\} V_c \left[B^*_{T,3}\right]_c \Gamma^c_{2,3} \quad \text{(A4.87)}$$

Balance on $[B^*_{i,1}]$ for $i \geq 3$:

$$\begin{aligned} d\left(V_c\left[B^*_{T,3}\right]_c \Gamma^c_{i,3}\right)/dt = {} & \left\{k^c_{pBB}\left[B^*_{i-2,3}\right]_c + k^c_{pAB}\left[A^*_{i-2,3}\right]_c\right\}[B]_c V_c - \left\{\frac{Q_{sm}}{m_{CPP}} + k^c_{pBA}[A]_c + k^c_{pBG}[G]_c\right\} V_c \left[B^*_{T,3}\right]_c \Gamma^c_{i,3} \\ & - \left\{k^c_{pBB}\ [B]_c + 2k^c_{tcBB}\left(\left[B^*_{T,0}\right]_c + \left[B^*_{T,1}\right]_c + \left[B^*_{T,3}\right]_c\right) + k^c_{tcBA}\left(\left[A^*_{T,0}\right]_c + \left[A^*_{T,1}\right]_c + \left[A^*_{T,3}\right]_c\right)\right\} V_c \left[B^*_{T,3}\right]_c \Gamma^c_{i,3} \\ & - \left\{k^c_{tdGB}\left[G^*_{T,3}\right]_c + k^c_{t,B}\left[CTA\right]_c + k^c_{tr,SB}\left[S\right]_c + k^c_{tr,GB}\left[G\right]_c + 2\pi d_p N_p \bar{D}_3 + K_p \bar{M}^c_n / M_u\right\} V_c \left[B^*_{T,3}\right]_c \Gamma^c_{i,3} \end{aligned} \quad \text{(A4.88)}$$

The global sum on all the species gives:

$$\begin{aligned} d\left(V_c\left[B^*_{T,3}\right]_c\right)/dt = {} & \left\{k^c_{GB}\left[G^*_{0,3}\right]_c + k^c_{pAB}\left[A^*_{T,3}\right]_c\right\}[B]_c V_c - \left\{\frac{Q_{sm}}{m_{CPP}} + k^c_{pBA}[A]_c + k^c_{pBG}[G]_c\right\} V_c \left[B^*_{T,3}\right]_c \\ & - \left\{2k^c_{tcBB}\left(\left[B^*_{T,0}\right]_c + \left[B^*_{T,1}\right]_c + \left[B^*_{T,3}\right]_c\right) + k^c_{tcBA}\left(\left[A^*_{T,0}\right]_c + \left[A^*_{T,1}\right]_c + \left[A^*_{T,3}\right]_c\right)\right\} V_c \left[B^*_{T,3}\right]_c \\ & - \left\{k^c_{tdGB}\left[G^*_{T,3}\right]_c + k^c_{t,B}\left[CTA\right]_c + k^c_{tr,SB}\left[S\right]_c + k^c_{tr,GB}\left[G\right]_c + 2\pi d_p N_p \bar{D}_3 + K_p \bar{M}^c_n / M_u\right\} V_c \left[B^*_{T,3}\right]_c \end{aligned} \quad \text{(A4.89)}$$

$$\begin{aligned} d\left(V_c\left[B^*_{T,3}\right]_c \eta^c_{1,3}\right)/dt = {} & \left\{2k^c_{pBB}\left[B^*_{T,3}\right]_c + k^c_{pAB}\left[A^*_{T,3}\right]_c\left(\lambda^c_{1,3} + 2\right) + 2k^c_{GB}\left[G^*_{0,3}\right]_c\right\}[B]_c V_c \\ & - \left\{\frac{Q_{sm}}{m_{CPP}} + k^c_{pBA}[A]_c + k^c_{pBG}[G]_c + 2k^c_{tcBB}\left(\left[B^*_{T,0}\right]_c + \left[B^*_{T,1}\right]_c + \left[B^*_{T,3}\right]_c\right)\right\} V_c \left[B^*_{T,3}\right]_c \eta^c_{1,3} \\ & - \left\{k^c_{tcBA}\left(\left[A^*_{T,0}\right]_c + \left[A^*_{T,1}\right]_c + \left[A^*_{T,3}\right]_c\right) + k^c_{tdGB}\left[G^*_{T,3}\right]_c\right\} V_c \left[B^*_{T,3}\right]_c \eta^c_{1,3} \\ & - \left\{k^c_{t,B}\left[CTA\right]_c + k^c_{tr,SB}\left[S\right]_c + k^c_{tr,GB}\left[G\right]_c + 2\pi d_p N_p \bar{D}_3 + K_p \bar{M}^c_n / M_u\right\} V_c \left[B^*_{T,3}\right]_c \eta^c_{1,3} \end{aligned} \quad \text{(A4.90)}$$

$$\begin{aligned} d\left(V_c\left[B^*_{T,3}\right]_c \eta^c_{2,3}\right)/dt = {} & \left\{k^c_{pBB}\left[B^*_{T,3}\right]_c\left(4\eta^c_{1,3} + 4\right) + k^c_{pABc}\left[A^*_{T,3}\right]_c\left(\lambda^c_{2,3} + 4\lambda^c_{1,3} + 4\right) + 4k^c_{GB}\left[G^*_{0,3}\right]\right\}[B]_c V_c \\ & - \left\{\frac{Q_{sm}}{m_{CPP}} + k^c_{pBA}[A]_c + k^c_{pBG}[G]_c + 2k^c_{tcBB}\left(\left[B^*_{T,0}\right]_c + \left[B^*_{T,1}\right]_c + \left[B^*_{T,3}\right]_c\right)\right\} V_c \left[B^*_{T,3}\right]_c \eta^c_{2,3} \\ & - \left\{k^c_{tcBA}\left(\left[A^*_{T,0}\right]_c + \left[A^*_{T,1}\right]_c + \left[A^*_{T,3}\right]_c\right) + k^c_{tdGB}\left[G^*_{T,3}\right]_c\right\} V_c \left[B^*_{T,3}\right]_c \eta^c_{2,3} \\ & - \left\{k^c_{t,B}\left[CTA\right]_c + k^c_{tr,SB}\left[S\right]_c + k^c_{tr,GB}\left[G\right]_c + 2\pi d_p N_p \bar{D}_3 + K_p \bar{M}^c_n / M_u\right\} V_c \left[B^*_{T,3}\right]_c \eta^c_{2,3} \end{aligned} \quad \text{(A4.91)}$$

*A4.1.3.9. Radicals with a terminal G**

Activated S5200 : $\left[G^*_{0,3}\right]_c$

$$d\left(V_c\ \left[G^*_{0,3}\right]_c\right)/dt = \left\{\left(k^c_{RG}+k^c_{RG,ng}\right)\left[R^*\right]_c + k^c_{trAG}\left(\left[A^*_{T,0}\right]_c+\left[A^*_{T,1}\right]_c+\left[A^*_{T,3}\right]_c\right)+k^c_{trBG}\left(\left[B^*_{T,0}\right]_c+\left[B^*_{T,1}\right]_c+\left[B^*_{T,3}\right]_c\right)\right\}[G]_c V_c$$
$$-\left\{\frac{Q_{sm}}{m_{CPP}}+k^c_{GA}\ [A]_c+k^c_{GB}\ [B]_c+k^c_{kdGA}\left(\left[A^*_{T,0}\right]_c+\left[A^*_{T,1}\right]_c+\left[A^*_{T,3}\right]_c\right)\right\}\ V_c\left[G^*_{0,3}\right]_c$$
$$-\left\{k^c_{kdGB}\left(\left[B^*_{T,0}\right]_c+\left[B^*_{T,1}\right]_c+\left[B^*_{T,3}\right]_c\right)+k^c_{t,G}\left[CTA\right]_c+k^c_{tr,SG}\left[S\right]_c\right\}V_c\left[G^*_{0,3}\right]_c \qquad \text{(A4.92)}$$

Balance on $[G^*_{i,3}]$ for $i \geq 1$:

$$d\left(V_c\left[G^*_{T,3}\right]_c\Pi^c_{i,3}\right)/dt = \left\{k^c_{pAG}\left[A^c_{T,0}\right]_c\Delta^c_{i,0}+k^c_{pBG}\left[B^c_{T,0}\right]_c\Gamma^c_{i,0}\right\}[G]_c V_c$$
$$-\left\{\frac{Q_{sm}}{m_{CPP}}+k^c_{kdGA}\left(\left[A^*_{T,0}\right]_c+\left[A^*_{T,1}\right]_c+\left[A^*_{T,3}\right]_c\right)+k^c_{kdGB}\left(\left[B^*_{T,0}\right]_c+\left[B^*_{T,1}\right]_c+\left[B^*_{T,3}\right]_c\right)\right\}V_c\left[G^*_{T,3}\right]_c\Pi^c_{i,3}$$
$$-\left\{k^c_{t,G}\left[CTA\right]_c+k^c_{tr,SG}\left[S\right]_c+2\pi d_p N_p\bar{D}_3+K_p\bar{M}^c_n/M_u\right\}V_c\left[G^*_{T,3}\right]_c\Pi^c_{i,3} \qquad \text{(A4.93)}$$

The sum of all species gives:

$$d\left(V_c\left[G^*_{T,3}\right]_c\right)/dt = \left\{\left(k^c_{RG}+k^c_{RG,ng}\right)\left[R^*\right]_c+k^c_{trAG}\left(\left[A^*_{T,0}\right]_c+\left[A^*_{T,1}\right]_c+\left[A^*_{T,3}\right]_c\right)+k^c_{trBG}\left(\left[B^*_{T,0}\right]_c+\left[B^*_{T,1}\right]_c+\left[B^*_{T,3}\right]_c\right)\right\}[G]_c V_c$$
$$+\left\{k^c_{pAG}\left[A^c_{T,0}\right]_c+k^c_{pBG}\left[B^c_{T,0}\right]_c\right\}[G]_c V_c-\left\{k^c_{GA}\left[A\right]_c+k^c_{GB}\left[B\right]_c\right\}V_c\left[G^*_{0,3}\right]_c$$
$$-\left\{\frac{Q_{sm}}{m_{CPP}}+k^c_{kdGA}\left(\left[A^*_{T,0}\right]_c+\left[A^*_{T,1}\right]_c+\left[A^*_{T,3}\right]_c\right)+k^c_{kdGB}\left(\left[B^*_{T,0}\right]_c+\left[B^*_{T,1}\right]_c+\left[B^*_{T,3}\right]_c\right)\right\}V_c\left[G^*_{T,3}\right]_c$$
$$-\left\{k^c_{t,G}\left[CTA\right]_c+k^c_{tr,SG}\left[S\right]_c+2\pi d_p N_p\bar{D}_3+K_p\bar{M}^c_n/M_u\right\}V_c\left[G^*_{T,3}\right]_c \qquad \text{(A4.94)}$$

$$d\left(V_c\left[G^*_{T,3}\right]_c\nu^c_{1,3}\right)/dt = \left(k^c_{pAG}\left[A^c_{T,0}\right]_c\lambda^c_{1,0}+k^c_{pBG}\left[B^c_{T,0}\right]_c\eta^c_{1,0}\right)[G]_c V_c$$
$$-\left\{\frac{Q_{sm}}{m_{CPP}}+k^c_{kdGA}\left(\left[A^*_{T,0}\right]_c+\left[A^*_{T,1}\right]_c+\left[A^*_{T,3}\right]_c\right)+k^c_{kdGB}\left(\left[B^*_{T,0}\right]_c+\left[B^*_{T,1}\right]_c+\left[B^*_{T,3}\right]_c\right)\right\}V_c\left[G^*_{T,3}\right]_c\nu^c_{1,3}$$
$$-\left\{k^c_{t,G}\left[CTA\right]_c+k^c_{tr,SG}\left[S\right]_c+2\pi d_p N_p\bar{D}_3+K_p\bar{M}^c_n/M_u\right\}V_c\left[G^*_{T,3}\right]_c\nu^c_{1,3} \qquad \text{(A4.95)}$$

$$d\left(V_c\ \left[G^*_{T,3}\right]_c\nu^c_{2,3}\right)/dt = \left(k^c_{pAG}\left[A^c_{T,0}\right]_c\lambda^c_{2,0}+k^c_{pBG}\left[B^c_{T,0}\right]_c\eta^c_{2,0}\right)[G]_c V_c$$
$$-\left\{\frac{Q_{sm}}{m_{CPP}}+k^c_{kdGA}\left(\left[A^*_{T,0}\right]_c+\left[A^*_{T,1}\right]_c+\left[A^*_{T,3}\right]_c\right)+k^c_{kdGB}\left(\left[B^*_{T,0}\right]_c+\left[B^*_{T,1}\right]_c+\left[B^*_{T,3}\right]_c\right)\right\}V_c\left[G^*_{T,3}\right]_c\nu^c_{2,3}$$
$$-\left\{k^c_{t,G}\left[CTA\right]_c+k^c_{tr,SG}\left[S\right]_c+2\pi d_p N_p\bar{D}_3+K_p\bar{M}^c_n/M_u\right\}V_c\left[G^*_{T,3}\right]_c\nu^c_{2,3} \qquad \text{(A4.96)}$$

A4.1.3.10. Balance on polymer having 0 graft

$$d\left(V_c\left[P_{T,0}\right]_c\right)/dt = -\left\{\frac{Q_{sm}}{m_{CPP}} + 2\pi d_p N_p \bar{D}_0\right\} V_c\left[P_{T,0}\right]_c + \left(k^c_{tcAA}\left[A^*_{T,0}\right]^2_c + k^c_{tcBB}\left[B^*_{T,0}\right]^2_c\right)V_c$$
$$+k^c_{tcAB}\left[A^*_{T,0}\right]_c\left[B^*_{T,0}\right]_c V_c + k^c_{tdGA}\left[G^*_{T,3}\right]_c\left[A^*_{T,0}\right]_c V_c + k^c_{tdGB}\left[G^*_{T,3}\right]_c\left[B^*_{T,0}\right]_c V_c$$
$$+\left\{k^c_{t,A}[CTA]_c + k^c_{tr,AG}[G]_c + k^c_{tr,AS}[S]_c\right\}V_c\left[A^*_{T,0}\right]_c$$
$$+\left\{k^c_{t,B}[CTA]_c + k^c_{tr,BG}[G]_c + k^c_{tr,BS}[S]_c\right\}V_c\left[B^*_{T,0}\right]_c - K_p\bar{M}^c_n/M_u V_c\left[P_{T,0}\right]_c \qquad \text{(A4.97)}$$

$$d\left(V_c\left[P_{T,0}\right]_c \mu^c_{1,0}\right)/dt = -\left\{\frac{Q_{sm}}{m_{CPP}} + 2\pi d_p N_p \bar{D}_0\right\} V_c\left[P_{T,0}\right]_c \mu^c_{1,0}$$
$$+\left(2k^c_{tcAA}\left[A^*_{T,0}\right]^2_c \lambda^c_{1,0} + 2k^c_{tcBB}\left[B^*_{T,0}\right]^2_c \eta^c_{1,0}\right)V_c + k^c_{tcAB}\left[A^*_{T,0}\right]_c\left[B^*_{T,0}\right]_c\left(\lambda^c_{1,0} + \eta^c_{1,0}\right)V_c$$
$$+k^c_{tdGA}\left[G^*_{T,3}\right]_c\left[A^*_{T,0}\right]_c\left(\nu^c_{1,3} + \lambda^c_{1,0}\right)V_c + k^c_{tdGB}\left[G^*_{T,3}\right]_c\left[B^*_{T,0}\right]_c\left(\nu^c_{1,3} + \eta^c_{1,0}\right)V_c$$
$$+\left\{k^c_{t,A}[CTA]_c + k^c_{tr,AG}[G]_c + k^c_{tr,AS}[S]_c\right\}V_c\left[A^*_{T,0}\right]_c \lambda^c_{1,0}$$
$$+\left\{k^c_{t,B}[CTA]_c + k^c_{tr,BG}[G]_c + k^c_{tr,BS}[S]_c\right\}V_c\left[B^*_{T,0}\right]_c \eta^c_{1,0} - K_p\bar{M}^c_n/M_u V_c\left[P_{T,0}\right]_c \mu^c_{1,0} \qquad \text{(A4.98)}$$

$$d\left(V_c\left[P_{T,0}\right]_c \mu^c_{2,0}\right)/dt = -\left\{\frac{Q_{sm}}{m_{CPP}} + 2\pi d_p N_p \bar{D}_0\right\} V_c\left[P_{T,0}\right]_c \mu^c_{2,0}$$
$$+\left(2k^c_{tcAA}\left[A^*_{T,0}\right]^2_c\left(2\lambda^c_{2,0} + 2\lambda^c_{1,0}\lambda^c_{1,0}\right) + 2k^c_{tcBB}\left[B^*_{T,0}\right]^2_c\left(2\eta^c_{2,0} + 2\eta^c_{1,0}\eta^c_{1,0}\right)\right)V_c$$
$$+k^c_{tcAB}\left[A^*_{T,0}\right]_c\left[B^*_{T,0}\right]_c\left(\lambda^c_{2,0} + 2\lambda^c_{1,0}\eta^c_{1,0} + \eta^c_{2,0}\right)V_c$$
$$+k^c_{tdGA}\left[G^*_{T,3}\right]_c\left[A^*_{T,1}\right]_c\left(\nu^c_{2,3} + 2\nu^c_{1,3}\lambda^c_{1,0} + \lambda^c_{2,0}\right)V_c + k^c_{tdGB}\left[G^*_{T,3}\right]_c\left[B^*_{T,1}\right]_c\left(\nu^c_{2,3} + 2\nu^c_{1,3}\eta^c_{1,0} + \eta^c_{2,0}\right)V_c$$
$$+\left\{k^c_{t,A}[CTA]_c + k^c_{tr,AG}[G]_c + k^c_{tr,AS}[S]_c\right\}V_c\left[A^*_{T,0}\right]_c \lambda^c_{2,0}$$
$$+\left\{k^c_{t,B}[CTA]_c + k^c_{tr,BG}[G]_c + k^c_{tr,BS}[S]_c\right\}V_c\left[B^*_{T,0}\right]_c \eta^c_{2,0} - K_p\bar{M}^c_n/M_u V_c\left[P_{T,0}\right]_c \mu^c_{2,0} \qquad \text{(A4.99)}$$

A4.1.3.11. Balance on polymer having one polyol graft

$$d\left(V_c\left[P_{T,1}\right]_c\right)/dt = -\left\{\frac{Q_{sm}}{m_{CPP}} + 2\pi d_p N_p \bar{D}_1\right\} V_c\left[P_{T,1}\right]_c$$
$$+\left(k^c_{tcAA}\left[A^*_{T,0}\right]_c\left[A^*_{T,1}\right]_c + k^c_{tcBB}\left[B^*_{T,0}\right]_c\left[B^*_{T,1}\right]_c\right)V_c$$
$$+k^c_{tcAB}\left[A^*_{T,0}\right]_c\left[B^*_{T,1}\right]_c V_c + k^c_{tcAB}\left[A^*_{T,1}\right]_c\left[B^*_{T,0}\right]_c V_c + k^c_{tdGA}\left[G^*_{T,3}\right]_c\left[A^*_{T,1}\right]_c V_c + k^c_{tdGB}\left[G^*_{T,3}\right]_c\left[B^*_{T,1}\right]_c V_c$$
$$+\left\{k^c_{t,A}[CTA]_c + k^c_{tr,AG}[G]_c + k^c_{tr,AS}[S]_c\right\}V_c\left[A^*_{T,1}\right]_c + \left\{k^c_{t,B}[CTA]_c + k^c_{tr,BG}[G]_c + k^c_{tr,BS}[S]_c\right\}V_c\left[B^*_{T,1}\right]_c$$
$$-K_p\bar{M}^c_n/M_u V_c\left[P_{T,1}\right]_c \qquad \text{(A4.100)}$$

$$d\left(V_c\left[P_{T,1}\right]_c \mu^c_{1,1}\right)/dt = -\left\{\frac{Q_{sm}}{m_{CPP}} + 2\pi d_p N_p \bar{D}_1\right\} V_c\left[P_{T,1}\right]_c \mu^c_{1,1}$$
$$+\left(k^c_{tcAA}\left[A^*_{T,0}\right]_c\left[A^*_{T,1}\right]_c\left(\lambda^c_{1,1}+\lambda^c_{1,0}\right)+k^c_{tcBB}\left[B^*_{T,0}\right]_c\left[B^*_{T,1}\right]_c\left(\eta^c_{1,1}+\eta^c_{1,0}\right)\right)V_c$$
$$+k^c_{tcAB}\left[A^*_{T,0}\right]_c\left[B^*_{T,1}\right]_c\left(\lambda^c_{1,0}+\eta^c_{1,1}\right)V_c + k^c_{tcAB}\left[A^*_{T,1}\right]_c\left[B^*_{T,0}\right]_c\left(\lambda^c_{1,1}+\eta^c_{1,0}\right)V_c$$
$$k^c_{tdGA}\left[G^*_{T,3}\right]_c\left[A^*_{T,1}\right]_c\left(\nu^c_{1,3}+\lambda^c_{1,1}\right)V_c + k^c_{tdGB}\left[G^*_{T,3}\right]_c\left[B^*_{T,1}\right]_c\left(\nu^c_{1,3}+\eta^c_{1,1}\right)V_c$$
$$+\left\{k^c_{t,A}[CTA]_c + k^c_{tr,AG}[G]_c + k^c_{tr,AS}[S]_c\right\}V_c\left[A^*_{T,1}\right]_c\lambda^c_{1,1}$$
$$+\left\{k^c_{t,B}[CTA]_c + k^c_{tr,BG}[G]_c + k^c_{tr,BS}[S]_c\right\}V_c\left[B^*_{T,1}\right]_c\eta^c_{1,1} - K_p\bar{M}^c_n/M_u\, V_c\left[P_{T,1}\right]_c\mu^c_{1,1} \qquad \text{(A4.101)}$$

$$d\left(V_c\left[P_{T,1}\right]_c \mu^c_{1,2}\right)/dt = -\left\{\frac{Q_{sm}}{m_{CPP}} + 2\pi d_p N_p \bar{D}_1\right\} V_c\left[P_{T,1}\right]_c \mu^c_{1,2}$$
$$+\left(k^c_{tcAA}\left[A^*_{T,0}\right]_c\left[A^*_{T,1}\right]_c\left(\lambda^c_{2,1}+2\lambda^c_{1,1}\lambda^c_{1,0}+\lambda^c_{2,0}\right)+k^c_{tcBB}\left[B^*_{T,0}\right]_c\left[B^*_{T,1}\right]_c\left(\eta^c_{2,1}+2\eta^c_{1,1}\eta^c_{1,0}+\eta^c_{2,0}\right)\right)V_c$$
$$+k^c_{tcAB}\left[A^*_{T,0}\right]_c\left[B^*_{T,1}\right]_c\left(\lambda^c_{2,0}+2\lambda^c_{1,0}\eta^c_{1,1}+\eta^c_{2,1}\right)V_c + k^c_{tcAB}\left[A^*_{T,1}\right]_c\left[B^*_{T,0}\right]_c\left(\lambda^c_{2,1}+2\lambda^c_{1,1}\eta^c_{1,0}+\eta^c_{2,0}\right)V_c$$
$$k^c_{tdGA}\left[G^*_{T,3}\right]_c\left[A^*_{T,1}\right]_c\left(\nu^c_{2,3}+2\nu^c_{1,3}\lambda^c_{1,1}+\lambda^c_{2,1}\right)V_c + k^c_{tdGB}\left[G^*_{T,3}\right]_c\left[B^*_{T,1}\right]_c\left(\nu^c_{2,3}+2\nu^c_{1,3}\eta^c_{1,1}+\eta^c_{2,1}\right)V_c$$
$$+\left\{k^c_{t,A}[CTA]_c + k^c_{tr,AG}[G]_c + k^c_{tr,AS}[S]_c\right\}V_c\left[A^*_{T,1}\right]_c\lambda^c_{2,1}$$
$$+\left\{k^c_{t,B}[CTA]_c + k^c_{tr,BG}[G]_c + k^c_{tr,BS}[S]_c\right\}V_c\left[B^*_{T,1}\right]_c\eta^c_{2,1} - K_p\bar{M}^c_n/M_u\, V_c\left[P_{T,1}\right]_c\mu^c_{2,1} \qquad \text{(A4.102)}$$

A4.1.3.12. Balance on Polymer having one S5200 graft

$$d\left(V_c\left[P_{T,3}\right]_c\right)/dt = -\left\{\frac{Q_{sm}}{m_{CPP}} + 2\pi d_p N_p \bar{D}_3\right\} V_c\left[P_{T,3}\right]_c$$
$$+\left(k^c_{tcAA}\left[A^*_{T,3}\right]_c\left[A^*_{T,0}\right]_c + k^c_{tcBB}\left[B^*_{T,3}\right]_c\left[B^*_{T,0}\right]_c\right)V_c$$
$$+k^c_{tcAB}\left[A^*_{T,3}\right]_c\left[B^*_{T,0}\right]_c V_c + k^c_{tcAB}\left[A^*_{T,0}\right]_c\left[B^*_{T,3}\right]_c V_c$$
$$+2k^c_{tdGA}\left[G^*_{T,3}\right]_c\left[A^*_{T,3}\right]_c V_c + 2k^c_{tdGB}\left[G^*_{T,3}\right]_c\left[B^*_{T,3}\right]_c V_c$$
$$+k^c_{tdGA}\left[G^*_{T,3}\right]_c\left(\left[A^*_{T,0}\right]_c + \left[A^*_{T,1}\right]_c\right)V_c + k^c_{tdGB}\left[G^*_{T,3}\right]_c\left(\left[B^*_{T,0}\right]_c + \left[B^*_{T,1}\right]_c\right)V_c$$
$$+\left\{k^c_{t,A}[CTA]_c + k^c_{tr,AG}[G]_c + k^c_{tr,AS}[S]_c\right\}V_c\left[A^*_{T,3}\right]_c$$
$$+\left\{k^c_{t,B}[CTA]_c + k^c_{tr,BG}[G]_c + k^c_{tr,BS}[S]_c\right\}V_c\left[B^*_{T,3}\right]_c + \left\{k^c_{tr,G}[CTA]_c + k^c_{tr,GS}[S]_c\right\}V_c\left[G^*_{T,3}\right]_c$$
$$-K_p\,\bar{M}^c_n/M_u\, V_c\left[P_{T,3}\right]_c \qquad \text{(A4.103)}$$

$$d\left(V_c\left[P_{T,3}\right]_c \mu^c_{1,3}\right)/dt = -\left\{\frac{Q_{sm}}{m_{CPP}} + 2\pi d_p N_p \bar{D}_3\right\} V_c\left[P_{T,3}\right]_c \mu^c_{1,3}$$
$$+\left(k^c_{tcAA}\left[A^*_{T,3}\right]_c\left[A^*_{T,0}\right]_c\left(\lambda^c_{1,3}+\lambda^c_{1,0}\right)+k^c_{tcBB}\left[B^*_{T,3}\right]_c\left[B^*_{T,0}\right]_c\left(\eta^c_{1,3}+\eta^c_{1,0}\right)\right)V_c$$

$$+k^c_{tcAB}\left[A^*_{T,3}\right]_c\left[B^*_{T,0}\right]_c\left(\lambda^c_{1,3}+\eta^c_{1,0}\right)V_c+k^c_{tcAB}\left[A^*_{T,0}\right]_c\left[B^*_{T,3}\right]_c\left(\lambda^c_{1,0}+\eta^c_{1,3}\right)V_c$$
$$+2k^c_{tdGA}\left[G^*_{T,3}\right]_c\left[A^*_{T,3}\right]_c\left(\nu^c_{1,3}+\lambda^c_{1,3}\right)V_c+2k^c_{tdGB}\left[G^*_{T,3}\right]_c\left[B^*_{T,3}\right]_c\left(\nu^c_{1,3}+\eta^c_{1,3}\right)V_c$$
$$+k^c_{tdGA}\left[G^*_{T,3}\right]_c\left(\left[A^*_{T,0}\right]_c\left(\nu^c_{1,3}+\lambda^c_{1,0}\right)+\left[A^*_{T,1}\right]_c\left(\nu^c_{1,3}+\lambda^c_{1,1}\right)\right)V_c$$
$$+k^c_{tdGB}\left[G^*_{T,3}\right]_c\left(\left[B^*_{T,0}\right]_c\left(\nu^c_{1,3}+\eta^c_{1,0}\right)+\left[B^*_{T,1}\right]_c\left(\nu^c_{1,3}+\eta^c_{1,1}\right)\right)V_c$$
$$+\left\{k^c_{t,A}\left[CTA\right]_c+k^c_{tr,AG}\left[G\right]_c+k^c_{tr,AS}\left[S\right]_c\right\}V_c\left[A^*_{T,3}\right]_c\lambda^c_{1,3}$$
$$+\left\{k^c_{t,B}\left[CTA\right]_c+k^c_{tr,BG}\left[G\right]_c+k^c_{tr,BS}\left[S\right]_c\right\}V_c\left[B^*_{T,3}\right]_c\eta^c_{1,3}$$
$$+\left\{k^c_{tr,G}\left[CTA\right]_c+k^c_{tr,GS}\left[S\right]_c\right\}V_c\left[G^*_{T,3}\right]_c\nu^c_{1,3}-K_p\bar{M}^c_n/M_u V_c\left[P_{T,3}\right]_c\mu^c_{1,3} \qquad \text{(A4.104)}$$

$$d\left(V_c\left[P_{T,3}\right]_c\mu^c_{2,3}\right)/dt=-\left\{\frac{Q_{sm}}{m_{CPP}}+2\pi d_p N_p\bar{D}_3\right\}V_c\left[P_{T,3}\right]_c\mu^c_{2,3}$$
$$+\left(k^c_{tcAA}\left[A^*_{T,3}\right]_c\left[A^*_{T,0}\right]_c\left(\lambda^c_{2,3}+2\lambda^c_{1,3}\lambda^c_{1,0}+\lambda^c_{2,0}\right)+k^c_{tcBB}\left[B^*_{T,3}\right]_c\left[B^*_{T,0}\right]_c\left(\eta^c_{2,3}+2\eta^c_{1,3}\eta^c_{1,0}+\eta^c_{1,0}\right)\right)V_c$$
$$+k^c_{tcAB}\left[A^*_{T,3}\right]_c\left[B^*_{T,0}\right]_c\left(\lambda^c_{2,3}+2\lambda^c_{1,3}\eta^c_{1,0}+\eta^c_{2,0}\right)V_c+k^c_{tcAB}\left[A^*_{T,0}\right]_c\left[B^*_{T,3}\right]_c\left(\lambda^c_{2,0}+2\lambda^c_{1,0}\eta^c_{1,3}+\eta^c_{2,3}\right)V_c$$
$$+2k^c_{tdGA}\left[G^*_{T,3}\right]_c\left[A^*_{T,3}\right]_c\left(\nu^c_{2,3}+2\nu^c_{1,3}\lambda^c_{1,3}+\lambda^c_{2,3}\right)V_c+2k^c_{tdGB}\left[G^*_{T,3}\right]_c\left[B^*_{T,3}\right]_c\left(\nu^c_{2,3}+2\nu^c_{1,3}\eta^c_{1,3}+\eta^c_{2,3}\right)V_c$$
$$+k^c_{tdGA}\left[G^*_{T,3}\right]_c\left(\left[A^*_{T,0}\right]_c\left(\nu^c_{2,3}+2\nu^c_{1,3}\lambda^c_{1,0}+\lambda^c_{2,0}\right)+\left[A^*_{T,1}\right]_c\left(\nu^c_{2,3}+2\nu^c_{1,3}\lambda^c_{1,1}+\lambda^c_{2,1}\right)\right)V_c$$
$$+k^c_{tdGB}\left[G^*_{T,3}\right]_c\left(\left[B^*_{T,0}\right]_c\left(\nu^c_{2,3}+2\nu^c_{1,3}\eta^c_{1,0}+\eta^c_{2,0}\right)+\left[B^*_{T,1}\right]_c\left(\nu^c_{2,3}+2\nu^c_{1,3}\eta^c_{1,1}+\eta^c_{2,1}\right)\right)V_c$$
$$+\left\{k^c_{t,A}\left[CTA\right]_c+k^c_{tr,AG}\left[G\right]_c+k^c_{tr,AS}\left[S\right]_c\right\}V_c\left[A^*_{T,3}\right]_c\lambda^c_{2,3}$$
$$+\left\{k^c_{t,B}\left[CTA\right]_c+k^c_{tr,BG}\left[G\right]_c+k^c_{tr,BS}\left[S\right]_c\right\}V_c\left[B^*_{T,3}\right]_c\eta^c_{2,3}$$
$$+\left\{\ {}^c_{tr,G}\left[\quad\right]_c+\ {}^c_{tr,GS}\left[\ \right]_c\right\}\ {}_c\left[\ {}^*_{T,3}\right]_c\nu^c_{2,3}-K_p\bar{M}^c_n/M_u V_c\left[P_{T,3}\right]_c\mu^c_{2,3} \qquad \text{(A4.105)}$$

A4.1.4. Balance on oligoradicals, dead polymer and moments within particles

A4.1.4.1. Balance on radicals R coming from initiator decomposition and transfers:*

$$d\left(V_p\left[R^*\right]_p\right)/dt=2f_p k^p_d\left[I\right]_p V_p-\left(\frac{Q_{sm}}{m_{CPP}}+k^p_{RA}\left[A\right]_p+k^p_{RB}\left[B\right]_p\right)\left[R^*\right]_p V_p$$
$$+\left(k^p_{tr,A}\left[A^*_{T,0}\right]_p+k^p_{tr,B}\left[B^*_{T,0}\right]_p\right)\left[CTA\right]_p V_p$$
$$+\left(k^p_{tr,A}\left(\left[A^*_{T,1}\right]_p+\left[A^*_{T,3}\right]_p\right)+k^p_{tr,B}\left(\left[B^*_{T,1}\right]_p+\left[B^*_{T,3}\right]_p\right)+k^p_{tr,G}\left[G^*_{T,3}\right]_p\right)\left[CTA\right]_p V_p$$

(A4.106)

A4.1.4.2. Radicals with a terminal A and having 0 graft*

Balance on $[A^*_{1,0}]_p$:

$$d\left(V_p\left[A^*_{T,0}\right]_p \Delta^p_{1,0}\right)/dt = 2\pi d_p N_p \bar{D}_0 \left[A^*_{T,0}\right]_c \Delta^c_{1,0} V_c + k^p_{RA}\left[R^*\right]_p [A]_p V_p$$
$$-\left\{\frac{Q_{sm}}{m_{CPP}} + k^p_{pAA}[A]_p + k^p_{pAB}[B]_p\right\} V_p \left[A^*_{T,0}\right]_p \Delta^p_{1,0}$$
$$-\left\{2k^p_{tcAA}\left(\left[A^*_{T,0}\right]_p + \left[A^*_{T,1}\right]_p + \left[A^*_{T,3}\right]_p\right) + k^p_{tcBA}\left(\left[B^*_{T,0}\right]_p + \left[B^*_{T,1}\right]_p + \left[B^*_{T,3}\right]_p\right)\right\} V_p \left[A^*_{T,0}\right]_p \Delta^p_{1,0}$$
$$-\left\{k^p_{tdGA}\left[G^*_{T,3}\right]_p + k^p_{t,A}[CTA]_p\right\} V_p \left[A^*_{T,0}\right]_p \Delta^p_{1,0} + K_p \bar{M}^c_n / M_u V_c \left[A^*_{T,0}\right]_c \Delta^c_{1,0} \qquad \text{(A4.107)}$$

Balance on $[A^*_{i,0}]_p$ for $i \geq 2$:

$$d\left(V_p\left[A^*_{T,0}\right]_p \Delta^p_{i,0}\right)/dt = 2\pi d_p N_p \bar{D}_0 \left[A^*_{T,0}\right]_c \Delta^c_{i,0} V_c$$
$$+\left(k^p_{pAA}\left[A^*_{T,0}\right]_p \Delta^p_{i-1,0}[A]_p + k^p_{pBA}\left[B^*_{T,0}\right]_p \Gamma^p_{i-1,0}[A]_p\right) V_p$$
$$-\left(\frac{Q_{sm}}{m_{CPP}} + k^p_{pAA}[A]_p + k^p_{pAB}\ [B]_p + 2k^p_{tcAA}\left(\left[A^*_{T,0}\right]_p + \left[A^*_{T,1}\right]_p + \left[A^*_{T,3}\right]_p\right)\right) V_p \left[A^*_{T,0}\right]_p \Delta^p_{i,0}$$
$$-\left(k^p_{tcAB}\left(\left[B^*_{T,0}\right]_c + \left[B^*_{T,1}\right]_c + \left[B^*_{T,3}\right]_c\right)\right) V_p \left[A^*_{T,0}\right]_p \Delta^p_{i,0}$$
$$-\left(k^p_{tdGA}\left[G^*_{T,3}\right]_p + k^p_{t,A}[CTA]_p\right) V_p \left[A^*_{T,0}\right]_p \Delta^p_{i,0} + K_p \bar{M}^c_n / M_u V_c \left[A^*_{T,0}\right]_c \Delta^c_{i,0} \qquad \text{(A4.108)}$$

Sum of all the species :

$$d\left(V_p\left[A^*_{T,0}\right]_p\right)/dt = \left(k^p_{RA}\left[R^*\right]_p [A]_p + k^p_{pBA}\left[B^*_{T,0}\right]_p [A]_p\right) V_p$$
$$-\left(\frac{Q_{sm}}{m_{CPP}} + k^p_{pAB}[B]_p + 2k^p_{tcAA}\left[A^*_{T,0}\right]_p\right) V_p \left[A^*_{T,0}\right]_p - \left(k^p_{tcAB}\left[B^*_{T,0}\right]_p + k^p_{t,A}[CTA]_p\right) V_p \left[A^*_{T,0}\right]_p$$
$$+2\pi d_p N_p \bar{D}_0 V_c \left[A^*_{T,0}\right]_c + K_p V_c \left[A^*_{T,0}\right]_c \lambda^c_{1,0} - k^p_{tdGA}\left[G^*_{T,3}\right]_p V_p \left[A^*_{T,0}\right]_p$$
$$-2k^p_{tcAA}\left(\left[A^*_{T,1}\right]_p + \left[A^*_{T,3}\right]_p\right) V_p \left[A^*_{T,0}\right]_p - \left(k^p_{tcAB}\left(\left[B^*_{T,1}\right]_p + \left[B^*_{T,3}\right]_p\right) + k^p_{t,A}[CTA]_p\right) V_p \left[A^*_{T,0}\right]_p$$
$$+\left\{2\pi d_p N_p \bar{D}_0 + K_p \bar{M}^c_n / M_u\right\} V_c \left[A^*_{T,0}\right]_c \qquad \text{(A4.109)}$$

$$d\left(V_p\left[A^*_{T,0}\right]_p \lambda^p_{1,0}\right)/dt = \left(k^p_{RA}\left[R^*\right]_p + k^p_{pAA}\left[A^*_{T,0}\right]_p + k^p_{pBA}\left[B^*_{T,0}\right]_p\left(\eta^p_{1,0}+1\right)\right)[A]_p V_p$$
$$-\left(\frac{Q_{sm}}{m_{CPP}} + k^p_{pAB}[B]_p + 2k^p_{tcAA}\left[A^*_{T,0}\right]_p\right) V_p \left[A^*_{T,0}\right]_p \lambda^p_{1,0}$$
$$-\left(k^p_{tcAB}\left[B^*_{T,0}\right]_p + k^p_{t,A}[CTA]_p\right) V_p \left[A^*_{T,0}\right]_p \lambda^p_{1,0} + \left(2\pi d_p N_p \bar{D}_0 + K_p \bar{M}^c_n / M_u\right) V_c \left[A^*_{T,0}\right]_c \lambda^c_{1,0}$$

$$-k^p_{tdGA}\left[G^*_{T,3}\right]_p V_p\left[A^*_{T,0}\right]_p \lambda^p_{1,0} - \left(2k^p_{tcAA}\left(\left[A^*_{T,1}\right]_p + \left[A^*_{T,3}\right]_p\right)\right)V_p\left[A^*_{T,0}\right]_p \lambda^p_{1,0}$$
$$-k^p_{tcAB}\left(\left[B^*_{T,1}\right]_p + \left[B^*_{T,3}\right]_p\right)V_p\left[A^*_{T,0}\right]_p \lambda^p_{1,0} \qquad \text{(A4.110)}$$

$$d\left(V_p\left[A^*_{T,0}\right]_p \lambda^p_{2,0}\right)/dt = \left(k^p_{RA}\left[R^*\right]_p + k^p_{pAA}\left[A^*_{T,0}\right]_p\left(2\lambda^p_{1,0}+1\right) + k^p_{pBA}\left[B^*_{T,0}\right]_p\left(\eta^p_{2,0}+2\eta^p_{1,0}+1\right)\right)[A]_p V_p$$
$$-\left(\frac{Q_{sm}}{m_{CPP}} + k^p_{pAB}[B]_p + 2k^p_{tcAA}\left[A^*_{T,0}\right]_p\right)V_p\left[A^*_{T,0}\right]_p \lambda^p_{2,0}$$
$$-\left(k^p_{tcAB}\left[B^*_{T,0}\right]_p + k^p_{t,A}[CTA]_p\right)V_p\left[A^*_{T,0}\right]_p \lambda^p_{2,0}$$
$$+\left(2\pi d_p N_p \bar{D}_0 + K_p \bar{M}^c_n/M_u\right)V_c\left[A^*_{T,0}\right]_c \lambda^c_{2,0} - k^p_{tdGA}\left[G^*_{T,3}\right]_p V_p\left[A^*_{T,0}\right]_p \lambda^p_{2,0}$$
$$-2k^p_{tcAA}\left(\left[A^*_{T,1}\right]_p + \left[A^*_{T,3}\right]_p\right)V_p\left[A^*_{T,0}\right]_p \lambda^p_{2,0} \; - k^p_{tcAB}\left(\left[B^*_{T,1}\right]_p + \left[B^*_{T,3}\right]_p\right)V_p\left[A^*_{T,0}\right]_p \lambda^p_{2,0}$$
(A4.111)

A4.1.4.3. Radicals with a terminal A and having one polyol graft*

Balance on $[A^*_{1,1}]_p$:

$$d\left(V_p\left[A^*_{T,1}\right]_p \Delta^p_{1,1}\right)/dt = 2\pi d_p N_p \bar{D}_1 V_c\left[A^*_{T,1}\right]_c \Delta^c_{1,1} - \left\{\frac{Q_{sm}}{m_{CPP}} + k^p_{pAA}[A]_c + k^p_{pAB}[B]_c\right\}V_p\left[A^*_{T,1}\right]_p \Delta^p_{1,1}$$
$$-\left\{2k^p_{tcAA}\left(\left[A^*_{T,0}\right]_p + \left[A^*_{T,1}\right]_p + \left[A^*_{T,3}\right]_p\right) + k^p_{tcBA}\left(\left[B^*_{T,0}\right]_p + \left[B^*_{T,1}\right]_p + \left[B^*_{T,3}\right]_p\right)\right\}V_p\left[A^*_{T,1}\right]_p \Delta^p_{1,1}$$
$$-\left\{k^p_{tdGA}\left[G^*_{T,3}\right]_p + k^p_{t,A}[CTA]_p\right\}V_p\left[A^*_{T,1}\right]_p \Delta^p_{1,1} + K_p \bar{M}^c_n/M_u V_c\left[A^*_{T,1}\right]_c \Delta^c_{1,1} \qquad \text{(A4.112)}$$

Balance on $[A^*_{i,1}]_p$ for $i \geq 2$:

$$d\left(V_p\left[A^*_{T,1}\right]_p \Delta^p_{i,1}\right)/dt = 2\pi\, d_p N_p \bar{D}_1\left[A^*_{T,1}\right]_c \Delta^c_{i,1} V_c + \left(k^p_{pAA}\left[A^*_{T,1}\right]_p \Delta^p_{i-1,1}[A]_p + k^p_{pBA}\left[B^*_{T,1}\right]_p \Gamma^p_{i-1,1}[A]_p\right)V_p$$
$$-\left(\frac{Q_{sm}}{m_{CPP}} + k^p_{pAA}[A]_p + k^p_{pAB}\;[B]_p + 2k^p_{tcAA}\left(\left[A^*_{T,0}\right]_p + \left[A^*_{T,1}\right]_p + \left[A^*_{T,3}\right]_p\right)\right)V_p\left[A^*_{T,1}\right]_p \Delta^p_{i,1}$$
$$-\left(k^p_{tcAB}\left(\left[B^*_{T,0}\right]_c + \left[B^*_{T,1}\right]_c + \left[B^*_{T,3}\right]_c\right)\right)V_p\left[A^*_{T,1}\right]_p \Delta^p_{i,1}$$
$$-\left(k^p_{tdGA}\left[G^*_{T,3}\right]_p + k^p_{t,A}[CTA]_p\right)V_p\left[A^*_{T,1}\right]_p \Delta^p_{i,1} + K_p \bar{M}^c_n/M_u V_c\left[A^*_{T,1}\right]_c \Delta^c_{i,1} \qquad \text{(A4.113)}$$

Sum of all the species :

$$d\left(V_p\left[A^*_{T,1}\right]_p\right)/dt = k^p_{pBA}\left[B^*_{T,1}\right]_p V_p[A]_p - k^p_{tdGA}\left[G^*_{T,3}\right]_p V_p\left[A^*_{T,1}\right]_p$$
$$-\left(\frac{Q_{sm}}{m_{CPP}} + k^p_{pAB}[B]_p + 2k^p_{tcAA}\left(\left[A^*_{T,0}\right]_p + \left[A^*_{T,1}\right]_p + \left[A^*_{T,3}\right]_p\right)\right)V_p\left[A^*_{T,1}\right]_p$$

$$-\left(k^{p}_{tcAB}\left(\left[B^{*}_{T,0}\right]_{c}+\left[B^{*}_{T,1}\right]_{c}+\left[B^{*}_{T,3}\right]_{c}\right)+k^{p}_{t,A}\left[CTA\right]_{p}\right)V_{p}\left[A^{*}_{T,1}\right]_{p}+2\pi d_{p}N_{p}\bar{D}_{1}V_{c}\left[A^{*}_{T,1}\right]_{c}$$
$$+K_{p}\bar{M}^{c}_{n}/M_{u}V_{c}\left[A^{*}_{T,1}\right]_{c} \qquad \text{(A4.114)}$$

$$d\left(V_{p}\left[A^{*}_{T,1}\right]_{p}\lambda^{p}_{1,1}\right)/dt=\left\{k^{p}_{pAA}\left[A^{*}_{T,1}\right]_{p}+k^{p}_{pBA}\left[B^{*}_{T,1}\right]_{p}\left(\eta^{p}_{1,1}+1\right)\right\}V_{p}\left[A\right]_{p}-k^{p}_{tdGA}\left[G^{*}_{T,3}\right]_{p}V_{p}\left[A^{*}_{T,1}\right]_{p}\lambda^{p}_{1,1}$$
$$-\left(\frac{Q_{sm}}{m_{CPP}}+k^{p}_{pAB}\left[B\right]_{p}+2k^{p}_{tcAA}\left(\left[A^{*}_{T,0}\right]_{p}+\left[A^{*}_{T,1}\right]_{p}+\left[A^{*}_{T,3}\right]_{p}\right)\right)V_{p}\left[A^{*}_{T,1}\right]_{p}\lambda^{p}_{1,1}$$
$$-\left(k^{p}_{tcAB}\left(\left[B^{*}_{T,0}\right]_{c}+\left[B^{*}_{T,1}\right]_{c}+\left[B^{*}_{T,3}\right]_{c}\right)+k^{p}_{t,A}\left[CTA\right]_{p}\right)V_{p}\left[A^{*}_{T,1}\right]_{p}\lambda^{p}_{1,1}$$
$$+\left(2\pi d_{p}N_{p}\bar{D}_{1}+K_{p}\bar{M}^{c}_{n}/M_{u}\right)V_{c}\left[A^{*}_{T,1}\right]_{c}\lambda^{c}_{1,1} \qquad \text{(A4.115)}$$

$$d\left(V_{p}\left[A^{*}_{T,1}\right]_{p}\lambda^{p}_{2,1}\right)/dt=\left\{k^{p}_{pAA}\left[A^{*}_{T,1}\right]_{p}\left(2\lambda^{p}_{1,1}+1\right)+k^{p}_{pBA}\left[B^{*}_{T,1}\right]_{p}\left(\eta^{p}_{2,1}+2\eta^{p}_{1,1}+1\right)\right\}V_{p}\left[A\right]_{p}-k^{p}_{tdGA}\left[G^{*}_{T,3}\right]_{p}V_{p}\left[A^{*}_{T,1}\right]_{p}\lambda^{p}_{2,1}$$
$$-\left(\frac{Q_{sm}}{m_{CPP}}+k^{p}_{pAB}\left[B\right]_{p}+2k^{p}_{tcAA}\left(\left[A^{*}_{T,0}\right]_{p}+\left[A^{*}_{T,1}\right]_{p}+\left[A^{*}_{T,3}\right]_{p}\right)\right)V_{p}\left[A^{*}_{T,1}\right]_{p}\lambda^{p}_{2,1}$$
$$-\left(k^{p}_{tcAB}\left(\left[B^{*}_{T,0}\right]_{c}+\left[B^{*}_{T,1}\right]_{c}+\left[B^{*}_{T,3}\right]_{c}\right)+k^{p}_{t,A}\left[CTA\right]_{p}\right)V_{p}\left[A^{*}_{T,1}\right]_{p}\lambda^{p}_{2,1}$$
$$+\left(2\pi d_{p}N_{p}\bar{D}_{1}+K_{p}\bar{M}^{c}_{n}/M_{u}\right)V_{c}\left[A^{*}_{T,1}\right]_{c}\lambda^{c}_{2,1} \qquad \text{(A4.116)}$$

A4.1.4.4. Radicals with a terminal A and having one S5200 graft*

Balance on $[A^{*}_{1,3}]_{p}$:

$$d\left(V_{p}\left[A^{*}_{T,3}\right]_{p}\Delta^{p}_{1,3}\right)/dt=2\pi d_{p}N_{p}\bar{D}_{3}V_{c}\left[A^{*}_{T,3}\right]_{c}\Delta^{c}_{1,3}-\left\{\frac{Q_{sm}}{m_{CPP}}+k^{p}_{pAA}\left[A\right]_{c}+k^{p}_{pAB}\left[B\right]_{c}\right\}V_{p}\left[A^{*}_{T,3}\right]_{p}\Delta^{p}_{1,3}$$
$$-\left\{2k^{p}_{tcAA}\left(\left[A^{*}_{T,0}\right]_{p}+\left[A^{*}_{T,1}\right]_{p}+\left[A^{*}_{T,3}\right]_{p}\right)+k^{p}_{tcBA}\left(\left[B^{*}_{T,0}\right]_{p}+\left[B^{*}_{T,1}\right]_{p}+\left[B^{*}_{T,3}\right]_{p}\right)\right\}V_{p}\left[A^{*}_{T,3}\right]_{p}\Delta^{p}_{1,3}$$
$$-\left\{k^{p}_{tdGA}\left[G^{*}_{T,3}\right]_{p}+k^{p}_{t,A}\left[CTA\right]_{p}\right\}V_{p}\left[A^{*}_{T,3}\right]_{p}\Delta^{p}_{1,3}+K_{p}\bar{M}^{c}_{n}/M_{u}V_{c}\left[A^{*}_{T,3}\right]_{c}\Delta^{c}_{1,3} \qquad \text{(A4.117)}$$

Balance on $[A^{*}_{i,1}]_{p}$ for $i \geq 2$:

$$d\left(V_{p}\left[A^{*}_{T,3}\right]_{p}\Delta^{p}_{i,3}\right)/dt=2\pi d_{p}N_{p}\bar{D}_{3}V_{c}\left[A^{*}_{T,3}\right]_{c}\Delta^{c}_{i,3}+\left(k^{p}_{pAA}\left[A^{*}_{T,3}\right]_{p}\Delta^{p}_{i-1,3}\left[A\right]_{p}+k^{p}_{pBA}\left[B^{*}_{T,3}\right]_{p}\Gamma^{p}_{i-1,3}\left[A\right]_{p}\right)V_{p}$$
$$-\left(\frac{Q_{sm}}{m_{CPP}}+k^{p}_{pAA}\left[A\right]_{p}+k^{p}_{pAB}\ \left[B\right]_{p}+2k^{p}_{tcAA}\left(\left[A^{*}_{T,0}\right]_{p}+\left[A^{*}_{T,1}\right]_{p}+\left[A^{*}_{T,3}\right]_{p}\right)\right)V_{p}\left[A^{*}_{T,3}\right]_{p}\Delta^{p}_{i,3}$$
$$-\left(k^{p}_{tcAB}\left(\left[B^{*}_{T,0}\right]_{c}+\left[B^{*}_{T,1}\right]_{c}+\left[B^{*}_{T,3}\right]_{c}\right)\right)V_{p}\left[A^{*}_{T,3}\right]_{p}\Delta^{p}_{i,3}$$
$$-\left(k^{p}_{tdGA}\left[G^{*}_{T,3}\right]_{p}+k^{p}_{t,A}\left[CTA\right]_{p}\right)V_{p}\left[A^{*}_{T,3}\right]_{p}\Delta^{p}_{i,3}+K_{p}\bar{M}^{c}_{n}/M_{u}V_{c}\left[A^{*}_{T,3}\right]_{c}\Delta^{c}_{i,3} \qquad \text{(A4.118)}$$

Sum of all the species :

$$d\left(V_p\left[A^*_{T,3}\right]_p\right)/dt = k^p_{pBA}\left[B^*_{T,3}\right]_p V_p[A]_p - k^p_{tdGA}\left[G^*_{T,3}\right]_p V_p\left[A^*_{T,3}\right]_p$$
$$-\left(\frac{Q_{sm}}{m_{CPP}} + k^p_{pAB}[B]_p + 2k^p_{tcAA}\left(\left[A^*_{T,0}\right]_p + \left[A^*_{T,1}\right]_p + \left[A^*_{T,3}\right]_p\right)\right)V_p\left[A^*_{T,3}\right]_p$$
$$-\left(k^p_{tcAB}\left(\left[B^*_{T,0}\right]_c + \left[B^*_{T,1}\right]_c + \left[B^*_{T,3}\right]_c\right) + k^p_{t,A}[CTA]_p\right)V_p\left[A^*_{T,3}\right]_p + 2\pi d_p N_p \bar{D}_3 V_c\left[A^*_{T,3}\right]_c$$
$$+ K_p \bar{M}^c_n / M_u V_c\left[A^*_{T,3}\right]_c \lambda^c_{1,3} \qquad \text{(A4.119)}$$

$$d\left(V_p\left[A^*_{T,3}\right]_p \lambda^p_{1,3}\right)/dt = \left\{k^p_{pAA}\left[A^*_{T,3}\right]_p + k^p_{pBA}\left[B^*_{T,3}\right]_p\left(\eta^p_{1,3}+1\right)\right\}V_p[A]_p - k^p_{tdGA}\left[G^*_{T,3}\right]_p V_p\left[A^*_{T,3}\right]_p \lambda^p_{1,3}$$
$$-\left(\frac{Q_{sm}}{m_{CPP}} + k^p_{pAB}[B]_p + 2k^p_{tcAA}\left(\left[A^*_{T,0}\right]_p + \left[A^*_{T,1}\right]_p + \left[A^*_{T,3}\right]_p\right)\right)V_p\left[A^*_{T,3}\right]_p \lambda^p_{1,3}$$
$$-\left(k^p_{tcAB}\left(\left[B^*_{T,0}\right]_c + \left[B^*_{T,1}\right]_c + \left[B^*_{T,3}\right]_c\right) + k^p_{t,A}[CTA]_p\right)V_p\left[A^*_{T,3}\right]_p \lambda^p_{1,3}$$
$$+\left(2\pi d_p N_p \bar{D}_1 + K_p \bar{M}^c_n / M_u\right)V_c\left[A^*_{T,3}\right]_c \lambda^c_{1,3} \qquad \text{(A4.120)}$$

$$d\left(V_p\left[A^*_{T,3}\right]_p \lambda^p_{2,3}\right)/dt = \left\{k^p_{pAA}\left[A^*_{T,3}\right]_p\left(2\lambda^p_{1,3}+1\right) + k^p_{pBA}\left[B^*_{T,3}\right]_p\left(\eta^p_{2,3} + 2\eta^p_{1,3} + 1\right)\right\}V_p[A]_p$$
$$-k^p_{tdGA}\left[G^*_{T,3}\right]_p V_p\left[A^*_{T,3}\right]_p \lambda^p_{2,3}$$
$$-\left(\frac{Q_{sm}}{m_{CPP}} + k^p_{pAB}[B]_p + 2k^p_{tcAA}\left(\left[A^*_{T,0}\right]_p + \left[A^*_{T,1}\right]_p + \left[A^*_{T,3}\right]_p\right)\right)V_p\left[A^*_{T,3}\right]_p \lambda^p_{2,3}$$
$$-\left(k^p_{tcAB}\left(\left[B^*_{T,0}\right]_c + \left[B^*_{T,1}\right]_c + \left[B^*_{T,3}\right]_c\right) + k^p_{t,A}[CTA]_p\right)V_p\left[A^*_{T,3}\right]_p \lambda^p_{2,3}$$
$$+\left(2\pi d_p N_p \bar{D}_3 + K_p \bar{M}^c_n / M_u\right)V_c\left[A^*_{T,3}\right]_c \lambda^c_{2,3} \qquad \text{(A4.121)}$$

A4.1.4.5. Radicals with a terminal B and having 0 graft*

Balance on $[B^*_{2,0}]_p$:

$$d\left(V_p\left[B^*_{T,0}\right]_p \Gamma^p_{2,0}\right)/dt = k^p_{RB}\left[R^*\right]_p[B]_p V_p - \left\{\frac{Q_{sm}}{m_{CPP}} + k^p_{pBA}[A]_p + k^p_{pBB}[B]_p\right\}V_c\left[B^*_{T,0}\right]_p \Gamma^p_{2,0}$$
$$-\left\{2k^p_{tcBB}\left(\left[B^*_{T,0}\right]_p + \left[B^*_{T,1}\right]_p + \left[B^*_{T,3}\right]_p\right) + k^p_{tcBA}\left(\left[A^*_{T,0}\right]_p + \left[A^*_{T,1}\right]_p + \left[A^*_{T,3}\right]_p\right)\right\}V_p\left[B^*_{T,0}\right]_p \Gamma^p_{2,0}$$
$$-\left\{k^p_{tdGB}\left[G^*_{T,3}\right]_p + k^p_{t,B}[CTA]_p\right\}V_p\left[B^*_{T,0}\right]_p \Gamma^p_{2,0}$$
$$+\left(2\pi d_p N_p \bar{D}_0 + K_p \bar{M}^c_n / M_u\right)V_c\left[B^*_{T,0}\right]_c \Gamma^c_{2,0}$$

(A4.122)

Balance on $[B^*_{i,0}]_p$ for $i \geq 3$

$$d\left(V_p\left[B^*_{T,0}\right]_p \Gamma^p_{i,0}\right)/dt = k^p_{pBB}\left[B^*_{i-2,0}\right]_p [B]_p V_p + k^p_{pAB}\left[A^*_{i-2,0}\right]_p [B]_p V_p$$
$$-\left\{\frac{Q_{sm}}{m_{CPP}} + k^p_{pBA}[A]_p + k^p_{pBB}[B]_p\right\} V_p\left[B^*_{T,0}\right]_p \Gamma^p_{i,0}$$
$$-\left\{2k^p_{tcBB}\left(\left[B^*_{T,0}\right]_p + \left[B^*_{T,1}\right]_p + \left[B^*_{T,3}\right]_p\right) + k^p_{tcBA}\left(\left[A^*_{T,0}\right]_p + \left[A^*_{T,1}\right]_p + \left[A^*_{T,3}\right]_p\right)\right\} V_p\left[B^*_{T,0}\right]_p \Gamma^p_{i,0}$$
$$-\left\{k^p_{tdGB}\left[G^*_{T,3}\right]_p + k^p_{t,B}[CTA]_p\right\} V_p\left[B^*_{T,0}\right]_p \Gamma^p_{i,0}$$
$$+\left(2\pi d_p N_p \bar{D}_0 + K_p \bar{M}^c_n / M_u\right) V_c\left[B^*_{T,0}\right]_c \Gamma^c_{i,0}$$

(A4.123)

The global sum on all the species gives:

$$d\left(V_p\left[B^*_{T,0}\right]_p\right)/dt = k^p_{RB}\left[R^*\right]_p [B]_p V_p + k^p_{pAB}\left[A^*_{T,0}\right]_p [B]_p V_p - \left\{\frac{Q_{sm}}{m_{CPP}} + k^p_{pBA}[A]_p\right\} V_p\left[B^*_{T,0}\right]_p$$
$$-\left\{2k^p_{tcBB}\left[B^*_{T,0}\right]_p + k^p_{tcBA}\left[A^*_{T,0}\right]_p + k^p_{t,B}[CTA]_p\right\} V_p\left[B^*_{T,0}\right]_p$$
$$+\left(2\pi d_p N_p \bar{D}_0 + K_p \bar{M}^c_n / M_u\right) V_c\left[B^*_{T,0}\right]_c$$
$$-\left\{2k^p_{tcBB}\left(\left[B^*_{T,1}\right]_p + \left[B^*_{T,3}\right]_p\right) + k^p_{tcBA}\left(\left[A^*_{T,1}\right]_p + \left[A^*_{T,3}\right]_p\right) + k^p_{tdGB}\left[G^*_{T,3}\right]_p\right\} V_p\left[B^*_{T,0}\right]_p$$

(A4.124)

$$d\left(V_p\left[B^*_{T,0}\right]_p \eta^p_{1,0}\right)/dt = \left\{2k^p_{pBB}\left[B^*_{T,0}\right]_p + k^p_{pAB}\left[B^*_{T,0}\right]_p \left(\lambda^p_{1,0} + 2\right) + 2k^p_{RB}\left[R^*\right]_p\right\}[B]_c V_p$$
$$-\left\{\frac{Q_{sm}}{m_{CPP}} + k^p_{pBA}[A]_p\right\} V_p\left[B^*_{T,0}\right]_p \eta^p_{1,0}$$
$$-\left\{2k^p_{tcBB}\left[B^*_{T,0}\right]_p + k^p_{tcBA}\left[A^*_{T,0}\right]_p + k^p_{t,B}[CTA]_p\right\} V_p\left[B^*_{T,0}\right]_p \eta^p_{1,0}$$
$$+\left(2\pi d_p N_p \bar{D}_0 + K_p \bar{M}^c_n / M_u\right) V_c\left[B^*_{T,0}\right]_c \eta^c_{1,0}$$
$$-\left\{2k^p_{tcBB}\left(\left[B^*_{T,1}\right]_p + \left[B^*_{T,3}\right]_p\right) + k^p_{tcBA}\left(\left[A^*_{T,1}\right]_p + \left[A^*_{T,3}\right]_p\right) + k^p_{tdGB}\left[G^*_{T,3}\right]_p\right\} V_p\left[B^*_{T,0}\right]_p \eta^p_{1,0}$$

(A4.125)

$$d\left(V_p\left[B^*_{T,0}\right]_p \eta^p_{2,0}\right)/dt = \left(k^p_{pBB}\left[B^*_{T,0}\right]_p \left(4\eta^p_{1,0} + 4\right) + k^p_{pAB}[B]_p V_p\left[A^*_{T,0}\right]_p \left(\lambda^p_{2,0} + 4\lambda^p_{1,0} + 4\right) + 4k^p_{RB}\left[R^*\right]_p\right)[B]_p V_p$$
$$-\left\{\frac{Q_{sm}}{m_{CPP}} + k^p_{pBA}[A]_p\right\} V_p\left[B^*_{T,0}\right]_p \eta^p_{2,0}$$
$$-\left\{2k^p_{tcBB}\left[B^*_{T,0}\right]_p + k^p_{tcBA}\left[A^*_{T,0}\right]_p + k^p_{t,B}[CTA]_p\right\} V_p\left[B^*_{T,0}\right]_p \eta^p_{2,0}$$

$$+\left(2\pi d_p N_p \bar{D}_0 + K_p \bar{M}_n^c / M_u\right) V_c \left[B_{T,0}^*\right]_c \eta_{2,0}^c$$
$$-\left\{2k_{tcBB}^p \left(\left[B_{T,1}^*\right]_p + \left[B_{T,3}^*\right]_p\right) + k_{tcBA}^p \left(\left[A_{T,1}^*\right]_p + \left[A_{T,3}^*\right]_p\right) + k_{tdGB}^p \left[G_{T,3}^*\right]_p\right\} V_p \left[B_{T,0}^*\right]_p \eta_{2,0}^p$$

(A4.126)

A4.1.4.6. Radicals with a terminal B and having one polyol graft*

Balance on $[B^*_{2,1}]_p$:

$$d\left(V_p \left[B_{T,1}^*\right]_p \Gamma_{2,1}^p\right)/dt = -\left\{\frac{Q_{sm}}{m_{CPP}} + k_{pBA}^p [A]_p + k_{pBB}^p [B]_p\right\} V_c \left[B_{T,1}^*\right]_p \Gamma_{2,1}^p$$
$$-\left\{2k_{tcBB}^p \left(\left[B_{T,0}^*\right]_p + \left[B_{T,1}^*\right]_p + \left[B_{T,3}^*\right]_p\right) + k_{tcBA}^p \left(\left[A_{T,0}^*\right]_p + \left[A_{T,1}^*\right]_p + \left[A_{T,3}^*\right]_p\right)\right\} V_p \left[B_{T,1}^*\right]_p \Gamma_{2,1}^p$$
$$-\left\{k_{tdGB}^p \left[G_{T,3}^*\right]_p + k_{t,B}^p [CTA]_p\right\} V_p \left[B_{T,1}^*\right]_p \Gamma_{2,1}^p$$
$$+\left(2\pi d_p N_p \bar{D}_1 + K_p \bar{M}_n^c / M_u\right) V_c \left[B_{T,1}^*\right]_c \Gamma_{2,1}^c$$

(A4.127)

Balance on $[B^*_{i,1}]_p$ for $i \geq 3$:

$$d\left(V_p \left[B_{T,1}^*\right]_p \Gamma_{i,1}^p\right)/dt = k_{pBB}^p \left[B_{i-2,1}^*\right]_p [B]_p V_p + k_{pAB}^p \left[A_{i-2,1}^*\right]_p [B]_p V_p$$
$$-\left\{\frac{Q_{sm}}{m_{CPP}} + k_{pBA}^p [A]_p\right\} V_p \left[B_{T,1}^*\right]_p \Gamma_{i,1}^p$$
$$-\left\{k_{pBB}^p [B]_p + 2k_{tcBB}^p \left(\left[B_{T,0}^*\right]_p + \left[B_{T,1}^*\right]_p + \left[B_{T,3}^*\right]_p\right) + k_{tcBA}^p \left(\left[A_{T,0}^*\right]_p + \left[A_{T,1}^*\right]_p + \left[A_{T,3}^*\right]_p\right)\right\} V_p \left[B_{T,1}^*\right]_p \Gamma_{i,1}^p$$
$$-\left\{k_{tdGB}^p \left[G_{T,3}^*\right]_p + k_{t,B}^p [CTA]_p\right\} V_p \left[B_{T,1}^*\right]_p \Gamma_{i,1}^p$$
$$+\left(2\pi d_p N_p \bar{D}_1 + K_p \bar{M}_n^c / M_u\right) V_c \left[B_{T,1}^*\right]_c \Gamma_{i,1}^c$$

(A4.128)

The global sum on all the species gives:

$$d\left(V_p \left[B_{T,1}^*\right]_p\right)/dt = k_{pAB}^p \left[A_{T,1}^*\right]_p [B]_p V_p - \left\{\frac{Q_{sm}}{m_{CPP}} + k_{pBA}^p [A]_p\right\} V_p \left[B_{T,1}^*\right]_p$$
$$-\left\{2k_{tcBB}^p \left(\left[B_{T,0}^*\right]_p + \left[B_{T,1}^*\right]_p + \left[B_{T,3}^*\right]_p\right) + k_{tcBA}^p \left(\left[A_{T,0}^*\right]_p + \left[A_{T,1}^*\right]_p + \left[A_{T,3}^*\right]_p\right)\right\} V_p \left[B_{T,1}^*\right]_p$$
$$-\left\{k_{tdGB}^p \left[G_{T,3}^*\right]_p + k_{t,B}^p [CTA]_p\right\} V_p \left[B_{T,1}^*\right]_p + \left(2\pi d_p N_p \bar{D}_1 + K_p \bar{M}_n^c / M_u\right) V_c \left[B_{T,1}^*\right]_c$$

(A4.129)

$$d\left(V_p \left[B_{T,1}^*\right]_p \eta_{1,1}^p\right)/dt = \left\{2k_{pBB}^p \left[B_{T,1}^*\right]_p + k_{pAB}^p \left[A_{T,1}^*\right]_p \left(\lambda_{1,1}^p + 2\right)\right\} [B]_p V_p - \left\{\frac{Q_{sm}}{m_{CPP}} + k_{pBA}^p [A]_p\right\} V_p \left[B_{T,1}^*\right]_p \eta_{1,1}^p$$
$$-\left\{2k_{tcBB}^p \left(\left[B_{T,0}^*\right]_p + \left[B_{T,1}^*\right]_p + \left[B_{T,3}^*\right]_p\right) + k_{tcBA}^p \left(\left[A_{T,0}^*\right]_p + \left[A_{T,1}^*\right]_p + \left[A_{T,3}^*\right]_p\right)\right\} V_p \left[B_{T,1}^*\right]_p \eta_{1,1}^p$$

$$-\left\{k^p_{tdGB}\left[G^*_{T,3}\right]_p + k^p_{t,B}\left[CTA\right]_p\right\}V_p\left[B^*_{T,1}\right]_p\eta^p_{1,1}$$
$$+\left(2\pi d_p N_p \bar{D}_1 + K_p\,\bar{M}^c_n/M_u\right)V_c\left[B^*_{T,1}\right]_c\eta^c_{1,1} \qquad \text{(A4.130)}$$

$$d\left(V_p\left[B^*_{T,1}\right]_p\eta^p_{2,1}\right)\Big/dt = \left\{k^p_{pBB}\left[B^*_{T,1}\right]_p\left(4\eta^p_{1,1}+4\right)+k^p_{pAB}\left[A^*_{T,1}\right]_p\left(\lambda^p_{2,1}+4\lambda^p_{1,1}+4\right)\right\}[B]_p V_p$$
$$-\left\{\frac{Q_{sm}}{m_{CPP}}+k^p_{pBA}[A]_p\right\}V_p\left[B^*_{T,1}\right]_p\eta^p_{2,1}$$
$$-\left\{2k^p_{tcBB}\left(\left[B^*_{T,0}\right]_p+\left[B^*_{T,1}\right]_p+\left[B^*_{T,3}\right]_p\right)+k^p_{tcBA}\left(\left[A^*_{T,0}\right]_p+\left[A^*_{T,1}\right]_p+\left[A^*_{T,3}\right]_p\right)\right\}V_p\left[B^*_{T,1}\right]_p\eta^p_{2,1}$$
$$-\left\{k^p_{tdGB}\left[G^*_{T,3}\right]_p+k^p_{t,B}\left[CTA\right]_p\right\}V_p\left[B^*_{T,1}\right]_p\eta^p_{2,1}$$
$$+\left(2\pi d_p N_p \bar{D}_1 + K_p\,\bar{M}^c_n/M_u\right)V_c\left[B^*_{T,1}\right]_c\eta^c_{2,1} \qquad \text{(A4.131)}$$

A4.1.4.7. Radicals with a terminal B and having one S5200 graft*

Balance on $[B^*_{2,3}]_p$:

$$d\left(V_p\left[B^*_{T,3}\right]_p\Gamma^p_{2,3}\right)\Big/dt = -\left\{\frac{Q_{sm}}{m_{CPP}}+k^p_{pBA}[A]_p+k^p_{pBB}[B]_p\right\}V_c\left[B^*_{T,3}\right]_p\Gamma^p_{2,3}$$
$$-\left\{2k^p_{tcBB}\left(\left[B^*_{T,0}\right]_p+\left[B^*_{T,1}\right]_p+\left[B^*_{T,3}\right]_p\right)+k^p_{tcBA}\left(\left[A^*_{T,0}\right]_p+\left[A^*_{T,1}\right]_p+\left[A^*_{T,3}\right]_p\right)\right\}V_p\left[B^*_{T,3}\right]_p\Gamma^p_{2,3}$$
$$-\left\{k^p_{tdGB}\left[G^*_{T,3}\right]_p+k^p_{t,B}\left[CTA\right]_p\right\}V_p\left[B^*_{T,3}\right]_p\Gamma^p_{2,3}$$
$$+\left(2\pi d_p N_p \bar{D}_3 + K_p\,\bar{M}^c_n/M_u\right)V_c\left[B^*_{T,3}\right]_c\Gamma^c_{2,3}$$

(A4.132)

Balance on $[B^*_{i,3}]_p$ for $i \geq 3$:

$$d\left(V_p\left[B^*_{T,3}\right]_p\Gamma^p_{i,3}\right)\Big/dt = k^p_{pBB}\left[B^*_{i-2,3}\right]_p[B]_p V_p + k^p_{pAB}\left[A^*_{i-2,3}\right]_p[B]_p V_p$$
$$-\left\{\frac{Q_{sm}}{m_{CPP}}+k^p_{pBA}[A]_p\right\}V_p\left[B^*_{T,3}\right]_p\Gamma^p_{i,3}$$
$$-\left\{k^p_{pBB}[B]_p+2k^p_{tcBB}\left(\left[B^*_{T,0}\right]_p+\left[B^*_{T,1}\right]_p+\left[B^*_{T,3}\right]_p\right)+k^p_{tcBA}\left(\left[A^*_{T,0}\right]_p+\left[A^*_{T,1}\right]_p+\left[A^*_{T,3}\right]_p\right)\right\}V_p\left[B^*_{T,3}\right]_p\Gamma^p_{i,3}$$
$$-\left\{k^p_{tdGB}\left[G^*_{T,3}\right]_p+k^p_{t,B}\left[CTA\right]_p\right\}V_p\left[B^*_{T,3}\right]_p\Gamma^p_{i,3}$$
$$+\left(2\pi d_p N_p \bar{D}_3 + K_p\,\bar{M}^c_n/M_u\right)V_c\left[B^*_{T,3}\right]_c\Gamma^c_{i,3}$$

(A4.133)

The global sum on all the species gives:

$$d\left(V_p\left[B^*_{T,3}\right]_p\right)/dt = k^p_{pAB}\left[A^*_{T,3}\right]_p[B]_p V_p - \left\{\frac{Q_{sm}}{m_{CPP}} + k^p_{pBA}[A]_p\right\}V_p\left[B^*_{T,3}\right]_p$$
$$-\left\{2k^p_{tcBB}\left(\left[B^*_{T,0}\right]_p + \left[B^*_{T,1}\right]_p + \left[B^*_{T,3}\right]_p\right) + k^p_{tcBA}\left(\left[A^*_{T,0}\right]_p + \left[A^*_{T,1}\right]_p + \left[A^*_{T,3}\right]_p\right)\right\}V_p\left[B^*_{T,3}\right]_p$$
$$-\left\{k^p_{tdGB}\left[G^*_{T,3}\right]_p + k^p_{t,B}[CTA]_p\right\}V_p\left[B^*_{T,3}\right]_p + \left(2\pi d_p N_p \bar{D}_3 + K_p \bar{M}^c_n/M_u\right)V_c\left[B^*_{T,3}\right]_c$$

(A4.134)

$$d\left(V_p\left[B^*_{T,3}\right]_p \eta^p_{1,3}\right)/dt = \left\{2k^p_{pBB}\left[B^*_{T,3}\right]_p + k^p_{pAB}\left[A^*_{T,3}\right]_p\left(\lambda^p_{1,3}+2\right)\right\}[B]_p V_p - \left\{\frac{Q_{sm}}{m_{CPP}} + k^p_{pBA}[A]_p\right\}V_p\left[B^*_{T,3}\right]_p \eta^p_{1,3}$$
$$-\left\{2k^p_{tcBB}\left(\left[B^*_{T,0}\right]_p + \left[B^*_{T,1}\right]_p + \left[B^*_{T,3}\right]_p\right) + k^p_{tcBA}\left(\left[A^*_{T,0}\right]_p + \left[A^*_{T,1}\right]_p + \left[A^*_{T,3}\right]_p\right)\right\}V_p\left[B^*_{T,3}\right]_p \eta^p_{1,3}$$
$$-\left\{k^p_{tdGB}\left[G^*_{T,3}\right]_p + k^p_{t,B}[CTA]_p\right\}V_p\left[B^*_{T,3}\right]_p \eta^p_{1,3}$$
$$+\left(2\pi d_p N_p \bar{D}_3 + K_p \bar{M}^c_n/M_u\right)V_c\left[B^*_{T,3}\right]_c \eta^c_{1,3} \qquad \text{(A4.135)}$$

$$d\left(V_p\left[B^*_{T,3}\right]_p \eta^p_{2,3}\right)/dt = \left\{k^p_{pBB}\left[B^*_{T,3}\right]_p\left(4\eta^p_{1,3}+4\right) + k^p_{pAB}\left[A^*_{T,3}\right]_p\left(\lambda^p_{2,3}+4\lambda^p_{1,3}+4\right)\right\}[B]_p V_p$$
$$-\left\{\frac{Q_{sm}}{m_{CPP}} + k^p_{pBA}[A]_p\right\}V_p\left[B^*_{T,3}\right]_p \eta^p_{2,3}$$
$$-\left\{2k^p_{tcBB}\left(\left[B^*_{T,0}\right]_p + \left[B^*_{T,1}\right]_p + \left[B^*_{T,3}\right]_p\right) + k^p_{tcBA}\left(\left[A^*_{T,0}\right]_p + \left[A^*_{T,1}\right]_p + \left[A^*_{T,3}\right]_p\right)\right\}V_p\left[B^*_{T,3}\right]_p \eta^p_{2,3}$$
$$-\left\{k^p_{tdGB}\left[G^*_{T,3}\right]_p + k^p_{t,B}[CTA]_p\right\}V_p\left[B^*_{T,3}\right]_p \eta^p_{2,3}$$
$$+\left(2\pi d_p N_p \bar{D}_3 + K_p \bar{M}^c_n/M_u\right)V_c\left[B^*_{T,3}\right]_c \eta^c_{2,3}$$

(A4.136)

A4.1.4.9. Balance on polymer having 0 Graft

$$d\left(V_p\left[P_{T,0}\right]_p\right)/dt = -\frac{Q_{sm}}{m_{CPP}}V_p\left[P_{T,0}\right]_p + 2\pi d_p N_p \bar{D}_0 V_c\left[P_{T,0}\right]_c + \left(k^p_{tcAA}\left[A^*_{T,0}\right]^2_p + k^p_{tcBB}\left[B^*_{T,0}\right]^2_p\right)V_p$$
$$+k^p_{tcAB}\left[A^*_{T,0}\right]_p\left[B^*_{T,0}\right]_p V_p$$
$$+\left\{k^p_{tdAG}\left[G^*_{T,3}\right]_p + k^p_{t,A}[CTA]_p\right\}V_p\left[A^*_{T,0}\right]_p + \left\{k^p_{tdBG}\left[G^*_{T,3}\right]_p + k^p_{t,B}[CTA]_p\right\}V_p\left[B^*_{T,0}\right]_p$$
$$+K_p V_c\left[P_{T,0}\right]_c \bar{M}^c_n/M_u$$

(A4.137)

$$d\left(V_p\left[P_{T,0}\right]_p \mu^p_{1,0}\right)/dt = -\frac{Q_{sm}}{m_{CPP}}V_p\left[P_{T,0}\right]_p \mu^p_{1,0} + 2\pi d_p N_p \bar{D}_0 V_c\left[P_{T,0}\right]_c \mu^c_{1,0}$$
$$+2\left(k^p_{tcAA}\left[A^*_{T,0}\right]^2_p \lambda^p_{1,0} + k^p_{tcBB}\left[B^*_{T,0}\right]^2_p \eta^p_{1,0}\right)V_p + k^p_{tcAB}V_p\left[A^*_{T,0}\right]_p\left[B^*_{T,0}\right]_p\left(\lambda^p_{1,0} + \eta^p_{1,0}\right)$$

$$+\left\{k_{tdAG}^{p}\left[G_{T,3}^{*}\right]_{p}+k_{t,A}^{p}\left[CTA\right]_{p}\right\}V_{p}\ \left[A_{T,0}^{*}\right]_{p}\lambda_{1,0}^{p}+\left\{k_{tdBG}^{p}\left[G_{T,3}^{*}\right]_{p}+k_{t,B}^{p}\left[CTA\right]_{p}\right\}V_{p}\left[B_{T,0}^{*}\right]_{p}\eta_{1,0}^{p}$$
$$+K_{p}\,\bar{M}_{n}^{c}/M_{u}\,V_{c}\left[P_{T,0}\right]_{c}\mu_{1,0}^{c} \qquad \text{(A4.138)}$$

$$d\left(V_{p}\left[P_{T,0}\right]_{p}\mu_{2,0}^{p}\right)/dt=-\frac{Q_{sm}}{m_{CPP}}V_{p}\left[P_{T,0}\right]_{p}\mu_{2,0}^{p}+2\pi d_{p}N_{p}\bar{D}_{0}V_{c}\left[P_{T,0}\right]_{c}\mu_{2,0}^{c}$$
$$+\left(k_{tcAA}^{p}\left[A_{T,0}^{*}\right]_{p}^{2}\left(2\lambda_{2,0}^{p}+2\lambda_{1,0}^{p}\lambda_{1,0}^{p}\right)+k_{tcBB}^{p}\left[B_{T,0}^{*}\right]_{p}^{2}\left(2\eta_{2,0}^{p}+2\eta_{1,0}^{p}\eta_{1,0}^{p}\right)\right)V_{p}$$
$$+k_{tcAB}^{p}V_{p}\left[A_{T,0}^{*}\right]_{p}\left[B_{T,0}^{*}\right]_{p}\left(\lambda_{2,0}^{p}+2\lambda_{1,0}^{p}\eta_{1,0}^{p}+\eta_{2,0}^{p}\right)$$
$$+\left\{k_{tdAG}^{p}\left[G_{T,3}^{*}\right]_{p}+k_{t,A}^{p}\left[CTA\right]_{p}\right\}V_{p}\ \left[A_{T,0}^{*}\right]_{p}\lambda_{2,0}^{p}+\left\{k_{tdBG}^{p}\left[G_{T,3}^{*}\right]_{p}+k_{t,B}^{p}\left[CTA\right]_{p}\right\}V_{p}\left[B_{T,0}^{*}\right]_{p}\eta_{2,0}^{p}$$
$$+K_{p}\,\bar{M}_{n}^{c}/M_{u}\,V_{c}\left[P_{T,0}\right]_{c}\mu_{2,0}^{c} \qquad \text{(A4.139)}$$

A4.1.4.10. Balance on polymer having one polyol graft

$$d\left(V_{p}\left[P_{T,1}\right]_{p}\right)/dt=-\frac{Q_{sm}}{m_{CPP}}V_{p}\left[P_{T,1}\right]_{p}+2\pi d_{p}N_{p}\bar{D}_{1}V_{c}\left[P_{T,1}\right]_{c}+K_{p}\,\bar{M}_{n}^{c}/M_{u}\,V_{c}\left[P_{T,1}\right]_{c}$$
$$+\left(k_{tcAA}^{p}\ \left[A_{T,0}^{*}\right]_{p}\left[A_{T,1}^{*}\right]_{p}+k_{tcBB}^{p}\left[B_{T,0}^{*}\right]_{p}\left[B_{T,1}^{*}\right]_{p}\right)V_{p}$$
$$+k_{tcAB}^{p}\ \left[A_{T,0}^{*}\right]_{p}\left[B_{T,1}^{*}\right]_{p}V_{c}+k_{tcAB}^{p}\left[A_{T,1}^{*}\right]_{p}\left[B_{T,0}^{*}\right]_{p}V_{p}$$
$$+k_{tdGA}^{p}\left[G_{T,3}^{*}\right]_{p}\left[A_{T,1}^{*}\right]_{p}V_{p}+k_{tdGB}^{p}\left[G_{T,3}^{*}\right]_{p}\left[B_{T,1}^{*}\right]_{p}V_{p}$$
$$+k_{t,A}^{p}\left[CTA\right]_{p}V_{p}\ \left[A_{T,1}^{*}\right]_{p}+k_{t,B}^{p}\left[CTA\right]_{p}V_{p}\left[B_{T,1}^{*}\right]_{p} \qquad \text{(A4.140)}$$

$$d\left(V_{p}\left[P_{T,1}\right]_{p}\mu_{1,1}^{p}\right)/dt=-\frac{Q_{sm}}{m_{CPP}}V_{p}\left[P_{T,1}\right]_{p}\mu_{1,1}^{p}+\left(2\pi d_{p}N_{p}\bar{D}_{1}+K_{p}\,\bar{M}_{n}^{c}/M_{u}\right)V_{c}\left[P_{T,1}\right]_{c}\mu_{1,1}^{c}$$
$$+\left(k_{tcAA}^{p}\ \left[A_{T,0}^{*}\right]_{p}\left[A_{T,1}^{*}\right]_{p}\left(\lambda_{1,1}^{p}+\lambda_{1,0}^{p}\right)+k_{tcBB}^{p}\left[B_{T,0}^{*}\right]_{p}\left[B_{T,1}^{*}\right]_{p}\left(\eta_{1,1}^{p}+\eta_{1,0}^{p}\right)\right)V_{p}$$
$$+k_{tcAB}^{p}\ \left[A_{T,0}^{*}\right]_{p}\left[B_{T,1}^{*}\right]_{p}\left(\lambda_{1,0}^{p}+\eta_{1,1}^{p}\right)V_{p}$$
$$+k_{tcAB}^{p}\left[A_{T,1}^{*}\right]_{p}\left[B_{T,0}^{*}\right]_{p}\left(\lambda_{1,1}^{p}+\eta_{1,0}^{p}\right)V_{p}+k_{tdGA}^{p}\left[G_{T,3}^{*}\right]_{p}\left[A_{T,1}^{*}\right]_{p}\left(\nu_{1,3}^{p}+\lambda_{1,0}^{p}\right)V_{p}$$
$$+k_{tdGB}^{p}\left[G_{T,3}^{*}\right]_{p}\left[B_{T,1}^{*}\right]_{p}\left(\nu_{1,3}^{p}+\eta_{1,0}^{p}\right)V_{p}$$
$$+k_{t,A}^{p}\left[CTA\right]_{p}V_{p}\ \left[A_{T,1}^{*}\right]_{p}\lambda_{1,1}^{p}+k_{t,B}^{p}\left[CTA\right]_{p}V_{p}\left[B_{T,1}^{*}\right]_{p}\eta_{1,1}^{p}$$

(A4.141)

$$d\left(V_{p}\left[P_{T,1}\right]_{p}\mu_{2,1}^{p}\right)/dt=-\frac{Q_{sm}}{m_{CPP}}V_{p}\left[P_{T,1}\right]_{p}\mu_{2,1}^{p}+\left(2\pi d_{p}N_{p}\bar{D}_{1}+K_{p}\,\bar{M}_{n}^{c}/M_{u}\right)_{1}V_{c}\left[P_{T,1}\right]_{c}\mu_{2,1}^{c}$$
$$+k_{tcAA}^{p}\ \left[A_{T,0}^{*}\right]_{p}\left[A_{T,1}^{*}\right]_{p}\left(\lambda_{2,1}^{p}+2\lambda_{1,1}^{p}\lambda_{1,0}^{p}+\lambda_{2,0}^{p}\right)V_{p}$$
$$+k_{tcBB}^{p}\left[B_{T,0}^{*}\right]_{p}\left[B_{T,1}^{*}\right]_{p}\left(\eta_{2,1}^{p}+2\eta_{1,1}^{p}\eta_{1,0}^{p}+\eta_{2,0}^{p}\right)V_{p}$$

$$+k_{tcAB}^{p}\left[A_{T,0}^{*}\right]_p\left[B_{T,1}^{*}\right]_p\left(\lambda_{2,0}^{p}+2\lambda_{1,0}^{p}\eta_{1,1}^{p}+\eta_{2,1}^{p}\right)V_p$$
$$+k_{tcAB}^{p}\left[A_{T,1}^{*}\right]_p\left[B_{T,0}^{*}\right]_p\left(\lambda_{2,1}^{p}+2\lambda_{1,1}^{p}\eta_{1,0}^{p}+\eta_{2,0}^{p}\right)V_p$$
$$+k_{tdGA}^{p}\left[G_{T,3}^{*}\right]_p\left[A_{T,1}^{*}\right]_p\left(\nu_{2,3}^{p}+2\nu_{1,3}^{p}\lambda_{1,1}^{p}+\lambda_{2,1}^{p}\right)V_p+k_{tdGB}^{p}\left[G_{T,3}^{*}\right]_p\left[B_{T,1}^{*}\right]_p\left(\nu_{2,3}^{p}+2\nu_{1,3}^{p}\eta_{1,1}^{p}+\eta_{2,1}^{p}\right)V_p$$
$$+k_{t,A}^{p}\left[CTA\right]_p V_p\ \left[A_{T,1}^{*}\right]_p\lambda_{2,1}^{p}+k_{t,B}^{p}\left[CTA\right]_p V_p\left[B_{T,1}^{*}\right]_p\eta_{2,1}^{p} \qquad \text{(A4.142)}$$

A4.1.4.11. Balance on polymer having one S5200 graft

$$d\left(V_p\left[P_{T,3}\right]_p\right)/dt=-\frac{Q_{sm}}{m_{CPP}}V_p\left[P_{T,3}\right]_p+\left(2\pi d_p N_p\bar{D}_3+K_p\,\bar{M}_n^c/M_u\right)V_c\left[P_{T,3}\right]_c$$
$$+\left(k_{tcAA}^{p}\left[A_{T,0}^{*}\right]_p\left[A_{T,3}^{*}\right]_p+k_{tcBB}^{p}\left[B_{T,0}^{*}\right]_p\left[B_{T,3}^{*}\right]_p\right)V_p$$
$$+k_{tcAB}^{p}\ \left[A_{T,0}^{*}\right]_p\left[B_{T,3}^{*}\right]_p V_c+k_{tcAB}^{p}\left[A_{T,3}^{*}\right]_p\left[B_{T,0}^{*}\right]_p V_p$$
$$+2k_{tdGA}^{p}\left[G_{T,3}^{*}\right]_p\left[A_{T,3}^{*}\right]_p V_p+2k_{tdGB}^{p}\left[G_{T,3}^{*}\right]_p\left[B_{T,3}^{*}\right]_p V_p+k_{tdGA}^{p}\left[G_{T,3}^{*}\right]_p\left(\left[A_{T,0}^{*}\right]_p+\left[A_{T,1}^{*}\right]_p\right)V_p$$
$$+k_{tdGB}^{p}\left[G_{T,3}^{*}\right]_p\left(\left[B_{T,0}^{*}\right]_p+\left[B_{T,1}^{*}\right]_p\right)V_p+k_{t,A}^{p}\left[CTA\right]_p V_p\left[A_{T,3}^{*}\right]_p+k_{t,B}^{p}\left[CTA\right]_p V_p\left[B_{T,3}^{*}\right]_p$$
(A4.143)

$$d\left(V_p\left[P_{T,3}\right]_p\mu_{1,3}^{p}\right)/dt=-\frac{Q_{sm}}{m_{CPP}}V_p\left[P_{T,3}\right]_p\mu_{1,3}^{p}+\left(2\pi d_p N_p\bar{D}_3+K_p\,\bar{M}_n^c/M_u\right)V_c\left[P_{T,3}\right]_c\mu_{1,3}^{c}$$
$$+\left(k_{tcAA}^{p}\left[A_{T,0}^{*}\right]_p\left[A_{T,3}^{*}\right]_p\left(\lambda_{1,0}^{p}+\lambda_{1,3}^{p}\right)+k_{tcBB}^{p}\left[B_{T,0}^{*}\right]_p\left[B_{T,3}^{*}\right]_p\left(\eta_{1,0}^{p}+\eta_{1,3}^{p}\right)\right)V_p$$
$$+k_{tcAB}^{p}\left[A_{T,0}^{*}\right]_p\left[B_{T,3}^{*}\right]_p\left(\lambda_{1,0}^{p}+\eta_{1,3}^{p}\right)V_p$$
$$+k_{tcAB}^{p}\left[A_{T,3}^{*}\right]_p\left[B_{T,0}^{*}\right]_p\left(\lambda_{1,3}^{p}+\eta_{1,0}^{p}\right)V_p+2k_{tdGA}^{p}\left[G_{T,3}^{*}\right]_p\left[A_{T,3}^{*}\right]_p\left(\nu_{1,3}^{p}+\lambda_{1,3}^{p}\right)V_p$$
$$+2k_{tdGB}^{p}\left[G_{T,3}^{*}\right]_p\left[B_{T,3}^{*}\right]_p\left(\nu_{1,3}^{p}+\eta_{1,3}^{p}\right)V_p$$
$$+k_{tdGA}^{p}\left[G_{T,3}^{*}\right]_p\left(\left[A_{T,0}^{*}\right]_p\left(\nu_{1,3}^{p}+\lambda_{1,0}^{p}\right)+\left[A_{T,1}^{*}\right]_p\left(\nu_{1,3}^{p}+\lambda_{1,1}^{p}\right)\right)V_p$$
$$+k_{tdGB}^{p}\left[G_{T,3}^{*}\right]_p\left(\left[B_{T,0}^{*}\right]_p\left(\nu_{1,3}^{p}+\eta_{1,0}^{p}\right)+\left[B_{T,1}^{*}\right]_p\left(\nu_{1,3}^{p}+\eta_{1,1}^{p}\right)\right)V_p$$
$$+k_{tr,A}^{p}\left[CTA\right]_p V_p\left[A_{T,3}^{*}\right]_p\lambda_{1,3}^{p}+k_{tr,B}^{p}\left[CTA\right]_p V_p\left[B_{T,3}^{*}\right]_p\eta_{1,3}^{p} \qquad \text{(A4.144)}$$

$$d\left(V_p\left[P_{T,3}\right]_p\mu_{2,3}^{p}\right)/dt=-\frac{Q_{sm}}{m_{CPP}}V_p\left[P_{T,3}\right]_p\mu_{2,3}^{p}+\left(2\pi d_p N_p\bar{D}_3+K_p\,\bar{M}_n^c/M_u\right)V_c\left[P_{T,3}\right]_c\mu_{2,3}^{c}$$
$$+\left(k_{tcAA}^{p}\ \left[A_{T,0}^{*}\right]_p\left[A_{T,3}^{*}\right]_p\left(\lambda_{2,3}^{p}+2\lambda_{1,3}^{p}\lambda_{1,0}^{p}+\lambda_{2,0}^{p}\right)+k_{tcBB}^{p}\left[B_{T,0}^{*}\right]_p\left[B_{T,3}^{*}\right]_p\left(\eta_{2,3}^{p}+2\eta_{1,3}^{p}\eta_{1,0}^{p}+\eta_{2,0}^{p}\right)\right)V_p$$
$$+k_{tcAB}^{p}\ \left[A_{T,0}^{*}\right]_p\left[B_{T,3}^{*}\right]_p\left(\lambda_{2,0}^{p}+2\lambda_{1,0}^{p}\eta_{1,3}^{p}+\eta_{2,3}^{p}\right)V_p$$
$$+k_{tcAB}^{p}\left[A_{T,3}^{*}\right]_p\left[B_{T,0}^{*}\right]_p\left(\lambda_{2,3}^{p}+2\lambda_{1,3}^{p}\eta_{1,0}^{p}+\eta_{2,0}^{p}\right)V_p$$
$$+2k_{tdGA}^{p}\left[G_{T,3}^{*}\right]_p\left[A_{T,3}^{*}\right]_p\left(\nu_{2,3}^{p}+2\nu_{1,3}^{p}\lambda_{1,3}^{p}+\lambda_{2,3}^{p}\right)V_p+k_{tdGB}^{p}\left[G_{T,3}^{*}\right]_p\left[B_{T,3}^{*}\right]_p\left(\nu_{2,3}^{p}+2\nu_{1,3}^{p}\eta_{1,3}^{p}+\eta_{2,3}^{p}\right)V_p$$

$$+k_{tdGA}^{p}\left[G_{T,3}^{*}\right]_{p}\left(\left[A_{T,0}^{*}\right]_{p}\left(\nu_{2,3}^{p}+2\nu_{1,3}^{p}\lambda_{1,0}^{p}+\lambda_{2,0}^{p}\right)+\left[A_{T,1}^{*}\right]_{p}\left(\nu_{2,3}^{p}+2\nu_{1,3}^{p}\lambda_{1,1}^{p}+\lambda_{2,1}^{p}\right)\right)V_{p}$$
$$+k_{tdGB}^{p}\left[G_{T,3}^{*}\right]_{p}\left(\left[B_{T,0}^{*}\right]_{p}\left(\nu_{2,3}^{p}+2\nu_{1,3}^{p}\eta_{1,0}^{p}+\eta_{2,0}^{p}\right)+\left[B_{T,1}^{*}\right]_{p}\left(\nu_{2,3}^{p}+2\nu_{1,3}^{p}\eta_{1,1}^{p}+\eta_{2,1}^{p}\right)\right)V_{p}$$
$$+k_{t,A}^{p}\left[CTA\right]_{p}V_{p}\left[A_{T,3}^{*}\right]_{p}\lambda_{2,3}^{p}+k_{t,B}^{p}\left[CTA\right]_{p}V_{p}\left[B_{T,3}^{*}\right]_{p}\eta_{2,3}^{p} \qquad \text{(A4.145)}$$

A4.2. The Gamma function

The Euler's gamma function is defined by the integral

$$\Gamma(x)=\int_{0}^{+\infty}e^{-t}t^{x-1}dt \qquad \text{(A4.146)}$$

or real integer and half integer arguments it is given by

$$\Gamma(1/2)=\sqrt{\pi} \qquad \text{(A4.147)}$$

$$\Gamma(1)=\int_{0}^{\infty}e^{-x}dx=\left[-e^{-x}\right]_{0}^{\infty}=1 \qquad \text{(A4.148)}$$

and the recurrence formula valid for all complex z (except negative integers and zero) is

$$\Gamma(z)=(z-1)\Gamma(z-1)=(z-1)! \qquad \text{(A4.149)}$$

Indeed for stricly positive integers (n > 1) :

$$\Gamma(n)=\int_{0}^{\infty}t^{n-1}d\left(-e^{-t}\right)=\left[-t^{n-1}e^{-t}\right]_{0}^{\infty}-\int_{0}^{\infty}(n-1)\left(-e^{-t}\right)t^{n-2}dt=(n-1)\Gamma(n-1) \qquad \text{(A4.150)}$$

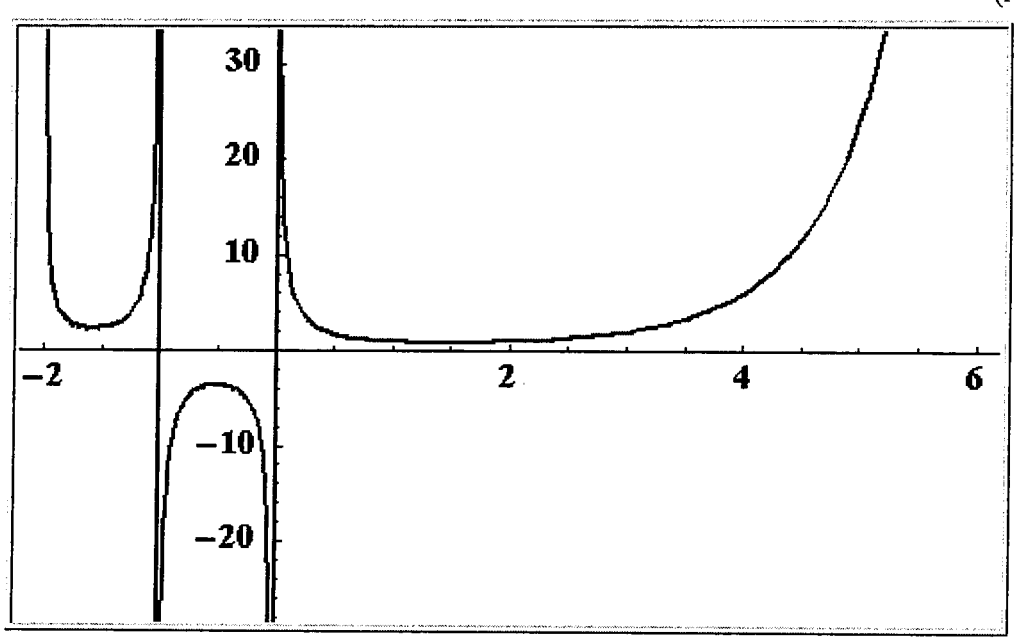

Figure A4.1 : The Euler's Gamma function

As explained in chapter 2, various mathematical functions may be employed to describe theoretically the molecular weight distributions : Gaussian, log-normal, Poisson or Gamma (also called Flory-Schulz) functions. The Gamma function is the recommanded one when a tail appears in the high molecular weights. The following procedure describes therefore how to obtain the theoretical molecular weight distribution following a Gamma function, when the numbre-average and the weight-average molecular weights are known.

The gamma distribution is $\varphi_n(t) = K t^n e^{-t/\tau}$, (A4.151)

where $\int_0^\infty \varphi_n(t)\,dt = 1 = \int_0^\infty K t^n e^{-t/\tau} dt = K \int_0^\infty (\tau y)^n e^{-y} \tau dy = K\tau^{n+1}\Gamma(n+1)$, (A4.152)

and finally $\varphi_n(t) = \dfrac{t^n e^{-t/\tau}}{\tau^{n+1}\Gamma(n+1)}$. (A4.153)

The moments of order one and two can therefore be calculated :

$$\mu_1 = \int_0^\infty t\varphi_n(t)\,dt = \int_0^\infty \frac{t^{n+1} e^{-t/\tau}}{\tau^{n+1}\Gamma(n+1)} dt = \tau \int_0^\infty \frac{y^{n+1} e^{-y}}{\Gamma(n+1)} dy = \tau \frac{\Gamma(n+2)}{\Gamma(n+1)} = \tau(n+1),$$

(A4.154)

$$\mu_2 = \int_0^\infty t^2\varphi_n(t)\,dt = \int_0^\infty \frac{t^{n+2} e^{-t/\tau}}{\tau^{n+1}\Gamma(n+1)} dt = \tau^2 \int_0^\infty \frac{y^{n+2} e^{-y}}{\Gamma(n+1)} dy = \tau^2 \frac{\Gamma(n+3)}{\Gamma(n+1)} = \tau^2 (n+2)(n+1).$$

(A4.155)

The variance is $\text{var} = \mu_2 - \mu_1^2 = (n+1)\tau^2 = \mu_1\tau$. (A4.156)

Therefore $\tau = \dfrac{\mu_2 - \mu_1^2}{\mu_1}$ and $n = \dfrac{2\mu_1^2 - \mu_2}{\mu_2 - \mu_1^2}$ if $\mu_2 < 2\mu_1^2$. (A4.157)

The numbre-average and weight-average molecular weigths are respectively defined as follows : $\bar{M}_n = \mu_1$ and $\bar{M}_w = \dfrac{\mu_2}{\mu_1}$.

Thus, τ and n can be calculated from $\bar{M}_n$ and $\bar{M}_w$:

$$\tau = \bar{M}_w - \bar{M}_n, \quad \text{(A4.158)}$$

$$n = \frac{2\bar{M}_n - \bar{M}_w}{\bar{M}_w - \bar{M}_n}. \quad \text{(A4.159)}$$

A4.3. Approximation to integrate derivative equations between t and t + Δt

In order to solve the equations of second order during the integration of the system exposed in chapter 4, it was required to calculate some variables at time t + Δt using the same variables at time t. In other words, the new values of the variables are approximated to be closed to the values of the previews step if the step of integration is small enough.

The mathematical justification of this numerical process is explained below.

Let us define a system of two derivative equations such that :

$dy/dt = g(y)$, is independent and, (A4.160)

$dx/dt = f(x,y)$, is instable by numerical integration. (A4.161)

The last equation must be solved by considering the QSSA, which leads to solve :

$$f(x,y) = 0. \tag{A4.162}$$

In order to determine x for a given y in a given space, the system is redefined :

$$x = \varphi(x,y), \tag{A4.163}$$

such that a series

$$x^{n+1} = \varphi(x^n, y), \tag{A4.164}$$

exists and converges for all y in the given space, that is to say that, the variable ψ defined in equation A4.165 exists :

$$|x^{n+1} - x| = \psi |x^n - x|, \tag{A4.165}$$

with $\psi < 1$.

It is assumed that with Δt = 0.1 s, we are very close to the convergence and therefore a single step is needed.

ANNEX 5

TABLES AND FIGURES OF CHAPTER 5

Table A5.1 : Comparison of the number-average molecular weights of experiments carried out at 140 °C obtained experimentally and given by the model.

Run n°	Mn (g/mol)		Relative difference (%)
	Model	Measurements	
4	4,61E+04	4,80E+04	4,0
5	1,65E+04	2,58E+04	36,0
6	3,89E+04	3,20E+04	21,6
7	1,60E+04	2,45E+04	34,7
12	4,96E+04	4,15E+04	19,5
13	1,77E+04	2,62E+04	32,4
14	4,19E+04	3,23E+04	29,7
15	1,67E+04	2,45E+04	31,8
18	3,71E+04	3,53E+04	5,1
19	1,40E+04	1,34E+04	4,5
20	3,15E+04	3,02E+04	4,3
21	1,34E+04	1,50E+04	10,7
26	3,97E+04	4,00E+04	0,8
27	1,49E+04	1,68E+04	11,3
28	3,34E+04	3,65E+04	8,5
29	1,41E+04	1,76E+04	19,9
30	1,41E+04	1,63E+04	13,5

Table A5.2 : Comparison of the number-average molecular weights of the experiments carried out at 120 °C obtained experimentally and given by the model.

Run n°	Mn (g/mol)		Relative difference (%)
	Model	Measurements	
1	1,66E+04	2,71E+04	38,7
2	4,05E+04	5,16E+04	21,5
3	1,60E+04	2,55E+04	37,3
8	4,94E+04	5,97E+04	17,3
9	1,75E+04	2,85E+04	38,6
10	4,29E+04	4,93E+04	13,0
11	1,68E+04	2,76E+04	39,1
16	3,25E+04	3,80E+04	14,5
17	1,33E+04	1,45E+04	8,3
22	3,89E+04	4,38E+04	11,2
23	1,42E+04	1,40E+04	1,4
24	3,39E+04	4,27E+04	20,6
25	1,38E+04	1,75E+04	21,1

Table A5.3 : Comparison of the weight-average molecular weights of the experiments done at 140 °C obtained experimentally and given by the model.

Run n°	Mw (g/mol)		Relative difference (%)
	Model	Measurements	
4	1,09E+05	2,24E+05	51,3
5	3,56E+04	8,16E+04	56,4
6	1,00E+05	1,53E+05	34,6
7	3,54E+04	9,45E+04	62,5
12	1,26E+05	2,06E+05	38,8
13	3,97E+04	8,49E+04	53,2
14	1,18E+05	1,55E+05	23,9
15	3,84E+04	9,60E+04	60,0
18	8,97E+04	9,88E+04	9,2
19	3,11E+04	3,33E+04	6,6
20	8,34E+04	9,00E+04	7,3
21	3,09E+04	3,68E+04	16,0
26	1,02E+05	1,18E+05	13,6
27	3,46E+04	3,93E+04	12,0
28	9,41E+04	1,26E+05	25,3
29	3,41E+04	4,29E+04	20,5
30	3,41E+04	4,20E+04	18,8

Table A5.4 : Comparison of the weight-average molecular weights of the experiments done at 120 °C obtained experimentally and given by the model.

Run n°	Mw (g/mol)		Relative difference (%)
	Model	Measurements	
1	3,77E+04	7,32E+04	48,5
2	1,12E+05	2,84E+05	60,6
3	3,76E+04	7,61E+04	50,6
8	1,30E+05	2,55E+05	49,0
9	4,12E+04	7,36E+04	44,0
10	1,27E+05	1,92E+05	33,9
11	4,10E+04	8,28E+04	50,5
16	9,05E+04	1,07E+05	15,4
17	3,17E+04	3,49E+04	9,2
22	1,02E+05	1,03E+05	1,0
23	3,37E+04	3,30E+04	2,1
24	9,80E+04	1,23E+05	20,3
25	3,40E+04	4,05E+04	16,0

Table A5.5 : Comparison of the quantities of solid of the experiments done at 140 °C obtained experimentally and given by the model.

Run n°	Solid (wt-%)		Relative difference (%)
	Model	Measurements	
4	39,5	39,9	1,0
5	38,6	39,3	1,8
6	39,5	39,9	1,0
7	39,7	39,3	1,0
12	39,3	39,2	0,3
13	38,9	38,5	1,0
14	39,7	39,8	0,3
15	39,3	39,5	0,5
18	35,1	33,5	4,8
19	34,8	30,8	13,0
20	35,9	35,2	2,0
21	35,8	34,3	4,4
26	35,5	34,9	1,7
27	35,3	31,3	12,8
28	36,2	37,3	2,9
29	36,1	34,9	3,4
30	36,1	36,9	2,2

Table A5.6 : Comparison of the quantities of solid of the experiments done at 120 °C obtained experimentally and given by the model.

Run n°	Solid (wt-%)		Relative difference (%)
	Model	Measurements	
1	38,8	39,3	1,3
2	39,9	39,3	1,5
3	39,4	38,4	2,6
8	39,5	38,9	1,5
9	38,9	41,6	6,5
10	39,9	39,3	1,5
11	39,4	38,9	1,3
16	35,8	36,1	0,8
22	35,1	38,7	9,3
23	34,6	39,9	13,3
24	36	37,1	3,0
25	35,7	32,1	11,2

Table A5.7 : Comparison of the quantities of residual acrylonitrile of the experiments done at 140 °C obtained experimentally and given by the model.

Run n°	Residual AN (wt-%)		Relative difference (%)
	Model	Measurements	
4	2,36	2,31	2,2
5	2,95	2,68	10,1
6	2,38	1,62	46,9
7	2,26	2,18	3,7
12	2,47	2,33	6,0
13	2,74	2,64	3,8
14	2,27	1,9	19,5
15	2,51	2,17	15,7
18	1,79	2,2	18,6
19	1,84	3,05	39,7
20	1,59	1,47	8,2
21	1,6	2,07	22,7
26	1,7	1,78	4,5
27	1,72	2,84	39,4
28	1,52	1,27	19,7
29	1,52	1,9	20,0
30	1,52	1,44	5,6

Table A5.8 : Comparison of the quantities of residual acrylonitrile of the experiments done at 120 °C obtained experimentally and given by the model.

Run n°	Residual AN (wt-%)		Relative difference (%)
	Model	Measurements	
1	2,71	2,67	1,5
2	2,02	1,8	12,2
3	2,33	2,15	8,4
8	2,27	2,51	9,6
9	2,65	3,05	13,1
10	2,05	1,93	6,2
11	2,32	2,26	2,7
16	1,44	1,74	17,2
17	1,5	2,83	47,0
22	1,58	2,26	30,1
23	1,68	3,91	57,0
24	1,4	1,39	0,7
25	1,44	2,68	46,3

Table A5.9 : Comparison of the conversions in residual acrylonitrile of the experiments done at 140 °C obtained experimentally and given by the model.

Run n°	Conversion AN (%)		Relative difference (%)
	Model	Measurements	
4	86,3	86,6	0,3
5	82,8	84,4	1,9
6	86,2	90,6	4,9
7	86,9	87,3	0,5
12	85,6	86,5	0,9
13	84,1	84,7	0,7
14	86,8	89,0	2,4
15	85,4	87,4	2,3
18	79,2	74,4	6,4
19	78,6	64,5	21,8
20	81,5	82,9	1,7
21	81,4	75,9	7,2
26	80,2	79,3	1,2
27	80,0	67,0	19,4
28	82,3	85,2	3,4
29	82,3	77,9	5,7
30	82,3	83,3	1,1

Table A5.10 : Comparison of the conversions in residual acrylonitrile of the experiments done at 120 °C obtained experimentally and given by the model.

Run n°	Conversion AN (%)		Relative difference (%)
	Model	Measurements	
1	84,2	84,5	0,3
2	88,3	89,5	1,4
3	86,5	87,5	1,2
8	86,8	85,4	1,6
9	84,6	82,3	2,8
10	88,1	88,8	0,8
11	86,5	86,9	0,4
16	83,3	79,8	4,4
17	82,6	67,1	23,1
22	81,6	73,7	10,7
23	80,5	54,5	47,5
24	83,7	83,8	0,1
25	83,3	68,8	20,9

Table A5.11 : Comparison of the quantities of residual styrene of the experiments done at 140 °C obtained experimentally and given by the model.

Run n°	Residual Sty (wt-%)		Relative difference (%)
	Model	Measurements	
4	1,8	3,36	46,4
5	2,42	4,22	42,7
6	1,46	3,37	56,7
7	1,85	3,21	42,4
12	2,24	3,51	36,2
13	2,5	3,9	35,9
14	1,73	3,22	46,3
15	1,94	3,57	45,7
18	11,8	10,3	14,6
19	15,7	10,7	46,7
20	9,62	9,43	2,0
21	11,2	9,57	17,0
26	9,34	9,94	6,0
27	13,5	10,1	33,7
28	6,83	9,13	25,2
29	9,55	9,2	3,8
30	7,78	9,2	15,4

Table A5.12 : Comparison of the quantities of residual styrene of the experiments done at 120 °C obtained experimentally and given by the model.

Run n°	Residual Sty (wt-%)		Relative difference (%)
	Model	Measurements	
1	4,17	2,29	82,1
2	3,11	1,73	79,8
3	3,57	1,92	85,9
8	3,49	2,31	51,1
9	4,05	2,37	70,9
10	3,14	1,72	82,6
11	3,54	1,94	82,5
16	9,8	9,57	2,4
17	10,1	15,3	34,0
22	10,6	11,7	9,4
23	11,1	18,1	38,7
24	9,56	7,51	27,3
25	9,83	12,9	23,8

Table A5.13 : Comparison of the conversions in residual styrene of the experiments done at 140 °C obtained experimentally and given by the model.

Run n°	Conversion Sty (%)		Relative difference (%)
	Model	Measurements	
4	87,0	93,0	6,5
5	83,6	90,6	7,7
6	86,9	94,3	7,8
7	87,6	92,8	5,7
12	86,4	91,3	5,4
13	84,9	90,3	6,0
14	87,5	93,3	6,2
15	86,2	92,5	6,8
18	70,1	65,7	6,6
19	68,9	54,4	26,7
20	72,6	72,0	0,8
21	72,2	67,4	7,0
26	71,1	72,8	2,4
27	70,6	60,8	16,3
28	73,5	80,1	8,3
29	73,3	72,2	1,4
30	73,3	77,4	5,3

Table A5.14 : Comparison of the conversions in residual styrene of the experiments done at 120 °C obtained experimentally and given by the model.

Run n°	Conversion Sty (%)		Relative difference (%)
	Model	Measurements	
1	83,8	91,1	8,0
2	87,9	93,3	5,7
3	86,2	92,6	6,9
8	86,5	91,0	5,0
9	84,3	90,8	7,2
10	87,8	93,3	5,9
11	86,3	92,5	6,7
16	71,5	72,2	0,9
17	70,6	55,5	27,2
22	69,2	66,0	4,8
23	67,7	47,4	42,9
24	72,2	78,2	7,6
25	71,4	62,5	14,3

Table A5.15 : Comparison of the quantities of residual NDM of the experiments done at 140 °C obtained experimentally and given by the model.

Run n°	Residual NDM (ppm)		Relative difference (%)
	Model	Measurements	
4	63,4	78	18,7
5	265	256	3,5
6	63	67,5	6,7
7	197	90	118,9
12	54,5	111	50,9
13	226	347	34,9
14	50,2	84	40,2
15	203	289	29,8
18	110	77	42,9
19	370	412	10,2
20	94,6	26	263,8
21	311	250	24,4
26	88,3	26	239,6
27	322	429	24,9
28	77,5	9	761,1
29	277	201	37,8
30	277	153	81,0

Table A5.16 : Comparison of the quantities of residual NDM of the experiments done at 120 °C obtained experimentally and given by the model.

Run n°	Residual NDM (ppm)		Relative difference (%)
	Model	Measurements	
1	353	414	14,7
2	82,4	25	229,6
3	291	277	5,1
8	81,9	96	14,7
9	318	375	15,2
10	71,5	40	78,8
11	268	270	0,7
16	108	14	671,4
17	342	135	153,3
22	114	60	90,0
23	389	435	10,6
25	315	149	111,4

Table A5.17 : Comparison of the conversions in residual NDM of the experiments done at 140 °C obtained experimentally and given by the model.

Run n°	Conversion NDM (%)		Relative difference (%)
	Model	Measurements	
4	95,8	94,8	1,0
5	94,1	94,3	0,2
6	95,8	95,5	0,3
7	95,6	98,0	2,4
12	96,4	92,6	4,1
13	95,0	92,3	2,9
14	96,7	94,4	2,4
15	95,5	93,6	2,0
18	92,7	94,9	2,3
19	91,8	90,8	1,0
20	93,7	98,3	4,7
21	93,1	94,4	1,4
26	94,1	98,3	4,2
27	92,8	90,5	2,6
28	94,8	99,4	4,6
29	93,8	95,5	1,8
30	93,8	96,6	2,9

Table A5.18 : Comparison of the conversions in residual NDM of the experiments done at 120 °C obtained experimentally and given by the model.

Run n°	Conversion NDM (%)		Relative difference (%)
	Model	Measurements	
1	92,2	90,8	1,5
2	94,5	98,3	3,9
3	93,5	93,8	0,3
8	94,5	93,6	1,0
9	92,9	91,7	1,4
10	95,2	97,3	2,2
11	94,0	94,0	0,0
16	92,8	99,1	6,3
17	92,4	97,0	4,7
22	92,4	96,0	3,7
23	91,4	90,3	1,1
25	93,0	96,7	3,8

Table A5.19 : Comparison of the compositions in acrylonitryle of the SAN copolymers of the experiments done at 140 °C obtained experimentally and given by the model.

Run n°	AN in SAN (wt-%)		Relative difference (%)
	Model	Measurements	
4	39,8	42,9	7,2
5	39,8	41,0	2,9
6	39,8	41,8	4,8
7	39,8	41,6	4,3
12	39,8	38,7	2,8
13	39,8	39,1	1,8
14	39,8	39,0	2,1
15	39,8	39,1	1,8
18	22,0	22,3	1,3
19	22,2	23,2	4,3
20	21,9	20,6	6,3
21	22,0	22,4	1,8
26	22,0	27,0	18,5
27	22,1	19,0	16,3
28	21,9	22,0	0,5
29	21,9	19,0	15,3
30	21,9	22,8	3,9

Table A5.20 : Comparison of the compositions in acrylonitryle of the SAN copolymers of the experiments done at 120 °C obtained experimentally and given by the model.

Run n°	AN in SAN (wt-%)		Relative difference (%)
	Model	Measurements	
1	40,1	41,0	2,2
2	40,1	41,2	2,7
3	40,1	41,1	2,4
8	40,1	39,0	2,8
16	22,5	22,4	0,4
17	22,6	23,4	3,4
22	22,8	26,0	12,3
23	22,9	25,0	8,4
24	22,5	22,0	2,3
25	22,6	17,0	32,9

Table A5.21 : Comparison of the quantities of copolymer SAN dissolved in the serum of the experiments done at 140 °C obtained experimentally and given by the model.

Run n°	SAN dissolved in serum (wt-%)		Relative difference (%)
	Model	Measurements	
4	0,58	0,78	26,0
5	1,31	0,98	33,7
6	0,82	1,46	44,0
7	1,44	1,43	0,7
12	0,77	0,93	17,7
13	1,51	1,26	19,8
14	0,95	1,35	29,7
15	1,78	1,60	11,3
18	0,70	0,97	27,5
19	1,63	1,14	43,0
20	0,93	1,68	44,4
21	1,97	1,45	35,9
26	0,82	1,12	26,9
27	1,78	1,39	28,1
28	1,03	1,77	41,8
29	2,08	1,94	7,2
30	2,08	3,06	32,0

Table A5.22 : Comparison of the quantities of copolymer SAN dissolved in the serum of the experiments done at 120 °C obtained experimentally and given by the model.

Run n°	SAN dissolved in serum (wt-%)		Relative difference (%)
	Model	Measurements	
1	0,85	0,71	19,0
2	0,48	1,03	53,2
3	1,04	1,07	2,8
8	0,44	0,80	45,1
9	0,98	0,74	31,9
10	0,56	0,87	35,3
11	1,14	1,01	12,9
16	0,60	1,45	58,9
17	1,37	1,48	7,4
22	0,49	0,86	42,6
23	1,21	1,66	27,1
24	0,63	1,53	58,6
25	1,42	1,85	23,2

Table A5.23 : Comparison of the proportions of copolymer SAN grafted in the serum of the experiments done at 140 °C obtained experimentally and given by the model.

Run n°	SAN grafted in serum (%)		Relative difference (%)
	Model	Measurements	
4	21,3	53,0	59,8
5	10,7	52,9	79,8
6	15,1	64,6	76,6
7	9,9	55,1	82,0
12	33,3	64,8	48,6
13	19,9	60,3	67,0
14	25,9	78,0	66,8
15	17,2	70,3	75,5
18	13,4	67,6	80,2
19	6,2	56,3	89,0
20	10,5	73,9	85,8
21	5,6	66,0	91,5
26	24,4	72,6	66,4
27	12,5	62,1	79,9
28	19,7	78,0	74,7
29	11,4	62,0	81,6
30	11,4	73,0	84,4

Table A5.24 : Comparison of the proportions of copolymer SAN grafted in the serum of the experiments done at 120 °C obtained experimentally and given by the model.

Run n°	SAN grafted in serum (%)		Relative difference (%)
	Model	Measurements	
1	4,8	56,6	91,4
2	8,1	58,4	86,2
3	4,4	52,5	91,6
8	24,7	58,8	58,0
9	12,7	81,1	84,3
10	19,6	85,4	77,0
11	11,7	73,7	84,1
16	4,0	76,7	94,8
17	2,0	55,6	96,4
22	13,0	51,1	74,6
23	6,0	45,1	86,8
24	10,9	74,9	85,4
25	5,9	54,6	89,2

Table A5.25 : Comparison of the proportions of copolymer SAN grafted in the whole CPP of the experiments done at 140 °C obtained experimentally and given by the model.

Run n°	SAN grafted in CPP (%)		Relative difference (%)
	Model	Measurements	
4	11,2	26,9	58,4
5	5,3	14,8	64,3
6	9,7	21,9	55,8
7	4,9	20,7	76,1
12	22,2	31,5	29,5
13	11,2	17,2	34,9
14	18,5	32,7	43,4
15	10,6	22,8	53,5
18	9,5	26,2	63,7
19	4,2	10,1	58,9
20	8,4	32,9	74,6
21	4,2	14,6	71,5
26	19,2	25,5	24,7
27	9,0	6,0	50,7
28	16,6	30,3	45,2
29	8,9	9,2	3,7
30	8,9	17,3	48,8

Table A5.26 : Comparison of the proportions of copolymer SAN grafted in the whole CPP of the experiments done at 120 °C obtained experimentally and given by the model.

Run n°	SAN grafted in CPP (%)		Relative difference (%)
	Model	Measurements	
1	2,3	9,8	76,5
2	4,8	38,0	87,4
3	2,4	13,6	82,6
8	15,1	-	-
9	7,1	9,0	21,3
10	13,3	34,7	61,7
11	7,1	14,0	49,6
16	3,2	26,2	88,0
17	1,6	10,8	85,6
22	9,7	16,8	42,0
23	4,5	5,8	23,3
24	9,0	23,4	61,8
25	4,7	7,1	34,1

Table A5.27 : Comparison of the quantities of polyol grafted to the solid of the experiments done at 140 °C obtained experimentally and given by the model.

Run n°	Polyol in solid (wt-%)		Relative difference (%)
	Model	Measurements	
4	2,40	3,14	23,6
5	3,11	2,01	54,7
6	2,45	4,25	42,4
7	3,00	3,08	2,6
12	4,41	2,90	52,1
13	6,18	2,30	168,7
14	4,36	4,10	6,3
15	6,19	3,50	76,9
18	2,53	2,80	9,6
19	2,90	2,50	16,0
20	2,63	3,50	24,9
21	3,05	3,40	10,3
26	4,78	2,50	91,2
27	5,97	2,20	171,4
28	4,90	3,10	58,1
29	6,17	2,80	120,4
30	6,17	3,70	66,8

Table A5.28 : Comparison of the quantities of polyol grafted to the solid of the experiments done at 120 °C obtained experimentally and given by the model.

Run n°	Polyol in solid (wt-%)		Relative difference (%)
	Model	Measurements	
1	1,35	1,59	15,1
2	1,16	1,77	34,5
3	1,45	2,03	28,6
8	3,02	2,60	16,2
9	3,97	1,70	133,5
10	3,06	3,10	1,3
11	4,13	2,40	72,1
16	0,96	2,80	65,7
17	1,15	2,70	57,4
22	2,49	2,01	23,9
23	3,08	2,37	30,0
24	2,62	2,50	4,8
25	3,34	2,50	33,6

Table A5.29 : Comparison of de Sauter diameters of the experiments done at 140 °C obtained experimentally and given by the model.

Run n°	D[3, 2] (micrometre)		Relative difference (%)
	Model	Measurements	
4	1,44	1,33	8,3
5	1,21	1,13	7,1
6	1,46	1,51	3,3
7	1,24	0,86	44,5
12	0,68	0,89	23,0
13	0,55	0,86	35,7
14	0,73	0,97	24,9
15	0,56	0,47	19,6

Table A5.30 : Comparison of de Sauter diameters of the experiments done at 120 °C obtained experimentally and given by the model.

Run n°	D[3, 2] (micrometre)		Relative difference (%)
	Model	Measurements	
1	1,35	0,87	55,2
2	1,50	1,11	35,1
3	1,25	0,95	32,0
8	0,51	1,62	68,6
9	0,43	0,94	54,7
10	0,51	1,00	48,5
11	0,41	0,82	50,6

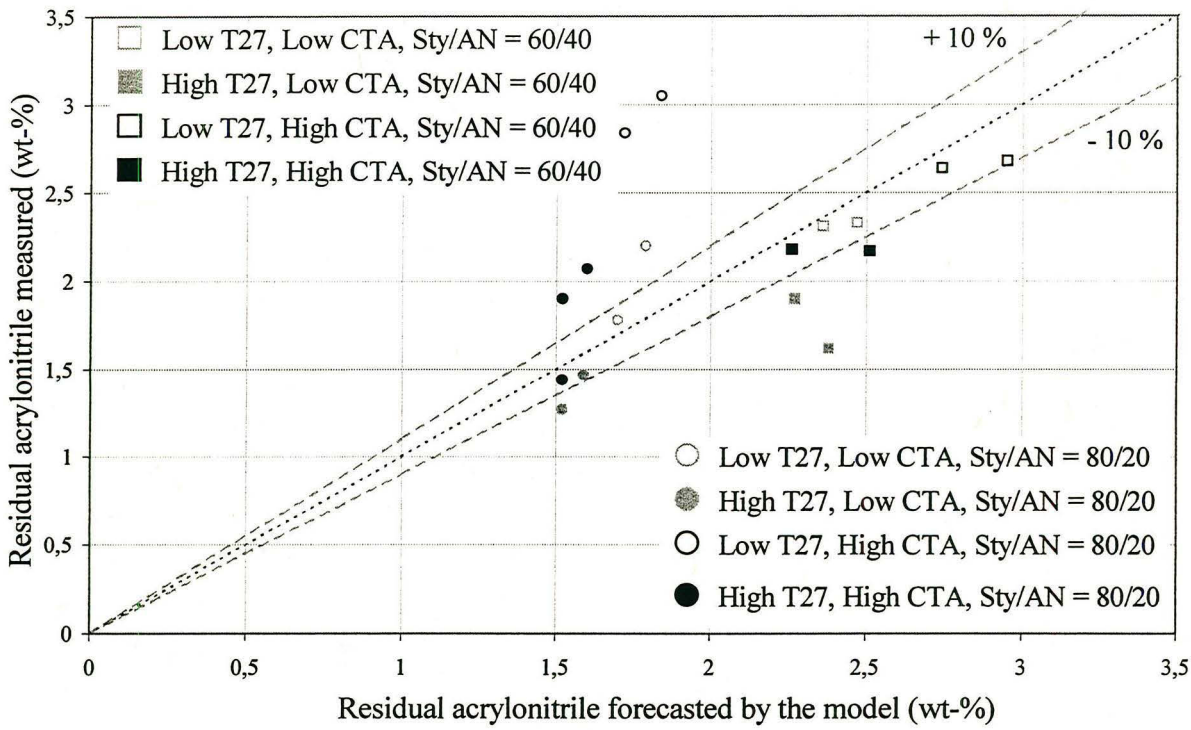

Figure A5.1. : Residual acrylonitrile : Measurements vs. modeling using the parameters identified at 140 °C

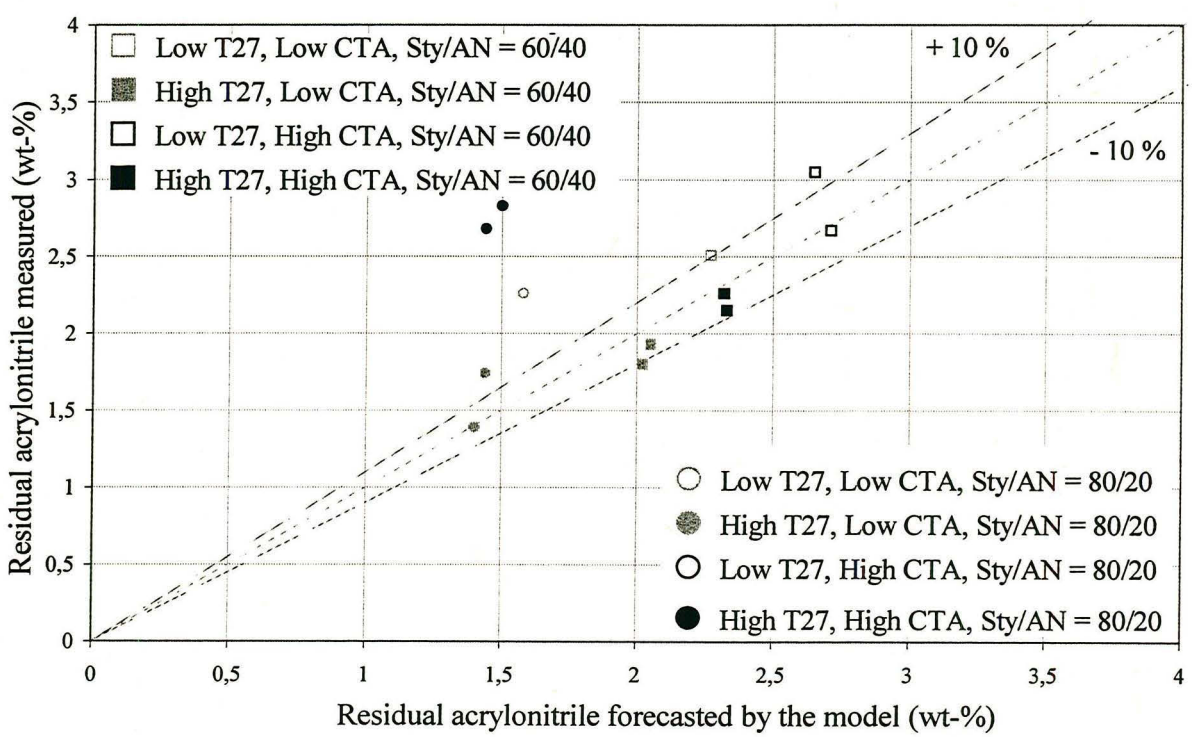

Figure A5.2. : Residual acrylonitrile : Measurements vs. modeling using the parameters identified at 120 °C

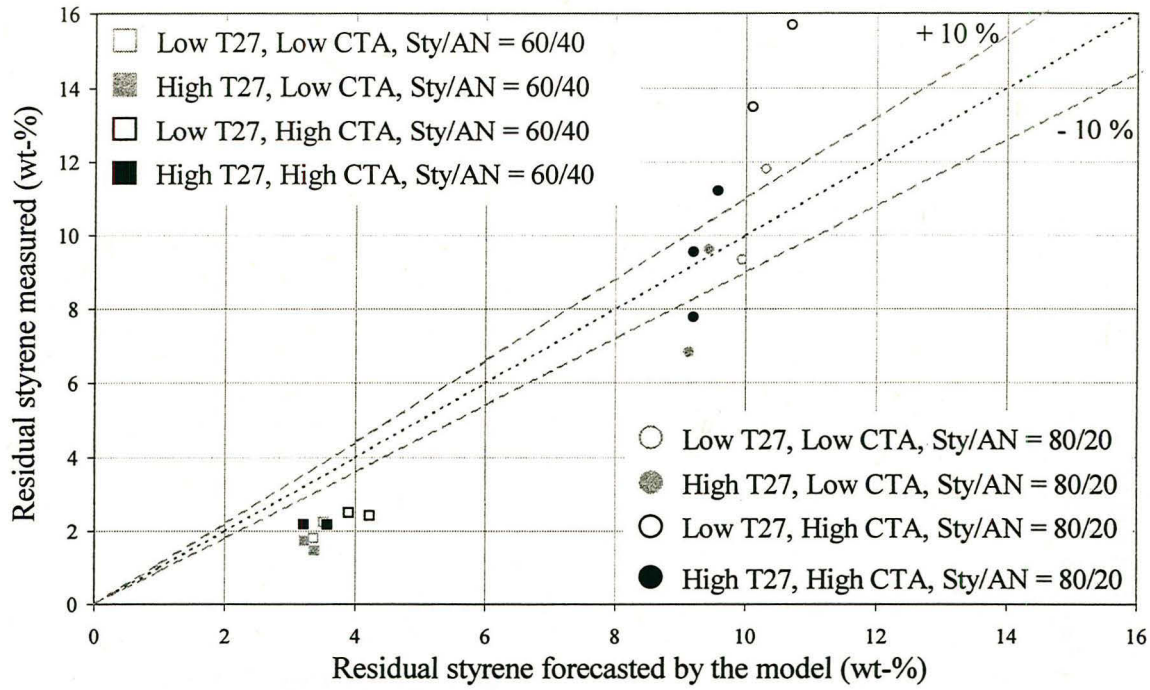

Figure A5.3. : Residual styrene : Measurements vs. modeling using the parameters identified at 140 °C

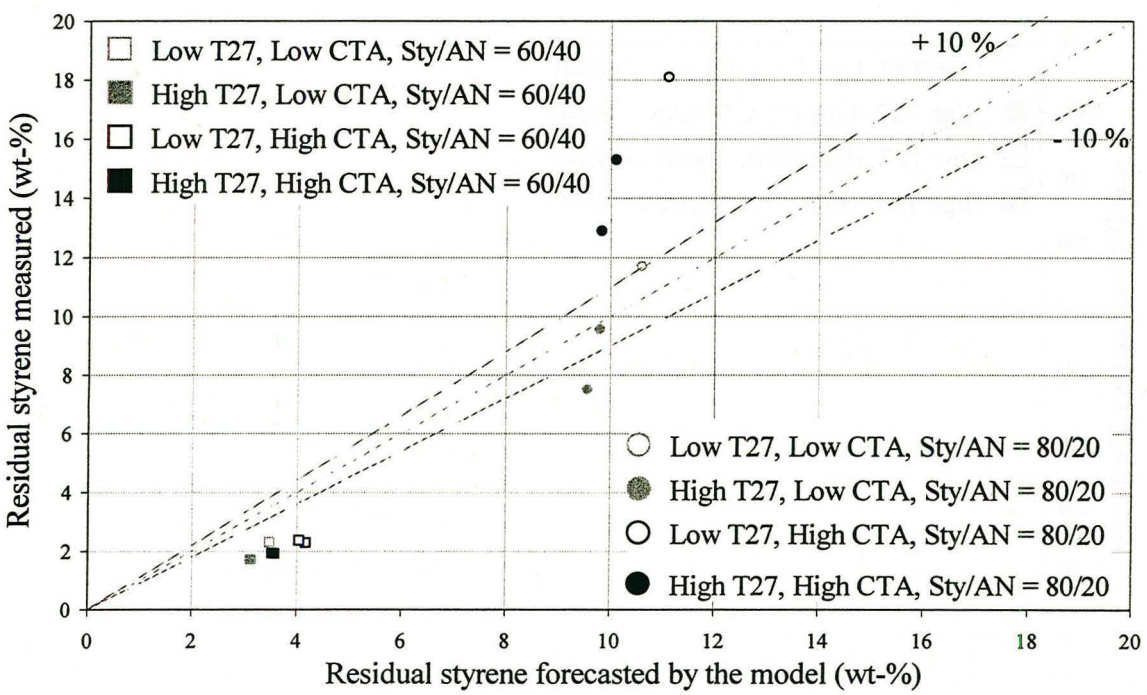

Figure A5.4. : Residual styrene : Measurements vs. modeling using the parameters identified at 120 °C

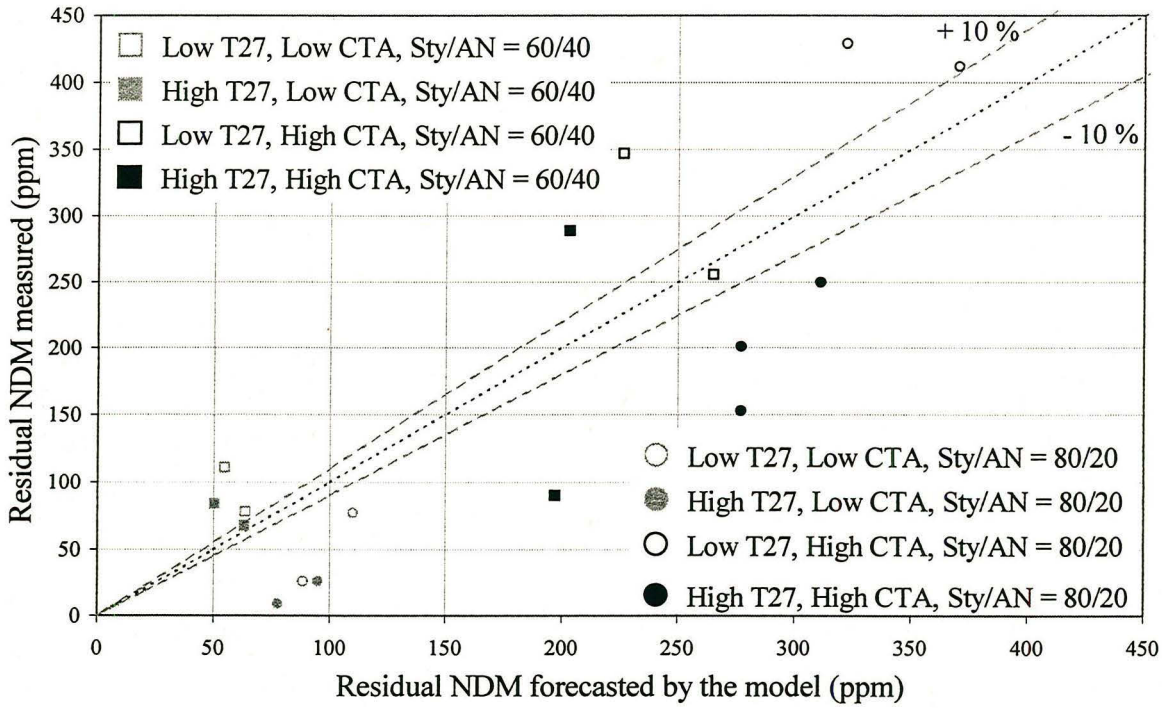

Figure A5.5. : Residual NDM : Measurements vs. modeling using the parameters identified at 140 °C

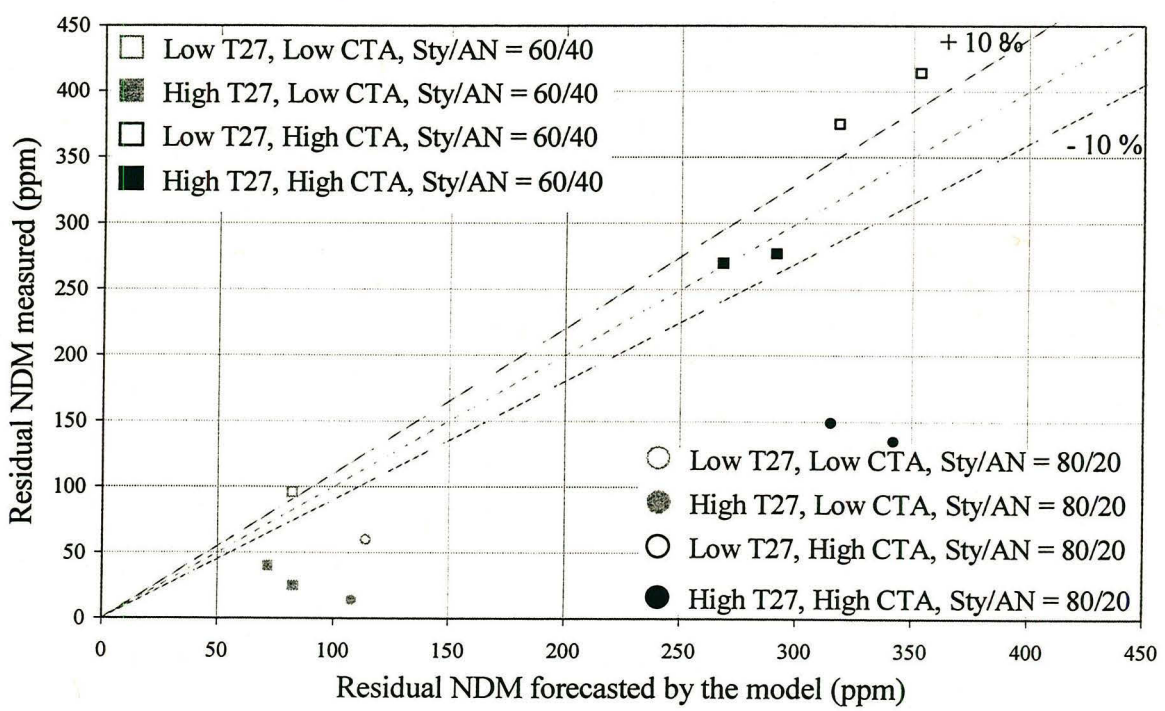

Figure A5.6. : Residual NDM : Measurements vs. modeling using the parameters identified at 140 °C

RESUME LONG

Ce travail est le résultat de la collaboration entre la société Dow Benelux à Terneuzen (NL) et l'équipe de procédés de polymérisation du Laboratoire des Sciences du Génie Chimique de Nancy. L'enjeu de ce travail est d'améliorer les connaissances concernant le procédé de fabrication des copolymères polyols produits par un procédé de copolymérisation en dispersion du système styrène/acrylonitrile en milieu polyol, afin d'améliorer les qualités du produit et de réduire le problème majeur qu'est l'agglomération des particules et l'encrassement des installations.

Ce travail étant destiné à la société Dow, ce document a été rédigé en anglais à sa demande. Ci-dessous un long résumé du travail permet de faire la synthèse de l'ensemble des résultats obtenus.

1. Généralité et contexte

1.1. Polymérisation en dispersion

La polymérisation en dispersion est un procédé hétérogène qui a été développé par la société Imperial Chemical Industries (Osmond et col.,1962). Ce procédé est considéré comme un cas particulier de polymérisation par précipitation et son origine est intimement liée au développement de l'industrie des peintures. En effet, le développement des résines en solution était limité par l'augmentation de la viscosité liée à la concentration en polymère et aux masses molaires des polymères.

Le procédé de polymérisation en émulsion en milieu aqueux constituait une alternative très intéressante puisqu'il permettait de produire des polymères de hautes masses molaires, avec une cinétique beaucoup plus importante qu'en solution, tout en s'affranchissant des restrictions sur la viscosité jusqu'à des extraits secs élevés. De plus, l'eau détient des avantages pratiques tels que l'ininflammabilité, la non toxicité et le caractère indolore. Cependant, l'eau s'accompagne aussi d'inconvénients dans le domaine des peintures : la chaleur latente d'évaporation de l'eau est élevée par rapport à la plupart des liquides organiques, allongeant les temps de séchage ; le point de congélation de l'eau est élevé en comparaison à celui de la plupart des liquides organiques, et malgré l'utilisation d'additifs adéquats, cela contribue à compliquer le transport et le stockage des polymères en émulsion ; l'utilisation d'émulsifiants tend à conférer au film une sensibilité résiduelle à l'eau qui conduit généralement à une dégradation de ses propriétés. La polymérisation en milieux organiques est donc directement issue de la recherche de nouveaux procédés de polymérisation à destination de l'industrie des peintures, et qui devaient conserver les avantages de la polymérisation en émulsion en s'affranchissant de l'eau comme milieu continu.

Ainsi, la polymérisation en dispersion nécessite typiquement quatre composants :

- un solvant : solvant des monomères mais précipitant du polymère formé,
- les monomères,
- le système amorceur soluble dans le solvant,

- un stabilisant stérique.

D'autres additifs peuvent être utilisés comme un agent de transfert, soluble dans le solvant.

Le milieu initialement formé par tous ces composés est alors une solution homogène. La polymérisation des monomères conduit ensuite à un système hétérogène du fait de l'insolubilité du polymère formé dans le milieu continu (communément appelé sérum). Le milieu réactionnel, initialement translucide, devient donc laiteux car les particules formées sont capables de diffuser la lumière.

La stabilisation des particules est assurée par la présence du stabilisant stérique. Ce stabilisant consiste en général en un copolymère greffé (préformé ou généré *in situ* par transfert ou copolymérisation avec un macromère soluble) qui s'adsorbe à la surface des particules et empêche leur agrégation. L'apparition d'un système hétérogène s'accompagne d'un partage des différentes espèces (monomères, amorceur, agent de transfert, stabilisant, solvant). Cela mène à l'existence de deux sites de polymérisations : le sérum et les particules.

Selon Kawaguchi (2000), l'histoire de la polymérisation en dispersion débute dans les années 1950. Jusque dans les années 1970, des hydrocarbures aliphatiques étaient utilisés comme phase continue dans presque toutes les polymérisation en dispersion. La première génération générait des dispersions organiques de particules de tailles inférieures au micromètre avec un fort taux de solide et une faible viscosité. Ces dispersions non aqueuses étaient employées pour les peintures et les encres. En comparaison, les polymérisations en dispersions apparues dans les années 1980 appartiennent à une deuxième génération. Elles utilisaient des solvants polaires comme phase continue et l'objectif était de préparer des suspensions de particules monodisperses de l'ordre du micromètre. La troisième génération est apparue dans les années 1990 avec les mêmes objectifs mais avec la production de particules fonctionnalisées et en prenant en compte les problèmes environnementaux, notamment en utilisant le CO_2 supercritique pour remplacer les solvants organiques.

1.2. Copolymères polyols

Les copolymères polyols (CPPs) sont produits par la société Dow Chemical, par voie radicalaire par copolymérisation en dispersion d'acrylonitrile et de styrène en milieu polyol, sur les sites de production de Freeport (Texas-USA), Terneuzen et Zwijndrecht (NL) en réacteur continu agité et en réacteur fermé agité. Le procédé batch a été développé en interne par Dow Chemical, tandis que les droits d'utiliser le procédé continu développé par la société Union Carbide ont été obtenus après l'acquisition d'une ancienne usine de British Petroleum en Belgique en juillet 1998.

Les CPPs sont utilisés depuis les années 1960 (Kuryla et al., 1965) comme matière première dans la fabrication des mousses polyuréthanes et ils sont devenus un des éléments clefs de l'industrie des polyuréthanes flexibles. Les applications les plus majeures sont dans l'industrie automobile avec la formulation de pièces moulées à haute résilience et de mousses de meilleure dureté. En effet, les CPPs augmentent la masse des mousses et diminuent les coûts de production de leurs procédés de fabrication. Cela se traduit alors par des économies d'énergie pendant la production de ces parties moulées à l'usage des sièges de voitures.

La nature et la structure du stabilisant est un des points clefs du procédé de polymérisation en dispersion. Les copolymères polyols produits lors de cette étude ont été réalisés en utilisant un stabilisant précurseur (S5200) ainsi qu'un stabilisant préformé (semence). Le macromère S5200 est le produit de la réaction d'une quantité de vinyltriméthoxysilane (VTMS) avec trois quantités

de polyéther triol. Puis, le stabilisant en lui-même est produit *in situ*, par greffage du S5200 sur les chaînes de copolymères SAN. Ce greffage est supposé avoir lieu par copolymérisation de la liaison Si-C=C du S5200 avec les monomères styrène et acrylonitrile. La réactivité du stabilisant précurseur avec le styrène et l'acrylonitrile est très faible et la réactivité du précurseur avec lui-même est considérée comme négligeable, ce qui remplit les conditions idéales pour former un bon stabilisant stérique. La semence, c'est-à-dire, le stabilisant préformé, est produite par la polymérisation radicalaire d'un excès de stabilisant précurseur avec les monomères. Ainsi, la semence contient à la fois des particules primaires de SAN insolubles et du SAN dissout dans le sérum.

Les fines dispersions de polymères sont stabilisées par le stabilisant qui s'adsorbe à la surface des particules. En effet, la partie SAN du copolymère greffé s'adsorbe sur les particules pendant que la partie polyol du S5200 forme une protection autour des particules les empêchant de s'approcher les unes des autres si suffisamment de stabilisant est adsorbé. Afin d'obtenir une dispersion stable, il est nécessaire que la phase continue soit un bon solvant du polymère adsorbé, et que la surface de toutes les particules soit complètement couverte par les greffons. De plus, le stabilisant doit être fermement attaché à la surface des particules et l'épaisseur de la barrière stérique doit être suffisante pour prévenir la floculation.

Cependant, d'autres mécanismes de greffage, appelés « greffage naturel », sont susceptibles d'intervenir. En effet, les radicaux issus de la décomposition de l'amorceur, ou toute autre espèce radicalaire présente dans le milieux, sont susceptible d'arracher un atome d'hydrogène à la chaîne polyol du solvant créant une nouvelle espèce radicalaire. Ainsi, le solvant polyol peut se comporter comme un agent de transfert, amorçant ensuite une nouvelle polymérisation avec les monomères présents. Ce type de mécanisme mène à la production *in situ* d'un macromère polyol-SAN, qui ne procure pas le même pouvoir stabilisant que le macromère S5200-SAN. Ceci montre que la nature et la structure du stabilisant est complexe et dépend des différentes conditions expérimentales.

1.3. Objectifs du travail

Les objectifs de ce travail étaient de tenter de répondre aux différentes questions se posant concernant le procédé continu de copolymérisation en dispersion de styrène et d'acrylonitrile en milieu polyol, et en particulier de mieux comprendre le système stabilisant et l'influence des conditions expérimentales sur les propriétés des copolymères polyols. Le système stabilisant est un point clef de ce type de procédé, or, d'importantes informations manquent quant à la structure du stabilisant produit *in situ* et l'épaisseur de la couche stabilisante. De plus, la majorité des constantes cinétiques qui interviennent dans le procédé ne sont pas connues, en particulier celles concernant le système stabilisant précurseur-styrène-acrylonitrile et la cinétique d'adsorption sur les particules de SAN. L'effet du greffage sur la stabilité et la viscosité du CPP doit aussi être éclairci. Un autre point important du procédé est le partage des monomères, de l'amorceur et de l'agent de transfert entre les deux phases.

L'objectif était ainsi d'étudier l'influence des conditions expérimentales sur les propriétés des copolymères polyols produits dans le but de mieux comprendre les différents mécanismes intervenants et de développer un modèle de tendances pour le procédé global.

2. Etude expérimentale du procédé

Une étude expérimentale du procédé a été effectuée afin de déterminer l'influence des conditions expérimentales sur les propriétés finales des copolymères polyols produits et de les relier entre elles.

2.1. Techniques expérimentales

Différents copolymères polyols ont été élaboré à l'aide d'un dispositif de laboratoire développé par Dow. La figure 1 présente le schéma de cette installation centrée autour d'un réacteur continu agité d'un volume de 0,5 L. La pression est maintenue supérieure à 3 bars grâce à une valve de régulation afin que les monomères restent liquides aux températures de travail utilisées comprises entre 120 °C et 140 °C. Ce réacteur est alimenté en mélange initial par une pompe à engrenage avec un débit de 25 g/min.

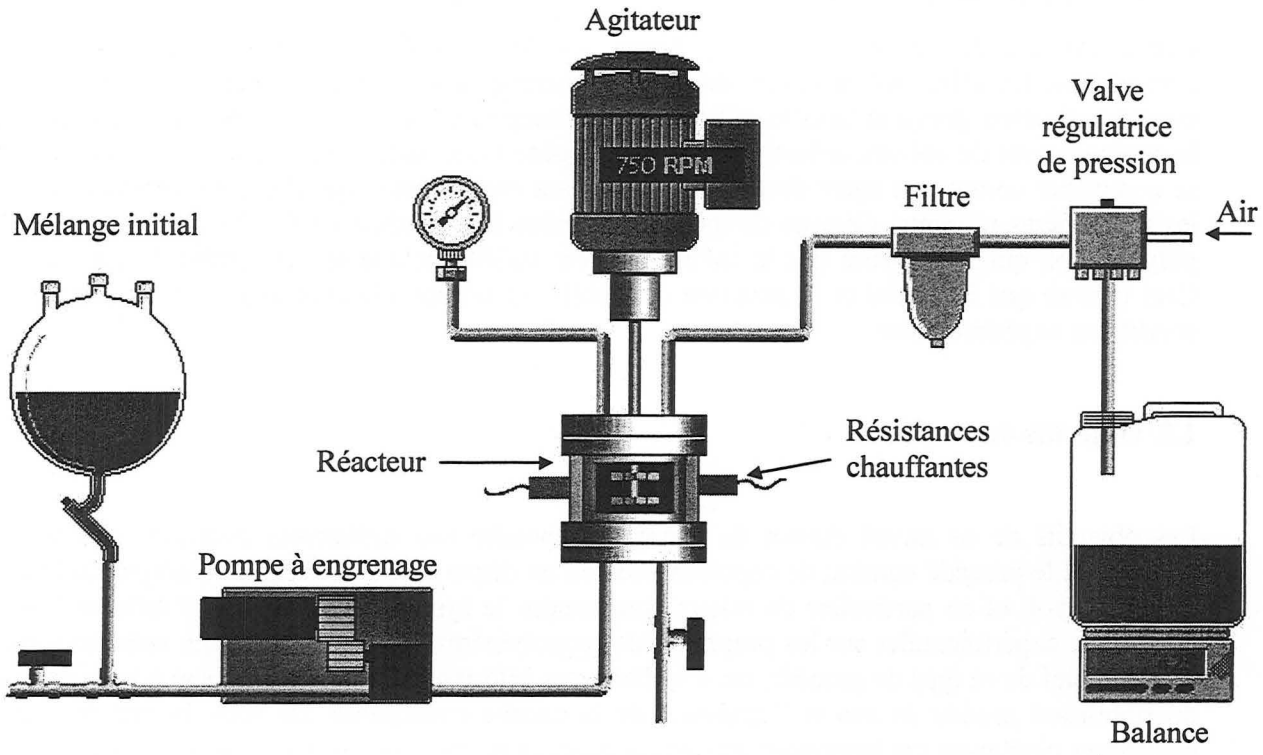

Figure 1. Schéma de l'installation

Le mélange initial est composé des ingrédients suivants :

- le solvant : le polyéther polyol,
- les monomères : 42 % en masses de styrène et d'acrylonitrile,
- l'amorceur (I),
- l'agent de transfert (CTA),

- le stabilisant précurseur (S5200),
- le stabilisant préformé (les semences).

Un plan d'expérience factoriel à deux niveaux (plus le centre) a été utilisé afin d'évaluer l'influence de la quantité de S5200, d'amorceur et d'agent de transfert, de la température ainsi que du rapport styrène/acrylonitrile.

Pour chaque expérience, des échantillons ont été collectés en régime permanent au bout de 13 temps de passages. Ces échantillons ont été analysés par le département d'analyses de la compagnie Dow à Terneuzen. Cette étude est extrêmement complexe et longue à mettre en œuvre. La figure 2 résume l'ensemble des mesures effectuées sur ces échantillons.

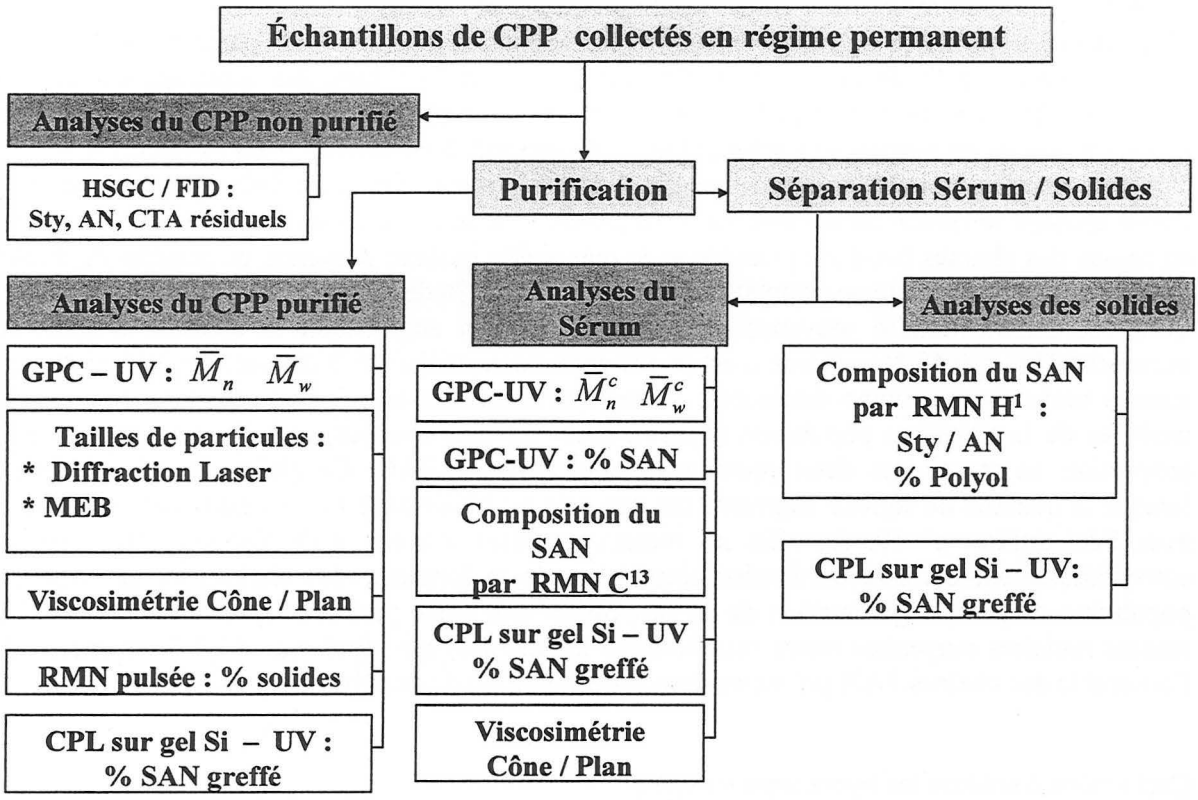

Figure 2 : Méthodes analytiques utilisées

2.2. Résultats

Les principaux résultats expérimentaux sont présentés ci-dessous. L'influence des différents paramètres expérimentaux sur les propriétés physiques des copolymères polyols sera présentée ainsi que les liens entre ses différentes propriétés.

2.2.1. Distributions de masses molaires

Les deux principaux paramètres qui influencent les distributions de masses molaires sont la quantité d'agent de transfert ainsi que le rapport styrène/acrylonitrile. C'est en effet le rôle de l'agent de transfert que de réduire les masses molaires et l'influence du rapport styrène/acrylonitrile est due au fait que l'augmentation de la quantité styrène dans le copolymère SAN diminue sa cristallinité due à l'acrylonitrile, rendant ce copolymère plus soluble dans la phase continue et favorisant la polymérisation en solution dans le sérum face à la polymérisation en masse dans les particules.

L'augmentation de la concentration en amorceur ainsi que l'augmentation de la température, en augmentant le nombre d'espèces radicalaires dans le milieu, réduisent légèrement les masses molaires moyennes. L'augmentation de la quantité de stabilisant précurseur, S5200, se traduit par une légère augmentation des masses molaires moyennes.

Un point important ressort de l'étude des distributions de masses molaires. En effet, il a été mis en évidence la présence de trois populations différentes de chaînes SAN par déconvolution de ces distributions à l'aide de fonctions Gamma (voir la présentation des fonctions Gamma en annexe A4.2). Comme le montre la figure 3 ainsi que le tableau 1 concernant la distribution de masses molaires en masses de l'échantillon n° 10 (réalisé avec Sty/AN = 60 /40 et CTA = 0,15 %), une première population représentant 1,2 % de la masse totale de SAN apparaît avec une masse molaire moyenne en nombre de 3550 g/mol. Une seconde population représentant 6,3 % en masse des chaînes SAN est présente avec une masse molaire moyenne en nombre de 10980 g/mol ainsi qu'une troisième population représentant 92,5 % de la masse totale des chaînes SAN avec une masse molaire moyenne de 83700 g/mol. En augmentant la quantité d'agent de transfert (CTA = 0,45 %) comme c'est le cas pour l'échantillon n° 9 (figure 4 et tableau 2), les masses molaires moyennes diminuent. Cette diminution est due à la diminution des masses molaires de la troisième population (chaînes SAN les plus longues) et à l'augmentation de la proportion en masse des deux premières populations de SAN. Ce phénomène est amplifié lorsque la quantité de styrène augmente comme cela est observable sur la figure 5 et le tableau 3 avec l'échantillon n° 19. En effet les masses molaires moyennes de l'échantillon réduisent considérablement par une diminution importante de la longueur des chaînes de la troisième population et par l'augmentation de la proportion des deux premières populations (dont les masses molaires moyennes restes sensiblement les mêmes) qui représente 44,4 % en masse de l'ensemble des chaînes SAN présentes dans cet échantillon de copolymère polyol.

Ceci amène à émettre les hypothèses suivantes :

(i) La première population correspond aux courtes chaînes de SAN produites par polymérisation en solution dans la phase continue,

(ii) La deuxième population correspond au stabilisant formé *in situ* dans la phase continue par greffage du S5200 avec le système styrène / acrylonitrile,

(iii) La troisième population correspond aux chaînes SAN produites dans les particules.

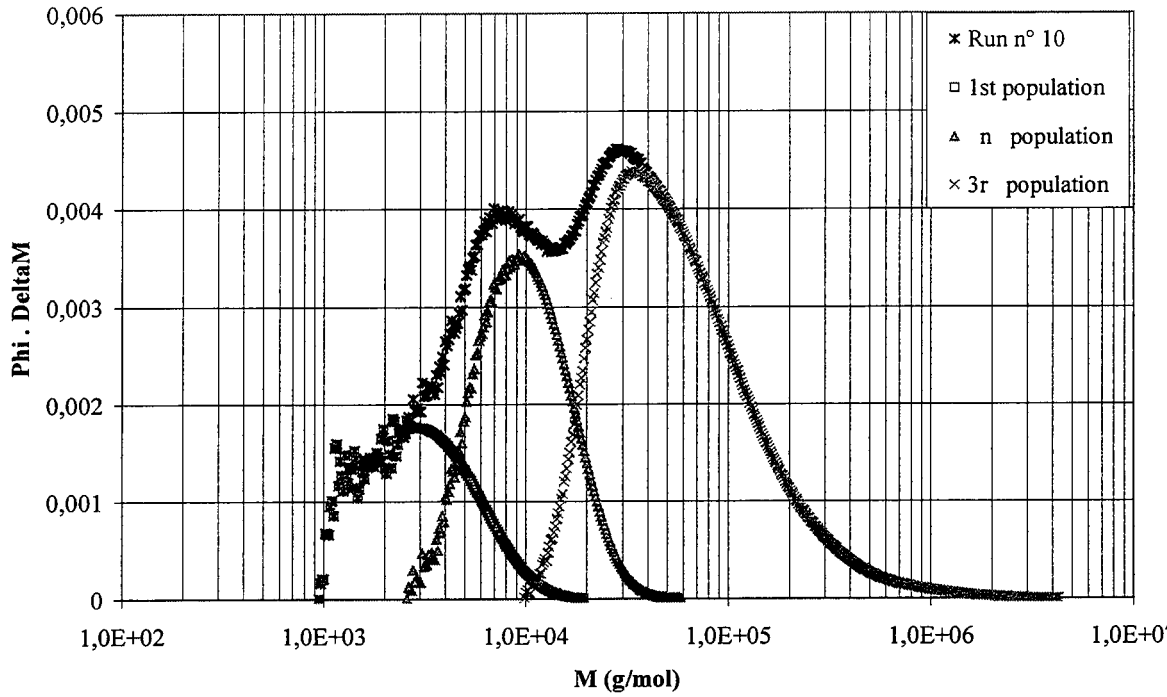

Figure 3 : Déconvolution de la distribution de masses molaires en masses de l'échantillon n° 10 réalisé avec Sty/AN=60/40, S5200 =3 wt-%, NDM = 0.15 wt-%, T27 = 0.20 wt-% et T=120 °C

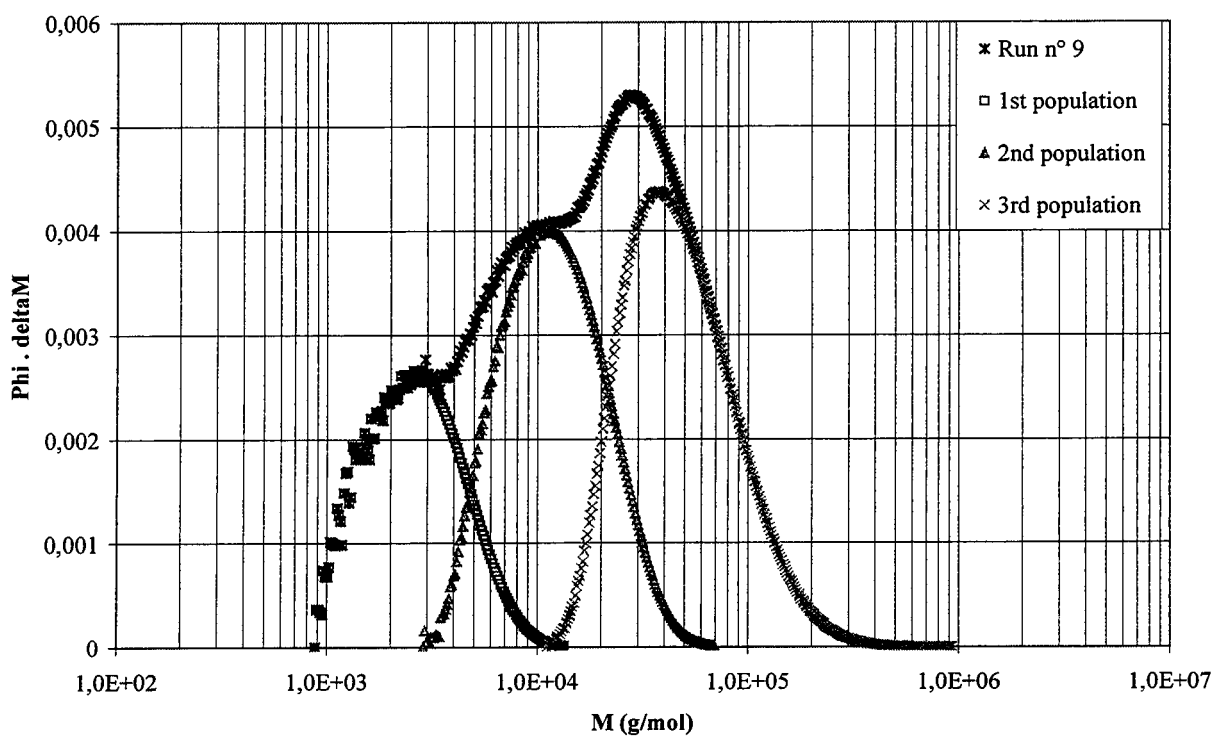

Figure 4 : Déconvolution de la distribution de masses molaires en masses de l'échantillon n° 9 réalisé avec Sty/AN=60/40, S5200 =3 wt-%, NDM = 0.45 wt-%, T27 = 0.10 wt-% et T=120 °C

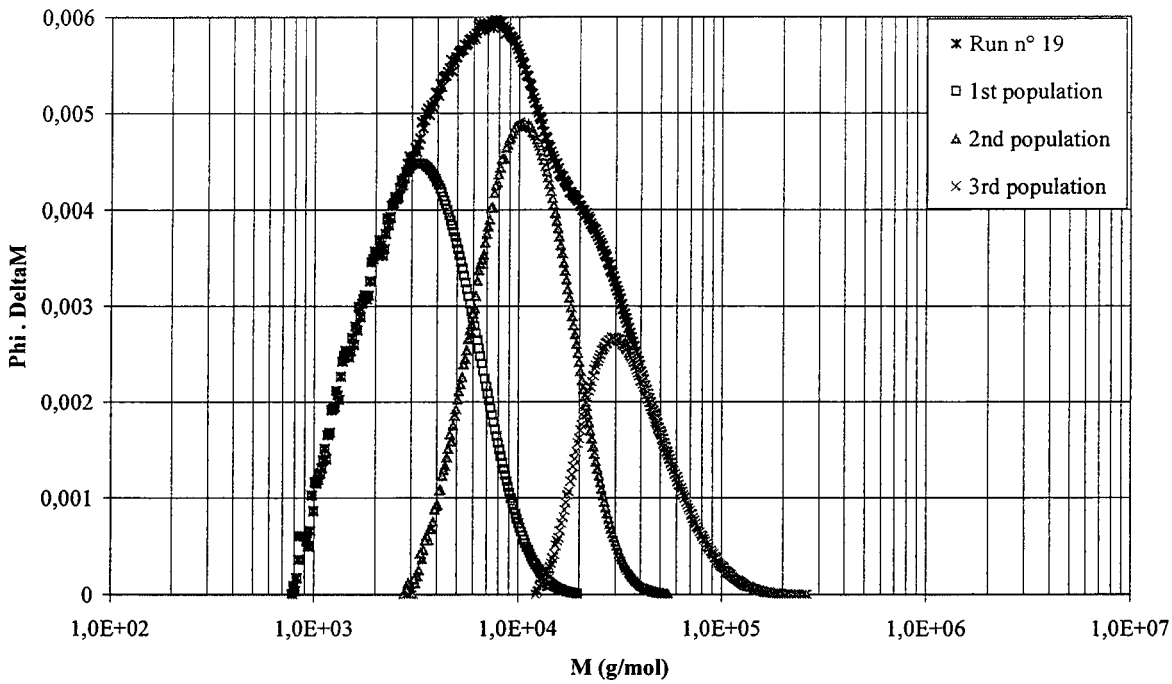

Figure 5 : Déconvolution de la distribution de masses molaires en masses de l'échantillon n° 19 réalisé avec Sty/AN=80/20, S5200 =1 wt-%, NDM = 0.45 wt-%, T27 = 0.10 wt-% et T=140 °C

Tableau 1 : Déconvolution des distributions de masses molaires de l'échantillon n°10

Population	1	2	3	Total
$\bar{M}_n$ (g/mol)	3550	10980	83700	49310
$\bar{M}_w$ (g/mol)	5030	14130	206230	191600
Mol-%	17	28.5	54.5	100
Wt-%	1.2	6.3	92.5	100

Tableau 2 : Déconvolution des distributions de masses molaires de l'échantillon n°9

Population	1	2	3	Total
$\bar{M}_n$ (g/mol)	3000	13800	57300	28500
$\bar{M}_w$ (g/mol)	3930	18660	88600	73600
Mol-%	21	37	42	100
Wt-%	2	17	81	100

Tableau 3. Déconvolution des distributions de masses molaires de l'échantillon n°19

Population	1	2	3	Total
$\bar{M}_n$ (g/mol)	3800	11900	39700	13400
$\bar{M}_w$ (g/mol)	5200	15100	51300	33300
Mol-%	41.2	39.2	19.6	100
Wt-%	11.1	33.3	55.6	100

2.2.2. Conversions et taux de solides

La conversion partielle en agent de transfert est comprise entre 90 et 100 % pour l'ensemble des expériences réalisées.

Le paramètre expérimental qui influence significativement la consommation en monomères est le rapport styrène / acrylonitrile car la vitesse de homopropagation du styrène étant inférieure à celle de l'acrylonitrile (Brandrupt & Immergut, 1989), et le site de la polymérisation étant dirigé vers la phase continue par la plus forte présence de styrène, la consommation de monomère est réduite dans les particules (avec notamment réduction de l'effet de gel) et les conversions sont plus faibles ainsi que la proportion de solides.

2.2.3. Distributions de tailles de particules

La diffraction laser a permis de déterminer les distributions de tailles de particules en volumes des échantillons produits. Les principaux paramètres influençant ces distributions sont le rapport styrène / acrylonitrile et la concentration en agent de transfert et en stabilisant précurseur S5200.

Les dispersions de particules les plus stables ont été obtenues avec Sty / AN = 60 / 40, CTA = 0,45 % et S5200 = 3 %. La figure 6 présente les distributions de particules en volumes des échantillons réalisés dans ces conditions. Une distribution bimodale est clairement visible avec une population de petites particules avec un diamètre de Sauter centré autour de 0,3 µm et une population de plus grosses particules avec un diamètre de Sauter centré autour de 1,7 – 2 µm. Les petites particules correspondent aux particules primaires et aux semences. Les images obtenues par le microscope électronique à balayage montrent des particules bien sphériques (figure 7).

Le diminution de la quantité de stabilisant précurseur S5200 entraîne l'apparition de particules de tailles dépassant les 10 µm (figure 8). Les images (figure 9) montrent qu'il s'agit en fait d'un artéfact produit par l'analyse des résultats de la diffraction laser : les particules sont moins bien stabilisées et certaines s'agglomèrent les unes aux autres.

La diminution de la quantité d'agent de transfert entraîne l'apparition d'agglomération plus importante comme cela est observable sur la figure 10. Les images (figure 11) montrent en effet que les particules ne sont pas parfaitement sphériques mais « bosselées » comme si elles s'étaient formées par l'agglomération de petites particules. Cette diminution de stabilité est donc liée à une augmentation des masses molaires moyennes.

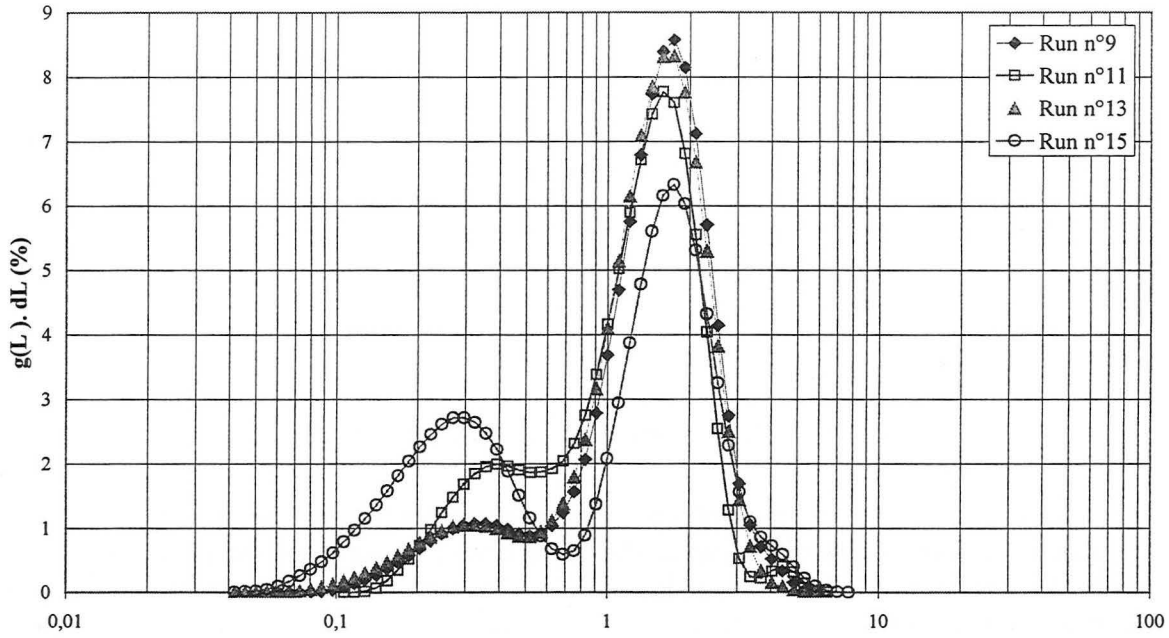

Figure 6 : Distribution volumique des tailles de particules des échantillons n° 9 (T27=0.1 et T=120°C), n°11 (T27=0.2 wt-% et T=140°C), n° 13 (T27=0.1 wt-% et T=140°C) et n°15 (T27=0.2 wt-% et T=140°C) réalisés avec Sty/AN=60/40, S5200 = 3 wt-% et NDM=0.45 wt-%.

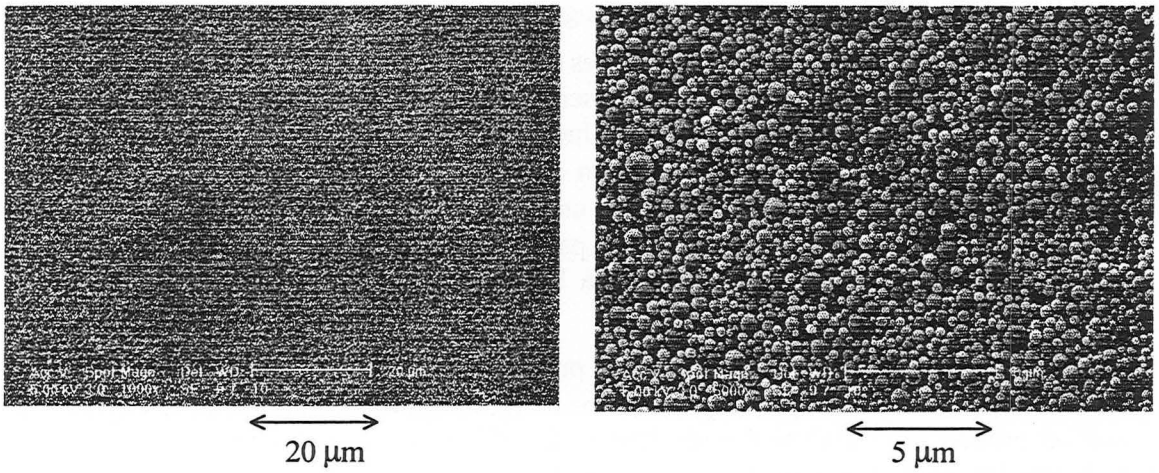

Figure 7 : Images SEM de l'échantillon n° 11 réalisées avec NDM =0.45 wt-%, T27 =0.20 wt-%, T=120°C, Sty/AN = 60/40 et S5200 =3 wt-%.

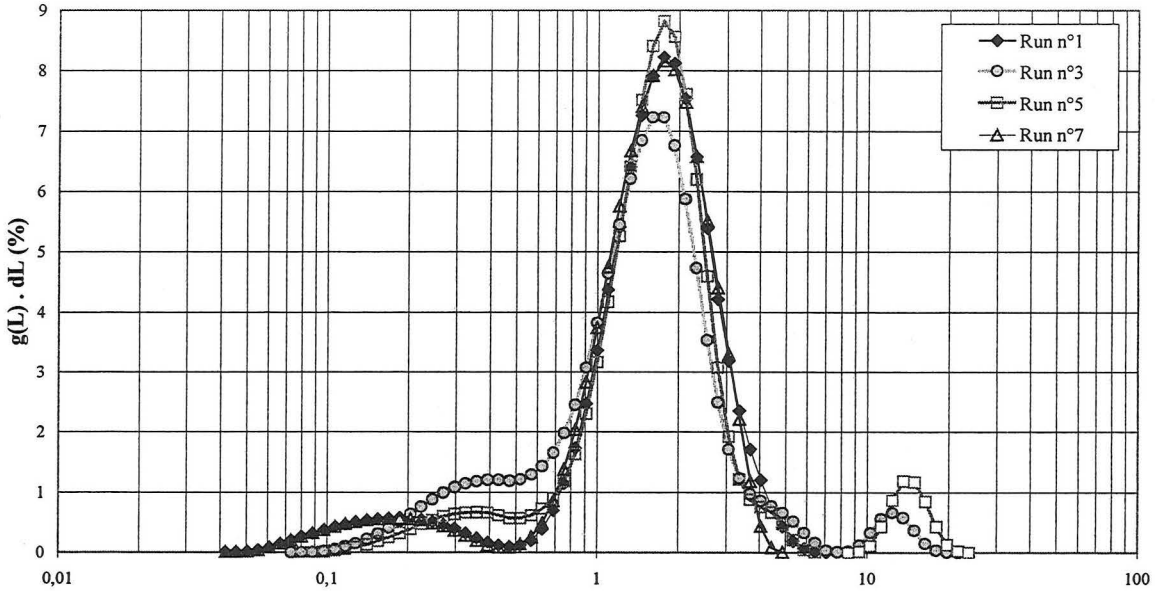

Figure 8 : Distribution volumique des tailles de particules des échantillons n° 1 (T27=0.1 wt-%. et T=120 °C), n°3 (T27=0.2 wt-%.et T = 140°C), n°5 (T27=0.1 wt-%. et T=140 °C) et n°7 (T27 =0.2 wt-%. et T =140 °C) réalisés avec Sty/AN=60/40, S5200 = 1 wt-% et NDM =0.45 wt-%.

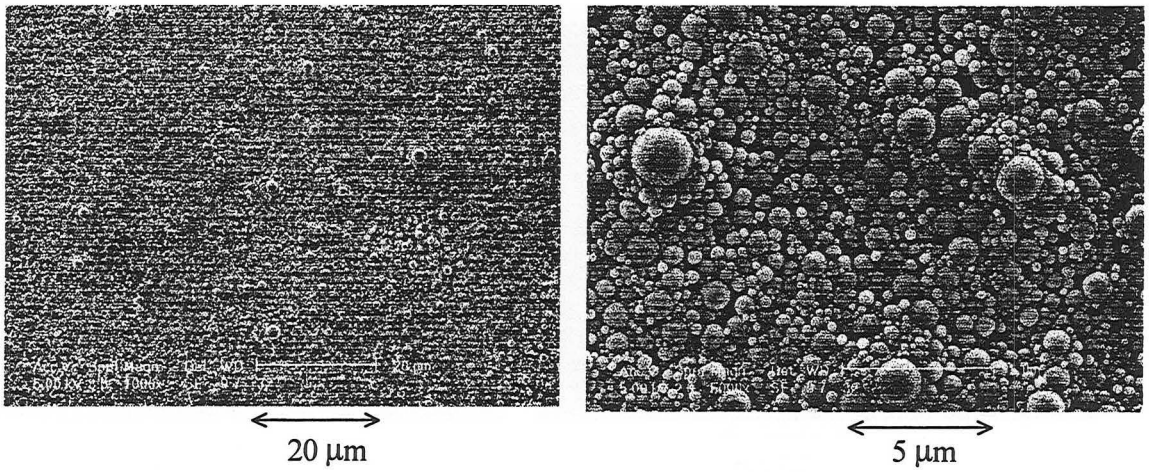

Figure 9 : Images SEM de l'échantillon n° 5 réalisé avec NDM =0.45 wt-%, T27 =0.10 wt-%, T = 140°C, Sty/AN = 60/40 et S5200 =1 wt-%.

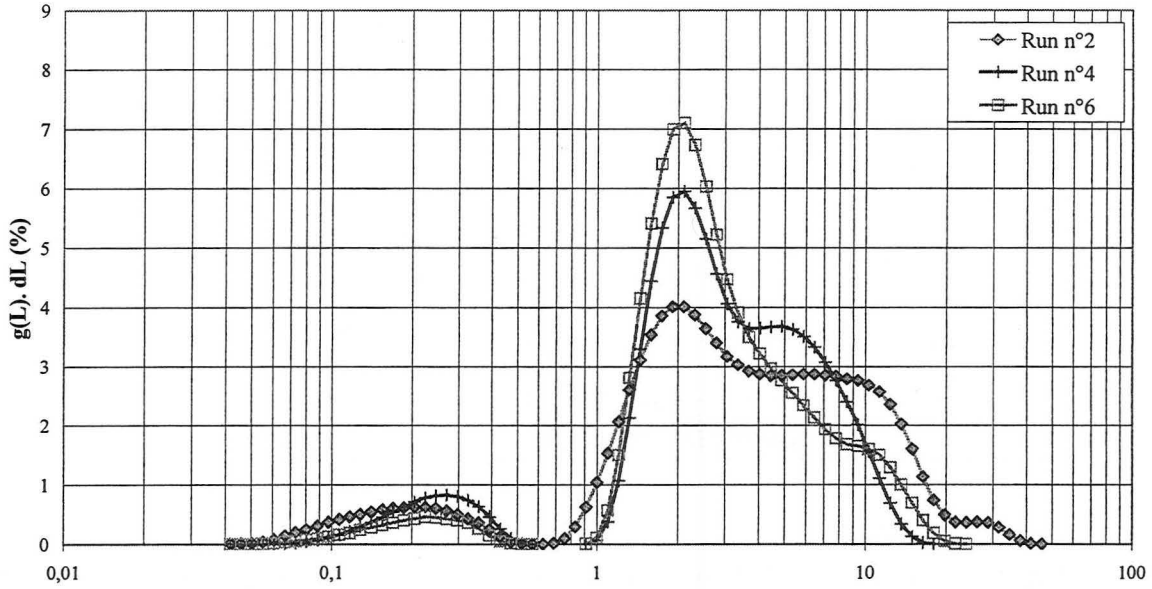

Figure 10 : Distribution volumique des tailles de particules des échantillons n° 2 (high T27 and low T), n°4 (low T27 and high T) and n°6 (high T27 and high T) done with Sty/AN=60/40, low S5200 (1 wt-%) and low NDM (0.15 wt-%).

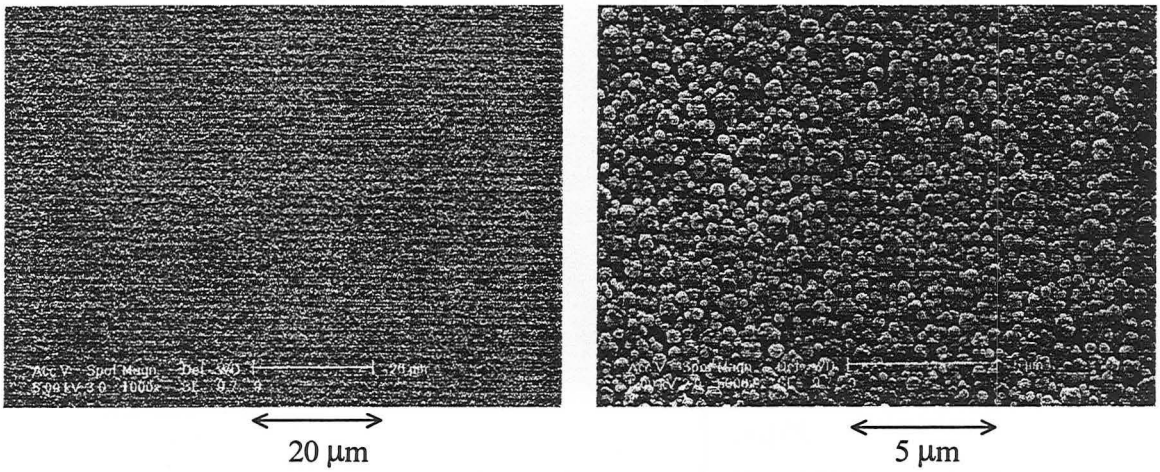

Figure 11 : Images SEM de l'échantillon n° 10 réalisé avec NDM =0.15 wt-%, T27 = 0.20 wt-%, T =120°C, Sty/AN = 60/40 et S5200 =3 wt-%.

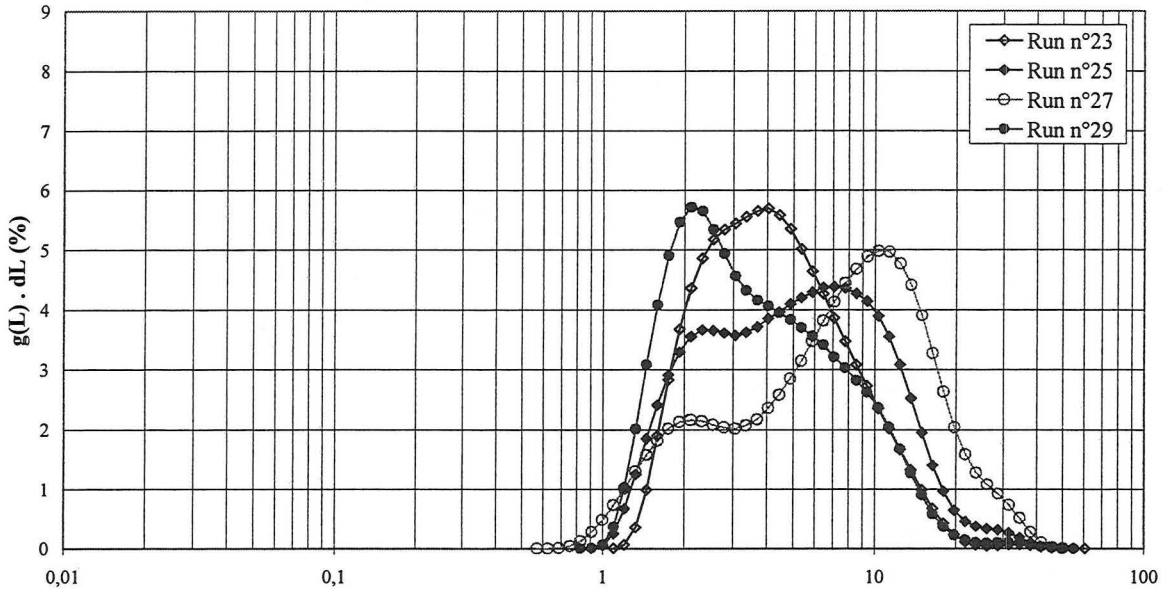

Figure 12 : Distribution volumique des tailles de particules des échantillons n° 23 (T27=0.1 wt-% et T=120°C), n°25 (T27=0.2 wt-% et T=120°C), n°27 (T27=0.1 wt-% et T=140°C) et n°29 (T27=0.2 wt-% et T=140°C) réalisés avec Sty/AN = 80/20, S5200 = 3 wt-% et NDM = 0.45 wt-%

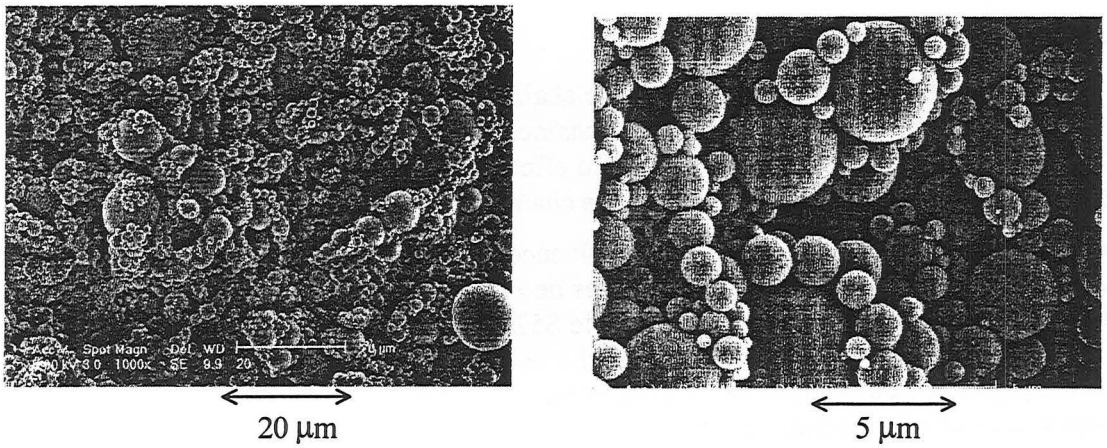

Figure 13 : Images SEM de l'échantillon n° 18 réalisé avec NDM = 0.15 wt-%, T27 = 0.10 wt-%, T = 140°C, Sty/AN = 80/20 et S5200 =1 wt-%.

En ce qui concerne le rapport styrène / acrylonitrile, toutes les expériences réalisées avec Sty / AN = 80 / 20 ont produit des copolymères polyols instables. La figure 12 montre des distributions de particules polymodales et les images de la figure 13 montrent des tailles de particules très diverses et des particules agglomérées les unes aux autres. Par conséquent, lorsque le site de polymérisation est orienté vers la polymérisation en solution dans la phase continue, les molécules de stabilisant contenant une proportion importante d'éléments styrène sont plus solubles dans le sérum et s'adsorbent plus difficilement à la surface des particules, réduisant la stabilisation des particules. Dans ces conditions, augmenter la quantité de stabilisant précurseur ne suffit pas à mieux stabiliser les particules car les molécules de SAN greffées restent dissoutes dans le sérum.

La température et la quantité d'amorceur n'ont pas une influence significative sur les distributions de tailles de particules en volume.

2.2.4. Viscosité

La viscosité des copolymères polyols doit dépendre, comme toute dispersion de particules, de la viscosité de la phase continue ainsi que du taux de particules présentes.

Une étude préliminaire menée par la société Dow et exposée dans le paragraphe 1.3 du chapitre 3, a montré l'augmentation de la viscosité du sérum avec l'augmentation du nombre de chaînes SAN greffées en solution. Cependant l'effet le plus important sur la viscosité des CPPs est l'augmentation de la quantité de chaînes SAN greffées dans la phase solide.

L'étude expérimentale qui a été menée montre que la viscosité des CPP est essentiellement influencée par la quantité d'agent de transfert et par le rapport styrène / acrylonitrile mettant en évidence le lien entre la viscosité de la dispersion de particules avec la longueur des chaînes SAN.

2.2.5. Greffage

L'influence principale sur le pourcentage de chaînes SAN greffées provient des deux paramètres qui influencent le plus la longueur de ces chaînes, c'est-à-dire, le rapport styrène / acrylonitrile ainsi que la quantité d'agent de transfert. En effet, une diminution des masses molaires entraîne également une diminution du pourcentage de chaînes greffées.

La figure 14 montre qu'il n'y a aucune influence significative du stabilisant précurseur S5200 sur le greffage. Cependant, l'étude des tailles de particules a permis de montré l'effet stabilisant du S5200. Cela amène donc à suggérer que le S5200 puisse stabiliser les particules en étant libre en solution par stabilisation par déplétion. La stabilité des particules provient dans ce type de stabilisation de la diminution de la concentration du polymère libre entre les deux particules lorsqu'elles sont très proches l'une de l'autre.

Cependant, les conditions expérimentales utilisées (amorceur de type peroxyde et solvant contenant des alcools instaurés) favorisent largement un greffage naturel, ce qui ne permet pas de conclure sur le mode de stabilisation du S5200.

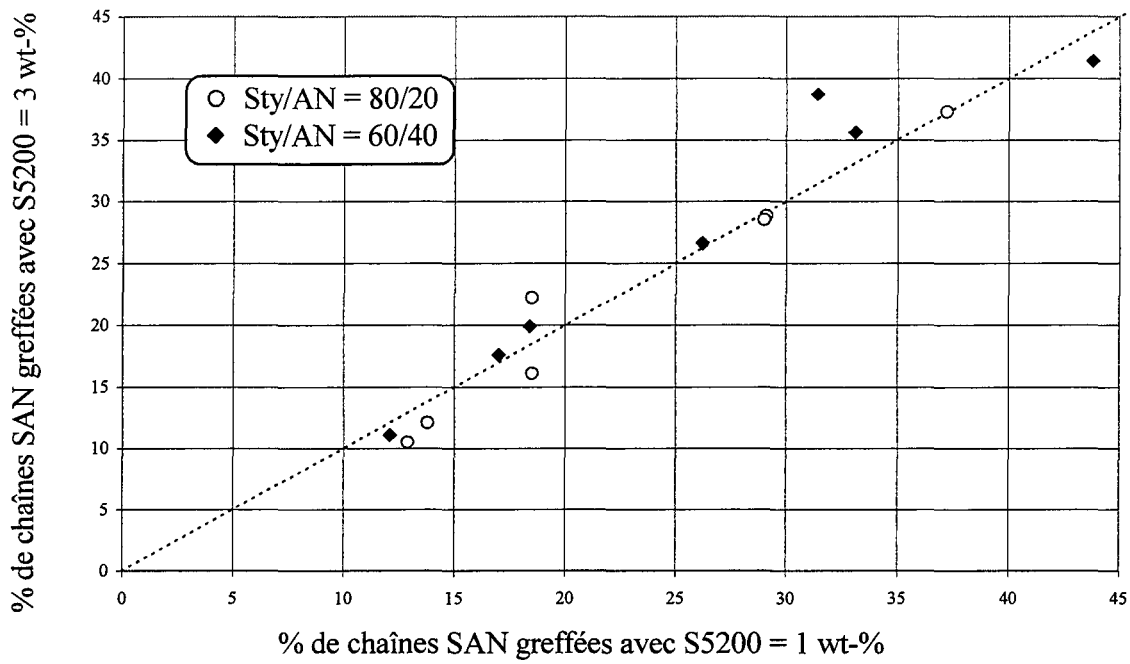

Figure 14 : Influence de la quantité de S5200 sur le % de chaînes SAN greffées dans les échantillons de CPP

2.3. Conclusions

Cette étude expérimentale a montré l'influence principale du rapport massique des monomères ainsi que de la concentration en agent de transfert. Ces deux paramètres expérimentaux agissent sur la solubilité du copolymère SAN dans la phase continue ainsi que sur le degré de polymérisation de ces chaînes. Ceci se répercute sur la solubilité du stabilisant stérique et sur son pouvoir à s'adsorber à la surface des particules et donc sur leur stabilité.

Il a été mis en évidence que la viscosité du produit ainsi que le pourcentage des chaînes greffées dépendent du degré de polymérisation des chaînes SAN produites dans les particules.

Les mesures effectuées sur le sérum donnent des informations importantes concernant le procédé, cependant, ces mesures sont dépendantes de la méthode utilisée pour séparer le sérum des particules et ne sont pas assez précises pour pouvoir procéder à une étude quantitative.

Enfin, il semblerait que le S5200 stabilise les particules plutôt par stabilisation par déplétion que par stabilisation stérique.

3. Modélisation du procédé

Le but de ce travail n'est pas de déterminer un modèle déterministe de ce procédé mais d'apporter un modèle de tendance pouvant prédire les principales propriétés des copolymères polyols. Cette modélisation se déroule en quatre étapes successives : l'écriture du modèle menant à un système d'équations non linéaires algébro-différentielles, dont la résolution constitue le simulateur. Les paramètres inconnus du modèle peuvent alors être identifiés par comparaisons à une série de résultats expérimentaux. La validation du modèle se fait finalement à l'aide d'expériences qui n'ont pas été utilisées pour réaliser l'identification paramétrique. Ces différentes étapes seront détaillées plus amplement ci-dessous avec également la présentation des résultats.

3.1. Ecriture du modèle

L'écriture du modèle passe par une série d'hypothèses concernant les mécanismes réactionnels dans la phase continue ainsi que dans les particules afin d'aboutir au schéma cinétique.

Les principales hypothèses prises en compte concernent le système styrène / acrylonitrile. Un modèle à effet terminal a été considéré afin de simplifier les calculs. De plus, comme cela est suggéré par la littérature, des coefficients de réactivités plus petits que l'unité ont été considérés ainsi que des terminaisons uniquement par combinaison.

Un effet de gel a été pris en compte à l'intérieur des particules dépendant de la composition du copolymère ainsi que de la proportion massique de polymère solide dans les particules.

Le dernier point important concerne les mécanismes de greffage. Afin de simplifier les calculs et comme semble l'indiquer certains résultats expérimentaux, l'hypothèse simplificatrice a été faite qu'il ne pouvait y avoir qu'un seul greffon par chaîne de SAN. Cependant, afin de tenir compte du greffage naturel, le modèle considère la possibilité que le stabilisant précurseur, S5200, ainsi que le polyéther polyol de la phase continue peuvent se greffer sur les chaînes de SAN.

Parallèlement, différents modèles complémentaires sont nécessaires en ce qui concerne la relation entre les deux phases, en particulier les transferts d'oligoradicaux de la phase continue vers les particules par précipitation ou par absorption, le partage des espèces et la stabilité des particules.

Ainsi, concernant la précipitation, un modèle de nucléation aggrégative a été préféré à un modèle de nucléation homogène car plus réaliste. Ainsi, les chaînes de polymère formées par polymérisation en solution dans la phase continue s'associent les unes aux autres au fur et à mesure que leur degré de polymérisation et que leur concentration augmente. La vitesse de précipitation proposée est donc proportionnelle à la concentration des oligoradicaux en solution et des masses molaires moyennes.

La vitesse d'absorption des oligoradicaux par les particules dépend de la concentration de ces espèces et de la surface totale des particules. Cette surface totale est calculée en faisant l'hypothèse que les particules sont entièrement couvertes par les greffons et sont donc toutes parfaitement stabilisées. Ceci, permet également d'estimer un diamètre moyen de particules en supposant ces particules sphériques et monodisperses. Le diamètre moyen estimé provient alors du rapport entre le volume total des particules et la surface totale des particules. Ce type de modèle est très simpliste mais un modèle plus complexe de prédiction des distributions de tailles de particules est prématuré à ce niveau de l'étude.

De plus, les deux phases sont supposées être en équilibre thermodynamique. Les coefficients de partage des monomères ont été évalués par chromatographie gazeuse. Le coefficient de partage de l'acrylonitrile est de 1, celui du styrène est de 0,9, marquant ainsi une petite affinité avec la phase continue. Le coefficient de partage de l'agent de transfert a été également mesuré comme étant égal à 0,98.

En ce qui concerne l'amorceur, étant donné que le temps de demi-vie de cet amorceur est très court par rapport au temps de passage dans le réacteur, l'hypothèse est faite que la totalité de l'amorceur est décomposée dès son entrée dans le réacteur, et qu'il n'y a donc pas d'amorceur à l'intérieur des particules. Les radicaux présents dans les particules proviennent donc exclusivement des oligoradicaux de la phase continue qui ont précipité ou qui ont été absorbés.

A partir de ces schémas cinétiques et de ces modèles complémentaires les vitesses réactionnelles sont calculées et un bilan de chaque espèce présent dans le milieu est effectué menant à un système d'équations non linéaires algébro-différentielles.

3.2. Simulation

A partir de ces équations, il est nécessaire d'estimer l'état du réacteur en régime permanent c'est à dire de déterminer la concentration de chaque espèce présente dans le milieu. Le simulateur qui a été développé intègre ce système d'équations de manière dynamique grâce à une méthode de Runge-Kutta. L'intégration a été réalisée sur 10000 s avec un pas de temps de 0,1 s. Le choix de ses deux paramètres est un compromis entre la précision des calculs et le temps de calcul qui doit être le plus court possible afin de permettre l'identification ultérieure des paramètres inconnus.

Il a été nécessaire de faire l'approximation de l'état quasi-stationnaire afin de supprimer les instabilités numériques qui perturbaient la résolution du système. Par conséquent, les vitesses de production de tous les radicaux sont considérées comme nulles et seule les équations différentielles liées aux monomères, à l'agent de transfert, à l'amorceur, au stabilisant précurseur, au polyéther polyol, au polymère mort et à ses moments sont considérées.

Connaissant l'état du système le simulateur calcule alors différentes données qui pourront être comparées aux données mesurées expérimentalement :

- Les masses molaires moyennes en nombre et en masse du CPP,
- Les conversions partielles en styrène, acrylonitrile et agent de transfert,
- Le pourcentage de solide présent dans le CPP purifié,
- La composition du copolymère SAN,
- La proportion massique de chaînes SAN dissoutes dans le sérum,
- La proportion de chaînes SAN greffées dans le CPP ainsi que dans le sérum,
- La quantité de polyol greffé sur le solide,
- Le diamètre moyen des particules.

Le simulateur permet alors de calculer ces données théoriques à partir de conditions expérimentales données. Cependant, 31 paramètres intervenant dans les différentes équations du système à résoudre sont inconnus. Il est ainsi nécessaire de procéder à l'identification de ces paramètres.

3.3. Identification paramétrique

3.3.1. Principe

Le programme effectuant l'identification paramétrique essaie de déterminer les meilleurs paramètres afin de réduire autant que possible l'écart entre les données théoriques proposées par le simulateur et les données qui ont été mesurées sur des échantillons réalisés dans les mêmes conditions.

L'algorithme itératif d'optimisation qui a été utilisé est un algorithme d'évolution dont le principe est le suivant : une population initiale est générée et chaque individu est généré à partir d'un domaine de recherche défini. Un individu est ici le vecteur contenant les différents paramètres à identifier. Le domaine de recherche est donc l'ensemble des domaines de recherches correspondant à chaque paramètre à identifier. Cette population forme un ensemble de solutions potentielles au problème d'optimisation. Une performance est associée à chaque solution potentielle c'est à dire à chaque individu par le biais d'une fonction d'évaluation déduite du critère d'optimisation. Dans le cas présent il s'agit de minimiser le logarithme de la somme des écarts entre données expérimentales et données théoriques au carré. Tant que la population ne convient pas ou que le critère d'arrêt n'est pas respecté, un processus de sélection, qui favorise la survie des individus les mieux adaptés au détriment des plus faibles, est effectué avec un renouvellement de la population par opérateurs génétiques (croisement, mutation).Cette approche itérative permet de faire évoluer les individus de génération en génération jusqu'à l'obtention d'une population solution la meilleure possible. La figure 15 schématise le principe général des algorithmes d'évolution.

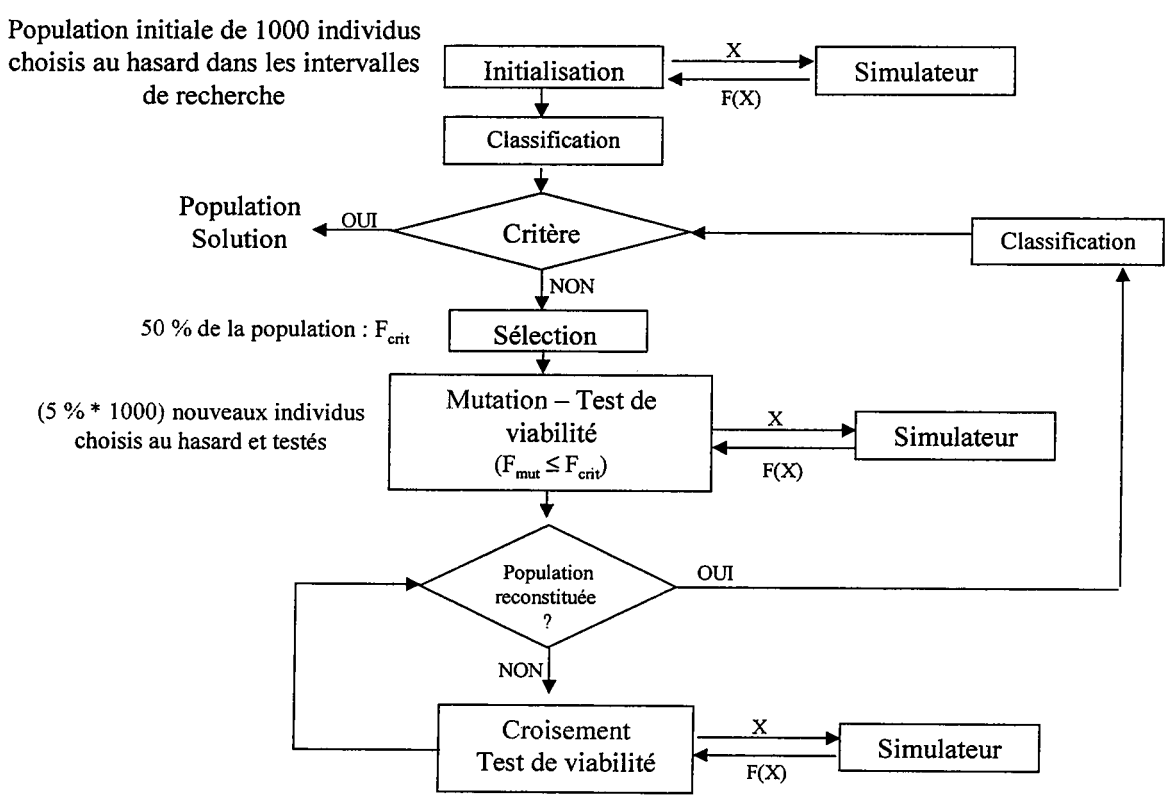

Figure 15 : Principe général de l'algorithme d'évolution utilisé

3.3.2. Résultats

L'identification paramétrique a d'abord été effectuée en négligeant les mécanismes de greffage naturels ainsi que l'absorption, ne laissant plus que 24 paramètres à déterminer. Les paramètres ont ensuite été identifiés à deux températures différentes : à 120 °C à l'aide de 145 mesures différentes ainsi qu'à 140 °C à l'aide de 195 mesures différentes. Les principaux résultats sont résumés ci-dessous.

3.3.2.1. Masses molaires moyennes

En comparant les masses molaires moyennes en nombre et en masse mesurées par GPC avec les celles données par le modèle permet de montrer que le modèle sous-estime ces masses molaires moyennes (voir figures 16 et17). Il faut cependant rappeler que les masses molaires moyennes théoriques prévoient les masses molaires théoriques en tenant compte de la présence d'acrylonitrile dans le copolymère. Or les mesures ayant été effectué à l'aide d'un étalonnage avec des standards de polystyrène surestiment les masses molaires. Cette déviation entre les valeurs mesurées en polystyrène par rapport aux valeurs absolues augmente avec la quantité d'acrylonitrile dans le copolymère. Ceci explique la plus grande déviation entre théorie et expérience due aux points correspondant aux expériences réalisées avec un rapport massique styrène / acrylonitrile = 60 / 40.

3.3.2.2. Taux de solides et conversions

Les figures 18 à 21 présentent les comparaisons entre les taux de solides et les conversions partielles en styrène, acrylonitrile et agent de transfert obtenus théoriquement et les mesures. Globalement le modèle estime correctement ces valeurs qui sont pour la plupart comprise dans les ± 5 % d'erreurs expérimentale attribuées à ces méthodes de mesures. uelques points sortent de cette marge d'erreur et correspondent en fait aux points correspondants aux expériences qui ont mené à des dispersions instables de particules.

3.3.2.3. Greffage : % de chaînes SAN greffées et % de polyol greffé

La figure 22 montre la comparaison entre les pourcentages de chaînes SAN greffées mesurés et les valeurs théoriques. Cette représentation montre que le modèle sous-estime le greffage. Cependant, il est à noter une importante erreur expérimentale sur les mesures ainsi que le fait que l'augmentation de la quantité de stabilisant précurseur, S5200, ne modifie pas sensiblement les résultats expérimentaux comme cela avait déjà été vu dans les chapitres précédents. Par conséquent le modèle essaie tente de prévoir un mécanisme qui semble se dérouler d'une manière différente.

Le pourcentage de polyol greffé sur le solide n'est pas non plus bien décrit par le modèle étant donné qu'il n'y a pas de variations de ces valeurs avec les variations de la quantité de S5200 (figure 23).

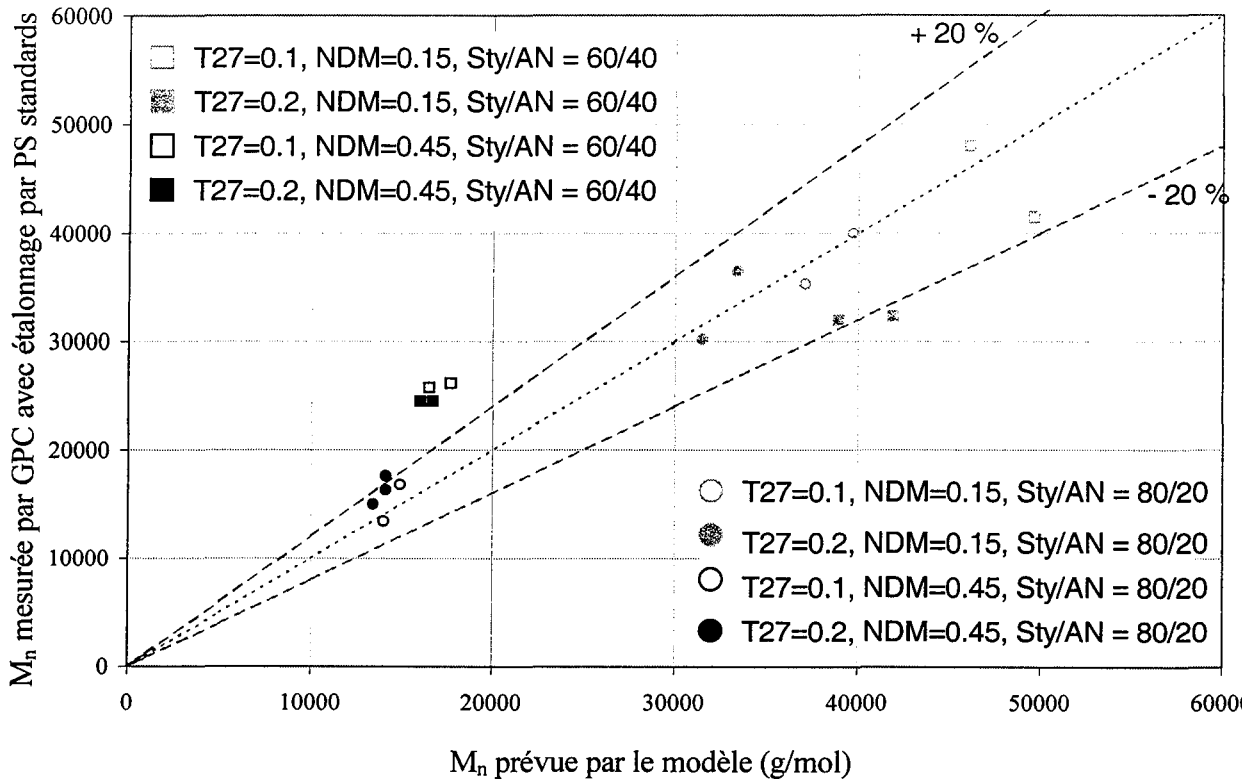

Figure 16 : Comparaison entre les masses molaires en nombres mesurées et prévues par le modèle utilisant les paramètres identifiés à T = 140 °C

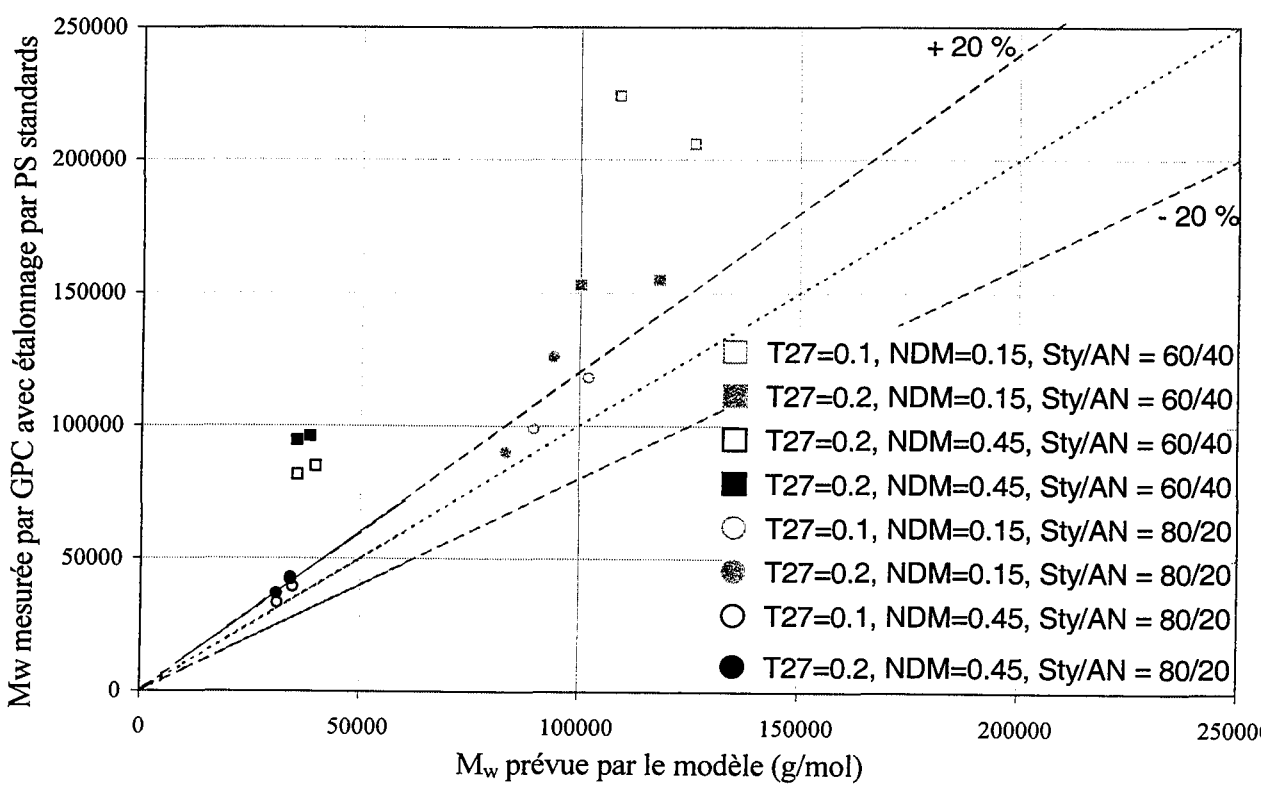

Figure 17 : Comparaison entre les masses molaires en masses mesurées et prévues par le modèle utilisant les paramètres identifiés à T = 140 °C

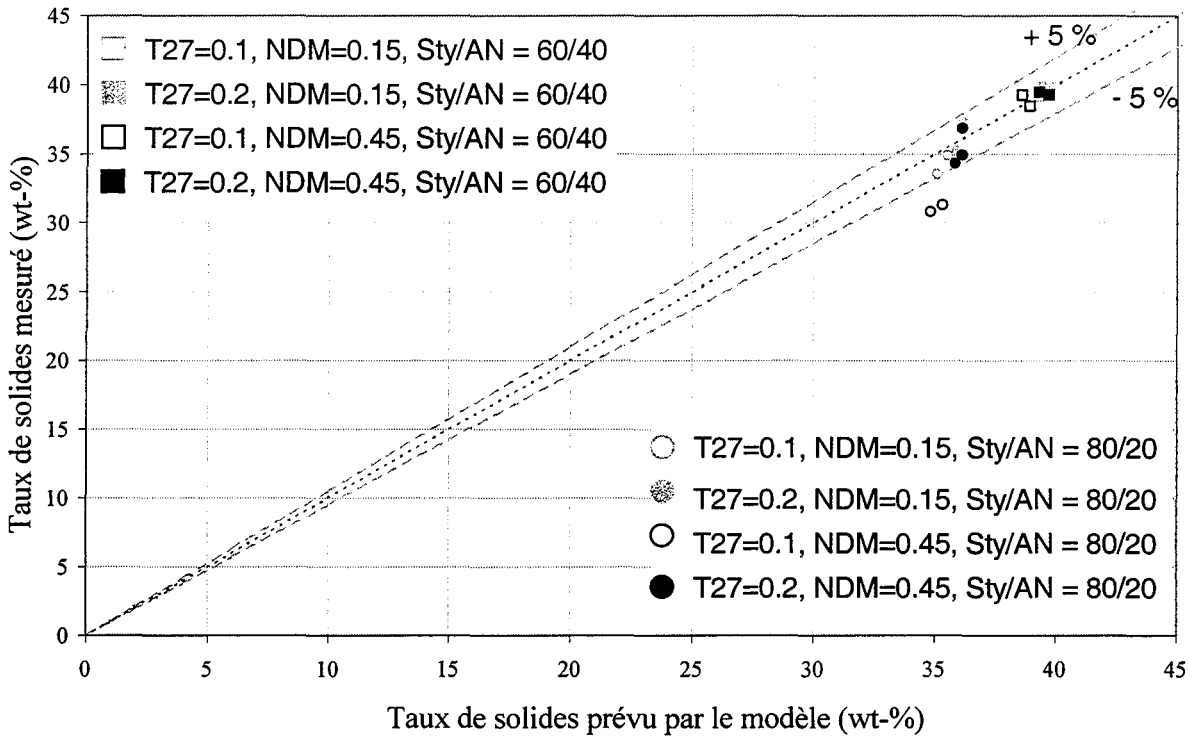

Figure 18 : Comparaison entre les taux de solides mesurés et prévus par le modèle utilisant les paramètres identifiés à T = 140 °C

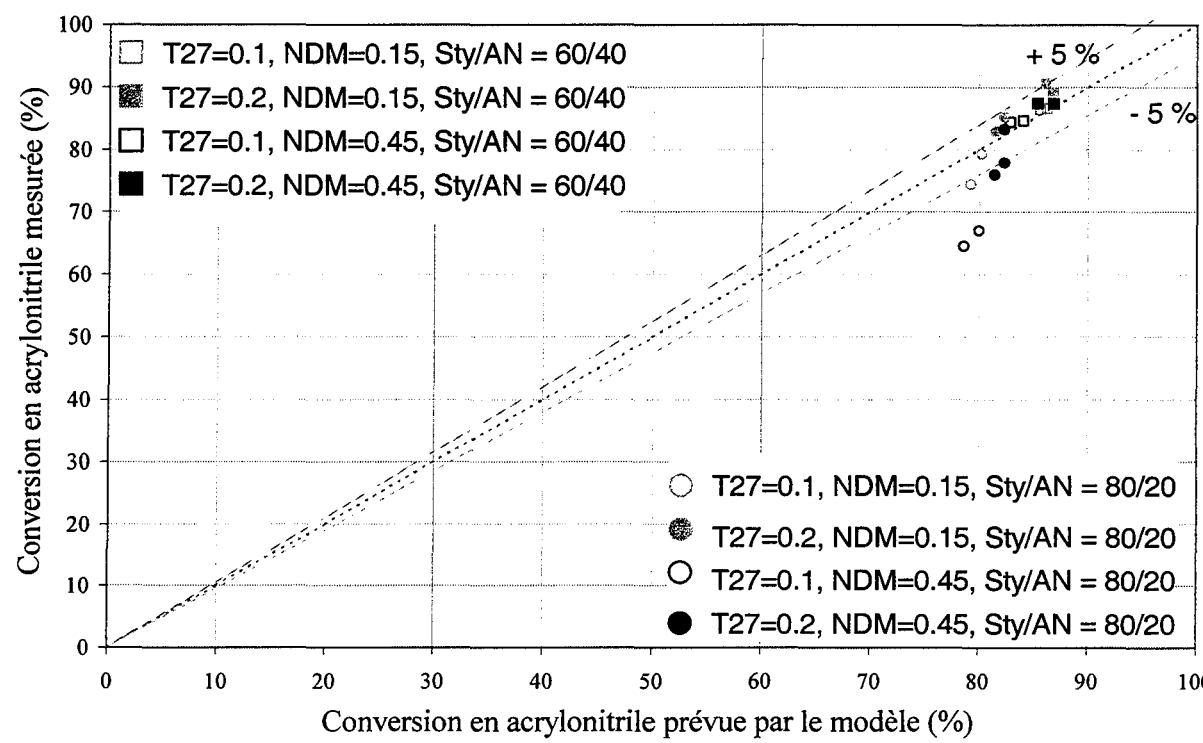

Figure 19 : Comparaison entre les conversions en acrylonitrile mesurées et prévues par le modèle utilisant les paramètres identifiés à T = 140 °C

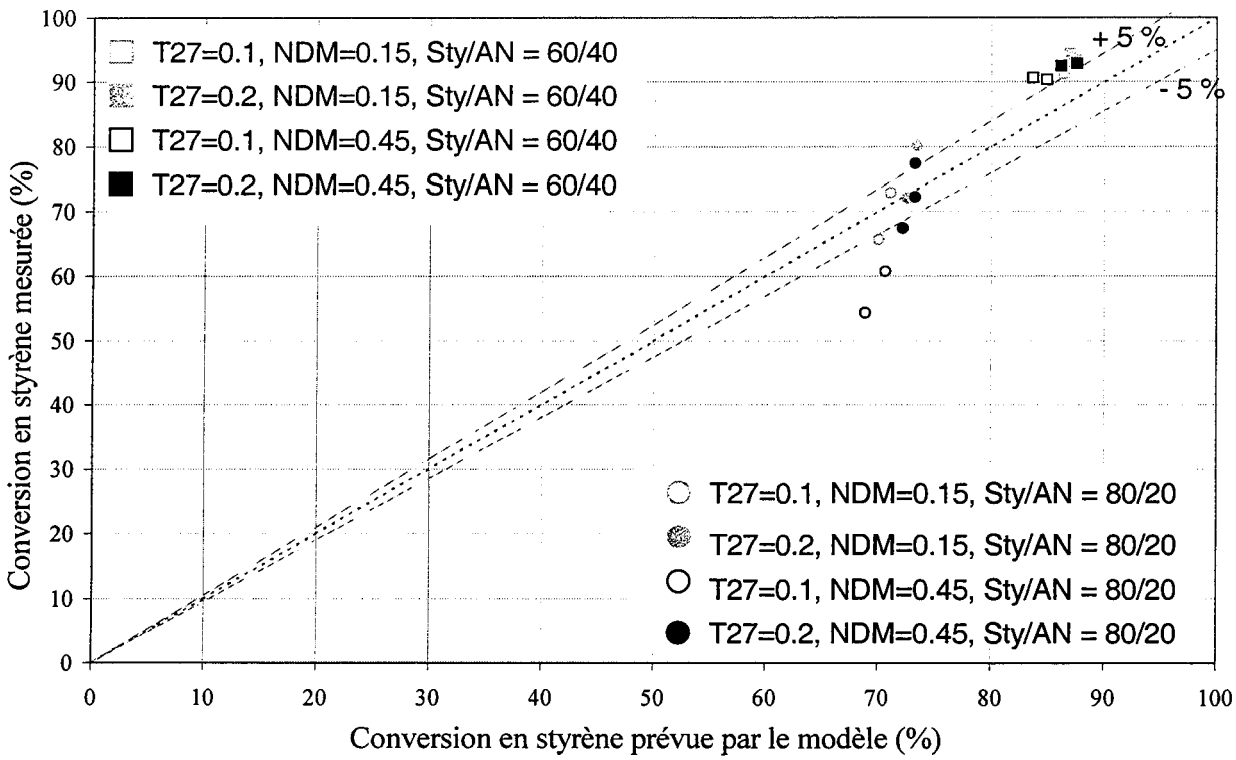

Figure 20 : Comparaison entre les conversions en styrènes mesurées et prévues par le modèle utilisant les paramètres identifiés à T = 140 °C

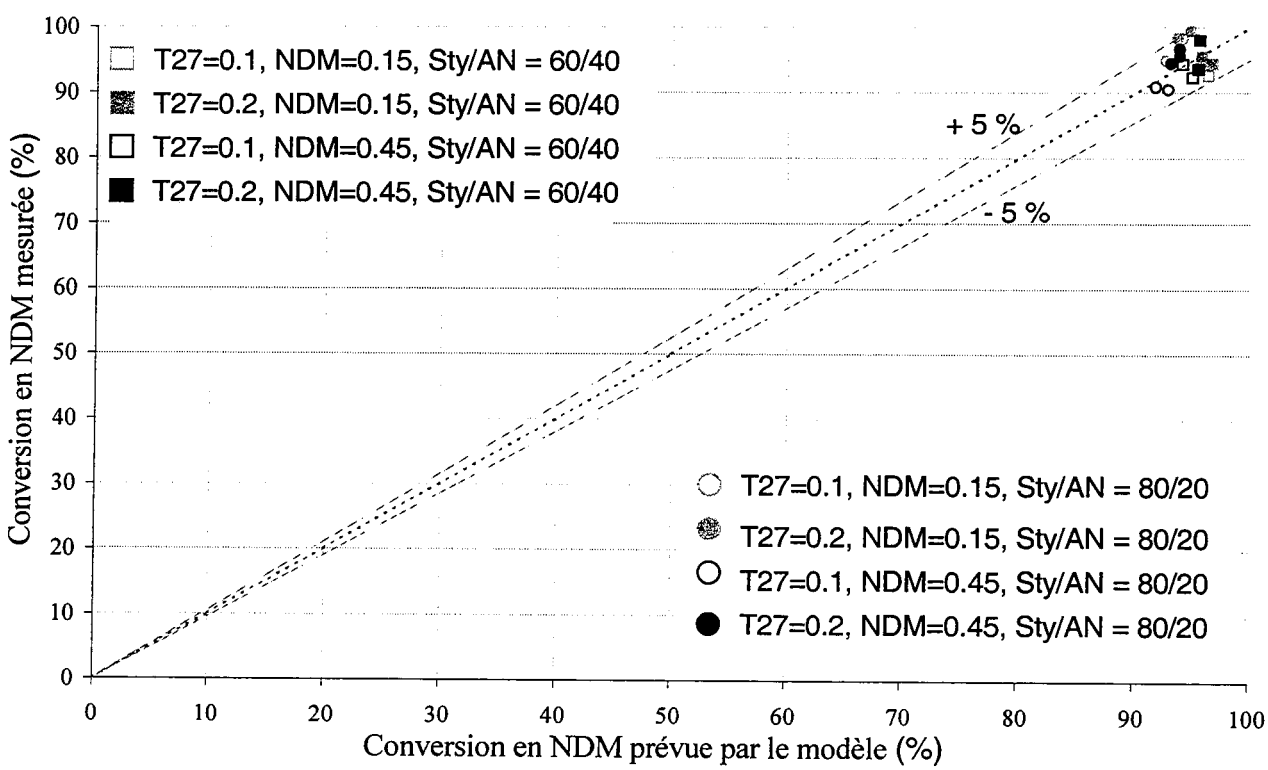

Figure 21 : Comparaison entre les conversions en NDM mesurées et prévues par le modèle utilisant les paramètres identifiés à T = 140 °C

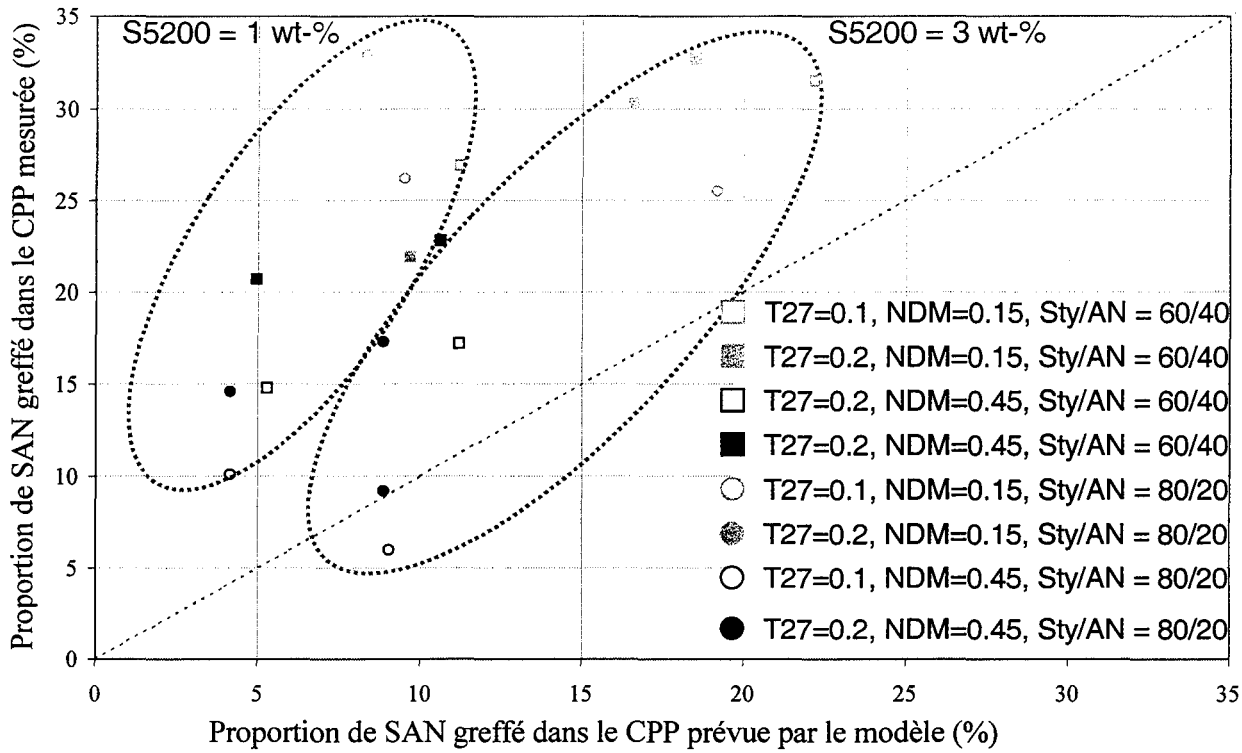

Figure 22 : Comparaison entre les proportions de chaînes SAN greffées mesurées et prévues par le modèle utilisant les paramètres identifiés à T = 140 °C

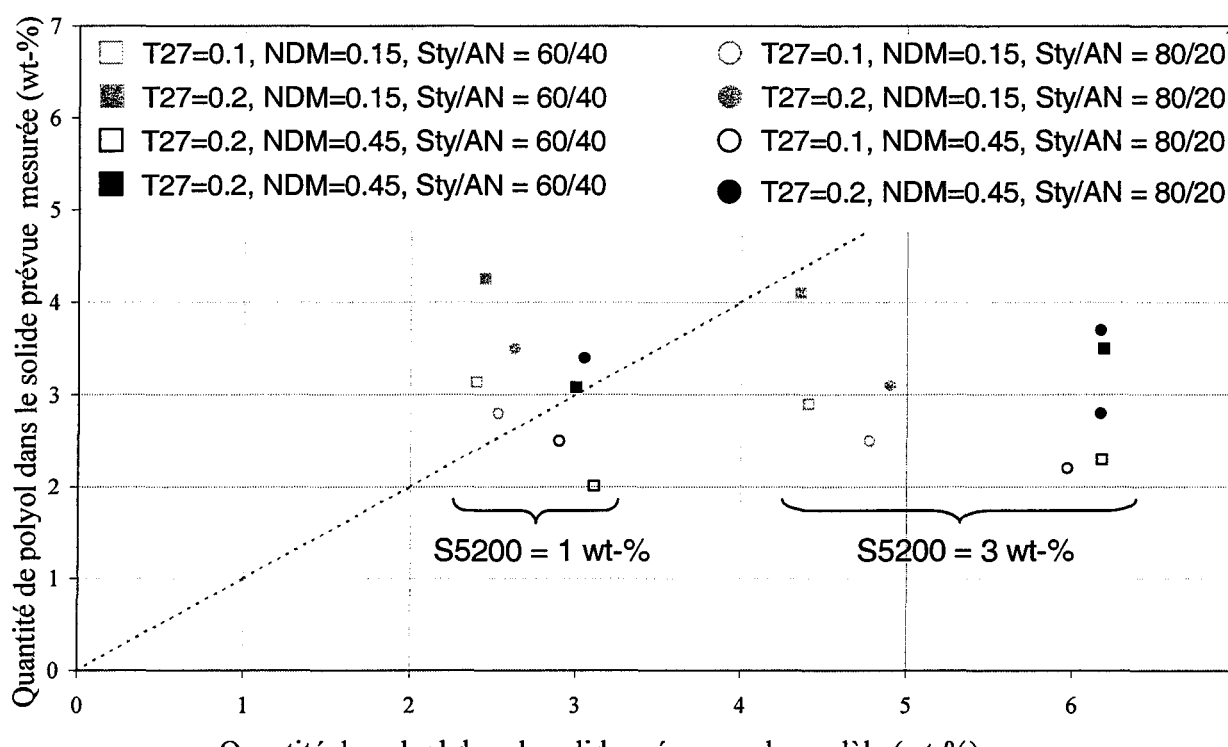

Figure 23 : Comparaison entre les quantités de polyol dans le solide mesurées et prévues par le modèle utilisant les paramètres identifiés à T = 140 °C

3.3.2.4.Diamètres moyens de particules

Seuls les diamètres de particules moyens estimés sur les échantillons obtenus avec 60 % de styrène ont été considérés pour l'identification, les copolymères polyols obtenus avec 80 % de styrène étant trop instables pour mesurer un diamètre moyen de particules significatif.

Comme cela est observable sur la figures 24, le modèle prévoit ces diamètres moyens avec un ordre de grandeur acceptable compte tenu de l'ensemble des approximations effectuées.

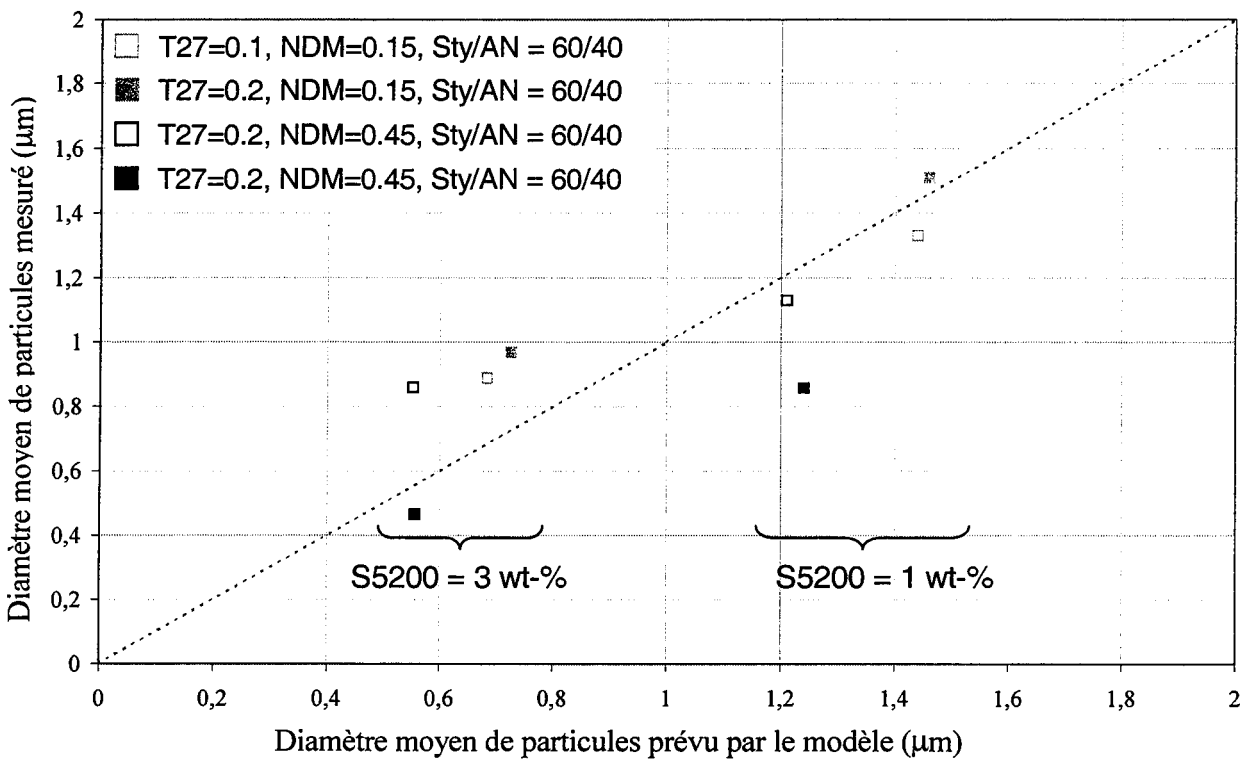

Figure 24 : Comparaison entre les tailles moyennes de particules mesurées et prévues par le modèle utilisant les paramètres identifiés à T = 140 °C

3.3.2.5. Greffage naturel et absorption

Le pourcentage de chaînes greffées étant sous-estimé par un modèle ne considérant que le greffage du S5200 sur les chaînes SAN, des tentatives d'identifier les paramètres cinétiques correspondant au greffage naturel ont été tentées. Cependant, cela n'a pas permit d'améliorer la prédiction du modèle car au lieu d'augmenter la quantité de greffage cela la fait diminuer car en effet cela a fait diminuer légèrement le degré de polymérisation des chaînes SAN. Ainsi, l'introduction dans le modèle de ce greffage naturel augmente le nombre de radicaux présents dans le milieu réduisant les masses molaires et par conséquent le pourcentage de chaînes greffées comme cela a été observé dans l'étude expérimentale.

De plus, l'introduction de coefficients de diffusion des oligoradicaux non nuls n'a pas permis d'obtenir de meilleurs résultats d'identification.

3.4. Premiers éléments de validation

La validation du modèle a été effectuée grâce aux expériences réalisées au centre du plan d'expérience c'est à dire avec les mesures réalisées sur les échantillons produits dans les conditions standards. Les paramètres à 130 °C ont été estimés en faisant la moyenne des paramètres obtenus à 120 °C et à 140 °C, qui sont très proches.

Le tableau 4 présente la comparaison entre les valeurs données par le simulateurs et les intervalles expérimentaux mesurés.

Tableau 4. : Données simulées comparées aux mesures réalisées dans les conditions standards

Données	Valeurs théoriques	Intervalle expérimental	Unité	Mesures provenant du tableau	Nombre de mesures effectuées
$\bar{M}_n$	25300	26000 - 37900	g mol^{-1}	A3.5	5
$\bar{M}_w$	59800	64100 - 98200	g mol^{-1}	A3.5	5
Solides	38.5	32.1 – 40.3	wt-%	A3.10	2
AN résiduel	1.85	1.58 – 2.17	wt-%	A3.10	2
Conversion en AN	85.7	83.2 – 87.7	%	A3.10	2
Sty résiduel	5.42	3.61 – 4.57	wt-%	A3.10	2
Conversion en Sty	82.0	84.8 – 88.0	%	A3.10	2
NDM résiduel	140	96.3 - 118	ppm	A3.10	1
Conversion en NDM	95.3	96.1 – 96.8	%	A3.10	1
Composition du SAN en AN	30.9	19.2 – 34.8	wt-%	A3.25	2
SAN dans le sérum	0.56	0.84 – 1.28	wt-%	A3.31	2
SAN greffé dans le sérum	24.2	42.1 – 93.2	%	A3.20	2
SAN greffé dans le CPP	16.2	12.9 – 19.3	%	A3.20	1
Polyol dans le solide	5.98	1.54 – 3.25	wt-%	A3.25	2
D[3, 2]	0.346	0.71 – 1.06	µm	A3.15	1

Les masses molaires moyennes semblent être légèrement sous-estimées mais il faut tenir compte du fait que les valeurs mesurées sont en polystyrène. Des mesures ont montré qu'avec des standards de SAN de composition sty / AN = 75 / 25 les valeurs absolues sont égales aux valeurs

mesurées en polystyrène multipliées par 0,8. Les conditions standards étant proches de cette composition, ce facteur 0,8 peut être une meilleure approximation des masses molaires moyennes et en l'appliquant aux résultats du tableau ci-dessus, les masses molaires prédites entrent bien dans l'intervalle expérimental.

De plus le pourcentage de solides, la composition du copolymère et les conversions partielles en styrène, acrylonitrile et agent de transfert sont acceptables.

La proportion de chaînes SAN greffées semble correctement estimée, cependant la proportion de polyol dans le solide est surestimée. Ceci met en évidence le fait que ce modèle simple de greffage ne permette pas de prévoir les mécanismes de greffage.

L'ordre de grandeur du diamètre moyen de particules est acceptable et inférieur au micromètre comme le sont les valeurs mesurées.

Conclusions et perspectives

Les objectifs de ce travail étaient d'apporter de meilleures connaissances sur le procédé de fabrication des copolymères polyols, en particulier en ce qui concerne les mécanismes de greffage, les cinétiques réactionnelles ainsi que le lien entre les conditions expérimentales et le site de la polymérisation et les conséquences sur les propriétés des CPPs.

Différents moyens ont été mis a disposition afin d'atteindre ces objectifs. Tout d'abord, une étude des conditions expérimentales sur les propriétés des copolymères polyols a été mis en œuvre nécessitant l'utilisation de méthodes analytiques les plus complètes possibles. Cette étude a permis d'améliorer la connaissance du procédé et d'aider à l'élaboration d'un modèle pouvant calculer les données qui sont mesurées. Un programme d'identification paramétrique suivant un algorithme d'évolution a permis de déterminer les paramètres inconnus de ce modèle aux deux températures de travail. Une validation de ce modèle a ensuite été effectuée grâce aux expériences réalisées dans les conditions standards.

Les conclusions principales concernant ce travail sont présentées ci-dessous. L'étude des distributions de masses molaires a mis en évidence la présence de trois populations de chaînes SAN. Une population de courtes chaînes produites par polymérisation en solution dans le sérum ainsi qu'une population de chaînes plus longues qui pourraient correspondre aux chaînes SAN greffées *in situ* par le stabilisant précurseur S5200. La troisième population de grandes masses molaires correspond au copolymère SAN produit par polymérisation en masse à l'intérieur des particules. L'augmentation de la quantité d'agent de transfert et de styrène dans le milieu réduit les masses molaires moyennes des CPPs en diminuant le degré de polymérisation des chaînes dans les particules et en augmentant la proportion d'espèces produites dans la phase continue, c'est à dire en déplaçant le site de la polymérisation vers la phase continue.

De plus la viscosité des copolymères polyols est directement liée aux masses molaires du copolymère SAN. Ainsi, le rapport styrène/acrylonitrile et la quantité d'agent de transfert sont les deux paramètres qui influencent majoritairement cette viscosité. Cependant, l'augmentation de la quantité d'amorceur et de la température augmente le nombre d'espèces radicalaires présentes dans le milieu et augmente également sensiblement la viscosité.

Les tailles de particules observées par diffraction laser sont polydisperses et des images obtenues par microscope électronique à balayage ont complété cette étude permettant de mettre en évidence l'instabilité des particules et la présence d'agglomérats en fonction des conditions expérimentales.

Il a été également observé que la quantité de stabilisant précurseur agissait sur la stabilité des dispersions de particules alors que la proportion de chaînes SAN greffées n'est pas modifiée. Il a donc été suggéré que le S5200 pourrait stabiliser les particules en étant libre en solution et non pas en étant greffé sur le SAN et qu'il agirait plutôt par stabilisation par déplétion. Il faut cependant rappeler que dans les conditions expérimentales utilisées un forte proportion du greffage est due à un greffage naturel, ne permettant pas de conclure sur l'effet du S5200 seul.

En conclusion de cette étude expérimentale, les paramètres expérimentaux qui influencent majoritairement les propriétés des copolymères polyols sont ceux qui interviennent sur le degré de polymérisation des chaînes SAN, dont dépendent le pourcentage d'espèces greffées ainsi que la viscosité du milieu.

En ce qui concerne la partie modélisation du procédé, les chapitres 4 et 5 montrent les différents outils qui ont été développés. Une série d'hypothèses effectuées concernant les mécanismes réactionnels et les transferts entre la phase continue et les particules ont permis d'aboutir à un système d'équations non-linéaires algébro-différentielles. Malgré la complexité du procédé, l'instabilité d'une partie des mesures et l'imprécision sur certaines mesures, l'identification paramétrique qui a été effectuée a permis de montrer que ce modèle permet de prévoir avec un ordre de grandeur correct les masses molaires moyennes, le taux de solide ainsi que les conversions en styrène, acrylonitrile et agent de transfert.

Les mécanismes de stabilisation des particules semblent par contre plus complexes que le modèle de greffage simplifié utilisé.

Différentes recommandations peuvent être apportées afin de prolonger ce travail.

(1) Premièrement, le plan expérimental et les conditions expérimentales devraient être réadaptée dans le but de limiter les problèmes d'instabilité ainsi que les mécanismes de greffage naturel. En particulier il serait recommandé de ne plus utiliser la composition Sty / AN = 80 / 20 car produisant des CPPs trop instables. Par contre il serait préférable d'utiliser des rapoorts Sty/AN = 70/30 et Sty/AN = 60/40. Afin de limiter la présence de greffage naturel il est possible d'utiliser comme solvant un polyéther polyol produit par catalyse avec le DMC pour réduire la quantité d'alcools insaturés ainsi que d'utiliser un amorceur de type AMBN (azo(bis-méthylbutyronitrile)). Ceci permettra d'observer plus précisément l'influence du stabilisant précurseur S5200.

(2) Deuxièmement, Il est nécessaire d'améliorer la précision de certaines mesures, en particulier de mieux estimer les masses molaires par rapport à des étalons de copolymères SAN de composition les plus proches possibles des composition utilisées. De plus, les données obtenues concernant le sérum étant dépendante des conditions de la séparation sérum/particules, ces valeurs ne sont pas quantitatives et ne permettent pas d'aider à l'identification paramétrique. Afin de gagner du temps sur les analyses, ces mesures ne sont pas nécessaires. De même la mesure de la composition du copolymère n'apporte pas d'information suffisamment pertinente pour aider à l'identification étant donné que cette composition ne dépend que de la composition du mélange initial dans un réacteur continu agité.

(3) Troisièmement, lorsque les résultats d'identification seront améliorés, il sera nécessaire d'estimer plus précisément la précision des paramètres estimés par l'identification paramétrique. Ainsi il serait également important d'étudier l'influence sur ces paramètres des caractéristiques de l'algorithme d'évolution (taille des populations, nombre de mutations, nombre d'individus remplacés) ainsi que des conditions d'intégration (le pas d'intégration et le temps final).

(4) Quatrièmement, d'autres paramètres expérimentaux pourraient être intégrer dans l'étude expérimentale comme le débit et la vitesse d'agitation.

(5) L'étape suivante serait de réduire ce modèle de tendances afin de simplifier le modèle de manière à ce qu'il puisse prédire des caractéristiques précises avec le but final d'effectuer une optimisation multicritère. En effet le but de cette modélisation est de déterminer numériquement l'ensemble des conditions expérimentales permettant de maximiser certaines propriétés comme la stabilité, le taux de solides, les conversions tout en minimisant d'autres caractéristiques comme la viscosité ou les coûts de production.

INSTITUT NATIONAL
POLYTECHNIQUE
DE LORRAINE

AUTORISATION DE SOUTENANCE DE THESE DU DOCTORAT DE L'INSTITUT NATIONAL POLYTECHNIQUE DE LORRAINE

o0o

VU LES RAPPORTS ETABLIS PAR :
Monsieur Brian Walta BROOKS, Professeur, Loughborough University, United Kingdom
Monsieur VAN DER WAL Hanno, Professeur, DOW Benelux N.V., The Netherlands

Le Président de l'Institut National Polytechnique de Lorraine, autorise :

Monsieur SALVADOR Bruno

NANCY BRABOIS
2, AVENUE DE LA
FORET-DE-HAYE
BOITE POSTALE 3
F - 54501
VANŒUVRE CEDEX

à soutenir devant un jury de l'INSTITUT NATIONAL POLYTECHNIQUE DE LORRAINE, une thèse intitulée :

« Etude expérimentale et modélisation du procédé continu ensemencé de copolymérisation en dispersion du système styrène/acrylonitrile en milieu polyol »

en vue de l'obtention du titre de :

DOCTEUR DE L'INSTITUT NATIONAL POLYTECHNIQUE DE LORRAINE

Spécialité : « Génie des procédés »

Fait à Vandoeuvre, le 14 juin 2004
Le Président de l'I.N.P.L.,
L. SCHUFFENECKER

TEL 33/03.83.59.59.59
FAX. 33/03.83.59.59.55

Étude Expérimentale et Modélisation du Procédé Continu Ensemencé de Copolymérisation en Dispersion du Système Styrène/Acrylonitrile en Milieu Polyol

Résumé

Ces travaux de recherche ont pour but d'étudier et de modéliser un procédé continu ensemencé de copolymérisation en dispersion d'acrylonitrile et de styrène en milieu polyol : l'influence des conditions expérimentales sur les propriétés physiques des copolymères polyols produits est examinée à dessein de mieux comprendre les mécanismes mis en jeu et de développer un modèle de tendances pour le procédé global.
La première partie concerne l'étude expérimentale du procédé. L'influence du rapport des compositions en styrène et acrylonitrile, la température de réaction et les concentrations en agent de transfert, amorceur et stabilisant précurseur, sur les propriétés des copolymères polyols, est étudiée. Cela permet d'établir les différentes relations existant entre la distribution de masses molaires, le niveau de greffage, la viscosité, la distribution de tailles de particules et le site de la polymérisation. Cette étude montre également la complexité des phénomènes de stabilisation de particules qui interviennent.
La seconde partie présente la modélisation du procédé ainsi que l'identification des paramètres inconnus de ce modèle. En effet, un modèle destiné à prévoir les masses molaires moyennes, les conversions ainsi que le niveau de greffage des copolymères polyols est développé malgré la complexité du procédé et le manque de précision de certaines des mesures. Un algorithme d'évolution permet, en utilisant un nombre important d'expériences, d'identifier ces paramètres. Une validation préliminaire du travail est effectuée et permet de définir avec plus de précision les futures voies de recherche dans le domaine.

Mots clés : Copolymérisation en dispersion, Modélisation, Algorithme d'évolution, Copolymère polyol

Experimental Study and Modeling of the Seeded Continuous Dispersion Copolymerization of the Styrene/Acrylonitrile System in Polyol Medium

Abstract

The aim of this work is to study and model the continuous seeded dispersion copolymerization of acrylonitrile with styrene in polyol medium : the influence of the process conditions on the physical properties of the copolymer polyols produced is investigated in order to better understand the different mechanisms involved and to develop a tendency model for the whole process.
The first part deals with the experimental study of the process. The influence of the styrene to acrylonitrile ratio, the temperature and the concentrations of the chain transfer agent, the initiator, and the precursor stabilizer, on the physical properties of copolymer polyols are studied. This allows to understand better the relationships between the molecular weight distributions, the grafting level, the viscosity, the particle size distributions, and the locus of polymerization. This study shows also the complexity of the phenomena involved in the particle stabilization.
The second part presents the modeling of the overall process and the identification of the parameters of this model. Indeed, a model intended to forecast the average molecular weights, the conversions and the grafting level in the copolymer polyols is developed in spite of the process complexity and the lack of accuracy of some of the measurements. An evolutionary algorithm allows then, with a consequent number of experiments realized, to identify the unknown parameters of this model. A preliminary validation of the work is presented and helps to define the ways to go further with this research.

Keywords : Dispersion polymerization, Modeling, Evolutionary algorithm, Copolymer polyol

Discipline : Génie des Procédés
Laboratoire de Recherche : Laboratoire des Sciences du Génie Chimique,
U.P.R.-C.N.R.S. 6811, 1 rue Grandville, BP 451, 54001 Nancy Cedex